SYNTHESIS, MODIFICATION, AND

APPLICATION OF MESOPOROUS

MATERIALS BASED ON MCM-41

By

ZEID ABDULLAH AL-OTHMAN

Bachelor of Science

King Saud University

Riyadh, Saudi Arabia

1997

Submitted to the Faculty of the
Graduate College of the
Oklahoma State University
in partial fulfillment of
the requirements for
the Degree of
DOCTOR OF PHILOSOPHY
December, 2006

SYNTHESIS, MODIFICATION, AND

APPLICATION OF MESOPOROUS

MATERIALS BASED ON MCM-41

Thesis Approved:

_____Dr. Allen W. Apblett _____
Thesis Adviser
_____Dr. K. Darrell Berlin _____

_____Dr. Neil Purdie _____

_____Dr. Gary Foutch_____

_____ Dr. A. Gordon Emslie _____
Dean of the Graduate College

ACKNOWLEDGMENTS

In the Name of Allah, Most Gracious, Most Merciful

Greatest thanks are first and foremost due to Allah (SWT) for giving me the health, ability, strength and blessing to make this work possible. My success in everything can only come from Allah. In Him I trust, and unto Him I turn.

I would like to thank all people who have helped me along the way. First of all, I wish to express my sincere appreciation and gratefulness to my thesis advisor, Dr. Allen W. Apblett, for his intelligent supervision, constructive guidance, inspiration and friendship over the years of my graduate studies and during my dissertation research work at Oklahoma State University.

I would also like to express my sincere gratitude to my committee members Dr. Darrell Berlin, Dr. Neil Purdie, and Dr. Gary Foutch, whose guidance, assistance and friendship have been very valuable to me during this investigation. I also wish to thank Dr. Darrell Berlin for his valuable guidance and discussions during this investigation.

I would like also to express my sincere gratitude to Dr. Margaret Eastman, the manager of Oklahoma statewide NMR facility and solid-state NMR, for recording the ^{13}C and ^{29}Si solid-state NMR spectra for my solid specimens and Mrs. Phoebe Doss, the manager of the electron microscopy laboratory at Oklahoma state university, for doing the SEM and TEM images. They were very cooperative and helpful in the work.

I would like also to seize this opportunity to thank all the faculty members of the Department of Chemistry at Oklahoma State University from whom I learned much

iv

during the time of my graduate studies. In addition, I thank the staff and secretaries of the Department of Chemistry for their kindness and cooperation.

I would also like to give my special thanks to my beloved parents for their love, supplications, patience, and support. I ask Allah to grant on you thy mercy even as you cherished me in childhood.

Profound appreciations and grateful honor to my wife, Afaf AL-Foraih, my children, Norah and Abdullah, for their love, patience, care, sacrifice, encouragement, cheerfulness and trust during my study. Thank you so much, I ask Allah to bless and take care of you.

I am extremely grateful to my brothers and sisters for their valuable suggestions, their strong encouragement at times of difficulty, love and understanding throughout the whole study.

I am grateful to my uncle, Abdulaziz AL-Foraih and Hasah AL-Saed, for their strong support at times of difficulty, love and understanding throughout the whole study.

I am particularly grateful to my faithful buddy Abdulaziz Bagabas for his constant encouragement, support, assistance, friendship, and advice. He was always available in person to help me on almost all the time.

I would like also to thank and appreciate Alan Piquett and Lisa Reilly for their help in correction and editing of my thesis.

I would like also to thank and appreciate the friendship and support of all of my lab-mates in Dr. Apblett's group.

I extend my thanks and gratitude to my close friends here in Stillwater, Oklahoma, for their encouragement and friendship.

I appreciate also the great help of my academic advisors, Dr. Sadedine Belarbi and Dr. Faleh Al-hogbani, at the Royal Embassy of Saudi Arabia Cultural Mission Attaché in Washington, D.C., USA.

Last but not least, I would like to express my thanks to all faculty member, colleagues, and staff at the Chemistry Department, King Saud University (KSU) for their assist and encouragement. I would like also to acknowledge the financial support of my sponsor King Saud University (KSU), Riyadh, Kingdom of Saudi Arabia.

I conclude these acknowledgements with the supplication of Prophet Solomon peace and blessing be upon him, as narrated by the Almighty Allah in The Holy Qur-ān in Sūrat An-Naml (Ants), verse 19, "O my Lord! So order me that I may be grateful for thy favors, which thou has bestowed on me and on my parents, and that I may work the righteousness that will please thee and admit me, by thy grace, to the ranks of thy righteous servants".

TABLE OF CONTENTS

CHAPTER FOUR   **PAGE**

SYNTHESIS OF MESOPOROUS MATERIALS BEARING DIAMINO FUNCTIONAL

CHAPTER FIVE   **PAGE**

SYNTHESIS OF MESOPOROUS MATERIALS BEARING METHACRYLATE

FUNCTIONAL GROUPS AND OTHER DERIVATIVES AND REMOVAL OF

CHAPTER SEVEN   **PAGE**

CHAPTER EIGHT   **PAGE**

FUNCTIONALIZED MESOPOROUS SURFACE WITH THIOL-FUNCTIONAL

GROUPS FOR HEAVY METAL RECOVERY.. 357

CHAPTER NINE   **PAGE**

PREPARATION OF MESOPOROUS MATERIALS BEARING BROMOPROPYL
FUNCTIONAL GROUPS AND AMINE DERIVATIVES FOR METAL ADSORPTION

LIST OF FIGURES

CHAPTER TWO   **PAGE**

CHAPTER FOUR   **PAGE**

LIST OF SCHEMES

LIST OF TABLES

CHAPTER ONE

INTRODUCTION, BACKGROUND, RATIONALE AND SCOPE OF THE STUDY

1.1. INTRODUCTION

The synthesis, characterization, and application of novel porous materials have

been strongly encouraged due to their wide range of applications in adsorption,

separation, catalysis, and sensors. The design, synthesis, and modification of porous

materials are in some aspects more challenging than the synthesis of dense materials.

Therefore, new strategies and techniques are continuously being developed for the

synthesis and structure-tailoring of mesoporous materials.[1,2]

Ordered mesoporous materials, based on MCM-41 (Mobile Crystalline Material),

are silicates obtained by hydrothermal synthesis and a liquid templating mechanism.[1,2]

Such materials exhibit remarkable features such as pores with well-defined sizes and

uniform shapes (with tunable channel diameter from 2.0 to 10.0 nm) that are ordered to

some degree over micrometer length scales to yield arrays of non-intersecting hexagonal

channels. The latter structures are readily identifiable by transmission electron

microscopy (TEM) images and X-ray powder diffraction (XRD) patterns, see Figure 1.1.

These materials possess high surface areas of about 1000 m^2/g as revealed from surface

area measurements. Mesoporous materials based on MCM-41 show excellent thermal,
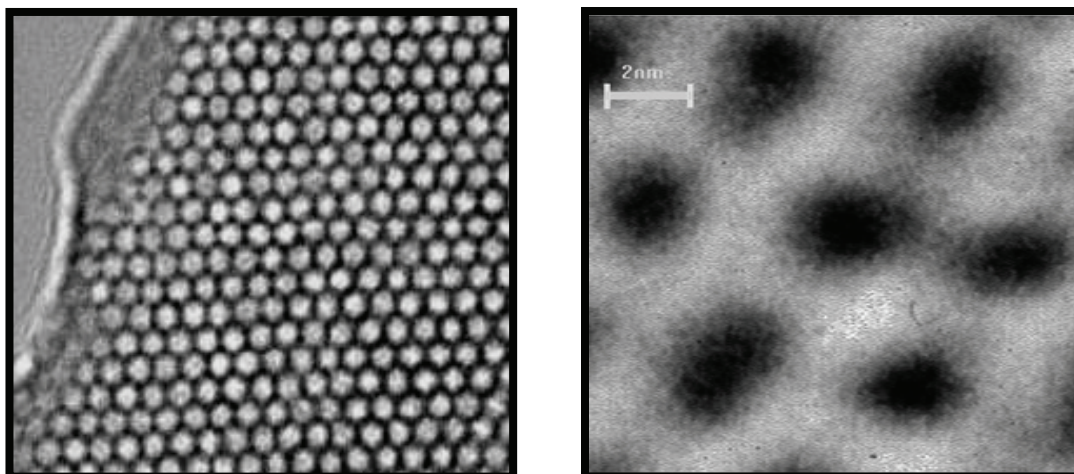
Figure 1.1. HRTEM images of MCM-41 with hexagonal channels.[2b]

hydrothermal, and hydrolytic stabilities.[3] The walls of the channels are amorphous SiO_2,

and the porosity can be as high as 80% of their total volume.[2,3] These materials can be

synthesized using anionic, cationic, or neutral surfactants or non-surfactant template

pathways. The diameter of the channels (pores) can be controlled to be within 2.0 nm to

10.0 nm by changing the length of the template molecule. Moreover, changing the silica

source [*e.g.,* fused silica, colloidal silica, tetraethylorthosilicate (TEOS)], surfactants

[*e.g.,* hexadecylamine (HDA), and cetyltrimethylammonium bromide (CTAB)], auxiliary

compounds [*e.g.,* 1,3,5- trimethylbenzene (TMB)], or reaction conditions, such as

solvent, temperature, aging time, reactant mole ratio, and the pH of the medium, will lead

to the production of new mesoporous systems with different pore sizes, pore volumes,

and wall thicknesses. At the same time, these changes will also affect the thermal,

hydrothermal, and mechanical stabilities of the materials.[1-3]

Functionalization of the surface of these mesoporous materials with organic or

inorganic functional groups leads to new physical and chemical properties. These

2

modified materials can be used in a variety of applications such as catalysis, adsorption, and separation as chromatographic column packing.

The scope of this thesis encompasses the development, characterization, and applications of ordered mesoporous materials, based on MCM-41. It is intended that this thesis will provide a comprehensive overview on synthesis, formation mechanisms, characterization, modification, and applications of mesoporous materials based on MCM-41 in order to identify significant trends.

In this research investigation, several ordered mesoporous materials have been synthesized using the previous reported procedures with some alterations. The resulting products will be denoted as OSU instead of MCM-41, and there will be numbers and letters following the symbol (OSU) which will be explained in the following chapters.

These materials have been characterized using several characterization techniques including X-ray powder diffraction (XRD), elemental analysis, diffuse reflectance infrared Fourier transform spectroscopy (DRIFTS), scanning electron microscopy (SEM), transmission electron microscopy (TEM), elemental analysis (EA), thermogravimetric analysis (TGA), solid-state ^{29}Si and ^{13}C nuclear magnetic resonance spectroscopy (NMR), and surface area analysis including pore size, pore volume, and pore size distribution (PSD) measurements. In addition, the as-synthesized materials have been subjected to derivitization reactions in order to modify their surface with functional groups of interest. Their adsorption efficiency and selectivity have been determined along with their applications in separation of heavy and transition metal ions, radioactive materials, and organic compounds.

The first chapter provides an introduction to the fundamental aspects of mesoporous materials. It includes a brief historical introduction to MCM-41, an overview of mesoporous materials, a brief beginning to the surfactant science, a general introduction to sol-gel science, a general review of modification methods for MCM-41, and a summary of some applications of these modified MCM-41 materials.

In addition to the introductory chapter, the thesis contains eight other chapters. The second chapter encompasses a thorough review of the recent published reports of methods for the preparation of ordered mesoporous materials. It also provides an in depth look into the chemistry involved in the mesoporous materials developed using the sol-gel process. The latter was the method of choice, with the aid of templates, used to prepare mesoporous materials based on MCM-41 in this research work. In addition, chapter two will describe in detail the synthesis and characterization of the different mesoporous materials that we have prepared. Several aspects will be highlighted including investigations of surfactant behavior and influence of other reaction conditions such as pH and temperature. Determination of the hydroxyl group concentration and the thermal, hydrothermal and mechanical stability of the produced mesoporous materials will also be discussed.

Chapters three to nine will be concerned with the modification of the as-synthesized mesoporous materials with functional groups of interest and the development of new methods for the modification of these mesoporous materials. A comprehensive review of recent published reports involving the methods used for modification of these ordered mesoporous materials will be provided. We prepared several modified mesoporous materials using variety methods (*i.e.* the post-synthesis grafting method and

the direct co-condensation method). These chapters illustrate the synthetic procedures of the modified materials as well as characterization of the products. In these chapters we aimed to maximize the functional group concentration on the surface. Several functional groups such as thiols, amines, and carboxylic acids were added to the surface of the as-synthesized mesoporous materials. Features that will be highlighted include examination of different organic functional groups and the influence of reaction conditions such as catalysis, solvent (water), and temperature.

Each of the seven chapters will include introductions to the application of the modified mesoporous materials in adsorption and separation of toxic materials. For example, heavy metal ions, radioactive materials, and organic compounds have been separated using these modified mesoporous materials. The adsorption capacity, selectivity, and separation efficiency will be reported, and the effect of pH of the media, temperature, and time on the adsorption and separation will be covered as well. Also, the competition effect of some metal ions of alkali and alkaline earth metals such as sodium (Na), potassium (K), magnesium (Mg), and calcium (Ca) with respect to the adsorption and separation of heavy metal ions and radioactive materials is reported. Various techniques were used in order to determine the adsorption and separation efficiency such as ultraviolet-visible spectroscopy (UV-Vis), inductively coupled plasma atomic emission spectroscopy (ICP), and atomic absorption spectroscopy (AAS).

1.2. HISTORICAL BACKGROUND

Porous materials are ubiquitous since, with the exception of metals and ceramics that are fired at high temperatures, all of the earth's solid contents are porous to some extent. As with the use of many other materials of practical importance, the applications

of clays, hides, wood and other porous materials do not have any well documented

beginning and certainly date back to prehistoric times. Such porous solids were almost

always used by early people in the form of the natural material or with some minor

modification (*e.g.,* heat treatment). For example, the ancient Egyptians used charcoal to

purify water.[4]

1.2.1. Development of Porous Materials

Zeolites and porous silicas are among the important porous materials for their

wide applications in separation and catalysis. Zeolites are members of a large family of

crystalline aluminosilicates. They were first discovered in 1756 by the Swedish scientist

Cronstedt when an unidentified silicate mineral was subjected to heat, these strange

minerals was found to bubble and froth, releasing bursts of steam. Therefore, he called

this mineral zeolite (in Greek, *zeo* = boiling and *lithos* = stone). In the nineteenth

century, zeolite minerals began to be well documented although there was a lack of the

general scientific interest. The term molecular sieve was derived from McBain[5] in 1931

when he found that chabazite, a mineral, had a property of selective adsorption of

molecules smaller than 5 Å in diameter. In other words, molecular sieves retain the

particles that fit within the channels and let the larger ones pass through. The term

"molecular sieves" is used to describe a class of materials that exhibit selective sorption

properties (*i.e.* that are able to separate a class of a mixture on the basis of molecular size

and shape). However, a few years later Barrer and coworkers[4b] studied the sorptive

properties of chabazite and other porous minerals and reported that nitrogen and oxygen

could be separated using a zeolite that had been treated to provide the necessary shape

selectivity for the discrimination between the molecular dimensions. Later, synthetic

6

zeolites began to be used in large amounts for the production of pure oxygen from air. Between 1949 and 1954, Breck and coworkers[4c] were able to synthesize a number of new zeolites (types A, X, and Y) which were produced in large scale to be used for the separation and purification of small molecules. Since then, the nomenclature of this kind of porous material has become universal. The success of synthesizing crystalline aluminosilicates, in particular the emergence of the new family of aluminophosphates[6] and silicoaluminophosphates,[7] made the concept of zeolites and molecular sieves more complicated. In other words, zeolites are crystalline aluminosilicates with molecular sieve properties.

The small pore entrances (diameters) in zeolites (*e.g.,* 0.4 nm in zeolite A) were attractive for commercial applications because they provided the opportunity for selective adsorption based on small differences in the size of gaseous molecules. In addition, these materials caught the attention of scientists who were interested in catalysis. At the beginning, the oil industry was reluctant to accept the idea, since it was thought that these materials have pores too small to be of interest for cracking activity (break down long hydrocarbon molecules into gasoline and other useful products). The zeolite marketing prospects were improved when Rosinski and coworkers[4] showed rare earth-containing zeolites have the ability to handle cracking activity. There has been, however, a continually growing interest in expanding the pore sizes of zeotype materials from the micropore region to mesopore region in response to the increasing demands in both industrial and fundamental studies. Examples are the separation of heavy metal ions, the separation and selective adsorption of large organic molecules from waste water, the formation of supramolecular assembly of molecular arrays, the encapsulation of metal

7

complexes in the frameworks, and the introduction of nanometer particles into zeolites and molecular sieves for electronic and optical applications.[8-10] Therefore, to meet these demands, numerous experiments to create zeotype materials with pore diameters larger than those of the traditional zeolites were carried out. Since it was thought that most of the organic templates used to synthesize zeolites affect the gel chemistry by filling the voids in the growing porous solid, many of these attempts used larger templates. It was not until 1982 that success was achieved by changing the synthesis gel compositions when the first so-called ultra large pore molecular sieve, $AlPO_4$-8, which contains 14-membered rings, was discovered.[6] Indeed, this not only broke the deadlock of the traditional viewpoint that zeolite molecular sieves could not be constructed with more than 12-membered rings, but also stimulated further investigations into other ultra large pore molecular sieves, such as VPI-5 with an 18-tetrahedral ring opening, cloverite, and JDF-20.[11-13] While these zeolites attracted much attention and were of scientific importance, they have not found any significant applications because of either their inherently poor stability, their weak acidity, or their small pore size (0.8-1.3 nm). As a consequence, they seem to be inferior compared to pillared layered clays.

Yanagisawa et al.[14] described in the early 1990s the synthesis of mesoporous materials that have characteristics similar to that of MCM-41. Their preparation method is based on the intercalation of long-chain (typically C-16) alkyltrimethylammonium cations, into the layered silicate kanemite, followed by calcination to remove the organic species, which is later called surfactants, yielding a mesoporous material. The silicate layers condensed to form a three-dimensional structure with nanoscale pores. ^{29}Si solid-state NMR spectroscopy indicated that a large number of the incompletely condensed

silica sites $Si(OSi)_3(OH)$ (Q^3) species were converted to the completely condensed silica sites $Si(OSi)_4$ (Q^4) species during the intercalation and calcination processes. The X-ray powder diffraction gave only an uninformative peak centered at extreme low angles. Unfortunately, there were no further characterization data available leading to an ignoring of Yanagisawa *et al.*'s results.

In 1992, researchers at Mobil Corporation discovered the M41S family of silicate/aluminosilicate mesoporous molecular sieves with exceptionally large uniform pore structures. This discovery has resulted in a worldwide resurgence in this area.[1,3] The synthesis of this family of mesoporous materials is based on the combination of two major sciences, sol-gel science and surfactant (templating) science. The template agent used is no longer a single, solvated organic molecule or metal ion, but rather a self-assembled surfactant molecular array as suggested initially.[3] Three different mesophases in this family have been identified, i.e., lamellar (MCM-50), hexagonal (MCM-41), and cubic (MCM-48) phases. The hexagonal mesophase, denoted as MCM-41, possesses highly regular arrays of uniform-sized channels whose diameters are in the range of 15-100 Å depending on the templates used, the addition of auxiliary organic compounds, and the reaction parameters.[3,15,16] The pores of this novel material are nearly as regular as zeolites, however, they are considerably larger than those present in crystalline materials such as zeolites, thus offering new opportunities for applications in catalysis,[17] chemical separation,[18] adsorption media,[19-25] and advanced composite materials.[26] MCM-41 has been investigated extensively because the other members in this family are either thermally unstable or difficult to obtain.[16]

1.3. DEFINITION AND CLASSIFICATION OF POROUS MATERIALS

The term porous material is used for all materials that are full of pores, channels, vessels, holes, or cavities which are deeper than they are wide and permit the movement of fluids or gases. An example of a porous material is sponge.[27] Porous materials created by nature or by synthetic design have found great utility in all aspects of human activities. Their pore structure is usually formed in the stages of crystallization or subsequent treatment and consists of isolated or interconnected pores that may have similar or different shapes and sizes. Porous materials with small pore diameters (0.3 nm to 10 μm) are being studied for their molecular sieving properties. The pore shape can be roughly approximated by any of the following three basic pore models, see Figure 1.2:[27]
a) Cylindrical pores, circular in cross section, b) Ink-bottled pores, having a narrow neck and wide body, and c) Slit-shaped pores with parallel plates.
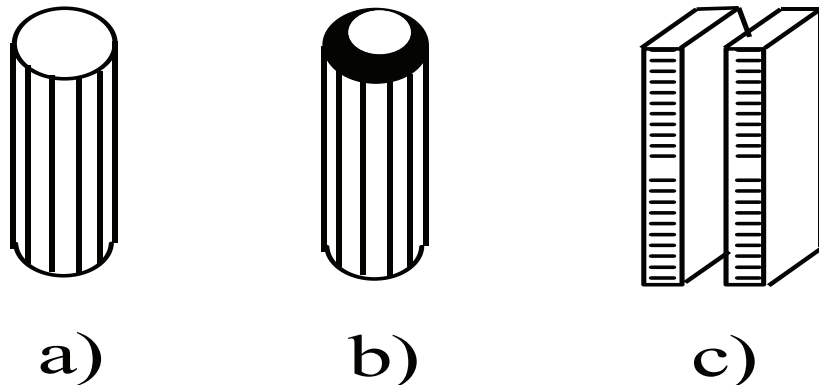
Figure 1.2. Pore shapes; a) cylindrical pores, b) ink-bottled pores, and c) slit-shaped pores.

Depending on the predominant pore sizes, the porous solid materials are classified by IUPAC to:[27]

1) Microporous materials, having pore diameters up to 2.0 nm,

2) Macroporous materials, having pore sizes exceeding 50.0 nm, and

3) Mesoporous materials, having pore sizes intermediate between 2.0 and 50.0 nm.

Figure 1.3. gives a few examples of porous materials that fit into these pore size regimes.
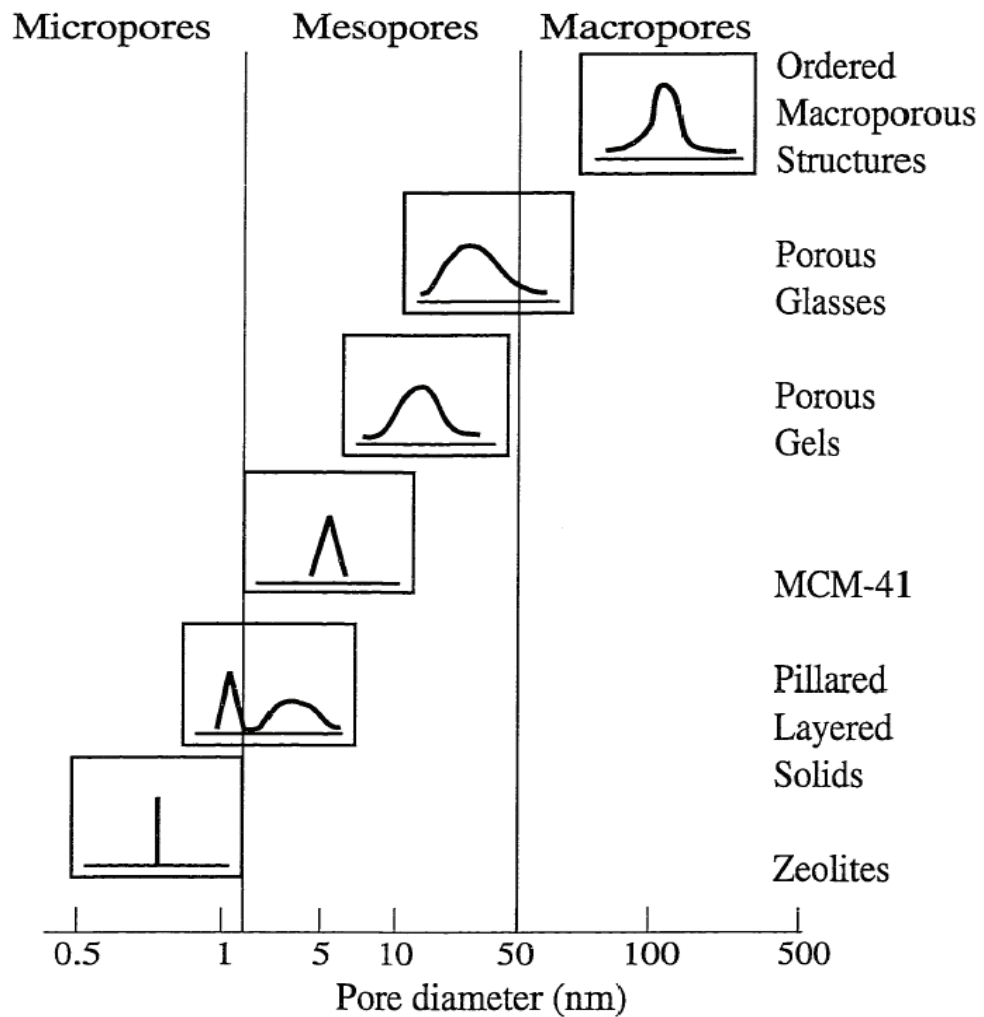
Figure 1.3. Schematic illustrating pore size distribution of some porous materials.[28]

As indicated, the pore size is generally specified as the pore width which is defined as the distance between the two opposite walls. Obviously, pore size has a precise meaning only when the geometrical shape is well defined. Porosity of a material is usually defined as the ratio of the volume of pores and voids to the volume occupied by the solid.[27,28]

Porous materials are also defined in terms of their adsorption properties. The term adsorption originally denoted the condensation of gas on a free surface as opposed to its entry into the bulk, as in absorption. However, this distinction is frequently not observed, and the uptake of a gas by porous materials is often referred to as adsorption or simply sorption, regardless of the physical mechanism involved. Adsorption of a gas by a porous material is described quantatively by an adsorption isotherm, the amount of gas adsorbed by the material at a fixed temperature as a function of pressure. Porous materials are most frequently characterized in terms of pore sizes derived from gas sorption data, and IUPAC conventions have been proposed for classifying pore sizes and gas sorption isotherms that reflect the relationship between porosity and sorption.[27] The IUPAC classification of adsorption isotherms is illustrated in Figure 1.4.[27] The six types of isotherm are characteristic of adsorbents that are microporous (type I), nonporous or macroporous (types II, III, and VI), or mesoporous (types IV and V).[27]
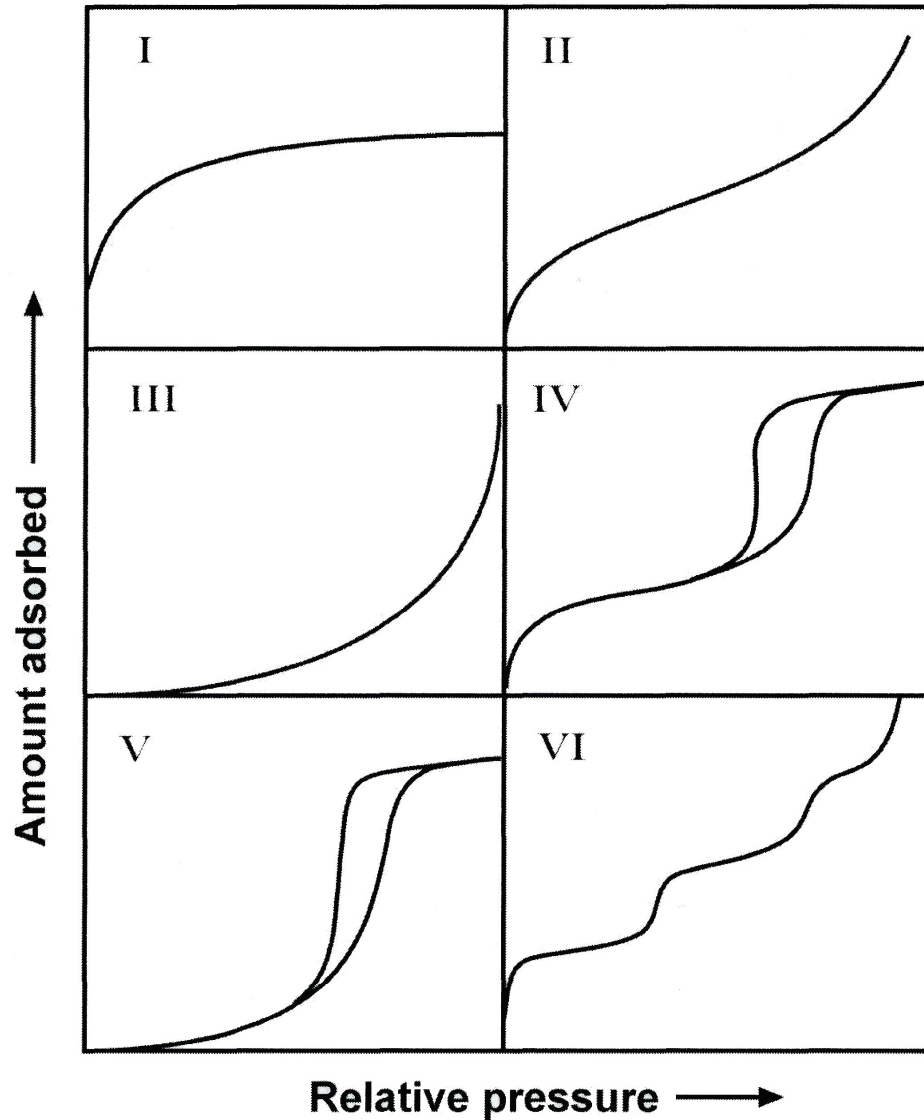
Figure 1.4. The IUPAC classification of adsorption isotherms showing both the adsorption and desorption pathways. Note the hysteresis in types IV and V.

The adsorption hysteresis in figure 1.4 (IV and V) are classified and are widely accepted that there is a correlation between the shape of the hysteresis loop and the texture (*e.g.,* pore size distribution, pore geometry, and connectivity) of a mesoporous material. An empirical classification of hysteresis loops was given by the IUPAC, which

is based on an earlier classification of hysteresis by De Boer.[27b,27c] Figure 1.5 shows the

IUPAC classification and according to the IUPAC, type H1 is often associated with

porous materials consisting of well-defined cylindrical-like pore channels or

agglomerates of approximately uniform spheres. Type H2 ascribes materials that are
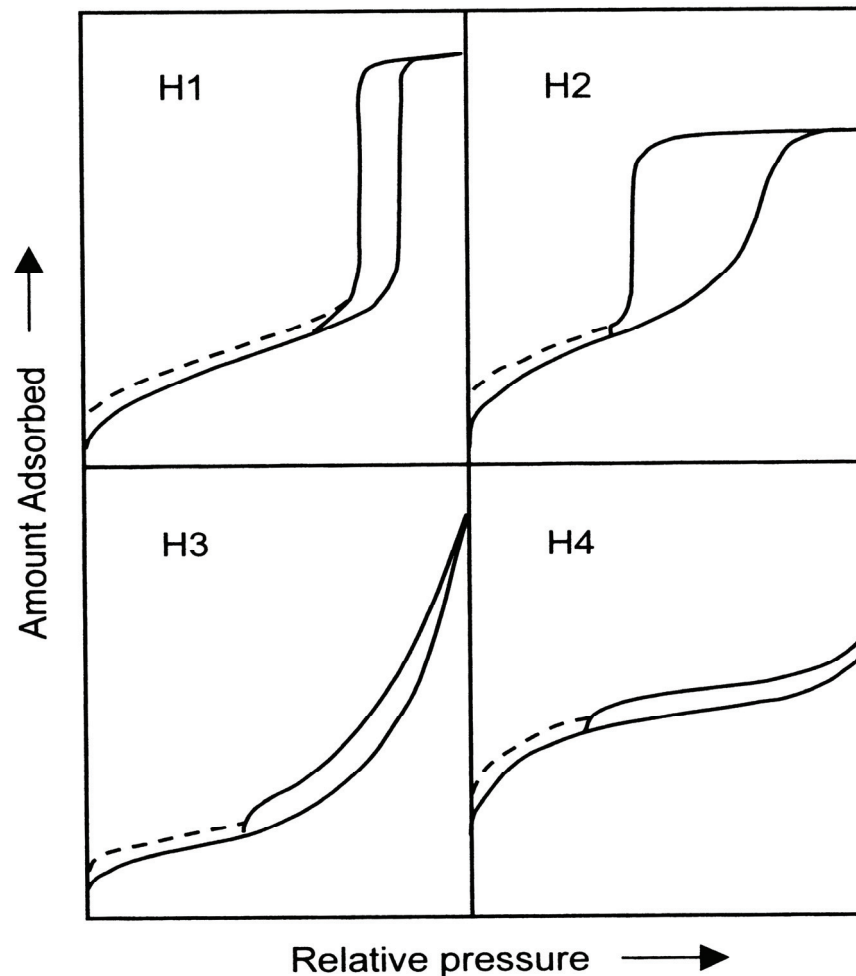
Figure 1.5. The relationship between the pore shape and the adsorption-desorption
isotherm.

often disordered and the distribution of pore size and shape is not well defined and also

indicate of bottleneck constrictions. Materials that give rise to H3 hysteresis have slit-

shaped pores (the isotherms revealing type H3 do not show any limiting adsorption at high P/P_o, which is observed with non-rigid aggregates of plate-like particles). The desorption curve of H3 hysteresis contains a steep associated with a forced of the hysteresis loop, due to the so-called tensile strength effect which is a phenomenon occurs for nitrogen at 77 K in the relative pressure range from 0.4 to 0.45. However, type H4 hysteresis is also often associated with narrow slit pores.[27d]

The dashed curves in the hysteresis loops shown in figure 1.5 reflect low-pressure hysteresis, which may be associated with the change in volume of the adsorbent, for example, the swelling of non-rigid pores or the irreversible uptake of molecules in pores of about the same width as that of the adsorptive molecule.[27d]

Porous materials can be structurally amorphous, paracrystalline, or crystalline. Amorphous materials, such as silica gel or alumina gel, do not possess long range order, whereas paracrystalline solids, such as γ- or η- Al_2O_3, are quasiordered as evidenced by the broad peaks on their X-ray diffraction patterns. Both classes of materials exhibit a broad distribution of pores predominantly in the mesoporous range. This broad pore size distribution limits the shape-selectivity and the effectiveness of the adsorbents, ion-exchangers, and catalysts prepared from amorphous and paracrystalline solids. The only class of porous materials possessing narrow pore size distributions or uniform pore sizes includes crystalline zeolites and related molecular sieves.[29,30]

Macroporous solids are not widely used as adsorbents and catalysts due to their low surface area and large non-uniform pores. Microporous and mesoporous solids, however, are widely used in adsorption, separation technology and catalysis. Owing to

the need for higher accessible surface area and pore volume for efficient chemical processes, there is a growing demand for new highly stable porous materials.[27,28]

1.4. AN OVERVIEW OF ORDERED MESOPOROUS MATERIALS (M41S)

Meso, the Greek prefix, meaning "in between", has been adopted by IUPAC to define porous materials with pore sizes between 2.0 and 50.0 nm.[31] These materials have received widespread interest because of their potential applications as supports for catalysis, separation, selective adsorption, novel functional materials, and use as hosts to confine guest molecules. These applications are possible due to the extremely high surface areas combined with large and uniform pore sizes of these mesoporous materials.[32] Furthermore, these materials have high thermal stability and high adsorption capacity. Mesopores are present in aerogels, and pillared layered clays which show disordered pore systems with broad pore-size distributions. A persistent demand has been developed for larger pores with well-defined pore structures.

The design and synthesis of organic, inorganic, and polymeric materials with controlled pore structure are important academic and industrial research projects. Many potential applications require specific pore size, so that the control of pore dimensions to within a portion of an angstrom can be the dividing line between success and failure. Zeolites and zeolite-like molecular sieves (zeotypes) often fulfill the requirements of ideal porous materials such as narrow pore size distribution and a readily tunable pore size in a wide range.[1] However, despite the many important commercial applications of zeolites, where the occurrence of a well-defined micropore system is desired, there has been a persistent demand for crystalline mesoporous materials because of their potential

applications as adsorbents, catalysts, separation media or hosts for bulky molecules for advanced materials applications.

Until the late 1980's, most mesoporous materials were amorphous and often had broad pore size distributions. In the early 1990s, Kresge et al.[1] reported the emergence of a new family of so-called "mesoporous molecular sieves", prepared by templating silica species with surfactant molecules leading to the formation of ordered mesoporous silica oxides. These new products, known under the group name M41S, with the hexagonal array of pore (MCM-41), being the most prominent member, dramatically expanded the range of pore sizes accessible in the form of an ordered pore system. In recent years, research in this area has been extended to many metal oxide systems other than silica and also to the novel organic-inorganic hybrid mesoporous materials.

These new silicate materials, with well defined pore sizes of about 2.0-10.0 nm, surpass the pore-size constraint (< 2.0 nm) of microporous zeolites. They also possess extremely high surface areas (> 700 $m^2\,g^{-1}$) and narrow pore size distributions. Instead of using small organic molecules as the templating compound, as in the case of zeolites, Mobil scientists employed long chain surfactant molecules as the structure-directing agent during the synthesis of these highly ordered materials.[1] Rather than an individual molecular directing agent participating in the ordering of the reagents forming the porous materials, assemblies of molecules, dictated by solution energetics, are responsible for the formation of these pore systems. This supramolecular directing concept has led to a family of materials whose structure, composition, and pore size can be tailored during synthesis by variation of the reactant stoichiometry, nature of the surfactant molecule, auxiliary chemicals, reaction conditions, or by post-synthesis functionalization

techniques. For example, MCM-41 contains regular arrangements of hexagonal pores in a honeycomb arrangement, MCM-48 which exhibits cubic symmetry that can be envisaged as a gyroid minimal surface[2,33] and MCM-50 is a layered silicate. Figure 1.6 shows the different structures.[31]

Figure 1.6. Schematic of the M41S materials: MCM-50 (layered), MCM-41 (hexagonal) and MCM-48 (Cubic).

Following the initial announcement of MCM-41, there has been a surge in research activity in this area.[34] Interestingly, Di Renzo *et al.*[35] recently found a patent from 1971 in which a synthesis procedure similar to the one used by the Mobil group was described as yielding "low-bulk density silica". The patent procedure was reproduced, and the product had all the features of a well-developed MCM-41 structure, as shown by transmission electron microscopy, X-ray diffraction, and nitrogen adsorption. However, in the original patent, only a few of the remarkable properties of the materials were actually described. It was the Mobil scientists who really recognized the spectacular features of these ordered mesoporous oxides.

Scientists have postulated that the formation of these molecular sieve materials is based on the concept of a structural directing agent or template. Templating has been defined as a process in which an organic species functions as a central structure about which oxide moieties organize into a crystalline lattice.[8,36,37] In other words, the template is a structure, usually organic, around which a material, often inorganic, nucleates and grows in a "skin-tight" manner, so that upon the removal of the templating structure, its geometric and electronic characteristics are replicated in the inorganic materials.[38a] The above definition has also been elaborated to include the role of the organic molecules such as:[8] (a) space-filling species, (b) structural directing agents, and (c) templates.

In the simplest case of space filling, the organic species merely serves to occupy voids about which the oxide crystallizes. Therefore, the same organic molecule can be used to synthesize a variety of structures. Structural direction requires that a specific framework be formed from a unique organic compound, but this does not imply that the resulting oxide structure mimics identically the form of the organic molecule. In true templating, however, in addition to the structural directing component, there is an intimate relationship between the oxide lattice and the organic form such that the synthesized lattice contains the organic fixed into position. Thus, the lattice reflects the geometry of the organic molecule.

In M41S materials, a liquid crystal templating (LCT) mechanism has been proposed by the Mobil scientists in which supramolecular assemblies of surfactant micelles (*e.g.,* alkyltrimethylammonium surfactants) act as structure directors for the formation of the mesophase, see Figure 1.7.[1,3] This mechanism behind the composite mesophase formation is best understood for the synthesis under high pH conditions.

Under these conditions, anionic silicate species, and cationic or neutral surfactant molecules, cooperatively organize to form hexagonal, lamellar, or cubic structures. In other words, there is an intimate relationship between the symmetry of the mesophases and the final products.[3]

The composite hexagonal mesophase is suggested to be formed by condensation of silicate species (formation of a sol-gel) around a preformed hexagonal surfactant array or by adsorption of silicate species onto the external surfaces of randomly ordered rod-like micelles through columbic or other type of interactions. Next these randomly ordered composite species spontaneously pack into a highly ordered mesoporous phase with an energetically favorable hexagonal arrangement, accompanied by silicate condensation. This process initiates the hexagonal ordering in both the surfactant template molecules and the final product as shown in Figure 1.7.[3]
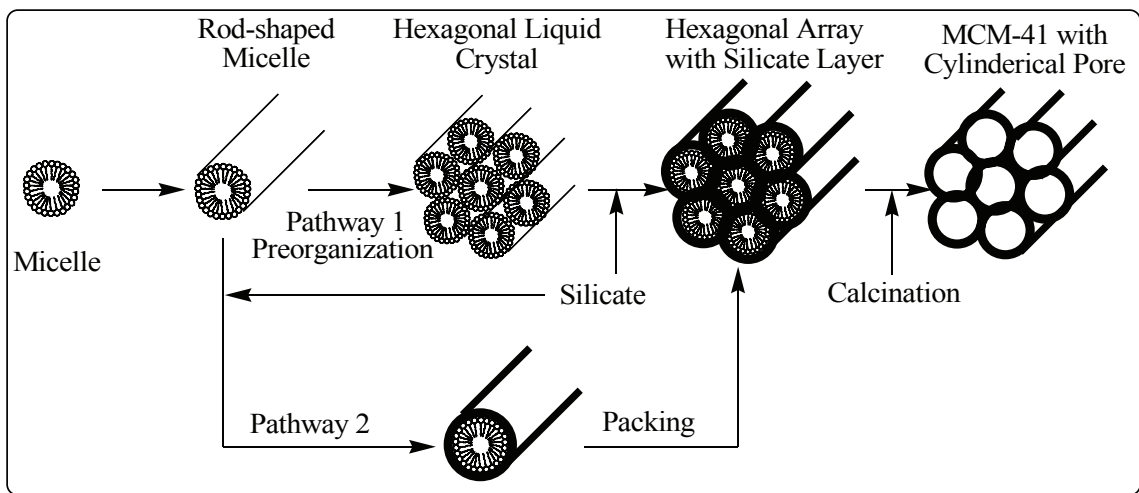
Figure 1.7. Schematic model of liquid crystal templating mechanism via two possible pathways.[3]

20

Several other researchers further revised this liquid crystal templating mechanism. Chen *et al.*,[38b] studied this mechanism by carrying out in situ ^{14}N NMR spectroscopy. They concluded that the randomly ordered rod-like organic micelles interact with silica species to form two or three monolayers of silica on the outer surfaces of the micelles. Then these composite species spontaneously self-organize into a long range ordered structure to form the final hexagonal packing mesoporous MCM-41. Moreover, they indicated that in the case of tetraethylorthosilicate as the silica sources, the concentration of the surfactant should be equal to or higher than the critical micelle concentration in order to obtain hexagonal MCM-41 materials.

In addition to the previous proposed mechanism, there are two other proposed liquid-crystal template mechanisms. The first mechanism was suggested by Monnier *et al.*[2] It is proposed that the surfactant is initially present in the lamellar phase regardless of the final product. This lamellar mesophase transforms to the hexagonal phase as the silicate network condenses and grows, see Figure 1.8 (i). The second mechanism was proposed by Steel *et al.*[38c] They suggested that, as the silicate source is introduced into the reaction gel, it dissolves into the aqueous regions around the surfactant molecules, and then promotes the organization of the hexagonal mesophase. The silicate first becomes ordered into layers between which the hexagonal mesophases of micelles are sandwiched. Further ordering of the silicate results in the layers wrinkling, closing together, and growing into hexagonal channels, see Figure 1.8 (ii).
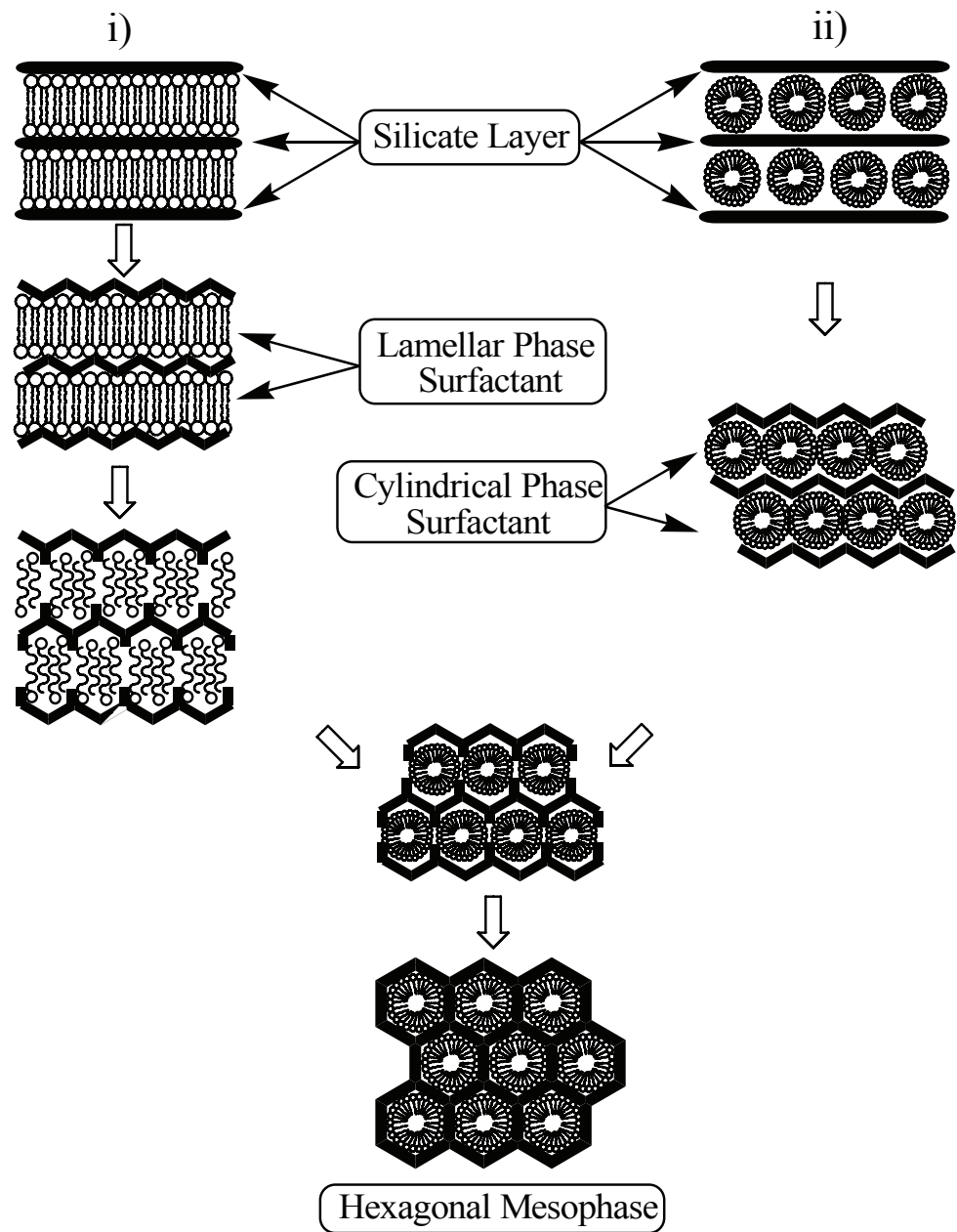
Figure 1.8. Schematic diagrams of the formation mechanism of MCM-41; i) is the proposed transformation mechanism by Monnier *et al.*[2] and ii) is the formation mechanism proposed by Steel *et al.*[38b]

1.4.1. Chemistry of Surfactant/Silicate Solution

The structural phase of these materials, schematically shown in Figure 1.9, is based on the fact that surfactant molecules manifest themselves as very active components with variable structures in accordance with increasing concentrations[28a]
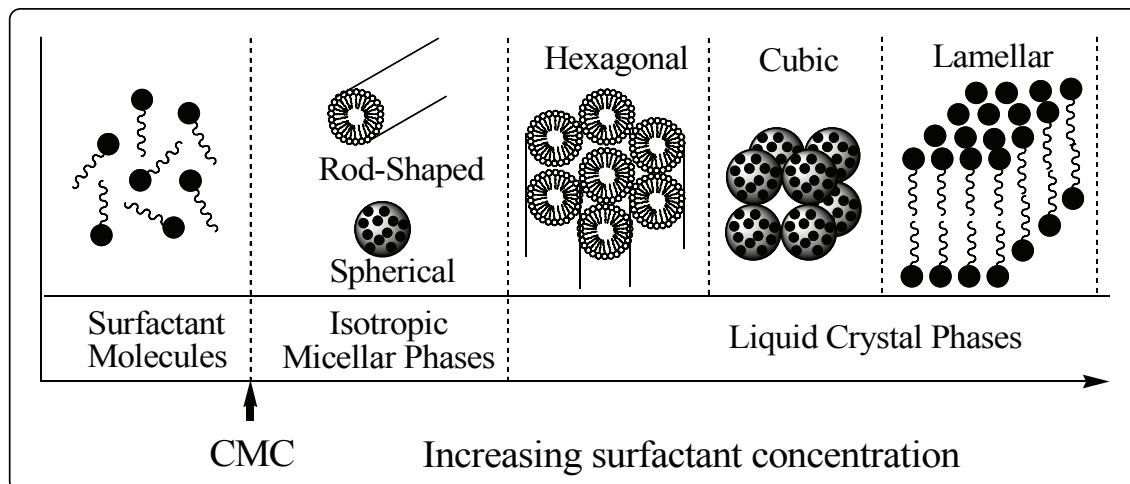
Figure 1.9. Phase sequence of surfactant-water binary system.[28a]

At low concentrations, the surfactants energetically exist as monomolecules. With increasing concentration, surfactant molecules aggregate together to form micelles in order to increase the system entropy since this increase is the major contributor to the negative ΔG^o.[28a, 29.39] This phenomenon is rationalized in the following way. Below the initial concentration threshold at which monoatomic molecules aggregate to form isotropic micelles which is called critical micellization concentration (CMC), the hydrocarbon tail constitutes a cavity in the water structure, this cavity is lined by water molecules which differ in their organization from that of the bulk water. The water becomes more "structured". Furthermore, the hydrocarbon tail is less free to move in the solvated molecule because of the surrounding water. On micelle formation, the bulk

23

structure of water is restored and the entropy of the water increases. In the micelle core, which is essentially liquid hydrocarbon, there is greater freedom for movement and so the entropy associated with the hydrocarbon tails also increases.[29,39]

The ability of surfactants to reduce surface or interfacial tension is expected to be directly related to the CMC. As the concentration process continues, hexagonal close packed arrays appear, producing the hexagonal phases.[39] The next step in the process is the coalescence of the adjacent, mutually parallel cylinders to produce the lamellar phase. In some cases, the cubic phase also appears prior to the lamellar phase. The cubic phase is generally believed to consist of complex, interwoven networks of rod-shaped aggregates.[40]

The formation of a particular phase in a surfactant aqueous solution at a given concentration depends not only on the concentrations but also on the nature of the surfactant itself such as the length of the hydrophobic carbon chain, hydrophilic head group, and counter ion in case of ionic surfactants. Moreover, it depends on the environmental parameters, such as pH, temperature, the ionic strength, solvent, and other additives (*i.e.* organic compounds). Generally, the CMC decreases with the increase of the surfactant chain length due to the increase of the magnitude of the negative free energy change of micellisation. Increasing the ionic strength in the solution and increasing the valence of the counter ions lead also to the reduction in the CMC. On the other hand, the CMC increases with increasing counter ion radius, pH, and temperature. Also, it is known that non-ionic surfactants generally exhibit lower CMC's than ionic surfactants.[39,40b] It is important to note that a high surfactant concentration, high pH, low

temperature, and low degree of silicate polymerization always supports the formation of cylindrical micelles as well as the hexagonal mesophases.[28]

The mesophases are formed by interaction of the organic parts with inorganic species, and thus both components play a crucial role in the assembly. The possible types of interactions between the organic and the inorganic parts that drive the formation of the mesophases depend on the charge on the surfactant, S^+ or S^-, on the inorganic species, I^+ or I^-, and the presence of mediating ions, i.e. X^- or M^+. All permutations enabling Columbic attraction are possible, i.e. S^+I^-, S^-I^+, $S^+X^-I^+$ or $S^-M^+I^-$. Subsequently, three other pathways were also discovered. Neutral (S^o) or nonionic (N^o) species can interact with uncharged inorganic species by hydrogen-bonding (S^oI^o or N^oI^o). Molecules with a covalent bond between the surfactant and inorganic parts were directly assembled (S-I), Figure 1.10 and Figure 1.11 illustrate the different interactions between the inorganic species and the surfactants. This formulation suggests the presence of a clearly defined interface between the organic and inorganic parts of the material.[42, 43a]
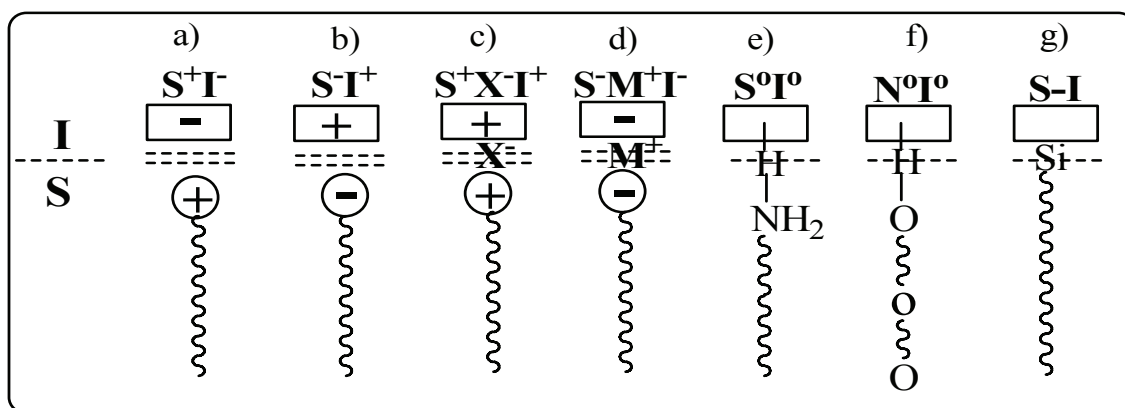
Figure 1.10. Interactions at the interface between the organic phase (S, N) and the inorganic phase (I) a-d) ionic interactions, e and f) hydrogen bonding, g) covalent bond
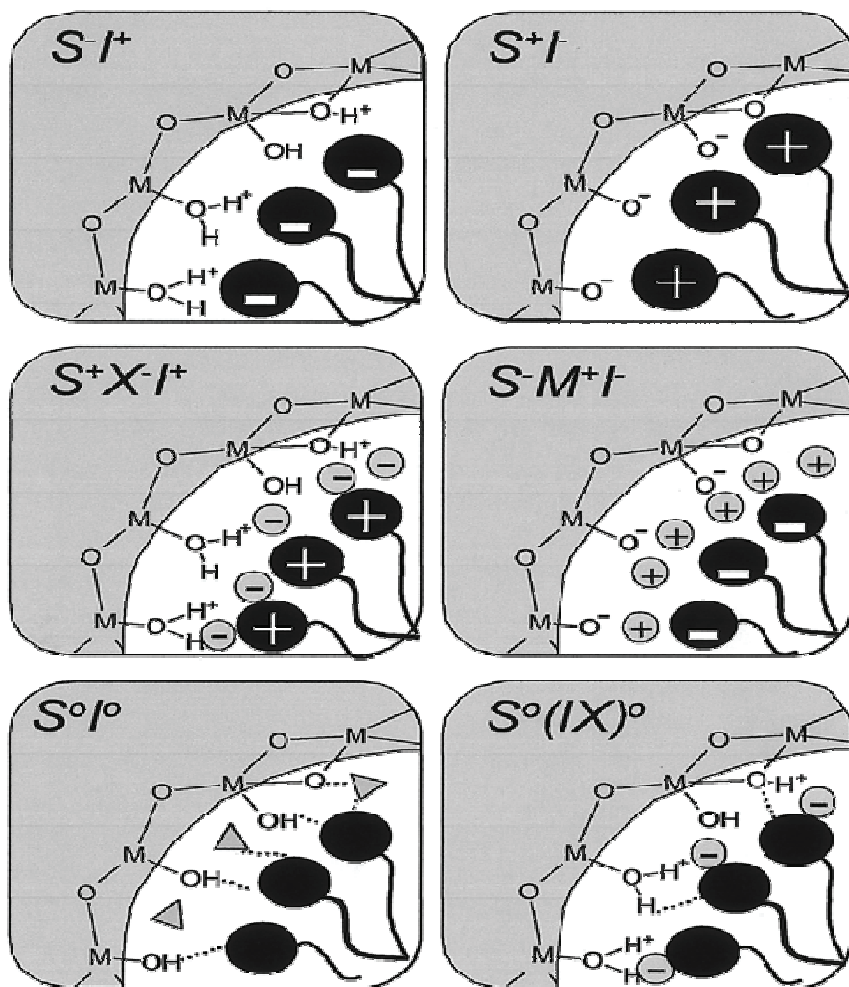
Figure 1.11. Schematic representation of the different types of silica-surfactant interfaces. S represents the surfactant molecule and I, the inorganic framework. M^+ and X^- represent the corresponding counterions. Solvent molecules are not shown, except for the I^0S^0 case (triangles); dashed lines correspond to H-bonding interactions.[43d]

The pore size in MCM-41 materials can be controlled from 1.5 to 10.0 nm by the hydrophobic alkyl chain length of the surfactants (altering the aggregation number and diameter) or with the aid of auxiliary organic compounds (*i.e.,* trimethylbenzene) as spacers and fillers. When the auxiliary organic species are added to the reaction gel, they

will be solubilized inside the hydrophobic regions of micelles, causing an increase in micelle diameter which will lead to an increase in the pore size of the final product.[41] Strong electrostatic interactions between the ionic surfactants and the inorganic species result in an MCM-41 matrix with pore wall thickness that is influenced by the type of surfactant and little by the pH conditions. Neutral template molecules, such as primary amines (with carbon tail lengths between C_8 and C_{18}), have also been employed to direct mesoporosity in silicates.[42] It is suggested that a neutral silicate would interact with micellar aggregates through hydrogen bonding between hydroxyl groups of hydrolyzed silicate species and the polar surfactant head-groups. The resultant framework structures are shown to have thicker silicate walls (*i.e.,* 1.5-3.0 nm) and therefore enhanced thermal and hydrothermal stability.[43,44] Other newly developed methods include the use of non-surfactant templates and copolymer precursor pathways.[45,46] The non-surfactant templated synthesis utilizes small organic molecules such as D-glucose, D-fructose, and dibenzoyl tartaric acid (DBTA) as the structure-directing agent.[11] By simply varying the concentration of the template molecules, mesoporous materials with different pore sizes (*i.e.,* 2.0-10.0 nm) can be obtained. The template can be easily removed by washing with water, solvent extraction, or calcination. These products possess high surface areas of ~1000 $m^2\ g^{-1}$, pore volumes as large as ~1.0 $cm^3\ g^{-1}$, and narrow pore size distributions. In addition to low cost, environmental friendliness, and easy removal of templates, this new approach also provides many other advantages such as mild synthesis conditions.[47]

Since the discovery of these ordered mesoporous materials formed by the self-cooperative assembly of inorganic species and organic surfactants, researchers have hoped to understand and improve their structures to obtain forms suitable for application

in adsorption, separation, catalysis, optical devices, and controlled polymerization inside their pores.[48]   Mesoporous silica, in its many forms, adsorbs a wide range of compounds. For this reason it has been widely used in chromatographic columns for the adsorption and separation of chemical species.

In the second chapter of this thesis, an overview of the preparative methods of the ordered mesoporous materials, based on MCM-41, will be covered and a description of the experimental methods that were used in this research will be provided.

1.4.2. An Overview of Sol-Gel Science Involved in the Synthesis of Mesoporous Silica

Organic/inorganic hybrid materials prepared by the sol-gel approach have rapidly become a fascinating new field of research in materials science. The explosion of activity in this area in the past two decades has resulted in tremendous progress in both the fundamental understanding of the sol-gel process and the development and applications of new organic/inorganic hybrid materials. Sol-gel chemistry has been investigated extensively since the 1970's, when sol-gel reactions were shown to produce a variety of inorganic networks.[49] Sol-gel reactions are those which convert an aqueous metal alkoxide $[M^{n+}(OR)_n]$ solution into an inorganic network.[49] The sol-gel method is also capable of producing homogeneous, high purity inorganic oxide glasses at room temperature, much lower than the high temperatures required by the conventional glass manufacturing process. For example, silica can be obtained from melt processing glass, but sol-gel method is more effective for the production of amorphous silica. Another advantage of sol-gel procedure is its ability to produce silica[1] in different forms such as molded gels,[50] spun fibers,[51] thin films,[52] molecular cages,[53] aerogels, xerogels,[54] and

mesoporous materials for a variety of applications such as gas, and liquid separations, optical coatings, protective films, membranes, and catalysis.[55-58] Therefore, changing the conditions of sol-gel polymerization and processing is helpful for controlling the bulk properties of silica. Among the advantages of using the sol-gel method is the availability of its raw materials in high purity. The modification of diverse properties of the inorganic network resulted from sol-gel reaction is possible through the incorporation of the inorganic compound into different organic polymers.

The two words sol and gel describe the sol-gel process, representing a process in which a sol changes into a gel.[59] A sol is defined as a colloid of small particles that are dispersed into a liquid. A gel, on the other hand, is a rigid non-fluid mass and is usually a substance made up of a continuous network including a continuous liquid phase.[56,57,60,61] Therefore, sol-gel reactions involve hydrolysis and condensation reactions of inorganic alkoxide monomers in order to develop colloidal particles (sol) and consequently convert them into a network (gel). A metal or metalloid element bound to various reactive ligands represents the precursor used to synthesize the colloids. Metal alkoxides are the reagents most used for this purpose due to their ease of hydrolysis in the presence of water. Alkoxysilanes, such as tetramethoxysilane (TMOS) and tetraethoxysilane (TEOS), are extensively used for the production of silica gels. Aluminates, titanates, and zirconates, however, are usually used for the synthesis of alumina, titania, and zirconia gels, respectively.

Figure 1.12 displays the involved hydrolysis and condensation reactions of TEOS. The hydrolysis step takes place by the addition of water to the TEOS solution under neutral, acidic, or basic conditions.
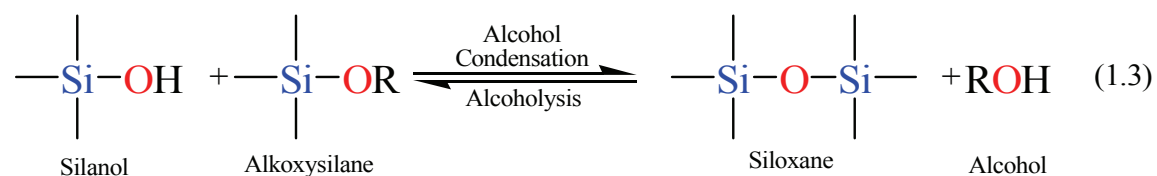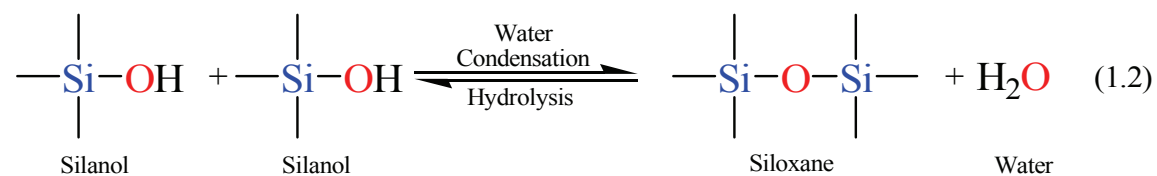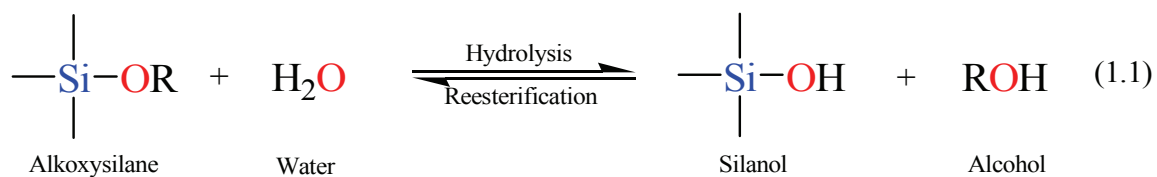
Figure 1.12. Sol-gel general reaction scheme

The hydrolysis step, equation 1.1 in Figure 1.12, leads to the generation of a silanol group (Si-OH). The mechanism of hydrolysis is catalyst dependent while its rate depends on the pH parameter, the water to alkoxide ratio, and the employed solvent.

Since alkoxysilanes are not water-soluble, an organic co-solvent is required to facilitate the hydrolysis step by mixing the alkoxysilane with the water in the reaction mixture.[61]

In the second step, the silanol group condense with either an alkoxide or another silanol group (the forward reactions in equations 1.2 and 1.3 in Figure 1.12) to build a strong siloxane linkage (Si-O-Si) with the loss of either an alcohol (ROH) or a water molecule. The siloxane hydrolysis and alcoholysis reactions (the reverse reactions in equations 1.2 and 1.3, respectively) break the siloxane bond, but along with the forward

reactions, the stepwise construction of the emerging network is permitted.[56,57,62] As the number of Si-O-Si bridges increases, the siloxane particles can aggregate into a sol, which disperse in the solution into small silicate clusters. Condensation of the latter silicate clusters leads to the formation of a network (a gel), trapping the water and the alcohol by-products. Removal of these trapped molecules from the formed gel-network by heat treatment under vacuum yield a vitrified, dense glass network. It is noteworthy to mention that hydrolysis and condensation reactions go on concomitantly, so that the full hydrolysis of tetraalkoxysilane to $Si(OH)_4$ does not necessarily occur before the beginning of condensation reactions.[56,62]

1.4.2.1. Factors Influencing the Sol-Gel Reaction

The hydrolysis and condensation reactions are affected by several factors. For example, these reactions become slower with increasing the electronegativity of the metal center of the alkoxide. The most influential factors are the water-to-alkoxide ratio, the type and the amount of the catalyst used, the type of the organic groups attached to the metal atom center, and the solvent.[61,62] The first three factors along with the relatively high electronegativity of silicon help for better control over the hydrolysis and condensation reactions, and thus over the structure of the resulting silica gel.[56,57]

1.4.2.1.1. Water-to-Alkoxide Ratio

It has been found that the silica content of the formed gel increases upon increasing the water-to-alkoxide ratio. Accordingly, one molecule of water is required for each alkoxide group to achieve full hydrolysis. Some researchers claimed that reesterification would occur faster than the hydrolysis reaction in case of using more than one molecule of water for every alkoxide group.[61] However, McCormick and

coworkers[62] worked over a wide range of water-to-alkoxide ratios and found no correlation between the water:alkoxide ratio and the achievement of complete hydrolysis. The latter result is logically correct because water is generated *in situ* during the reaction.

The water-condensation step (equation 1.2 in Figure 1.12), on the basis of LeChâtelier's principle, is anticipated to be hindered by increasing the water-to-alkoxide ratio. However, investigations of the impact of water-to-alkoxide ratio on the condensation step were contrary to the theoretical expectation. The condensation step was found to be accelerated upon increasing the water-to-alkoxide ratio due to the increase in the solubility of silica and in the concentration of the hydroxyl ion catalyst. Moreover, it was found that alcohol condensation to produce alcohol (equation 1.3) was promoted upon employing a water:alkoxide ratio less or equal to 2, while water condensation was promoted at higher ratios.[56,57,62]

The water-to-alkoxide also influences the structure of the resultant gel network. It was established that high water:alkoxide ratios led to more rigid gel network via the prevention of contraction upon drying. The latter network rigidity was a result of the completion of hydrolysis and the occurrence of auxiliary condensation upon the presence of surplus amount of water.[56,57,62]

1.4.2.1.2. Type and Amount of Catalyst

The rates and mechanisms of hydrolysis and condensation reactions are strongly affected by the identity of the catalyst. In acid catalysis (Figure 1.13), the first step in hydrolysis (equation 1.4) is electrophilic attack of the proton on an alkoxide oxygen atom, leading to the development of a positive charge on it. This electrophilic attack also makes the bond between the silicon center and the attacked oxygen (Si—O) more

polarized and facilitates its breakage for the departure of alcohol leaving group.[64] The rate-controlling step in acid hydrolysis (equation 1.5) is an S_N^2 nucleophilic attack of water oxygen on the silicon from the backside. This latter nucleophilic attack results in the formation of a pentacoordinate transition state in which the silicon center is partially bonded to both of —OH_2 and —OHR while the incoming group (attacking water molecule), the silicon center, and the leaving group (departing alcohol molecule) lie on an axis that is perpendicular on the plane in which the silicon center and the other three alkoxide groups lie.[62]

$$\text{(1.4)}$$

$$\text{(1.5)}$$
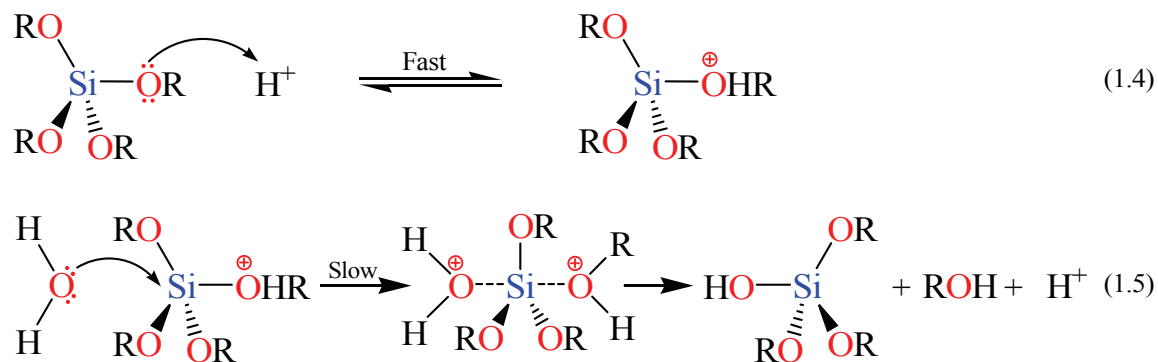
Figure 1.13. Hydrolysis mechanism of an alkoxysilane using acidic catalyst.[62]

The two-step acid promotion for hydrolysis reaction and sol formation mechanism is known as "A2 sols".[56,57,62] The presence of bulky or long alkyl substituents decreases the rate of the hydrolysis reaction by hindering the Walden inversion of the S_N^2 transition state.[65] It was also found that the hydrolysis reaction was first-order with respect to water concentration under acidic conditions. Accordingly, an increase in the water to alkoxide

ratio resulted in an increase in the rate of hydrolysis. However, the enthalpy of the hydrolysis declined upon increasing extent of hydrolysis.

The condensation rate and mechanism, as mentioned earlier, were found to depend on the pH of the reaction. For instance the condensation reactions (equations 1.2 and 1.3 in Figure 1.12) become irreversible at low pH because the solubility of silica and its rate of dissolution are insignificant. The mechanism of condensation under acidic conditions is depicted in Figure 1.14 (*vide infra*).[62] The first step is the fast step and is an electrophilic attack of the proton on the oxygen of the silanol group. This attack makes

$$(1.6)$$

$$(1.7)$$
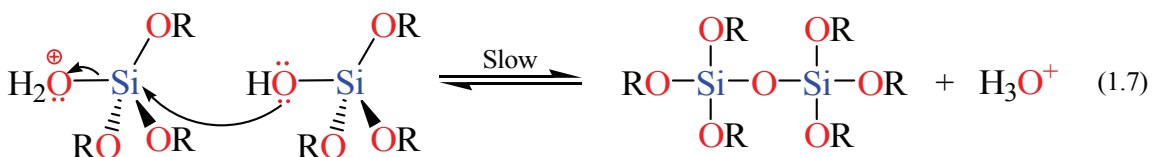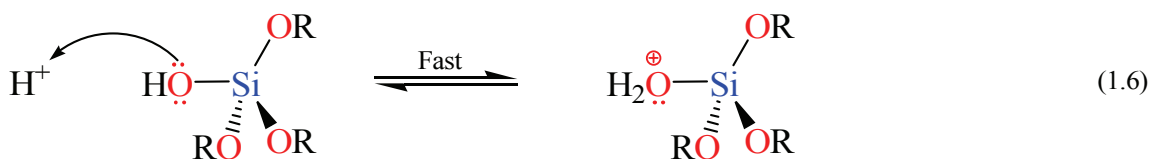
Figure 1.14. Condensation mechanism of an alkoxysilane using acidic catalyst.[56,62]

the silanol oxygen positively charged. The second step is the formation of a siloxane bridge via the loss of a hydronium cation (the catalyst) as a result of the condensation between a protonated silanol group with unprotonated one. Noticeably, the first steps in both hydrolysis and condensation reactions are similar.

When a base catalyst is used for the formation of silica, the hydroxide ion serves as a nucleophile that attacks the silicon atom center of the tetraalkoxysilane in an S_N^2

hydrolysis step. The result of this step is a silanol and alkoxide ion. Abstraction of the

silanol proton by the hydroxide ion is the first step in the condensation process, leading to

the formation of siloxide ion and water. A siloxane linkage is then formed through the

S_N^2 attack of the latter ion on the silicon center of silanol. This step regenerates the

hydroxide ion catalyst and is the rate-determining step of the condensation reactions. The

hydrolysis and condensation reactions mechanisms are shown below in Figure 1.15.[56,57]

Base Promotion Hydrolysis

(1.8)

Base Promotion Condensation

(1.9)

(1.10)
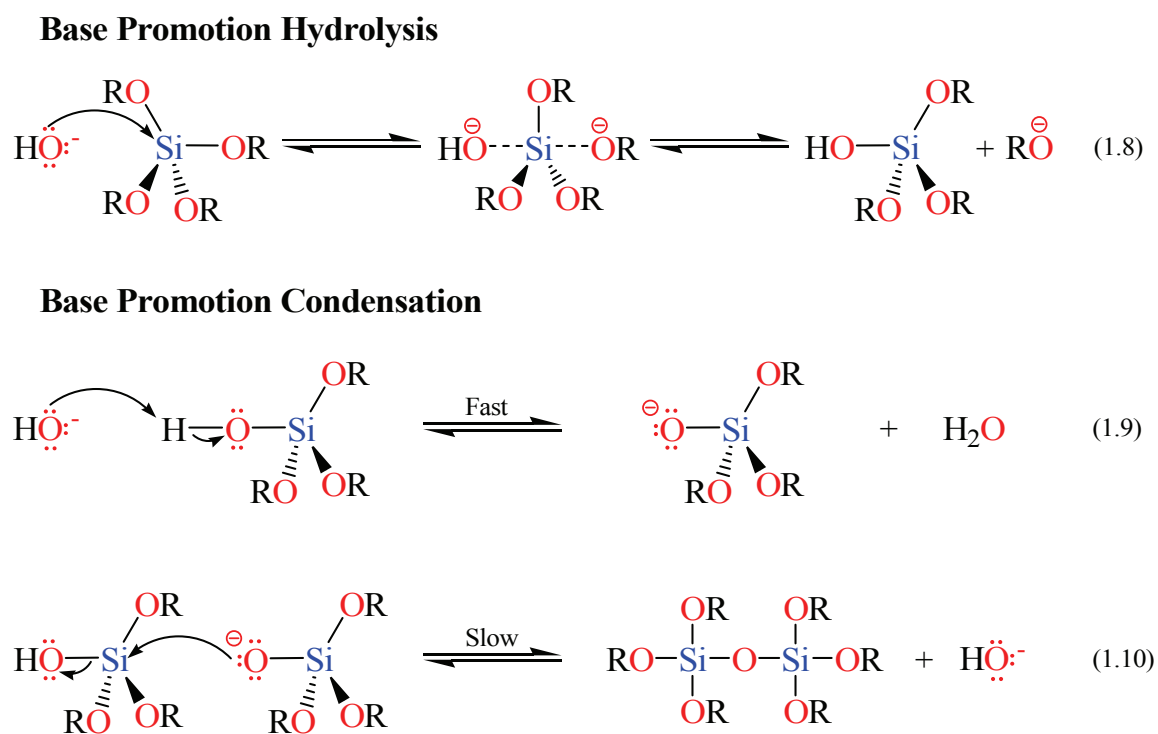
Figure 1.15. Hydrolysis and condensation mechanisms of an alkoxysilane using basic catalyst.

McCormick and coworkers[63] performed sol-gel reactions over a wide range of

acid concentration. Their results showed no effect of the acid concentration on the

35

structure of the resulting sol-gel. This conclusion was supported by ^{29}Si NMR
spectroscopy study which showed that the sol-gels obtained at different concentrations of
the acid catalyst had similar spectra, indicating their possession of similar structures.
However, McCormick and coworkers showed that a specific amount of the acid catalyst
was necessary to initiate the reaction. Therefore, the existence of this minimum amount
of the catalyst allowed the self-propagation. In addition, on the basis of gelation time and
the fact that condensation rate is inversely related to gelation time, it was found that 0.07
M of acid resulted in the lowest condensation rate.[56,57]

Most inorganic alkoxides hydrolyze and condensate very rapidly in the absence of
catalyst. In contrast, the hydrolysis of alkoxysilanes is so slow that it necessitates the
addition of either an acid or base catalyst, see Figure 1.16.
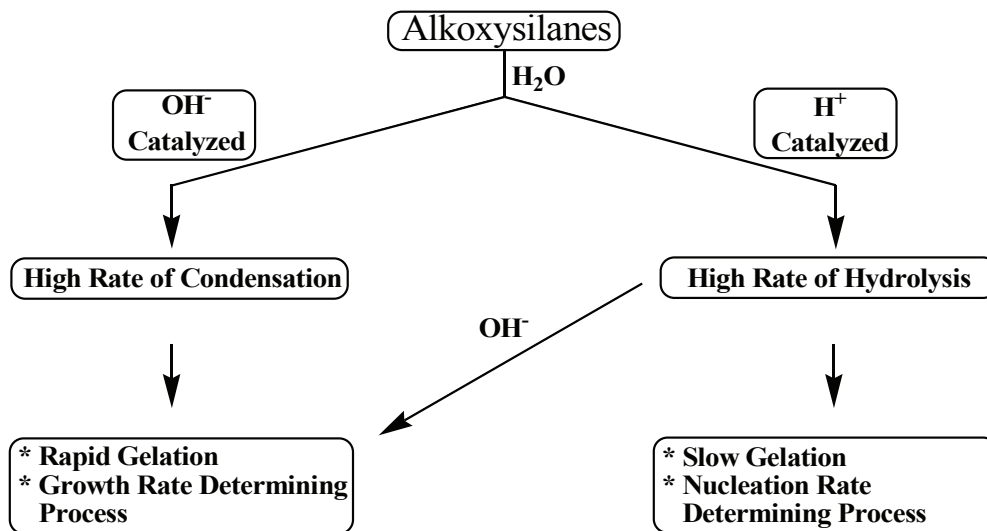
Figure 1.16. Effect of catalyst on hydrolysis and condensation.

When an acid catalyst is employed, the rate-controlling step is the particle nucleation and the fast step is the hydrolysis. This fact leads to the production of more linear-like networks with less siloxane bonds and high concentrations of silanol groups, and hence, minimally branched polymeric species. On the other hand, base catalyst hydrolyzes the alkoxide hydrolysis faster than a acids and prevents the quick aggregation of sol particles resulting in highly dense materials with fewer silanol groups in the overall network.[56,57]

The rates of both of the hydrolysis and condensation reactions depends strongly on the pH parameter as shown in Figure 1.17.[56,57,60,61] For instance, at pH ≈ 7, molecular
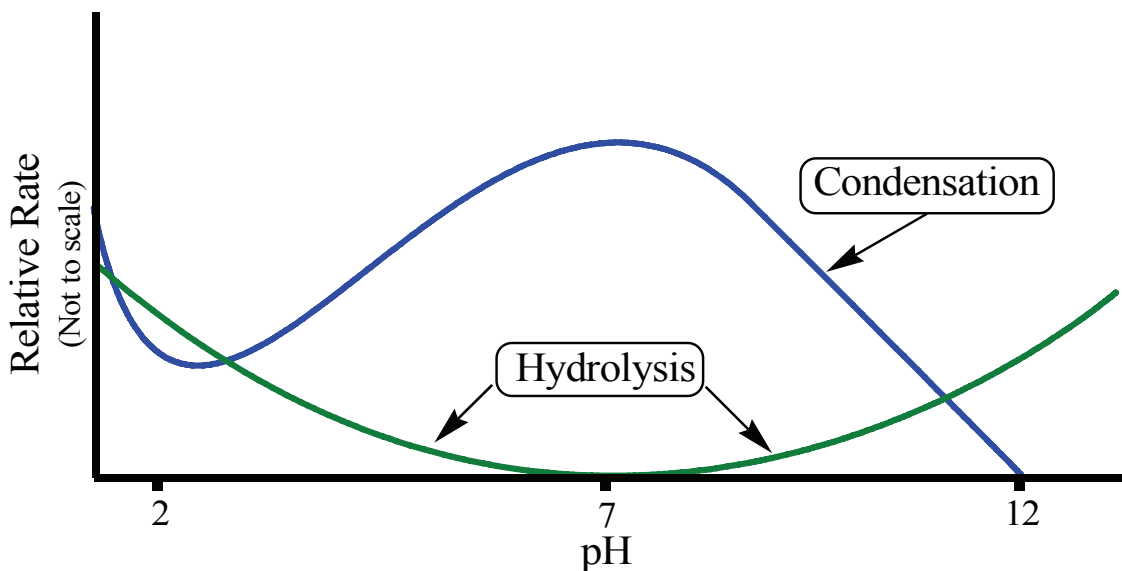
Figure 1.17. Effect of pH on hydrolysis and condensation rates.

hydrolysis takes place at a slow rate, while molecular condensation occurs at a fast one. This inverse relationship between the rates of the hydrolysis and condensation reactions controls both the kinetics of the reaction and the ultimate network structure.

1.4.2.1.3. Type of Network Modifier

Co-polymerization of silicon alkoxide monomers with others that have organic groups directly bonded to their silicon atoms leads to the formation of what is called organically modified silicates. The co-polymerization process modifies the network connectivity. Organic groups lead to coordination centers with functionality less than four and influence the reactivity of the alkoxy groups, and therefore, the connectivity of the sol-gel network in two ways. The first effect is the reduction of the rate of diffusion, and hence, the decrease of the degree of connectivity within the network due to the presence of bulky alkyl groups attached to the silicon centers. In other words, the steric hindrance created by the bulky groups impedes the diffusion together of partially hydrolyzed molecules required for the formation of siloxane bonds. The second effect is an increase of the surface area of the gel polymer, as a result of the presence of the bulky alkyl groups.[61] The higher surface area leads to higher silanol concentration in the gels. This produces a branching effect in the sol-gel network. In addition to these two points, steric effects caused by the presence of bulky or long alkyl substituents influenced the rate of the hydrolysis reaction by hindering the inversion of the $S_N{}^2$ transition state.[64]

1.4.2.1.4. Solvent Effects

Solvents other than water and simple alcohols are rarely used for gelation, so that their effect is not considered seriously. However, addition of external solvents may significantly affect the hydrolysis and condensation rates. These solvents, excluding water and alcohol co-solvent, are known as drying control chemical additives (DCCAs) and include tetrahydrofuran (THF), formamide (FA), and dimethylformamide (DMF).

These solvents are employed besides alcohol for slow drying of the silica monolithic gel. In bulk films, slow drying prevents the film from cracking.[61,64]

The solvent identity can strongly influence the condensation rate. For instance, protic solvents apparently have little or no effect on condensation rates in case of acid catalysis. On the other hand, polar, aprotic solvents, such as THF, FA, and DMF, solvate the protonated silanol $(Si\text{-}OH_2^+)$ under acidic conditions. The solvation of this cation is possible via directing the negative end of the solvent molecule towards the cation and donating their lone pair electrons to the unoccupied molecular orbitals of the cation. This solvation process stabilizes the transition state and increases the rate of condensation. The DCCAs are useful for the synthesis of inorganic, uniform gel networks within a membrane template because DCCAs allow molecular diffusion but postpones the reaction. However, when a DCCA is absent, the overall reaction rate is high in comparison to the slow diffusion process, resulting in highly non-uniform geometrical distribution of silicate.[56,57]

1.4.2.1.5. Sol Aging Effect on Network Structure

The physical and chemical alterations which take place in wet gels due to the continuation of condensation reactions are termed "aging". However, the term "sol aging" identifies the permissible time duration for the prolongation of condensation reactions before gelation. Sol aging is beneficial for controlling the size and the structure of sol polymers. Sol aging, however, is affected by several factors such as temperature, dilution, and pH. Elevation of temperature usually results in increasing reaction rate while increasing dilution leads to deceleration of the reaction. The pH parameter, on the other hand, has a pronounced impact on the distribution of condensation products

because variation of pH causes changes in reaction rate, solubility of silica, and the distribution of silicate species. Several spectroscopic techniques such as the silicon-29 nuclear magnetic resonance spectroscopy (^{29}Si NMR), small angle X-ray scattering (SAXS), Fourier transform infrared (FTIR) and Raman spectroscopies have been exploited to investigate the effect of sol aging on the size and distribution of silicate species when employing either an acidic or basic catalyst. The first technique, for instance, revealed that increasing degree of condensation via sol aging under basic conditions led to gradual shift of the chemical shifts to the Q^4 region (the region of fully condensed silicate) implying the attainment of a more cross-linked silicate. However, the ^{29}Si NMR spectrum was mainly composed of Q^2 and Q^3 signals under acidic condition, even if long sol aging was applied. This result is parallel with the acidic promotion mechanism in which the acid catalyst makes the condensation between the least acidic sites at the ends of chains and between low molecular weight species more feasible than between the more acidic sites at the middle of chains and between high molecular weight species.[56,57,62]

1.4.2.1.6. Gelation and Aging Effect

Gelation results in the "freezing" of the configuration of a sol even though the structure continues to develop to a small extent during the aging after gelation. For silica derived from TEOS, gelation takes place after 80-85% of reaction progress. The high conversion of TEOS upon gelation was explained on the basis of the formation of compact double three-membered rings (D3R) which were more kinetically stable than chain extension under the A2 sol mechanism. However, spectroscopic studies based on

^{29}Si NMR and Raman revealed the existence of cyclic species with the prevalence of cyclic tetramers but no evidence for the presence of cyclotrisiloxanes.[56,57]

The gel is subject to spontaneous shrinkage by ejecting of the solvent from its pores. This phenomenon is called *syneresis*, which is driven by the continuous condensation reactions and coarsening. However, the rate of *syneresis* reaches its minimum at the isoelectric point (IEP) of silica, the point at which the mobility of silica particles is zero, because of the minimization of the rate of condensation at this point. Coarsening takes place because the variation of the solubility between surfaces with different radii of curvature. Accordingly, smaller particles having high solubility dissolve and precipitate onto larger particles or on necks between particles with high solubility. On the basis of the emergence of coarsening, it can be inferred that coarsening leads to reduction in interfacial area and increase in the strength of the network. However, coarsening does not occur under the A2 mechanism due to the lower solubility of silica under the acidic conditions.[56,57]

The *syneresis* caused by condensation reaction is irreversible and its amount depends on the solvent used for gelation. The extent of the *syneresis* is reflected by the density of the resultant gel. Irreversible *syneresis* in pure TEOS gels, for instance, increased from 1% in pure EtOH to about 16% in pure H_2O. On the other hand, the density of the gels synthesized under similar conditions increased from 1.71 g/cm in the former solvent to about 2.18 g/cm in the latter solvent.[56,57]

Reduction of the huge solid/liquid interfacial area by the gel network may also cause *syneresis*. This kind of *syneresis*, however, is partially reversible. For example, changing the solvent from decane to water caused a decrease in the pore size in titania

gels from 7.5 to 3 nm. The pore was then re-expanded to its original size upon introducing decane again. Overall, microstructural changes resulting from *syneresis* have a strong influence on the microstructural development during drying process.[56,57]

1.4.2.1.7. Drying Effect

The drying process is imperative for obtaining of dense, rigid gels. Capillary tension occurs inside pores with the beginning of the drying process. This capillary tension makes the gel network contract. The network contraction quits when the capillary tension is balanced by the gel rigidity. This balancing point is called the critical point because it establishes the final pore size and volume in the gel. The minimum attainable pore size for microporous materials, for example, is established by the competition between the continued condensation reactions and capillary stresses. The former factor causes an increasing in the rigidity of the network, and opposes the latter factor which serves as a collapsing mechanism. The pore volume, under these circumstances, declines with the reduction in the pore size.[56,57]

1.5. AN OVERVIEW OF MODIFICATION OF AS-SYNTHESIZED MCM-41

Besides the extension from silicate to non-silica mesoporous materials, one other important way of modifying the physical and chemical properties of mesoporous silica materials has been by the incorporation of organic and inorganic components, either on the silicate surface, inside the silicate wall, or trapped within the channels, Figure 1.18 illustrates the functional groups in the internal pore surface.
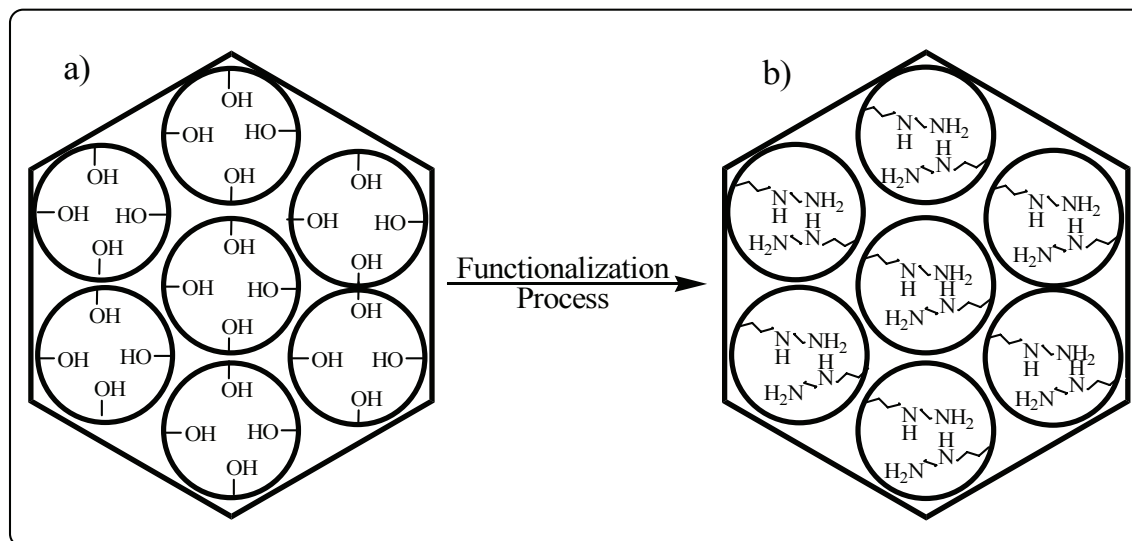
Figure 1.18. A diagram illustrating; a) unmodified pore walls and b) the presence of the functional groups on the pore walls.

Introduction of organic groups (functionalization) in the mesoporous materials permits the tuning of surface properties (e.g., hydrophilicity, hydrophobicity, acidity, bascity and binding to guest molecules), alteration of the surface reactivity, protection of the surface from chemical attack, hydrophobization of the surface by silylation to preclude water attack, and modification of the bulk properties of the materials while at the same time stabilizing the materials towards hydrolysis. Surface functionalized mesoporous materials are of great interest because of their potential applications in various areas such as catalysis, adsorption, chromatography, nanotechnology, metal ion extraction, and imprinting for molecular recognition. For example, a mesoporous silica having thiol groups on the pore surface showed high adsorption efficiency for heavy metals such as Hg, Ag, and Cd ions.[65] Sulfonic acid groups grafted on mesoporous materials, as another example, exhibited high catalytic activity for selective formation of bulky organic molecules.[66]

Mesoporous materials are interesting supports for organic functional groups due to their high surface area, large and uniform pore size, and narrow pore size distribution. While the silica framework provides thermal and mechanical stability, the surface organic moieties provide control of interfacial and bulk materials properties such as flexibility and optical properties.

Various literature reports describe methods for functionalizing the interior pore surfaces of mesoporous solids such as MCM-41 and SBA-15.[67-80] These hybrid materials are generally synthesized via two methods.[81] The first one is the post-synthesis grafting method in which pore wall surface of the pre-fabricated inorganic mesoporous materials is modified with organosilane compounds after the surfactant removal. The mesoporous materials possess silanols (Si-OH) groups that facilitate the attaching of the organic functions to the surface. Silylation is the most commonly used reaction for the surface modification.[80] Moreover, esterification is another reaction to carry out surface modification.[82a,b] The silylation reaction method is achieved by one of the following reactions, shown in Figure 1.19.[80]

$$\equiv Si-OH \quad + \quad Cl-SiR_3 \quad \longrightarrow \quad \equiv Si-OSiR_3 \quad + \quad HCl \cdot Base \qquad (1.11)$$

$$\equiv Si-OH \quad + \quad R'O-SiR_3 \quad \longrightarrow \quad \equiv Si-OSiR_3 \quad + \quad HOR' \qquad (1.12)$$

$$2 \equiv Si-OH \quad + \quad HN(SiR_3)_2 \longrightarrow 2 \equiv Si-OSiR_3 \quad + \quad NH_3 \qquad (1.13)$$
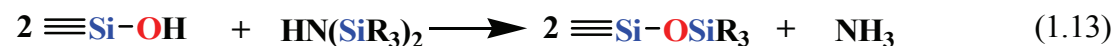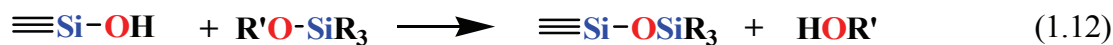
Figure 1.19. The silylation reaction for the modification of the surface of the mesoporous silica

The original structure of the mesoporous support is typically maintained after modification of the surface. Silylation occurs on all surface groups of the silica including the free or geminal silanols. However, hydrogen-bonded silanol groups are less accessible to the modification because of the formation of hydrophilic networks.[82c] In the post-synthesis grafting method, the host materials should be completely dried before adding the modification precursors in order to avoid the self-condensation of the precursors in the presence of water.

The second method for the modifying of the internal surface of the mesoporous materials is the direct synthesis. This method is based on the co-condensation of a tetraalkoxysilane (siloxane) and one or more organoalkoxysilane precursors with Si-C bonds through a sol-gel process. Siloxane precursors work as the main framework of the mesoporous materials while the organoalkoxysilane precursors contribute to the building of the framework and work as functional groups on the surface.[68,69,71,72] The direct synthesis has advantage over the grafting method in which the former produce mesoporous materials with high loading of the functional groups.[68,69]

Grafting of the mesopore surface with both passive[3,82] (*i.e.,* alkyl and phenyl) and reactive[67] (*i.e.,* amines, nitriles, thiol, halides *etc.*) surface groups has been studied. The former can be used to tailor the accessible pore sizes and increase surface hydrophobicity while the latter for increasing hydrophilicity and permits further functionalization. Multiple grafting has also been investigated. In order to minimize involvement of the external surface in reaction processes and to optimize selectivity, researchers have tried to graft to the external surface first through passive groups, before functionalizing the internal silanol groups.[83] Co-condensation using ionic,[71] neutral surfactant,[84] and non-

surfactant templates[85] have all been demonstrated. Each of the two functionalization methods has certain advantages. If uniform surface coverage with organic groups is desired in a single step, the direct method may be the first choice. It also provides better control over the amount of organic groups incorporated in the structure. However, products obtained by post-synthesis grafting are often structurally better defined and hydrolytically more stable. Although pore sizes can be controlled to some extent by both methods, it is more easily achieved by grafting.[68,69]

A recent development in functionalization of mesoporous materials has been the study of organic-inorganic species covalently bonded inside the mesoporous wall structure. The surfactant templated synthesis of these materials uses a precursor that has two trialkoxysilyl groups connected by an organic bridge.[86-88] The new technique allows stoichiometric incorporation of organic groups into silicate networks, resulting in higher loading of organic functional groups than by the grafting or direct synthesis method. The only major problem with this approach is the lack of chemicals that have the two trialkoxysilyl groups.[86-88] By introducing suitable functional groups onto the surface of these mesoporous materials, tunability of the mechanical, surface chemical, electronic, optical, or magnetic properties of the hybrid composite may be possible.[86,88]

In the chapters three to nine, we will report the synthesis of modified mesoporous materials with different functional groups (*e.g.,* amino, thiol, carboxyl, vinyl, and other interesting functional groups) using the two methods of functionalization. Moreover, these chapters will include characterization methods and the results and discussion of the interesting results.

1.6. AN OVERVIEW OF THE APPLICATION OF MCM-41 IN
ENVIRONMENTAL POLLUTION CONTROL PROCESSES

Contamination of water streams by transition metals, heavy metals, and radioactive compounds (*e.g.,* nickel, copper, lead, mercury, cadmium, uranium, and thorium) remains a concern in the field of environmental remediation. These materials enter the environment through a variety of avenues that include: mining, nuclear power plants, and industrial processing plants. Furthermore, some natural waters contain naturally high concentration levels of metals.[89] The presence of even low concentrations (ppb) of some heavy metals or radioactive substrates in natural water systems can have a harmful effect on both wildlife and humans. However, at these low concentrations of metal ions the sample often requires pre-concentration before analysis can be undertaken. Adsorption onto solid substrates (*e.g.,* activated carbons, zeolites, aluminas, and silicas) provides one of the most effective means for adsorption, separation and removal of trace pollutants (heavy metal ions, radioactive compounds, *etc.*) from aqueous streams.[89-91] A wide variety of novel materials can be prepared through the chemical modification of ordered mesoporous materials, MCM-41, since numerous organic and inorganic functionalities can be used for this purpose. In addition to their use in chromatographic separations that forms the main body of chapter four, they have been increasingly used as heterogeneous catalysts in liquid phase organic reactions. It is the characteristics of these materials, such as their viability and environmental safety, which makes them alternatives to traditional absorbent materials such as activated charcoal and zeolites. Their use as efficient materials for the selective adsorption and separation, and high capacity uptake of

trace metals from aqueous systems is due to their unique characteristics such as high surface area, large pore size and presence of reactive groups on the surfaces.[89,92]

Many of the more recent advances have been focused in the use of modified silicas for clean technology. One area of research in which modified silicas are used for clean technology applications, other than catalysis, is in the adsorption, separation, removing and analysis of trace components in aqueous systems. A wide variety of analytical techniques have been developed to separate and determine trace metal concentrations in natural water.[89] Several methods have been employed in the adsorption and separation of metal ions from aqueous solutions, such as activated charcoal, zeolites, clays, solvent extraction using a chelating agent [90] and the use of polymeric resins.[91] These methods suffer from a number of drawbacks. The use of activated charcoal, zeolites and clays showed low loading capacities and relatively small metal ion binding constants.[92] However, the use of chelating reagents (*i.e.* iminodiacetate resin) is time consuming, whereas organic resins possess low surface area and low mechanical stabilities, and the time taken for the metal ion to be complexed can be of the order of hours. Conventional methods such as precipitation are unfavourable especially when dealing with large volumes of matter which contains heavy metal ions in low concentration. Typically these ions are precipitated as hydrated metal oxides or hydroxides or sulfides using calcium oxide. Precipitation is accompanied by flocculation or coagulation, and one major problem is the formation of large amounts of sediments containing heavy metal ions. In addition, these methods are often unselective towards the metal being analyzed, with interference from alkaline earth metals being particularly problematic.[93] In recent years, the use of modified mesoporous silica in the pre-

concentration and separation of trace metal ions has been investigated.[94-96] Modified silica gels offer the advantages of high surface areas and increased chemical and mechanical stability. Nitrogen-containing organic groups have been shown selectively to bind first row transition metals from solutions.[97,98] Thus, Marshall and Mottola [93] prepared an immobilized quinolin-8-ol complex for the pre-concentration and separation of copper(II) ions. By varying the pH of the solution, a variety of transition metal(II) ions could selectively be extracted, even in the presence of alkali and alkaline earth metal ions. This makes the material useful for separation and analysis of trace metals in natural waters where alkaline earth metals would be expected.

Separation of transition metals, heavy metal ions or radioactive materials from aqueous streams is one of the most significant and fascinating problems to be challenged, severely hampered by the presence of a large excess of competing ionic species. Therefore, the materials to be used for the adsorption and separation of these toxic substances are required to be specific enough to discriminate the transition metals or heavy metal ions or the radioactive compounds from other benign metal cations such as Mg^{2+}. The criteria can be met by the smart choice of the functional groups and environmental conditions. For example, there are factors that affect the adsorption and selectivity such as the pH and ionic strength of the water medium, the concentration ratio of the metal ion to the adsorbent, and the agitation time.[95,96,98]

A suitable sorbent should fulfill some preliminary conditions: 1) cheap and easily available, 2) high capacity for toxic metals at the actual pH-value of the wastewater, 3) effective separation of sorbent from water phase after sorption of the targeted materials. In other words, the sorbent should be insoluble in water, 4) it should be stable against

physical and chemical degradation in order to permit long-term recycling procedures and to avoid contamination of the water, and 5) it must have a rapid rate of uptake .[95-98]

The last part of chapters three to nine of this thesis will show in detail the application of our modified mesoporous materials in adsorption, separation, and removing of toxic materials. Moreover, the effect of competitive ions and pH of the medium, and selectivity will be considered in this study.

1.7. REFERENCES

1. Kresge, C. T.; Leonowicz, M. E.; Roth, W. J.; Vartuli, J. C.; Beck, J. S. Ordered Mesoporous Molecular Sieves Synthesized by a Liquid-Crystal Template Mechanism. *Nature* **1992**, *359*, 710-712.

2. (a) Monnier, A.; Schüth, F.; Huo, Q.; Kumar, D.; Margolese, D.; Maxwell, R. S.; Stucky, G. D.; Krishnamurty, M.; Petroff, P.; Firoouzi, A.; Janicke, M.; Chmelka, B. F. Cooperative Formation of Inorganic-organic Interfaces in the Synthesis of Silicate Mesostructures. *Science* **1993,** *261*(5126), 1299-303. (b) Karakassides, M. A.; Bourlinos, A.; Petridis, D.; Coche-Guerente, L.; Labbe, P. Synthesis and Characterization of Copper Containing Mesoporous Silicas. *J. Mater. Chem.* **2000,** *10*(2), 403-408.

3. Beck, J.S.; Vartuli, J.C.; Roth, W.J.; Leonowicz, M. E.; Kresge, C. T.; Schmitt, K. D.; Chu, C. T. W.; Olson, D. H.; Sheppard, E. W. McCullen, S. B.; Higgins, J. B.; Schlenkert, J. L. A New Family of Mesoporous Molecular Sieves Prepared with Liquid Crystal Templates. *J. Am. Chem. Soc.* **1992**, *114*(27), 10834-43.

4. (a) Schüth, F.; Sing, K.S.W.; Weitkamp, J. Ed., *Handbook of Porous Solids Vol.1*; Wiley-VCH Verlag GmbH & Co. KGaA: Weinheim, Germany, 2002, pp 3, 18, 585. (b)Barrer, R. M.; Brook, D. W. Molecular Diffusion in Chabazite, Mordenite, and Levynite. *Trans. Faraday Soci.* **1953,** *49,* 1049-59. (c) Breck, D. W.; Eversole, W. G.; Milton, R. M.. New Synthetic Crystalline Zeolites. *J. Am. Chem. Soci.* **1956,** *78,* 2338-2339.

5. McBain, J. W. Ed., *The Sorption of Gases and Vapors by Solids*; Routledge and Sons: London, 1932, pp 169.

6. Wilson, S. T.; Lok, B. M.; Messina, C. A.; Cannan, T. R.; Flanigen, E. M. Aluminophosphate Molecular Sieves: A New Class of Microporous Crystalline Inorganic Solids. *J. Am. Chem. Soc*. **1982**, *104*, 1146-1147.

7. Lok, B. M.; Messina, C. A.; Lyle Patton, R.; Gajek, R. T.; Cannan, T. R.; Flanigen, E. M. Silicoaluminophosphate Molecular Sieves: Another New Class of Microporous Crystalline Inorganic Solids. *J. Am. Chem. Soc*. **1984**, *106*, 6092-6093.

8. Davis, M. E.; Lobo, R. F. Zeolite and Molecular Sieve Synthesis. *Chem. Mater*. **1992**, *4*, 756-768.

9. Mitchell, P. C. H. Zeolite-Encapsulated Metal Complexes: Biomimetic Catalysts. *Chem. Ind*. **1991**, 308-310.

10. Ozin, G. A. Nanochemistry: Synthesis in Diminishing Dimensions. *Adv. Mater*. **1992**, *10*, 612-649.

11. Davis, M. E.; Saldarriaga, C.; Montes, C.; Garces, J.; Crowder, C. A Molecular Sieve with Eighteen-Membered Rings. *Nature* **1988**, *331*, 698-702.

12. Estermann, M.; Mccusker, L. B.; Baerlocher, Ch.; Merrouche, A.; Kessler, H. A Synthetic Gallophosphate Molecular Sieves with a 20-Tetrahedral-Atom Pore Opening. *Nature* **1991**, *352*, 320-323.

13. Jones, R. H.; Thomas, J. M.; Chen, J.; Xu, R.; Huo, Q.; Li, S.; Ma, Z.; Chippindale, A. M. Structure of an Unusual Aluminium Phosphate ([$Al_5P_6O_{24}H]^{2-}$ $2[N(C_2H_5)_3H]^+$ $2H_2O$) JDF-20 with Large Elliptical Apertures. *J. Solid State Chem.* **1993**, *102*, 204-208.

14. Yanagisawa, T.; Schimizu, T.; Kiroda, K.; Kato, C. The Preparation of Alkyltrimethylammonium-Kanemite Complexes and their Conversion to Mesoporous Materials. *Bull. Chem. Soc. Jpn.* **1990**, *63*, 988-992.

15. Dubois, M.; Gulik-krzywicki, Th.; Cabane, B. Growth of Silica Polymer in a Lamelar Mesophase. *Langmuir* **1993**, *9*, 673-680.

16. Vartuli, J. C.; Schmitt, K. D.; Kresge, C. T.; Roth, W. J.; Leonowicz, M. E.; McCullen, S. B.; Hellring, S. D.; Beck, J. S.; Schlenker, J. L.; Olson, D. H.; Sheppard, E. W. Effects of Surfactant/Silica Molar Ratios on the Formation of Mesoporous Molecular Sieves: Inorganic Mimicry of Surfactant Liquid-Crystal Phases and Mechanistic Implications. *Chem. Mater*. **1994**, *6*(12), 2317-2326.

17. Corma, A.; Martinez, A.; Martinez-Soria, V.; Monton, J. B. Hydrocracking of Vacuum Gasoil on the Novel Mesoporous MCM-41 Aluminosilicates Catalysts. *J. Catal*. **1995**, *153*, 25-31.

18. Thomas, J. M. The Chemistry of Crystalline Sponges. *Nature* **1994**, *368*, 289-290.

19. Rathousky, J.; Zukai, A.; Franke, O.; Schulz-Ekloff, G. Adsorption on MCM-41 Mesoporous Molecular Sieve. Part 1. Nitrogen Isotherms and Parameters of the Porous Structure. *J. Chem. Soc., Faraday Trans*. **1994**, *90*, 2821-2826.

20. Rathousky, J.; Zukai, A.; Franke, O.; Schulz-Ekloff, G. Adsorption on MCM-41 Mesoporous Molecular Sieve. Part 2. Cyclopentane Isotherms and their Temperature Dependence. *J. Chem. Soc., Faraday Trans*. **1995**, *91*, 937-940.

21. Llewellyn, P. C.; Schuth, F.; Grillet, Y.; Rouqoerol, F.; Rouquerol, J.; Unger, K. K. Water Sorption on Mesoporous Aluminosilicate MCM-41. *Langmuir* **1995**, *11*, 574-577.

22. Branton, P. J.; Hall, P. G.; Sing, K. S. W. Physisorption of Nitrogen and Oxygen by MCM-41, a Model Mesoporous Adsorption. *J. Chem. Soc., Chem. Commun*. **1993**, *16,* 1257-1258.

23. Branton, P. J.; Hall, P. G.; Sing, K. S. W.; Reichert, H.; Schuth, F.; Unger, K. K. Physisorption of Argon, Nitrogen and Oxygen by MCM-41, a Model Mesoporous Adsorbent. *J. Chem. Soc., Faraday Trans*. **1994**, *90*, 2965-2967.

24. Branton, P. J.; Hall, P. G.; Treguer, M.; Sing, K. S. W. Adsorption of Carbon Dioxide, Sulfur Dioxide and Water Vapor by MCM-41, a Model Mesoporous Adsorbent. *J. Chem. Soc., Faraday Trans*. **1995**, *91*, 2041-2043.

25. Feuston, B. P.; Higgins, J. B. Physical Sorption of Argon, Nitrogen and Oxygen by MCM-41, a Model Mesoporous Adsorbent. *J. Phys. Chem*. **1994**, *98*, 4459.

26. Huber, C.; Moller, K.; Bein, T. Reactivity of A Trimethylstannyl Molybdenum Complex in Mesoporous MCM-41. *J. Chem. Soc., Chem. Commun*. **1994**, *22,* 2619-2620.

27. (a) Rouquerol, F.; Rouquerol, J.; Sing, K. Ed., *Adsorption by Powders & Porous Solids*, Academic Press: San Diego, CA USA, 1999. pp 8, 191, 416, 439, 442. (b) Sing, K. S. W.; Everett, D. H.; Haul, R. A. W.; Moscou, L.; Pierotti, R. A.; Rouquerol, J.; Siemieniewska, T. Reporting Physisorption Data for Gas/solid Systems with Special Reference to the Determination of Surface Area and Porosity. *Pure Appl. Chem.* **1985,** *57*(4), 603-19. (c) Broekhoff, J. C. P. Mesopore Determination from Nitrogen Sorption Isotherms: Fundamentals, Scope, Limitations. *Stud. Surf. Sci. Catal.* **1979**, *3*(2), 663-84. (d) Shields, J. E.; Lowell, S.; Thomas, M.

A.; Thommes, M. *Characterization of Porous Solids and Powders: Surface Area, Pore Size and Density*. Fourth Ed. Kluwer Academic Pub. USA, 2004. pp. 43-45.

28. (a) Zhao, X. S.; Lu, G. Q.; Millar, G. J. Advances in Mesoporous Molecular Sieve MCM-41 *Ind. Eng. Chem. Res.* **1996,** *35,* 2075-2090. (b) Barton, T. J.; Bull, L. M.; Klemperer, W. G.; Loy, D. A.; McEnaney, B.; Misono, M.; Monson, P. A.; Pez, G.; Scherer, G. W.; Vartuli, J. C.; Yaghir, O. M. Tailored Porous Materials *Chem. Mater.***1999,** *11,* 2633-2656.

29. Bergna, H. E. Ed., The Colloid Chemistry of Silica, *Adv. Chem. Ser.* V. 234, ACS, Washington, D.C., 1994.

30. Wefers, K.; Misra, C. Oxides and Hydroxides of Aluminum, Alcoa Technical Paper No. 19, Alcoa Laboratories, **1972,** 52.

31. Behrens, P. Mesoporous Inorganic Solids. *Adv. Mater.* **1993,** *5*(2), 127-132.

32. Sing, K. S. W.; Everett, D. H.; Haul, R. A. W.; Moscou, L.; Pierotti, R. A.; Rouquerol, J.; Siemienieska, T. Reporting Physisorption Data for Gas/solid Systems with Special Reference to the Determination of Surface Area and Porosity. *Pure. Appl. Chem.* **1985,** *57*(4), 603-619.

33. Alfredsson, V.; Anderson, M. W. Structure of MCM-48 Revealed by Transmission Electron Microscopy. *Chem. Mater.* **1996,** *8*, 1141-1146.

34. (a) Ciesla, U.; Schüth, F. Ordered Mesoporous Materials. *Micropor. Mesopor. Mater.* **1999,** *27*, 131-149. (b) Ying, J. Y.; Mehnert, C. P.; Wong, M. S. Synthesis and Applications of Supramolecular-templated Mesoporous Materials. *Angew. Chem. Int. Ed.* **1999,** *38*(1/2), 56-77. (c) Linden, M.; Schacht, S.; Schüth, F.; Steel, A.; Unger, K. K. Recent Advances in Nano- and Macroscale Control of Hexagonal, Mesoporous Materials. *J. Porous Mater.* **1998,** *5*(3/4), 177-193. (d) Schüth, F. Superstructures of Mesoporous Silicas. *Curr. Opin. Coll. Inter. Sci.* **1998,** *3*(2), 174-180. (e) Sayari, A.; Liu, P. Non-silica Periodic Mesostructured Materials: Recent Progress. *Micropor. Mater.* **1997,** *12*(4-6), 149-177.

35. Di Renzo, F.; Cambon, H.; Dutarte, R. A 28-year-old Synthesis of Micelle-templated Mesoporous Silica. *Micropor. Mater.* **1997,** *10*(4-6), 283-286.

36. Flaigen, E. M.; Patton, R. L.; Wison, S. T. Structural, Synthetic and Physicochemical Concepts in Aluminophosphate-based Molecular Sieves. *Stud. Surf. Sci. Catal.* **1988,** *37*, 13-27.

37. Lok, B. M.; Cannon, T. R.; Messina, C. A. The Role of Organic Molecules in Molecular Sieve Synthesis. *Zeolites* **1983,** *3*(4), 282-291.

38. (a) Sayari, A. Periodic Mesoporous Materials: Synthesis, Characterization and Potential Applications. *Stud. Surf. Sci. Catal.* **1996,** *102*, 1-46. (b) Chen, C. Y.; Burkett, S. L.; Li, H. X.; Davis, M. E. Studies on Mesoporous Materials. II. Synthesis Mechanism of MCM-41. *Micro. Mater.* **1993,** *2*(1), 27-34. (c) Steel, A.; Carr, S. W.; Anderson, M. W. [14]N NMR Study of Surfactant Mesophases in the Synthesis of Mesoporous Silicates. *J. Chem. Soc., Chem. Commun.* **1994,** *13,* 1571-1572.

39. Lawrence, M. J. Surfactant Systems: Their Use in Drug Delivery. *Chem. Soc. Rev.* **1994,** *23*(6), 417-424.

40. (a) Fromherz, P. Micelle Structure: A Surfactant-Block Model. *Chem. Phys. Lett.* **1981,** *77*(3), 460-466. (b) Myers, D. Surfactant Science and Technology, VCH: New York, 1992.

41. McCusker, L. B.; Baerlocher, E. J.; Bulow, M. The Triple Helix Inside the Large-Pore Aluminophosphate Molecular Sieve VPI 5. *Zeolites* **1991,** *11*(4), 308-313.

42. Tanev, P. T.; Pinnavaia, T. J. A Neutral Templating Route to Mesoporous Molecular Sieves. *Science* **1995,** *267*(5199), 865-867.

43. (a) Bagshaw, S. A.; Prouzet, E.; Pinnavaia, T. J. Templating of Mesoporous Molecular Sieves by Nonionic Polyethylene Oxide Surfactants. *Science* **1995,** *269*(5228), 1242-1244. (b) Attard, G. S.; Glyde, J. C.; Goltner, C.. Liquid-crystalline Phases as Templates for the Synthesis of Mesoporous Silica. *Nature* **1995,** *378*(6555), 366-368. (c) Bagshaw, S. A.; Pinnavaia, T. J. Mesoporous Alumina Molecular Sieves. *Angew. Chem. Int. Ed.* **1996,** *35*(10), 1102-1105. (d) Soler-Illia, G. J.; Sanchez, C.; Lebeau, B.; Patarin, J. Chemical Strategies to Design Textured Materials: from Microporous and Mesoporous Oxides to Nanonetworks and Hierarchical Structures *Chem. Rev.,* 2002, *102* (11), 4093-4138.

44. Zhao, D.; Huo, Q.; Feng, J.; Chmelka,, B. F.; Stucky, G. D. Nonionic Triblock and Star Diblock Copolymer and Oligomeric Surfactant Syntheses of Highly Ordered, Hydrothermally Stable, Mesoporous Silica Structures. *J. Am. Chem. Soc.* **1998,** *120*(24)*,* 6024-6036.

45. (a) Wei, Y.; Jin, D.; Ding, T.; Shih, W.-H.; Liu, X.; Cheng, S. Z. D.; Fu, Q. A Non-Surfactant Templating Route to Mesoporous Silica Materials. *Adv. Mater.* **1998,** *10*(4), 313-316. (b) Wei, Y.; Xu, J.; Dong, H.; Dong, J.; Qiu, K.; Jansen-Varnum, S. A. Preparation and Physisorption Characterization of D-Glucose-Templated Mesoporous Silica Sol-Gel Materials. *Chem. Mater.* **1999,** *11*(8), 2023-2029.

46. Chan, V. Z.-H.; Hoffman, J.; Lee, V. Y.; Iatrou, H.; Avgeropoulos, A.; Hadjichristidis, N.; Miller, R. D.; Thomas, E. L. Ordered Bicontinuous Nanoporous and Nanorelief Ceramic Films from Self Assembling Polymer Percursors. *Science* **1999,** *286*(5445), 1716-1719.

47. (a) Wei, Y.; Xu, J.; Feng, Q.; Dong, H.; Lin, M. Encapsulation of Enzymes in Mesoporous Host Materials via the Nonsurfactant-templated Sol-gel Process. *Mater. Lett.* **2000,** *44*(1), 6-11. (b) Xu, J.; Dong, H.; Feng, Q.; Wei, Y. *Polym. Prep.* **2000,** *41*(1)*,* 1042; 1044; 1046. (c) Wei, Y.; Xu, J.; Feng, Q.; Lin, M.; Dong, H.; Zhang, W.; Wang, C. A Novel Method for Enzyme Immobilization: Direct Encapsulation of Acid Phosphatase in Nanoporous Silica Host Materials. *J. Nanosci. Nanotechnol.* **2001,** *1*(1), 83-93.

48. Alsyouri, H. M.; Lin, Y. S. Effects of Synthesis Conditions on Macroscopic and Microscopic Properties of Ordered Mesoporous Silica Fibers. *Chem. Mater.* **2003,** *15*(10)*,* 2033-2039.

49. Nogami, M.; Moriya, Y. Glass Formation Through Hydrolysis of Silicon Acetate $(Si(OC_2H_5)_4)$ with Ammonium Hydroxide and Hydrochloric Acid Solution. *J. Non-Cryst. Solids.* **1980,** *37*(2), 191-201.

50. Wei, Y.; Jin, D.; Yang, C.; Wei, G. A Fast Convenient Method to Prepare Hybrid Sol-Gel Materials with Low Volume-Shrinkages. *J. Sol-Gel Sci. Tech.* **1996,** *7*(3), 191-201.

51. Brinker, C. J.; Sehgal, R.; Hietala, S. L.; Deshpande, R.; Smith, D. M.; Loy, D.; Ashley, C. S. Sol-Gel Strategies for Controlled Porosity Inorganic Materials. *J. Memb. Sci.* **1994,** *94*(1-3), 85-102.

52. Zusman, R.; Beckman, D. A.; Zusman, I.; Brent, R. L. Purification of Sheep Immunoglobulin G using Protein A Trapped in Sol-gel Glass. *Anal. Biochem.* **1992,** *201*(1), 103-106.

53. Hobson, S. T.; Shea, K. J. Bridged Bisimide Polysilsesquioxane Xerogels: New Hybrid Organic-Inorganic Materials. *Chem. Mater.* **1997,** *9*(2), 616-623.

54. Yoldas, B. E. Hydrolytic Polycondensation of Tetra(ethoxy)silane (Si(OC₂H₅)₄) and Effect of Reaction Parameters. *J. Non-Cryst. Solids,* **1986,** *83*(3), 375-390.

55. Wen, J.; Wilkes, G. L. Novel Abrasion Resistant Inorganic/Organic Coating Materials Based on Functionalized Diethylenetriamine, Glycerol and Diols. *Poly. Mater. Sci. Eng.* **1995,** *73,* 429-430.

56. Brinker, C.; Scherer, G. Sol-Gel Science: The Physics and Chemistry of Sol-Gel Processing. Academic Press, Inc.: New York, 1990.

57. Brinker, C. Jeffrey. Sol-Gel Processing of Silica. *Adv. Chem. Ser.* **1994,** *234*(Colloid Chemistry of Silica), 361-402.

58. Brinker, C. J. Hydrolysis and Condensation of Silicates: Effects on Structure. *J. Non-Cryst. Solids,* **1988,** *100*(1-3), 31-50.

59. Yoldas, B. E. Modification of Polymer-Gel Structures. *J. Non-Cryst. Solids,* **1984,** *63*(1-2), 145-154.

60. Ng, L. V.; Thompson, P.; Sanchez, J.; Macosko, C. W.; McCormick, A. V. Formation of Cagelike Intermediates from Nonrandom Cyclization during Acid-Catalyzed Sol-Gel Polymerization of Tetraethyl Orthosilicate. *Macromolecules* **1995,** *28*(19), 6471-6476.

61. Wen, J.; Wilkes, G. L. Organic/Inorganic Hybrid Network Materials by the Sol-Gel Approach. *Chem. Mater.* **1996,** *8*(8), 1667-1681.

62. Hench, L. L.; West, J. K. The Sol-Gel Process. *Chem. Rev.* **1990,** *90*(1), 33-72.

63. Schmidt, H.; Scholze, H.; Kaiser, A. Principles of Hydrolysis and Condensation Reaction of Alkoxysilanes. *J. Non-Cryst. Solids.* **1984,** *63*(1-2), 1-11.

64. Julbe, A.; Balzer, C.; Barthez, J. M.; Guizard, C.; Larbot, A.; Cot, L. Effect of Non-ionic Surface Active Agents on TEOS-derived Sols, Gels and Materials. *J. Sol-Gel Sci. Tech.* **1995,** *4*(2), 89-97.

65. (a) Mercier, L.; Pinnavaia, T. J. Access in Mesoporous Materials. Advantages of a Uniform Pore Structure in the Design of a Heavy Metal Ion Adsorbent for Environmental Remediation. *Adv. Mater.* **1997,** *9*(6), 500-3. (b) Feng, X.; Fryxell, G. E.; Wang, L.-Q.; Kim, Y. A.; Liu, J.; Kemner, K. M. Functionalized Monolayers on Ordered Mesoporous Supports. *Science* **1997,** *276*(5314), 923-926.

66. Van Rhijn, W. M.; DeVos, D. E.; Sels, B. F.; Bossaert, W. D.; Jacobs, P. A. Sulfonic Acid Functionalized Ordered Mesoporous Materials as Catalysts for Condensation and Esterification Reactions. *Chem. Commun.* **1998,** *3,* 317-318.

67. Diaz, J. F.; Balkus, K. J., Jr.; Bedioui, F.; Kurshev, V.; Keva, L. Synthesis and Characterization of Cobalt-Complex Functionalized MCM-41. *Chem. Mater.* **1997,** *9*(1), 61-67.

68. Lim, M. H.; Stein, A. Comparative Studies of Grafting and Direct Syntheses of Inorganic-Organic Hybrid Mesoporous Materials. *Chem. Mater.* **1999,** *11*(11)*,* 3285-3295.

69. Mercier, L.; Pinnavaia, T. J. Direct Synthesis of Hybrid Organic-Inorganic Nanoporous Silica by a Neutral Amine Assembly Route: Structure-Function Control

by Stoichiometric Incorporation of Organosiloxane Molecules. *Chem. Mater.* **2000,** *12*(1)*,* 188-196.

70. Brown, J.; Richer, R.; Mercier, L. One-step Synthesis of High Capacity Mesoporous Hg^{2+} Adsorbents by Non-ionic Surfactant Assembly. *Micropor. Mesopor. Mater.* **2000,** *37*(1-2)*,* 41-48.

71. Fowler, C. E.; Burkett, S. L.; Mann, S. Synthesis and Characterization of Ordered Organosilica-Surfactant Mesophases with Functionalized MCM-41-type Architecture. *Chem. Commun.* **1997,** *18,* 1769-1770.

72. Macquarrie, D. J.; Jackson, D. B.; Tailland, S.; Utting, K. A. Organically Modified Hexagonal Mesoporous Silicas (HMS) - Remarkable Effect of Preparation Solvent on Physical and Chemical Properties. *J. Mater. Chem.* **2001,** *11*(7)*,* 1843-1849.

73. Mori, Y.; Pinnavaia, T. J. Optimizing Organic Functionality in Mesostructured Silica: Direct Assembly of Mercaptopropyl Groups in Wormhole Framework Structures. *Chem. Mater.* **2001,** *13*(6)*,* 2173-2178.

74. Yiu, H. H. P.; Botting, C. H.; Botting, N. P.; Wright, P. A. Size Selective Protein Adsorption on Thiol-functionalized SBA-15 Mesoporous Molecular Sieve. *Phys. Chem. Chem. Phys.* **2001,** *3*(15)*,* 2983-2985.

75. Lin, V.S.-Y.; Radu, D.R.; Han, M.-K.; Deng, W.; Kuroki, S.; Shanks, B.H.; Pruski, M. Oxidative Polymerization of 1,4-Diethynylbenzene into Highly Conjugated Poly(phenylene butadiynylene) within the Channels of Surface-Functionalized Mesoporous Silica and Alumina Materials. *J. Am. Chem. Soc.* **2002,** *124*(31)*,* 9040-9041.

76. Mbaraka, I.K.; Radu, D.R.; Lin, V.S.-Y.; Shanks, B.H. Organosulfonic Acid-functionalized Mesoporous Silicas for the Esterification of Fatty Acid. *J. Cat.* **2003,** *219*(2)*,* 329-336.

77. Huh, S.; Wiench, J. W.; Yoo, J. C.; Pruski, M.; Lin, V. S. Y. Organic Functionalization and Morphology Control of Mesoporous Silicas via a Co-Condensation Synthesis Method. *Chem. Mater.* **2003,** *15*(22)*,* 4247-4256.

78. Wirnsberger, G.; Scott, B. J.; Stucky, G. D. pH Sensing with Mesoporous Thin Films. *Chem. Commun.* **2001,** *1,* 119-120.

79. Uusitalo, A. M.; Pakkanen, T. T.; Iiskola, E. I. Immobilization of $CrCl_3(THF)_3$ on A Cyclopentadienyl Surface of Silica. *J. Mol. Cat. A: Chemical* **2000,** *156*(1-2)*,* 181-193.

80. Anwander, R. SOMC@PMS. Surface Organometallic Chemistry at Periodic Mesoporous Silica. *Chem. Mater.* **2001,** *13*(12)*,* 4419-4438.

81. (a) Stein, A.; Melde, B, J.; Schroden, R. C. Hybrid Inorganic-Organic Mesoporous Silicates-Nanoscopic Reactors coming of Age. *Adv. Mater.* **2000,** *12*(19), 1403-1419. (b) Inagaki, S.; Guan, S.; Fukushima, Y.; Ohsuna, T.; Terasaki, O. Novel Ordered Mesoporous Materials with Hybrid Organic-inorganic Network in the Frameworks. *Stud. Surf. Sci. Catal.* **2000,** 129, 155-162.

82. (a) Beck, J. S.; Calabro, D. C.; McCullen, S. B.; Pelrine, B. P.; Schmitt, K. D.; Vartuli, J. C. Method for Functionalizing Synthetic Mesoporous Crystalline Material, Mobil Oil Corp., USA 1992. (b) Kimura, T.; Saeki, S.; Sugahara, Y.; Kuroda, K. A. Organic Modification of FSM-Type Mesoporous Silicas Derived from Kanemite by Silylation. *Langmuir* **1999,** *15*(8), 2794-2798. (c) Zhao, X. S.; Lu, G. Q. Modification of MCM-41 by Surface Silylation with Trimethylchlorosilane and Adsorption Study.

J.Phys. Chem. B. **1998,** *102*(9), 1556-1561. (d) Inagaki, S.; Fukushima, Y.; Kuroda, K. Synthesis of Highly Ordered Mesoporous Materials from a Layered Polysilicate. *J.*Chem. Soc. Chem. Commun. **1993,** 8, 680-682.

83. (a) Shephard, D. S.; Zhou, W.; Maschmeyer, T.; Matters, J. M.; Roper, C. L.; Parsons, S.; Johnson, B. F. G.; Duer, M. J. Site-directed Surface Derivatization of MCM-41: use of High-resolution Transmission Electron Microscopy and Molecular Recognition for Determining the Position of Functionality within Mesoporous Materials. *Angew. Chem. Int. Ed.* **1998,** *37*(19), 2719-2723. (b) De Juan, F.; Ruiz-Hitzky, E. Selective Functionalization of Mesoporous Silica. *Adv. Mater.* **2000,** *12*(6), 430-432. (c) Aronson, B. J.; Blanford, C. F.; Stein, A. Solution-Phase Grafting of Titanium Dioxide onto the Pore Surface of Mesoporous Silicates: Synthesis and Structural Characterization. *Chem. Mater.* **1997,** *9*(12), 2842-2851.

84. (a) Macquarrie, D. J. Direct Preparation of Organically Modified MCM-Type Materials. Preparation and Characterization of Aminopropyl-MCM and 2-Cyanoethyl-MCM. *Chem. Commun.* **1996,** *16,* 1961-1962. (b) Koya, M.; Nakajima, H. Hybrid Inorganic-organic Mesoporous Molecular Sieves. *Stud. Surf. Sci. Catal.* **1998,** *17*, 243-248. (c) Richer, R.; Mercier, L. Direct Synthesis of Functionalized Mesoporous Silica by Nonionic Alkylpolyethylene Oxide Surfactant Assembly. *Chem. Commun.*1998, *16,* 1775-1777.

85. (a) Wei, Y.; Feng, Q.; Xu, J.; Dong, H.; Qiu, K.-Y.; Jansen, S. A.; Yin, R.; Ong, K. Polymethacrylate-Silica Hybrid Nanoporous Materials: A Bridge between Inorganic and Polymeric Molecular Sieves. *Adv. Mater.* **2000,** *12*(19), 1448-50. (b) Feng, Q.; Xu, J.; Dong, H.; Li, S.; Wei, Y. Synthesis of Polystyrene-Silica Hybrid Mesoporous Materials via the Nonsurfactant-template Sol-gel Process. *J. Mater. Chem.* **2000,** *10*(11), 2490-2494.

86. Inagaki, S.; Guan, S.; Fukushima, Y.; Ohsuma, T.; Terasaki, O. Novel Mesoporous Materials with a Uniform Distribution of Organic Groups and Inorganic Oxide in Their Frameworks. *J. Am. Chem. Soc.* **1999,** *121*(41)*,* 9611-9614.

87. Melde, B. J.; Holland, H. T.; Blanford, C. F.; Stein, A. Mesoporous Sieves with Unified Hybrid Inorganic/Organic Frameworks. *Chem. Mater.* **1999,** *11*(11), 3302-3308.

88. Asefa, T.; MacLachlan, M. J.; Coombs, N.; Ozin, G. A. Periodic Mesoporous Organosilicas with Organic Groups inside the Channel Walls. *Nature* **1999,** *402*(6764), 867-871.

89. Rubin, A. J. *Aqueous-Environmental Chemistry of Metals*, Ann Arbor Science Publishers Inc., Ann Arbor, Michigan, 1974.

90. R. W. Frei (Editor) and O. Hutzinger, *Analytical Aspects of Mercury and Other Heavy Metals in the Environment*, Gordon and Breach Science Publishers, London, 1975.

91. Krenkel, P. A. (Editor), *Heavy Metals in the Aquatic Environment*, Pergamon Press: Oxford, 1975.

92. Mercier, L.; Pinnavaia, T. J. Heavy Metal Ion Adsorbents Formed by the Grafting of a Thiol Functionality to Mesoporous Silica Molecular Sieves: Factors Affecting Hg(II) Uptake *Environ. Sci. Technol.,***1998,** *32*(18), 2749 -2754.

93. Marshall, M. A.; Mottola, H. A. Performance Studies under flow Conditions of Silica-Immobilized 8-Quinolinol and its Application as A Preconcentration Tool in

Flow Injection/atomic Absorption Determinations. *Anal. Chem.*, **1985,** *57*(3)*,* 729-733.

94. Leyden, D. E.; Luttrell, G. H. Preconcentration of Trace Metals using Chelating Groups Immobilized via Silylation. *Anal. Chem.*, **1975,** *47*(9)*,* 1612-1617.

95. Bresson, C.; Menu, M. J.; Dartiguenave, M.; Dartiguenave, Y. N,S Ligands for Preconcentration or Elimination of Heavy Metals. Synthesis and Characterization of Aminoethanethiols and Aminoethanethiol-modified Silica Gel. *J. Chem. Res.*, **1998,** *490*(8), 1919-1932.

96. Prasad, B. B.; Sundd, S. Silica Gel-Bonded Cationic Polyelectrolyte with Ferron as Counterion. Application to Preconcentration or Elimination of Trace Metals. *Bull. Chem. Soc. Jpn.*, **1995,** *68*(2)*,* 559-565.

97. Dias, F.; Newton, L; Gushikem, Y.; Rodrigues, E.; Moreira, J. C.; Polito, W. L. Structure of Copper Complexes Adsorbed on a Silica Gel Surface Chemically Modified with Benzimidazole. *J. Chem. Soc., Dalton Trans.*, **1994,** *9,* 1493-1497.

98. Dias, F.; Newton, L. Adsorption of Copper(II) and Cobalt(II) Complexes on a Silica Gel Surface Chemically Modified with 3-Amino-1,2,4-triazole. *Colloids Surf. A: Phys. Eng.,* **1998,** *144,* 219-227.

CHAPTER
TWO

SYNTHESIS OF MESOPOROUS MATERIALS BASED ON MCM-41 SILICAS

Abstract

We describe a simple method for controlling the channel diameter of the mesoporous molecular sieve MCM-41 in the range from 40.9 to 51.1 Å and the wall thickness in the 15.2-21.1 Å range while using the same gel mixture. This is achieved by varying the synthesis temperature from 25-100 $^\circ$C and reaction times from 1-14 days. The mole ratio, use of catalyst, and additives used were also varied. The unit cell parameter, channel diameter, thickness of the channel wall, surface area, degree of polymerization and grain morphology were monitored by X-ray diffraction, N_2 adsorption, solid state ^{29}Si magic-angle-spinning NMR, Fourier transform infrared (FT-IR) spectroscopy, UV-Visible spectrophotometer, scanning electron microscopy (SEM) and transmission electron microscopy (TEM).

Mesoporous materials with wider and thicker-walled channels and higher degree of polymerization are prepared at room temperature and at longer reaction times. The thick-wall mesoporous material, designated OSU-6, has higher thermal, hydrothermal and mechanical stabilities, and higher surface area than conventionally prepared MCM-41 silica. The material with the thickest channel wall (21.1 Å) can withstand calcination to nearly 1000 $^\circ$C with little structural damage. We suggest a mechanism for the increase

of wall thickness and channel diameter. Fascinating morphological features involving tubes and vesicles, up to 1500 nm in diameter are observed.

2.1. INTRODUCTION

2.1.1 Background

Mesoporous silica materials made by the use of self-assembled surfactants as templates have attracted a lot of interest in recent years. The family of highly ordered mesoporous siliceous materials, designated as M41S (MCM-41, MCM-48 and MCM-50), has the highest priority as new potential molecular sieves and supporting materials.[1,2] Parallel to the development of M41S materials, many other ordered mesophases with similar properties have been synthesized (*e.g.,* HMS,[3,4] FSM-16,[5] PCH,[6] SBA,[7] MSU,[8] and KIT.[9]) Several research groups have reported successful applications of these semi-crystalline silica zeolites. Mesostructured silicas with incorporated or grafted functional active groups or transition metals have been reported to have outstanding selective separation and catalytic activities because the porous network facilitates mass transfer of reactants to the active sites.[4]

The discovery of mesoporous MCM-41 materials by researchers at Mobil in 1992 has stimulated research in separation, selective adsorption, stationary phases in chromatography, pre-concentration of trace metals, heterogeneous catalysis,[10] in biochemistry as immobilization supports for enzymes,[11] in membranes, sensors, and in biological applications (immobilization, recognition, drug delivery, *etc.*),[11] agents for sequestering nuclear waste heavy metals, luminescent materials for laser and optical devices applications[12] and controlled polymerization inside their pores.[13] The presence of large and tunable uniform pores opens up the possibility for shape-selective conversions

of bulky molecules and pharmaceutical products.[14] Furthermore, surface-modified

mesoporous molecular sieves might find other potential applications, such as gas[15] and

liquid chromatographic separations. For this latter application, different methods have

been tested to synthesize mesoporous silica particles with spherical shapes and a narrow

pore size distribution.[16,17]

The usual procedure for the formation of mesostructured silica is to employ

surfactants as the structure-directing agents and a simple organosilicate compound, such

as tetramethylorthosilicate (TMOS) or tetraethylorthosilicate (TEOS), as the silica

source. These can be regarded as tetraesters of silicic acid, $Si(OH)_4$ which polymerizes

very easily and has never been isolated. The silicic acid esters are often referred to as

alkoxides. They are not soluble in water, but can be dissolved in a mixture of water and a

water miscible organic solvent. They are hydrolyzed when the pH is reduced or

increased causing the ester bond to cleave, generating an alcohol and a free silanol group.

The silanol group is reactive and undergoes condensation reactions with other silanol

groups. Depending on the pH and the presence of salts, the condensation may lead to

particle growth and/or gelation *via* processes that are relatively well understood.[18]

The structure formed is influenced by a number of parameters: choice of precursor,

choice of surfactant, presence of specific ions, condensation rate, which in turn, is mainly

governed by the pH and the temperature used. It seems that a low reaction rate favors

formation of a well-ordered crystalline material. For instance, faceted single crystals of

mesoporous materials with cubic geometry were obtained by running the reaction for one

week at 0 °C, instead of shorter time at room temperature in which case a less ordered

product was obtained.[19] It is likely that the control of crystal morphology that can be

obtained by low temperature is due to the reaction then proceeding under thermodynamically controlled conditions, which is not always the case otherwise.[20]

2.1.2. Properties (Advantages and Disadvantages)

The mesoporous materials initially appeared to be the holy grail sought after by zeolite chemists of the time. They possessed extremely high surface areas and easily accessible, regular arrays of uniform pores. Most importantly, the pore sizes exceeded those attainable in zeolites and they could be tuned in the nanometer range (15-100 Å) by choosing an appropriate surfactant templating system, sometimes with a co-solvent or swelling agent. Moreover, it is possibly to functionalize their surfaces for particular applications. Thus, novel catalysts, sorbents, sensors, and host materials for large guest molecules were envisioned. Furthermore, MCM-41 has a rigid structure and so avoids the swelling problems encountered with some other adsorbents. However, the original mesoporous silicates and aluminosilicates exhibited a number of limitations, including lower thermal, hydrothermal and mechanical stability and lower reactivity than zeolites with comparable compositions. They possessed relatively thin walls, which prevented incorporation of secondary pores within the walls, they only formed fine particles, and they have low amounts of hydroxyl groups.[21] Yet, the ability to manipulate structures of porous solids on a nanometer scale in a controlled way proved to be so important to the research community that many of these limitations have been addressed and overcome in the last few years. For example, the hydrothermal stability of mesoporous silicates has been improved by adding salts to the synthesis mixture,[22] or by producing materials with thicker walls.[3,7,8,23-29] Structures with uniform pore sizes can now be formed throughout most of the mesopore size range.[21]

The advantages of ordered silicate mesoporous materials for separation applications include a regular array of uniform pores, controllable pore size, and the ability to functionalize the surface for particular separations.[30] Potential separation applications for MCM-41 include mercury removal from waste streams.[31,32] However, the stability of these materials in aqueous solutions is of concern. Although the properties of M41S materials have been widely investigated, only limited studies have been performed after their exposure to aqueous solutions. Most of these studies have focused on the hydrothermal stability of the materials by assessing their structure before and after treatment in boiling water for up to 48 h.[33,34] However, it is important that the pore structure integrity is retained throughout repeated adsorption and regeneration cycles (generally performed around room temperature) if these materials are to be economically employed in separation processes involving aqueous solutions. Recent work has shown that the M41S materials are modified by prolonged exposure to water and water vapor, leading to decrease structural regularity, pore shape uniformity, pore size, and pore volume.[34-37] Basic solutions in particular cause major loss of structure with much larger pores and decreased surface areas found in materials immersed for short periods, *e.g.,* several hours.[38,39] Little change was observed in the properties for materials exposed to neutral or acidic solutions over periods up to 48 h.[38,39] Water immersion was found to have greater impact on the structure as the temperature of the solution was increased in the range 298-373 K.[22] This low stability restricts the life of M41S materials in aqueous solutions, and has limited the range of applications for these materials.

Gusev *et al.,*[40] reported experimental data on the mechanical stability of the silica mesoporous material MCM-41. Using X-ray diffraction and nitrogen adsorption they

showed that the ordered mesoporous structure of MCM-41 can be affected considerably by mechanical compression at pressures as low as 850 atmospheres and essentially can be destroyed at 2200 atmospheres.

2.2. LITERATURE REVIEW

Bearing in mind large-scale industrial applications, one has to take into account the critical conditions imposed on molecular sieves. It is recognized that the thermal, hydrothermal, and mechanical stabilities are crucial parameters for potential applications. The powders are usually compressed into pellets and have to withstand extreme reaction and regeneration conditions. Moreover, these materials have to have a high number of hydroxyl groups on the surface in order to use them for further modification and functionalization reactions.

The MCM-41 materials consist of uniform, hexagonal arrays of mesopores with pore diameter between 20 and 100 Å. They show extraordinary high surface areas and narrow pore size distributions.[1,2] The ability to grow size and shape specific forms of ordered mesoporous solids, such as hexagonally ordered MCM-41 silica, by subtle modifications of the synthesis conditions is an important consideration in the use of these new materials for technological applications. The pore size of MCM-41 can be controlled by varying the alkyl chain length of the surfactant molecules used as template in the synthesis or by adding auxiliary hydrocarbons to the synthesis mixture, such as alkylated benzene (*e.g.,* trimethylbenzene), which are solubilized into the internal hydrophobic region of the templating aggregates (micelles) which will increase the size of the micelle, also pore size uniformity and long range structural ordering of MCM-41 can be modified by changing the pH when preparing the gel.[1,2,41-43] Moreover, the

hydrothermal and mechanical stabilities can be modified by changing the reaction conditions such as pH, temperature, aging time, and composite ratio of silica. MCM-41 can be synthesized in different morphologies including rods, thin films, spheres, and curved shapes.[44]

Many synthesis methods and post treatment methods for MCM-41 have been published from 1992 to date. Some other mesophases similar to MCM-41 have also been developed such as SBA-n,[7,26] MSU-n,[3,8] and KT-n.[9] Synthesis of MCM-41 mesoporous materials has been accomplished using a variety of routes.

The aim of this investigation was the synthesis of mesoporous silica materials based on MCM-41 with high surface areas, large pore sizes, narrow pore size distribution, and high thermal, hydrothermal, and mechanical stabilities. Another important objective is to have high hydroxyl group content in the resulting materials. In order to obtain these goals, several factors that affect the characteristics of the MCM-41 were studied and the effect of each factors on the final product were defined.

2.2.1. Synthesis Components

2.2.1.1. Source of Silica

A silicon atom in a silica or silicate product can be attached to between zero and four other silicon atoms *via* siloxane (Si-O-Si) bonds. TEOS and other simple alkoxides are examples of silica sources that do not contain any siloxane bonds and colloidal silica is an example of a source of silica where the majority of silicon atoms have four neighbors linked by siloxane bonds. The silicon atoms on the periphery of the silica nanoparticle usually have three siloxane bridges and one silanol group. The coordination pattern is usually determined by ^{29}Si-NMR and it is customary to use $Si(Q^n)$ as the

nomenclature for signals from silicon atoms coordinated by n siloxane bonds. Thus, TEOS gives only the $Si(Q^o)$ signal and colloidal silica gives mostly the $Si(Q^4)$ signal. Water glass can show all five signals, with signals from higher coordination increasing with increasing SiO_2 to Na_2O ratio, *i.e.*, decreasing pH. It has been shown that silica sources that display $Si(Q^4)$ signals are unsuitable as starting materials for the synthesis of mesoporous materials. For instance, colloidal silica and high ratio water glass were found not to give a mesoporous material under conditions where low ratio water glass and TEOS gave hexagonal mesoporous silica.[45] However, if the colloidal silica was first treated with alkali to reach a SiO_2 to Na_2O ratio of two, it could be used as a starting material for mesoporous silica. This silica source gave no $Si(Q^4)$ NMR signal. Klotz *et al.*,[46] showed the importance of the $Si(Q^n)$ distribution in the formation of ordered mesostructured silica and the effects of aging the synthesis solution on the $Si(Q^n)$ distribution. They found that a solution with a predominance of $Si(Q^1)$ species in the initial stage of the synthesis resulted in an ordered mesophase and that the disappearance of the order was related to the presence of $Si(Q^3)$ species in the initial stage of the synthesis. It thus seems that the presence of low condensed, $Si(Q^{n<3})$, species in the initial synthesis solution is a prerequisite for obtaining ordered mesoporous silica.

2.2.1.2. Surfactants and Additives

Several different experimental procedures for the preparation of mesostructured silica covered a wide variety of different surfactants and additives. The choice of surfactant is very important because it governs the size of the pores, as well as the thickness of the walls, and the symmetry of the mesoporous material. The two main classes used are cationics and nonionics. Anionic surfactants, which constitute the largest

surfactant class, have rarely been employed as a template for mesostructured silica,[47] whereas the fourth surfactant class, zwitterionics, do not seem to have been used at all with inorganic silica sources. There are also examples of the use of combinations of surfactants from different classes, such as cationic and nonionic.[48] Cationic surfactants of the type $C_nH_{2n+1}(CH_3)_3N^+X^-$, with n being 12–16 and X being Br or Cl, were used in the first experiments to produce mesoporous silica from an alkoxide precursor[1,2] and similar surfactants have been used in a large number of subsequent reports with TEOS or other organosilicates as the starting material. Cationic surfactants have also been employed for the preparation of mesoporous silica from an inorganic silica source and most of these studies have been performed under neutral to alkaline conditions,[49-53] although examples from the acidic side have also been published.[45]

Kresge and coworkers[1,2] reported the first self-assembly process to synthesis MCM-41 involving electrostatic interaction between positively charged quaternary ammonium micelles as surfactant (S^+) and inorganic silica anions (I^-) as framework precursors. They suggested a liquid crystal templating mechanism where surfactant molecules act as templates. This method applied an ionic surfactant route. The synthesis experiment was done under acidic conditions and at temperatures of about 100 ^{o}C. The surfactant was not recovered, but simply burned off by calcinations at elevated temperatures. The resulting MCM-41 showed hexagonal arrays of one dimensional pores with pore size ranging approximately from 1.5 to 10 nm and a surface area of ~ 1000 m^2/g. Since then, researchers have aimed to expand the synthesis conditions in order to improve these materials and identifying synthesis mechanisms. Huo *et al.*,[54] reported a generalized approach to the synthesis of periodic mesoporous materials using cationic and anionic

surfactants under a range of pH < 7 and pH 10-13. They reported that, the cationic

surfactants (S^+) are useful for the structuring of negatively charged inorganic species (I^-).

On the other hand, anionic surfactants (S^-) such as alkylsulfonate surfactants, have been

employed for structuring cationic inorganic species (I^+). Organic-inorganic combinations

with identically charged partners (*i.e.,* S^+ and I^+ or S^- and I^-) are possible, but then the

formation of the mesostructures is mediated by the counter-charged ions which must be

present in stoichiometric amounts $S^+X^-I^+$ (where $X^- = Cl^-$ or Br^-) or $S^-M^+I^-$ (where $M^+ =$

Na^+ or K^+) mechanisms have been demonstrated.[54,55] It was concluded in cases where the

degree of condensation of the oligomeric ions, which form the walls, is low, the removal

of the surfactants (templates) leads to the collapse of the ordered mesostructures.

Moreover, the study showed clearly that similar surfactants in acidic medium produce

mesoporous structures with similar, but slightly larger *d*-spacings than those obtained by

basic medium synthesis.[56]

  Shio *et al.,*[52] prepared fine mesoporous silica powders by adding an acid to a

solution of a mixture of sodium metasilicate and a surfactant of the type

$C_nH_{2n+1}(CH_3)_3N^+Cl^-$, with *n* being 18 or 22. The procedure gave particles with not only

the pore diameter and the specific surface area varying with the length of the long alkyl

chain of the surfactant but, also the particle size and shape. Stearyl (*n* = 18) gave a pore

diameter of 3.0 nm and a specific surface area (BET surface) of 1050 m^2 g^{-1} while

behenyl (*n* = 22) gave a pore diameter of 3.5 nm and a surface area of 900 m^2 g^{-1}. Since

in the liquid crystal that serves as a template for the mesoporous material the surfactants

assemble in head-out double layers, the pore diameter should reflect twice the length of

the hydrophobic tail of the surfactant because the pores should equal the size of the

hydrophobic domains of the liquid crystal. The values obtained, 3.0 and 3.5 nm, are perfectly reasonable for alkyl chains of 2×18 and 2×22 carbon atoms. While the powder particles made with the stearyl-based surfactant were cubes with a dimension of around 100 nm, the particles made with the behenyl-based surfactant were rod-like with a length of 300–500 nm and a diameter of *ca.* 50 nm.

Setoguchi *et al.*,[45] performed the synthesis of hexagonal mesoporous silica by adding water glass to a highly acidic solution of different cationic surfactants. Two surfactant series were tested, $C_nH_{2n+1}(CH_3)_3N^+X^-$, with *n* being 14, 16 or 18 and X being Cl or Br, and $C_{16}H_{33}Pyr^+X^-$, with Pyr being pyridyl and X being Cl or Br. Both the mean pore diameter and the *d*-spacing obtained from X-ray diffraction increased with increasing alkyl chain length of the first series of surfactants, which is in accordance with expectations since, as mentioned above, the pore diameter should reflect twice the length of the hydrophobic tail of the surfactant. The overall highest quality product was obtained with hexadecylpyridinium chloride as the surfactant.

Recently a cationic Gemini surfactant, $(C_{12}H_{25}N^+(CH_3)_2–(CH_2)_2–N^+(CH_3)_2$ $C_{12}H_{25})$ $2Br^-$, was used for making mesoporous silica with cubic geometry (space group *Ia3d*) from sodium silicate.[50] Gemini surfactants are known to self-assemble at much lower concentration than their monomeric counterparts so they should be interesting as structure-directing agents. The material obtained was of high quality as evidenced by small angle X-ray diffraction, determination of specific BET surface area (991 $m^2\ g^{-1}$), and by assessment of the pore size distribution. It would have been interesting to compare the results with corresponding experiments using the monomeric surfactant, *i.e.*, $C_{12}H_{25}N^+(CH_3)_3$ Br^-.

It is noteworthy that the surfactant counterion seems not to be of importance. Similar structures are reported for chloride and bromide as counterion. This is somewhat surprising since the physical chemistry of a self-assembled cationic surfactant in water is usually strongly influenced by the choice of counterion. Bromide is, for instance, more strongly bound than chloride or acetate to micelles and monolayers of cationic surfactants, which leads to differences in critical micelle concentration at lower concentration and in phase behavior at higher concentration. The reason why the surfactant counterion is not important in the formation of mesoporous silica is probably that formation of the mesoporous material involves a cooperative interaction between the surfactant cation and a growing silicate prepolymer, as discussed below. Thus, the type of counterion is not important since it is being replaced by silicate, which then serves as an inorganic, polymeric counterion for the surfactant.[18]

Tanev et al.,[3] have synthesized mesoporous MCM-41 using a neutral surfactant templating route ($S^o I^o$). In the neutral surfactant templating approach, a self-assembly between neutral surfactants S^o (e.g., primary amine) and neutral inorganic precursors I^o (e. g., tetraethyl orthosilicate (TEOS)) is based on hydrogen bonding. This approach affords mesostructures with larger wall thicknesses, small scattering domain sizes, and complementary textural mesoporosities. The thicker pore walls improve the thermal and hydrothermal stability of the mesopore framework, and the small crystallite domain size introduces textural mesoporosity, which facilitates accessing the framework-confined mesopores. A great advantage of this synthesis route with respect to that developed by Mobil researchers was that the neutral pathway allows for the facile recovery of the template from the mesopores by simple solvent extraction and the formation of

frameworks with a much higher surface silanol concentration compared to those of their electrostatically assembled and calcined counterparts.[56] Complete template recovery is not possible for MCM-41 prepared using the conventional approach because of the strong electrostatic interactions between ionic surfactants and the charged framework.[1,2]

Corma *et al.*,[57] studied the preparation of mesoporous materials, MCM-41, under highly acidic synthesis conditions. They reported that the formation of $S^+X^-I^+$ type interactions occurred and that the removal of the surfactant is easy by simply washing with water at room temperature. The facile removal of the surfactant indicates the weak interaction between the surfactant and the inorganic silica. They suggest that the mesostructures are formed by $I^oX^-S^+$ interactions, giving a neutral structure instead of the positively charged framework that was proposed previously by Huo and coworker.[54]

Sayari *et al.*,[58] reported the effect of the length of the hydrocarbon chain of the surfactant on the pore sizes and the final structure. They concluded that the pore size can be tailored by changing the length of the hydrocarbon chain. In other words, increasing the length will lead to an increase in the pore size. In their experiment alkylhexadecyldimethylammonium derivatives, *i.e.,* $(C_{16}H_{33})(C_nH_{2n+1})(CH_3)_2N^+$ were used and they concluded that a hexagonal phase was obtained for n = 1, 3, 5, 7, while a lamellar phase was obtained for all other templates, see Figure 2.1.
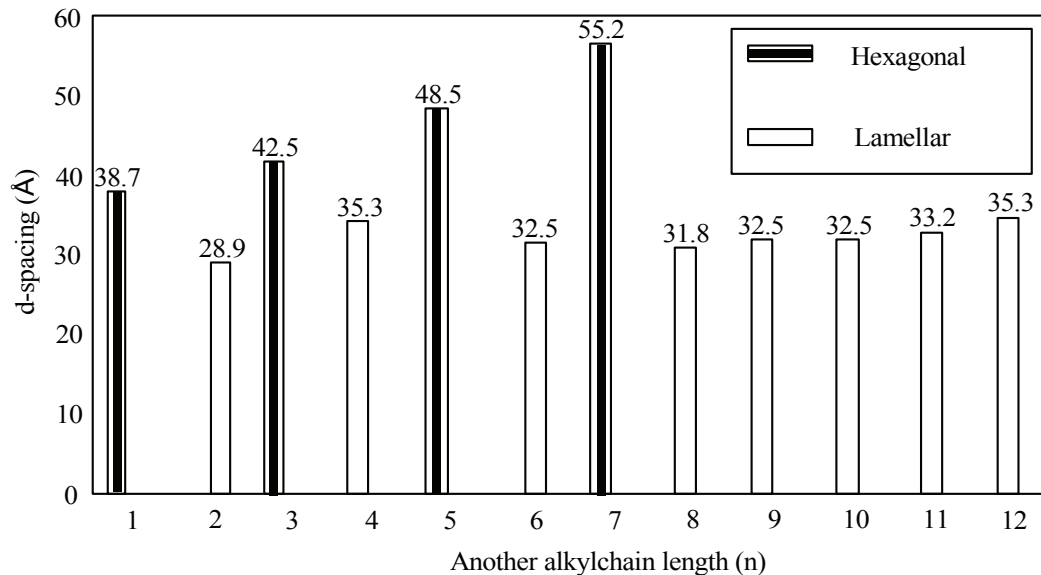
Figure 2.1. Influence of another alkyl chain length (n) of $(C_{16}H_{33})(C_nH_{2n+1})(CH_3)_2N^+$ on the mesophase and the d_{100} spacing.

The d_{100} spacing of the hexagonal MCM-41 increases by ~ 2.45 Å with the increasing of the carbon number (n) by one atom, which is much higher than the 1 Å /Carbon atom reported by Beck *et al.*[2] In the latter study, the alkyl chain lengths of quaternary ammonium surfactants $(C_nH_{2n+1})(CH_3)_3N^+$ (n = 8,9,10,12,14,16) were found to result in MCM-41 materials that exhibited increasing XRD d-spacing (d_{100}) and an increase in pore size of 1 Å /Carbon atom with increasing length of the surfactants.

One other possibility to expand the pore size of the mesoporous materials is the addition of organic molecules into the synthesis medium, in particular 1,3,5-trimethylbenzene (mesitylene). Beck *et al.,*[2] studied the effect of the addition of the auxiliary organic, mesitylene (MES), to MCM-41 synthesis mixtures on the pore size. This study indicated a proportional increase between the amount of the mesitylene added with both the pore sizes and the d-spacing of the XRD d_{100} peak. However, above a certain concentration of the additive, the resulting MCM-41 had wide pore size

distribution. However, Ulagappan and Rao[59] reported the synthesis of MCM-41 with different pore sizes utilizing alkanes of different chain lengths together with the surfactant as a template. The characterization of the results suggests that the surfactant molecules in the micelle are fully extended and the size of such micelles increased with the chain length of the n-alkane at least until the molecule has 15 carbon atoms, as shown in Figure 2.2.

a   b
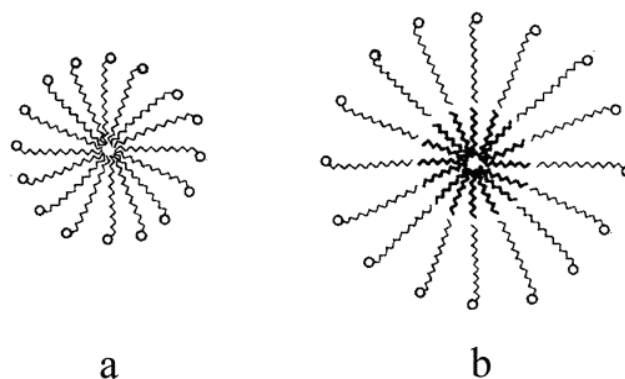
Figure 2.2. Schematic drawing of a micelle of surfactant molecules: (a) in the absence of a solubilizing agent and (b) in the presence of n-alkanes as solubilizing agents.[59]

Namba *et al.,*[60] prepared silica MCM-41 materials hydrothermally by using 1,3,5-trimethylbenzene or 1,3,5-triisopropylbenzene as an auxiliary chemical. The BJH pore size of MCM-41 increased up to 12 nm with increasing amounts of mesitylene. However, MCM-41 materials prepared with mesitylene displayed irregular pore arrangements and a half of these materials exhibited low thermal and hydrothermal stabilities. On the other hand, MCM-41 materials prepared with 1,3,5-triisopropylbenzene as an auxiliary chemical displayed regular pore arrangements and high thermal and hydrothermal stabilities, but their BJH pore sizes did not go over 4.0 nm. MCM-41 prepared with a 3:1 mixture of 1,3,5-triisopropylbenzene and mesitylene

displayed regular pore arrangements and high thermal and hydrothermal stabilities. Its BJH pore size was 4.7 nm.

Moreover, Namba et al.,[61] prepared MCM-41 materials hydrothermally by using template mixtures of hexadecyltrimethylammonium/dodecyltrimethylammonium with various molar ratios. The MCM-41 materials thus prepared were highly ordered and their pore sizes can be finely controlled by changing the molar ratio of the two surfactants. However, removal of surfactants requires high temperature which leads to low hydroxyl group concentration. Also they did not show high thermal, hydrothermal and mechanical stabilities.

Nonionic surfactants containing polyoxyethylene chains, either block copolymers of the polyoxyethylene-polyoxypropylene-polyoxyethylene type (often referred to as EO–PO–EO polymers) or fatty alcohol ethoxylates, C_nH_{2n+1}-$(EO)_m$, with n typically being 12–18 and m being 5–8, have been widely used as structure-directing agents in the formation of mesoporous silica using TEOS or other alkoxides as the silica source.[25,62-65] These types of nonionic surfactants have also been used in the synthesis of mesoporous silica from inorganic silica sources and both hexagonal and cubic structures have been prepared.[17,66-74] The nonionic surfactants have most often been used under acidic to neutral conditions. The hydrophilic–lipophilic balance of these surfactants is strongly affected by the temperature, which makes it possible to govern the type of liquid crystalline structure formed in water solutions by temperature adjustments.

Kipkemboi et al.,[75] have demonstated how the mesostructure obtained with EO–PO–EO block copolymers as structure-directing agents is influenced by the temperature and by the hydrophilic domain length. An increase in temperature leads to dehydration

of the polyoxyethylene chains, causing a reduction of the size of this block. This results

in a change of the spontaneous curvature of the surfactant film. For low surfactant

concentrations increase temperature will lead to a transition from less elongated to more

elongated micelles while for high surfactant concentration a transition from micellar

cubic, *via* hexagonal and lamellar, to bicontinuous cubic liquid crystals occurs. One

would expect that the temperature-controlled mode of self-assembly in solution would be

transferred to the corresponding structures in the mesoporous material. This has been

found to be the case for TEOS as the silica source.[75]

Shrinkage of the hydrophilic domains of the templating surfactant means that the

volume where the silica wall is being formed is reduced. This would be expected to lead

to thinner walls of the mesoporous material. It is now experimentally verified that this is

true, *i.e.*, an increase in temperature for systems based on surfactants containing

polyoxyethylene chains leads to a decrease of the wall thickness. The mesopore diameter

is only slightly affected by variations in temperature; however, because it is governed by

the size of the hydrophobic domain *i.e.*, the PO block, which is not much influenced by

the temperature.[75]

Coleman and Attard[76] studied the effects of surfactant concentration on the

regularity and morphology of mesoporous silica prepared in the tetramethyl orthosilicate

(TMOS)/Brij 56/HCl (0.5 *M*) system. For a fixed weight ratio of 1.8 TMOS:1.0 Brij 56,

they found that very low surfactant concentrations gave a disordered structure but when

increasing the surfactant concentration the order rapidly increased and resulted in a

hexagonal mesopore structure. On further increasing of the surfactant concentration the

hexagonal structure became progressively more disordered and wormhole-like structures

were obtained. When reaching a surfactant concentration that would give lyotropic phases in the surfactant/water binary system, the order of the mesoporous silica structure returned upon increasing the surfactant concentration, and reached a maximum at the same ratio as the hexagonal phase appeared in the binary system. At higher surfactant concentrations the order of the mesoporous silica structure again decreased. Taking into account that the presence of HCl and $SiO_x(OH)_{4-2x}$ species will induce (relatively small) changes in the binary phase diagram these can be used as useful guides for predicting the mesoporous structure of the silica. In the synthesis of mesoporous silica from micellar solutions the order was found to depend much on the surfactant concentration. Here the addition of the silicate precursor results in phase separation in the form of small domains having a pseudoliquid crystal structure that act as a mold for the forming silica network. However, for both routes it is only possible to obtain ordered mesostructures through the correct proportions of TMOS, surfactant and water.

2.2.1.3. Role of Acid and Base Catalysts (pH)

The pH of the medium plays a crucial role in the synthesis of M41S materials. By controlling the pH of the initial synthesis mixture, MCM-41 materials with increased wall thicknesses of 16 to 27 Å were prepared.[77] Ryoo *et al.,*[42] reported the synthesis of highly ordered MCM-41 by adding acetic acid to the reaction system to shift the equilibrium between the reactants and the mesophases formed toward the desired direction. They suggested that the MCM-41 phase was in dynamic equilibrium with the reactants. Therefore, the addition of acid to the reaction mixture was proposed to neutralize the hydroxyl and shift the equilibrium toward the positive direction.

Ryoo *et al.,*[22] reported that improved hydrothermal stability could be achieved by adjusting the gel pH several times during the hydrothermal crystallization process. However, this pH adjustment is a tedious process and the high pressure crystallization reaction has to be interrupted repeatedly.

Sierra *et al.,*[17] reported that isometric particles of mesoporous SiO_2 could be synthesized between 25 °C and 45 °C from reaction mixtures containing silicic acids, NaCl and a nonionic surfactant (Triton X 100). The particle size decreases from some tens of micrometers to < 1 μm when the pH increases from 1.85 to 6.0. At pH < 3.5, a glassy material forms that cements particles together. The particle size distribution narrows at higher pH and at long reaction times (several days). A spheroidal shape is favored by low pH and high temperature, and a more polyhedral shape appears at high pH that is independent of the temperature. This behavior could be related to the polycondensation rate of the silicic acids, the lifetime and disorder of the micelles, or to the micelles-silicic acid interactions.

Coustel *et al.,*[77] reported that the control of aluminosilicate activity during synthesis of MCM-41 leads to thicker pore walls, and hence to improved thermal and hydrothermal stabilities. The most probable model for formation of MCM 41 materials assumes aggregation of silica-coated micelles and the thickness of the silicate coating at the micelle surface can be varied by changing the activities of the aluminosilicate units in solution.

On the alkaline side, Kim *et al.,*[66,67,68] have developed a synthetic method using nonionic surfactants, such as *tri*-block copolymers and alcohol ethoxylates, and a reaction solution at near neutral pH conditions. The surfactant together with acetic acid, used in an amount

equimolar to the hydroxide content of the sodium silicate, was added to a sodium silicate solution to create the reactive solution. At molar ratios of $H_2O/Si = 230$ and surfactant/Si $= 0.008–0.017$ the procedure resulted in a thermally stable 2D hexagonal mesostructured silica, MSU-H. The reaction time was 20 hours at fixed temperatures of 308, 318 and 333 K, where the different temperatures generated different pore sizes in the hexagonal structure.

Increasing the pH increases the charge density of the silica. This favors electrostatic interactions between the surfactants and the silica, which can be taken advantage of when using cationic surfactants. Han *et al.*,[49] used a mixture of two cationic surfactants as a template for the synthesis of rod-like mesoporous silica with hexagonal symmetry. In the procedure, ethyl acetate was added to a dilute solution of a mixture of sodium silicate and the surfactants to obtain the desired pH due to hydrolysis of the ester. The reaction was allowed to proceed at 353 K for 72 h, followed by calcination. The reported specific BET surface area was about 760 $m^2 \ g^{-1}$.

Several papers deal with synthesis under very acidic conditions and the results obtained are generally good. Setoguchi *et al.*,[45] reported that their acidic synthesis generated the largest mesopore volume and the highest surface area with cationic surfactants. Studies on the use of nonionic surfactants under acidic conditions have been reported by Kim *et al.*[69,70] By using *di-* and *tri*-block copolymers together with sodium metasilicate as the silica source, different mesostructures, such as 2D hexagonal, 3D hexagonal, and 3D cubic, were obtained. With blends of different amphiphilic block copolymers and through variations in the hydrophilic–hydrophobic balance achieved by

changing the size of the hydrophilic blocks, the mesostructured phase was controlled with considerable accuracy.

The possibility of controlling the morphology of mesostructured particles has been investigated in several publications using sodium silicate as the silica source.[71,72,78,79] Experiments using the *tri*-block copolymer Pluronic P123 as a nonionic surfactant resulted in a monodisperse rodlike SBA-15 structure with high mesoscopic order. Only a very limited range of synthesis conditions could be used, however. The molar ratio of SiO_2/HCl/P123/H_2O was 1/7.84/0.0017/252 and the reaction was run at 303 K for 6 hours.[72] There are also reports on the formation of single crystals of mesoporous silica with a reaction mixture composed of cationic surfactant/SiO_2/NaOH/H_2SO_4 in a molar ratio of 1/2.15/1.67/4.35–8.90 in a very dilute water solution under static conditions for 2–4 days at 30 °C. Chao *et al.,*[78,79] produced SBA-1 mesoporous silica in the form of single crystals. The crystal shape (spheres, decaoctahedrons or cubes) was governed by varying the pH between 1 and 2. The results were explained by the fact that both the dilute conditions and the pH used, which is close to the isoelectric point of SiO_2, leads to a slow condensation rate. From the viewpoint of crystallization kinetics, the crystal morphology is determined by the relative rate of growth of different crystal faces, with the slow-growing surface dominating the final shape.

Gross *et al.,*[80] found that both the activation energy for annealing the surfactant/silica composite into a more ordered hexagonal structure and the activation energy for phase transition into a lamellar phase depended on the pH of the synthesis solution under alkaline conditions. Materials made at a lower alkaline pH showed the lowest activation

energy for annealing but the highest for phase transition. It was postulated that materials

prepared at lower pH get a more condensed framework thus requiring hydrolysis of more

siloxane linkages for phase transition to occur.

Boissière et al.,[81] explored a two-step synthesis approach for mesoporous MSU-X silica.

In the first step, mildly acidic conditions (pH 2–4) were employed to avoid uncontrolled

silica condensation and obtain a stable solution of micellar hybrid objects made of both

surfactant micelles and small silica oligomers. The second step of the synthesis consisted

of the condensation of the silica particles, and was performed either by increasing the pH

of the solution to neutral values or by addition of small amounts of fluoride. The addition

of fluorides leads to better control of both the nanostructure and the particle morphology.

2.2.1.4. Temperature and Aging

Elder et al.,[82] synthesized silica molecular sieves closely related to MCM-41 at

ambient temperature. The resulting materials were characterized and showed high

hydrothermal, thermal, and mechanical stability when compared with the results reported

by Stucky et al.,[83] who synthesized MCM-41 at 25 $^{\circ}$C in an alkaline preparation and

noted a lack of hydrothermal, thermal, and mechanical stability of this material compared

to that obtained from a heated preparation. Elder et al.,[82] suggested that the stability of

these materials is due to the condensation reaction which occurs during aging in the case

of reaction at ambient temperature. They concluded there was a relationship between

aging and stability of the final product.

Chen et al.,[84] studied the effect of calcination on the condensation using ^{29}Si

NMR on MCM-41 samples and reported an increase in the number of Q^4 sites over Q^3

and Q^2 sites upon calcination, showing that further reactions have occurred.

Elder *et al.*,[82] compared the shrinkages of the mesoporous materials prepared at ambient temperature and these prepared at high temperature after calcination. They found more silanol groups in the sample prepared at ambient temperature than that of the heated one. Moreover, the surface area measurements of the unheated preparation and heated preparation showed that these materials have surface areas close to each other.

Cheng *et al.*,[85] described a simple method of controlling the channel diameter of the mesoporous molecular sieve MCM-41 in the 26.1-36.5 Å range and the wall thickness in the 13.4-26.8 Å range while using the same gel mixture. This is achieved by varying the synthesis temperature in the 70-200 °C range and/or reaction times in the 0.5-96 h range. MCM-41 with wider and thicker-walled channels was prepared at higher temperature and at longer reaction times. Thick-wall MCM-41 has higher thermal stability but lower surface area. The material with the thickest channel wall ever reported (26.8 Å) can withstand calcination at nearly 1000 °C with little structural damage. The authors suggest a mechanism for the increase of wall thickness and channel diameter. Fascinating morphology features involving sealed silicate tubes and vesicles up to 1200 Å in diameter are observed.

Cheng *et al.*,[86] reported that a highly crystalline MCM-41 with a very narrow pore size distribution (1.5 Å), high surface area (1185 m^2/g), large grain size and thick channel walls (~ 17 Å) was prepared in alkali-free media by use of tetramethylammonium hydroxide as the source of base. The properties of the product depend on the source and concentration of the reactants, the gel aging time, temperature, and duration of synthesis. The initially produced hexagonal phase is transformed into the lamellar phase and then into an amorphous phase. In the 150 °C synthesis, the most stable product is amorphous

SiO_2. The synthesis is conveniently monitored by pH measurement. Gel aging, during which a spatial distribution of silicate polyanions and micellar cations is established, is essential for preparing high-quality MCM-41. Surfactants with the same cationic organic group but different counteranions alter the synthesis. The degree of polymerization of SiO_2 is also important. Highly basic gels favor the lamellar product; when the gel is weakly basic the quality of MCM-41 is lower as insufficient TMAOH is available to dissolve the SiO_2. The result of excess SiO_2 is similar but even more pronounced. Purely lamellar products are made at low SiO_2 concentrations, when the gel is more strongly basic. The best quality MCM-41 was prepared from a gel of molar composition SiO_2:0.19 $Me_4N^+OH^-$:0.27 CTABr:40 H_2O (with CTABr/SiO_2 = 0.27, similar to the ratio in the solid product) aged at 20 °C for 24 h and synthesis lasting for 48 h.

2.2.1.5. Hydrolysis and Condensation

In the preparation of large-pore MCM-41 type materials, the order of adding swelling agents and the nature of siloxane precursors had a significant influence on the pore diameters. When a swelling agent (mesitylene) was added to the template solution before addition of siloxane precursors, the pore size of the MCM-41 type materials did not increase. However, an increase in the pore size of MCM-41 type materials was attained by adding the swelling agents to the reaction bottle in which TEOS was already partially polymerized in the template solution. Since TEOS hydrolyzed and condensed in a period of ~ 20 min, the initial mesostructure was only weakly polymerized when mesitylene was added after 5.0 min. The loosely condensed framework could be easily expanded by swelling agents within the micellar arrays. Pore sizes of MCM-41 type samples could not be increased when precursors with methoxy groups were employed.[33]

Due to the fast hydrolysis and condensation of these precursors in the template solution, the framework became rigid quickly, which may have prevented expansion of the pore size.[33]

2.2.1.6. Addition of Salt and Post-Synthesis Treatments

Variations of the synthetic methods, such as addition of salt or post-synthesis treatments have been shown to improve the stability of M41S materials.[21,30,35,38,87] The relatively low wall thickness of these materials contributes to their lack of stability, so thicker-walled materials also show improved stability.[21] Modification of mesoporous silicates to include hydrophobic organic components on the pore surfaces or within the walls, either by co-condensation or post-synthesis grafting, has been found to improve their stability in the presence of water.[21,36,88] This has also been shown to improve the materials' structural stability and thereby their mechanical stability under compression.[37,88] Lim and Stein[33] demonstrated that a vinyl-functionalized MCM-41 sample prepared by post-synthesis grafting had greater hydrothermal stability than untreated MCM-41 when placed in boiling water for 24 h. However, the functionalized sample was still noticeably degraded in this time with a significant broadening of the pore size distribution in the range of 3-8 nm and a 49% increase in the pore volume. Application of MCM-41 in separation processes involving solution contact will require significantly longer term stability than has been exhibited by these modified samples to date, with minimal changes to the porous structure.

Kawi *et al.,*[89] reported that the mesoporous framework of MCM-41 synthesized in their lab was remarkably stabilized in boiling H_2O for one week by simply substituting structural Al into the framework or introducing nonstructural Al species onto the pore

surface of MCM-41. They found that the enhancement of the stability of MCM-41 is attributed to two major factors: the effect of randomness in the pore structure (due to structural Al species in the framework) in enhancing the thermodynamic stability of the mesostructural framework as well as the effect of the protective surface composite layer (due to the nonstructural Al-species on the pore surface) in preventing the covered surface hydroxyl groups from undergoing hydrolysis with H_2O molecules.

Jun et al.,[90] reported that the hydrothermal stability study of mesoporous silica molecular sieves MCM-48 increases if the as-synthesized materials containing surfactant are heated in an aqueous solution of salts. Although the optimum treatment conditions depended on details of the synthetic procedures, this post-synthesis technique led to a significant improvement in the hydrothermal stability of various MCM-48 materials that were synthesized using cationic surfactants alone or cationic-neutral surfactant mixtures. These results were concluded to be due to the restructuring effects of the pore walls as demonstrated by magic angle spinning ^{29}Si NMR spectroscopy, nitrogen adsorption and SEM.

Ryoo et al.,[22] reported that the hydrothermal stability of MCM-41 was improved remarkably by using various salts such as sodium chloride, potassium chloride, sodium acetate, and tetrasodium salt of EDTA during the hydrothermal crystallization process performed at 370 K. High-quality MCM-41 samples obtained by using the salt effect indicated negligible structural losses as judged by X-ray diffraction during heating for 12 h in boiling water.

Kim et al.,[91] reported on the improvement of hydrothermal stability of mesoporous silica using salt solutions. The salt effect has been reinvestigated to solve

problems of poor reproducibility. It turned out that the time-dependent effect was missing in the previous reports. The salt effect required approximately 10 days of treatment at 373 K to give its full effect. The time dependence was a critical factor for the improvement of the hydrothermal stability.

Das et al.,[92] reported that significant improvement in the hydrothermal stability of MCM-41 can be achieved by simply adding different tetraalkylammonium or sodium ions to the synthesis gel and without the necessity of multiple pH adjustment steps as mentioned by Ryoo and coworker.[22] Although the exact roles of these additional cations are still not clear, their presence seems to facilitate increased condensation of the silanol groups during the formation of the mesostructure. The highly condensed silica wall is considered to have better structural stability under hydrothermal treatment conditions.

The addition of inorganic and organic salts (sodium chloride, sodium acetate, sodium fluoride, tetraalkylammonium ions, EDTA) during the crystallization process of the pure silica material[22,90-92] and post-synthesis hydrothermal restructuring in water[93] were reported to enhance the stability in boiling water. Other effective modifications are the complete or partial hydrophobization of the surface by silylation to preclude water attack.[88] The structural stability of silica materials can be improved by increasing the wall thickness and enhancing the local ordering of the amorphous walls.[94] Such thicker-walled and more stable mesoporous silicas were prepared by using a two-step synthetic method or long crystallization times. Other reports have illustrated that incorporated or grafted Al MCM-41 and Al MCM-48 have higher mechanical and hydrothermal stabilities.[89,95,96]

2.2.1.7. Synthetic Strategies

As mentioned above, several other synthetic strategies for silica mesostructures have been successfully developed. These materials have slightly different properties than M41S materials, and these differences could lead to an enhancement of the thermal, hydrothermal, and mechanical stabilities. The framework wall thicknesses of HMS and SBA mesostructures are claimed to be consistently larger than those of MCM-41 and MCM-48.[23,97]

Alternative synthetic approaches have been reported for the preparation of mesoporous silicate from layered silicates. These materials are designated PCH[6] and FSM[5] and consist of walls that are more condensed and ordered than the walls of M41S materials.

A number of stability studies have already been carried out. The hydrothermal stability in boiling water has been tested on siliceous and Al-grafted MCM-41[89,95] and pure MCM-48.[90] Furthermore, the steam resistances of pure, Al-grafted,[95] and Al-incorporated[96] MCM-41 and pure have been investigated. In addition, O'Brien *et al.,*[40] and Hartmann *et al.,*[98] focused on the mechanical stabilities of both MCM-41 and MCM-48, whereas the thermal stabilities of MCM-41 and FSM were tested by Inagaki.[99] However, the various stability tests reported were performed under different conditions. This variation in experimental parameters makes it difficult to make a systematic comparison between the different tests on one hand and the several silica materials on the other. In addition, the reported stability experiments were performed only on M41S materials. Cassiers *et al.,*[100] reported the first systematic and comparative study of the thermal, hydrothermal, and mechanical stabilities of the most important mesoporous

materials, in particular, the molecular sieves MCM-41, MCM-48, HMS, FSM-16, PCH, and SBA-15, and it can be considered as a basis for further investigations of the stability of mesoporous materials.

2.2.2. Surfactants Removal

The conventional method of surfactant removal by calcination affects the surface area, pore size and pore volume of the M41S material. To avoid such shortcomings, several methods have been employed to extract the template molecules including solvent extraction[101,102] and supercritical fluid extraction.[103] In case of solvent extraction, a very large amount of organic solvent is required to extract the alkyltrimethylammonium templates from MCM-41 and mostly, the extraction needs to be followed by a calcination step to remove the remaining surfactant. However, recently, Antochshuk and Jaroniec[104] developed an efficient extraction procedure to remove the template from MCM-41 using trialkylchlorosilanes. The simultaneous removal of a surfactant template and attachment of trialkylsilyl groups has been successfully achieved and resulting in the synthesis of mesoporous hydrophobic materials of highly uniform pore structure. One should notice that the resulting silica is coated with silanes. The use of the supercritical fluid extraction method results in the recovery of the template and a material with improved physical properties compared to calcined MCM-41. Vansant *et al.*,[105] developed an efficient method extracting up to 90% of the surfactant from the mesoporous materials in acidified methanol. The template could be reused several times, without degradation of the surfactant or the produced MCM. Also in this case, it is shown that the extracted materials have a narrower pore size distribution and a larger average pore radius.

Although the electrostatically bound surfactant in MCM-41 can be removed by ion exchange,[8] the exchange process requires strong acid conditions, so there is little or no advantage of ion exchange over surface rehydroxylation after calcination.

The initial method for preparation of the MCMs involved high temperature calcination (typically 550-650 $^{\circ}$C) to remove the ionic template. Such a requirement precludes this method from the preparation of MCM-type materials containing organic functional groups. Recently, Tanev and Pinnavaia published details of non-ionic routes to the MCMs, in which an amine[3] or a polyethylene oxide[8] was used as a template. Such templates can be removed by extraction with hot solvents such as ethanol, and avoid the necessity of calcination.

Mercier and Brown, *et al.,*[31,106,107] used a neutral surfactant as a template to overcome the lack of hydroxyl group. The neutral surfactant could be removed by solvent extraction. The amount of surface hydroxyl group loss by this procedure was much less than that by calcination or ion exchange. Moreover, because of the absence of a framework charge, the surfactant molecules can be removed from the channels by solvent extraction and recycled. This facile removal of the surfactant optimizes the number of surface hydroxyl groups that are available on the pore walls for an organosilane functionalization.[106] As a result, repeated hydrolysis and silylation reactions were not required for this procedure.

2.3. HYDROXYL (SILANOL) GROUPS AND THEIR DETERMINATION

2.3.1. Hydroxyl Groups Identification

The surface characteristics of silica are important in the study of functionalization of the silica surface via silylation reactions. The silica surface consists of a combination

of different types of hydroxyl (*i.e.* silanol) groups and of siloxane bridges whose relative

concentrations depend on the calcination temperature as well as on the ambient humidity

and storage time. The distribution of silanols on the amorphous silica surface has been

shown to be random by simulations based on the dehydration of crystalline β-

cristobalite.[108] There are isolated and geminal silanols on the silica surface which can be

linked through hydrogen bridges depending on the distance between the silanols and the

local geometric structure.[107,109] The geminal silanols consist of two hydroxyl groups

attached to one silicon atom, while the single isolated silanols consist of one hydroxyl per

silicon atom. Hydrogen-bonded hydroxyls can be further divided into weakly and

strongly bonded hydroxyls. The weakly bonded hydroxyls are also called internal or

intraglobular hydroxyls which occur throughout the particle structure in almost all kinds

of amorphous silicas.[109] These bulk silanols are said to be inaccessible to water even

though the distinction between internal and surface silanols is ambiguous. Hydrogen-

bonded water molecules or physisorbed water may also be adsorbed onto all types of

surface hydroxyl groups.[109]

These silanol groups are often characterized by IR spectroscopy. Different types

of hydroxyl groups are seen in the OH-stretching region of the IR spectrum. Isolated (Si-

OH) and geminal (Si-$(OH)_2$) are reported at around 3740 cm^{-1} in the IR spectrum while

the broad band at 3200–3600 cm^{-1} is assigned to hydrogen-bonded silanol species.[101]

Several authors observed a shoulder of the 3740 cm^{-1} band at ≈ 3710 cm^{-1}.[41] A

distinction is therefore made between the terminal silanol groups at 3740 cm^{-1} and the

internal groups at 3710 cm^{-1}.

2.3.2. Hydroxyl Groups Determination

The amount of free silanol groups in comparable mesoporous materials can vary substantially, depending upon factors such as the use of heat, acid catalyst, aging period, and on how the material has been treated. For example, treatment with base can result in marked increase in number of the silanol groups. The number of reactive silanol groups, in turn, can be a factor in determining the capacity of the surface for chemical modification. Where the modification relies on covalent derivitization of silanol groups, the degree of modification that can be achieved might be limited by the amount of reactable silanol groups that are available for reaction.

The adsorption capacity of MCM-41 for polar molecules (*e.g.,* H_2O, methanol) at a relatively low vapor pressure is, to a large extent, related to the density of surface silanol groups (SiOH), which are also responsible for ion exchange and post-modification, such as silylation[2] and chemical deposition.[110] It is, therefore, desirable to evaluate the surface chemistry of MCM-41 type materials qualitatively and quantitatively in terms of its SiOH groups.

The hydroxyl group content of silica can be determined by several different chemical and physical methods.[109] Thermogravimetry (TG) is an example of a simple and inexpensive physical method.[111,112] The most important parameters to be considered in the thermogravimetric measurements of silica are the heating rate and the end point of the measurement. It is usually preferred to keep the former as low as possible, while having the latter high enough to ensure a total dehydroxylation of silica. It has been stated that temperatures higher than 600 °C are required to remove all intraglobular hydroxyls.[109] When heating silica samples to 1100 °C, the amount of isolated hydroxyls

diminishes considerably, but for the removal of the rest of the silanols temperatures higher than 1200 °C are required.[113] In the TG method, it is also important to find an appropriate way to distinguish between the dehydroxylation and dehydration phenomena in the thermograms. The distinction can be made with the help of differential thermogravimetry (DTG) or differential thermal analysis (DTA).[109,112] Curve fitting of the DTG profile reveals that the desorption of physisorbed water from silica surface is complete by 120 °C when heated at a rate of 10 °C min^{-1} in a 150 ml min^{-1} nitrogen flow.[109] However, according to Zhuravlev[114,115], the threshold temperature corresponding to a complete dehydration and the beginning of dehydroxylation is estimated to be 190±10 °C, so a small amount of physically adsorbed water remains on the surface up to ca. 200 °C. In addition, it has been shown by NMR techniques that drying at 110 °C not only removes the physisorbed water but dehydroxylates some of the silanol groups.[116] As a conclusion, it seems obvious that the dehydration and dehydroxylation reactions overlap to some extent.

Temperature-programmed desorption (TPD) of pyridine is another potential method for determining the distribution of energetically heterogeneous SiOH sites over silica surfaces.[117-120] The lone-pair electrons of the nitrogen atom in the pyridine ring interact strongly with surface SiOH groups through hydrogen bonding.[119] Different types of SiOH groups (free and hydrogen-bonded) exhibit different activation energies of desorption and thus can be differentiated.[101]

Solid-state ^{29}Si nuclear magnetic resonance (^{29}Si NMR) experiments employing magic-angle spinning (MAS) with or without cross polarization (CP) have been shown previously to be reliable means for quantitatively characterizing the nature of various

solid surfaces, in particular that of amorphous silica.[121-127] The fact that the CP process

discriminates against ^{29}Si nuclei far away from protons makes this technique a sensitive

method for measuring Si-OH groups. Relaxation studies in the literature[122,124,125] have

shown that the resonances of those silicons to which OH groups are directly connected,

and silicons in the attached silane groups (*e.g.,* $Si(CH_3)_3$) can be measured quantitatively.

By means of ^{29}Si CP/MAS NMR spectroscopy the isolated and hydrogen bonded silanol

species are differentiated from the geminal hydroxyl groups since the former are Q^3

species with a chemical shift of around -100 ppm whereas the latter is Q^2 seen at around -

90 ppm.[101,123] In addition, the intensities of those silicons which are used for quantitative

analysis are not affected by the presence of water molecules,[125] and therefore preparation

of a completely anhydrous sample is not a prerequisite.[101]

In the ^{29}Si NMR method, the silanol groups on the mesoporous surface are

derivatized with a substituent that can be detected by ^{29}Si NMR such as the trimethylsilyl

group. Silicon atoms in the this moiety show peaks at ~ 12 ppm. After

trimethylsilylation, a Q^3 silanol is converted to a silicon atom surrounded by four other

silicons Q^4, and thus this will show peaks at around -110 ppm. The trimethylsilyl silicon

atom concentration is equal to the silanol concentration, so the peak area relative to the

total of Q^4 silicons after silylation will present the percentage of silanol silicon atoms or

at least the percent converted.

Zhao *et al.,*[101] used trimethylchlorosilane as silylating agent to probe the surface

hydroxyl groups of MCM-41. The samples were pre-treated at different calcination

temperatures prior to silylation. Due to dehydroxylation, the amount of isolated silanol

groups increases with the temperature of calcination. Also the degree of silylation was

found to linearly increase with increasing calcination temperature prior to silylation. The

IR band at around 3738 cm^{-1} of the silylated MCM-41 samples decreased with the

increment of the pre-treatment temperature. From these observations it was concluded

that only the isolated and geminal hydroxyl groups on the surface of MCM-41 react with

the chlorosilane. However no direct observation leading to this conclusion was given.

Wouters et al.,[128] developed a new, alternative procedure to evaluate the degree of

silylation from the ^{29}Si MAS NMR spectrum. The Q^2, Q^3 and Q^4 resonances of MCM-41

are usually found at around −90 ppm, −100 ppm and −110 ppm respectively, see Table

2.1. The silicon atom of the trimethylsilyl group is seen at around 15 ppm. From the

relative peak areas of the spectra, the silanol concentration [SiOH] and the degree of

silylation [Me$_3$Si] per gram of dry MCM-41 (mol/g) can be obtained from the formula:[128]

$$[SiOH] = ((I_{Q^3} + 2 \times I_{Q^2})/(60 \times I_{Q^4} + 69 \times I_{Q^3} + 78 \times I_{Q^2}))$$

$$[Me_3Si] = ((I_{Me3Si})/(60 \times I_{Q^4} + 69 \times I_{Q^3} + 78 \times I_{Q^2}))$$
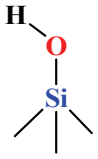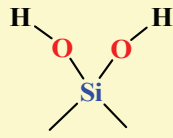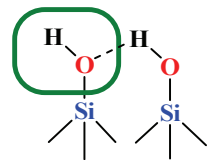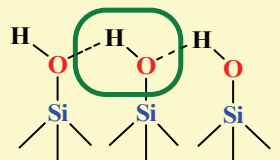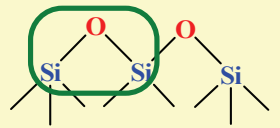
I_i represents the line intensity of the various silicon lines in the solid state ^{29}Si MAS

NMR spectrum. These formulas can be rationalized when it is assumed that each ^{29}Si

atom has an equal contribution to the intensity, which is the case when proper relaxation

occurs during the consecutive pulses. The denominator of both equations relates to the

chemical composition of the dry MCM-41 sample. The ^{29}Si MAS NMR signal areas are

therefore multiplied by the respective molecular weight of Q^4, Q^3, and Q^2. The

numerator weighs the I_i lines relative to the dry MCM-41. Note that the absolute

intensities of the Si lines are not required.[128] No external reference is needed when the

degree of silylation is determined from the ^{29}Si MAS NMR spectrum. This is in contrast

to the proton measurement.[128]

^{1}H MAS NMR is a more simple and direct way of measuring the total OH content given a known reference sample and can approximately separate the isolated and hydrogen-bonded SiOH groups.[127] ^{1}H MAS NMR is a bulk method able to detect all the OH groups in the sample.

Previously, ^{29}Si–^{1}H CP/MAS NMR spectroscopy of silylated samples was used to determine the total silanol content of MCM-41 and amorphous silica.[41] The weight gain due to silylation is required in this approach. This can be determined by elemental analysis in an additional experiment. Wouters *et al.,*[128] suggest a method that can provide both the amount of silylating agent attached to MCM-41 and the silanol content from a single measurement.

Fourier transform infrared (FT-IR) spectroscopy has been extensively used in previous studies to investigate the surface nature of MCM-41, see Table 2.1.[41,129,130] Ishikawa *et al.,*[129] recently studied the types and concentrations of SiOH groups over mesoporous silica FSM-16 (which is similar to MCM-41) using FT-IR and gravimetric methods. Both free and hydrogen-bonded SiOH groups, with O-H stretching vibration bands at around 3740 and 3600-3500 cm^{-1}, respectively, were observed and the number of SiOH groups per nm^2, α_{OH}, was determined to be 3.3. Llewellyn *et al.,*[130] reported on the interaction of water with aluminosilicate MCM-41 and concluded that the α_{OH} was 1.2. Jentys *et al.,*[41] reported that besides surface SiOH groups, inside the lattices, Si-OH groups can also be detected which gives an IR absorbance at 3715 cm^{-1}. Though widely used, FTIR cannot discriminate between single and geminal Si-OH groups and trapped water also is difficult.[101]

Table 2.1. Surface Silanol and Siloxane Types with Their 29Si CP/MAS NMR and FTIR Peak Position and Names.[113,131]

^{29}Si CP MAS NMR (Peak Position)	FTIR Spectra (Peak Position)	Assignment (Description)	Structure (Silanol and Siloxane groups)
Q^3 Single ~ -100 ppm	Free 3745±10 cm^{-1} (SiO-H) 950±10 cm^{-1} (Si-OH)	Isolated (Single)	
Q^2 Geminal ~ -90 ppm	Free 3745±10 cm^{-1} (SiO-H)	Geminal	
Q^3 Single ~ -100 ppm	Bridged (Hydrogen-bond) 3715±5 cm^{-1}	Weakly interacting vicinal	
Q^3 Single ~ -100 ppm	Bridged (Hydrogen-bond) 3520±20 cm^{-1}	Strongly interacting vicinal	
Q^3 ~ -100 ppm	Internal 3650±5 cm^{-1}	Internal silanol (Intraglobular)	---
Q^4 ~ -110 ppm	1000-1100 cm^{-1} (stretching) 525±10 and 460±10 cm^{-1} (bending)	Siloxane (–Si–O–Si–)	

Ultraviolet spectroscopy (UV) is one of the methods that have been used to determine the number of reactive hydroxyl (silanol) groups on the silica surface. In this method a titration reagent binds substantially to reactive silanol groups on the silica

surface through an ionic interaction in a manner that is essentially stoichiometric, and the known binding stoichiometry between the titration reagent and reactable silanol groups is used to calculate the concentration of reactable silanol groups on the silica surface. It is sometimes desirable to use a titration reagent for which the binding stoichiometry between the titration reagent and the reactable silanol groups is known, *e.g.,* a binding stoichiometry of 1:1. In order to achieve a 1:1 binding stoichiometry, the reagent radius should not be larger than the midpoint spacing between the silanol groups.

Methodology can be used to determine the effectiveness of a procedure used to modify a silica surface. For example, the number of free silanol groups in a material can be determined before and after chemical modification, and the difference used as a measure of the extent of reaction. Alternatively, the number of free silanol groups can be determined prior to modification, and then the extent of modification determined by measuring the presence of the functional group that was introduced. For example, if the modifying group includes a thiol moiety, the extent of modification can be determined by assaying for thiol content, *e.g.,* by reaction with 5,5'-Dithio-bis(2-nitrobenzoic acid) and spectrophometric quantification of the colored product. In this way, one can determine any correlation between the number of reactive silanol groups and extent of modification.

The term "reactive silanol groups" refers to silanol groups that are on the silica surface and positioned in a manner such that they are available for chemical reaction. Silanol groups that are not reactive are not detected by this method, and are in most instances are not relevant since they will not participate in reactions with modifying groups or otherwise affect the chemistry at the silica surface.

The titration reagent can be any molecule that is capable of quantitatively binding to reactable silanol groups on a silica surface. Preferably, it is a molecule that is small enough that it's binding to a silanol group will not shield adjacent silanol groups on the surface from interacting with the titration reagent. That is, the titration reagent should be small enough such that its binding to a reactive silanol group does not substantially block any other reactive silanol group on the surface from reaction with another molecule of the titration reagent. Of course, depending upon the steric properties of the molecule, *e.g.,* it's 3-dimensional structure, in some cases larger molecules will function effectively.

In addition, it is preferable that the titration reagent include a group that enables detection and quantification of the titration reagent. Cyclohexylamine is a relatively small molecule that can be detected by UV spectroscopy since it absorbs strongly at 226 nm. Furthermore, the molecule reacts specifically with the silanol group under appropriate conditions, *e.g.,* in the presence of cyclohexane.

In general, a wide variety of titration reagents can be used. Some preferred examples include cations, which bind to reactive silanol groups through an ionic interaction. Examples are amines that are protonated (positively charged) by silanol groups to give ammonium cations. The amine can be primary, secondary, tertiary or quaternary amines, including alkyl quaternary amines.

When an amine or other cationic titration reagent is used, the molecule should include at least one R group that is detectable. For example, this group can be an aromatic ring, *e.g.,* a benzene derivative such as aniline or pyridine, or a detectable functional group having conjugated double bonds capable of fluorescence, *e.g.,* anthracene, phenanthrene, naphthalene, *etc*.

The silanol titration solution uses titration reagent and a solvent in which the reagent is soluble, and in which the reagent binds quantitatively to reactive silanol groups. Typically, the binding should be electrostatic as opposed to covalent binding, and the solvent should be chosen accordingly. Thus, where the titration reagent is charged and the interaction electrostatic, the polarity of the solvent should be such that it promotes electrostatic interaction, *e.g.,* of low to medium polarity. Electrostatic interactions are enhanced by reduced polarity of the solvent, and reduced when the solvent is highly polar and/or contains salt or other charged constituents. For example, this can be achieved with benzenetriethylamine by using a low molecular weight alcohol such as methanol as the solvent. Other solvents of similar polarity could also be used provided the titration reagent is sufficiently soluble in the solvent. In some embodiments an aqueous solvent is used with an organic solvent wash. Regardless, the solvent must support the ionic state of the silanol and the titration reagent.

Detection can be achieved by any of a number of techniques. As exemplified in the examples, one can use a titration reagent with a detectable group that absorbs UV radiation. Other modes of detection could also be used, such as visible, atomic absorption, atomic emission, flame emission detection, fluorescence or mass spectrometry. The reagent may detect directly or a detection agent such as a color forming reagent may be added to make the displacement reagent detectable.

The amount of bound titration reagent is determined by detecting the reagent in a manner that allows for its quantification. For example, if the titration reagent is detected by absorbance, the absorbance can be used to quantify the amount of titration reagent using Beer's Law, which states that there is a linear relationship between absorbance and

concentration. Thus, concentration of reagent can be determined using the absorbance coefficient, if that is known. Alternatively, a standard of known concentration can be prepared, and the absorbance of bound titration reagent determined by comparison with the standard. The standard and sample should be tested at a concentration wherein the relationship between absorbance and concentration is linear.

Most of the silica used in chemical applications is synthetic and is generally amorphous. Depending on the method and specific parameters of preparation, certain physical properties such as surface area, pore volume, pore size and particle size are to some extent controllable. The number, size and morphology of the pores largely influence the water desorption.[109] The ratio between the quantities of surface and bulk OH groups depends on the pretreatment of the sample and on the size of the silica globules.[132] According to Zhuravlev's data[133] on over 100 different silica samples, the silanol number of totally hydroxylated silica is between 4.2 and 5.7 OH groups/nm^2 regardless of the origin and structural characteristics of silica. Zhuravlev's measurements were performed using a deuterium-exchange method with mass spectrometric analysis which is able to distinguish between the surface and bulk hydroxyls.[114,133] Recently, De Farias and Airoldi[111] showed the TGA method to be a satisfactory way to determine the hydroxyl group content of silica samples having different surface areas. They heated the silica samples at a rate of 5 °C min^{-1} to 1100 °C and calculated the remaining silanol groups attached to silica gel at 1100 °C. The silanol numbers in their samples, which were untreated or were rehydroxylated by acid treatments, ranged from 4.3 to 6.7 OH groups/nm^2.[111] The silanol numbers determined by the TGA method are larger

99

than the ones determined by deuterium-exchange, because both surface and bulk hydroxyls are included.

2.4. RESEARCH GOALS

Based on the literature, the intention of this investigate was to synthesize mesoporous materials based on MCM-41 in both acidic and basic systems using hydrochloric acid to adjust the pH of the reaction in the acidic system and using aqueous ammonia in the basic system. Tetraethylorthosilicate (TEOS) was used as the silica source. In addition, different surfactants were explored including anionic, cationic and neutral ones. The surfactant/silica mole ratio was adjusted in order to optimize the properties of the product. The effect of different organic additives used such as 1,3,5-trimethylbenzene and decane were also explored. Temperature and aging time were varied from 25 to 100 $^{\circ}$C and from 1 to 14 days, respectively.

A simple method for quantification of the hydroxyl group content in an unknown silica sample was also developed. For this, the OH groups content of a series of different types of mesoporous silicas were measured by the adsorption of a proper probe molecule such as cyclohexylamine or proton-sponge. The results were compared those from solid state ^{29}Si NMR which served as a reliable reference method.

Previously, the fact that various stability tests were performed under different conditions and that each different synthesis of the same material corresponds a different structure with its own properties such as stability and nature of surface makes it difficult to systematically compare the different tests on one hand, and the several silica materials on the other hand. Therefore, in this study, focus was placed on the thermal,

hydrothermal and mechanical stability of the most important mesoporous materials, in particular the mesoporous molecular sieves designated OSU-6 below.

2.5. EXPERIMENTAL

2.5.1. Materials

The chemicals used in this part of the thesis are as follow: tetraethylorthosilicate [$(Si(OCH_2CH_3)_4)$ 98.0%, Aldrich] and tetramethylorthosilicate [$(Si(OCH_3)_4)$ 98.0%, Aldrich] as silica sources. Cetyltrimethylammonium bromide [$(CH_3(CH_2)_{15}N(CH_3)_3Br)$ 98.0%, Aldrich], n-Hexadecylsulfuric acid, sodium salt [$(CH_3(CH_2)_{15}OSO_3^-Na^+)$, contains *ca.* 40% Sodium Stearylsulfate, TCI America], and 1-hexadecylamine [$(CH_3(CH_2)_{15}NH_2)$ 90.0%, Aldrich] were the templates (surfactants). 1,3,5-trimethylbenzene [(mesitylene, (C_9H_{12})) 98.0%, TCI] and dodecane [$(C_{12}H_{26})$ 99.0%, Aldrich] were the organic additives. Cyclohexylamine [$(C_6H_{13}N)$ 99%, Aldrich] and proton-sponge [1,8-bis(dimethylamino)naphthalene $(C_{14}H_{18}N_2)$, Aldrich] were the probe molecules for hydroxyl group determination. Absolute ethyl alcohol [(C_2H_6O) 99.5% A.C.S. reagent, Pharmco, USA], isopropyl alcohol [(C_3H_8O) 99.8% HPLC-UV Grade, Pharmco, USA], hydrochloric acid (HCl), and distilled water were used as solvents. All chemicals were purchased and used without further purification. Structures of some starting materials are shown in Scheme 2.1.
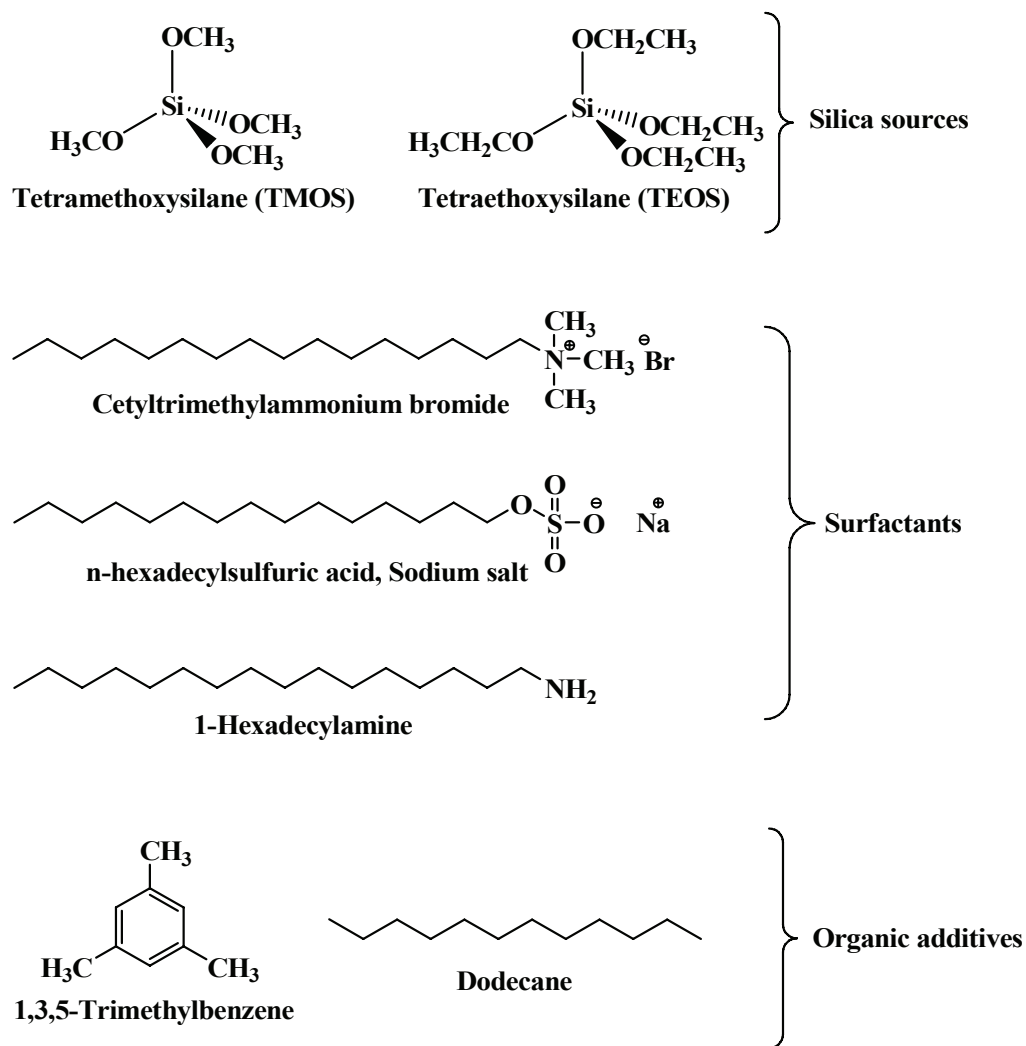
Scheme 2.1. Structures of some starting materials that are used in this research

2.5.2. Synthesis Methods

Mesoporous molecular sieves with the MCM-41 structure were synthesized using a variety of methods in order to find the best approach for obtaining high quality samples. The factors affecting synthesis of mesoporous materials based on MCM-41 such as silica sources, organic surfactants (templates), silica/surfactant ratios, additives, solvents,

temperatures, pH values, aging time, drying process, and template removal were varied for different synthetic methods as described in the literature.[84]

2.5.2.1. Synthesis of Mesoporous Material (OSU-1) Using Neutral Surfactant

The mesoporous material OSU-1 was synthesized as described below following the reported literature procedure by Tuel *et al.,*[135] with some alteration. This synthesis method involves preparation and mixing of two mixtures. The first solution is prepared by dissolving 7.23g (0.03 mol) of the neutral surfactant 1-hexadecylamine (HDA) in 65 ml (3.6 mol) of distilled H_2O at room temperature in a 250-ml Erlenmeyer flask, sonicated for a few minutes and left under magnetic stirring for one hour until a white homogenous suspension formed. At the same time, a second solution is prepared that consists of 19.5g (0.1 mol, $d = 0.934$ g/cm^3) of the silica source, tetraethylorthosilicate (TEOS), 28 ml (0.6 mol) of ethanol (EtOH) and 6 ml (0.1 mol) of isopropanol (Iso-PrOH) mixed together in a 250-ml closed Erlenmeyer flask under magnetic stirring at room temperature for about 30 minutes. The two solutions were then mixed at room temperature under stirring for about 30 minutes in a 250-ml closed Erlenmeyer flask. After 5 minutes of stirring of this mixture, 4 ml of the auxiliary organic mesitylene was added as the last ingredient. This amount of the mesitylene corresponded to 1:1 ratio with the surfactant. After that, the stirring was stopped and the reaction was left to age for 14 days at room temperature under static conditions. The gel compositions were SiO_2: 6 EtOH: Iso-PrOH: 0.3 HDA: 36 H_2O: 0.3 MES. The resulting white solid was recovered by centrifugation, and washed with distilled water and ethanol (three times) in order to remove all the residual surfactant and additives using a fine sintered-glass filter

funnel. Then, the synthesized mesoporous material was dried at room temperature under vacuum for around 48 hours. The yield was 24.61g (~ 92%).

The IR absorptions in cm^{-1} (KBr) are 3359(w), 3301(w), 2920(s, sh), 2850(s, sh), 1597(m), 1467(m, sh), 1377(w), 1236(s, br), 1062(s, br), 958(m), and 795(m) cm^{-1}. Solid-state ^{29}Si CPMAS NMR δ (ppm) are -91.2(Q^2), -100.6(Q^3) and -109.8(Q^4).

The resulting material was given the designation OSU-1. The organic template was removed using both the calcination and HCl-ethanol extraction methods. A small amount (1.0g) of the obtained synthesized sample, OSU-1, was taken and washed five times with a hot solution of HCl-ethanol in order to remove the surfactant (HDA) and the mesitylene. After washing, the material was dried under vacuum, and then characterized. This material was labeled OSU-1-W where W indicates HCl-ethanol washing. IR (cm^{-1}, KBr) are 3746(vs, sh), 3533(m, br), 1863(w), 1692(w), 1642(w), 1213(s, br), 1027(s, br), 962(m), and 812(m). Solid-state ^{29}Si CP/MAS NMR δ (ppm) are -91.4(Q^2), -101.5(Q^3), and -109.4(Q^4).

Another part of the synthesized sample, OSU-1 material, was taken and calcined by heating in a programmed furnace at 550 ^{0}C (according to the TGA result) in air for 12 hours at rate of 2 ^{o}C/min in order to remove the organic species. After cooling to room temperature, the calcined sample was characterized and was designated OSU-1-C where C indicates calcination. IR (cm^{-1}, KBr) are 3743(m, sh), 3635(w, br), 3541(w, br), 1627(w), 1062(s, br), 976(m), and 808(m). Solid-state ^{29}Si CP/MAS NMR δ (ppm) are -100.4(Q^3) and -110.6(Q^4).

2.5.2.2. Synthesis of Mesoporous Silica OSU-2 Using Neutral Surfactant

The mesoporous material OSU-2 was synthesized following the same preparation method used for the synthesis of the mesoporous silica OSU-1 with changing of the organic additive. First, a mixture was prepared by dissolving 7.23 g (0.03 mol) of the neutral surfactant 1-hexadecylamine (HDA) in 65 ml (3.6 mol) of distilled H_2O at room temperature in a 250-ml Erlenmeyer flask, sonicated for a few minutes and left under magnetic stirring for one hour until a white homogenous suspension formed. At the same time, a second solution was prepared by mixing 19.5 g (0.1 mol, $d = 0.934$ g/cm^3) of the silica source, tetraethylorthosilicate, 28 ml (0.6 mol) of ethanol and 6 ml (0.1 mol) of isopropanol together in a 250-ml closed Erlenmeyer flask under magnetic stirring at room temperature for about 30 minutes. The two solutions were then mixed at room temperature under stirring for about 30 minutes in a 250-ml closed Erlenmeyer flask. After roughly five minutes, 5.0g (0.03 mol) of the auxiliary organic dodecane was added to the stirred mixture. After that, the stirring was stopped and the reaction was left to age for 14 days at room temperature under static conditions in the closed Erlenmeyer flask. The gel composition was SiO_2: 6 EtOH: Iso-PrOH: 0.3 HDA: 36 H_2O: 0.3 Dodecane. The resulting white solid was recovered by filtration and washed with distilled water and ethanol (three times) in order to remove all the residual surfactant and additive. Then, the synthesized mesoporous material was dried at room temperature under vacuum for around 48 hours. The yield of this material, identified as OSU-2, was 24.85g (~ 93%).

The FT-IR absorptions (cm^{-1}, KBr) are 3359(w), 3293(w), 2918(s, sh), 2850(s, sh), 1593(w), 1467(m, sh), 1378(w), 1232(s, br), 1072(s, br), 966(m) and 794(m). Solid-state ^{29}Si CP/MAS NMR δ (ppm) are -108.9(Q^4), -100.2(Q^3), and -89.5(Q^2).

The organic template was removed using both calcination and HCl-ethanol extraction methods. A small amount (1.0g) of OSU-2 was taken and washed five times with a hot solution of HCl-ethanol in order to remove the surfactant and dodecane to give the material OSU-2-W. IR (cm^{-1}, KBr) are 3743(vs, sh), 3530(m, br), 1234(s, br), 1053(s, br), 978(m), and 806(m). Solid-state ^{29}Si CP/MAS NMR δ (ppm) are -109.8(Q^4), -100.4(Q^3), and -91.1(Q^2).

Another sample of the OSU-2 silica was taken and calcined by heating in a programmed furnace at 550 ^{0}C in air for 12 hours at rate of 2 ^{o}C/min in order to remove the organic components. After cooling to room temperature, the calcined sample was characterized and was designated OSU-2-C (C; calcination). IR (cm^{-1}, KBr) are 3739(m, sh), 3635(w, br), 3541(w, br), 1060(s, br), 946(m), and 807(m). Solid-state ^{29}Si CP/MAS NMR δ (ppm) are -110.4(Q^4), -100.8(Q^3).

2.5.2.3. Synthesis of Mesoporous Material Using Cationic Surfactant (OSU-3)

The mesoporous material OSU-3 was synthesized as described below. An amount of 11 g (0.03 mol) of the cationic surfactant cetyltrimethylammonium bromide (CTAB) in 65 ml (3.6 mol) of distilled H$_2$O at room temperature in a 250-ml Erlenmeyer flask, was sonicated for a few minutes and left under magnetic stirring for one hour until a white homogenous suspension formed. At the same time, a second solution was prepared that consisted of 19.5 g (0.1 mol, d = 0.934 g/cm^3) of tetraethylorthosilicate, 28 ml (0.6 mol) of ethanol (EtOH) and 6.0 ml (0.1 mol) of isopropanol (Iso-PrOH) mixed together in a 250-ml closed Erlenmeyer flask under magnetic stirring at room temperature for about 30 minutes. The two solutions were then mixed at room temperature under stirring for about 30 minutes in a 250-ml closed Erlenmeyer flask. 4.0 ml (0.03 mol) of

the auxiliary organic mesitylene was added after 5 minuets of stirring. After that, the stirring was stopped and the reaction was left to age for 14 days at room temperature under static conditions in the closed Erlenmeyer flask. The gel composition was SiO_2: 6 EtOH: Iso-PrOH: 0.3 CTAB: 36 H_2O: 0.3 MES. The resulting white solid was filtered off and washed with distilled water and ethanol (three times) in order to remove all the residual surfactant and additive. Then, the product was dried at room temperature under vacuum for around 48 hours to give 28.5g (~ 93.5%) of OSU-3 silica. The IR absorptions (cm^{-1}, KBr) are 3458(m), 2918(s, sh), 2850(s, sh), 1467(m, sh), 1377(w, sh), 1238(s, br), 1063(s, br), 958(m), 798(m), and 721(m, sh). Solid-state ^{29}Si CP/MAS NMR δ (ppm) are -109.1(Q^4), -100.5(Q^3), and -88.9(Q^2).

The organic template was removed using both the calcination and HCl-ethyl alcohol extraction methods. A small amount (1.0g) of the OSU-3 was washed five times with a hot solution of HCl-ethanol in order to remove the surfactant and mesitylene. The OSU-3-W silica thus obtained. IR (cm^{-1}, KBr) are 3741(vs, sh), 3526(m, br), 1025(s, br), 954(m), and 799(m). Solid-state ^{29}Si CP/MAS NMR δ (ppm) are -109.1(Q^4), -101.4(Q^3), and -91.8(Q^2).

Another sample of the OSU-3 material was converted to OSU-3-C by calcining at 550 $^{\circ}$C in air for 12 hours to remove the organic species. IR (cm^{-1}, KBr) are 3738(m, sh), 3628(w, br), 3538(w, br), 1060(s, br), 964(m), and 791(m). Solid-state ^{29}Si CP/MAS NMR δ (ppm) are -110.6(Q^4), and -101.1(Q^3).

2.5.2.4. Synthesis of Mesoporous Material Using Anionic Surfactant (OSU-4)

The mesoporous material OSU-4 was synthesized as described below. First, the surfactant suspension was prepared by dissolving 10 g (0.03 mol) of the anionic

surfactant n-Hexadecylsulfuric acid, sodium salt (HDSA) in 65 ml (3.6 mol) of distilled H_2O at room temperature in a 250-ml Erlenmeyer flask, sonicating for a few minutes then magnetically stirred for one hour until a white homogenous suspension formed. At the same time, a second solution was prepared by mixing 19.5 g (0.1 mol) of tetraethylorthosilicate, 28 ml (0.6 mol) of ethanol and 6 ml (0.1 mol) of isopropanol together in a 250-ml closed Erlenmeyer flask under magnetic stirring at room temperature for about 30 minutes. The two solutions were then mixed at room temperature under stirring for about 30 minutes in a 250-ml closed Erlenmeyer flask. After five minutes, 4 ml (0.03 mol) of the auxiliary organic mesitylene was added to the stirred reaction mixture. After that, the stirring was stopped and the reaction mixture was left to age for 14 days at room temperature in a closed Erlenmeyer flask. The gel composition was SiO_2: 6 EtOH: Iso-PrOH: 0.3 HDSA: 36 H_2O: 0.3 MES. The resulting white solid was recovered by filtration and washed with distilled water and ethanol (three times) in order to remove all the residual surfactant and additives. Then, the synthesized mesoporous material was dried at room temperature under vacuum for around 48 hours. The yield of OSU-4 was 27.9 g (~ 94.6%). The IR absorptions (cm^{-1}, KBr) are 3347(m), 2926(s, sh), 2850(s, sh), 1466(m, sh), 1449(m), 1370(w), 1243(s, br), 1103(s, br), 1063(s, br), 977(m) and 802(m). Solid-state ^{29}Si CP/MAS NMR are δ (ppm) -109.4(Q^4), -100.4(Q^3), and -91.1(Q^2).

The organic template was removed using both calcination and HCl-ethanol extraction methods. 1.0g of OSU-4 was washed five times with hot solution of HCl-ethanol in order to remove the surfactant and the additive. This gave the material that was designated OSU-4-W (W; HCl-ethanol washing). IR (cm^{-1}, KBr) are 3740(vs, sh),

3529(m, br), 1037(s, br), 960(m), and 809(m). Solid-state ^{29}Si CP/MAS NMR δ (ppm) are -109.7(Q^4), -99.9(Q^3), and -91.6(Q^2).

Another portion of the OSU-4 material was calcined at 550 ^{o}C in air for 12 hours in order to remove the organic components and produce the silica that was labeled OSU-4-C (C; calcination). IR (cm^{-1}, KBr) are 3739(m, sh), 3531(w, br), 1059(s, br), 966(m), and 811(m). Solid-state ^{29}Si CP/MAS NMR δ (ppm) are -110.2(Q^4) and -101.1(Q^3).

2.5.2.5. Synthesis of Mesoporous Material Using Neutral Surfactant (OSU-5)

The mesoporous material OSU-5 was synthesized as described below following the same preparation method mentioned above in the synthesis of the mesoporous material OSU-1 with some modification in the molar ratio of the reactants, adding of organic additive, and use of catalyst. This synthesis method involves preparation and mixing of two mixtures. The first solution was prepared by dissolving 16.0 g (0.067 mol) of the surfactant 1-hexadecylamine (HDA) in 65 ml (3.6 mol) of distilled H_2O at room temperature in a 250-ml Erlenmeyer flask, sonicating for a few minutes and then stirring for one hour until a white homogenous suspension had formed. An amount of 1.0 M of HCl was added to the first mixture as a catalyst and until the pH of the mixture was around 4.5. At the same time, a second solution was prepared by mixing 32.0 g (0.15 mol) of tetraethylorthosilicate, 28 ml (0.6 mol) of ethanol and 6 ml (0.1 mol) of isopropanol in a 250-ml closed Erlenmeyer flask by magnetic stirring at room temperature for about 30 minutes. The two solutions were then mixed at room temperature and were stirred for about 30 minutes in a 500-ml closed Erlenmeyer flask. After five minutes, 11.0 g (0.067 mol) of the auxiliary organic dodecane was added to the stirred mixture. After that, the stirring was stopped, 100 ml of distilled water was added

109

to the mixture, the flask was swirled to mix, and then the reaction was left to age for 14 days at 25 $^\circ$C under static conditions.

The resulting gel composition was SiO_2: 4 EtOH: 0.67 Iso-PrOH: 0.45 HDA: 29.5 H_2O: 0.45 Dodecane. The resulting solid was recovered by filtration, washed with distilled water and ethanol (three times) using a fine sintered-glass filter funnel. Then, the synthesized mesoporous material was dried at room temperature under vacuum for 48 hours. Finally, the product was weighed and characterized. The yield of OSU-5 was 46.5 g (~ 97%). IR (cm^{-1}, KBr) are 3356(w), 3305(w), 2923(s, sh), 2853(s, sh), 1597(m), 1467(m, sh), 1376(w), 1226(s, br), 1080(s, br), 964(m) and 795(m). Solid-state ^{29}Si CP/MAS NMR δ (ppm) are -108.6(Q^4), -100.4(Q^3), and -90.5(Q^2).

The organic template was removed using both calcination and HCl-ethanol extraction methods. A small sample (1.0 g) of OSU-5 was washed five times with hot solution of HCl-ethanol to produce OSU-5-W silica. IR (cm^{-1}, KBr) are 3746(vs, sh), 3564(m, br), 1628(w), 1090(s, br), 977(m), and 805(m). Solid-state ^{29}Si CP/MAS NMR δ (ppm) are -109.2(Q^4), -100.6(Q^3), and -91.4(Q^2).

Another sample of OSU-5 material was calcined at 550 $^\circ$C in air for 12 hours. After cooling to room temperature, the calcined sample was characterized and labeled OSU-5-C. IR (cm^{-1}, KBr) are 3745(m, sh), 3635(w, br), 3533(w, br), 1213(s, br), 1061(s, br), 981(m), and 808(m). Solid-state ^{29}Si CP/MAS NMR δ (ppm) are -110.6(Q^4), and -101.2(Q^3).

2.5.2.6. Synthesis of Mesoporous Material Using Neutral Surfactant (OSU-6)

The mesoporous material, OSU-6, was formed using neutral primary amine micelles and neutral inorganic species via hydrogen-bond interactions at room

temperature under acidic conditions. The neutral surfactant used here is the organic

primary amine, 1-hexadecylamine (HDA). The procedure for the synthesis is described

below and followed the same procedure as that for OSU-1 with some alteration in the

mole ratio of the reactants, adding of organic additive, and use of catalyst. The first

solution was prepared by dissolving 16.0 g (0.067 mol) of the surfactant 1-

hexadecylamine (HDA) in 65 ml (3.6 mol) of distilled H_2O at room temperature in a 250-

ml Erlenmeyer flask, sonicating for a few minutes and magnetically stirring for one hour

until a white homogenous suspension formed. 1.0 M of HCl was added to the first

mixture until the pH of the mixture was approximately 4.5. At the same time, a second

solution was prepared by mixing 32.0 g (0.15 mol) of tetraethylorthosilicate, 28 ml (0.6

mol) of ethanol and 6 ml (0.1 mol) of isopropanol in a 250-ml closed Erlenmeyer flask

under magnetic stirring at room temperature for about 30 minutes. The two solutions

were then mixed at room temperature with stirring for about 30 minutes in a 500-ml

closed Erlenmeyer flask. 9.0 ml of the auxiliary organic mesitylene was added to the

stirred reaction mixture after five minutes. After that, the stirring was stopped and 100

ml of distilled water was added to the mixture, the mixture was swirled to mix, and was

then left to age for 14 days at 25 ^{o}C under static conditions.

The gel composition was SiO_2: 4 EtOH: 0.67 Iso-PrOH: 0.45 HDA: 29.5 H_2O:

0.45 MES. The resulting solid was recovered by filtration, washed with distilled water

and ethanol (three times) using a fine filter funnel. Then, the synthesized mesoporous

material was dried at room temperature under vacuum for 48 hours. The yield of OSU-6

was 44.85 g ($\sim$ 93.5%). IR (cm^{-1}, KBr) are 3734(w), 3291(s, br), 2926(s, sh), 2855(s, sh),

1624(w), 1588(m), 1489(m), 1465(m, sh), 1378(w), 1192(s, br), 1074(s, br), 949(s),

807(s), 682(w), and 562(m). Solid-state ^{29}Si CP/MAS NMR δ (ppm) are -110.7(Q^4), -100.9(Q^3), and -91.6(Q^2).

The organic template was removed using both the calcination and HCl-ethyl alcohol extraction methods. 1.0 g of OSU-6 was washed five times with a hot solution of HCl-ethanol in order to remove the organic components. The product after washing was characterized and designated OSU-6-W. IR (cm^{-1}, KBr) are 3746(vs, sh), 3548(m, br), 1633(w), 1206(s, br), 1031(s, br), 976(m), 813(m), and 704(w). Solid-state ^{29}Si CP/MAS NMR δ (ppm) are -109.7(Q^4), -101.4(Q^3), and -90.3(Q^2).

Another sample of OSU-6 material was calcined at 550 $^{\circ}$C in air for 12 hours to remove the organic species. After cooling to room temperature, the calcined sample was characterized and is referred to as OSU-6-C. IR (cm^{-1}, KBr) are 3744(m, sh), 3635(w, br), 3508(w, br), 1625(w), 1201(s, br), 1057(s, br), 975(m), and 805(m). Solid-state ^{29}Si CP/MAS NMR δ (ppm) are -109.5(Q^4), and -101.6(Q^3).

2.5.3. Removal of Organic "Templates" from As-Synthesized Mesoporous Materials

The organic "template" molecules were removed by contacting the synthesized mesoporous samples three to five times with a 1.0 *M* HCl solution in ethanol at 70 °C for about one hour or with a 1.0 *M* HCl solution in diethyl ether at 25 °C. The solid-to-liquid ratio was 100 ml/g.[84] The second method was to calcine the mesoporous materials at the temperature required for complete removed of the organics as referred by TGA analysis.[1,2] Each method has different advantages and disadvantages. For example, the calcination method will lead to highly condensed mesoporous materials that unfortunately have low hydroxyl group concentration on the surface. The washing

method provides higher hydroxyl group concentration but decreased degree of condensation.

Notably, if the main objective of the synthesis of these materials is to modify them with functional groups, then the first method, extraction with HCl/ethanol, will be recommended in order to maximize the number of available surface silanol groups in purely siliceous mesoporous materials. The alternative surfactant removal methods, calcination and heating/washing, lead to condensation of silanol groups, resulting in fewer anchoring sites.

2.6. CHARACTERIZATION OF THE AS-SYNTHESIZED MESOPOROUS MATERIALS

There are a wide variety of techniques available for the characterization of mesoporous silicas. In general, they can be divided into two distinct areas; (i) characterization of the physical structure, (ii) chemical characterization. Thus, through the combination of several techniques, an accurate picture of the mesoporous silicas can be obtained. In this section a range of the most commonly used techniques will be discussed briefly.

The mesoporous materials were characterized using a variety of techniques. The X-ray powder diffraction (XRD) patterns were obtained on a Bruker AXS D-8 Advance diffractometer using Cu K radiation ($\lambda = 0.154056$ nm) at 40 kV and 30 mA within the 2θ range of 1.2 to 10. The samples were prepared as a thin, flat layer in a plastic holder. The main index peak (100) of MCM-41 appears at around 2 degrees (2θ), and the other index peaks (110) and (200) are at around 3 and 5 degrees (2θ), respectively. Data were

collected with the resolution of 0.02° with step time of 8.2 sec. at 25 $^{\circ}$C. The interplanar

spacing (d, nm) was calculated using Bragg's equation of the formula:

$$d_{100} = \lambda / 2 \cdot \text{Sin } \theta$$

where d_{100} is the interplanar distance (nm), λ is a wavelength of Cu K_{α} radiation and θ is

the position of the first low-angle peak (degrees). By using the main index peak position,

the pore size of MCM-41 can be calculated by the following equations:

$$d_{100} = \lambda / 2 \cdot \text{Sin } \theta_{100}$$

$$a = 2 \ (\sqrt{3}) \ d_{100} - 1(\text{nm}) \text{ or } a = 2 \ d_{100} / (\sqrt{3})$$

where a is the pore size in nanometers (nm). The wall thickness can be calculated by

determining the difference between the lattice parameter determined by X-ray diffraction

and the pore size obtained by nitrogen adsorption analysis.

The diffuse reflectance infrared Fourier transform (DRIFT) spectra were recorded

on a Nicolet Magna 750 FTIR. The spectra were collected for all samples in the range

from 400 to 4000 cm^{-1}. The samples were ground powders diluted with potassium

bromide in an approximate ratio of 1:4.

Thermogravimetric analyses (TGA) were performed on a Seiko ExSTAR 6200

TG/DTA instrument using between 2 mg and 30 mg samples and a flow of dry air of 100

ml/min. The temperature was ramped from 25 $^{\circ}$C to ~ 800 $^{\circ}$C at a rate of 2 $^{\circ}$C/min. Bulk

pyrolyses at different temperatures were executed in ambient air in a temperature-

programmable muffle furnace employing a temperature ramp of 2 $^{\circ}$C/min.

Textural properties (surface areas, pore sizes, pore volumes, and pore size

distribution) were determined at -196 °C using Brunauer-Emmett-Teller (BET)[139,140]

multilayer nitrogen adsorption method in a conventional volumetric technique by a

Quantachrome Nova 1200 instrument and Quantachrome Autosorb-3B automated gas adsorption system. All samples were degassed for 16 h at 100-150 $^{\circ}$C prior to adsorption. This temperature range was chosen from the TGA data in order to avoid the degradation of the immobilized surface groups or templating organic molecules while at the same time removing adsorbed gases and water. The surface area was calculated using the BET six-point surface area measurement method based on adsorption data in the partial pressure (P/P_o) range 0.05 to 0.3 and the pore volume was determined from the amount of N_2 adsorbed at $P/P_o = ca.$ 0.99. The calculation of pore size was performed using the Barrett-Joyner-Halenda (BJH) method applied to the adsorption data of the N_2 sorption isotherms.[139,140]

A JEOL JXM 6400 Scanning Electron Microscope (SEM) equipped with an Evex Analytical Imaging System was used to study the morphology, shape, and size of the particles of the synthesized mesoporous materials. The SEM was operated at accelerating voltages between 10 kV to 25 kV and working distances from 8 to 48 mm. The magnification range from 100x to 30000x. Samples were mounted using a conductive carbon double sided sticky tape (Scotch brand) on an aluminum stub. A thin (*ca.* 10 nm) coating of gold/palladium was deposited onto the samples in order to reduce the effects of charging, using a Balzers MED 010 sputter coater.

A JEOL JEM 100 CX II Transmission Electron Microscope (TEM) was used to study the shape, and size of the pores of the mesoporous materials. The TEM was operated at a voltage of 80 kV with a modified specimen stage with objective lens parameters C_s (spherical aberration coefficient) = 0.41 mm and C_c (chromatic aberration coefficient) = 0.95 mm, giving an interpretable point resolution of *ca.* 0.185 nm.

Samples for analysis were prepared by placing a small amount of the mesoporous

material samples into a Beam capsule. Each capsule was then filled top with Polybed

812 resin and polymerized at 60 $^{\circ}$C for 48 hours in a polymerization oven. The blocks

were sectioned in thin sections of about 70 nm thickness using a Sorvall MT 5000

Ultramicrotome with a Diatome diamond knife. The sections were taken and placed on

150 mesh Formvar-coated nickel grids. The images were recorded at magnifications

ranging from 58000X to 190000X.

Solid-state ^{29}Si nuclear magnetic resonance (NMR) spectra were recorded on a

Chemagnetics CMX-II solid-state NMR spectrometer operating at resonance frequencies

of 59.79 MHz for ^{29}Si nucleus. Several signals are typically observed in the ^{29}Si NMR

spectra which correspond to silicon atoms in different chemical environments. ^{29}Si

CP/MAS NMR spectra of silicate show distinct resonances for siloxane [Q^n =

Si(OSi)$_n$(OH)$_{4-n}$, n = 2–4] and organosiloxane [T^m = RSi(OSi)$_m$(OH)$_{3-m}$, m = 1–3]

centers, such as siloxane Q^4 [($\equiv$Si-O-)$_4$Si*] (*ca.* -110 ppm), single silanol Q^3 [($\equiv$Si-O-

)$_3$Si*-OH] (*ca.* -100 ppm), geminal silanol Q^2 [($\equiv$Si-O-)$_2$Si*(-OH)$_2$] (*ca.* -90 ppm) or

silicon from attached alkylsilane ligands – M [($\equiv$Si-O-)Si*(R)R$^{'}_2$]. The single pulse ^{29}Si

NMR experiment is equally sensitive to all silicon atoms and can provide information

about the ratio between siloxane (Q^4) and silanol (Q^3) groups in different samples.

Measurements were performed at room temperature with a Chemagnetics CMX-II solid-

state NMR spectrometer 5 mm double resonance magic-angle spinning probe and the

chemical shifts are given in ppm from external tetramethylsilane. The ^{29}Si cross-

polarization/magnetic-angle spinning (CP/MAS) experiments were 1000-2000. The ^{29}Si

CP/MAS spectra were acquired in a 5.0 mm zirconia rotor spinning at 6 kHz utilizing a

quasi-adiabatic cross-polarization pulse sequence using a 5.0 s pulse delay, a 9.0 ms

contact time, a 7.0 μs pulse width and at least 3000 scans. Proton decoupling was used

during acquisition.[136]

Ultraviolet-visible spectra were recorded on a Perkin Elmer UV/VIS spectrometer

Lambda EZ 201 in the range 200-800 nm using 10 mm quartz cuvettes.

Thermal, hydrothermal and mechanical stabilities of the as-synthesized

mesoporous materials were determined using nitrogen adsorption and small-angle X-ray

diffraction (XRD) measurements after employing thermal tests up to 1000 $^\circ$C,

hydrothermal tests in boiled water up to 35 hours, and compression pressures from 111 to

555 MPa.

The mesoporous MCM-41 materials were pyrolyzed in a temperature

programmable, muffle furnace under ambient air at temperatures that corresponded to

completion of decomposition steps observed by TGA experiments. The solid product

obtained at every thermal decomposition step was characterized by FTIR and XRD

analyses.

2.7. DETERMINATION OF ADSORPTION PARAMETERS

Specific surface areas of the materials under study were calculated using the BET

method.[137,138] These calculations were performed via computer according to the

following linear equation:

$$\frac{P/P_o}{X \cdot (1 - P/P_o)} = \frac{1}{X_{monolayer} \cdot C} + \frac{(C - 1)}{X_{monolayer} \cdot C} \cdot (P/P_o)$$

where X is the amount adsorbed at the relative pressure, (P/P_o), $X_{monolayer}$ is the monolayer

capacity, and C is an empirical constant. Solving this equation requires plotting

$(P/P_o)/(X(1-P/P_o))$ vs. (P/P_o), where X and (P/P_o) are the values that are measured by

instrument. The slope of the straight line (the adsorption points are selected in the region of the monolayer formation) is equal to $(C-1)/(X_{monolayer} \cdot C)$ and the intercept is $1/(X_{monolayer} \cdot C)$. The adsorption data in a narrow range of relative pressures ($P/P_o = 0.05 - 0.3$) were used to calculate the surface area (S_{BET}, m^2/g). In order to avoid overlapping with the capillary condensation step, which can appear at the relatively low pressures for modified samples, the pressure in some cases were adjusted to the range ($P/P_o = 0.05-0.15$). The two equations, slopes and intercepts, can be solved and find the C and $X_{monolayer}$ values. The BET surface areas (S_{BET}, m^2/g) were calculated using the following equation:

$$S_{BET} = X_{monolayer} \cdot (N_{Avogadro} / V_{molar}) \cdot {}^{S}N_2$$

where $X_{monolayer}$ (m^3 STP/g) is the BET monolayer capacity, $N_{Avogadro}$ is the Avogadro number (6.022×10^{23} mol^{-1}), V_{molar} is the molar volume of gas at STP (0.0224 m^3/mol) and ${}^{S}N_2$ is the nitrogen cross-sectional area (1.62×10^{-19} m^2). The nitrogen cross-sectional area (${}^{S}N_2$) was previously calculated using the density of liquid nitrogen and an assumption of the ideal surface in the bulk liquid.[139]

The total pore volume was evaluated from the total volume of nitrogen adsorbed at the relative pressure close to unity ($P/P_o = 0.99$), assuming that the pores are then filled with liquid adsorbate.

Differential pore size distributions were evaluated from adsorption branches of nitrogen isotherms using the BJH method with the corrected form of the Kelvin equation for capillary condensation in cylindrical pores: [139-141]

$$r(P/P_o) = \frac{0.416}{Log(P/P_o)} + t(P/P_o) + 0.3$$

where r is the pore radius in nm, P is the equilibrium vapor pressure, P_o is the saturation vapor pressure, $t(P/P_o)$ is the statistical film thickness curve (t-curve) as a function of the relative pressure (P/P_o) and an additional term in the above equation (equal to 0.3) denotes empirical correction made in the Kelvin equation.[141] The position of the peak maximum on the pore size distribution is referred as the pore width (w, nm).

2.8. DETERMINATION OF SILANOL GROUPS (Si-OH) ON THE SURFACE

The surface species are essential for the silylation reaction. Due to the different synthetic procedures for preparation of the mesoporous materials, a high variability in the amount of hydroxyl species is observed. As mentioned earlier, there are many different methods to determine the concentration of silanol groups on the mesoporous materials such as solid state ^{29}Si NMR and UV-Vis spectroscopy. In this study two different methods were employed; first one is the UV-Vis. method employing two different probing molecules (Cyclohexylamine and proton-sponge), and the second method is ^{29}Si CP/MAS NMR.

2.8.1. Cyclohexylamine as Determination Probe for the Hydroxyl Groups

The total hydroxyl (silanol) groups content in the synthesized mesoporous materials were calculated from the Langmuir adsorption isotherm using cyclohexylamine as an adsorbate (a titration agent). The concentration of non-adsorbed base in equilibrium with the concentration of the adsorbed base on the surface of solid (C) was determined from the difference in the UV absorption before and after the adsorption of the titrating agent on the mesoporous surface. A solution of approximately 4.3 x 10^{-3} M cyclohexylamine in cyclohexane ($\lambda_{max} \approx 226$ nm) was prepared. A sample of 10 ml of the cyclohexylamine solution was added to a specific amount of mesoporous material in a

20-ml glass vial. This mixture was then stirred for 12 hours, then filtered using a syringe filter of 0.45 μm after which the UV absorption was measured at the λ_{max} of the cyclohexylamine solution to give the equilibrium concentration (C) and the amount of the base adsorbed per gram of the mesoporous material (X). The number of acidic sites, hydroxyl groups, on the surface of the mesoporous expressed in μmol/g is equal to the amount of the adsorbate adsorbed by the mesoporous material to form a monolayer (X_m), which is equal to the reciprocal of the slope of the straight line obtained from the plot of C/X versus C according to the Langmuir equation:

$$C/X = C/ X_m + b/ X_m$$

where b is a characteristic constant of the adsorbent under study state which can be determined experimentally by dividing the intercept by the slope.

2.8.2. Proton-Sponge as Determination Probe for Hydroxyl Group

The total numbers of hydroxyl groups (silanol) on the surface of the synthesized mesoporous materials were determined from the Langmuir adsorption isotherm using proton-sponge as an adsorbate (a titration agent). Unlike cyclohexylamine, proton-sponge will not react with Lewis acid sites and so can give a more accurate measure of silanol concentration. The concentration of non-adsorbed base in equilibrium with the concentration of the adsorbed base on the surface of solid (C) was determined from the difference in the UV absorption before and after the adsorption of the titrating agent on the mesoporous surface. A solution of approximately 1.0×10^{-4} M proton-sponge in cyclohexane ($\lambda_{max} \approx 328$ nm) was prepared. A sample of 10 ml of the proton-sponge solution was added to a specific amount of mesoporous material in a 20-ml glass vial. This mixture was then stirred for 12 hours, the mixture was filtered off using syringe

filters of 0.45 μm and then the UV absorption was measured at the λ_{max} of the proton-sponge solution ($\lambda_{max} \approx 328$ nm) to give the equilibrium concentration (C) and the amount of the base adsorbed per gram of the mesoporous material (X). The number of acidic sites on the surface of the mesoporous expressed in μmol/g is equal to the amount of the adsorbate adsorbed by the mesoporous material to form a monolayer (X_m), which is equal to the reciprocal of the slope of the straight line obtained from the plot of C/X versus C according to the Langmuir equation.

2.8.3. Solid State ^{29}Si CP/MAS NMR

By means of ^{29}Si MAS NMR spectroscopy the total hydroxyl (silanol) groups can be determine using Wouters et al.,[128] technique. The samples were pre-treated (evacuated) prior to measurement. The procedure to evaluate the total amount of hydroxyl groups is developed from the ^{29}Si MAS NMR spectrum makes use of the relative peak areas of the spectra at Q^2, Q^3 and Q^4 that are usually found at around -90 ppm, -100 ppm, and -110 ppm respectively. From these data, the silanol concentration [SiOH] per gram of dry MCM-41 (mol/g) can be obtained from the formula:[128]

$$[SiOH] = ((I_Q{}^3 + 2 \times I_Q{}^2)/(60 \times I_Q{}^4 + 69 \times I_Q{}^3 + 78 \times I_Q{}^2))$$

I_i represents the line intensity of the various silicon lines in the solid state ^{29}Si MAS NMR spectrum.

2.9. THERMAL, HYDROTHERMAL, AND MECHANICAL STABILITIES STUDIES

The as-synthesized mesoporous materials were subjected to thermal, hydrothermal and mechanical studies in order to investigate their abilities to withstand

conditions such as high temperature environments, hydrothermal reactions with water at elevated temperature, or compression into a pellet form.

2.9.1. Thermal Stability Investigation

In this investigation, the as-synthesized mesoporous materials were subjected to heat (calcination) in air at different temperatures based on the TGA results. All samples were calcined at a heating rate of 2 $^\circ$C/min and kept at the end temperature for 8 hours. The product after each calcination temperature was characterized using two different techniques; the XRD and surface area analysis (BET) in order to differentiate between the final and starting mesoporous materials and identity thermal stability limit at which their framework collapses, See Table 2.2.

Table 2.2. Effect of thermal treatments on the surface area (BET) and pore diameter.

Sample	Temperature ($^\circ$C)					
	25	550	750	850	900	950
OSU-6-W	1283[a]	1180[a]	1023[a]	862[a]	491[a]	125[a]
	51.1[b]	47.8[b]	44.3[b]	41.7[b]	31.2[b]	26.1[b]
OSU-6-C	1211[a]	1196[a]	1066[a]	897[a]	578[a]	231[a]
	47.2[b]	45.6[b]	43.1[b]	38.7[b]	33.6[b]	24.8[b]

[a] Surface area in m^2/g and [b] pore diameter in Å.

2.9.2. Hydrothermal Stability Investigation

Hydrothermal stability tests were carried out for all the mesoporous materials. This study was done by boiling them in distilled water for times ranging from 1 hour to 35 hours, see Table 2.3. The product at each set time was characterized after drying by XRD and surface area measurements. This study identifies the effects of hydrothermal reactions and determines the hydrothermal stability limit of these materials before their framework re-hydrolyzed and collapses.

Table 2.3. Hydrothermal effects on the surface area (BET) and pore diameter.

Sample	Time of boiling Treatment (hour)					
	0	10	20	25	30	35
OSU-6-W	1283^a	1176^a	1064^a	928^a	618^a	168^a
	51.1^b	43.8^b	39.6^b	37.2^b	28.4^b	16.5^b
OSU-6-C	1211^a	1188^a	1104^a	978^a	818^a	568^a
	47.2^b	45.1^b	42.6^b	39.2^b	33.4^b	26.5^b

^{a} Surface area in m^2/g and ^{b} pore diameter in Å.

It is conceivable that water adsorbed onto silanol groups causes the hydrolysis of nearby Si–O–Si bonds, resulting in the collapse of the ordered structure. The enhanced hydrophobicity of the surface resulting from the decreased density of silanol groups is favorable for hindering attack by water, and protect those Si–O–Si bonds from hydrolysis, resulting in a significant increase in hydrothermal stability.[142]

2.9.3. Mechanical Stability Investigation

Mechanical tests were performed by pelletizing each synthesized mesoporous powder sample into a die with a diameter of 13 mm at a pressure range from 111 to 555 MPa, see Table 2.4. The pressure was increased in steps of 111 MPa and was kept constant for 2 min. After that these compressed materials were characterized by the XRD and surface area analysis (BET). It is not surprising that the much thicker pore walls and the highly polymerized walls are less affected by this systematic mechanical cleavage process.

Table 2.4. Mechanical pressure effect on the surface area (BET) and pore diameter.

Sample	Pressure Applied (MPa)					
	0	111	333	444	500	555
OSU-6-W	1283^a	1062^a	968^a	721^a	486^a	223^a
	51.1^b	47.3^b	44.6^b	41.4^b	38.2^b	32.3^b
OSU-6-C	1211^a	1182^a	1048^a	866^a	529^a	292^a
	47.2^b	45.9^b	44.9^b	42.3^b	41.6^b	39.3^b

^{a} Surface area in m^2/g and ^{b} pore diameter in Å.

2.10. RESULTS AND DISCUSSION

All of the synthesized mesoporous silicas have the hexagonal structure of MCM-41. However, they show slight differences in surface areas, pore sizes (diameters), pore size distributions, and wall thicknesses. Of all of the synthesized materials, OSU-6, OSU-6-W, and OSU-6-C will be discussed in detail in this chapter due to their unique characteristics as will be seen later.

2.10.1. Identification of the Textural Properties (Physical characterization)

The physical structure of silica gel (high surface area, large pore volume, *etc.*) is one of the major reasons for its effectiveness as a catalyst support material and a chromatography media. However, these features can be altered significantly during preparation (*i.e.* change in pH, temperature, use of template, *etc.*). Variations in surface areas, pore volumes and pore sizes (as well as their distribution) have a significant effect on the resulting material. It is therefore necessary to accurately characterize the physical nature of the resulting material.

I. X-ray Diffraction Measurements (XRD)

The quality of X-ray powder diffraction (XRD) patterns reported in the literature for MCM-41 varies widely.[1-4,54] In general, line widths of the XRD patterns increase upon calcination, indicating a loss of long-range structural order. Variability in the long-range structural order greatly inhibits not only the interpretation of spectroscopic or other characterization studies of these novel materials, but also restricts practical applications requiring structural integrity.[1-4]

Typical XRD patterns of all the OSU samples obtained in this research before calcination or/and washing with HCl-ethanol exhibited XRD patterns with a very intense

(100) diffraction peak and two weak (110) and (200) peaks, which are characteristic of the hexagonal, MCM-41 type, phase.[1,2] High intensities of the higher-order diffraction peaks were observed for all of the mesoporous silicas prepared in this investigation. This can originate from two sources, as explained by Schüth *et al.,*[143] First, a high ratio of pore size versus wall thickness produces higher relative intensities for higher-order diffractions. In the case of the materials synthesized here, the wall thickness is almost half the pore size. Second, these relative intensities are also influenced by the roughness of the pore walls. In the OSU materials, this roughness can be considered to be quite small due to the small amount or absence of micropores near the wall surface as indicated from the surface area analysis. A low microporosity (as in our samples) will result in high relative intensities.

XRD patterns for the as-synthesized mesoporous materials, OSU-6, (surfactant-containing), calcined (OSU-6-C), and HCl-ethanol extracted (OSU-6-W) are shown in Figure 2.3. They feature three well-resolved intense reflections despite the fact that the patterns were recorded on a powder diffractometer using rather short counting times (one hour for scan from 2θ from $1.2°$ to $10°$) and therefore the background noise was relatively large.

The as-synthesized OSU-6 has three diffraction peaks that correspond to *d*-spacings of 100, 110, and 200 of 62.70, 34.62, and 25.24 Å. In the case of calcined OSU-6, the XRD shows three diffraction peaks corresponding to the *d*-spacing of 100, 110, and 200 with intensities for the strong peak at 59.10 Å and for the two weak peaks at 28.36 and 18.14 Å.
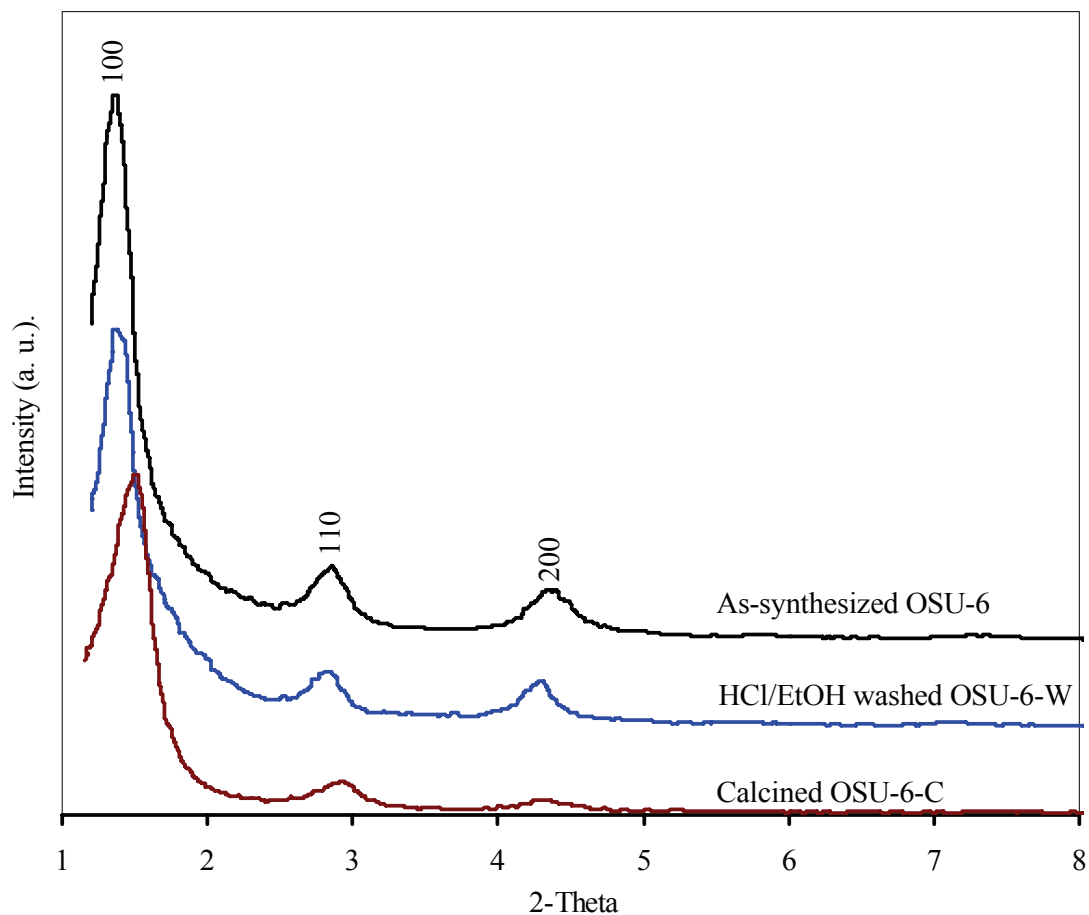
Figure 2.3. Powder XRD patterns for as-synthesized OSU-6, calcined OSU-6-C, and HCl/ethanol extracted OSU-6-W samples. The spectra are shifted vertically for clarity.

In the HCl-ethanol extracted (OSU-6-W) these three diffraction peaks corresponding to the *d*-spacing of 100, 110, and 200 occur at 62.4, 31.70, and 21.74 Å, respectively. The intensity of the d_{100} reflection in HCl-ethyl alcohol extracted sample is higher than that of the calcined sample while the as-synthesized sample shows higher intensity than both samples. Thus, the removal of the template by HCl-ethanol extraction preserves pore of the crystallinity of the mesoporous materials. The decrease in the intensity (lower d_{100} value) is expected because the HCl-ethanol extraction of the

surfactant leads to some condensation, especially, acid-catalyzed condensation of silanol is well known.

The main index peak position of the hexagonal unit cell was used to calculate the pore size of the mesoporous material using the following equations;

$$d_{100} = \lambda / 2 \cdot \sin \theta_{100}$$

$$a = 2 \, d_{100} / (\sqrt{3})$$

The pore sizes calculated using the above equation for the three mesoporous samples are shown in Table 2.5. The differences in the pore sizes indicate a lattice contraction of about 0.3 Å upon extraction of surfactant using HCl-ethanol mixture and also the results indicate a lattice contraction of about 3.6 Å upon calcination at 550 $^{\circ}$C. These results show an agreement with the fact that calcination will increase the condensation degree and lead to the shrinkage of the frameworks.

For all samples under study, the unit cell contraction upon washing and calcination was small (below 10%, see Table 2.5).[144]

II. Nitrogen Adsorption-desorption Measurements (BET)

The BET specific surface area, S_{BET}, calculated using nitrogen adsorption data in the relative adsorption range from 0.04 to 0.2 was used to avoid inclusion of the data points considerably affected by the capillary condensation in primary mesopores of the sample.[145]

Nitrogen adsorption/desorption isotherms measurements (surface areas, pore sizes, pore size distribution, and pore volumes) of all the calcined samples and the HCl-ethanol extracted ones are shown in Table 2.5.

Table 2.5. Textural Properties Determined from Nitrogen Adsorption-Desorption Experiments at 77 K and XRD Powder Measurements.

Sample	Specific surface area $(m^2/g)^a$	Total pore volume $(cm^3/g)^b$	Average pore size $(Å)^c$	d_{100} $(Å)^d$	Wall Thickness $(Å)^e$
OSU-1-W	1063	0.96	47.2	54.6	15.8
OSU-1-C	988	0.74	41.6	50.1	16.2
OSU-2-W	1022	0.93	46.6	53.5	15.2
OSU-2-C	964	0.69	40.9	48.9	15.6
OSU-3-W	1051	0.96	44.3	54.2	18.3
OSU-3-C	1036	0.86	42.1	53.0	19.1
OSU-4-W	1089	0.95	45.1	55.3	18.7
OSU-4-C	1073	0.90	43.4	53.9	18.9
OSU-5-W	1167	1.10	48.6	58.2	18.6
OSU-5-C	1123	0.92	44.3	55.6	19.9
OSU-6-W	1283	1.24	51.1	62.4	20.9
OSU-6-C	1211	0.98	47.2	59.1	21.1

[a] Specific BET surface area. [b] BJH desorption cumulative pore volume of pores between $d_p = 15$ Å and 200 Å; all samples were pretreated at 100-150 ^{o}C under vacuum. [c] Pore diameter according to the maximum of the BJH pore size distribution calculated from the desorption branch of the isotherm. [d] d index at Miller Index of 100 in the XRD. [e] wall thickness from the difference between pore diameter and lattice dimension (a).

All the materials prepared in this investigation show high surface areas (BET) ranging from 900 m^2/g to 1300 m^2/g, the largest surface areas in this list of materials are OSU-6-W and OSU-6-C which were prepared using neutral surfactant (*n*-hexadecylamine) and 1,3,5-trimethylbenzene as an additive. OSU-6-W and OSU-6-C have the highest surface areas of all mesoporous materials prepared in this investigation and considered as the highest and much better quality among all MCM-41 mesoporous materials.[1-4,40,100]
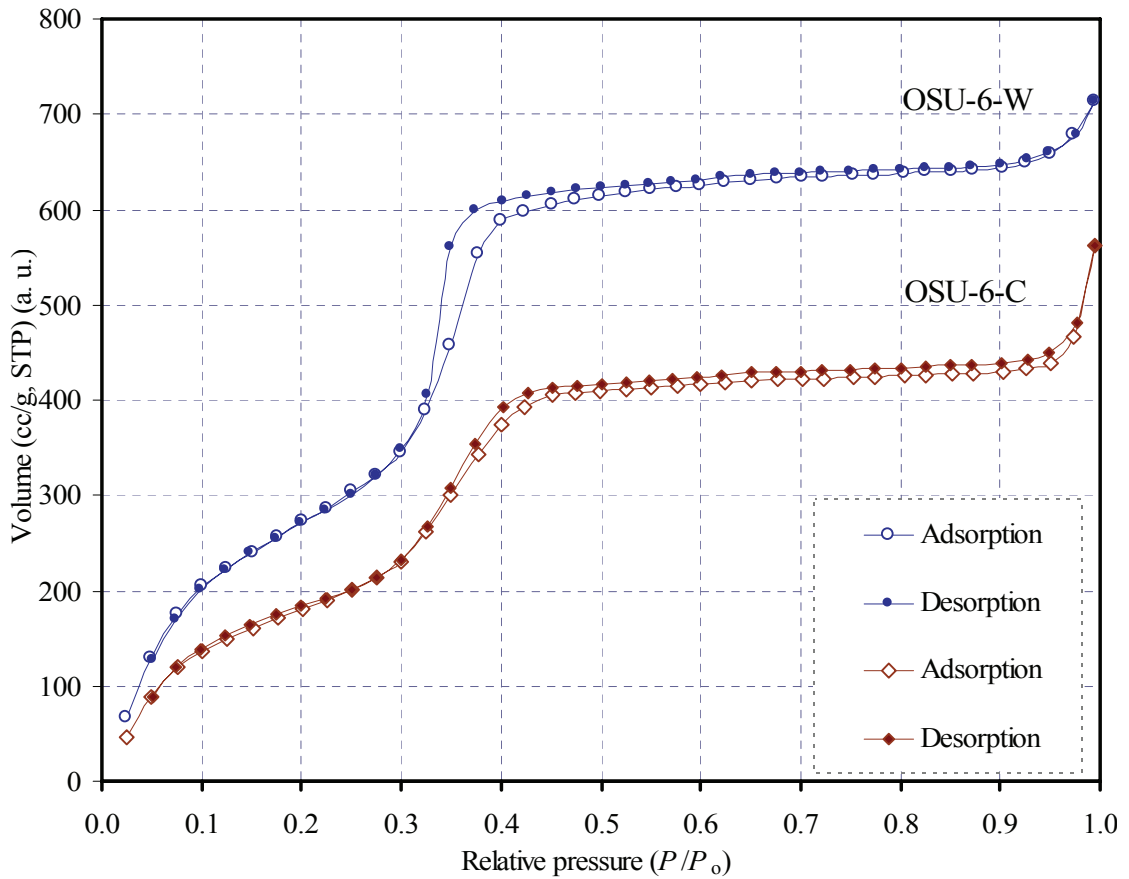
Figure 2.4. Nitrogen adsorption-desorption isotherms at 77 K obtained on Ethanol-HCl washed mesoporous OSU-6-W and calcined mesoporous OSU-6-C. The isotherm data are shifted vertically for the sake of clarity.

Figure 2.4 shows the adsorption-desorption isotherm of the HCl-ethanol washed OSU-6-W and calcined OSU-6-C materials. Figure 2.4 enables the calculation of the specific surface areas, pores volume, and pore size distributions. The nitrogen adsorption by OSU-6-W and OSU-6-C at relatively low pressures, P/P_o, is from the adsorption of a monolayer of N_2 on the walls of the mesopores and there is no evidence of any micropores presence. It shows a typical reversible type IV adsorption isotherm as defined by IUPAC.[146] The sharp inflection between relative pressure $P/P_o = 0.3$ and 0.4

corresponds to capillary condensation within uniform mesopores. The sharpness of this step reflects the uniformity in the pore size distribution. Also, the fact that the initial region can be extrapolated back to the origin confirms the absence of any detectable micropore filling at low P/P_o. Therefore, a very uniform mesoporous system without micropore structure is observed in the HCl/EtOH washed and calcined samples. The adsorption and desorption cycle did not show large hysteresis loops which can be attributed to the small size of the particles as confirmed by SEM and TEM as we will see later.[145,147,148]

The BJH plot of the derivative of the pore volume per unit weight with respect to the pore diameter (dV/dD) versus the pore diameter is shown in Figure 2.5. The pore size distribution of this sample is very narrow (FWHM = 3.5 Å) and the average pore diameter is 51.1 and 47.2 Å for OSU-6-W and OSU-6-C, correspondingly.
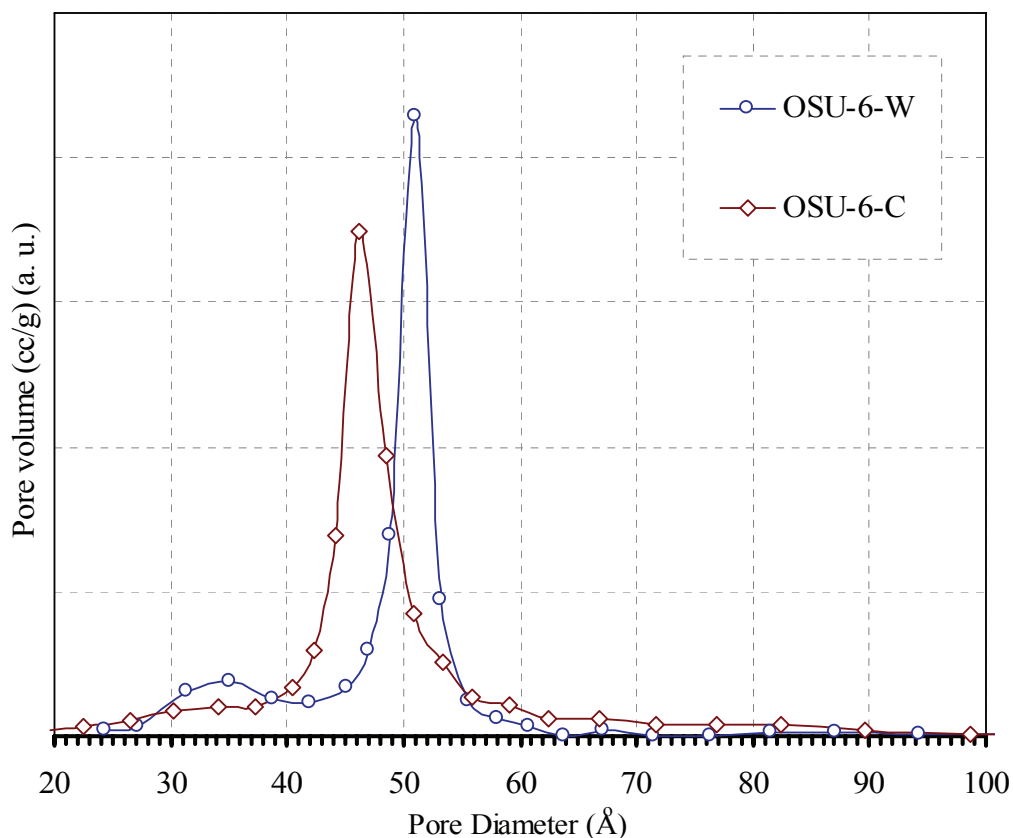
Figure 2.5. Pore size distributions of the two samples, OSU-6-W (max at 51.1 Å) and OSU-6-C (max at 47.2 Å), calculated by the Barrett–Joyner–Halenda method.

Combining the results from XRD and N_2 adsorption/desorption, the prepared mesoporous materials have pore sizes of ~ 51.1 Å and wall thickness of ~ 20.9 Å for OSU-6-W and ~ 47.2 Å and wall thickness of ~ 21.1 Å for OSU-6-C.

The pH of the initial synthesis had an effect on the final products. The XRD patterns in Figure 2.3 show that at pH ≈ 4.5, only the mesophase with hexagonal array was obtained. At pH higher than 11.0, we could not obtain any mesophase structures, indicating that at high pH the silica frameworks dissolve faster than the polymerization or precipitation of silicas. Therefore, the synthesis and formation of mesoporous materials depend on the initial pH of the synthesis gels.

III. Thermogravimetric Analysis (TGA)

The TGA results for the as-synthesized mesoporous materials are illustrated in Figure 2.6. This sample shows three distinct weight loss steps. The first weight loss step at 25-120 $^{\circ}$C ($\sim$ 4.5% lost) is due to desorption of water and alcohol. The second weight loss step between 120 and 220 $^{\circ}$C ($\sim$ 33.5% lost) is indicating the combustion and decomposition of the organic template and the additive. The third step at above 220 $^{\circ}$C ($\sim$ 15% lost) and believed to be related to water losses upon condensation of hydroxyl (silanol) groups to form siloxane bonds.
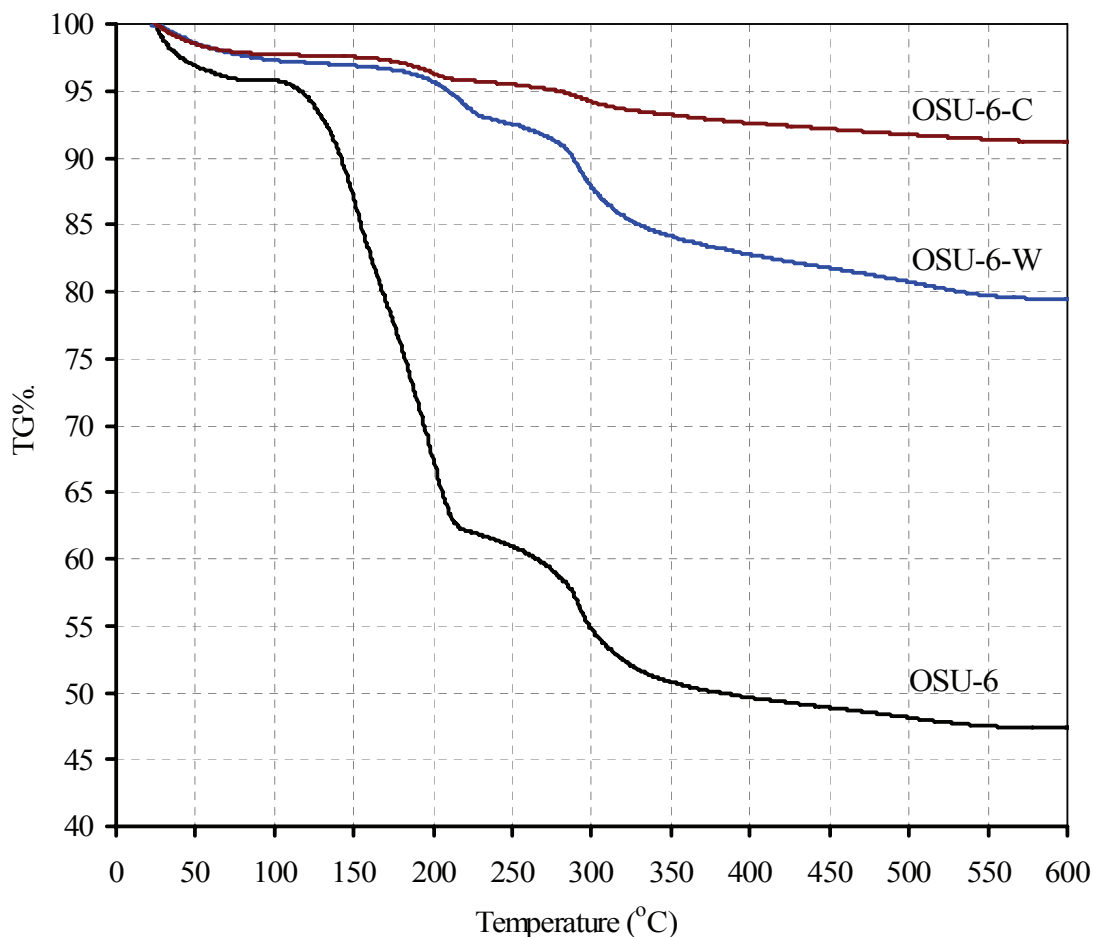
Figure 2.6. TGA of the as-synthesized mesoporous, OSU-6, the HCl/EtOH washed mesoporous OSU-6-W, and the calcined mesoporous OSU-6-C.

The TGA results for the calcined (OSU-6-C) and HCl-ethanol (OSU-6-W) mesoporous materials are also illustrated in Figure 2.6. The calcined sample shows a small change in weight and is present in this figure in order to compare with the TGA of the mesoporous sample after removing of the surfactant with the HCl-ethanol extraction method. In the TGA curve of the latter sample there are three distinct weight loss steps. The first weight loss step at 25-150 ^{o}C (~ 3.0% lost) is due to desorption of water and alcohol on the surface and inside the pores. The second step at around 150 ^{o}C (~ 4.5%) is assumed to be associated with water inside the pores or to the condensation of silanol groups on the surfaces. The third step at around 240 ^{o}C (~ 14.5%) is believed to be related to water losses upon condensation of silanol groups to form siloxane bonds. This result confirms the presence of high concentration of silanol groups in the mesoporous silica prepared by removing the surfactant using HCl-ethanol extraction method.

The TGA results of the unwashed sample and the HCl-ethanol washed sample indicate evidence for the presence of the silanol groups in the washed sample. Moreover, it confirms that the third step in the TGA analysis of unwashed samples is related to the condensation of silanol groups and losing of water molecules.

The thermogravimetric curves of the six mesoporous silicas studied are depicted in Figure 2.7. As previously established, there are three distinct mass loss steps in the TGA traces for the silicas.[109] The first step is gradual and is most probably due to the removal of physisorbed water from the silica surface. The second step is abrupt and is believed to be related to the combustion and decomposition of the organic templates and the additives. The third step is broader and is considered to correspond to slow condensation of silanols. From the literature,[109] it is known that upon heating of silica,

hydrogen-bonded hydroxyls are released first quite rapidly in the temperature range 200-300°C and isolated hydroxyls more slowly at higher temperatures.

Unfortunately, the removal of different types of hydroxyls, *e.g.* isolated and hydrogen-bonded, takes place during one continuous mass loss step so that distinguishing them is not possible from the thermograms. A third, rather flat peak at about 700-1000 °C can also be observed in the TGA curves of all the silicas, but it is presumably not characteristic for any specific type of OH group. It might be due to the dehydroxylation of final OH groups before collapse of the porous structure after which no more OH groups are close enough and able to react on the external surface of the silica particles.
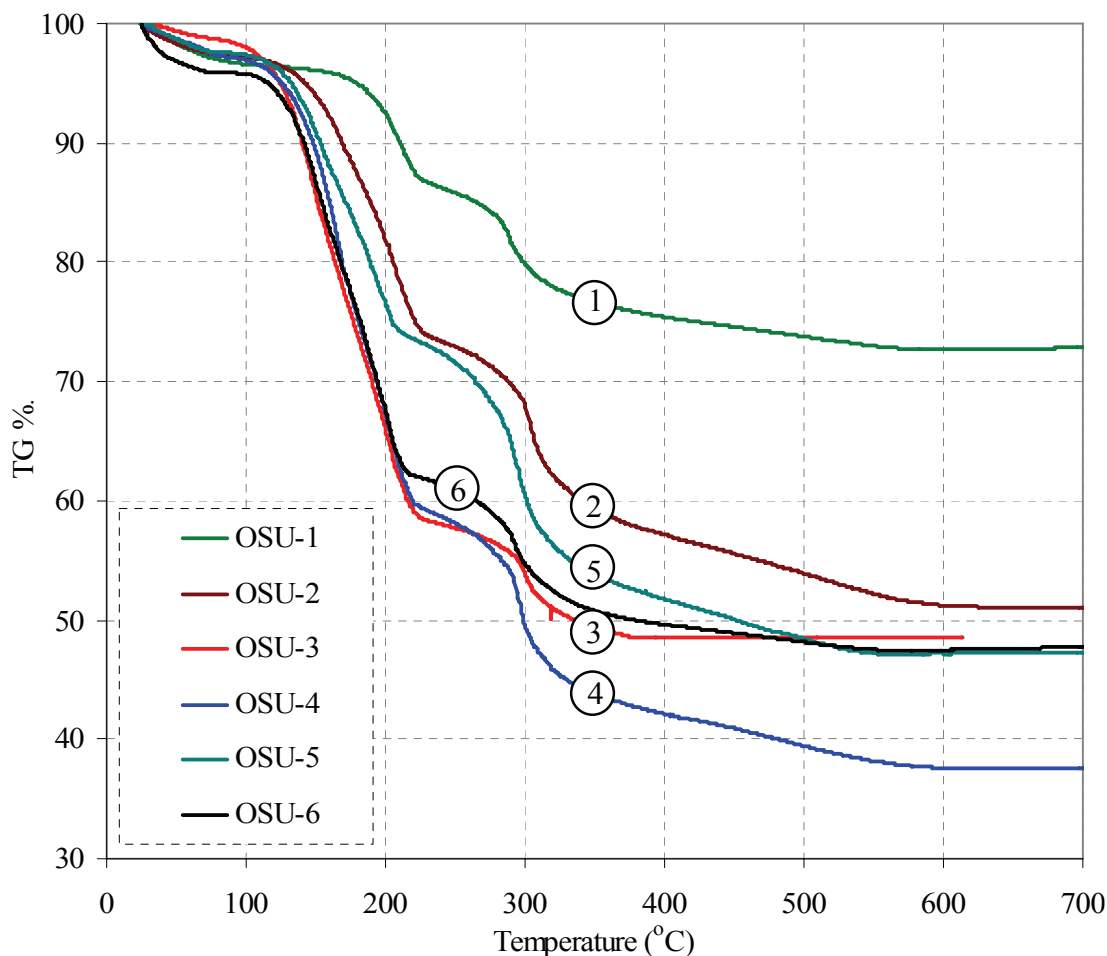
Figure 2.7. TGA of the as-synthesized mesoporous materials, OSU-1 to OSU-6.

2.10.2. Recognition of Chemical Structure (Chemical Characterization)

The techniques employed for the physical characterization of mesoporous silica materials are, in the main, applicable to all mesoporous silicas. However, this is not the case when investigating the chemical nature of the same materials. The range of techniques available is large. Therefore, the aim of this section is to briefly discuss the most commonly used techniques for chemical characterization. To obtain an accurate picture of the nature of the mesoporous silica surface a combination of techniques should be employed.

I. Solid State ^{29}Si CP/MAS NMR

The solid-state ^{29}Si nuclear magnetic resonance (NMR) spectra of the mesoporous materials before and after calcination also for the sample washed with HCl-ethanol to remove the surfactants are shown in Figure 2.8. The ^{29}Si NMR spectra of these samples are broad. The as-synthesized sample exhibits three partially resolved ^{29}Si NMR peaks at -110.7, -100.9, and -91.6 ppm which are related to the Q^4, Q^3, and Q^2 environments, respectively. The calcined sample at 550 $^{\circ}$C shows ^{29}Si CP/MAS NMR peaks at -109.5 and -101.6 ppm (Q^4, Q^3 environments) and after heating the sample to 700 $^{\circ}$C only one peak at -110.8 ppm related to Q^4 is present. The treated sample with HCl-ethanol solution shows ^{29}Si CP/MAS NMR peaks at -109.7, -101.4, and -90.3 ppm with higher intensities of the Q^3 and Q^2 at the expense of Q^4 as compared to the as-synthesized and calcined materials.
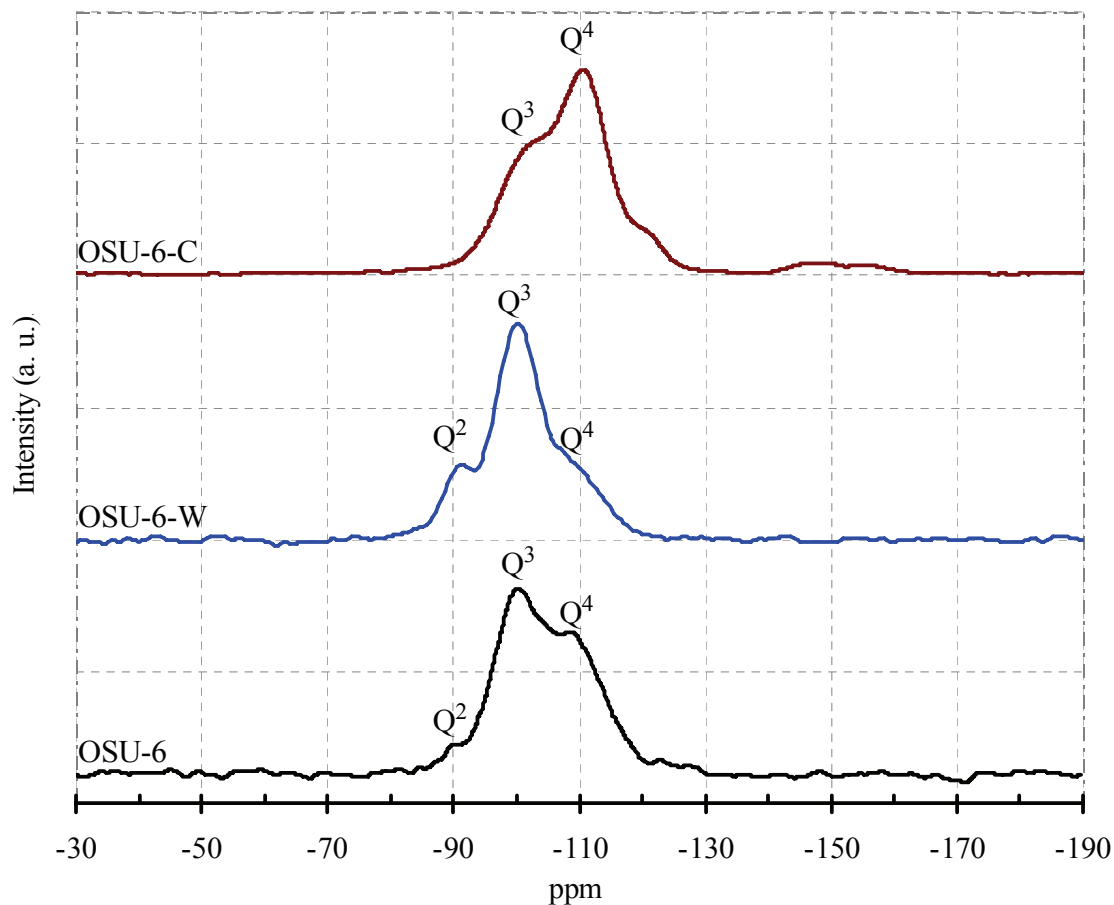
Figure 2.8. Solid state ^{29}Si CP/MAS NMR spectra of; As-synthesized OSU-6, HCl/EtOH washed mesoporous silica, OSU-6-W, and the calcined OSU-6-C.

This result provides evidence for the presence of high concentration of silanol groups on the surface of the sample treated with HCl-ethanol compared with the calcined sample. Moreover, it shows a decrease in the silanol groups (increase in the condensation degree) with increasing the calcination temperature. Accurate Q^3/Q^4 ratios determined from deconvolution of spectra recorded are given in Table 2.6.

Table 2.6. The Q^3/Q^4 ratios determined from deconvolution of ^{29}Si CP/MAS NMR spectra recorded.

Sample	Q^4 (%)	Q^3 (%)	Q^2 (%)	Q^3/Q^4
OSU-1-W	44.56	53.31	2.13	1.19
OSU-1-C	84.04	15.96	0.00	0.18
OSU-2-W	43.52	55.18	1.30	1.27
OSU-2-C	80.88	19.12	0.00	0.24
OSU-3-W	40.67	57.30	2.03	1.41
OSU-3-C	77.83	22.17	0.00	0.28
OSU-4-W	40.05	58.71	1.24	1.47
OSU-4-C	71.81	28.19	0.00	0.39
OSU-5-W	19.51	78.40	2.10	4.02
OSU-5-C	67.70	32.30	0.00	0.48
OSU-6-W	14.38	71.73	13.89	4.99
OSU-6-C	65.10	31.87	3.04	0.49

The Q^3/Q^4 ratios provide important information regarding the structure and mechanism of formation of the silicate walls. First, there is a substantial difference in the Q^3/Q^4 ratio between layered mesoporous silicas and the other M41S materials. Note that upon calcination of the hexagonal material the Q^3/Q^4 ratio is reduced, indicating increased condensation of the silicate structure. This also exhibits itself as a weight loss at temperatures in excess of 200 $^{\circ}$C in the TGA analysis (Figure 2.7). Indeed the Q^3/Q^4 ratio of *ca.* 1.0 suggests a wall composed of two Q^4 layers bordered by one Q^3 layer.[136]

II. Fourier Transform Infrared Spectroscopy (FT-IR)

The template or surfactant content of the hexagonal mesoporous silica can be identifying using FT-IR. Figure 2.9 shows the FT-IR spectra of as-synthesized, HCl/EtOH extracted, and the calcined mesoporous samples, OSU-6, OSU-6-W, and OSU-6-C, respectively. The absorptions at around 2926, 2855, 1465 and 1378 cm^{-1} are ascribed to stretching vibrations of methyl groups in HDA molecules. The absorption at 3291 cm^{-1} is ascribed to stretching vibration of the amine groups, but because of the large

and broad peak of the hydroxyl groups and water this peak was not clear. In the infrared

spectrum of the as-synthesized sample shown in Figure 2.9 (A), these peaks are easily

observed, indicating the existence of HDA molecules. The FT-IR spectra of the calcined

mesoporous sample at 550 °C is shown in Figure 2.9 (B), it shows no peaks related to the

surfactant. This means the surfactant is completely removed from the pores of the

mesoporous material. Figure 2.9 (C) shows the FT-IR spectra of the mesoporous sample

after extraction of the surfactant with HCl-Ethanol. The peaks related to the HAD have

disappeared which indicates the extraction with HCl-ethanol can totally remove HAD

molecules from as-synthesized mesoporous materials.[149,150]
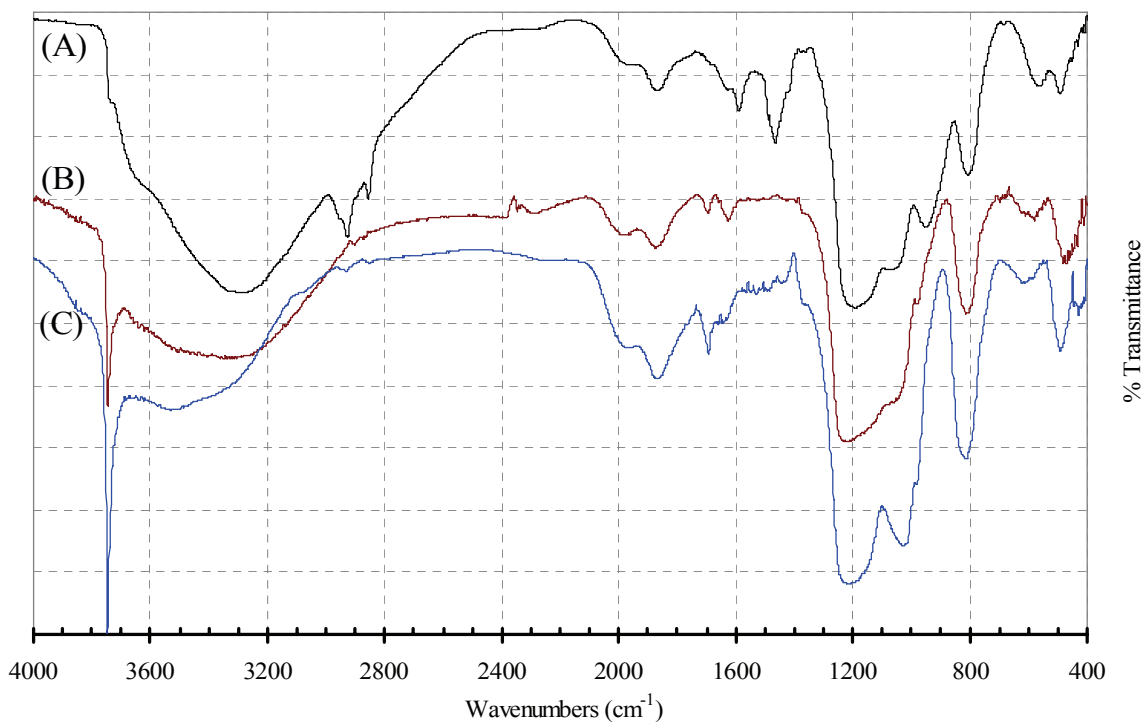
Figure 2.9. FT-IR spectra of (A) as-synthesized sample OSU-6, (B) calcined sample (OSU-6-C, and (C) HCl-ethanol washed sample (OSU-6-W).

The spectra of calcined and HCl/EtOH extracted OSU-6 consist of a sharp band at

3744 and 3746 cm^{-1}, respectively, typical of amorphous silica due to isolated hydroxyl

(silanol) groups and a very broad band appearing around 3500-3550 cm^{-1}. The latter was

assigned to hydrogen-bonded silanol groups. Upon activation the maximum of the 3550

cm^{-1} band is slightly blue-shifted and the intensity decreases due to condensation of

hydrogen-bonded silanol groups.[151]

The FT-IR spectra did not show any peaks related to the organic additive, 1,3,5-

trimethylbenzene. This is due to the extensive washing of the as-synthesized sample with

a mixture of ethanol and water also due to the drying process under vacuum. The FT-IR

spectra of the sample calcined at 550 $^{\circ}$C, Figure 2.9 (B), show a low intensity of the peak

at around 3744 cm^{-1} which is related to silanol groups or hydroxyl groups. This means a

low concentration of silanol groups on the surface. In comparison with the FT-IR spectra

of the well washed with HCl/EtOH sample, Figure 2.9 (C), the peaks associated with the

silanol groups in the latter sample have high intensity (high concentration) than that of

the former sample which support the other results from the TGA, solid state ^{29}Si NMR,

and UV-Visible spectrophotometer measurements.

FT-IR spectra for as-synthesized mesoporous materials prepared from silicon

alkoxides (TEOS) are different from those of fumed silica, and from those of other

amorphous SiO_2, whose network is relatively complete. The assignment of the major IR

absorption bands is well established from experimental studies of the vibrations of

amorphous silica. The components at 1192 and 1074 cm^{-1} arise from the stretching

frequency of the SiO_4 tetrahedral unit ($\equiv$ Si-O-Si $\equiv$), while the 807 cm^{-1} band is due to ($\equiv$

Si-O-Si $\equiv$) bending modes. The band at 1624 cm^{-1} is due to the bending vibration of

molecular H_2O that is adsorbed by hydrogen bonding with terminal ($\equiv$ Si-OH) groups.[149,150] This band, unfortunately, is also present on hygroscopic silica powders, although with only small intensity. One important feature of the OSU-6 material is the occurrence of an absorption band at 949 cm^{-1}, similar to that in MCM-41, which is due to the silicon-oxygen stretching vibration of ($\equiv$ Si-OH, non-bridging) bonds in the alkoxides gels, which is not present in many other silicas. Heat treatment reduces the concentration of non-bridging ($\equiv$ Si-OH) bonds, especially above 550 $^{\circ}$C.[149,150] Moreover, the absorption peaks around 562 and 456-469 cm^{-1} are attributed to the Si-O-Si bending vibration.[149,150]

The FT-IR of the calcined mesoporous sample, OSU-6-C, shows an absorption component at around 1201(s, br), 1057(s, br) and 805(m) cm^{-1} that arise from the stretching and bending modes of the SiO_4 tetrahedral unit, respectively. The absorption peak that appears at 1625 cm^{-1} is attributed to the H-O-H bending vibration of molecularly adsorbed water.[149,150] The band near 975 cm^{-1} has been attributed to the stretching vibration of non-bridging ($\equiv$ Si-OH), and its frequency and intensity is different than that for the as-synthesized OSU-6. The position of this vibration is known to vary with the nature of the silica from which the spectra were recorded. Many silicas calcined at high temperature show very few non-bridging oxygen atoms, therefore, the structure is similar to that of an unbroken silica network. After suspension of the silica in water it can show the stretching vibration of non-bridging ($\equiv$ Si-OH) in IR spectra because of the hydrolysis of tetrahedral surface units. A significant shift from 949 cm^{-1} to 975 cm^{-1} occurs as the hydrogen-bonded H_2O is removed during equilibrium in a furnace, after calcination. The shift to higher frequency is expected for ($\equiv$ Si-OH) groups

without H_2O, as the effective mass of the OH is reduced when H_2O is lost due to calcination.[149,150] Moreover, the absorption peaks around 486 cm^{-1} are attributed to the Si-O-Si bending vibration.[149,150]

In the case of OSU-6-W, the absorption bands at around 1206(s, br), 1031(s, br) and 813(m) cm^{-1} arise from the stretching and bending modes of the SiO_4 tetrahedral unit, respectively. The band at around 1633(w) is due to the bending mode of SiO-H, and the band at around 976(m) cm^{-1} is due to the stretching vibration of non-bridging silanol groups.[149,150] The frequency and intensity of the band at 976 cm^{-1} are different from that of OSU-6 and OSU-6-C. As expected, a significant shift from 949 cm^{-1} to 976 cm^{-1} occurs as the hydrogen-bonded H_2O is removed during equilibrium in a vacuum. The infrared spectrum also displays absorption peaks around 496 cm^{-1} are attributed to the Si-O-Si bending vibration.[149,150]

2.10.3. Morphology, Shape, and Size of Particles

I. Scanning Electron Microscope (SEM)

The morphology, shape, and size of the particles of the as-synthesis mesoporous materials were characterized by high resolution scanning electron microscopey (SEM). Mesoporous materials with different morphologies can be synthesized by changing reaction conditions or ingredients. Increasing the amount of TEOS in the synthesis results in a morphologic shift starting from micron-sized spheres of approximately 1μm in size at low silica concentration, to the same type of spheres but in a lower amount on the surface of randomly shaped aggregated particles, to completely randomly shaped aggregated particles, and finally to the formation of macrospheres when using the highest silica concentration. The shift in morphology can be explained by the rate of the phase

separation as explained in the colloidal phase separation mechanism.[152] At lower silica

concentration, the rate of phase separation will be slower, due to a lower rate of silica

condensation. In this case, the morphology will be controlled by the surface free energy,

resulting in a higher curvature of the particles.[152] At higher silica concentrations, the

formation of the randomly shaped particles will occur from a competition between the

surface free energy and the total free energy. Finally, the macrospheres will form

through a further condensation between the preformed silica particles resulting in one

large particle, still minimizing its surface free energy. Figure 2.10 show the SEM images

of several mesoporous materials which show well defined edges and spherical shapes.

Scanning electronic microscopy (SEM) images showed that the particle sizes of OSU-6,

OSU-6-W and OSU-6-C were in the range of 250-1500 nm.

The SEM images Figure 2.10 (A and B) of the mesoporous OSU-6 show a narrow

particle size distribution and well defined spherical particles. The same characteristics

are shown in the SEM images C and D of the mesoporous OSU-6-W. However, in the

case of the calcined mesoporous OSU-6-C, the particles exhibited shrinkage and

aggregation as shown in Figure 2.10 (E and F).
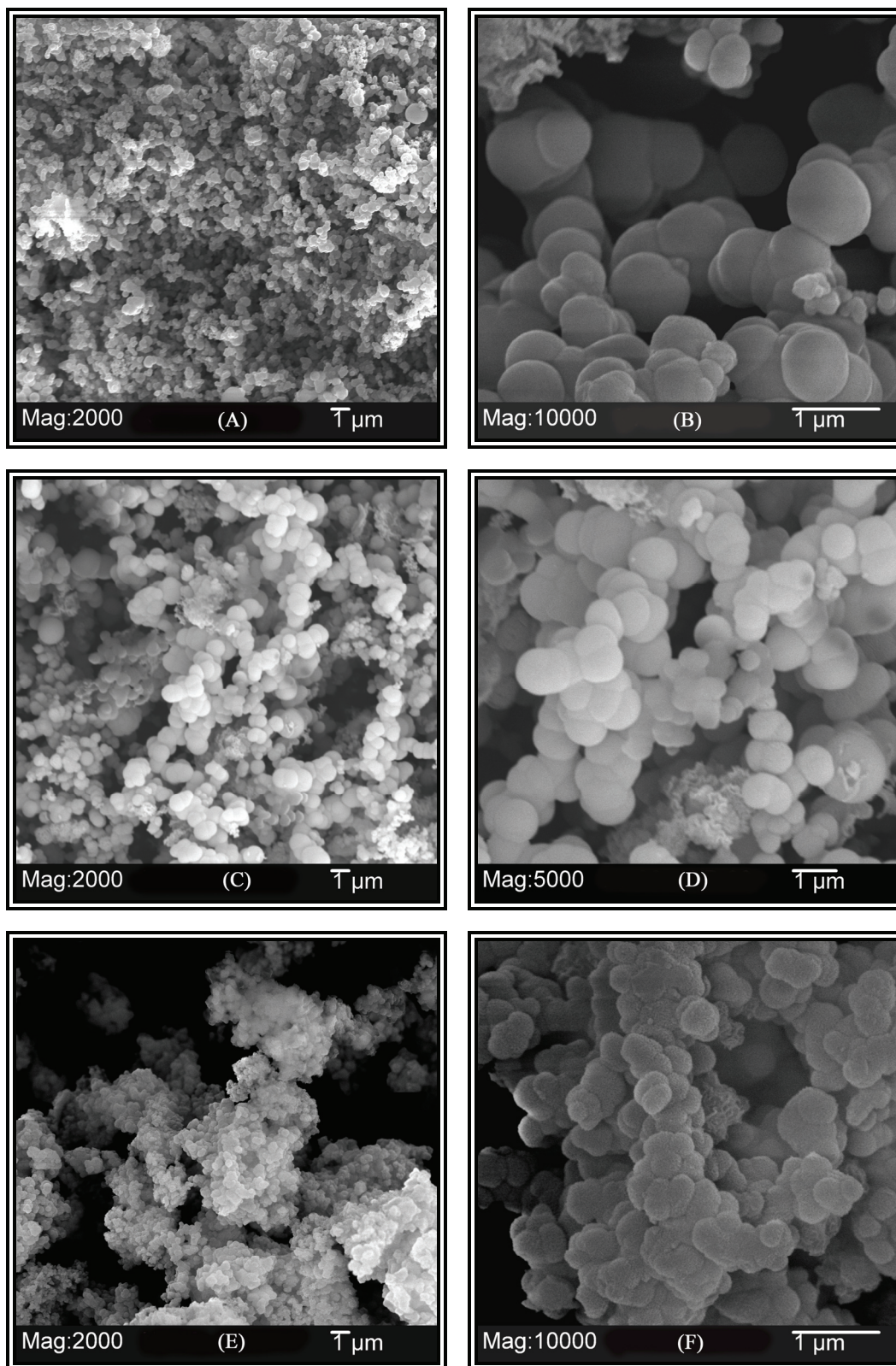
Figure 2.10. SEM Images of the as-synthesized mesoporous silica OSU-6 (A and B), HCl/EtOH washed OSU-6-W (C and D), and calcined OSU-6-C (E and F).

143

II. Transmission Electron Microscopy (TEM)

TEM images for selected calcined as well as EtOH/HCl washed samples are shown in Figure 2.11 and Figure 2.12. The unit cell parameters obtained from the TEM images were close to those evaluated using XRD, indicating a proper calibration of electron microscopy magnification. The pore wall thickness was usually found to be larger for uncalcined samples than for the calcined ones,[153,154] which is probably related to the shrinkage of the structure upon calcination. It can be seen in Figure 2.11 that the OSU-6-W pores are approximately hexagonal. Materials of lower degree of structural ordering may exhibit larger deviations from the hexagonal pore shape. However, this feature requires further verification, since the samples were crushed before their TEM imaging. It should also be noted that in comparison to the uncalcined (for instance the EtOH/HCl washed) samples, the calcined ones, OSU-6-C, appeared to have slightly lower degree of pore structure ordering.

Figures 2.11 and Figure 2.12 show the TEM images of two mesoporous materials which show well defined channels and walls. Moreover, they can be used to estimate the channels size and shape, and walls thickness. High resolution TEM images for selected particles along [100], [111], and [110] directions correspond well with reported MCM-41 images. Along the [100] direction the TEM micrograph shows uniform pore structures, the image on the [111] direction shows a well defined hexagonal arrangement and the image on the [110] direction shows a very regular pattern. Along the [100] and [111] directions channels are observed, but along the [110] direction the contrast variation is due to changes in electron density. Therefore, the [100] and [111] projections reflect the

actual shape and structure of the channels, while the regularity of the TEM image in the

[110] direction in indicates a uniform channel system.
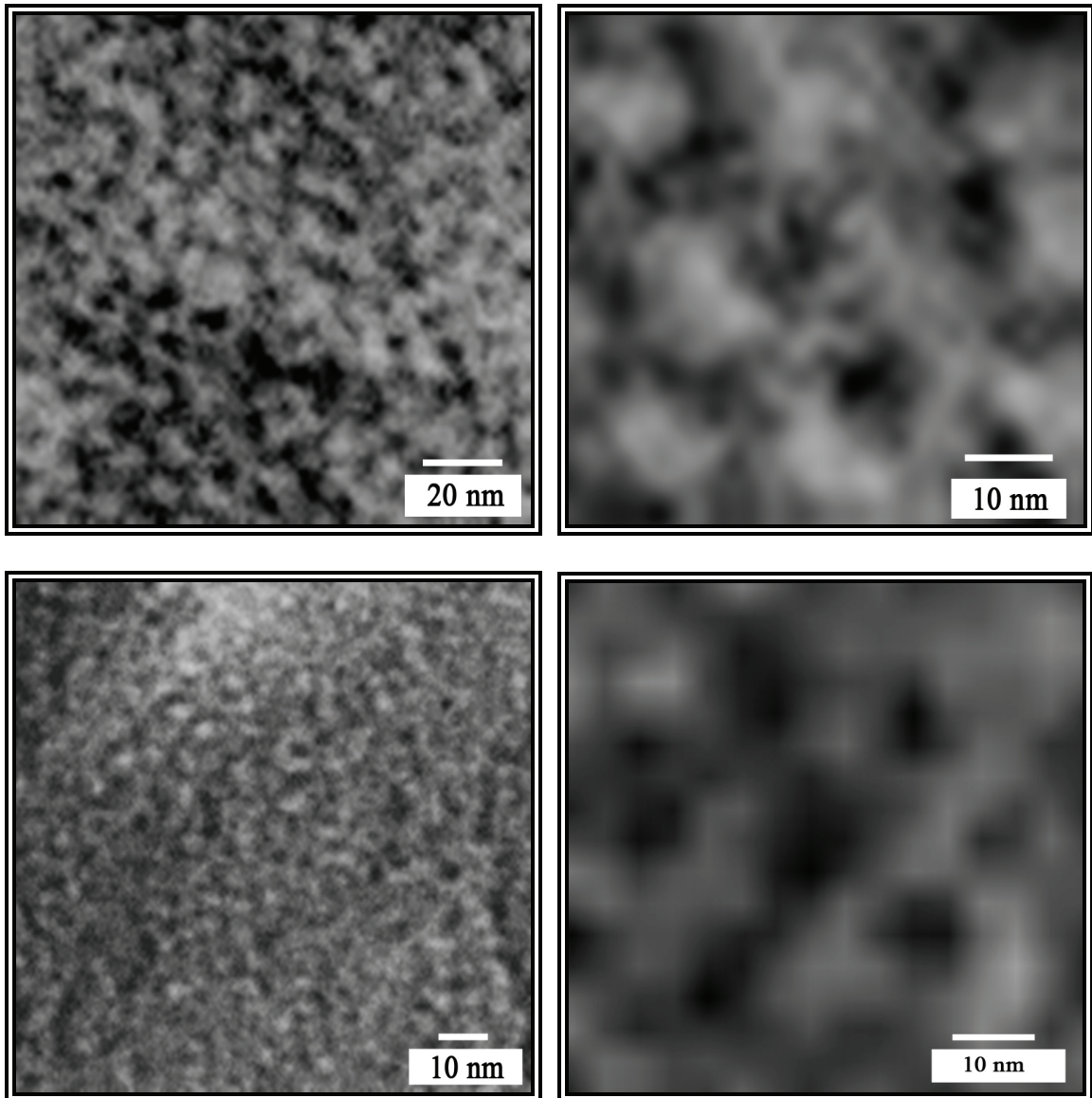
Figure 2.11. Transmission electron microscopy images for selected OSU samples: (a) OSU-6-W EtOH/HCl washed and (b) OSU-6-C calcined. These images show the hexagonal array. The pore diameters are *ca.* 50 Å.
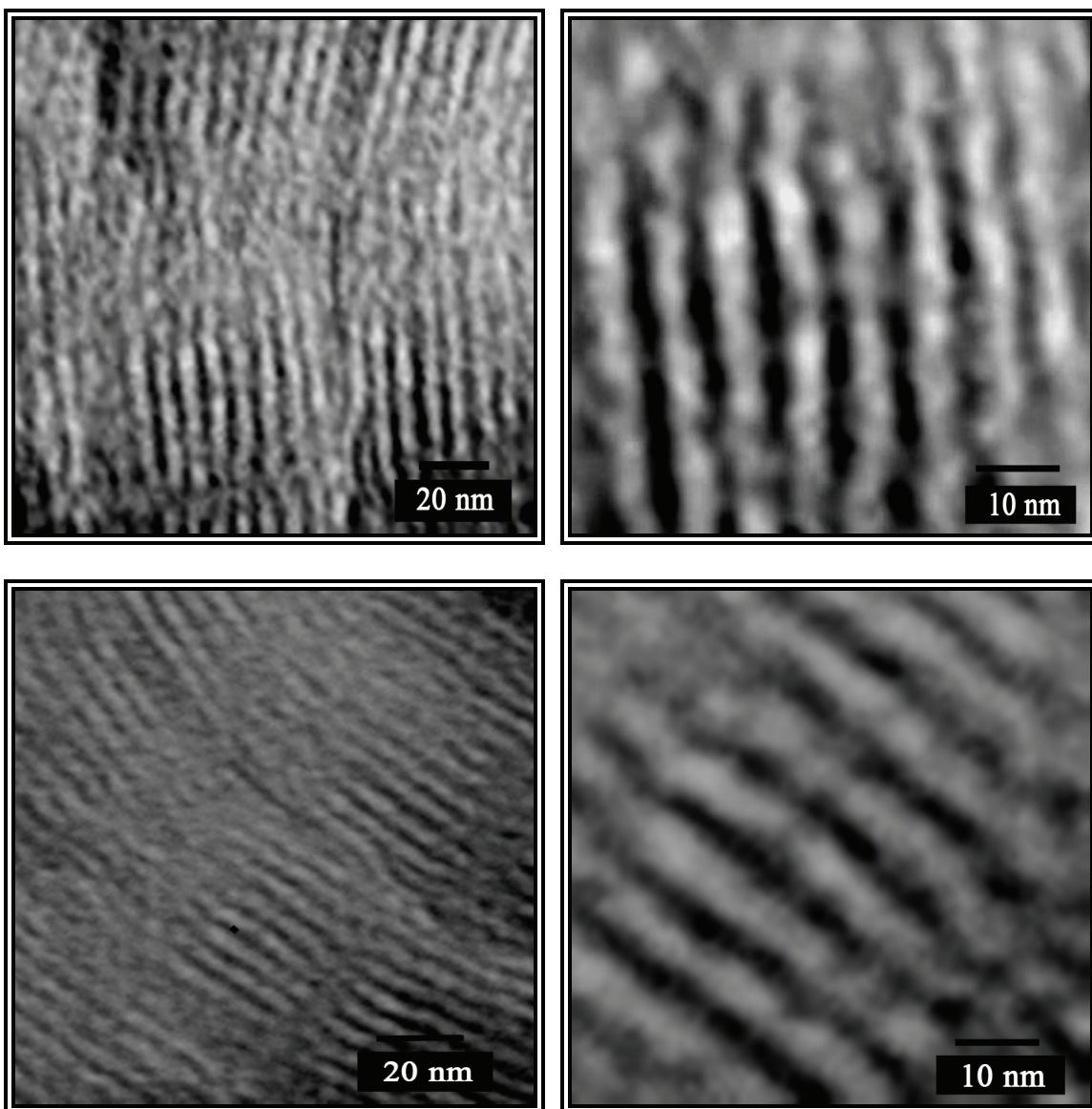
Figure 2.12. TEM images of mesoporous silica, OSU-6-W and OSU-6-C, show the pore diameter and wall thickness. The pore diameters are *ca.* 50 Å and wall thicknesses are *ca.* 20 Å.

2.10.3. Hydroxyl Group Concentration

The total hydroxyl group contents of several mesoporous materials obtained from the various synthetic routes are listed in Table 2.7. The listed values were obtained from the adsorption of cyclohexylamine and proton-sponge and from the solid state ^{29}Si NMR.

The data in Table 2.7 indicate that the hydroxyl groups on the surface of the synthesized mesoporous materials have widely variable total number of hydroxyl groups. These differences can be mainly attributed to the both variations in specific surface area and the availability and concentration of the active sites, and the structure of hydroxyl species on the surface.

Table 2.7. Total amount of hydroxyl (silanol) groups using Ultraviolet Titration and ^{29}Si CP/MAS NMR deconvolution results.

Sample	[SiOH] mmol/g (molecule/nm^2)		
	Cyclohexylamine	Proton-Sponge	Solid state ^{29}Si NMR
OSU-1-W	10.34 (5.86)	8.02 (4.54)	8.83 (5.00)
OSU-1-C	3.61 (2.20)	2.53 (1.54)	2.59 (1.58)
OSU-2-W	9.73 (5.73)	8.04 (4.73)	8.68 (5.11)
OSU-2-C	3.73 (2.33)	2.87 (1.79)	3.10 (1.94)
OSU-3-W	10.31 (5.91)	8.65 (4.95)	9.08 (5.20)
OSU-3-C	4.51 (2.62)	3.12 (1.81)	3.58 (2.08)
OSU-4-W	10.44 (5.77)	7.71 (4.26)	9.17 (5.07)
OSU-4-C	5.36 (3.01)	4.11 (2.31)	4.51 (2.53)
OSU-5-W	13.81 (6.56)	10.43 (4.96)	12.25 (5.82)
OSU-5-C	6.16 (3.30)	4.54 (2.43)	5.13 (2.75)
OSU-6-W	15.92 (7.47)	11.86 (5.56)	14.43 (6.77)
OSU-6-C	7.23 (3.59)	5.87 (2.92)	6.28 (3.12)

The proton-sponge measurements more closely reflected those of the solid state

NMR than do the cyclohexylamine measurements. This likely reflects that the latter

method also measures Lewis acid sites (*i.e.,* low valent Si atoms). Also the solid state

NMR results tend to be higher than the chemisorption, possibly reflecting internal OH

groups.

2.10.4. Stability Studies

2.10.4.1. Thermal Stability

Table 2.2 and Figure 2.13 show the surface areas and pore diameters calculated

from N_2 adsorption-desorption measurements and XRD for all solvent extracted and

thermally calcined mesoporous samples. As mentioned before, all the synthesized

materials, solvent-extracted and calcined samples, exhibit well-defined reflections at d_{100}

in their XRD patterns that are characteristic for hexagonal mesostructures. The surface

areas and pore diameters of all the solvent-extracted mesoporous materials gradually

decrease as the calcination temperature increases. However, the reduction in the surface

areas and pore diameters of all samples are small up to certain point after which the

reduction dramatically increases. The relative decrease in surface areas and pore

diameters are presented in Figure 2.13. In the case of the calcined mesoporous samples,

the surface areas and pore diameters were not affected by heat prior to 550 ^{o}C. However,

beyond this point the reduction occurs. From the thermal treatment study, these

mesoporous materials, in general, show high thermal stability compared with other

prepared MCM-41 materials as investigated by Cassiers *et al.,*[100] who reported that when

the M41S materials prepared with TEOS are subjected to a calcination temperature of

750 ^{o}C, they suffer an ~ 75% decrease in BET surface area, whereas, in the case of the

OSU-6-W and OSU-6-C mesoporous materials prepared in our laboratory using TEOS as silica source, around 80% of the initial surface area still remains after calcination at 750 ^{o}C for both samples. Moreover, unit cell contraction is almost negligible when the calcination temperature is increased from 550 to 850 ^{o}C (from 58.4 to 54.3 Å for OSU-6-W and from 59.1 to 54.6 Å for OSU-6-C). The synthesis conditions used by Cassiers *et al.*[100] are to some extent the same for the OSU materials prepared with TEOS.
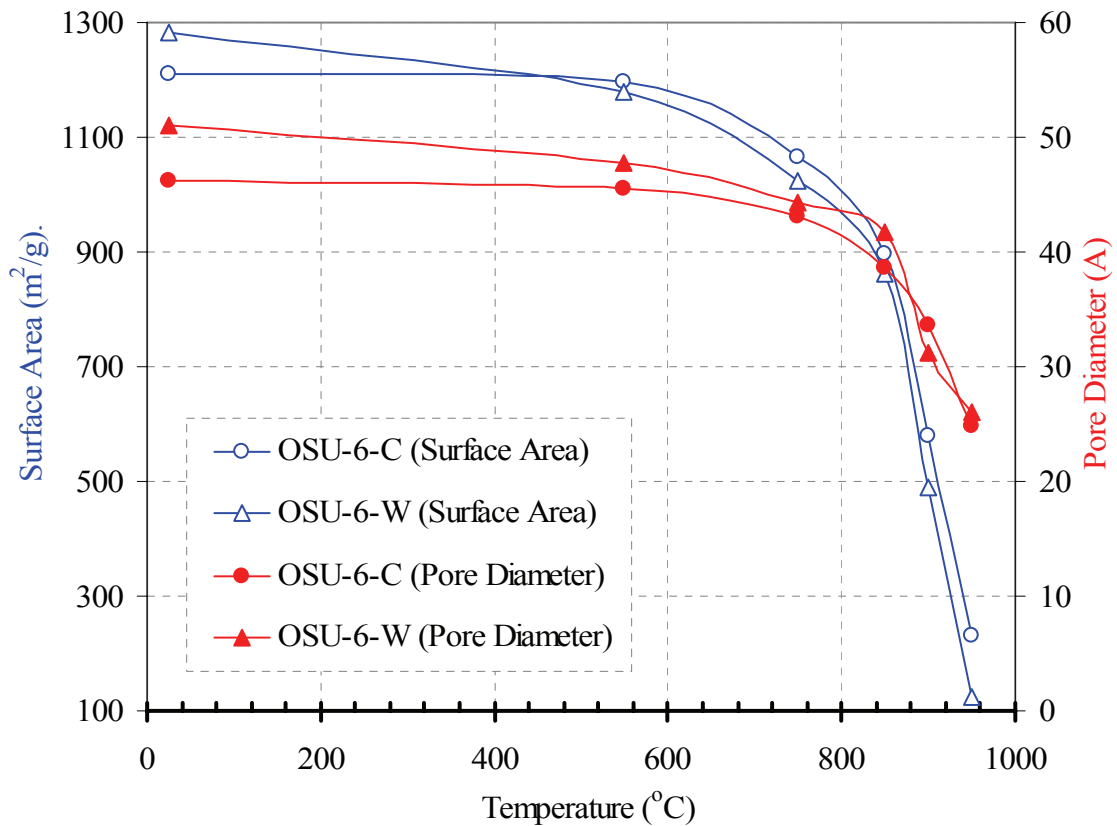
Figure 2.13. The thermal stability study illustrated by the effect of temperature on the surface areas and pore sizes of OSU-6-W and OSU-6-C mesoporous samples.

The differences in thermal stability are likely due to the difference in the wall thickness, Table 2.5, where the wall thickness of our materials is two times larger than that of the MCM-41 material prepared by others.[100] However, the other mesoporous silicas listed in Table 2.5 show a similar thermal stability trend to that of OSU-6-W and OSU-6-C, but their relative drop in surface areas are larger. For both samples, OSU-6-W and OSU-6-C, at a calcination temperature of 550 ^{o}C, the surface area is reduced to around ~ 80% of its initial value. However, at higher temperature big differences in surface area are noticed. At 850 ^{o}C, around ~ 75% of the initial surface area still remains. Figure 2.13 provides further evidence that the thermal stability of OSU-6 is higher than that of the other prepared mesoporous samples. All samples show the d_{100} reflection in the XRD diffraction pattern at a calcination temperature of 850 ^{o}C, but it disappears at 1000 ^{o}C as a result of the complete collapse of the framework's mesopores. From the surface area measurements, at a calcination temperature of 850 ^{o}C, only a small shrinkage of the BJH diameter (from 51.1 to 41.7 Å for OSU-6-W and from 47.2 to 38.7 Å for OSU-6-C) and a slight diminution of pore volume can be observed (see Table 2.2). Furthermore, the higher thermal stability of other OSU mesoporous materials compared to hexagonal TEOS-made materials with the same wall thickness can be attributed to the higher regular arrangement in the silica walls.[99]

2.10.4.2. Hydrothermal Stability

The hydrothermal stabilities of template-free mesoporous materials, calcined (OSU-6-C) and HCl-Ethanol washed (OSU-6-W) samples, were studied by boiling the samples in distilled water at various times ranging from 1 to 35 hours. The physical properties of the two mesoporous materials before and after the various hydrothermal

treatments are listed in Table 2.3. The changes in the surface areas and pore sizes of both samples were note noticeable at lower treatment time up to 25 hours, while small decreases in both the surface areas and pore sizes were observed with increasing time of treatment beyond this point, see Figure 2.14.
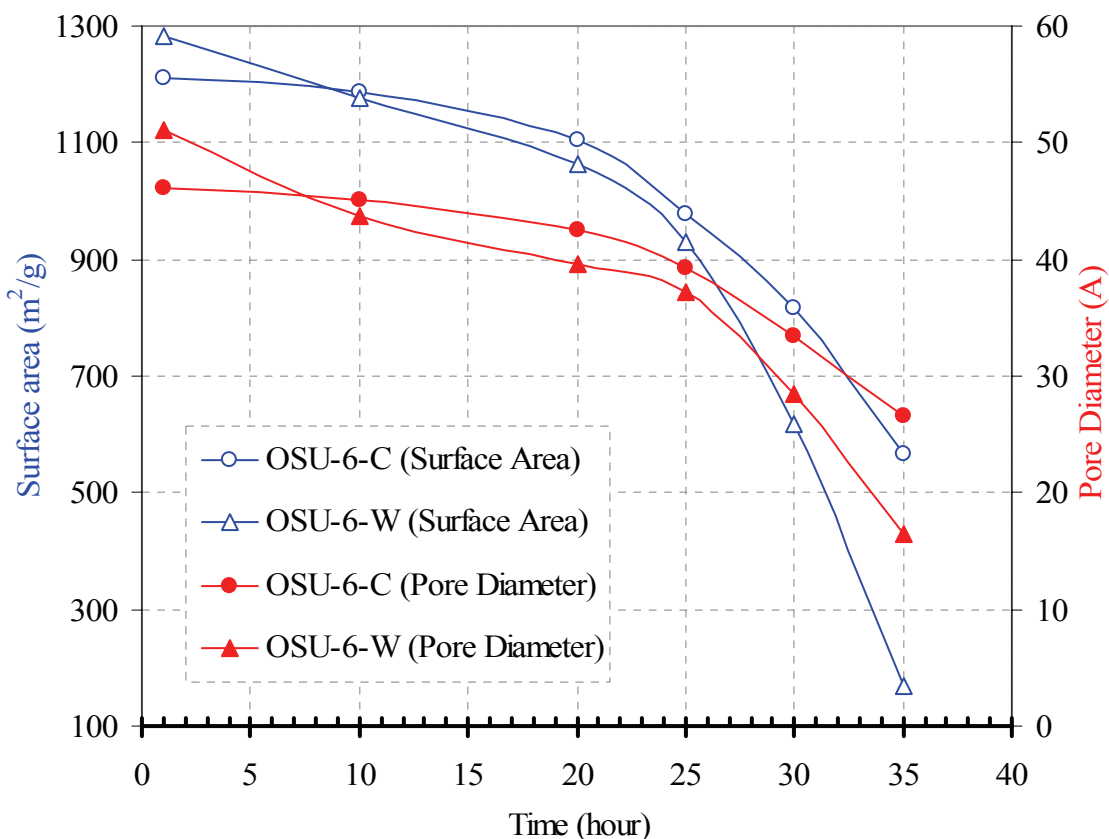
Figure 2.14. The hydrothermal stability study illustrated by the effect of boiling water on the surface areas and pore sizes of OSU-6-W and OSU-6-C mesoporous samples.

At about 25-30 hour treatment, more significant reduction occurs in both parameters for the two samples. At about 35 hours treatment, large reductions occur in both parameters for these two samples. These reductions are believed to be due to the rehydration of the siloxane groups (Q^4) and the formation of silanol groups (Q^3) and geminal silanol groups (Q^2) as confirmed by the solid state ^{29}Si NMR spectra of OSU-6-

C, Figure 2.15.[155] Moreover, from the pattern of the hydrothermal reaction it indicates a self-catalytic reaction.
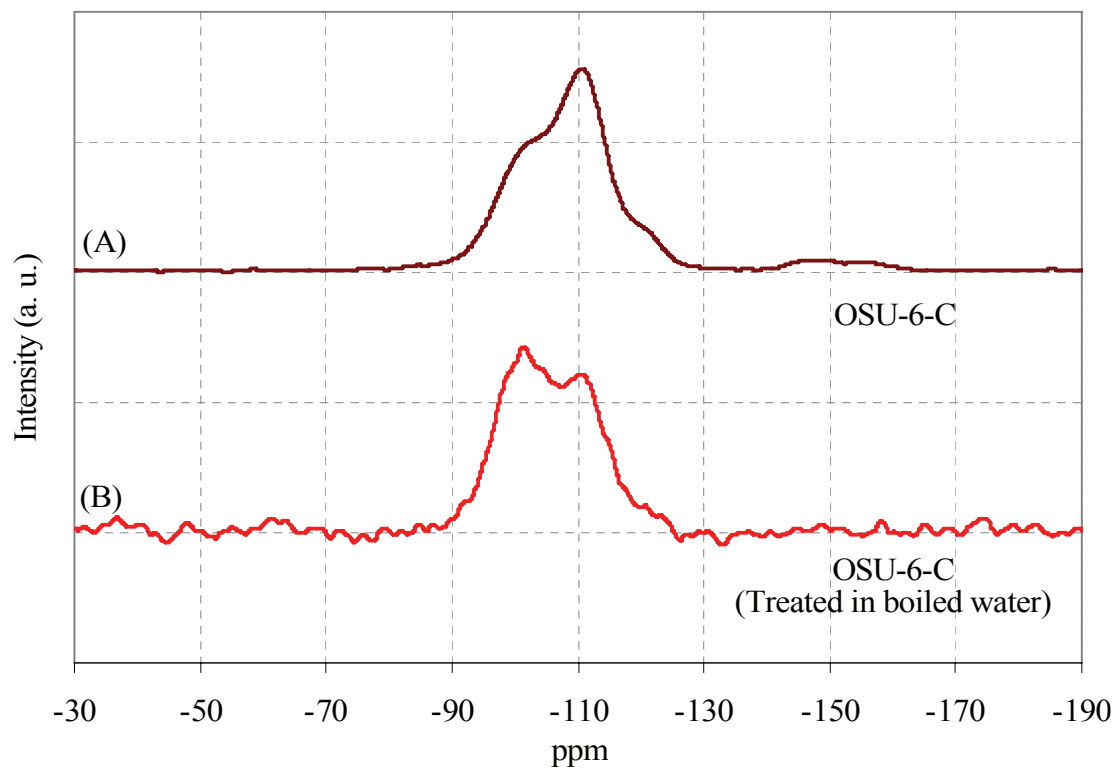
Figure 2.15. Solid state ^{29}Si CP/MAS NMR of OSU-6-C boiled in water for 35 hours.

These results indicate that the deformation of the mesoporous silicas by hydrothermal reactions does not follow the same trends as the thermal treatment. The calcined and washed samples have similar hexagonal ordering and comparable wall thicknesses and, therefore, behave similarly when calcined. However, OSU-6-W is much less hydrothermally stable than OSU-6-C. This difference can be explained by the differences in hydroxyl group contents, condensation degree of the silica wall, and to some degree, wall thickness. Chen *et al.*,[93] reported that the degree of polymerization in

the silica walls plays a crucial role in the hydrothermal stability by comparing a post-synthetically restructured MCM-41 with a non-restructured MCM-41. Moreover, one should note the difference in hydrothermal stability between OSU-6-W and OSU-6-C samples and MCM-41(T) material reported previously which displayed a hydrothermal stability less that 16 hours.[100] Despite the fact that these materials are synthesized with the same silica source (TEOS), OSU-6-W and OSU-6-C are hydrothermally much more stable than MCM-41(T) which showed a 87% loss in surface area (from 1128 to 145 m^2/g) after 16 hours hydrothermal treatement. It is reasonable to suggest that this higher hydrothermal stability of OSU-6-W and OSU-6-C materials are a result of the thicker pore walls (Table 2.5.) and is in agreement with the results reported in other papers.[94] It is believed that the structural degradation is caused by the hydrolysis of Si-O-Si bonds.[100,156] If the walls are thin, as in the case of MCM-41(T) (thicknesses of ~10 Å, which corresponds to only a few $[SiO_4]^{4-}$ groups), these structures collapse easily by hydrolysis. A possible explanation for the low structural damage under mild steaming conditions is the different pore structure and curvature, which results in a different nature of surface silanol groups.[155]

Figure 2.16 presents the XRD patterns of samples that were hydrothermally treated in boiling distilled water for 35 hours. The XRD intensity and the number of reflections were used to estimate the hydrothermal stability of the samples. The OSU-6-C sample still exhibited long-range order with one reflection detected after treatment in boiling water for 35 hour. The intensity of the d_{100} reflection decreased by about 50%, and the d_{100} spacing contracted considerably (~ 10 Å). The higher hydrothermal stability of the OSU-6-C sample was attributed to an enhancement of the wall thickness. The

hydrothermal stability can be increased be grafting with groups that have hydrophobic nature, which will protect the walls from the attack by water. The low Q^3/Q^4 ratio implies a less condensed silica wall structure of OSU-6-W compared to siliceous OSU-6-C, as well as the presence of more unprotected Si-OH groups, see Table 2.6.[33]
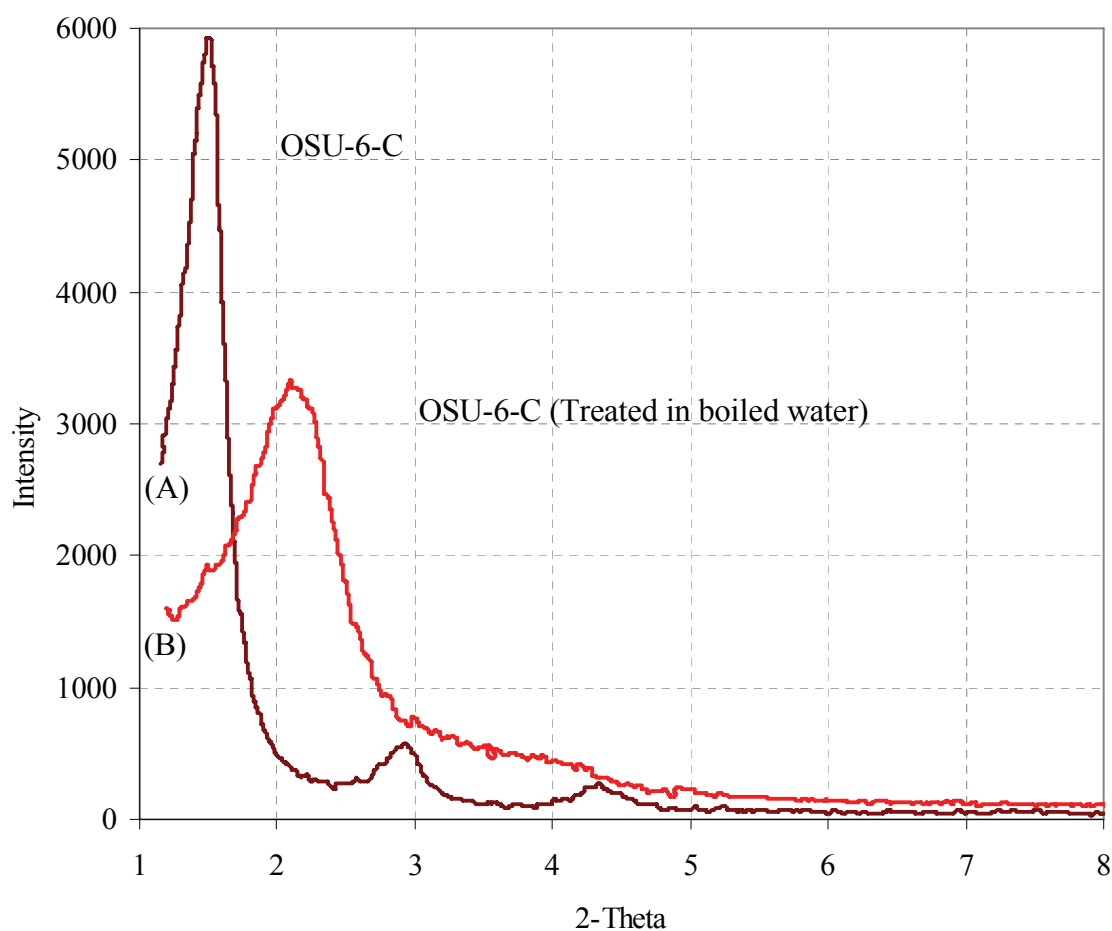
Figure 2.16. Powder XRD patterns of (A) OSU-6-C and (B) OSU-6-C after 35 hour hydrothermal treatment in boiling water.

2.10.4.3. Mechanical Stabilities

The mechanical stabilities of template-free, calcined and HCl-ethanol washed OSU-6 samples, were studied under different compression pressures (111, 333, 444, 500,

and 555 MPa). Table 2.4 and Figure 2.17 show the effect of compression on the surface

areas and pore sizes of these materials. The surface areas were noticed to be reduced

with increasing pressure until about 555 MPa where all mesoporous materials under

study lost the mesoporous structure and collapsed.
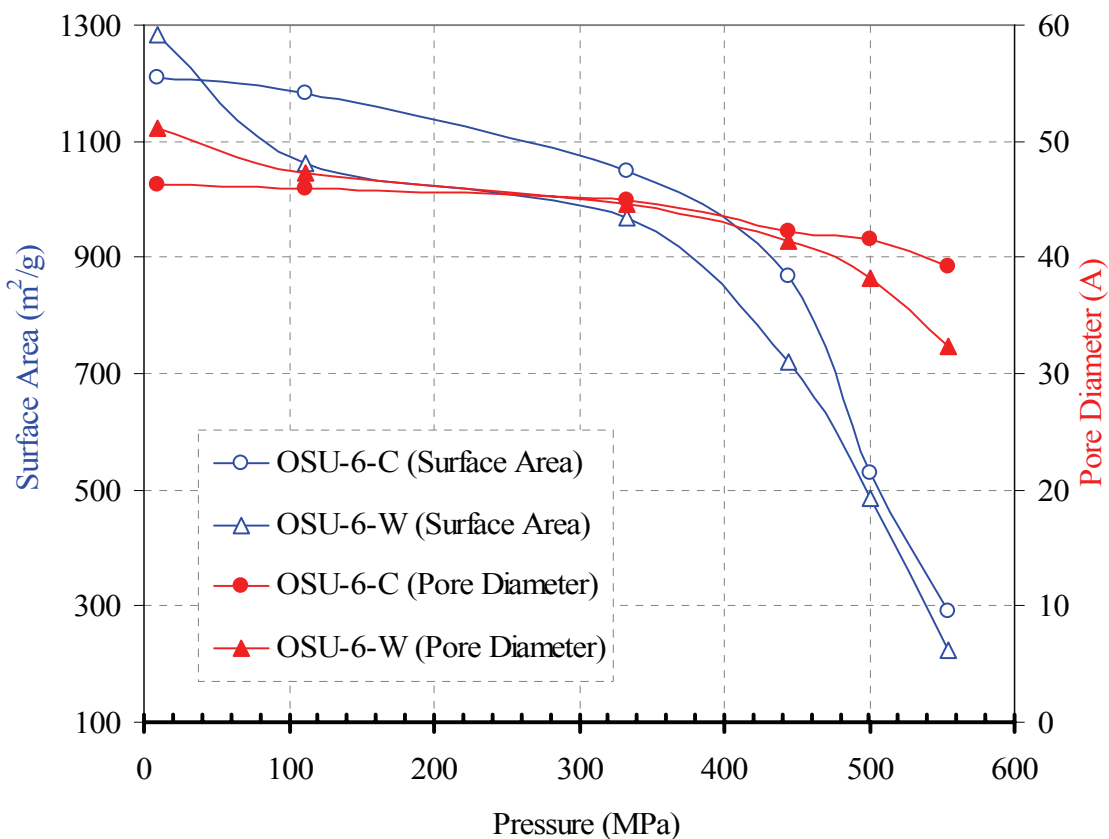
Figure 2.17. The mechanical stability study illustrated by the effect of compression on
the surface areas and pore sizes of OSU-6-W and OSU-6-C mesoporous samples.

The pore sizes calculated from the XRD d-spacing of the samples after each

compression indicate small reduction in the pore sizes that can be neglected. The slight

effect of the compression on the pore diameter indicates only minimal pore deformation

upon compression. This indicates either that some of the pores are blocked by other

particles of the same material or that less stable pores are completely collapsed due to compression while the residual pores are totally unaffected.

MCM-41(T)[100] has wall thickness of around 10 Å, which corresponds to only 3 $[SiO_4]^{4-}$ layers, whereas OSU-6-W and OSU-6-C have wall thicknesses of 20.9 and 21.1 Å, corresponding to around 7 $[SiO_4]^{4-}$ layers. Furthermore, as mentioned above, OSU-6-C has very condensed silica walls. Consequently, it is not surprising that the much thicker pore walls of OSU-6-C and the highly polymerized walls are less affected by this systematic mechanical cleavage process than the MCM-41(T) which collapses at 370 MPa. Nevertheless, it should be emphasized that both OSU-6-W and OSU-6-C show an extremely low intensity peak in the X-ray diffraction patterns after a pelletizing pressure of 555 MPa despite their good stability at a mechanical pressure at 500 MPa. The large porosity and the absence of a stabilizing crystal structure can explain the relatively slight differences in the final mechanical stabilities of all studied materials. However, these materials show good mechanical stabilities when compare to zeolites.[100,157,159]

A more detailed examination of the physical data permits a closer look at the influence of unilateral pressure on the structural properties of the mesoporous materials. As can be seen in Figure 2.17, the specific surface areas are reduced in both cases, whereas the BJH pore diameter and the cell parameter are slightly affected. Furthermore, the pore size distributions for these materials are only slightly broadened, which indicates only minimal pore deformation upon compression. This indicates either that some of the pores are blocked by other particles of the same material or that less stable pores are completely collapsed due to compression while the residual pores are totally unaffected.

2.11. CONCLUSIONS

Many new mesoporous materials based on hexagonal MCM-41 silicas have been synthesized and characterized using a variety of techniques. These mesoporous materials have been synthesized following a templated technique demonstrated by the presence of characteristic X-ray diffraction peaks, nitrogen adsorption-desorption isotherms, and TEM images. Mesoporous systems of regular mesopores and high surface areas were confirmed. The mesoporous materials prepared in this investigation exhibit hexagonal mesostructure with large wall thickness.

The current study showed that the applied synthetic procedures allow for tailoring of pore sizes and wall thicknesses and are suitable for preparation of high-quality mesoporous materials. It was shown that the pore wall thickness estimated on the basis of N_2 adsorption/XRD data is in acceptable agreement with the results of TEM. The latter technique indicates somewhat larger pore wall thickness, which can be attributed, at least in part, to the nature of the evaluation procedures. Both of these approaches consistently show that the pore wall thickness for the samples tend to increase as the pore size increases. In calculations of the pore wall thickness on the basis of adsorption/XRD data, it needs to be kept in mind that the pores of the OSU mesoporous materials are likely to be hexagonal rather than circular, although it is not fully clear if this conclusion is general or just extends over certain OSU silicas.

These materials show large pore sizes of about 51 Å, narrow pore size distributions (3.5 Å), high surface areas of up to 1283 m^2/g, and wall thicknesses of about 21 Å.

Neutral amine surfactant assembly is a most convenient synthesis methodology, allowing the one-step preparation of mesostructure materials in which both organic loading and pore dimensions can be accurately tuned by reagent stoichiometry control. Unlike electrostatic S^+I^-, S^-I^+, or $S^+X^-I^+$ mesostructure formation mechanisms, the S^0I^0 templating mechanism involved in the formation of OSU silica mesoporous molecular sieves allows the complete removal and recovery of neutral amine assembly surfactants from the mesostructures by HCl-ethanol extraction. In addition, the resulting materials retain a very large surface silanol concentration suitable for the anchoring of functional groups by post-synthesis grafting method.

Removal of the templating molecules by calcination in air resulted in a partial contraction of the mesopores. Solvent-extracted materials were thermally stable and could be calcined at 550 ^{o}C in air without modification of the coordination or structure, however, a small lattice contraction was noticed.

After activation (removal of surfactant), these materials reveal promising properties as packing materials in chromatography and as catalyst supports based on their extremely high surface area and easy accessibility of the pore system. Nevertheless, despite many advantages of using the materials, leaching of active grafted species or incorporated active elements and collapsing of the mesoporous structure may occur as a result of the conditions during separation or catalysis process. A key issue for the applicability of these mesoporous materials is associated with the thermal, and more importantly the hydrothermal and mechanical stabilities. Important improvements were realized by developing these materials with thicker and more condensed silicate walls.

These mesoporous materials exhibit high thermal stability of up to 950 $^{\circ}$C before the complete collapsing of the structure. The thermal stability is found to be strongly related to the wall thickness which is affected by the silica/surfactant ratio, aging time and catalyst as can be compared with previous work.

High hydrothermal stabilities at boiling degree of water for up to 35 hour were observed for these mesoporous materials. These hydrothermal stabilities were found to be influenced mainly by the wall thickness and the degree of condensation (hydroxyl concentration).

No remarkable trends could be observed for the mechanical stability of the HCl-ethanol washed and calcined samples (*e.g.,* OSU-6-W and OSU-6-C). The mesoporosity is essentially lost for all mesostructures at pelletizing pressure approximately 555 MPa. Nevertheless, these ordered mesoporous structures show an inferior mechanical stability compared to zeolites, which may result from their large porosity and the absence of a stabilizing crystal structure.

Finally, these mesoporous materials show high thermal, hydrothermal and mechanical stability comparable with those prepared previously from the same starting materials. This can be explained by their three times thicker pore walls and more highly condensed silica walls in the case of calcined samples. The synthetic routes presented are thus very promising for preparing high quality template-free mesoporous silicas.

2.12. REFERENCES

1. Kresge, C. T.; Leonowics, M. E.; Roth; W. J.; Vartulli, J. C.; Beck, J. S.. Ordered mesoporous molecular sieves synthesized by a liquid-crystal template mechanism. *Nature* **1992,** *359*(6397), 710-712.

2. (a) Beck, J. S.; Vartuli, J. C.; Roth, W. J.; Leonowics, M. E.; Kresge, C. T.; Schmitt, K. D.; Chu, C. T.-W.; Olson, D. H.; Sheppard, E. W.; McCullen, S. B.; Higgings, J. B.; Schlenker, J. L.. A new family of mesoporous molecular sieves prepared with liquid crystal templates. *J. Am. Chem. Soc.* **1992,** *114*(27), 10834-10843. (b) Vartuli, J. C.; Schmitt, K. D.; Kresge, C. T.; Roth, W. J.; Leonowicz, M. E.; McCullen, S. B.; Hellring, S. D.; Beck, J. S.; Schlenker, J. L.; Olson, D. H.; Sheppard, E. W.. Effect of Surfactant/Silica Molar Ratios on the Formation of Mesoporous Molecular Sieves: Inorganic Mimicry of Surfactant Liquid-Crystal Phases and Mechanistic Implications. *Chem. Mater.* **1994,** *6*(12), 2317-2326.

3. Tanev, P. T.; Pinnavaia, T. J.. A neutral templating route to mesoporous molecular sieves. *Science* **1995,** *267*(5199), 865-867.

4. Tanev, P. T.; Chibwe, M.; Pinnavaia, T. J.. Titanium-containing mesoporous molecular sieves for catalytic oxidation of aromatic compounds. *Nature* **1994,** *368*(6469), 321-323.

5. Inagaki, S.; Fukushima, Y.; Kuroda, K. Synthesis of highly ordered mesoporous materials from a layered polysilicate. *J. Chem. Soc., Chem. Commun.* **1993,** *8,* 680-682.

6. Galarneau, A.; Barodawalla, A.; Pinnavaia, T. J.. Porous clay heterostructures formed by gallery-templated synthesis. *Nature* **1995,** *374*(6522), 529-531.

7. Zhao, D.; Feng, J.; Huo, Q.; Melosh, N.; Frederickson, G. H.; Chmelka, B. F.; Stucky, G. D.. Triblock copolymer syntheses of mesoporous silica with periodic 50 to 300 angstrom pores. *Science* **1998,** *279*(5350), 548-552.

8. Bagshaw, S. A.; Prouzet, E.; Pinnavaia, T. J.. Templating of mesoporous molecular sieves by nonionic polyethylene oxide surfactants. *Science* **1995,** *269*(5228), 1242-1244.

9. Ryoo, R.; Kim, J. M.; Ko, C. H.; Shin, C. H.. Disordered Molecular Sieve with Branched Mesoporous Channel Network. *J. Phys. Chem.* **1996,** *100*(45), 17718-17721.

10. Moller, K.; Bein, T.. Inclusion Chemistry in Periodic Mesoporous Hosts. *Chem. Mater.* **1998,** *10*(10), 2950-2963.

11. Diaz, J. F.; Balkus, K. J., Jr.. Enzyme immobilization in MCM-41 molecular sieve. *J. Mol. Catal. B*: *Enzymatic* **1996,** *2*(2-3), 115-126.

12. Xu, W.; Luo, Q.; Wang, H.; Francesconi, L. C.; Stark, R. E.; Akins, D. L.. Polyoxoanion Occluded within Modified MCM-41: Spectroscopy and Structure. *J. Phys. Chem. B*, **2003,** *107*(2), 497-501.

13. Llewellyn, P. L.; Ciesla, U.; Decher, H.; Stadler, R.; Schueth, F.; Unger, K. K.. MCM-41 and Related Materials as Media for Controlled Polymerization Processes. *Stud. Surf. Sci. Catal.* **1994,** *84*, 2013-2020.

14. Corma, A.; Fornés, V.; Navarro, M. T.; Pérez-Patiente, J.. Acidity and stability of MCM-41 crystalline aluminosilicates. *J. Catal.* **1994,** *148*(2), 569-574.

15. Raimondo, M.; Perez, G.; Sinibaldi, M.; De Stefanis, A.; Tomlinson, A. A. G.. Mesoporous M41S materials in capillary gas chromatography. *Chem. Commun.* **1997,** *15,* 1343-1344.

16. Grün, M.; Kurganoz, A. A.; Schacht, S.; Schütz, F.; Unger, K. K. Comparison of an ordered mesoporous aluminosilicate, silica, alumina, titania and zirconia in normal-phase high-performance liquid chromatography. *J. Chromatogr. A* **1996,** *740*(1), 1-9.

17. Sierra, L.; Lopez, B.; Guth, J.-L. Preparation of mesoporous silica particles with controlled morphology from sodium silicate solutions and a non-ionic surfactant at pH values between 2 and 6. *Microporous Mesoporous Mater.* **2000,** *39*(3), 519-527.

18. Berggren, A.; Palmqvist, A. E. C.; Holmberg, K.. Surfactant-templated mesostructured materials from inorganic silica. *Soft Matter* **2005,** *1*(3), 219-226.

19. Sakamoto, Y.; Kaneda, M.; Terasaki, O.; Zhao, D.; Kim, J. M.; Stucky, G. D.; Shin, H. J.; Ryoo, R.. Direct imaging of the pores and cages of three-dimensional mesoporous materials. *Nature* **2000,** *408*(6811), 449-453.

20. Che, S.; Sakamoto, Y.; Terasaki, O.; Tatsumi, T.. Control of crystal morphology of SBA-1 mesoporous silica. *Chem. Mater.* **2001,** *13*(7), 2237-2239.

21. Stein, A.; Melde, B. J.; Schroden, R.. Hybrid Inorganic-organic Mesoporous Silicates Nanoscopic Reactors Coming of Age. *Adv. Mater.* **2000,** *12*(19), 1403-1419.

22. Ryoo, R.; Jun, S.. Improvement of Hydrothermal Stability of MCM-41 Using Salt Effects during the Crystallization Process. *J. Phys. Chem. B* **1997,** *101*(3), 317-320.

23. Tanev, P. T.; Pinnavaia T.. Mesoporous Silica Molecular Sieves Prepared by Ionic and Neutral Surfactant Templating: A Comparison of Physical Properties. *J. Chem. Mater.* **1996,** *8*(8), 2068-2079.

24. Prouzet, Eric; Pinnavaia, Thomas J. Assembly of mesoporous molecular sieves containing wormhole motifs by a nonionic surfactant pathway: control of pore size by synthesis temperature. *Angew. Chem., Int. Ed. Engl.* **1997,** *36*(5), 516-518.

25. Kim, S. S.; Zhang, W.; Pinnavaia, T. J.. Ultrastable Mesostructured Silica Vesicles. *Science* **1998,** *282*(5392), 1302-1305.

26. Huo, Q.; Leon, R.; Petroff, P. M.; Stucky, G. D.. Mesostructure design with gemini surfactants: supercage formation in a three-dimensional hexagonal array. *Science* **1995,** *268*(5215), 1324-1327.

27. Zhao, D.; Yang, P.; Huo, Q.; Chmelka, B.; Stucky, G. D.. Topological construction of mesoporous materials. *Curr. Opin. Solid State Mater. Sci.* **1998,** *3*(1), 111-121.

28. Zhao, D.; Huo, Q.; Feng, J.; Chmelka, B.; Stucky, G. D.. Nonionic triblock and star diblock copolymer and oligomeric surfactant syntheses of highly ordered, hydrothermally stable, mesoporous silica structures. *J. Am. Chem. Soc.* **1998,** *120*(24), 6024-6036.

29. Schmidt-Winkel, P.; Lukens, W. W.; Yang, P.; Margolese, D. I.; Lettow, J. S.; Ying, J. Y.; Stucky, G. D.. Microemulsion templating of siliceous mesostructured cellular foams with well-defined ultralarge mesopores. *Chem. Mater.* **2000,** *12*(3), 686-696.
30. Kisler, J. M.; Gee, M. L.; Stevens, G. W.; O'Connor, A. J.. Comparative study of silylation methods to improve the stability of silicate MCM-41 in aqueous solutions. *Chem. Mater.* **2003,** *15*(3), 619-624.
31. Mercier, L.; Pinnavaia, T. J.. Access in mesoporous materials. Advantages of a uniform pore structure in the design of a heavy metal ion adsorbent for environmental remediation. *Adv. Mater.* **1997,** *9*(6), 500-503.
32. Feng, X.; Fryxell, G. E.; Wang, L.-Q.; Kim, A. Y.; Liu, J.; Kemner, K. M. Functionalized Monolayers on Ordered Mesoporous Supports. *Science* **1997,** *276*(5314), 923-926.
33. Lim, M. H.; Stein, A. Comparative Studies of Grafting and Direct Syntheses of Inorganic-Organic Hybrid Mesoporous Materials. *Chem. Mater.* **1999,** *11*(11), 3285-3295.
34. Yamamoto, K.; Tatsumi, T.. Organic functionalization of mesoporous molecular sieves with Grignard reagents. *Micropor. Mesopor. Mater.* **2001,** *44-45,* 459-464.
35. Ribeiro Carrott, M. M. L.; Estevao Candeias, A. J.; Carrott, P. J. M.; Unger, K. K.. Evaluation of the Stability of Pure Silica MCM-41 toward Water Vapor. *Langmuir* **1999,** *15*(26), 8895-8901.
36. Zhao, X. S.; Audsley, F.; Lu, G.. Irreversible Change of Pore Structure of MCM-41 upon Hydration at Room Temperature. *J. Phys. Chem. B* **1998,** *102*(21), 4143-4146.
37. Igarashi, Naoko; Tanaka, Yoshinori; Nakata, Shin-Ichi; Tatsumi, Takashi. Increased stability of organically modified MCM-41 synthesized by a one-step procedure. *Chem. Letters* **1999,** *1,* 1-2.
38. Landau, M. V.; Varkey, S. P.; Herskowitz, M.; Regev, O.; Pevzner, S.; Sen, T.; Luz, Z.. Wetting stability of Si-MCM-41 mesoporous material in neutral, acidic and basic aqueous solutions. *Micropor. Mesopor. Mater.* **1999,** *33*(1-3), 149-163.
39. Trong, O. D., Zaidi, S. M. J., Kaliaguine, S.. Stability of mesoporous aluminosilicate MCM-41 under vapor treatment, acidic and basic conditions. *Micropor. Mesopor. Mater.* **1998,** *22*(1-3), 211-224.
40. Gusev, V. Y.; Feng, X.; Bu, Z.; Haller, G. L.; O'Brien, J. A. Mechanical Stability of Pure Silica Mesoporous MCM-41 by Nitrogen Adsorption and Small-Angle X-ray Diffraction Measurements. *J. Phys. Chem.* **1996,** *100*(6), 1985-1988.
41. (a). Jentys, A.; Kleestorfer, K.; Vinek, H.. Concentration of Surface Hydroxyl Groups on MCM-41. *Micropor. Mesopor. Mater.* **1999,** *27,* 321-328. (b). Jentys, A.; Pham, N. H. Vinek, H.. Nature of hydroxy groups in MCM-41. *J. Chem. Soc., Faraday Trans.* **1996,** *92*(17), 3287-3291.
42. Ryoo, R.; Kim, J.. Structural Order in MCM-41 Controlled by Shifting Silicate Polymerization Equilibrium. *J. Chem. Soc., Chem. Commun.* **1995,** *7,* 711-712.
43. Mokaya, R.; Zhou, W.; Jones, W.. Restructuring of mesoporous silica: high quality large crystal MCM-41 via a seeded recrystallization route. *J. Mater. Chem.* **2000,** *10*(5), 1139-1145.
44. Alsyouri, H. M.; Lin, Y. S.. Effects of Synthesis Conditions on Macroscopic and Microscopic Properties of Ordered Mesoporous Silica Fibers. *Chem. Mater.* **2003,** *15*(10), 2033-2039.

45. Setoguchi, Y. M.; Teraoka, Y.; Moriguchi, I.; Kagawa, S.; Tomonaga, N.; Yasutake, A.; Izumi, J.. Rapid room temperature synthesis of hexagonal mesoporous silica using inorganic silicate sources and cationic surfactants under highly acidic conditions. *J. Porous Mater.* **1997,** *4*(2), 129-134.

46. Klotz, M.; Ayral, A.; Guizard, C.; Cot, L.. Synthesis conditions for hexagonal mesoporous silica layers. *J. Mater. Chem.*, **2000,** *10,* 663-669.

47. Che, S.; Garcia-Bennett, A. E.; Yokoi, T.; Sakamoto, K.; Kunieda, H.; Terasaki, O.; Tatsumi, T.. A novel anionic surfactant templating route for synthesizing mesoporous silica with unique structure. *Nat. Mater.*, **2003,** *2*(12), 801–805.

48. Newalkar, B. L.; Katsuki, H.; Komarneni, S.. Microwave-hydrothermal synthesis and characterization of microporous–mesoporous disordered silica using mixed-micellar-templating approach. *Micropor. Mesopor. Mater.*, **2004,** *73*(21), 161–170.

49. Han, S.; Hou, W.; Dang, W.; Xu, J.; Hu, J.; Li, D.. Synthesis of rod-like mesoporous silica with hexagonal appearance using sodium silicate as precursor. *Colloid Polym. Sci.,* **2004,** *282*(7), 761–765.

50. Xu, J.; Han, S.; Hou, W.; Dang, W.; Yan, X.. Synthesis of high-quality MCM-48 mesoporous silica using cationic Gemini surfactant C12-2-12. *Colloids Surf., A*, **2004,** *248*(1-3), 75–78.

51. Frasch, J.; Lebeau, B.; Soulard, M.; Patarin, J.; Zana, R.. In Situ Investigations on Cetyltrimethylammonium Surfactant/Silicate Systems, Precursors of Organized Mesoporous MCM-41-Type Siliceous Materials. *Langmuir*, **2000,** *16*(23), 9049–9057.

52. Shio, S.; Kimura, A.; Yamaguchi, M.; Yoshida, K.; Kuroda, K.. Morphological control of ordered mesoporous silica: formation of fine and rod-like mesoporous powders from completely dissolved aqueous solutions of sodium metasilicate and cationic surfactants. *Chem. Commun.*, **1998,** 2461–2462.

53. Park, S. -E.; Kim, D. S.; Chang, J. -S.; Kim, W. Y.. Synthesis of MCM-41 using microwave heating with ethylene glycol. *Catal. Today*, **1998,** *44*(1-4), 301–308.

54. Huo, Q.; Margolese, D. I.; Ciesla, U.; Feng, P.; Gier, T. E.; Sieger, P.; Leon, R.; Petroff, P. M.; Schuth, F.; Stucky, G. D.. Generalized synthesis of periodic surfactant/inorganic composite materials. *Nature* **1994**, *368*(6469), 317-321.

55. Huo, Q.; Margolese, D. I.; Ciesla, U.; Demuth, D. G.; Feng, P.; Gier, T. E.; Sieger, P.; Forouzi, A.; Chmelka, B. F.; Schuth, F.; Stucky, G. D.. Organization of Organic Molecules with Inorganic Molecular Species into Nanocomposite Biphase Arrays. *Chem. Mater.* **1994**, *6*(8), 1176-1191.

56. Mercier, L.; Pinnavaia, T. J. Direct Synthesis of Hybrid Organic-Inorganic Nanoporous Silica by a Neutral Amine Assembly Route: Structure-Function Control by Stoichiometric Incorporation of Organosiloxane Molecules. *Chem. Mater.* **2000,** *12*(1), 188-196.

57. Corma, A.. From Microporous to Mesoporous Molecular Sieve Materials and Their Use in Catalysis. *Chem. Rev.* **1997,** *97*(6), 2373-2419.

58. Sayari, A.; Karra, V. R.; Reddy, J. S.; Moudrakovski, I.. Synthesis, characterization and modification of MCM-41 molecular sieves. *Mater. Res. Soc. Symp. Proc.* **1995,** *371,* 81-86.

59. Ulagappan, N.; Rao, C. N. R.. Evidence of supramolecular organization of alkane and surfactant molecules in the process of forming mesoporous silica. *J. Chem. Soc., Chem. Commun.* **1996,** *24,* 2759-2760.

60. Namba, S.; Mochizuki, A. Effect of auxiliary chemicals on preparation of silica MCM-41. *Res. Chem. Interm.* **1998,** *24*(5), 561-570.

61. Namba, S.; Mochizuki, A.; Kito, M.. Fine control of pore size of highly ordered MCM-41 by using template mixtures of dodecyltrimethylammonium bromide/hexadecyltrimethylammonium bromide with various molar ratios. *Chem. Letters* **1998,** *7,* 569-570.

62. Holmberg, K.. Surfactant-templated nanomaterials synthesis. *J. Colloid Interface Sci.*, **2004,** *274*(2), 355–365.

63. Palmqvist, A. E. C.. Synthesis of ordered mesoporous materials using surfactant liquid crystals or micellar solutions. *Curr. Opin. Colloid & Interface Sci.* **2003,** *8*(2), 145-155.

64. Patarin, J.; Lebeau, B.; Zana, R.. Recent advances in the formation mechanisms of organized mesoporous materials. *Curr. Opin. Colloid Interface Sci.* **2002,** *7*(1,2), 107-115.

65. Attard, G. S.; Glyde, J. C.; Göltner, C. G.. Liquid-crystalline phases as templates for the synthesis of mesoporous silica. *Nature*, **1995,** *378*(6555), 366–368.

66. Kim, S. -S.; Pauly, T. R.; Pinnavaia, T. J.. Non-ionic surfactant assembly of ordered, very large pore molecular sieve silicas from water soluble silicates. *Chem. Commun.*, **2000,** 1661–1662.

67. Kim, S. -S.; Pauly, T. R.; Pinnavaia, T. J.. Non-ionic surfactant assembly of wormhole silica molecular sieves from water soluble silicates. *Chem. Commun.*, **2000,** 835–836.

68. Kim, S. S.; Karkamkar, A.; Pinnavaia, T. J.; Kruk, M.; Jaroniec, M.. Synthesis and Characterization of Ordered, Very Large Pore MSU-H Silicas Assembled from Water-Soluble Silicates. *J. Phys. Chem. B,* **2001,** *105,* 7663–7670.

69. Kim, J. M.; Sakamoto, Y.; Hwang, Y. K.; Kwon, Y. U.; Terasaki, O.; Park, S. E.; Stucky, G. D.. Structural Design of Mesoporous Silica by Micelle-Packing Control Using Blends of Amphiphilic Block Copolymers. *J. Phys. Chem. B,* **2002,** *106*(10), 2552–2558.

70. Kim, J. M.; Stucky, G. D.. Synthesis of highly ordered mesoporous silica materials using sodium silicate and amphiphilic block copolymers. *Chem. Commun.*, **2000,** 1159–1160.

71. Kosuge, K. K. N.; Takemori, M.. One-Step Preparation of Porous Silica Spheres from Sodium Silicate Using Triblock Copolymer Templating. *Chem. Mater.*, **2004,** *16,* 4181–4186.

72. Kosuge, K. S. T.; Kikukawa, N.; Takemori, M.. Morphological Control of Rod- and Fiberlike SBA-15 Type Mesoporous Silica Using Water-Soluble Sodium Silicate. *Chem. Mater.*, **2004,** *16*(5), 899–905.

73. Sierra, L.; Guth, J. L.. Synthesis of mesoporous silica with tunable pore size from sodium silicate solutions and a polyethylene oxide surfactant. *Micropor. Mesopor. Mater.*, **1999,** *27*(2-3), 243–253.

74. Boissiere, C.; Larbot, A.; Prouzet, E.. Synthesis of Mesoporous MSU-X Materials Using Inexpensive Silica Sources. *Chem. Mater.*, **2000,** *12*(7), 1937–1940.

75. Kipkemboi, P.; Fogden, A.; Alfredsson, V.; Flodstrom, K.. Triblock Copolymers as Templates in Mesoporous Silica Formation: Structural Dependence on Polymer Chain Length and Synthesis Temperature. *Langmuir* **2001,** *17*(17), 5398–5402.

76. Coleman, N. R.; Attard, G. S.. Ordered mesoporous silicas prepared from both micellar solutions and liquid crystal phases. *Micropor. Mesopor. Mater.* **2001**, *44-45,* 73–80.

77. Coustel, N.; Renzo, F. D.; Fajula, F.. Improved stability of MCM-41 through textural control. *J. Chem. Soc., Chem. Commun.* **1994**, *8,* 967-968.

78. Chao, M. -C.; Lin, H. -P.; Wang, D. -S.; Mou, C. Y.. Synthesis of SBA-1 mesoporous silica crystals with tunable pore size using sodium silicate and alkyltrimethylammonium surfactants. *Chem. Lett.*, **2004,** *33*(4), 374–375.

79. Chao, M. -C.; Wang, D. -S.; Lin, H. -P.; Mou, C. -Y.. Control of single crystal morphology of SBA-1 mesoporous silica. *J. Mater. Chem.*, **2003,** *13,* 2853–2854.

80. Gross, A. F.; Ruiz, E. J.; Le, V. H.; Tolbert, S. H.. The role of silica chemistry in controlling phase transitions in silica/surfactant composite materials. *Micropor. Mesopor. Mater.* **2001,** *44-45*, 785–791.

81. Boissière, C.; Larbot, A.; van der Lee, A.; Kooyman, P. J.; Prouzet, E.. A New synthesis of mesoporous MSU-X silica controlled by a two-step pathway. *Chem. Mater.* **2000,** *12*(10), 2902–2913.

82. Edler, K. J.; White, J. W.. Room-temperature Formation of Molecular Sieve MCM-41. *J. Chem. Soc., Chem. Commun.* **1995,** *2,* 155-156.

83. Stucky, G. D.; Monnier, A.; Schueth, F.; Huo, Q.; Margolese, D.; Kumar, D.; Krishnamurty, M.; Petroff, P.; Firouzi, A.; *et al.* Molecular and atomic arrays in nano- and mesoporous materials synthesis. *Mol. Cryst. Liq. Cryst.* **1994,** *240,* 187-200.

84. (a) Chen, C. Y.; Li, H. X.; Davis, M. E.. Studies on mesoporous materials. I. Synthesis and characterization of MCM-41. *Micropor. Mater.* **1993,** *2*(1), 17-26. (b) Chen, C. Y.; Burkett, S. L.; Li, H. X.; Davis, M. E. Studies on mesoporous materials. II. Synthesis mechanism of MCM-41. *Micropor. Mater.* **1993,** *2*(1), 27-34.

85. (a) Cheng, C. F.; Zhou, W. Z.; Park, D. H.; Klinowski, J.; Hargreaves, M.; Gladden, F.. Controlling the channel diameter of the mesoporous molecular sieve MCM-41. *J. Chem. Soc., Faraday Trans.* **1997**, *93*(2), 359-363. (b) Cheng, C. F.; Luan, Z.; Klinowski, J.. The Role of Surfactant Micelles in the Synthesis of the Mesoporous Molecular Sieve MCM-41. *Langmuir* **1995,** *11*(7), 2815-2819.

86. Cheng, C. F.; Park, D. H.; Klinowski, J.. Optimal parameters for the synthesis of the mesoporous molecular sieve [Si]-MCM-41. *J. Chem. Soc., Faraday Trans.* **1997**, *93*(1), 193-197.

87. Edler, K. J.; White, J. W.. Preparation dependent stability of pure silica MCM-41. *J. Mater. Chem.* **1999,** *9* (10), 2611-2615.

88. Koyano, K., Tatsumi, T, Tanaka, Y, Nakata, S.. Stabilization of Mesoporous Molecular Sieves by Trimethylsilylation. *J. Phys. Chem. B* **1997,** *101*(46), 9436-9440.

89. Kawi, S.; Shen, S.-C.. Effects of structural and non-structural Al species on the stability of MCM-41 materials in boiling water. *Mater. Lett.* **2000,** *42*(1-2), 108-112.

90. Jun, S.; Kim, J. M.; Ryoo, R.; Ahn, Y.-S.; Han, M.-K. Hydrothermal stability of MCM-48 improved by post-synthesis restructuring in salt solution. *Microporous Mesoporous Mater.* **2000,** *41*(1-3), 119-127.

91. Kim, J. M.; Jun, S.; Ryoo, R. Improvement of Hydrothermal Stability of Mesoporous Silica Using Salts: Reinvestigation for Time-Dependent Effects. *J. Phys. Chem. B* **1999,** *103* (30), 6200-6205.

92. Das, D.; Tsai, C.-M.; Ceng, S. Improvement of hydrothermal stability of MCM-41 mesoporous molecular sieve. *J. Chem. Soc., Chem. Commun.* **1999,** *4,* 473-474.

93. Chen, L.; Horiuchi, T.; Mori, T.; Maeda, K.. Post-synthesis Hydrothermal Restructuring of M41S Mesoporous Molecular Sieves in Water. *J. Phys. Chem. B* **1999,** *103*(8), 1216-1222.

94. Mokaya, R.. Improving the Stability of Mesoporous MCM-41 Silica via Thicker More Highly Condensed Pore Walls. *J. Phys. Chem. B* **1999,** *103*(46), 10204-10208.

95. Mokaya, R.; Jones, W.. Aluminosilicate mesoporous molecular sieves with enhanced stability obtained by reacting MCM-41 with aluminum chlorohydrate. *J. Chem. Soc., Chem. Commun.* **1998,** *17,* 1839-1840.

96. Shen, S.-C.; Kawi, S.. Understanding of the Effect of Al Substitution on the Hydrothermal Stability of MCM-41. *J. Phys. Chem. B* **1999,** *103*(42), 8870-8876.

97. Kruk, M.; Jaroniec, M.; Ko, C. H.; Ryoo, R.. Characterization of the Porous Structure of SBA-15. *Chem. Mater.* **2000,** *12*(7), 1961-1968.

98. Hartmann, M.; Bischof, C.. Mechanical Stability of Mesoporous Molecular Sieve MCM-48 Studied by Adsorption of Benzene, n-Heptane, and Cyclohexane. *J. Phys. Chem. B* **1999,** *103*(30), 6230-6235.

99. Inaki, Y.; Yoshida, H.; Kimura, K.; Inagaki, S.; Fukushima, Y.; Hattori T. Photometathesis activity and thermal stability of two types of mesoporous silica materials, FSM 16 and MCM 41. *Phys. Chem. Chem. Phys.* **2000,** *2*(22), 5293-5297.

100. Cassiers, K.; Linssen, T.; Mathieu, M.; Benjelloun, M.; Schrijnemakers, K.; Van Der Voort, P.; Cool, P.; Vansant, E. F.. A Detailed Study of Thermal, Hydrothermal, and Mechanical Stabilities of a Wide Range of Surfactant Assembled Mesoporous Silicas. *Chem. Mater.* **2002,** *14*(5), 2317-2324.

101. Zhao, X. S.; Lu, G. Q.; Whittaker, A. K.; Millar, G. J.; Zhu, H. Y.. Comprehensive Study of Surface Chemistry of MCM-41 Using ^{29}Si CP/MAS NMR, FTIR, Pyridine-TPD, and TGA. *J. Phys. Chem. B* **1997,** *101*(33), 6525-6531.

102. Hitz, S.; Prins, R.. Influence of Template Extraction on Structure, Activity, and Stability of MCM-41 Catalysts. *J. Catal.* **1997,** 168, 194-206.

103. Kawi, S.; Lai. M. W.. Supercritical fluid extraction of surfactant template from MCM-41. *Chem. Commun.* **1998,** 1407-1408.

104. Antochshuk, V.; Jaroniec, M.. Simultaneous modification of mesopores and extraction of template molecules from MCM-41 with trialkylchlorosilanes*. Chem. Commun.* **1999,** 2373-2374.

105. Benjelloun, M.; Van Der Voort, P.; Cool, P.; Collart, O.; Vansant, E. F.. Reproducible synthesis of high quality MCM-48 by extraction and recuperation of the gemini surfactant. *Phys. Chem. Chem. Phys.* **2001,** 3, 127-131.

106. Mercier, L.; Pinnavaia, T. J.. Heavy Metal Ion Adsorbents Formed by the Grafting of a Thiol Functionality to Mesoporous Silica Molecular Sieves: Factors Affecting Hg(II) Uptake. *Environ. Sci. Technol.,* **1998,** *32*(18), 2749-2754.

107. Brown, J.; Mercier, L.; Pinnavaia, T. J.. Selective adsorption of Hg^{2+} by thiol-functionalized nanoporous silica. *Chem. Commun.* **1999,** *5*(1), 69-70.
108. Branda, M. M.; Montani, R. A.; Castellani, N. J.. The Distribution of Silanols on the Amorphous Silica Surface: A Monte Carlo Simulation. *Surf. Sci.* **2000,** *446*, L89.
109. Vansant, E. F.; Van Der Voort, P.; Vrancken, K. C.. Characterization and Chemical Modification of the Silica Surface, Elsevier, Amsterdam, **1995,** (Chapters 1–6).
110. McCullen, S. B.; Vartuli, J. C. McCullen, S. B.; Vartuli, J. C.. Stabilization of synthetic mesoporous crystalline material, and the material obtained. 1992, 21 pp. Cont.-in-part of U.S. Ser. No. 625,245.
111. De Farias, R. F.; Airoldi, C.. Thermogravimetry as a reliable tool to estimate the density of silanols on a silica gel surface. *J. Thermal Anal.* **1998,** *53*(3), 751-756.
112. Huhn, H. J.. Thermoanalytical characterization of amorphous synthetic silicic acids. *J. Thermal Anal.* **1988,** *33*(3), 851-856.
113. Hoffmann, P.; Knözinger, E.. Novel aspects of mid and far IR Fourier spectroscopy applied to surface and adsorption studies on SiO_2. *Surf. Sci.* **1987,** *188*(1-2), 181-198.
114. Zhuravlev, L. T. Characterization of amorphous silica surface. *React. Kinet. Catal. Lett.* **1993,** *50*(1-2), 15-25.
115. Zhuravlev, L. T.. Structurally bound water and surface characterization of amorphous silica. *Pure Appl. Chem.* **1989,** *61*(11), 1969-1976.
116. Bermudez, V. M.. Proton nuclear magnetic resonance technique for determining the surface hydroxyl content of hydrated silica gel. *J. Phys. Chem.* **1970,** *74*(23), 4160-4161.
117. Gillis-D'Hamers, I.; Cornelissens, I.; vrancken, K. C.; Van Der Voort, P.; Vansant, E. F. Modeling of the hydroxyl group population using an energetic analysis of the temperature-programmed desorption of pyridine from silica gel. *J. Chem. Soc., Faraday Trans*. **1992**, *88* (5), 723-727.
118. Vansant, E. F.; Van Der Voort, P.; Vrancken, K. C. Characterization and Chemical Modification of the Silica Surface. *Stud. Surf. Sci. Catal.* **1995**, *93*, 109-119.
119. Schrader, G. L.; Cheng, C. P. Laser Raman spectroscopy of cobalt-molybdenum/γ-aluminum oxide catalysts. Characterization using pyridine adsorption. *J. Phys. Chem*. **1983**, *87*(19), 3675-3681.
120. Nikiel, L.; Zerda, T. W. Adsorption of pyridine on silica gels. *J. Phys. Chem*. **1991**, *95*(10), 4063-4069.
121. Fyfe, C. A.; Gobbi, G. C.; Kennedy, G. J. Quantitatively reliable silicon-29 magic-angle spinning nuclear magnetic resonance spectra of surfaces and surface-immobilized species at high field using a conventional high-resolution spectrometer. *J. Phys. Chem*. **1985**, *89*(2), 277-281.
122. Sindorf, D. W.; Maciel, G. E. Silicon-29 CP/MAS NMR studies of methylchlorosilane reactions on silica gel. *J. Am. Chem. Soc.* **1981**, *103*(14), 4263-4265.
123. Sindorf, D. W.; Maciel, G. E.. Silicon-29 nuclear magnetic resonance study of hydroxyl sites on dehydrated silica gel surfaces, using silylation as a probe. *J. Phys. Chem.* **1983**, *87*(26), 5516-5521.

124. Sindorf, D. W.; Maciel, G. E.. Cross-polarization magic-angle-spinning silicon-29 nuclear magnetic resonance study of silica gel using trimethylsilane bonding as a probe of surface geometry and reactivity. *J. Phys. Chem*. **1982,** *86*(26), 5208-5219.

125. Sindorf, D. W.; Maciel, G. E.. ^{29}Si NMR study of dehydrated/rehydrated silica gel using cross polarization and magic-angle spinning. *J. Am. Chem. Soc*. **1983**, *105*(6), 1487-1493.

126. Maciel, G. E.; Sindorf, D. W.; Bartuska, V. J. Silicon-29 NMR study of the surface of silica gel by cross polarization and magic-angle spinning. *J. Am. Chem. Soc*. **1980**, *102*(25), 7606-7607.

127. Haukka, S.; Lakomaa, E. L.; Root, A.. An IR and NMR study of the chemisorption of $TiCl_4$ on silica. *J. Phys. Chem*. **1993,** *97*(19), 5085-5094.

128. Wouters, B. H.; Chen, T.; Dewilde, M.; Grobet, P. J. Reactivity of the surface hydroxyl groups of MCM-41 towards silylation with trimethylchlorosilane. Micropor. Mesopor. Mater. **2001,** *44-45,* 453-457.

129. Ishikawa, T.; Matsuda, M.; Yasukawa, A.; Kandori, K.; Inagaki, S.; Fukushima, T.; Kondo, S.. Surface silanol groups of mesoporous silica FSM-16. *J. Chem. Soc., Faraday Trans*. **1996**, *92*(11), 1985-1989.

130. Llewellyn, P. C.; Schüth, F.; Grillet, Y.; Rouqoerol, F.; Rouquerol, J.; Unger, K. K.. Water Sorption on Mesoporous Aluminosilicate MCM-41. *Langmuir* **1995**, *11*(2), 574-577.

131. Van der Voort, P.; Gillis-D'Hamers, I.; Vrancken, K. C.; Vansant, E. F.. Effect of porosity on the distribution and reactivity of hydroxyl groups on the surface of silica gel. *J. Chem. Soc., Faraday Trans*. **1991,** *87*(24), 3899-3905.

132. Davydov, V.; Kiselev, A. V.; Zhuravlev, L. T.. Study of the surface and bulk hydroxyl groups of silica by Infrared spectra and D_2O-exchange. *Trans. Faraday Soc*. **1964,** *60,* 2254-2264.

133. Zhuravlev, L. T.. Concentration of hydroxyl groups on the surface of amorphous silicas. *Langmuir* **1987,** *3*(3), 316-318.

134. Linssen, T.; Cassiers, K.; Cool, P.; Vansant, E. F.. Mesoporous templated silicates: an overview of their synthesis, catalytic activation and evaluation of the stability. *Adv. Coll. Inter. Sci*. **2003,** *103*(2), 121-147.

135. Tuel, A.; Gontier, S.. Synthesis and Characterization of Trivalent Metal Containing Mesoporous Silicas Obtained by a Neutral Templating Route. *Chem. Mater*. **1996,** *8*(1), 114-122.

136. Steel, A.; Carr, S. W.; Anderson, M. W. ^{29}Si solid-state NMR study of mesoporous M41S materials. *Chem. Mater*. **1995,** *7*(10), 1829-1832.

137. Brunauer, S.; Emmett, P. H.; Teller, E.. Adsorption of gases in multimolecular layers. *J. Am. Chem. Soc*. **1938,** *60,* 309-319.

138. Rouquerol, J.; Avnir, D.; Fairbridge, C. W.; Everett, D. H.; Haynes, J. H.; Pernicone, N.; Ramsay, J. D. F.; Sing, K. S. W.; Unger, K. K.. Recommendations for the characterization of porous solids. *Pure Appl. Chem*. **1994,** *66*(8), 1739-1758.

139. Emmett, P. H.; Brunauer, S.. The use of low-temperature van der Waal adsorption isotherms in detg. the surface area of iron synthetic ammonia catalysts. *J. Am. Chem. Soc*. **1937,** *59,* 1553-1564.

140. (a) Barrett, E. P.; Joyner, L. G.; Halenda, P. P. The determination of pore volume and area distributions in porous substances. I. Computations from nitrogen

isotherms. *J. Am. Chem. Soc.* **1951,** *73,* 373-380. (b) Horvath, G.; Kawazoe, K. Method for the calculation of effective pore size distribution in molecular sieve carbon *J. Chem. Eng. Jpn.* **1983**, *16*, 470-475.

141. Kruk, M.; Jaroniec, M.; Sayari, A. Application of Large Pore MCM-41 Molecular Sieves To Improve Pore Size Analysis Using Nitrogen Adsorption Measurements. *Langmuir* **1997,** *13*(23), 6267-6273.-97

142. Yang, H.; Zhang, G.; Hong, X.; Zhu, Y. Silylation of Mesoporous Silica MCM-41 with the Mixture of $Cl(CH_2)_3SiCl_3$ and CH_3SiCl_3: Combination of Adjustable Grafting Density and Improved Hydrothermal Stability. *Micropor. Mesopor. Mater.* **2004,** *68*(1-3), 119-125.

143. Sauer, J.; Marlow, F.; Schüth, F.. Simulation of powder diffraction patterns of modified ordered mesoporous materials. *Phys. Chem. Chem. Phys.* **2001**, *3*(24), 5579-5584.

144. Jaroniec, M.; Kruk, M.; Shin, H. J.; Ryoo, R.; Sakamoto, Y.; Terasaki, O.. Comprehensive characterization of highly ordered MCM-41 silicas using nitrogen adsorption, thermogravimetry, X-ray diffraction and transmission electron microscopy. *Micropor. Mesopor. Mater.* **2001,** *48*(1-3), 127-134.

145. Sing, K. S. W.; Everett, D. H.; Haul, R. A. W.; Moscou, L.; Pierotti, R. A.; Rouquerol, J.; Siemieniewska, T.. Reporting physisorption data for gas/solid systems with special reference to the determination of surface area and porosity. *Pure Appl. Chem.* **1985,** *57*(4), 603-619.

146. Brunauer, S.; Deming, L. S.; Deming, W. E.; Teller, E.. A theory of the van der Waals adsorption of gases. *J. Am. Chem. Soc.* **1940,** *62,* 1723-1732.

147. Romero, A. A.; Alba, M. D.; Zhou, W.; Klinowski, J.. Synthesis and Characterization of the Mesoporous Silicate Molecular Sieve MCM-48. *J. Phys. Chem. B* **1997,** *101*(27), 5294-5300.

148. Luan, Zhaohua; He, Heyong; Zhou, wuzong; Cheng, Chi-Feng; Klinowski, Jacek. Effect of structural aluminum on the mesoporous structure of MCM-41. *J. Chem. Soc., Faraday Transactions* **1995,** *91*(17), 2955-2959.

149. Hayakawa, S.; Hench, L. L.. AM1 study on infra-red spectra of silica clusters modified by fluorine. *J. Non-Cryst. Solids* **2000,** *262*(1-3), 264-270.

150. Husung, R. D.; Doremus, R. H.. Infrared transmission spectra of four silicate glasses before and after exposure to water. *J. Mater. Res.* **1990,** *5*(10), 2209-2217.

151. Geidel, E.; Lechert, H.; Dobler, J.; Jobic, H.; Calzaferri, G.; Bauer, F. Characterization of mesoporous materials by vibrational spectroscopic techniques. *Micropor. Mesopor. Mater.* **2003,** *65*(1), 31-42.

152. Yu, C.; Fan, J.; Tian, B.; Zhao, D.. Morphology Development of Mesoporous Materials: a Colloidal Phase Separation Mechanism. *Chem. Mater.* **2004**, *16*(5), 889-898.

153. Inagaki, S.; Sakamoto, Y.; Fukushima, Y.; Terasaki, O. Pore Wall of a Mesoporous Molecular Sieve Derived from Kanemite *Chem. Mater.* **1996**, *8*(8), 2089-2095.

154. Alfredsson, V.; Keung, M.; Monnier, A.; Stucky, G. D.; Unger, K. K.; Schuth, F. High-resolution transmission electron microscopy of mesoporous MCM-41 type materials. *J. Chem. Soc., Chem. Commun.* **1994**, 8, 921-922.

155. Landmesser, H.; Kosslick, H.; Storek, W.; Fricke, R. Interior surface hydroxyl groups in ordered mesoporous silicates. *Solid State Ionics* **1997**, *101-103*(1), 271-277.
156. Tatsumi, T.; Koyano, K. A.; Tanaka, Y.; Nakata, S.. Mechanochemical collapse of M41S mesoporous molecular sieves through hydrolysis of siloxane bonds. *Chem. Lett.* **1997,** *5,* 469-470.
157. Bosacek, V.; Dubinin, M. M.; Kadlec, O.; Murdmaa, K. O.; Navratil, V. Destruction of synthetic zeolite crystals in pressure processing. *Doklady Akademii Nauk SSSR* **1967,** *174*(1), 117-120.
158. Gregg, S. J.; Langford, J. F.. Study of the effect of compaction on the surface area and porosity of six powders by measurement of nitrogen sorption isotherms. J. *Chem. Soc., Faraday Trans*. **1977**, *73*(5), 747-759.

CHAPTER
THREE

SYNTHESIS OF MESOPOROUS MATERIALS BEARING γ-AMINO-
FUNCTIONAL GROUPS AND OTHER DERIVATIVES

Abstract

γ-Aminopropyl-functionalized mesoporous OSU-6-W materials were synthesized via post-synthesis grafting of 3-aminopropyltrimethoxysilane (APTMS) with the surfactant-extracted mesoporous silica, OSU-6-W. At the maximum level of silylation with APTMS, the solid state ^{29}Si CP/MAS NMR measurements of the two modified samples, OSU-6-W-APTMS-1 and OSU-6-W-APTMS-2, thus obtained indicate that the organosilanes silicon atoms are different from each other. These measurements indicate that the surface coverage of γ-aminopropyl anchored to silanol groups on the surface of OSU-6-W were not the same. Moreover, the results from the UV-Visible spectroscopy and titration of the two modified samples show good agreement with that of the solid state ^{29}Si CP/MAS NMR and elemental analysis.

The γ-aminopropyl-functionalized mesoporous material was subjected to a reaction with ethylenediaminetetraacetic acid (EDTA) in order to introduce new active groups to the modified sample. The second modification shows about ~ 65% of the EDTA was anchored to the amine functional groups.

All materials were characterized using various techniques such as Fourier transform infrared spectroscopy (FTIR), X-ray powder diffraction (XRD), scanningelectron microscopy (SEM), solid state ^{13}C and ^{29}Si NMR spectroscopy, elemental analysis (EA), surface area analysis (BET), and UV-Visible spectroscopy.

Adsorption experiments of Cu^{2+}, Zn^{2+}, Cd^{2+} and UO_2^{2+} were conducted in order to investigate the capacity and selectivity of the synthesized materials. The cations adsorbed on the γ-aminopropyl-functionalized samples, and the adsorption capacities were increased with an increase in the surface density of amino groups and affected by the pH of the medium, surface areas, and pore sizes.

3.1. INTRODUCTION

3.1.1. Contaminants and Environmental Concern

A considerable amount of industrial waste water is contaminated with heavy metals such as lead, zinc, copper, antimony, chromium and nickel and radioactive ions such as radioisotopes of uranium, cobalt, thorium, strontium and cesium. These metals become contaminants in aqueous systems as the result of activities including chemical manufacture, smelting, electroplating, wood treating, industrial and medical use of radioisotopes, *etc*. When such metals are used, metal discharges in aqueous streams severely damage the environment by posing risk to wild life and human health, and have become a worldwide environmental concern.[1]

The successful treatment of low level radioactive effluent also presents a major challenge to the nuclear industry. Therefore, improved methods for removing heavy metals or radioactive isotope ions rapidly and efficiently from contaminated industrial aqueous solutions are highly desired.

Existing metal removal methods include standard, conventional techniques such as evaporation, precipitation, electrolytic techniques, membrane separation, and fixed and movable bed ion exchange. These methods generally need large and complicated facilities due to various equipment and reagents used in a series of treatments so they are not economical or efficient enough in most cases. Adsorption is a simple and facile technique, which is adaptable to personal and portable use for water supply. Adsorption techniques have been reported for the removal of pollutant metal cations using activated carbon[1,2], polymers[3], zeolites[4,5], and clays.[6,7] On the other hand, the removal of toxic materials is much more difficult because cations with a similar structure and size, such as sodium, potassium, calcium, and magnesium, often coexist in nature in high concentrations. Although the adsorptive removal of toxic substances from solution using conventional adsorbents, such as activated carbon[8,9], zeolite[10], and alumina oxides[11], have been reported, they are not selective and effective. The interest in the development of cost-effective methods for the removal and recovery of metal ions from contaminated waters has greatly increased because of the ecological awareness of the role of metals in the environment. Searching for effective adsorbents for the removal of these materials is important for environmental remediation.

3.1.2. Modification of OSU-6-W with 3-Aminopropyltrimethoxysilane

Since the discovery of a new family of mesoporous molecular sieves M41S[12,13] and FSM-16[14] with tailorable pore sizes ranging from 2.0 to 10 nm and with surface areas often exceeding 1000 m^2/g, these materials have attracted much attention in the field of catalysis, separation and adsorption. Unlike zeolites, the pore size of mesoporous silica is large enough to accommodate a variety of large molecules, and the high density of silanol

groups on the pore walls is beneficial to the introduction of functional groups with high coverage.[15] Several kinds of surface modification have been conducted for providing new functions for the surfaces.[16-19] Chemical surface modification of periodic mesoporous silicas via covalent bonding of organic molecules has been achieved using two general strategies. The post-synthesis procedure was the first to be used as it was already described in the early work on Mobil M41S[13] and Toyota FSM-16[20] silicas. Subsequently, co-condensation procedures were introduced by Burkett *et al.*,[21] and Macquarrie *et al.*[16] Both methods were discussed in details in chapter one.

Aminoorganosilanes have the general formula H_2N-R-$Si(OR')_3$. They differ from the general organosilanes in carrying an amino-functional group in the organic chain. This group is responsible for the specific chemical reaction behavior and high reactivity of the aminosilane molecules. The electron-rich nitrogen centre of the amine group can enter into hydrogen bonding interactions with hydrogen donating groups, such as hydroxyl groups or other amines. Mixing of an aminosilane with silica gel results in fast adsorption, by hydrogen bonding of the amine to a surface hydroxyl group.[22] After adsorption, the amine group can catalyze the condensation of the silicon side of the molecule with a surface silanol. Thus, siloxane bonds with the surface may be formed in the absence of water.[23,24] For other silanes the siloxane bond formation requires an initial hydrolysis of the methoxy or ethoxy groups or the addition of a catalyst to the reaction mixture.[25]

The modified silica may be used as such, or after a secondary treatment with an active group. Pure aminosilane-modified silica gel is used as a stationary phase in liquid and gas chromatography.[26,27] Trace levels of metals, such as copper, in aqueous solution

are separated and concentrated before analysis. Aminosilane-modified silica serves very well for this process.[28,29] The aminosilane-silica couple is used for the reinforcement of natural and synthetic rubbers and elastomers.[30]

The amino group may also serve as an active site on the silica surface to bind other molecules. These molecules may impart new interaction capacities to the surface. The bonding of metal complexes on aminosilane-silica allowed the production of a variety of heterogeneous catalysts.[31] Aminosilane modified silica layers are used as a starting layer for integrated circuit build-up.[32]

All of these applications explain the wide interest in the chemistry of aminosilane-modified silica. A fundamental understanding of the reaction mechanism may assist the further optimization of all these uses. Besides this, there is a large interest in the development of new applications of the aminosilane-modified silicas.

Functionalized mesoporous silica with a high density of amino groups and well-defined mesochannels that can enhance the accessibilities of molecules is required to achieve high production when applied as catalyst such as solid-base catalysts for Knoevenagel and aldol condensations,[33] and to accomplish high capacity and selectivity when applied as adsorbent and separation for harmful heavy metal cations, such as cobalt, copper and zinc.[34-37]

To ensure the effectiveness of the hybrid materials in exploiting the intrinsic reactivity of the organofunctional groups, these moieties must keep their activity upon immobilization, they must be accessible to the external solution, and mass transfer to and from these active sites should be as fast as possible. As highlighted in recent investigations, this is especially important in heterogeneous catalysis for ensuring high

efficiency and turnover,[19,38-45] as well as in removal of toxic substances (especially heavy metals) to improve the performance of remediation processes and environmental containment technologies,[28,35,46-66] and also in electrochemical applications for which diffusion is often the rate-determining step.[67-71] It is expected that the increase in the density of functional groups while retaining of the open space would result in a higher activity. Therefore, high loading of functional groups in mesoporous silicas has received much attention.[72-76] Uniform surface modification with functional groups is desired so that the coverage of functional groups on the surface may increase without adversely affecting the diffusion of molecules in the mesopore. The syntheses of amino-functionalized mesoporous silicas prepared *via* direct co-condensation and post-synthesis grafting methods have been numerously demonstrated.[77-80] Macquarrie and his co-workers reported on the differences in reactivity of aminopropyl groups in the neutral amine surfactant-templated mesoporous silica prepared between grafting and co-condensation routes.[81,82]

3.1.3. Immobilization of EDTA

The large number of primary amino groups with high reactivity enables a variety of chemical modification by immobilizing some ligands with high affinity for specific metal ions onto silica matrices of the mesoporous material by chemical modification. Such modification is expected to further improve the adsorption characteristics of the mesoporous materials.[72-78]

There has been much recent interest in the separation and removal of heavy and transition metal ions. The separation and extraction of the metals are usually carried out via liquid-liquid extraction using several organic-soluble extractants. Such processes,

however, require large amounts of harmful organic solvents (*e.g.,* benzene) as diluents and encounter the problem that a third (emulsion) phase appears in some cases during process operation. A process for the separation of metals that can be operated simply without the requirement of organic solvents is therefore required. Various investigations have been reported on the separation of metals by the use of various kinds of organic materials modified with several chelating ligands, such as cross-linked polystyrene with ethylenediaminetetraacetic acid (EDTA), diethylenetriaminepentaacetic acid (DTPA),[83] and *o*-vanillinsemicarbazone[84] and chitosan with EDTA or DTPA.[85] These "chelating resins" are insoluble in organic and aqueous solvents. When the resins are added to aqueous solution, metal ions are coordinated by the ligands on the surface of the resins. The resulting resins, loaded with metals, can then be recovered simply by decantation. For industrial applications, less expensive materials are preferable as the supports for the chelating ligands. In the present work, widely used inorganic adsorbents, such as mesoporous molecular sieves similar to MCM-41, will be used as the supporting materials.

3.1.4. Aim of Study

This investigation focused on maximizing the functional group concentration (coverage) of the mesoporous surfaces while keeping the pore size as large as possible. This can be accomplished by using mesoporous silica with large pore size, high surface area, and high concentration of hydroxyl (silanol) groups. However, high thermal, hydrothermal, and mechanical stabilities are also required. The control of the synthesis conditions and use of catalyst were found to have a significant impact on the final products.

One goal was to immobilize some active groups (*e.g.,* EDTA) that impart new activity to the materials. In addition to the synthesis, the testing of these modified materials as adsorbents for the separation and removal of harmful pollutants such as heavy metal ions and radioactive materials was also an objective.

3.2. EXPERIMENTAL

3.2.1. Materials

The chemicals were purchased from commercial sources and were used without any further purification. These chemical are as follow: 3-aminopropyltrimethoxysilane [($H_2N(CH_2)_3Si(OCH_3)_3$) 97.0%, Aldrich], toluene 99.8% HPLC grade, ethyl alcohol, triethylamine (TEA, 99%, Aldrich), salicylaldehyde (2-hydroxybenzaldehyde) reagent grade, Aldrich 98%, diethylether, 0.01 *M* hydrochloric acid (HCl), 0.10 *M* sodium hydroxide (NaOH), phenolphthalein [ACS reagent, Aldrich] , acetic anhydride (Fluke), ethylenediaminetetraacetic tetrasodium salt (Avocado), pyridine (Aldrich 99.0%), acetic acid, and distilled water. The structures of some of these compounds are shown in Scheme 3.1.
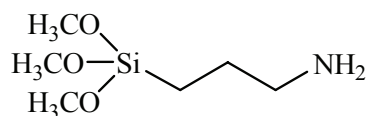
3-Aminopropyltrimethoxysilane
(APTMS)
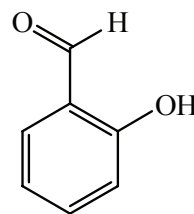
Salicylaldehyde (2-Hydroxybenzaldehyde)
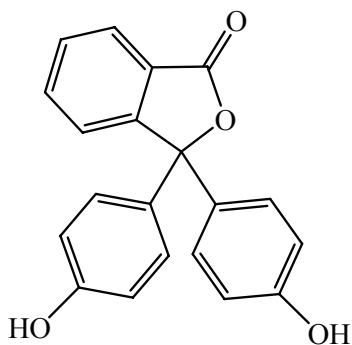
Phenolphthalein
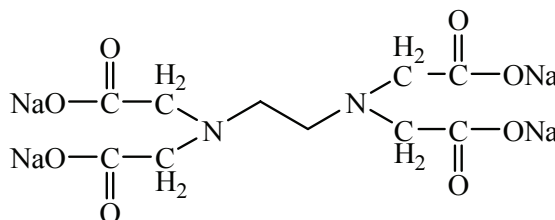
Ethylenediaminetetraacetic tetrasodium salt
(EDTA)

Scheme 3.1. The structures of some of the starting materials.

3.2.2. Characterization

In addition to the characterization techniques that were discussed previously in detail in Chapter 2, solid state ^{13}C NMR and elemental analysis (EA) were used for the characterization of the functionalized ordered mesoporous materials.

Solid state ^{13}C CP/MAS NMR spectra were obtained with a Chemagnetics CMX-II solid-state NMR spectrometer operating at 75.694 MHz for carbon-13 and a Chemagnetics 5mm double resonance magic-angle spinning probe. Carbon-13 cross-polarization/magic-angle spinning (CP/MAS) was carried out with a quasi-adiabatic sequence (1) using two pulse phase modulation (TPPM) decoupling (2) at 50-75 kHz. At

least 3600 scans were acquired with a delay of 1.0 s between scans. The MAS samples were collected in a 5.0 mm zirconia rotor spinning at 6.0 kHz, maintained to within a range of +/- 5.0 Hz or less with a Chemagnetics speed controller, utilizing a quasi-adiabatic cross-polarization pulse sequence using a 1.0 s pulse delay, a 1.0 ms contact time, and a 5.0 μs pulse width. The C-13 CP contact pulse of 1.0 millisecond length was divided into 11 steps of equal length with ascending radiofrequency field strength, while the H-1 contact pulse had constant radiofrequency field strength.

Chemical elemental analysis for C and N was used to measure the amount of functional groups in the samples. The elemental analysis was carried out on a LECO TruSpec Carbon and Nitrogen Analyzer.

All the adsorption measurements were carried out using a UV-Visible spectrophotometer or inductive coupled plasma atomic emission spectroscopy. UV-Visible spectra were recorded on a Perkin Elmer (Lambda EZ 201) spectrometer in the range from 200-800 nm, while the ICP analysis were performed on a Spectro CIROS ICP Spectrometer.

3.2.3. Preparation

3.2.3.1. Pretreatment of the Mesoporous OSU-6-W

Mesoporous silica materials were synthesized as discussed in chapter two of this thesis. The HCl-ethanol washed mesoporous silica OSU-6-W has a surface area of 1283 m^2/g and an average pore size of ~ 51 Å, as determined by the Nitrogen adsorption-desorption technique and transmission electron microscopy (TEM). It was activated prior to the functionalization step. This activation step is to remove water and other materials from the mesoporous channels. The activation process takes place by refluxing around

10 g of the mesoporous silica in 50 ml of dry toluene for 4 hrs under dry atmosphere, washing with dry toluene, and drying at 100 °C under vacuum. Toluene was dried using molecular sieves (5A, beads, 4-8 mesh).

3.2.3.2. Introducing γ-Amino Functional Groups into the Mesoporous Surfaces

γ-Amino-functional groups were chemically attached to the mesoporous OSU-6-W material surfaces by means of the post-synthesis grafting method. Two synthetic procedures were applied which are based on a combination of different synthetic methods used by previous researchers.

I. Reaction of the Mesoporous Silica with 3-Aminopropyltrimethoxysilane in a One Step Reaction (OSU-6-W-APTMS-1)

Mesoporous silica-supported γ-aminopropyl functional groups, with 1:1 mole ratio, was prepared by refluxing 3.0 g (~ 50 mmol) of the activated mesoporous silica (OSU-6-W) with 50 mmol (9.0 ml) of 3-aminopropyltrimethoxysilane (APTMS) in 100 ml of dry toluene in a 250-ml round-bottom flask for 48 hrs under dry atmosphere. A drying tube was attached to the reflux apparatus to minimize the influence of moisture. The chemical reaction and reflux setup are shown in Scheme 3.2 and Figure 3.1, respectively. The refluxed mixture was then cooled down to room temperature. The resulting light brown solid was filtered off with a fine filter funnel, washed plentifully with toluene three times (3 X 50 ml), and then ethanol, to wash away any excess APTMS. The product became white after the filtration and washing processes. The white solid was then dried at 80 °C under vacuum for 24 hrs in an integrated chemical dryer (CHEM-DRY®). The reaction yielded 5.04 g (72.2%, taking to account the production of methanol).
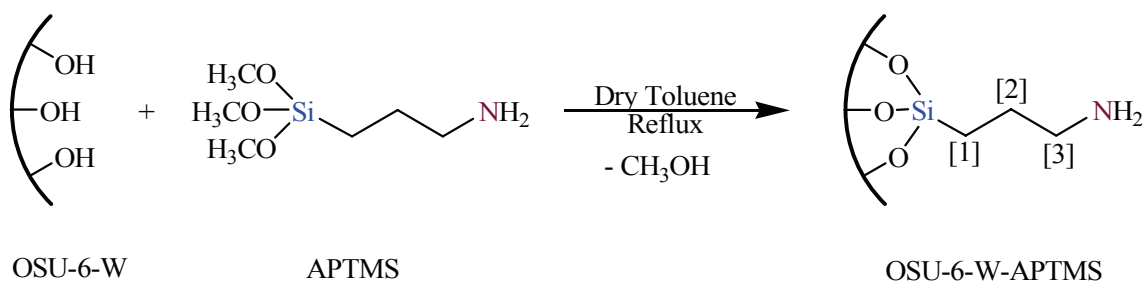
Scheme 3.2. Schematic illustration of the general chemical reaction and the carbon atom position as described in the solid state ^{13}C CP/MAS NMR.

A 30 ml of the filtrate solution was reserved for the functional group determination and the reminder of the solution was placed in a 500-ml beaker which was then left in a fume hood under direct air for evaporation of the solvent (toluene, ethanol, and methanol). A brownish sticky-solid formed from the filtrated solution. About 3.19 g of the solid was collected from the latter solution. IR (cm^{-1}) (KBr) of the main product: 3737(m), 3604(m, br), 3357(s, br), 3297(s, br), 3016(s, sh), 2923(s, sh), 2851(s, sh), 1862(w), 1640(m, sh), 1595(m, sh), 1542(m, sh), 1482(m, sh), 1432(w), 1361(m, sh), 1307(m, sh), 1150(s, br), 1055(s, br), 962(s, sh), 800(m, sh), 728(w), and 575(w). Solid-state ^{29}Si CP/MAS NMR: δ (ppm) -51.9 (T^1), -59.3 (T^2), -67.1 (T^3), -100.5 (Q^3) (w), and -110.3 (Q^4). Solid-state ^{13}C CP/MAS NMR: δ (ppm) 9.7($\equiv$Si-CH$_2$-CH$_2$-)[1], 25.6($\equiv$Si-CH$_2$-CH$_2$-)[2], 23.3($\equiv$Si-OCH$_3$), and 43.4($\equiv$Si-CH$_2$-CH$_2$-CH$_2$-NH$_2$)[3], see Scheme 3.2. Elemental analysis: C (11.21%) and N (3.72%).
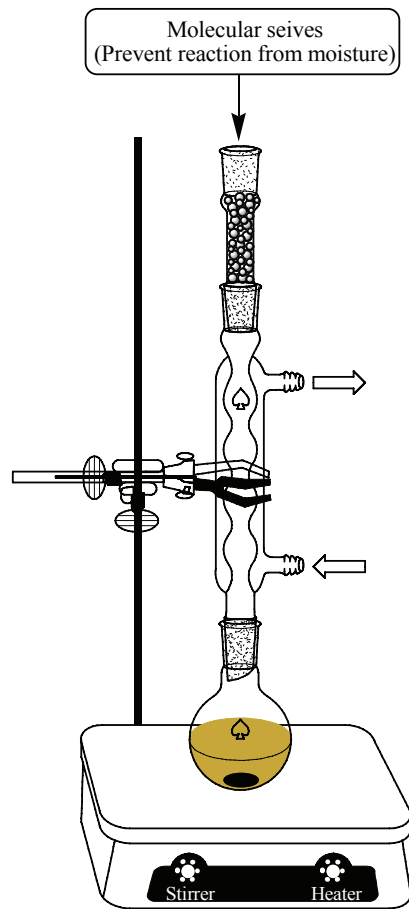
Figure 3.1. The reflux instrument setup for the modification synthesis.

II. Reaction of the Mesoporous Silica with 3-Aminopropyltrimethoxysilane in a Three Step Reaction (OSU-6-W-APTMS-2)

In this procedure aminopropyl-derivatized mesoporous silica was synthesized in three steps. The first step involved refluxing 3.0 g (50 mmol) of the activated mesoporous silica (OSU-6-W) with 25 mmol (~ 4.5 ml) of APTMS in 100 ml of dry toluene in a 250-ml round-bottom flask for 48 hrs under dry atmosphere. After that, the refluxed mixture was then cooled down to room temperature. The resulting light brown solid was filtered off with a fine filter funnel, washed copiously with toluene three times (3 X 50 ml), and then ethanol, to rinse away any surplus APTMS which changed the

products color to white after filtration. The white solid yield was then dried at 80 °C

under vacuum for 24 hrs in a chem-Dry apparatus. In the second step, resulting product

was placed in a 125-ml Erlenmeyer flask and stirred with 50 ml of distilled water at about

80 °C for around five hours in order to hydrolyze the methoxy groups. After cooling to

room temperature, the sample was centrifuged down to recover the solid product, the

water was decanted off, and the mesoporous silica was dried at 80 °C under vacuum for

24 hours. In the third step, the hydrated mesoporous silica was then suspended in 100 ml

of dried toluene in a 250-ml round-bottom flask, treated with 25 mmol (~ 4.5 ml) of

APTMS, and taken to reflux for 48 hours under dry atmosphere. After cooling to room

temperature, the reaction mixture (light brown) was filtered with a fine filter funnel. The

solid was washed copiously with toluene (3 X 50 ml) and then ethanol, to rinse away any

excess APTMS then dried at 80 °C under vacuum for 24 hours. The final product was

white and its yield was 5.73 g. The filtrates from the first and third steps were collected

and 30 ml of the total filtrate mixture was reserved for the functional group concentration

determination. The remainder of the filtrate solution was placed in a 500-ml beaker

which was then left in a fume hood for evaporation of the solvent. A light brown sticky

solid formed in a yield of 2.08 g. IR (cm^{-1}) (KBr) of the main product: 3359(s, sh),

3302(s, sh), 2920(s, sh), 2850(s, sh), 1873(w), 1638(m), 1600(m, sh), 1535(s, sh), 1467(s,

sh), 1408(m), 1392(m, sh), 1236(s, br), 1188(s, br), 1062(s, br), 993(m, br), 795(m, sh),

and 721(m, sh). Solid-state ^{29}Si CP/MAS NMR: δ (ppm) -57.3 (T^2), -66.6 (T^3), -100.6

(Q^3)(w, br), and -110.3 (Q^4). Solid-state ^{13}C CP/MAS NMR: δ (ppm) 10.6($\equiv$Si-CH_2-

CH_2-)[1], 26.1($\equiv$Si-CH_2-CH_2-)[2], and 43.6($\equiv$Si-CH_2-CH_2-CH_2-NH_2)[3]. Elemental

analysis: C (16.13%) and N (5.33%).

3.2.3.3. Immobilizing EDTA onto the γ-Amino Functionalized Mesoporous Silica

Ethylenediaminetetraacetic acid (EDTA) anhydride was prepared according to the procedure of Inoue *et al.*,[86] as shown in Scheme 3.3. Surface modification of the adsorbent OSU-6-W-APTMS-2 with the EDTA was carried out as follows (Scheme 3.3): 0.5 g of the modified mesoporous silica, OSU-6-W-APTMS-2, was stirred with 2.0 g of EDTA anhydride in ethanol/acetic acid solution (50%, 50 ml) in a 125-ml round-bottom flask for 12 hours at around 70 °C under reflux. After cooling, the solid product was isolated by filtration and washed with acetone/water and dried under vacuum for a day.

FT-IR spectra of the yield showed a distinctive absorption at 1640-1725 cm^{-1}, attributable to amide and carboxylic groups, thus suggesting that the chelating ligands had been anchored successfully on the surface of the adsorbents.

a)

b)
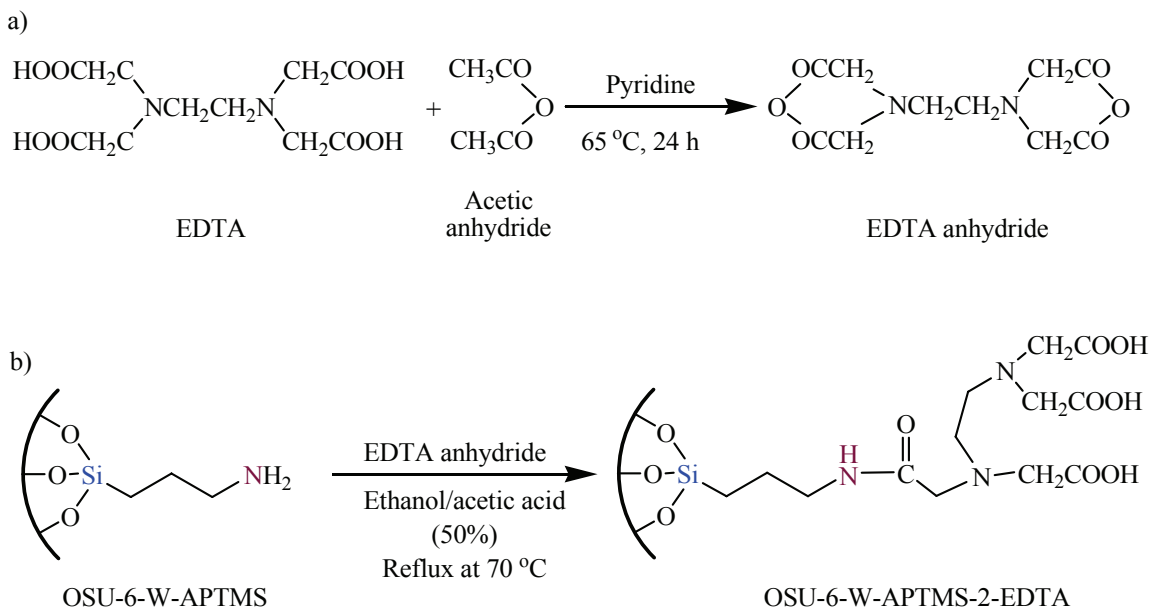
Scheme 3.3. Schematic diagram for the immobilization of EDTA on the OSU-6-W-APTMS-2 mesoporous material surface

3.2.4. Metal Uptake Experiments

The adsorption and separation experiments were conducted by shaking five different amounts (25, 50, 75, 100, and 125 mg) of the amino-functionalized mesoporous silica systems, OSU-6-W-APTMS-(1&2), each in a different glass vial for 4 hours with 10 ml of 100 ppm of aqueous solution of the appropriate metal(II)nitrate ions (Cu^{2+}, Zn^{2+}, and Cd^{2+}). Measurement of the metal ion concentration was carried out by allowing the insoluble complex to settle down, withdrawing an appropriate volume of the supernatant using a micropipette and then filtrating using a 0.45µm membrane syringe. The metal ion uptake was calculated as mmol of M^{2+}/g ligand. A linear range of the calibration curve for each metal was used in order to calculate the unknown concentration.

3.3. RESULTS AND DISCUSSION

3.3.1. Mesoporous OSU-6-W Modified with Amino Groups

The mesoporous silicas, OSU-6-W-APTMS-(1 and 2), with amino functional groups were prepared by the post-synthesis method from the reaction of the ordered mesoporous silica, OSU-6-W, with 3-aminopropyltrimethoxysilane using two different procedures of grafting. The aminated ordered mesoporous silicas prepared by these methods show good yields with excellent surface coverages. The properties of these materials are strongly dependent on the modification procedure used.

The ordered mesoporous silica, OSU-6-W, and the two modified samples, OSU-6-W-APTMS-1 and OSU-6-W-APTMS-2, were investigated using a variety of techniques. The most informative of these are cross-polarization/magic angle spinning nuclear magnetic resonance (CP/MAS NMR) and Fourier transform infrared (FT-IR) spectroscopies, X-ray powder diffraction (XRD), surface area analysis (BET), and

elemental analysis (EA). The NMR studies are mainly focused on the ^{29}Si and ^{13}C

nuclei. In the FT-IR, the CH_2 stretching modes provide a quantitative measure of the

surface concentration of the silane, while the Si-O, Si-O-Si, and N-H stretch/deformation

modes yield valuable structural information.

3.3.1.1. Identification of the Textural Properties (Physical Characterization)

As previously discussed (Chapter two), the physical structure of silica gels (high

surface area, large pore volume, *etc.*) is one of the major reasons for their effectiveness as

a support material. Variations in surface areas, pore volumes and pore sizes (as well as

their distribution) have a significant effect on the resulting material. This includes the

dispersion of the active groups and the ease in which reagents can diffuse to the active

site. It is therefore necessary to accurately characterize the physical nature of the

resulting material.

I. X-ray Powder Diffraction (XRD)

The X-ray diffraction patterns (XRD) in the range of 1.0-10.0º of pristine

HCl/EtOH washed ordered mesoporous material, OSU-6-W, and the two functionalized

samples, OSU-6-W-APTMS-1 and OSU-6-W-APTMS-2, are shown in Figure 3.2. The

XRD patterns of the samples show strong (100) peaks and proportional (110) and (200)

peak intensities, confirming the presence of the hexagonal structures and suggesting that

the modification process does not affect the framework integrity of the ordered

mesoporous OSU-6-W.[12,13,16] It is also to be noted that the (100) peak gradually shifts to

higher angles with increasing the amount of functional group on the surface from OSU-6-

W-APTMS-1 to OSU-6-W-APTMS-2, indicating an effective decrease of the OSU-6-W

pore diameter, which can be understood in terms of excluded volumes associated with the

silylation of the OSU-6-W surface walls.
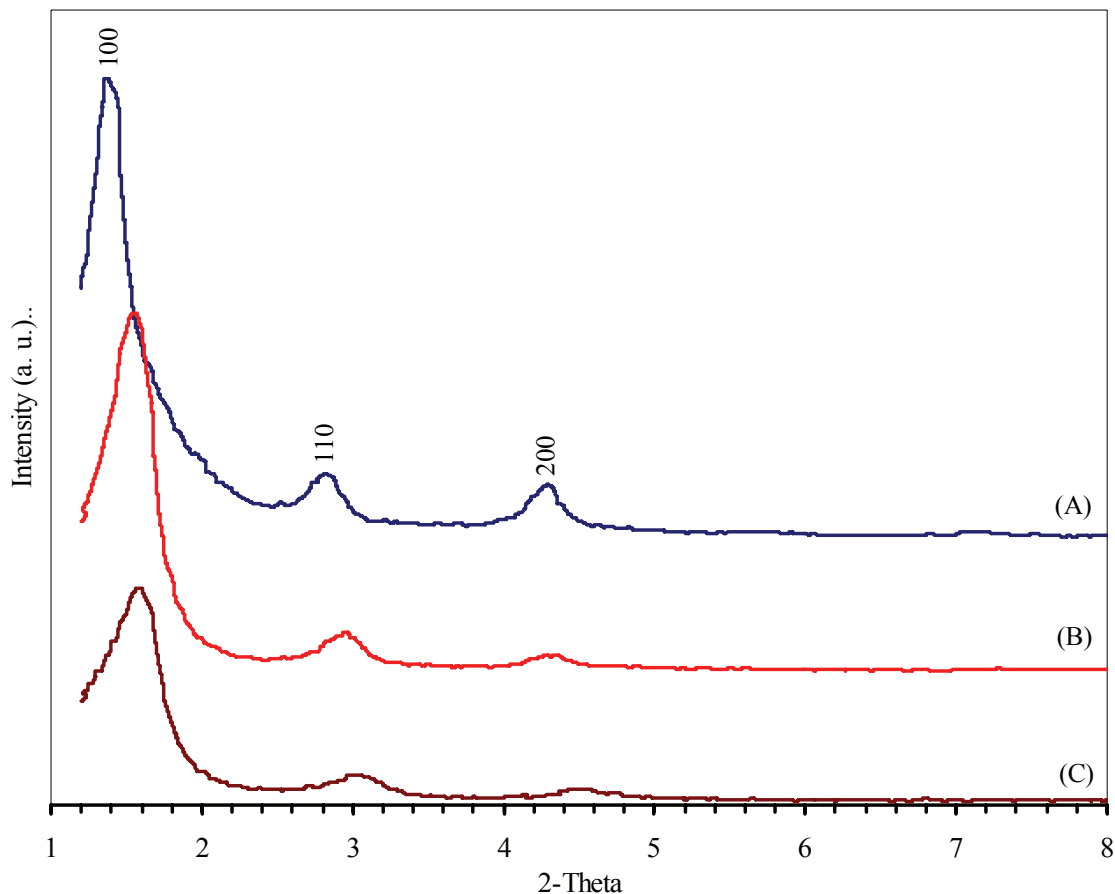
Figure 3.2. XRD patterns in the range of 1.0-10.0º of; (A) pristine HCl-Ethanol washed ordered mesoporous material, OSU-6-W, and the functionalized OSU-6-W with 3-aminopropyltrimethoxysilane: (B) OSU-6-W-APTMS-1 and (C) OSU-6-W-APTMS-2. The spectra are shifted vertically for the sake of clarity.

According to the average pore diameter of the material from the surface area

measurements, an average thickening of the walls of about 27.8 Å in the case of OSU-6-

W-APTMS-2 is indicated. This statistically would correspond to an extra layer of Si-O-

Si homogeneously spread on the original wall (20.9 Å Thickness). It can also be noticed

that the d_{100} peak has become broader with the increase in the loading of the functional

groups, indicating a slight alteration of the ordering of the mesoporous structure and more functional groups on the surface.

II. Nitrogen Adsorption-desorption Measurements

Figure 3.3 shows the nitrogen adsorption-desorption isotherms performed at 77K for the OSU-6-W silica before and after grafting with γ-aminopropyl trimethoxysilane. The textural properties of these materials are summarized in Table 3.1. The curve corresponding to the pure mesoporous silica, OSU-6-W, is typical for MCM-41 mesoporous materials with hexagonal channel arrays.[12,13] These are type IV isotherms showing a sharp, reversible step at ~ 0.3-0.4 P/P_o, typical of the N_2 filling of uniform mesopores, with an average pore diameter of about 51 Å, total pore volume of 1.24 cm^3/g, and a surface area of 1283 m^2/g. The saturation plateau is very clearly defined, indicating that the external surface of the sample is relatively small. The mesoporosity is filled for a very small range of relative pressure, confirming the very narrow pore size distribution. After reaction with the coupling agent, the nitrogen adsorption-desorption experiments yielded a Brunauer-Emmett-Teller (BET) surface area of 1023 m^2/g and a total pore volume of 0.98 cm^3/g for the OSU-6-W-APTMS-1 sample, and a surface area of 709 m^2/g and a total pore volume of 0.66 cm^3/g for the OSU-6-W-APTMS-2 sample. The BET isotherms for both modified samples also showed type IV isotherms. The adsorption isotherm curves obtained show that the total adsorbed amounts (taken at P/P_o = 0.99) have diminished, as have the specific surface area. The uptake corresponding to the filling of the mesopores has shifted to lower relative pressures indicating a reduction of the pore diameter from 51.1 to 43.6 Å for OSU-6-W-APTMS-1 and from 51.1 to 36.2 Å for OSU-6-W-APTMS-2.
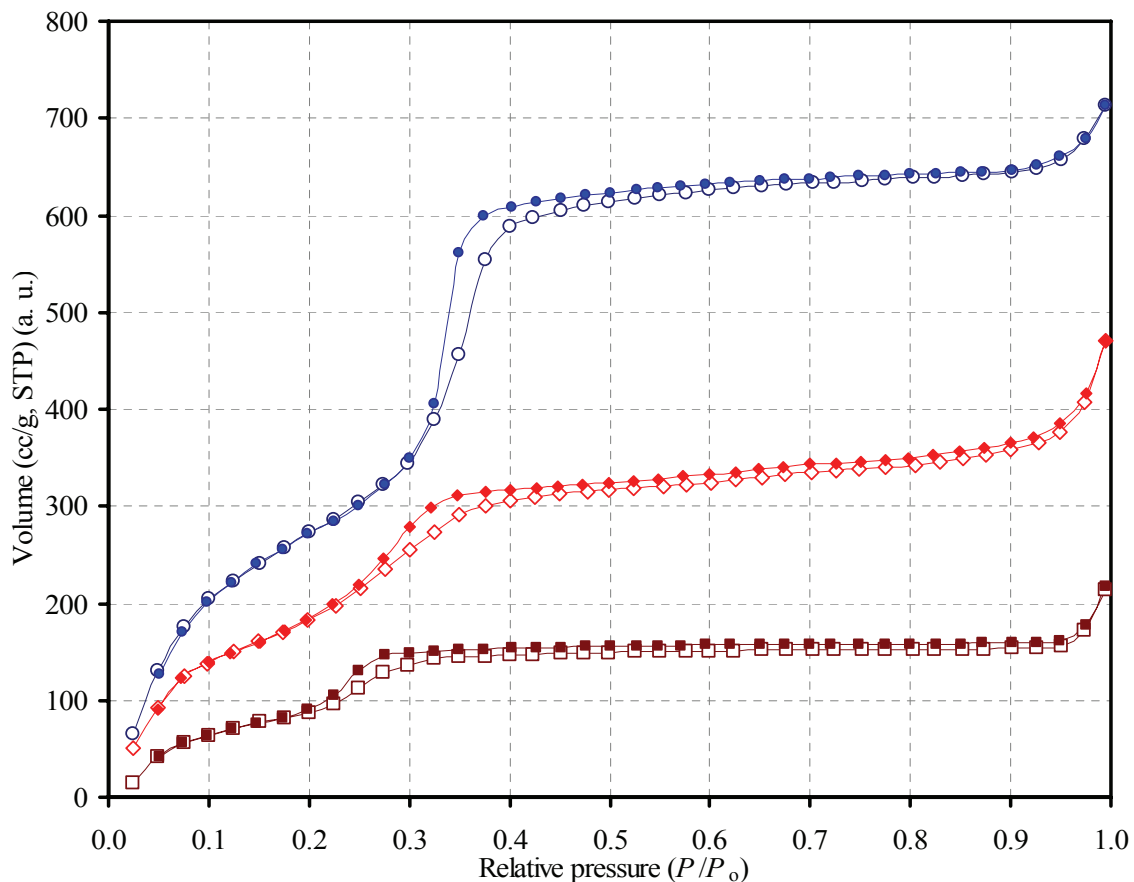
Figure 3.3. Nitrogen adsorption-desorption isotherms of (○) OSU-6-W, (◊) OSU-6-W-APTMS-1, and (□) OSU-6-W-APTMS-2. Open symbols: adsorption; closed symbols: desorption. The isotherm data are shifted vertically for the sake of clarity.

Both the surface area and the total pore volume of both samples dropped significantly compared with the un-functionalized sample, OSU-6-W. The decrease of the pore volume of the material after silanization is the direct consequence of the silanization process filling the mesopores. However, this quite large decrease may also be due to some pore blocking due to partial surface polymerization at the mouths of some mesopores, possibly with silsequioxane polymer. Most of the decrease of the specific surface area can be accounted for the mass uptake during the grafting of organic species into the pore structure.

The BET isotherms, Figure 3.3, of the modified samples show small hysteresis loops. A narrow hysteresis loop on the steep low-pressure portion of the isotherm may be due to nitrogen filling slit-like micropores in the regions between adjacent organic groups and the silica wall.[87] A second narrow hysteresis loop on the horizontal portion is assigned to the *ca*. 43.6 and 36.2 nm wide mesopores of the major channel structure. The reduction in total pore volume and shift in the pore size distribution peak from 51.1 to 43.6 and 36.2 Å, Figure 3.4, imply a reduction in the free channel space as the amino groups were deposited on the walls inside the mesoporous channel.
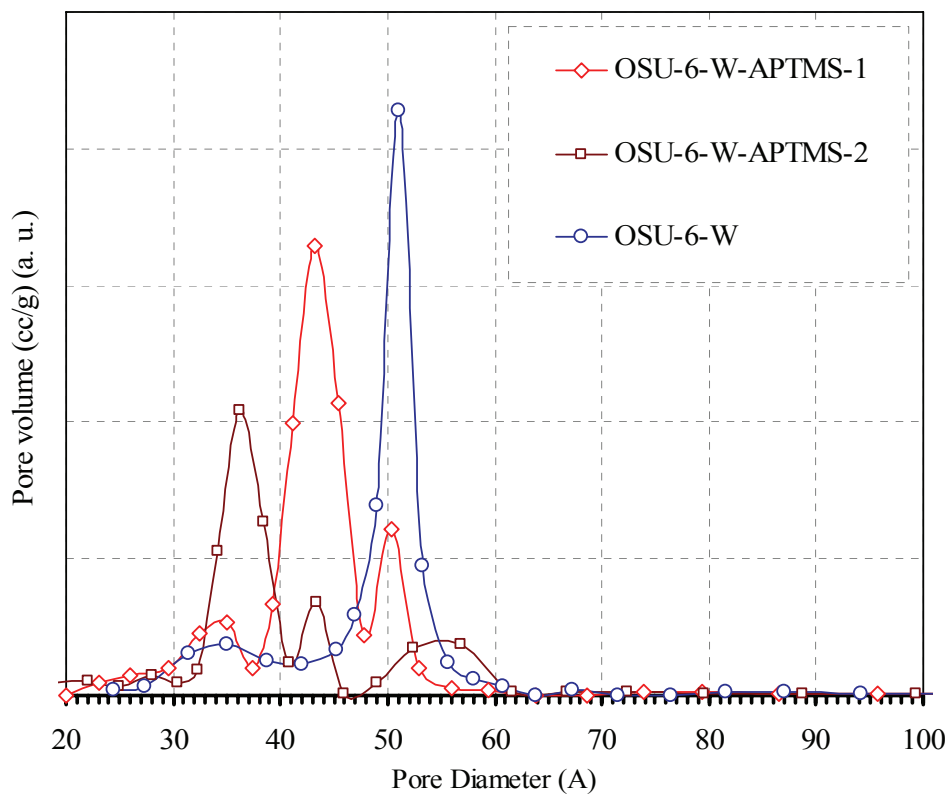
Figure 3.4. The pore size distribution of (○) OSU-6-W (max at 51.1 Å), (◊) OSU-6-W-APTMS-1 (max at 43.6 Å), and (□) OSU-6-W-APTMS-2 (max at 36.2 Å)

Combining the results of XRD with the results of the nitrogen adsorption-desorption isotherms demonstrate that after the silylation reaction the pore size of functionalized OSU-6-W was narrowed from *ca.* 51.1 Å to *ca.* 43.6 Å for the modified OSU-6-W-APTMS-1 and to *ca.* 36.2 Å for the modified OSU-6-W-APTMS-2. An opening of *ca.* 36.2 Å is sufficiently large to allow all metal ions and most small organic molecules to be incorporated into the functionalized samples.

Table 3.1. Textural Properties Determined from Nitrogen Adsorption-desorption Experiments at 77 K and Powder XRD Measurements.

Sample	Specific surface area (m^2/g)	Total pore volume (cm^3/g)	Average pore size (Å)	d_{100} (Å)	Wall Thickness (Å)
OSU-6-W	1283	1.24	51.1	62.4	20.9
OSU-6-W-APTMS-1	1023	0.98	43.6	57.7	23.0
OSU-6-W-APTMS-2	709	0.66	36.2	55.4	27.8

3.3.1.2. Identification of Functional Groups (Chemical Characterization)

The techniques employed for the physical characterization of the modified silica materials are, in the main, applicable to all modified silicas. However, this is not the case when investigating the chemical nature of these materials. The range of techniques available is large and very much dependent on the modified silica under investigation. Therefore, the aim of this section is to briefly discuss the most commonly used techniques for chemical characterization. To obtain an accurate picture of the nature of the active species on the silica surface a combination of techniques should be employed. There are three important points that should be addressed in order to achieve this: (i) stability, (ii) loading, and (iii) structure of the active species.

I. Solid State ^{29}Si CP/MAS NMR Spectroscopy

Solid state ^{29}Si CP/MAS NMR is a sensitive and reliable technique for qualitative and quantitative determination of both Si-OH groups on solid surfaces and the total loading of the functional groups on the silica surfaces.[15,16] Figure 3.5 shows the solid state ^{29}Si CP/MAS NMR spectra for HCl-Ethanol washed mesoporous silica, OSU-6-W (A), the modified OSU-6-W-APTMS-1 (B), and the modified OSU-6-W-APTMS-2 (C) samples.
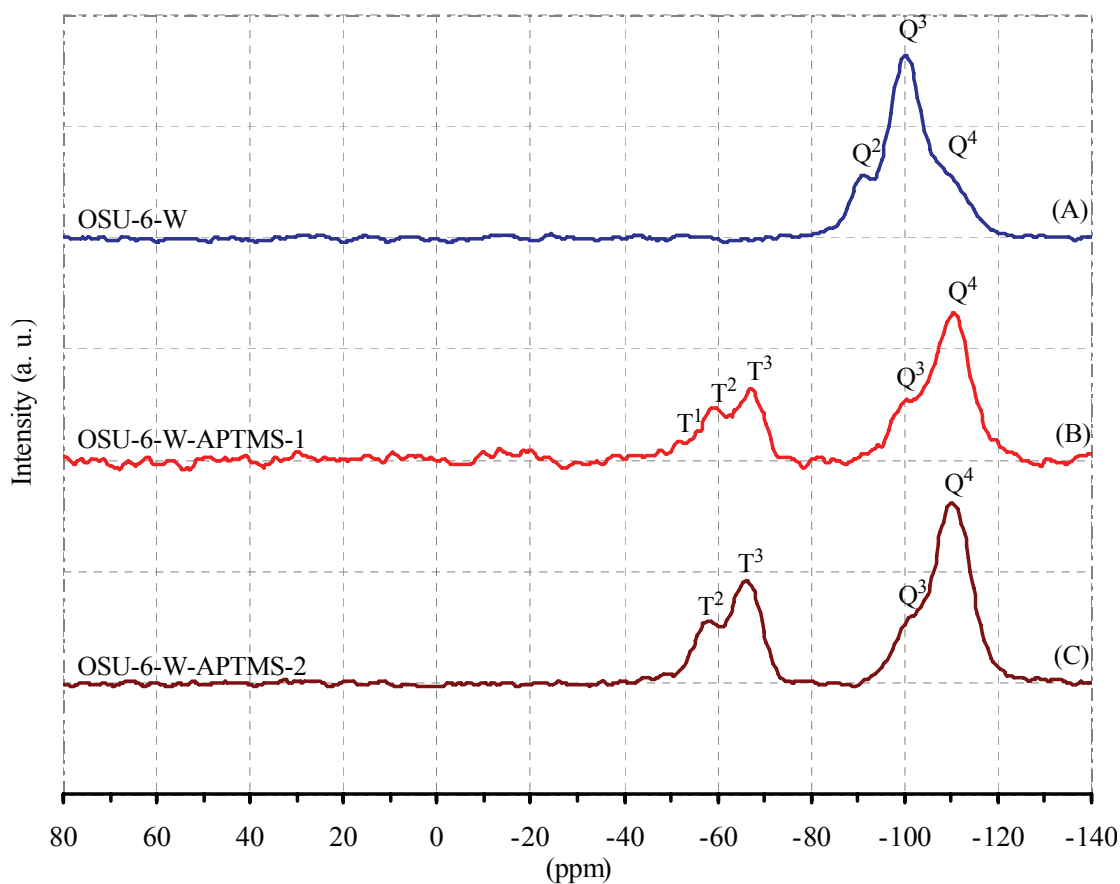
Figure 3.5. ^{29}Si CP/MAS NMR spectra of; (A) HCl-Ethanol washed mesoporous silica, OSU-6-W, (B) the modified OSU-6-W-APTMS-1, and (C) the modified OSU-6-W-APTMS-2.

Multipeak curve fitting indicates that for the HCl/EtOH washed sample, OSU-6-W, without silylation, three peaks can be identified in the vicinity of -100 ppm. According to Sindorf et al.,[88] the three peaks are composed of a low intensity peak at -91.2 ppm, which corresponds to surface silicon atoms with two siloxane bonds and two geminal silanol groups (either single or hydrogen-bonded), represented as $(SiO)_2*Si(OH)_2$ and labeled in Figure 3.5 as a Q^2 silicon; a peak at -100.4 ppm attributed to surface silicon atoms with three siloxane bonds and one (isolated) silanol group, represented as $(SiO)_3*Si$-OH and labeled in Figure 3.5 as a Q^3 silicon; and a resonance at -107.9 ppm attributed to surface silicon atoms with four siloxane bonds, i.e., $(SiO)_4*Si$, and labeled in Figure 3.5 as a Q^4 silicon.

The two amino functionalized samples, (B) and (C), show two peaks that are located near -100 and -110 ppm, corresponding to Q^3 and Q^4 silicon environments. Additionally, the OSU-6-W-APTMS-1 sample has another three peaks at -51.9, -59.3, and -67.1 ppm corresponding to T^1, T^2, and T^3 silicon environments, whereas the OSU-6-W-APTMS-2 sample has another two peaks at -57.3 (T^2), and -66.6 ppm (T^3). All peaks were identified by multipeak curve fitting. Scheme 3.4 illustrates all silicon atom environments.[35]
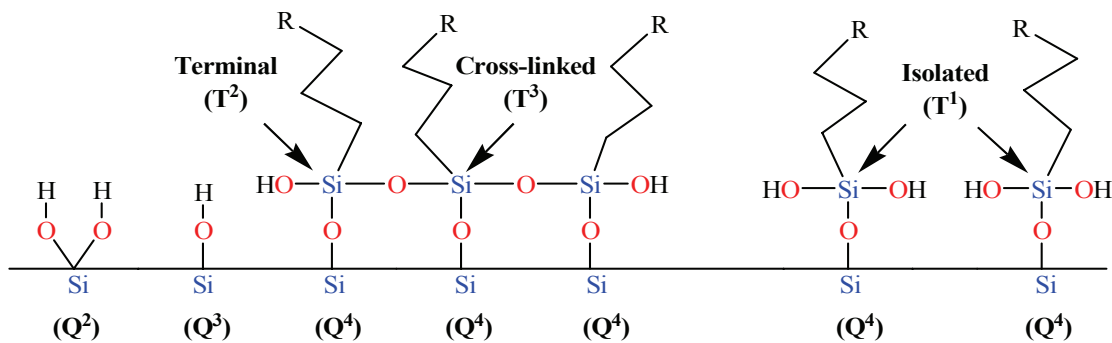
Scheme 3.4. Schematic illustration of different silicon atom environments.

The silylated samples, OSU-6-W-APTMS-1 and OSU-6-W-APTMS-2, show changes in relative intensities of the silicon atom resonances in the locality of -100 ppm when compared to OSU-6-W starting material. In particular, the relative intensity for the Q^3 silicon resonance labeled at around -100 ppm undergoes a significant decrease with increasing the amount of functional groups on the surface as compared to the Q^4 silicon resonance at *ca.* -110 ppm. This difference in relative intensity is attributable to reactions of surface Si-OH groups with APTMS that lead to the formation of more Si-O-Si bonds. By comparison between the two modified samples, the intensity of the peak at around -100 ppm is smallest for OSU-6-W-APTMS-2 sample providing evidence of greater functionalization of this sample.

The additional peaks lying in the range from -40 to -70 ppm, as shown in Figure 3.5, occur only for the silylated samples. These arise from the silicon atoms of the silylating reagent. There are three of these new peaks in case of the OSU-6-W-APTMS-1, Figure 3.5 (B). The three resonances indicate three different environments for the siloxane groups in the functionalized monolayer. The three resonances, as depicted in Figure 3.5 (B), can be assigned as the following: (i) the resonance at *ca.* -51.9 ppm arises from isolated SiO_3 groups that are not bound to any neighboring siloxanes, (ii) the resonance at *ca.* -59.3 ppm arises from terminal groups that are only bound to one neighboring siloxane, and (iii) the resonance at *ca.* -67.1 ppm arises from cross-linked groups that are bound to two neighboring siloxanes, see Scheme 3.4.

In the case of the OSU-6-W-APTMS-2, Figure 3.5 (C), there are two resonances that indicate two different environments for the siloxane groups in the functionalized monolayer. The two resonances, as depicted in Figure 3.5 (C), can be assigned as

follows: (i) the resonance at *ca.* -57.3 ppm arises from terminal groups that are only

bound to one neighboring siloxane, and (ii) the resonance at *ca.* -66.6 ppm arises from

cross-linked groups that are bound to two neighboring siloxanes. It can be noted that the

intensities of these peaks indicate different structures and surface coverages for the two

silylated samples. The dominant peak in the OSU-6-W-APTMS-1 and OSU-6-W-

APTMS-2 spectra is attributed to the cross-linked siloxane group. The surface coverage

of the functionalized monolayer of OSU-6-W is estimated to be greater in the OSU-6-W-

APTMS-2 sample than in the OSU-6-W-APTMS-1 sample. This conclusion is based on

the higher intensity of the peak for T^3 for the former sample compared to the latter. Also,

the absence of the peak for T^1 in the spectrum of OSU-6-W-APTMS-2 is evidence for

higher loading and greater homogeneity of the functional groups on the surface. OSU-6-

W-APTMS-1 has peaks that are slightly more than that of an approximately 50% surface

coverage sample while the OSU-6-W-APTMS-2 has peaks with intensities that are higher

than that of an approximately 75% surface coverage sample previously reported in

literature.[35] On this basis the surface coverage of the functionalized monolayer of

mesoporous OSU-6-W-APTMS-2 is estimated to be greater than 75%.[35]

Solid state ^{29}Si CP/MAS NMR spectra show distinct resonances for siloxane [Q^n

= Si(OSi)$_n$(OH)$_{4-n}$, $n = 2–4$] and organosiloxane [T^m = RSi(OSi)$_m$(OH)$_{3-m}$, $m = 1–3$]

centers, with T^3 predominant over T^2 and T^1 organosiloxane centers, Figure 3.5,

indicating that the condensation of the amino groups into the wall structure of the

mesoporous silica was extensive. In general, the quantitative determination of

organosilane content from the peak intensities indicated that the level of functionalization

corresponded to the organosilane content used in the reaction mixture as well as the

reaction conditions. The width of the T^m peaks is similar to those of the Q^n species, suggesting that the local environments are comparable in terms of steric hindrance.

II. Solid State ^{13}C CP/MAS NMR Spectroscopy

The presence of covalently linked organic moieties bearing amine groups in the derivitized OSU-6-W mesoporous silicas was also confirmed by the solid state ^{13}C CP/MAS NMR spectroscopy.[15,16] Figure 3.6 shows the solid state ^{13}C CP/MAS NMR spectra for amino-functionalized mesoporous materials. Figure 3.6 (A) shows resonances for the OSU-6-W-APTMS-1 sample at δ (ppm) values of 9.7($\equiv$Si-CH_2-), 25.6($\equiv$Si-CH_2-CH_2-), 23.3($\equiv$Si-OCH_3), and 43.4(-CH_2-NH_2), whereas Figure 3.6 (B) shows resonances related to the OSU-6-W-APTMS-2 sample at δ (ppm) values of 10.6($\equiv$Si-CH_2-), 26.1($\equiv$Si-CH_2-CH_2-), and 43.6(-CH_2-NH_2). These data confirmed that the γ-aminopropyl groups were not damaged by either functionalization method. Peaks corresponding to the organosiloxane moieties are relatively broad, indicating restricted mobility of the functional groups attached to the siloxane framework. The presence of a small peak at around 23.3 ppm indicates the presence of a small amount of methoxy groups, which in turn confirms the low loading of the functional groups in the OSU-6-W-APTMS-1 sample. The low intensity of the peaks of the latter material compared to OSU-6-W-APTMS-2 also reflects lower surface loading from the one-step method.
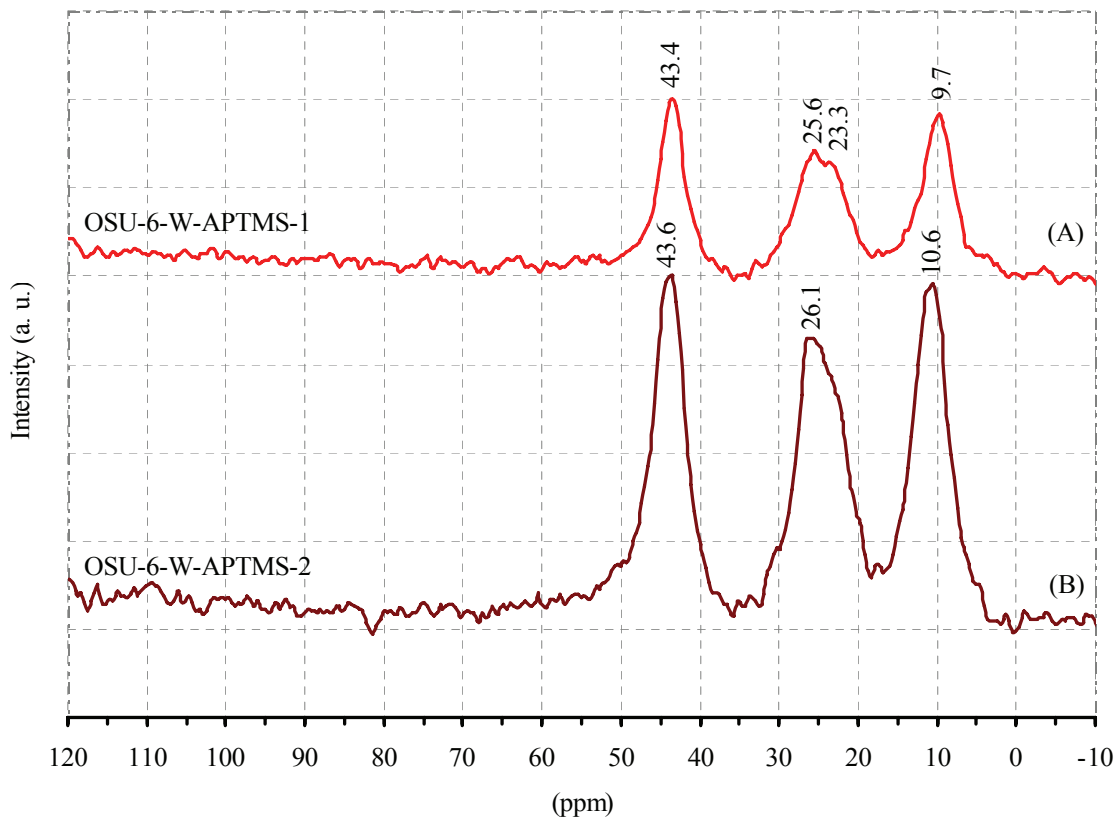
Figure 3.6. Solid state ^{13}C CP/MAS NMR spectra of the modified samples with Amine Groups, (A) OSU-6-W-APTMS-1, and (B) OSU-6-W-APTMS-2.

There are two consequences of leaving two out of the three methoxy groups unreacted with surface hydroxyls: (1) these groups cannot react with other silanes and (2) they partially screen neighboring surface hydroxyls from oncoming silanes as well. If water is present in the solution, hydrolysis of some methoxy groups allows their polymerization in the solution or polymerization with the surface-immobilized silanes, the so-called horizontal polymerization. The new approach developed in this work hydrolyzes only the methoxy groups of immobilized amine functional groups after initial silanization and washing. The resulting hydroxyls circumvent the two problems

mentioned above as well as eliminate the unwanted vertical polymerization. The

procedure is described by the cartoon in Scheme 3.5.
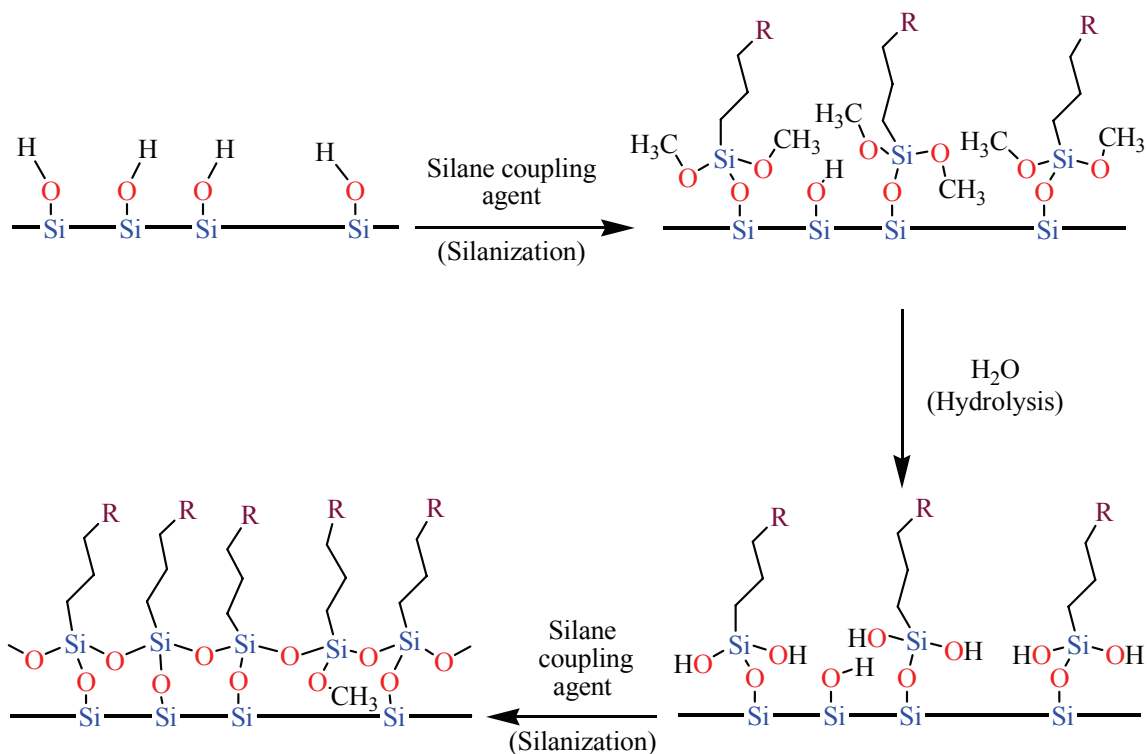
Scheme 3.5. General Silanization Mechanism and Effect of Water.[89]

Alternating silanization and washing in water enhances the maximum surface

density of silanes by at least 30%.[89] Moreover, it appears that one treatment in water

produces as large an effect as a few consecutive ones and the vertical polymerization,

which could in theory start from unreacted methoxy groups after the second silanization,

does not take place. It is known that amines catalyze reactions between methoxysilanes

and hydroxyl groups on silica[90] which suggests that aminomethoxysilanes would

immobilize on silica more efficiently. The ability to form a pseudo-five-membered ring

in γ-aminosilanes, as shown in Scheme 3.6,[91] offers a possibility for self-catalytic

reaction enhancement for the APTMS aminosilanes.[90]
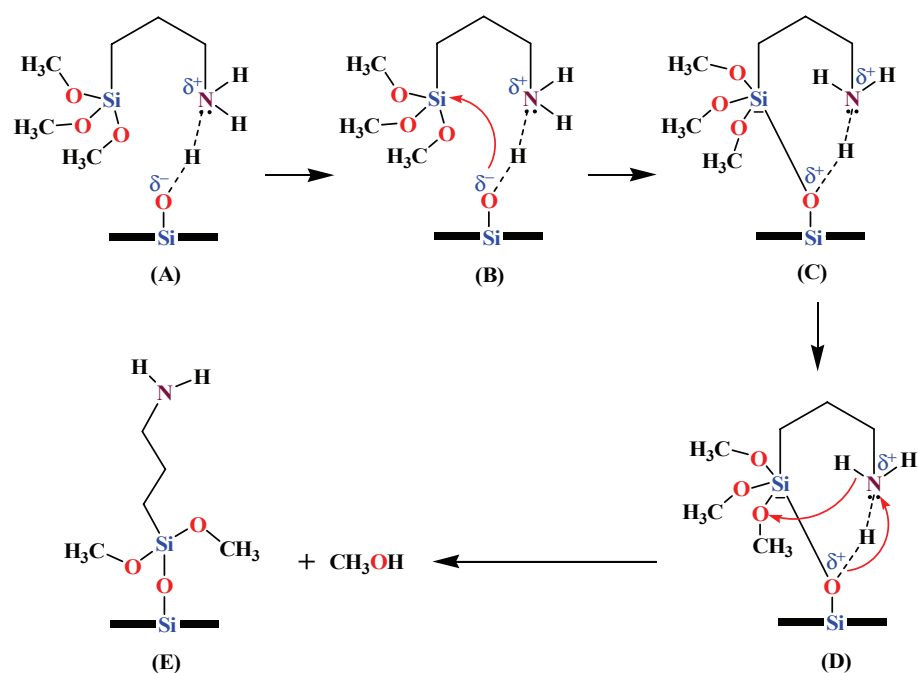
Scheme 3.6. Mechanistic description of amine catalysis of silylation reaction: (A) adsorption of 3-Aminopropyltrimethoxysilane through amino-group, (B) nucleophilic attack of SiO(δ-) on silicon, (C) heptacoordinate intermediate resulting from attack, (D) proton abstraction by methoxy leaving group with electrophilic assistance by amine, and (E) silylated surface with generation of methanol.[91]

III. Fourier Transform Infrared Spectroscopy (FT-IR)

The functional groups contained by the samples were also identified using FT-IR. Figure 3.7 shows the FT-IR spectra of the two modified samples along with the unmodified mesoporous OSU-6-W. The O-H bond stretching bands of silanol groups were observed at 3200-3800 cm^{-1}. Silanol groups on the silica surface of OSU-6-W exist as several types, such as isolated, hydrogen bonded, and geminal types of silanol.[15] The IR absorption bands of these silanol groups correspond to the peaks at 3740, 3200–3600, and 3715 cm^{-1}, respectively. For OSU-6-W, the concentration of surface silanol groups were reported to be 14.43 mmol/g (6.77 molecule/nm^2) in chapter two.
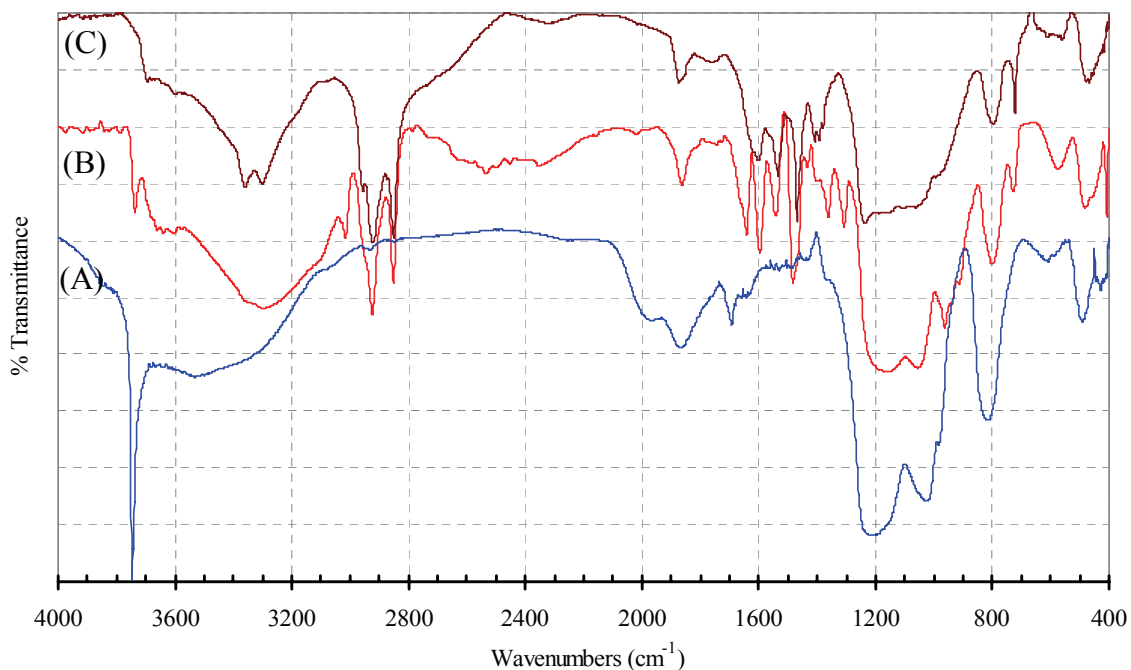
Figure. 3.7. The infrared spectra (IR) of OSU-6-W (curve A), OSU-6-W-APTMS-1 (curve B), and OSU-6-W-APTMS-2 (curve C).

The results showed that the surface silanol group was mainly of the isolated type, IR absorption bands for which were observed at 3746 cm^{-1}. Si-O bond stretching was detected at 976 cm^{-1}. The siloxane, -(SiO)$_n$-, peak appeared as a broad peak at 1000-1200 cm^{-1}, see description in chapter two (2.10.2.2).[92]

In general, the functionalized silicas with 3-aminopropyltrimethoxysilane show an IR peak for the CH$_2$ rocking vibration of Si-CH$_2$R at around 700 cm^{-1}. Broad NH$_2$ stretching at 3250–3450 cm^{-1}, an N-H deformation peak at 1640–1560 cm^{-1}, C-H stretching of methyl groups at 3000-2840 and 1450 cm^{-1}.[63,92] The efficiency of the grafting process is demonstrated by a significant decrease in the silanol bands at around 3746 cm^{-1}, with an association increase of new bands characteristic of the immobilized aminopropyl groups. These bands were attributed to both the symmetric and asymmetric

stretching of CH_3 and CH_2 groups in OSU-6-W-APTMS-1; $\nu_{as}(CH_3) = 3026$ cm^{-1}, $\nu_{as}(CH_2) = 2920$ cm^{-1}, $\nu_s(CH_2) = 2850$ cm^{-1}, CH_2 scissor at 1467 cm^{-1}, CH_3 bending at 1371 cm^{-1}, CH_3 bending vibration at 1307 cm^{-1}, and for the NH_2 at $\nu_{as} = 3359$ cm^{-1}, $\nu_s = 3302$ cm^{-1}. The IR spectra for OSU-6-W-APTMS-2 show peaks at 2923 and 2851 cm^{-1} assigned for the $\nu_{as}(CH_2)$ and $\nu_s(CH_2)$, and peaks at 3357 and 3297 cm^{-1} for the asymmetric and asymmetric stretching of NH_2.[92] When comparing the intensities of the IR peaks in the modified samples, it was concluded that the second sample had a higher concentration of functional groups than the first modified sample in accord with the solid state ^{29}Si and ^{13}C NMR and elemental analysis results.

3.3.1.3. Determination the Total Surface Loading of the Mesoporous Silica with the γ-Aminopropyl Functional Groups

Concentration of the functional groups on the surface is one of the important aspects of these materials, so determining the number of the functional group is one of the objectives for validation of the synthetic methods.

I. Spectrophotometric Analysis Method

The amount of aminosilane deposited on the surface was quantified using two variables. The surface loading (*l*) expresses the amount of deposited molecules in mmol/g. The number of molecules deposited per nm^2 is given by the surface coverage (*C*). Both values use the mass of the pure mesoporous silica before modification as a reference.[93]

For the quantitative analysis of the aminosilane in toluene solution a spectrophotometric analysis method was used. The determination of APTMS by means

of a color reaction with salicylaldehyde with the addition of a small amount of diethylether in an aprotic solvent such as toluene has been reported.[93]

After filtration of the modified sample, part of the filtrate was taken and transferred into three 10-ml vail samples. A 150 µl portion of salicylaldehyde and 150 µl of diethylether were added to each sample. The amine group reacts with salicylaldehyde, forming a yellow Schiff's base with $\lambda_{max} = 404$ nm. This reaction usually reaches equilibrium after one hour. All three samples were taken and the absorbance at $\lambda_{max} = 404$ nm was measured after one hour. APTMS concentration was calculated using a linear calibration curve.[93]

The total deposited amount (l) was calculated by subtracting the residual amount of aminosilane in the solvent after reaction from the initially added amount. This value includes chemical and physical deposition in the surface of the mesoporous material. The surface coverage (C) was calculated by ratioing the loading (l) to the specific surface area (S_{BET}) of the sample. Multiplication by Avogadro's number ($N_A = 6.022 \times 10^{23}$ molecules/mole) yields units of molecules/nm^2:[93]

$$C = (l / S_{BET}) \cdot N_A$$

For the OSU-6-W-APTMS-1, an average coverage of 2.76 APTMS molecules/nm^2 was calculated, while the OSU-6-W-APTMS-2 sample has an average coverage of 4.88 APTMS molecules/nm^2. The FTIR and the solid state ^{13}C and ^{29}Si CP/MAS NMR spectra of the OSU-6-W-APTMS-1 and OSU-6-W-APTMS-2 analyses demonstrated that the aminosilane was adsorbed almost exclusively by chemical reaction with surface hydroxyls. The coating formed by reaction of the silica with APTMS under dry conditions has been calculated.

II. Indirect Acid-base Titration

Another quantitative analysis of the amount of amine ligands immobilized on the mesoporous silica samples was achieved by indirect acid-base titration, Scheme 3.8. A 25 mg portion of each aminated silica sample was shaken with a 25 ml portion of aqueous 0.01 M hydrochloric acid solution for 24 h at 25 °C. The excess HCl was then titrated with a 0.10 M aqueous sodium hydroxide standard solution in the present of phenolphthalein indicator that changes its color from colorless in the acidic solution to red color in the alkaline solution.
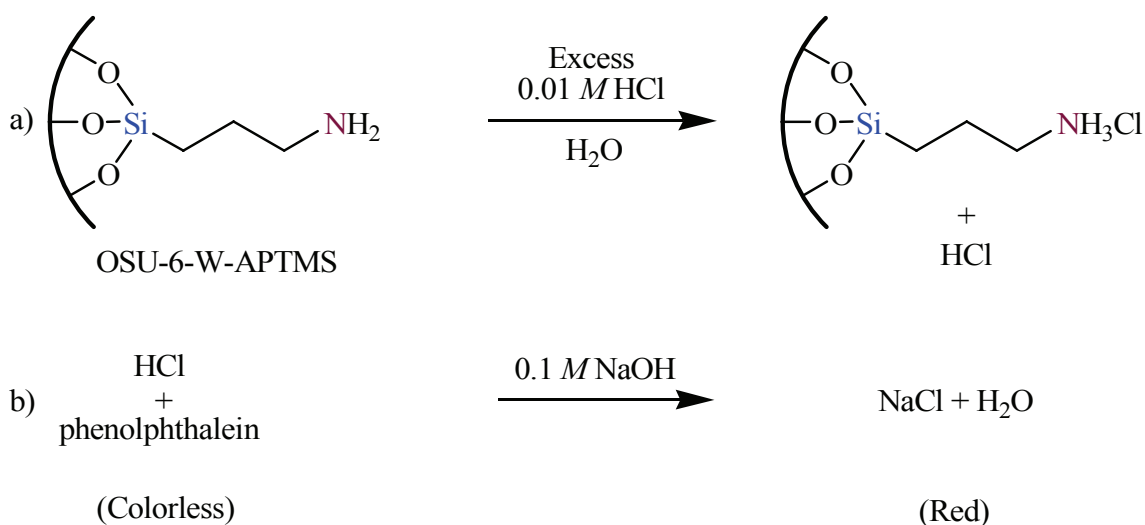
Scheme 3.8. Schematic illustration of the amino-functional determination using acid-base titration

The results of titration show good agreement with that of the spectrophotometric analysis method. It gives an amount of 2.24 group/nm^2 for the OSU-6-W-APTMS-1 and an amount of 4.93 group/nm^2 for the OSU-6-W-APTMS-2 sample.

III. Elemental Analysis (Combustion Analysis)

Carbon analysis was carried out for both modified samples. The concentration of attached groups was determined as follows:[94,95]

$$C \text{ (groups/nm}^2) = 6\text{x}10^5 \, P_C / [(1200n_C - WP_C)S_{BET}]$$

where C is the concentration of attached groups, which contain carbon; P_C is the percentage of carbon in the sample, n_C is the number of carbon atoms in the attached group (counted as C_3), W is the corrected formula mass of the modifier (counted as $C_3H_8NO_3Si$) and S_{BET} is the specific surface area of the unbonded substrate (1283 m^2/g), see Table 3.2.

Table 3.2. Carbon and nitrogen elemental analysis, and concentration of amine groups.

Sample	C %	N %	Surface Area (m^2/g)	[APTMS] (group/nm^2)
OSU-6-W	0.10	0.06	1283	---
OSU-6-W-APTMS-1	11.21	3.72	1023	2.50
OSU-6-W-APTMS-2	16.13	5.33	709	5.26

IV. Solid state ^{29}Si CP/MAS NMR Spectrum

A new, alternative procedure to evaluate the degree of silylation was developed using the ^{29}Si CP/MAS NMR spectrum.[96] The Q^2, Q^3 and Q^4 of OSU-6-W are found at -91.2, -100.4, and -107.9 ppm respectively, Figure 3.5 (A). The silicon atom of the silylating agent APTMS is seen at -51.9, -59.3, -67.1, -92.6, -100.5, and -110.3 ppm for OSU-6-W-APTMS-1 sample and at -57.3, -66.6, -100.6, and -110.3 ppm for OSU-6-W-APTMS-2 sample, Figure 3.5 (B and C). The relative peak areas of the spectra are given

in Table 3.3. From these data, the silanol concentration [SiOH] and the degree of

silylation [APTMS] per gram of dry OSU-6-W (mol/g) can be obtained from the formula:

$$[SiOH] = ((I_{Q}^{3} + 2 \times I_{Q}^{2})/(60 \times I_{Q}^{4} + 69 \times I_{Q}^{3} + 78 \times I_{Q}^{2}))$$

$$[APTMS] = ((I_{APTMS})/(60 \times I_{Q}^{4} + 69 \times I_{Q}^{3} + 78 \times I_{Q}^{2}))$$

I_i represents the line intensity of the various silicon lines in the ^{29}Si MAS NMR spectrum.

These formulas can be rationalized when it is assumed that each ^{29}Si atom has an equal

contribution to the intensity, which is the case when proper relaxation occurs during the

consecutive pulses. The denominator of both equations relates to the chemical

composition of the dry OSU-6-W sample. The ^{29}Si CP/MAS NMR signal areas are

therefore multiplied by the respective molecular weight of Q^4, Q^3, and Q^2. The

nominator weighs the I_i lines relative to the dry OSU-6-W. Note that the absolute

intensities of the silicon lines are not required.

Table 3.3. Solid state ^{29}Si CP/MAS NMR deconvolution results

Sample	Q^4 (%)	Q^3 (%)	Q^2 (%)	[SiOH] (mmol/g)	[SiOH] (molecule/nm²)	[APTMS] (group/nm²)
OSU-6-W	14.38	71.73	13.89	14.43	6.77	---
OSU-6-W-APTMS-1	60.84	31.44	7.72	7.29	4.3	2.47
OSU-6-W-APTMS-2	82.98	17.01	0	2.76	2.06	4.71

The difference in silanol concentration before and after silylation will relatively

be equal to the concentration of the functional groups. No external reference is needed

when the degree of silylation is determined from the ^{29}Si CP/MAS NMR spectrum, this

in contrast to the proton measurement. This method can provide both the amount of

silylating agent attached to OSU-6-W and the silanol content from a single measurement. The concentration of the functional groups for both silylated samples calculated using this method show high agreement with that found by the other methods, see Table 3.3.

In this work a significantly large coverage of functional groups (4.71 molecule/nm^2) is obtained compared with the results in the literature (2.53 molecule/nm^2).[97] This difference probably arises from the difference in pore sizes, 5.1 vs 3.6 nm, respectively, and the water treatment step in the silylation process. The larger pores can avoid a steric congestion of the silane molecules. The treatment with water easily induces the full coverage of adsorbed water, which allows the formation of hydroxy silanes to result in the assembly and aggregation of the molecules that are still mobile on the surface and finally fixed by the silanol or siloxane. Thus, in the presence of water, the aminosilane molecules are attached beyond the density of isolated silanols (total silanol concentration including isolated and geminal is 6.77 OH groups/nm^2). So the total coverage is controlled by the specific surface area and pore size of the silica, rather than the hydroxyl group content.

3.3.2. Mesoporous OSU-6-W-APTMS-2 Immobilized with EDTA

3.3.2.1. Identification of Functional Groups of OSU-6-W-APTMS-2-EDTA

I. Infrared Spectroscopy (FT-IR)

Identification of the modified mesoporous silica with immobilized EDTA, was carried out by FT-IR spectroscopy. Carbonyl groups of amides and carboxylic groups were confirmed by the strong absorptions at 1644 and 1725 cm^{-1}, respectively. These peaks validate the immobilization of the EDTA active groups to the amino functional groups.

II. Elemental Analysis

The carbon and nitrogen content increased comparing with the OSU-6-W-APTMS-2 sample from 16.13% to 27.04% for the total carbon and from 5.33% to 9.56% for the total nitrogen. These data confirm the attachment of the EDTA to the amine groups.

III. Surface Area Analysis

The BET measurement shows a noticeable decrease in the surface area from 709 m^2/g to 496 m^2/g.

3.3.2.2. Determination the Total Surface Loading of the Silica with the EDTA Groups

I. Indirect Acid–base Titration

A quantitative analysis of the amount of carboxylic ligands immobilized on the mesoporous silica sample was measured by means of an acid-base titration to evaluate the extent of introduction of the functional groups of EDTA into mesoporous matrices.

The quantitative analysis of the amount of carboxylic acid was achieved as follows: A 25 mg portion of the immobilized modified silica with EDTA was shaken with a 25 ml portion of aqueous 0.01 M NaOH solution for 24 h at 25 °C. The excess NaOH was then titrated with an aqueous 0.10 M HCl standard solution in the presence of phenolphthalein that changes its color from red in the basic solution to colorless in the acidic solution.

Approximately, 65% of the aminosilane were immobilized with EDTA (2.9 molecule/nm^2). The low extent of introduction of EDTA when compared with that in the case of chitosan (85%)[86] might be attributable to the steric hindrance of bulky EDTA

molecules or repulsion between the functional groups since the distance between the adjacent primary amino groups in OSU-6-W-APTMS-2 is much closer than that in chitosan.[86] However, the high surface area and other advantages of the mesoporous silicas over the organic polymer make the use of modified silica more practical and efficient.

3.3.3. Metal Uptake Study

3.3.3.1. Transition Metal Ions (Cu^{2+}, Zn^{2+}, and Cd^{2+})

I. Uptake Capacities

The uptake capacities of the mesoporous silicas with immobilized monoamine ligand systems were investigated using different amount of the absorbents, OSU-6-W-APTMS-(1&2), and one constant concentration of copper, zinc, and cadmium ions (100 ppm) at pH 5.5, 6.0, and 7.0, respectively. These acidities were selected based on previous reports of optimal pH for adsorption.[55] The results are shown in Figures 3.8 and 3.9. The tendency of these divalent metal ions to chemisorb to the monoamine ligand system at the optimum conditions increases in the order: $Cd^{2+} < Zn^{2+} < Cu^{2+}$. For both functionalized samples, it is shown that the uptake of all metal increases with an increase of the amount of absorbent. Moreover, the uptake capacities increase with the increasing of the total coverage of the surface with the functional groups from OSU-6-W-APTMS-1 to OSU-6-W-APTMS-2. The maximum uptakes were calculated from the Langmuir adsorption isotherms. The uptake capacities are listed in Table 3.4. The uptake capacities of the OSU-6-W-APTMS-1, Figure 3.8, are correlated to the approximate formation of 2 Cd^{2+}: 3 NH_2, an approximate 1 Zn^{2+}: 1 NH_2, and 1.2 Cu^{2+}: 1 NH_2

complexes. The absorption of greater than one copper ion per amine may be due to inclusion of anionic copper nitrate complexes as counterions.
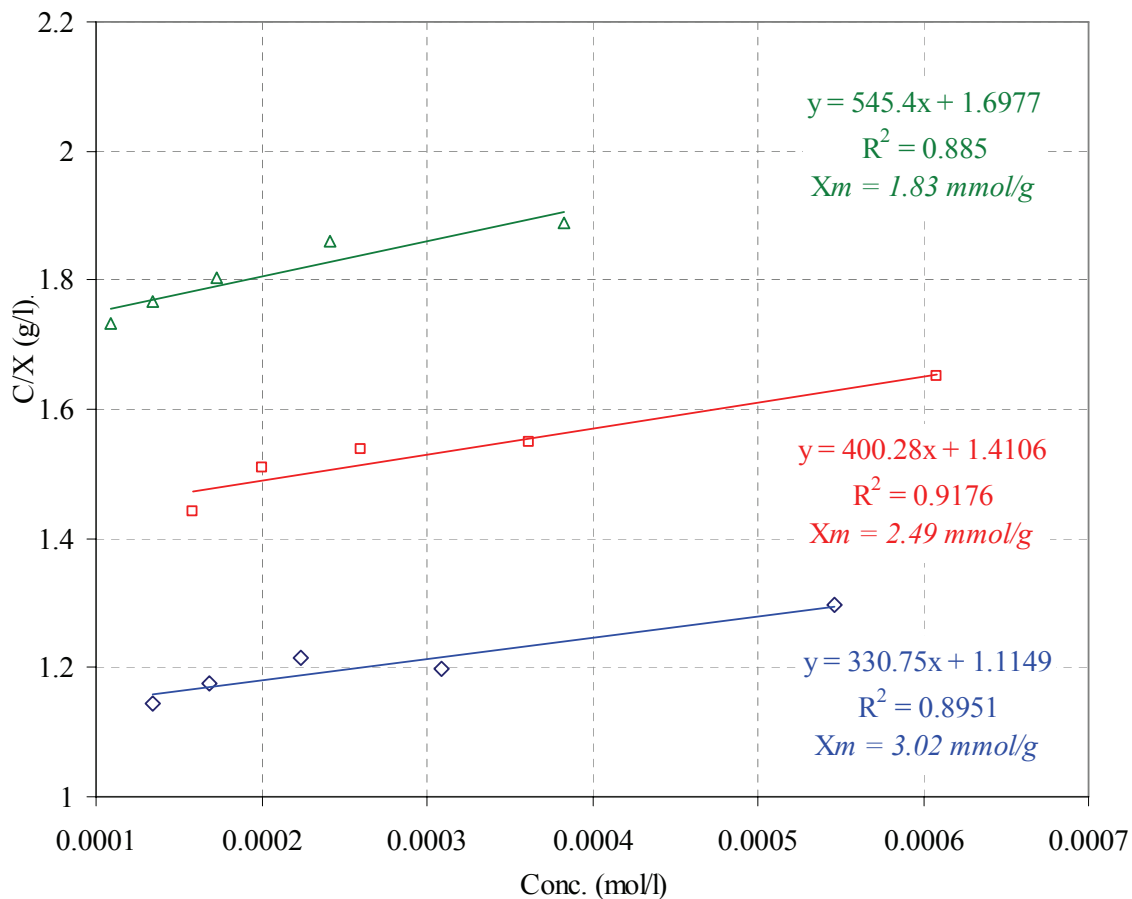
Figure 3.8. The Langmuir adsorption isotherms of ($\Diamond$) Cu^{2+}, ($\square$) Zn^{2+}, and (Δ) Cd^{2+} ions adsorbed by OSU-6-W-APTMS-1 absorbent.

In the case of OSU-6-W-APTMS-2, Figure 3.9, the stoichiometry of uptake per amine group changed. The cadmium uptake corresponded to formation of 1 Cd^{2+}: 2 NH_2 complex. The uptake of zinc exceeded this to give a ratio of Zn^{2+}: NH_2 of 1:1.3 which is likely a mixture of 1:1 and 1:2 complexes. Again, the number of copper ions exceeded the number of amine groups with a ration of 1.4 Cu^{2+} : 1 NH_2.
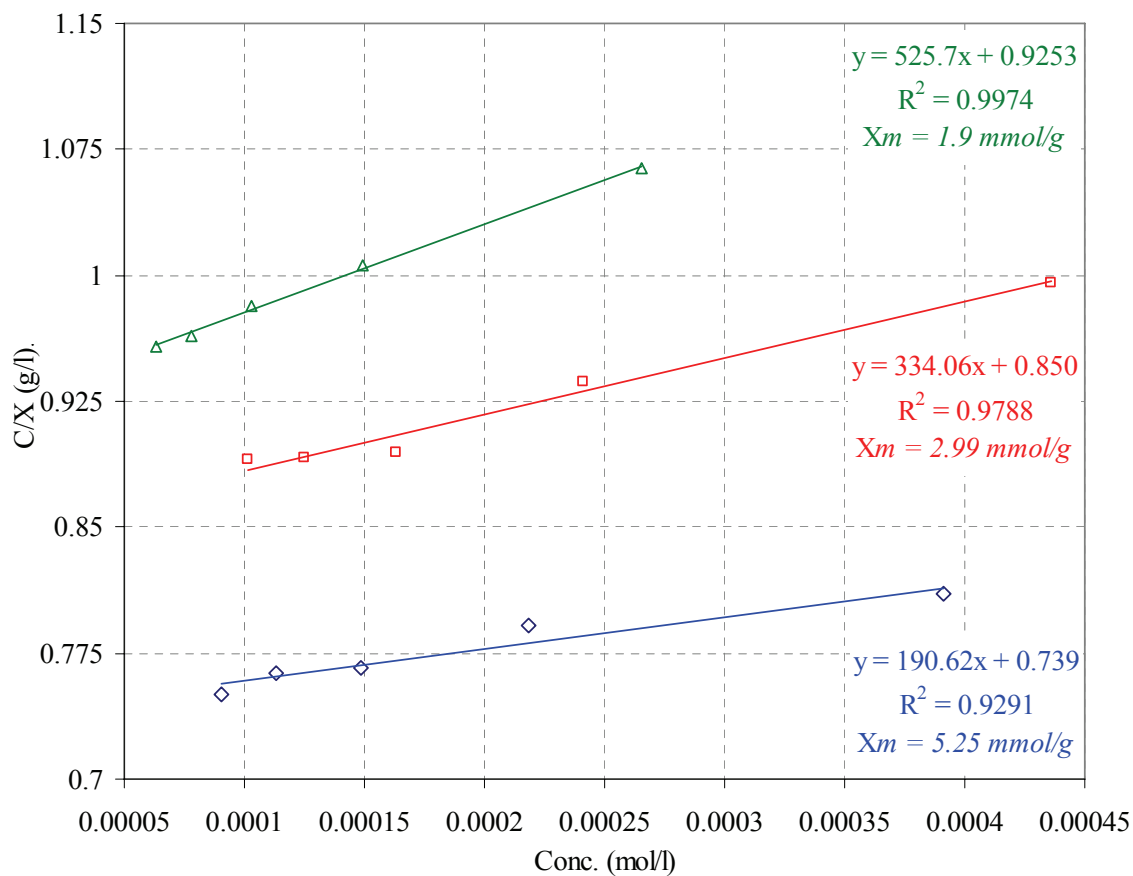
Figure 3.9. The Langmuir adsorption isotherms of (◊) Cu^{2+}, (□) Zn^{2+}, and (Δ) Cd^{2+} ions adsorbed by OSU-6-W-APTMS-2 absorbent.

Table 3.4. The uptake capacities from the Langmuir adsorption isotherms.

Adsorbent	Uptake capacity (mg/g)		
	Cu^{2+}	Zn^{2+}	Cd^{2+}
OSU-6-W-APTMS-1	191.9	162.9	205.7
OSU-6-W-APTMS-2	333.6	195.6	213.6

II. Adsorbent Regeneration

Treatment of the copper loaded material with an aqueous solution of 2.0 *M* HCl three times with stirring for one hour resulted in the complete removal of the bound Cu^{2+}

from the structure, regenerating the adsorbent for further metal ion uptake. The

regenerated material showed a high metal ion uptake capacity of 95% of the original

material. This result is better than that reported for acid-regenerated P-$(CH_2)_3NH_2$,[55]

where the metal ion uptake capacity of the acid-regenerated P-$(CH_2)_3NH_2$ dropped

dramatically to about 75% of its original adsorption capacity. This suggests that, our

materials have high stabilities toward acid leaching of the functional groups.

These results show the outstanding promise of these materials for adsorption and

separation processes. These amino-functionalized materials show higher metal ion

uptake than the aminosilyl derivitized materials produced prepared by El-Nahhal *et al.*[55]

The reason behind the high capacities of our modified samples are the high surface areas,

large pore sizes which make the diffusion easy, and the high coverage of the functional

amine groups on the surfaces. Moreover, our materials show high stability toward

leaching.

3.3.3.2. Radioactive Material (UO_2^{2+})

I. Uptake Capacity

The uptake capacity of the EDTA functionalized silicas was investigated using

different amount of absorbent, OSU-6-W-APTMS-2-EDTA, and one constant

concentration of uranium ions (100 ppm) at pH 6.5. The results are shown in Figure

3.10. The uranium ions have a high tendency to be chemisorbed by the carboxylic

ligand. The maximum uptake was calculated from the Langmuir adsorption isotherm to

be 534.1 mg of UO_2^{2+}/g of absorbent.
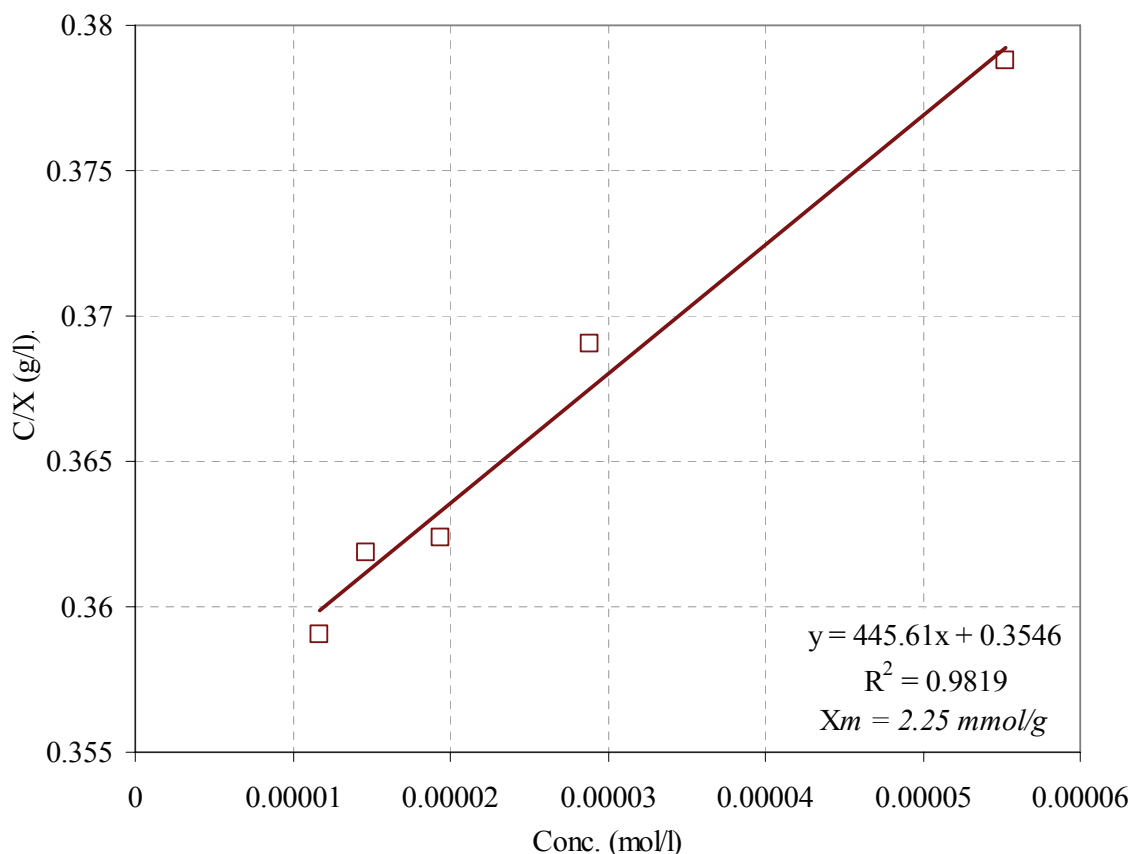
Figure 3.10. The Langmuir adsorption isotherms of UO_2^{2+} ions adsorbed by OSU-6-W-APTMS-2-EDTA absorbent.

The uptake of uranyl ions by OSU-6-W-APTMS-2-EDTA can be compared with the glycine immobilized material, OSU-6-W-TMSPMA-2-Glycine discussed in chapter five. In the adsorption study of the former sample, the uptake was 2.24 mmol/g while the latter sample shows less adsorption capacity of 1.3 mmol/g. This mostly correlates with the differences in the surface areas (496 m^2/g and 279 m^2/g, respectively) and may be due to the concentrations of immobilized ligands. However, both show excellent recovery of the uranium ions.

3.4. CONCLUSION

Water has a big influence along with surface area, pore size, pore volume, and silanol concentration, on the mechanism of monolayer formation and therefore on the structure of monolayer that can be obtained on a silica surface. It was demonstrated that hydrolysis of the remaining methoxy groups on the initial immobilized silane layer by water followed by another silanization yields enhanced surface density of silanes with improved cross polymerization and without complications of vertical polymerization. The improved technique allows surface concentration of amino-functional groups of around 4.71group/nm^2, almost 1.6 times higher than what is possible without water treatment.[89]

An alternative explanation for the affect of the water treatment effect might imply that, instead of steric hindrance, it could arise from the different ways silanes physisorb to the surface. Aminosilanes are known for forming hydrogen bonding with surface hydroxyl using all four active groups: three methoxy groups and amine. It was claimed[92] that, depending on aminosilane concentration, orientation of physisorbed silane can change from primarily a methoxy group attached at low concentration to an amine bonded orientation at high concentration. One may argue that the additional treatment with water primarily eliminates improperly oriented aminosilanes, which did not succeed in forming a Si-O-Si bond with the surface.[89]

OSU-6-W-APTMS-2 was chemically modified with EDTA prepared by interacting anhydrides of EDTA with the amine active group grafted on the mesoporous silica surface. The material was found to have high affinity for uranium ions.

By the aid of the excellent adsorption characteristics of the chemically modified silicas for some metal ions, separation application can be further investigated for different metal ions and the selectivity for metal ion in a mixture.

3.5. REFERENCES

1. S.D. Faust and O.M. Ali, Chemistry of Water Treatment, Butterworth, Boston (1983).
2. Mohan, D.; Guputa, V. K.; Srivastava, S. K.; Chander, S.. Kinetics of mercury adsorption from wastewater using activated carbon derived from fertilizer waste. *Colloids Surf. A* **2001,** *177*(2-3), 169-181.
3. Navarro, R. R.; Sumi, K.; Matumura, M.. Improved metal affinity of chelating adsorbents through graft polymerization. *Water Res.* **1999,** *33*(9), 2037-2044.
4. Huang, C. P.; Hao, O. J.. Removal of some heavy metals by mordenite. *J. Environ. Technol. Lett.* **1989,** *10*(10), 863-874.
5. Zamzow, M. J.; Eichbaum, B. R.; Sandgren, K. R.; Shanks, D. E.. Removal of heavy metals and other cations from wastewater using zeolites. *Separ. Sci. Technol.* **1990,** *25*(13-15), 1555-1569.
6. Mercier, L.; Pinnavaia, T. J.. A functionalized porous clay heterostructure for heavy metal ion (Hg^{2+}) trapping. *Micropor. Mesopor. Mater.* **1998,** *20*(1-3), 101-106.
7. Celis, R.; Hermosin, M. C.; Cornejo, J.. Heavy metal adsorption by functionalized clays. *Environ. Sci. Technol.* **2000,** *34*(21), 4593-4599.
8. Gupta, S. K.; Chen, K. Y.. Arsenic Removal by Adsorption. *J. Water Pollut. Control Fed.* **1978,** *50*(3 Part 1), 493-506.
9. Huang, C. P.; Fu, P. L. K.. Treatment of Arsenic(V)-Containing Water by The Activated Carbon Process. *J. Water Pollut. Control Fed.* **1984,** *56*(3 Part 1), 233-242.
10. Haggerty, G. M.; Bowman, R. S.. Sorption of chromate and other inorganic anions by organo-zeolite. *Environ. Sci. Technol.* **1994,** *28*(3), 452-458.
11. Wu, C. H.; Kuo, C. Y.; Lin, C. F.; Lo S. L.. Modeling competitive adsorption of molybdate, sulfate, selenate, and selenite using a Freundlich-type multi-component isotherm. *Chemosphere* **2002,** *47*(3), 283-292.
12. Kresge, C. T.; Leonowicz, M. E.; Roth, W. J.; Vartuli, J. C.; Beck, J. S. Ordered Mesoporous Molecular Sieves Synthesized by A Liquid-Crystal Template Mechanism. *Nature* **1992,** *359*(6397), 710-712.
13. Beck, J. S.; Vartuli, J. C.; Roth, W. J.; Leonowicz, M. E.; Kresge, C. T.; Schmitt, K. D.; Chu, C. T. W.; Olson, D. H.; Sheppard, E. W.; McCullen, S. B.; Higgins, J. B.; Schlenker, J. L. A new family of mesoporous molecular sieves prepared with liquid crystal templates. *J. Am. Chem. Soc.* **1992,** *114*(27), 10834-10843.
14. Inagaki, S.; Fukushima, Y.; Kuroda, K.. Synthesis of highly ordered mesoporous materials from a layered polysilicate *J. Chem. Soc., Chem. Commun.*, **1993,** 680-681.
15. Zhao, X. S.; Lu, G. Q.; Whittaker, A. J.; Millar, G. J.; Zhu, H. Y.. Comprehensive Study of Surface Chemistry of MCM-41 Using ^{29}Si CP/MAS NMR, FTIR, Pyridine-TPD, and TGA *J. Phys. Chem. B*, **1997,** *101*(33), 6525-6531.
16. Macquarrie, D. J. Direct Preparation of Organically Modified MCM-type Materials. Preparation and Characterization of Aminopropyl-MCM and 2-Cyanoethyl-MCM. *Chem. Commun.*, **1996,** *16,* 1961-1962.
17. Moller, K.; Bein, T. Inclusion Chemistry in Periodic Mesoporous Hosts. *Chem. Mater.*, **1998,** *10*(10), 2950–2963.
18. Asefa, T.; MacLachlan, M. J.; Coombs, N.; Ozin, G. A. Periodic Mesoporous Organosilicas with Organic Groups Inside the Channel Walls. *Nature*, **1999,** *402,* 867-871.

19. Brunel, D. Functionalized Micelle-templated Silicas (MTS) and their use as Catalysts for Fine Chemicals *Microporous Mesoporous Mater.* **1999,** *27*(2-3), 329-344.
20. Yanagisawa, T.; Shimizu, T.; Kuroda, K.; Kato, C. The Preparation of Alkyltrimethylammonium-kanemite Complexes and their Conversion to Microporous Materials *Bull. Chem. Soc. Jpn*. **1990,** *63*(4), 988-992.
21. Burkett, S. L.; Sims, S. D.; Mann, S. Synthesis of Hybrid Inorganic-organic Mesoporous Silica by Co-condensation of Siloxane and Organosiloxane Precursors *Chem. Commun.* **1996,** *11,* 1367-1368.
22. Vrancken, K. C.; Possemiers, K.; Van Der Voort, P.; Vansant, E. F. Surface modification of silica gels with aminoorganosilanes. *Colloids and Surfaces, A: Physicochemical and Engineering Aspects* **1995,** *98*(3), 235-241.
23. Vrancken, K. C.; Van der Voort, P.; Gillis-D'Hamers, I.; Vansant, E. F.; Grobet, P.. Influence of water in the reaction of γ-aminopropyltriethoxysilane with silica gel: a Fourier-transform infrared and cross-polarization magic-angle-spinning nuclear magnetic resonance study. *J. Chem. Soc., Faraday Trans.* **1992,** *88*(21), 3197-3200.
24. Kallury, K. M. R.; Macdonald, P. M.; Thompson, M.. Effect of Surface Water and Base Catalysis on the Silanization of Silica by (Aminopropyl)alkoxysilanes Studied by X-ray Photoelectron Spectroscopy and ^{13}C Cross-Polarization/Magic Angle Spinning Nuclear Magnetic Resonance. *Langmuir* **1994,** *10*(2), 492-499.
25. Blitz, J. P.; Murthy, R. S.; Leyden, D. E. Ammonia-catalyzed silylation reactions of Cab-O-Sil with methoxymethylsilanes. *J. Am. Chem. Soc.* **1987,** *109*(23), 7141-7145.
26. Smith, R. M.. Gas and Liquid Chromatography in Analytical Chemistry; John Wiley & Sons, New York, 1988; pp. 17.
27. Porsch, B.; Kratka, J. Chromatographic stability of silica-based aminopropyl-bonded stationary phases. *J. Chromatogr.* **1991,** *543*(1), 1-7.
28. Leyden, D. E.; Luttrell, G. H.. Preconcentration of trace metals using chelating groups immobilized via silylation. *Anal. Chem.* **1975,** *47*(9), 1612-1617.
29. Taylor, I.; Howard, A. G.. Measurement of primary amine groups on surface-modified silica and their role in metal binding. *Anal. Chim. Acta* **1992,** *271*(1), 77-82.
30. Deschler, U.; Kleinschmit, P.; Panster, P.. 3-Chloropropyltrialkoxysilane - a key component for the industrial preparation of organofunctional silane and polysiloxane. *Angew. Chem.* **1986,** *98*(3), 237-253.
31. T.J. Pinnavaia, J.G-S. Lee and M. Abedini, in D.E. Leyden and W.T. Collins (Eds.), Gordon and Breach Science Publ., New York, 1988, p. 35.
32. Helbert, J. H. and Saha, N. Silanes and Other Coupling Agents, VSP, Utrecht, The Netherlands, 1992, pp. 439.
33. Angeletti, E.; Canepa, C.; Martinetti, G.; Venturello, P.. Amino Groups Immobilized on Silica Gel: An Efficient and Reusable Heterogeneous Catalyst for the Knoevenagel Condensation. *J. Chem. Soc., Perkin. Trans.* **1989,** *1,* 105–107.
34. Liu, A. M.; Hidajat, K.; Kawi, S.; Zhao, D. Y.. A New Class of Hybrid Mesoporous Materials with Functionalized Organic Monolayers for Selective Adsorption of Heavy Metal Ions. *Chem. Commun.*, **2000,** *13,* 1145–1146.
35. Feng, X.; Fryxell, G. E.; Wang, L.-Q.; Kim, A. Y.; Liu, J.; Kemner, K. M.. Functionalized Monolayers on Ordered Mesoporous Supports. *Science*, **1997,** *276*(5314), 923–926.

36. Antochshuk, V.; Jaroniec, M.. 1-Allyl-3-propylthiourea Modified Mesoporous Silica for Mercury Removal. *Chem. Commun.*, **2002,** *3,* 258–259.
37. Fryxell, G. E.; Liu, J.; Hauser, T. A.; Nie, Z.; Ferris, K. F.; Mattigod, S.; Gong, M.; Hallen, R. T.. Design and Synthesis of Selective Mesoporous Anion Traps. *Chem. Mater.*, **1999,** *11*(8), 2148–2154.
38. Shephard, D. S.; Zhou, W.; Maschmeyer, T.; Matters, J. M.; Roper, C. L.; Parsons, S.; Johnson, B. F. G.; Duer, M. J. Site-Directed Surface Derivatization of MCM-41: Use of High-Resolution Transmission Electron Microscopy and Molecular Recognition for Determining the Position of Functionality within Mesoporous Materials. *Angew. Chem., Int. Ed. Engl.* **1998,** *37*(19), 2719-2723.
39. Maschmeyer, T.; Oldroyd, R. D.; Sankar, G.; Thomas, J. M.; Shannon, I. J.; Klepetko, J. A.; Masters, A. F.; Beattie, J. K.; Catlow, C. R. A. Designing a solid catalyst for the selective low-temperature oxidation of cyclohexane to cyclohexanone. *Angew. Chem., Int. Ed. Engl.* **1997,** *36*(15), 1639-1642.
40. Brunel, D.; Cauvel, A.; Fajula, F.; Di Renzo, F.. MCM-41 type silicas as supports for immobilized catalysts. *Stud. Surf. Sci. Catal.* **1995,** *97,* 173-180.
41. Corma, A.. From Microporous to Mesoporous Molecular Sieve Materials and Their Use in Catalysis. *Chem. Rev.* **1997,** *97*(6), 2373-2419.
42. Bellocq, N.; Abramson, S.; Lasperas, M.; Brunel, D.; Moreau, P. Factors Affecting the Efficiency of Hybrid Chiral Mesoporous Silicas used as Heterogeneous Inorganic-Organic Catalysts in the Enantioselective Alkylation of Benzaldehyde. *Tetrahedron: Asymmetry* **1999,** *10*(16), 3229-3241.
43. Lim, M. H.; Stein, A.. Comparative Studies of Grafting and Direct Syntheses of Inorganic-Organic Hybrid Mesoporous Materials. *Chem. Mater.* **1999,** *11*(11), 3285-3295.
44. Price, P. M.; Clark, J. H.; Macquarrie, D. J.. Modified Silicas for Clean Technology. *Dalton* **2000,** *2,* 101-110.
45. Clark, J. H.; Macquarrie, D. J.; Wilson, K.. Functionalised Mesoporous Materials for Green Chemistry. *Stud. Surf. Sci. Catal.* **2000,** *129,* 251-264.
46. Cooper, C.; Burch, R. Mesoporous Materials for Water Treatment Processes *Water Res.* **1999,** *33*(18), 3689-3694.
47. Zaporozhets, O.; Gawer, O.; Sukhan, V. The interaction of Fe (II), Cu (II) and Ag (I) ions and their complexes with 1,10-phenanthroline adsorbed on silica gel *Colloids Surf., A* **1999**, *147*(3), 273-281.
48. Singh, R.; Khwaja, A. R.; Gupta, B.; Tandon, S. N.. Uptake and Extraction Chromatographic Separation of Mercury(II) by Triisobutylphosphine Sulfide (TIBPS) Sorbed on Silica Gel and Decontamination of Mercury Containing Effluent. *Talanta* **1999**, *48*(3), 527-535.
49. Kham, K.; Deratani, A.; Sebille, B. Kinetics of copper(II) ion fixation on modified silicas bearing some organic complexant functions *New J. Chem.* **1987**, *11*(10), 709-714.
50. Hoorn, H. J.; De Joode, P.; Driessen, W. L.; Reedijk, J. Metal-binding affinity of a series of bis(2-pyridylalkyl)amines immobilized on silica *Recl. Trav. Chim. Pays-Bas* **1996**, *115*(3), 191-197.

51. Vieira, E. F. S.; Simoni, J. A.; Airoldi, C. Interaction of cations with SH-modified silica gel: thermochemical study through calorimetric titration and direct extent of reaction determination *J. Mater. Chem.* **1997**, *7*(11), 2249 - 2252.

52. Bresson, C.; Menu, M.-J.; Dartiguenave, M.; Dartiguenave, Y. Triethoxysilyl-substituted aminoethanethiol ligands for zinc and cadmium complexes and aminoethanethiol-modified silica gel. Evaluation of the corresponding supported molecular trap for metallic pollutant uptake (Cd^{2+}, Hg^{2+} and Pb^{2+}). *J. Environ. Monit.* **2000**, *2*(3), 240-247.

53. Fonseca, M. G.; Oliveira, A. S.; Airoldi, C. Silylating Agents Grafted onto Silica Derived from Leached Chrysotile *J. Colloid Interface Sci.* **2001**, *240*(2), 533-538.

54. Dai, S.; Burleigh, M. C.; Shin, Y.; Morrow, C. C.; Barnes, C. E.; Xue, Z.. Imprint Coating: A Novel Synthesis of Selective Functionalized Ordered Mesoporous Sorbents *Angew. Chem., Int. Ed. Engl.* **1999**, *38*(9), 1235-1239.

55. El-Nahhal, I. M.; Zaggout, F. R.; El-Ashgar, N. M. Uptake of divalent metal ions (Cu^{2+}, Zn^{2+} and Cd^{2+}) by polysiloxane immobilized monoamine ligand system *Anal. Lett.* **2000**, *33*(10), 2031-2053.

56. Im, H.-J.; Yang, Y.; Allain, L. R.; Barnes, C. E.; Dai, S.; Xue, Z. Functionalized Sol-Gels for Selective Copper(II) Separation *Environ. Sci. Technol.* **2000,** *34*(11), 2209-2214.

57. Nesterenko, P. N.; Ivanov, A. V.; Galeva, N. A.; Seneveratne, G. B. C. Complexing and acid-base properties of silica gels modified with oligoethyleneamines *J. Anal. Chem.* **1997,** *52*(8), 736-742.

58. Dias Filho, N. L.. Adsorption of Copper(II) and Cobalt(II) Complexes on a Silica Gel Surface Chemically Modified with 3-Amino-1,2,4-triazole. *Colloids and Surfaces, A: Physicochemical and Engineering Aspects* **1998,** *144*(1-3), 219-227.

59. Mahmoud, M. E. Selective solid phase extraction of mercury(II) by silica gel-immobilized-dithiocarbamate derivatives *Anal. Chim. Acta* **1999**, *398*(2-3), 297-304.

60. Broudic, J.-C.; Conocar, O.; Moreau, J. J. E.; Meyer, D.; Wong Chi Man, M. New hybrid silica based materials for the solid–liquid extraction of actinides *J. Mater. Chem.* **1999**, *9*(10), 2283-2285.

61. Ma, W. X.; Liu, F.; Li, K. A.; Chen, W.; Tong, S. Y. Preconcentration, separation and determination of trace Hg(II) in environmental samples with aminopropylbenzoylazo-2-mercaptobenzothiazole bonded to silica gel *Anal. Chim. Acta* **2000**, *416*(2), 191-196.

62. Soliman, E. M.; Mahmoud, M. E.; Ahmed, S. A. Synthesis, characterization and structure effects on selectivity properties of silica gel covalently bonded diethylenetriamine mono- and bis-salicyaldehyde and naphthaldehyde Schiff's bases towards some heavy metal ions *Talanta* **2001**, *54*(2), 243-253.

63. Lee, B.; Kim, Y.; Lee, H.; Yi, J. Synthesis of functionalized porous silicas via templating method as heavy metal ion adsorbents: the introduction of surface hydrophilicity onto the surface of adsorbents *Microporous Mesoporous Mater.* **2001**, *50*(1), 77-90.

64. Moller, K.; Bein, T. Inclusion Chemistry in Periodic Mesoporous Hosts. *Chem. Mater.* **1998**, *10*(10), 2950-2963.

65. Lim, M. H.; Blanford, C. F.; Stein, A. Synthesis of Ordered Microporous Silicates with Organosulfur Surface Groups and Their Applications as Solid Acid Catalysts *Chem. Mater.* **1998,** *10*(2), 467- 470.

66. Diaz, I.; Marquez-Alvarez, C.; Mohino, F.; Perez-Pariente, J.; Sastre, E. Combined Alkyl and Sulfonic Acid Functionalization of MCM-41-Type Silica *J. Catal.* **2000**, *193*(2), 283-294.

67. Collinson, M. M. Analytical applications of organically modified silicates *Mikrochim. Acta* **1998**, *129*(3-4), 149-165.

68. Walcarius, A. Analytical Applications of Silica-Modified Electrodes. A Comprehensive Review *Electroanalysis* **1998,** *10*(18), 1217-1235.

69. Walcarius, A. Electroanalysis with Pure, Chemically Modified and Sol-Gel-Derived Silica-Based Materials *Electroanalysis* **2001**, *13*(8-9), 701-718.

70. Walcarius, A.; Lüthi, N.; Blin, J.-L.; Su, B.-L.; Lamberts, L. Electrochemical evaluation of polysiloxane-immobilized amine ligands for the accumulation of copper(II) species *Electrochim. Acta* **1999**, *44*(25), 4601-4610.

71. Etienne, M.; Bessière, J.; Walcarius, A. Voltammetric detection of copper(II) at a carbon paste electrode containing an organically modified silica. *Sens. Actuators, B* **2001**, *76*(1-3), 531-538.

72. Zhao, X. S.; Lu, G. Q. Modification of MCM-41 by Surface Silylation with Trimethylchlorosilane and Adsorption Study, *J. Phys. Chem. B*, **1998,** *102*(9), 1556- 1561.

73. Zemanian, T. S.; Fryxell, G. E.; Liu, J.; Mattigod, S.; Franz, J. A.; Nie, Z.. Deposition of Self-Assembled Monolayers in Mesoporous Silica from Supercritical Fluids. *Langmuir*, **2001,** *17*(26), 8172-8177.

74. Kruk, K.; Asefa, T.; Jaroniec, M.; Ozin, G. A.. Metamorphosis of Ordered Mesopores to Micropores: Periodic Silica with Unprecedented Loading of Pendant Reactive Organic Groups Transforms to Periodic Microporous Silica with Tailorable Pore Size *J. Am. Chem. Soc.* **2002,** *124*(22), 6383-6392.

75. Beaudet, L.; Hossain, K. Z.; Mercier, L.. Direct Synthesis of Hybrid Organic-Inorganic Nanoporous Silica Microspheres. 1. Effect of Temperature and Organosilane Loading on the Nano- and Micro-Structure of Mercaptopropyl-Functionalized MSU Silica *Chem. Mater.* **2003,** *15*(1), 327-334.

76. Mori, Y.; Pinnavaia, T. J.. Optimizing Organic Functionality in Mesostructured Silica: Direct Assembly of Mercaptopropyl Groups in Wormhole Framework Structures *Chem. Mater.* **2001,** *13*(6), 2173-2178.

77. Díaz, J. F.; Balkus, K. J.; Bediouui, F.; Kurshev, V.; Kevan, L.. Synthesis and Characterization of Cobalt-Complex Functionalized MCM-41, *Chem. Mater.* **1997,** *9*(1), 61-67.

78. Fryxell, G. E.; Lin, Y.; Wu, H.; Kemner, K. M.. Environmental Applications of Self-Assembled Monolayers on Mesoporous Supports (SAMMS). *Stud. Surf. Sci. Catal.* **2002,** *141,* 583-590.

79. Bourlinos, A. B.; Karakostas, T.; Petridis, D.. "Side Chain" Modification of MCM-41 Silica through the Exchange of the Surfactant Template with Charged Functionalized Organosiloxanes: An Efficient Route to Valuable Reconstructed MCM-41 Derivatives, *J. Phys. Chem. B*, **2003,** *107*(4), 920-925.

80. Muñoz, A.; Rámila, A.; Pérez-Pariente, J.; Díaz, I.; Vallet-Regí, M.. MCM-41 Organic Modification as Drug Delivery Rate Regulator, *Chem. Mater.* **2003,** *15*(2), 500-503.

81. Macquarrie, D. J.; Rocchia, M.; Onida, B.; Garrone, E.; Lentz, P.; Nagy, J. B.; Brunel, D.; Blanc, A. C.; Fajula, F. Comparison of 3-Aminopropylsilane Linked to MCM-41- and HMS-type Silicas Synthesized under Biphasic and Monophasic Conditions. *Stud. Surf. Sci. Catal.* **2001,** *135,* 4849-4856.

82. Brunel, D.; Blanc, A. C.; Garrone, E.; Onida, B.; Rocchia, M.; Nagy, J. B.; Macquarrie, D. J.. Spectroscopic Studies on Aminopropyl-containing Micelle Templated Silicas. Comparison of Grafted and Co-condensation routes. *Stud. Surf. Sci. Catal.* **2002,** *142B,* 1395-1402.

83. Takeda, K.; Akiyama, M.; Kawakami, F.; Sasaki, M. Recovery of Highly-Purified Rare Earth Elements Using Newly-Synthesized Chelating Resins, *Bull. Chem. Soc. Jpn.* **1986**, *59*(7), 2225-2232.

84. Jain, V. K.; Handa, A.; Sait, S. S.; Shrivastav, P.; Agrawal, Y. K. Pre-concentration, Separation and Trace Determination of Lanthanum(III), Cerium(III), Thorium(IV) and Uranium(VI) on Polymer Supported *o*-Vanillinsemicarbazone, *Anal. Chim. Acta* **2001**, *429*(2), 237-246.

85. Inoue, K.; Yoshizuka, K.; Ohto, K. Adsorption Separation of Some Metal Ions by Complexing Agent Types of Chemically Modified Chitosan. *Anal. Chim. Acta* **1999**, *388*(1-2), 209-218.

86. Inoue, K.; Ohto, K.; Yoshizuka, K.; Yamaguchi, T.; Tanaka, T. Adsorption of Lead(II) Ion on Complexane Types of Chemically Modified Chitosan. *Bull. Chem. Soc. Jpn.* **1997**, *70*(10), 2443-2447.

87. Sing, K. S. W.; Everett, D. H.; Haul, R. A. W.; Moscou, L.; Pierotti, R. A.; Rouquerol, J.; Siemieniewska, T. Reporting Physisorption Data for Gas/Solid Systems with Special Reference to the Determination of Surface Area and Porosity. *Pure and Applied Chemistry* **1985,** *57*(4), 603-619.

88. Sindorf, D. W.; Maciel, G. E. Cross-Polarization Magic-Angle-Spinning Silicon-29 Nuclear Magnetic Resonance Study of Silica Gel Using Trimethylsilane Bonding as a Probe of Surface Geometry and Reactivity. *J. Phys. Chem.* **1982**, *86*(26), 5208-5219.

89. (a) Krasnoslobodtsev, A. V.; Smirnov, S. N.. Effect of Water on Silanization of Silica by Trimethoxysilanes. *Langmuir* **2002,** *18*(8), 3181-3184. (b) Brzoska, J. B.; Azouz, I. Ben; Rondelez, F. Silanization of Solid Substrates: A Step toward Reproducibility. *Langmuir* **1994,** *10*(11), 4367-4373.

90. White, L. D.; Tripp, C. P. An Infrared Study of the Amine-Catalyzed Reaction of Methoxymethylsilanes with Silica, *J. Colloid Interface Sci.* **2000,** *227*(1), 237-243.

91. Blitz, J. P.; Murthy, R. S. Shreedhara; Leyden, D. E. The Role of Amine Structure on Catalytic Activity for Silylation Reactions with Cab-O-Sil, *J. Colloid Interface Sci.* **1988,** *126*(2), 387-392.

92. Piers, A. S.; Rochester, C. H. Infrared Study of the Adsorption of 1-Aminopropyltrialkoxysilanes on Silica at the Solid/Liquid Interface *J. Colloid Interface Sci.* **1995**, *174*(1), 97-103.

93. Vrancken, K. C.; Van Der Voort, P.; Possemiers, K.; Vansant, E. F. Surface and Structural Properties of Silica Gel in the Modification with γ-Aminopropyltriethoxysilane. *J. Colloid and Interface Sci.* **1995,** *174*(1), 86-91.

221

94. Sander, L. C.; Wise, S. A. Recent advances in bonded phases for liquid chromatography. *Crit. Rev. Anal. Chem.* **1987,** *18*(4), 299-415.
95. Unger, K. K. Packings and Stationary Phases in Chromatographic Techniques, Marcel Dekker, Moscow (1990).
96. Wouters, B. H.; Chen, T.; Dewilde, M.; Grobet, P. J.. Reactivity of the surface hydroxyl groups of MCM-41 towards silylation with trimethylchlorosilane. *Micropor. Mesopor. Mater.* **2001,** *44-45,* 453-457.
97. Macquarrie, D. J.; Jackson, D. B.; Mdoe, J. E. G.; Clark, J.H.. Organomodified hexagonal mesoporous silicates. *New J. Chem.* **1999,** *23*(5), 539-544.

CHAPTER
FOUR

SYNTHESIS OF MESOPOROUS MATERIALS BEARING DIAMINO

FUNCTIONAL GROUPS

Abstract

Diamino-functionalized mesoporous OSU-6-W material was synthesized via post-synthesis grafting of *N*-[3-(trimethoxysilyl)propyl]ethylenediamine (TMSPEDA). At the maximum level of silylation with TMSPEDA, the solid state ^{29}Si CP/MAS NMR measurements of the two modified samples, OSU-6-W-TMSPEDA-1 and OSU-6-W-TMSPEDA-2, thus obtained indicate that the Si atoms containing Si-C bonds accounted for about 2.54 and 4.48 molecule/nm^2, respectively. The results from elemental analyses of the two modified samples show good agreement with that of the solid state ^{29}Si CP/MAS NMR. These materials were characterized using a variety of techniques including Fourier transform infrared spectroscopy (FTIR), X-ray powder diffraction (XRD), scanning electron microscope (SEM), ^{13}C and ^{29}Si solid state NMR spectroscopy, elemental analysis (EA), surface area analysis (BET), and UV-Vis spectroscopy. The adsorptions of Cu^{2+}, Co^{2+}, UO_2^{2+}, and Th^{4+} by the derivitized silicas were conducted in order to investigate their capacities and selectivity. The cations adsorbed on the diamino-functionalized samples and the adsorption capacity was increased with an increase in the surface density of amino groups.

4.1. INTRODUCTION

The removal of heavy metal ions from wastewater has been the subject of extensive industrial research. The recovery of heavy or valuable metals in process water or wastewater can often result in considerable cost savings.[1-3] Two approaches can be used for the removal of heavy metal ions from aqueous solutions depending on the concentration of metal ions in the aqueous solutions. High concentrations of heavy metal ions can be precipitated as hydroxides and removed by filtration, while low concentrations of metal ions can be removed from aqueous solutions using ion exchange resins, membranes, or adsorbents.[1]

A number of adsorptive compounds are capable of capturing metal ions from aqueous solution, among which are activated charcoal and clays. Among the inherent disadvantages of these materials are their wide distribution of pore size, heterogeneous pore structure, low selectivity for heavy metal ions, and relatively low loading capacities. In order to circumvent these limitations, some promising heavy metal adsorbents have been prepared via the immobilization of ion-chelating agents on inorganic supports,[1-3] or via the coupling of chelating ligands to a solid support, such as inorganic oxides and organic polymers.[4-15] These adsorbents have relatively high loading capacities. In addition, selectivity for a targeted metal ion can be increased by the proper selection of chelating ligands.

The recent discovery of mesoporous molecular sieves has stimulated a renewed interest in adsorbent and catalyst design, and a number of papers have been published in this area.[16,17] Applications of mesoporous silicas as heavy metal ion adsorbents have also been studied recently.[7-15]

Functionalized mesoporous silica with a high density of diamino groups and well-defined mesochannels that can enhance the accessibilities of molecules is required to achieve high production when applied as a catalyst[18] and to reach high capacity and selectivity when applied as an adsorbent for harmful heavy metal cations.[8,13]

This investigation has focused on the application of the cationic functionalized silica as adsorbents for the separation and removal of pollutant materials such as heavy and transition metal ions, which cause problems in drinking water-supplies from groundwater. Amino-functionalized mesoporous silicas show notable adsorption capacities for heavy and transition metal ions from solution.[19,20]

The modified silica may be used as such, or after a secondary treatment. Pure diaminosilane-modified silica gel is used as a stationary phase in liquid and gas chromatography.[21,22] In this application, TMSPEDA is often used, because of the high coordination capacity of the bifunctional organic chain.

The bonding of metal complexes on the diaminosilane-silica allowed the production of heterogeneous catalysts. Various types of catalysts have been developed.[23]

All these applications explain the wide interest in the chemistry of diaminosilane-modified silica. A fundamental understanding of the reaction mechanism may assist the further optimization of all these uses.

4.2. EXPERIMENTAL

4.2.1. Materials

The chemicals used in this part of the thesis are as follow: N-[3-(trimethoxysilyl)propyl]ethylenediamine [$((CH_3O)_3Si(CH_2)_3NHCH_2CH_2NH_2$) 97.0%,

Aldrich], and toluene 99.8% HPLC grade (dried with 5A molecular sieves), ethyl alcohol, and distilled water.

4.2.2. Characterization

The synthesized products were characterized using several techniques including X-ray powder diffraction (XRD), surface area analysis (BET), solid state C-13 and Si-29 NMR spectroscopy, and Fourier transform infrared (FT-IR) spectroscopies. The full descriptions are mentioned in chapter two and three of this thesis.

4.2.3. Preparation

4.2.3.1. Activation of the Mesoporous OSU-6-W

The mesoporous silica material, OSU-6-W, was synthesized as discussed in chapter two of this thesis. It has a surface area of around 1283 m^2/g and an average pore size of ~ 51 Å. This mesoporous silica was activated prior to the functionalization step by refluxing around 6.0 g of the mesoporous silica in 50 ml of dry toluene for 4 hrs under dry atmosphere, washing with dry toluene, and the dring at 100 °C under vacuum.

4.2.3.2. Introduction of Diamino Functional Groups onto the Mesoporous Surface

Propylethylenediamine groups were attached to the mesoporous OSU-6-W material by means of the post-synthesis grafting method. Two synthetic procedures were applied which are based on a combination of different synthetic techniques used by previous researchers.

I. Reaction of the Mesoporous Silica with N-[3-(Trimethoxysilyl)propyl]ethylene-diamine in a One Step Reaction (OSU-6-W-TMSPEDA-1)

Mesoporous silica-supported propylethylenediamine was prepared by refluxing 3.0 g (~ 50 mmol) of the activated mesoporous silica (OSU-6-W) with 50 mmol (~ 11.0

ml) of *N*-[3-(trimethoxysilyl)propyl]ethylenediamine (TMSPEDA) in 100 ml of dry toluene in a 250-ml round-bottom flask for 48 hrs under dry atmosphere, scheme 4.1. The mixture was then cooled to room temperature and then the resulting light brown mixture was filtered with a fine filter funnel. The solid was washed three times with toluene (3 X 50 ml) and then ethanol to rinse away any leftover TMSPEDA. During washing the light brown solid turned white. The white solid was then dried at 80 °C under vacuum for 24 hrs in a ChemDry apparatus. The reaction yielded 4.39 g of the main product. The filtrate solution, on the other hand, was placed in a 500-ml beaker which was then left in a fume hood to evaporate and yield a brownish solid. About 3.84 g of the sticky solid was collected.

IR (cm^{-1}) (KBr) of the main product: 3739(m), 3613(m, br), 3356(s, br), 3038(w), 2939(m, sh), 2886(m, sh), 2824(m), 1665(s, sh), 1594(w), 1493(w), 1458(m), 1354(m), 1231(s, sh), 1070(s, sh), 953(m), 801(m), 682(w), 556(m), and 476(s). Solid-state ^{29}Si CP/MAS NMR: δ (ppm) -58.7 (T^2), -66.0 (T^3), -99.9 (Q^3), and -109.7 (Q^4). Solid-state ^{13}C CP/MAS NMR: δ (ppm) 11.7 (≡Si-*C*H$_2$-)[1], 22.9 (≡Si-CH$_2$-*C*H$_2$-)[2], 33.8 (≡Si-CH$_2$-CH$_2$-*C*H$_2$-NH-)[3], 41.1 (-*C*H$_2$-NH-*C*H$_2$-CH$_2$-NH$_2$)[4], and 51.6 (-CH$_2$-NH-CH$_2$-*C*H$_2$-NH$_2$)[5].[24] Elemental analysis: C (16.32%) and N (6.47%).
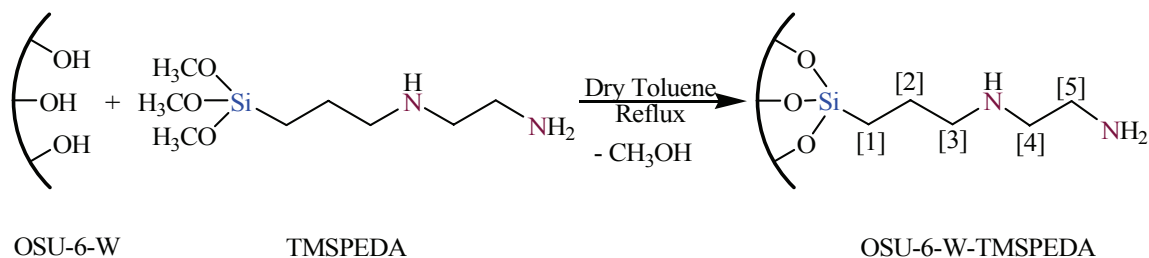
Scheme 4.1. Scheme to illustrate carbon atom position as described in the ^{13}C CP/MAS NMR

II. Reaction of the Mesoporous Silica with *N*-[3-(Trimethoxysilyl)propyl]ethylene-diamine in a Three Step (OSU-6-W-TMSPEDA-2)

In this procedure, mesoporous silica-supported propylethylenediamine was performed in three steps. The first step followed the same procedure used for OSU-6-W-TMSPEDA-1 but with TMSPEDA: OSU-6-W mole ratio of 1:2. After drying, the solid product was placed in a 125-ml Erlenmeyer flask and stirred with 50 ml of distilled water for five hours. The mixture was filtered to recover a white solid which was washed with dry toluene and dried at 80 °C under vacuum for 24 hours. In the third step, the silica was reacted at reflux with a solution of 25 mmol (~ 5.5 ml) of TMSPEDA in 100 ml of dry toluene in a 250-ml round-bottom flask for 48 hrs under a dry atmosphere. After cooling, the resulting solid was isolated by filtration with a fine filter funnel, washed plentifully with toluene (3 X 50 ml) and ethanol then dried at 80 °C under vacuum for 24 hours. The final product was a white solid obtained in a yield of 4.96 g. The filtrate solution was evaporated to yield 3.78 g of a sticky-solid brown solid formed from the filtrated solution.

IR (cm^{-1}) (KBr) of the main yield: 3618(w, br), 3286(s, br), 3265(s, br), 2933(s), 2879(s), 1598(s), 1464(s), 1438(w), 1371(w), 1313(m), 1201(s, br), 1119 (s, br), 1084(s, br), 966(m, br), 802(m), 729(w, sh), 694(w, sh), 579(w), and 465(m). Solid-state ^{29}Si CP/MAS NMR: δ (ppm) -59.7 (T^2), -68.1 (T^3), -99.6 (Q^3) (w), and -111.8 (Q^4). Solid-state ^{13}C CP/MAS NMR: δ (ppm) 11.4 ($\equiv$Si-*CH$_2$*-CH$_2$-)[1], 23.8 ($\equiv$Si-CH$_2$-*CH$_2$*-)[2], 41.1 ($\equiv$Si-CH$_2$-CH$_2$-*CH$_2$*-NH-)[3] and (-*CH$_2$*-NH-CH$_2$-CH$_2$-NH$_2$)[4], and 51.6(-CH$_2$-NH-*CH$_2$*-*CH$_2$*-NH$_2$)[5]. Elemental analysis: C (21.56%) and N (8.59%).

4.2.4. Metal Ions Adsorption Study

The adsorption and separation experiments were conducted as follows; five different amounts (25-125 mg) of the functionalized mesoporous silica, OSU-6-W-TMSPEDA-2, were shaken for 4 hours with 10 ml of 100 ppm solutions of Cu^{2+}, Co^{2+}, UO_2^{2+}, and Th^{4+} using 20-ml glass vials for each metal ion separately. Measurement of the metal ion concentration was carried out by allowing the insoluble complex to settle down and filter an appropriate volume of the supernatant using a 0.45µm syringe filter. The metal ion uptake was calculated as mmol of M^{n+}/g ligand. Inductively coupled plasma atomic emission spectroscopy (ICP-AES) was used to measure the concentration of the metals.

4.3. RESULTS AND DISCUSSION

The ordered mesoporous silicas, OSU-6-W modified with ethylenediamine functional groups were prepared by post-synthesis method from the reaction of the ordered mesoporous silica, OSU-6-W, with TMSPEDA using two different preparation procedures. Diamine-derivitized mesoporous silicas prepared by these methods were obtained in good yield and had excellent surface coverage. The properties of these materials are strongly dependent on the preparation procedure and starting materials.

4.3.1. Identification of the Textural Properties (Physical Characterization)

I. X-ray Powder Diffraction (XRD)

The pristine HCl-Ethanol washed ordered mesoporous material, OSU-6-W, and the two functionalized samples with TMSPEDA [OSU-6-W-TMSPEDA-1 and OSU-6-W-TMSPEDA-2) were characterized by XRD. The resulting diffraction patterns in the range of 1.0-10.0º are shown in Figure 4.1.
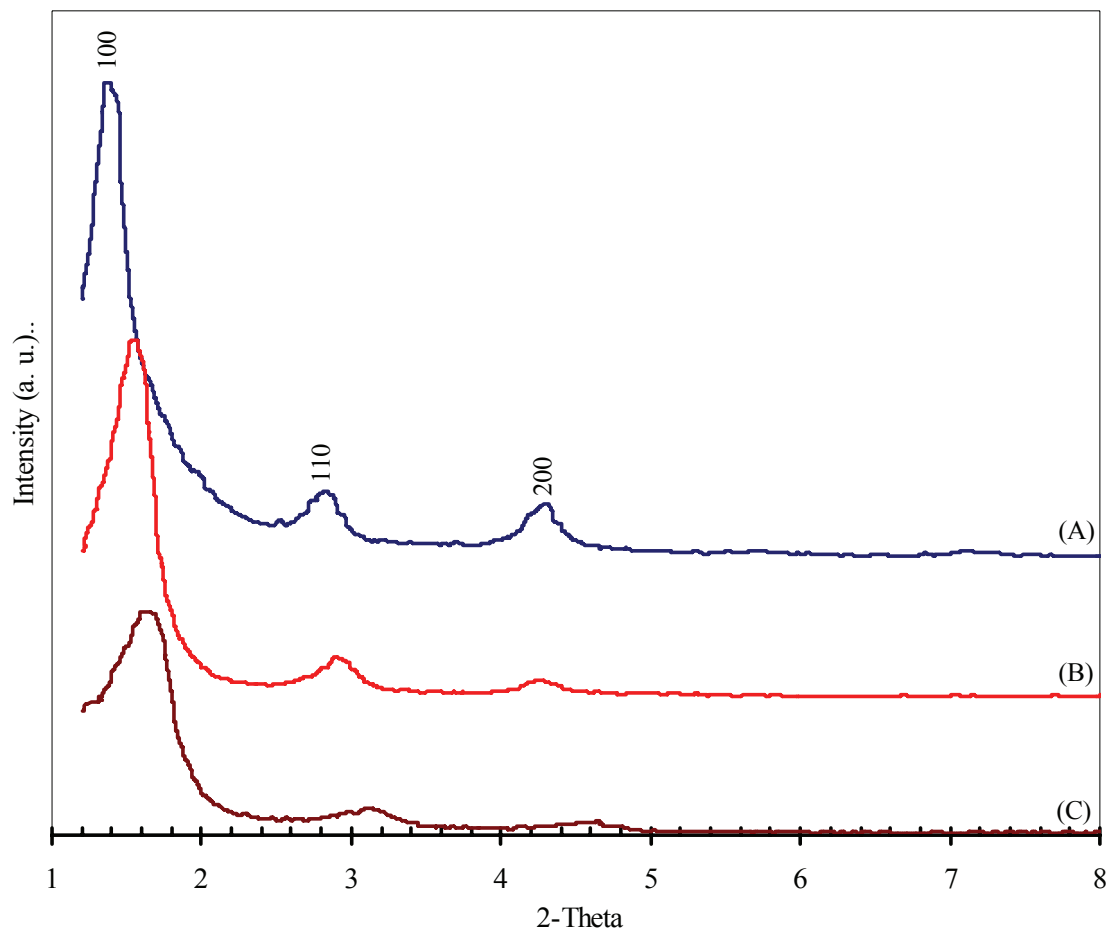
Figure 4.1. XRD patterns in the range of 1.0-10.0º of; (A) pristine HCl-Ethanol washed ordered mesoporous material, OSU-6-W, (B) OSU-6-W-TMSPEDA-1, and (C) OSU-6-W-TMSPEDA-2. The spectra are shifted vertically for the sake of clarity.

The XRD patterns of the samples show strong (100) peaks and smaller (110) and (200) peak intensities, suggesting that the modification process does not strongly affect the framework integrity of the ordered mesoporous OSU-6-W. It can also be noted that the (100) peak gradually shifts to higher angles with increasing of the functional group content of the OSU-6-W-TMSPEDA-1 to OSU-6-W-TMSPEDA-2, indicating an effective decrease of the pore diameter. This can be understood in terms of the volume

excluded as the silylation of the OSU-6-W surface walls takes place. According to the

average pore diameter of the material from the surface area measurements, this indicates

an average thickening of the walls of about 25.9 Å in the case of OSU-6-W-TMSPEDA-

2, which statistically would correspond to at least one extra layer of Si-O-Si

homogeneously spread on the original wall (~ 21.0 Å). It also can be noticed that the d_{100}

peak has become broader with the increase in the loading of the functional groups,

indicating a slight alteration of the ordering of the mesoporous structure as more

functional groups are added to the surface.

II. Nitrogen Adsorption-Desorption Measurements

Figure 4.2 shows the nitrogen adsorption-desorption isotherms performed at 77 K

for the various materials and their textural properties are summarized in Table 4.1. The

curve corresponding to pure silica is typical for mesoporous materials with a hexagonal

channel array. This is type IV isotherm that show a sharp, reversible step at ~ 0.3-0.4

P/P_0, typical of the N_2 filling of uniform mesopores, with an average pore diameter of

about 51 Å and a surface area of 1283 m^2/g.

After introduction of the functional groups, the nitrogen adsorption-desorption

experiments yielded a Brunauer-Emmett-Teller (BET) surface area of 983 m^2/g and a

total pore volume of 0.91 cm^3/g for the OSU-6-W-TMSPEDA-1 sample, and a surface

area of 691 m^2/g and a total pore volume of 0.58 cm^3/g for the OSU-6-W-TMSPEDA-2

sample.
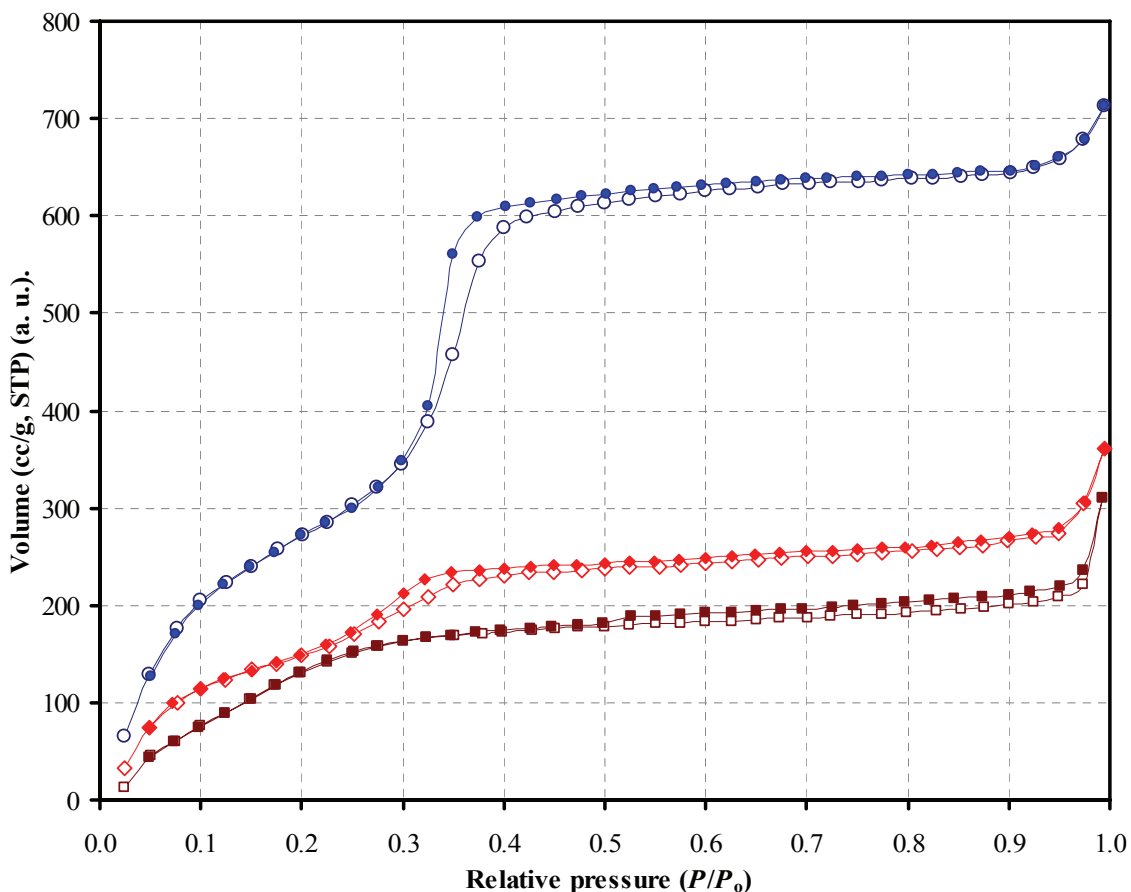
Figure 4. 2. Nitrogen adsorption-desorption isotherms of (○) OSU-6-W, (◊) OSU-6-W-TMSPEDA-1, and (□) OSU-6-W-TMSPEDA-2. Open symbols: adsorption; closed symbols: desorption. The isotherm data are shifted vertically for the sake of clarity.

The BET isotherms for both samples also showed type IV isotherms. The adsorption isotherm curves obtained show that the total adsorbed amounts (taken at P/P_o = 0.99) have diminished, as has the specific surface areas. The uptake corresponding to the filling of the mesopores has shifted to lower relative pressures indicating a reduction of the pore diameter (from 51.1 to 41.3 Å for OSU-6-W-TMSPEDA-1 and from 51.1 to 33.8 Å for OSU-6-W-TMSPEDA-2). An opening of *ca.* 33.8 Å is sufficiently large

enough to allow all metal ions and most small organic molecules to be incorporated into

the pore channels. Both the surface area and the total pore volume of both samples have

dropped significantly compared with the un-functionalized sample, OSU-6-W (BET

surface area 1283 m^2/g; total pore volume 1.24 cm^3/g). The decrease of the mesoporous

volume of the material after silanization is the direct consequence of the silanization

process filling the mesopores. However, this quite large decrease probably can also be

attributed to some pore blocking due to partial surface polymerization at the mouths of

some mesopores, possibly with silsequioxane polymers. Most of the decrease of the

specific surface area can be accounted for the uptake of organic species into the pore

structure.

Table 4.1. Textural Properties Determined from Nitrogen Adsorption-desorption
Experiments at 77 K and Powder XRD Measurements.

Sample	Specific surface area (m^2/g)	Total pore volume (cm^3/g)	Average pore size (Å)	d_{100} (Å)	Wall Thickness (Å)
OSU-6-W	1283	1.24	51.1	62.4	20.9
OSU-6-W-TMSPEDA-1	983	0.91	41.3	55.9	23.2
OSU-6-W-TMSPEDA-2	691	0.58	33.8	51.7	25.9

The pore size distribution measurements, Figure 4.3, show narrow pore size

distributions for all samples. The highest pore size distribution was found to correspond

to the OSU-6-W-TMSPEDA-1 and it is in the range of 5.0±1.0 Å.
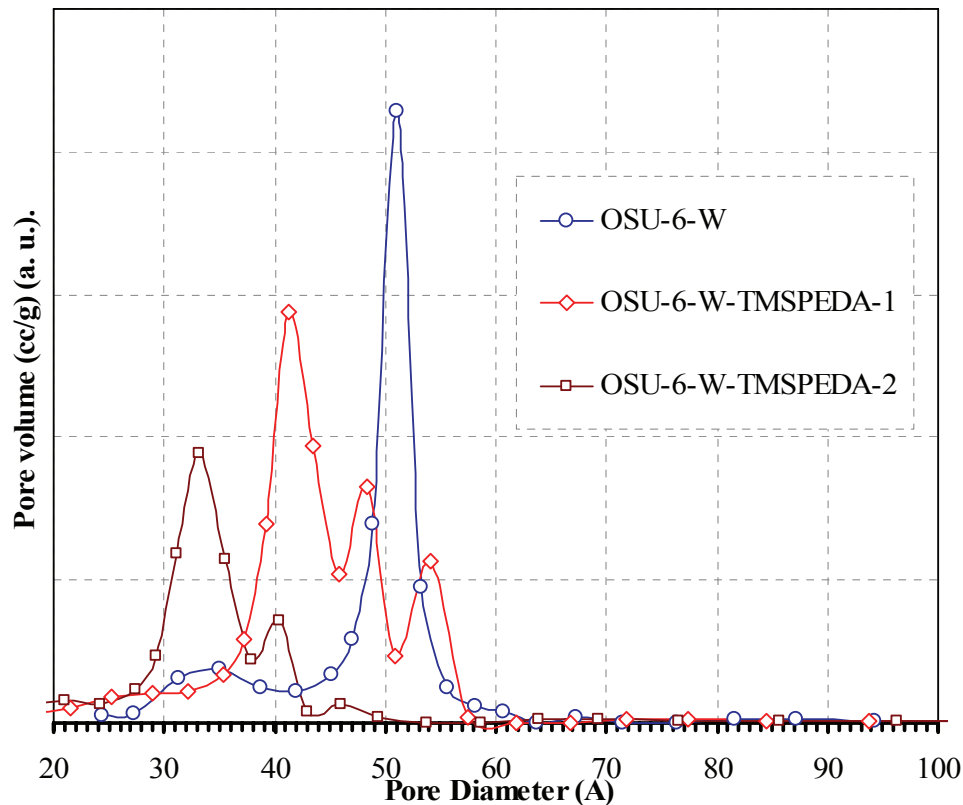
Figure 4. 3. The pore size distribution of (○) OSU-6-W (max at 51.1 Å), (◊) OSU-6-W-TMSPEDA-1 (max at 41.3 Å), and (□) OSU-6-W-TMSPEDA-2 (max at 33.8 Å).

4.3.2. Identification of Functional Groups (Chemical Characterization)

I. Solid State ^{29}Si CP/MAS NMR Spectroscopy

Figure 4.4 shows the solid state ^{29}Si CP/MAS NMR spectra for the unmodified mesoporous silica, OSU-6-W, and the two modified samples, OSU-6-W-TMSPEDA-1, and OSU-6-W-TMSPEDA-2.
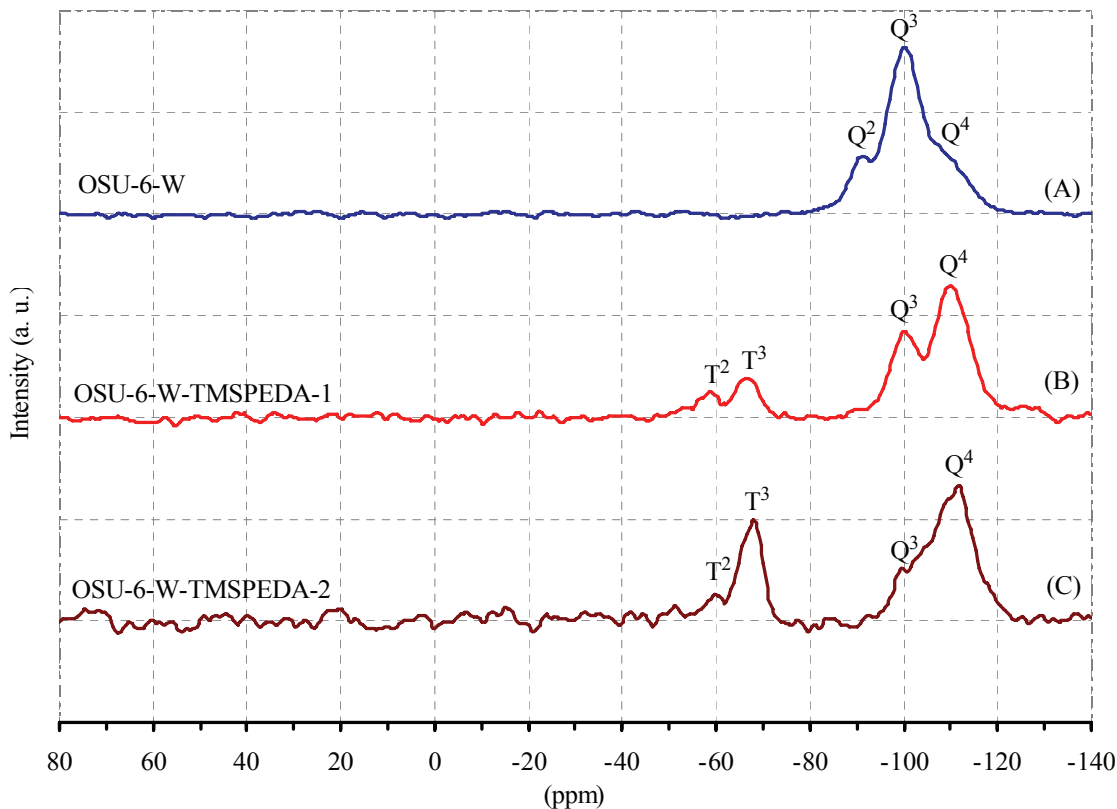
Figure 4.4. Solid state ^{29}Si CP/MAS NMR spectra of; (A) HCl-Ethanol washed mesoporous silica, OSU-6-W, (B) the modified OSU-6-W-TMSPEDA-1, and (C) the modified OSU-6-W-TMSPEDA-2.

As discussed previously, OSU-6-W has three peaks: low intensity peak at -91.2 ppm, which is due to Q^2 surface silicon atoms with two siloxane bonds and two geminal silanol groups; a peak at -100.4 ppm attributed to Q^3 surface silicon atoms with three siloxane bonds and one (isolated) silanol group; and a resonance at -107.9 ppm attributed to surface Q^4 silicon atoms with four siloxane bonds.

The two functionalized samples, Figure 4.4(B) and (C), show two peaks with locations near -100 and -110 ppm, corresponding to Q^3 and Q^4 silicon environments. In addition, the OSU-6-W-TMSPEDA-1 sample contains another two peaks at -58.7 and -

66.0 ppm corresponding to T^2 and T^3 silicon environments, while the OSU-6-W-TMSPEDA-2 sample shows another two peaks at -59.7 (T^2) and -68.1 ppm (T^3). All peaks were identified by multipeak curve fitting.

OSU-6-W-TMSPEDA-1 and OSU-6-W-TMSPEDA-2 show changes in the relative intensities of the silicon atom resonances in the locality of -100 ppm when compared to the signals for the OSU-6-W sample. In particular, the relative intensity for the Q^3 silicon resonance at around -100 ppm undergoes a significant decrease with increasing degree of functionalization. This difference in relative intensity is attributable to reactions of surface Si-OH groups with TMSPEDA molecules that lead to the formation of more Si-O-Si bonds. When the spectra of the two modified samples are compared to each other, the intensity of the peak at around -100 ppm is significantly less intense in the OSU-6-W-TMSPEDA-2 sample.

The additional peaks lying in the range from -50 to -70 ppm, as shown in Figure 4.4, occur only for the silylated sample since they are due to the organic silane groups. There are two of these peaks observed in case of the OSU-6-W-TMSPEDA-1, Figure 4.4 (B). These two resonances can be assigned as follows: (i) the resonance at *ca.* -58.7 ppm arises from terminal groups that are only bound to one neighboring siloxane, and (ii) the resonance at *ca.* -66.0 ppm arises from cross-linked groups that are bound to two neighboring siloxanes. In the case of the OSU-6-W-TMSPEDA-2, Figure 4.4 (C), there are two resonances that indicate two different environments for the siloxane groups in the functionalized monolayer. The two resonances can be assigned as follows: (i) the resonance at *ca.* -59.7 ppm arises from terminal groups that are only bound to one neighboring siloxane and (ii) the resonance at *ca.* -68.1 ppm arises from cross-linked

groups that are bound to two neighboring siloxanes. It is to be noted that the intensities of these peaks indicate that for both samples both the amount and structure of the grafted groups are different. Nevertheless, the dominant peak on the OSU-6-W-TMSPEDA-1 and OSU-6-W-TMSPEDA-2 is attributed to the cross-linked siloxane group. OSU-6-W-TMSPEDA-2 has much stronger terminal silicon resonances than OSU-6-W-TMSPEDA-1 which indicate more surface coverage with aminosilane. It also has a relatively large T^3 peak and a very small T^2 peak indicating a more complete function of a polymerized siloxane monolayer with fewer defects.

Solid state ^{29}Si CP/MAS NMR spectra show distinct resonances for siloxane [Q^n = Si(OSi)$_n$(OH)$_{4-n}$, $n = 2$–4] and organosiloxane [T^m = RSi(OSi)$_m$(OH)$_{3-m}$, $m = 1$–3] centers, with T^3 predominant over T^2 and T^1 organosiloxane centers, Figure 4.4, indicating that the condensation of the methoxy groups with silanol groups of the mesoporous silica was extensive. The width of the T^m peaks is similar to those of the Q^n species, suggesting that the local environments are comparable in terms of steric hindrance.[25] Solid state ^{29}Si NMR revealed a high degree of silane cross-linking and a surface population of 4.48 groups/nm^2 for OSU-6-W-TMSPEDA-2 and 2.54 groups/nm^2 for OSU-6-W-TMSPEDA-1.

II. Solid State ^{13}C CP/MAS NMR Spectroscopy

The presence of covalently linked organic moieties bearing diamine groups in the as-synthesized OSU-6-W mesoporous silicas were also confirmed by ^{13}C CP/MAS solid state NMR spectroscopy.[24] Figure 4.5 shows the solid state ^{13}C CP/MAS NMR spectra for diamino-functionalized mesoporous materials, OSU-6-W-TMSPEDA-1 and OSU-6-W-TMSPEDA-2.
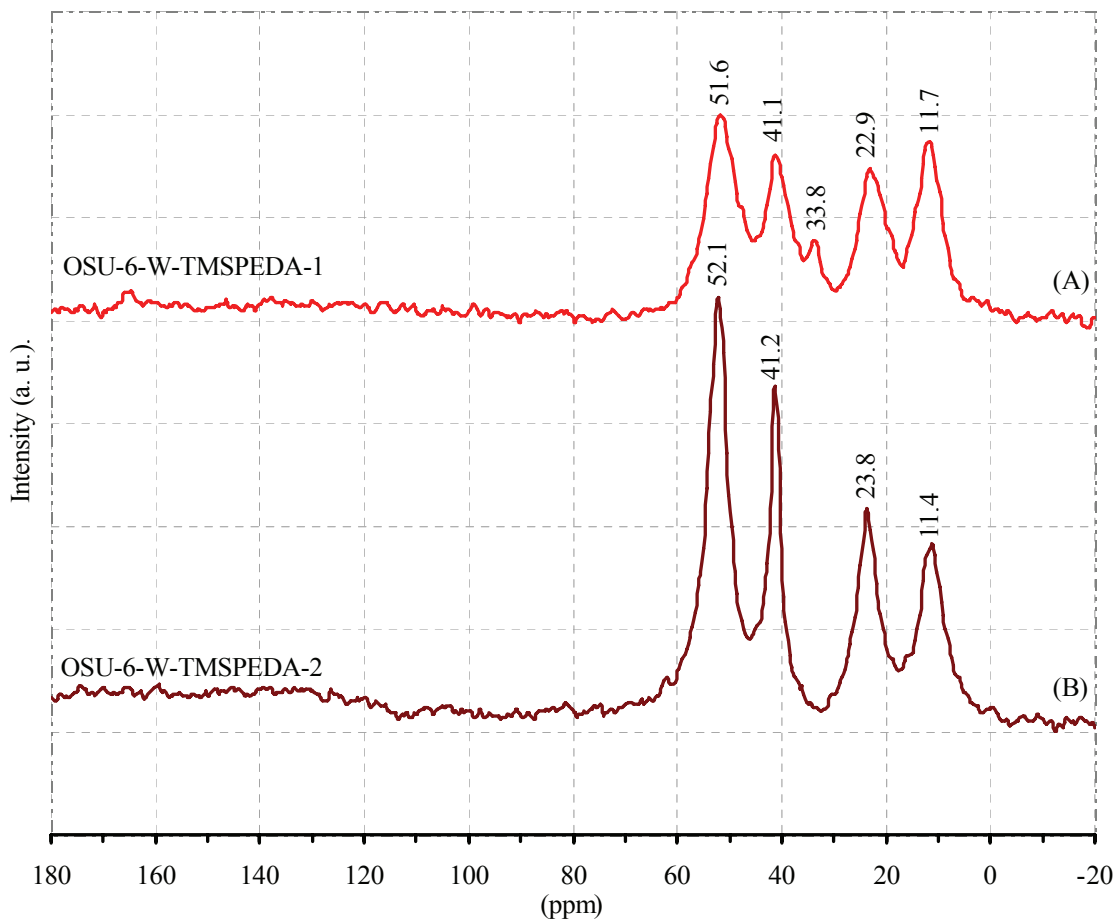
Figure 4.5. Solid state ^{13}C CP/MAS NMR spectra of the modified samples with diamine groups, (A) OSU-6-W-TMSPEDA-1, and (B) OSU-6-W-TMSPEDA-2.

The spectra of the first modified sample shows resonances at δ values of 11.7, 22.9, 41.1, and 51.6 ppm. These are due to the carbon atoms in (≡Si-CH$_2$-), (≡Si-CH$_2$-CH$_2$-), (≡Si-CH$_2$-CH$_2$-CH$_2$-NH-) and (-NH-CH$_2$-CH$_2$-NH$_2$), and (-CH$_2$-NH$_2$), respectively. The spectra of the second sample shows peaks at δ of 11.4, 23.8, 41.1, 51.6 ppm attributable to the carbon atoms in (≡Si-CH$_2$-CH$_2$-), (≡Si-CH$_2$-CH$_2$-), (≡Si-CH$_2$-CH$_2$-CH$_2$-NH-) and (-NH-CH$_2$-CH$_2$-NH$_2$), and (-CH$_2$-NH$_2$), respectively. The peaks corresponding to the organosiloxane moieties are relatively broad, indicating restricted

mobility of the functional groups attached to the siloxane framework. The low intensity of the peaks in OSU-6-W-TMSPEDA-1 sample compared to that in OSU-6-W-TMSPEDA-2 indicates a lower surface coverage. Moreover, from the spectrum, there are no peak indicates the presence of methoxy groups which means high hydrolysis and condensation of the functional groups on the surface of both samples.

III. Fourier Transform Infrared Spectroscopy (FT-IR)

Infrared spectroscopy was employed as an important tool to characterize the functional groups of the products. The vibrational spectra obtained from solid samples confirmed the success of the grafting reactions since they displays bands that are very close to those observed when propylethylenediamine functional group was previously incorporated into similar materials.

The infrared spectra obtained for OSU-6-W-TMSPEDA-1 and OSU-6-W-TMSPEDA-2 hybrids are shown in Figure 4.6. Typical silica bands associated with the main inorganic backbone can be clearly observed such as: (i) a large broad band between 3600 and 3200 cm^{-1}, and a band at 3740 cm^{-1} attributed to the presence of the O-H stretching frequency of silanol groups bonded to the inorganic structure, and also to the remaining adsorbed water, (ii) the intense band related to the siloxane stretching of these groups at 1100 cm^{-1}, (iii) a band assigned Si-O-H bending frequency near 950 cm^{-1}, and (iv) a band assigned O-Si-O vibration mode near 800 cm^{-1}. Additional bands are also observed in both spectra that confirm the presence of organic pendant groups in these materials. Generally, the functionalized silicas with trimethoxysilylpropylethylene-diamine show the CH_2 rocking vibration of $Si-CH_2R$ appearing at around 692 cm^{-1}, broad NH_2 stretching absorptions at 3250-3450 cm^{-1}, an N-H deformation peak at 1640-1560

239

cm^{-1}, and a C-H stretching and bending of methyl groups at 3000-2840 and 1450 cm^{-1}, respectively.[26-30]
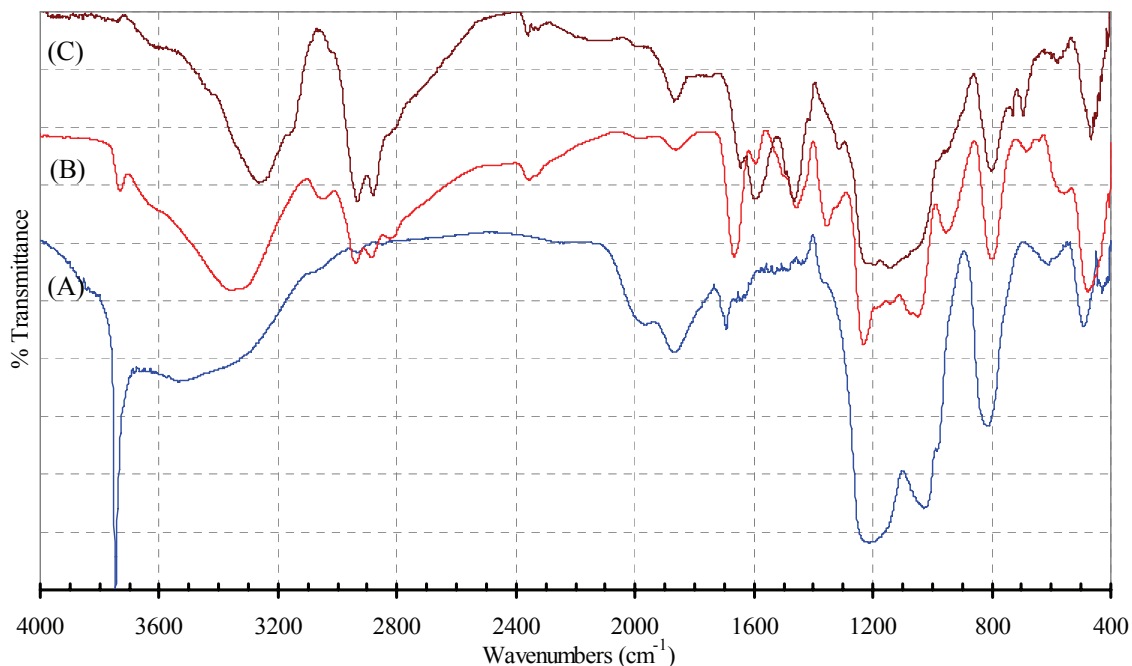
Figure 4.6. Infrared spectra of (curve A) OSU-6-W, (curve B) OSU-6-W-TMSPEDA-1, and (curve C) OSU-6-W-TMSPEDA-2.

The two diamine derivitized silicas, OSU-6-W-TMSPEDA-1 and OSU-6-W-TMSPEDA-2 were characterized by infrared spectroscopy and compared to the corresponding unmodified OSU-6-W. All spectra showed a large band around 3000-3500 cm^{-1} due to adsorbed water. The efficiency of the grafting process is demonstrated by a significant decrease in the silanol bands at around 3740 cm^{-1}, with an associated increase of new bands characteristics of the immobilized propylethylenediamine groups. These bands were attributed to both the symmetric and asymmetric stretching of active groups in OSU-6-W-TMSPEDA-1; $v_{as}(CH_2) = 2939$ cm^{-1}, $v_s(CH_2) = 2886$ cm^{-1}, CH$_2$

scissor at 1458 cm^{-1}, CH$_3$ bending vibration at 1354 cm^{-1}, NH$_2$ (v_{as} = 3356 cm^{-1}), and

NH$_2$ bending vibration at 1665 cm^{-1}, in OSU-6-W-TMSPEDA-2; v_{as}(CH$_2$) = 2933 cm^{-1}, v_s(CH$_2$) = 2879 cm^{-1}, CH$_2$ scissor at 1464 cm^{-1}, NH$_2$ (v_{as} = 3286 cm^{-1}, v_s = 3265 cm^{-1}), and

NH$_2$ bending vibration at 1598 cm^{-1}.[31,32] When comparing the intensities of the IR peaks

in the modified samples, it can be concluded that the second sample has a higher

concentration of functional groups.

4.3.3. Estimation of the Total Surface Loading of the Ordered Mesoporous Silica with the Propylethylenediamine Functional Groups

As discussed in chapter three, the concentration of the functional groups on the

surface is one of the most important aspects of these materials. Therefore, determination

of the degree of the functionalization is highly necessary.

The amount of functional group deposited on the surface was quantified using two

variables. The surface loading (*l*) expresses the amount of deposited molecules in

mmol/g. The number of molecules deposited per nm^2 is given by the surface coverage

(*C*). Both values use the mass of the pure mesoporous silica before modification as a

reference.

I. Elemental Analysis

Carbon and nitrogen elemental analysis was carried out for both modified

samples. The concentration of attached groups was determined as follows:[33,34]

$$C \text{ (groups/nm}^2) = 6\text{x}10^5\, P_C / [(1200 n_C - W P_C) S_{BET}]$$

where *C* is the concentration of attached groups, which contain carbon; P_C is the

percentage of carbon in the sample, n_C is the number of carbon atoms in the attached

group (counted as C$_5$), *W* is the corrected formula mass of the modifier (counted as

$C_5H_{13}N_2O_3Si$), and S_{BET} is the specific surface area of the pristine substrate (1283 m^2/g).

Table 4.2 shows the results.

Table 4.2. Carbon and nitrogen elemental analysis, and concentration of propyl ethylene diamine functional groups

Sample	C %	N %	Surface Area (m^2/g)	TMSPEDA (group/nm^2)
OSU-6-W	0.10	0.06	1283	---
OSU-6-W-TMSPEDA-1	16.32	6.47	983	2.36
OSU-6-W-TMSPEDA-2	21.56	8.59	691	4.63

II. Solid State ^{29}Si CP/MAS NMR Spectrum

The procedure described in chapter 3 was used to determine the degree of silylation of the functionalized silicas.[35] The results are given in Table 4.3.

The change in silanol concentration before and after silylation found to be equal to the concentration of the functional groups indicating that each diaminosilane condensed with a single surface hydroxyl. Also, the concentration of the functional groups for both silylated samples calculated using this method show high agreement with that of elemental analysis.

Table 4.3. Solid state ^{29}Si CP/MAS NMR deconvolution results

Sample	Q^4 (%)	Q^3 (%)	Q^2 (%)	[SiOH] (mmol/g)	[SiOH] (molecule/nm^2)	[TMSPEDA] (group/nm^2)
OSU-6-W	14.38	71.73	13.89	14.43	6.77	---
OSU-6-W-TMSPEDA-1	56.35	44.64	0.00	6.91	4.23	2.54
OSU-6-W-TMSPEDA-2	81.48	18.51	0.00	3.00	2.29	4.48

4.3.4. Metal Ions Adsorption Study

I. Transition Metal Ions Adsorption (Cu^{2+} and Co^{2+})

The uptake capacity of the modified mesoporous silica, OSU-6-W-TMSPEDA-2, toward transition metal ions was investigated using five different amounts of the adsorbent (ranging from 25 to 125 mg) and one constant concentration of the metal under study; copper ions (100 ppm) at pH 5.5 and cobalt ions (100 ppm) at pH 6.5. The results are shown in Figure 4.7. The maximum uptake of each metal was calculated from the Langmuir adsorption isotherms. The uptake capacity was found to be 9.10 mmol Cu^{2+}/g (578.3 mg/g) and 5.14 mmol Co^{2+}/g of the adsorbent (303 mg/g).
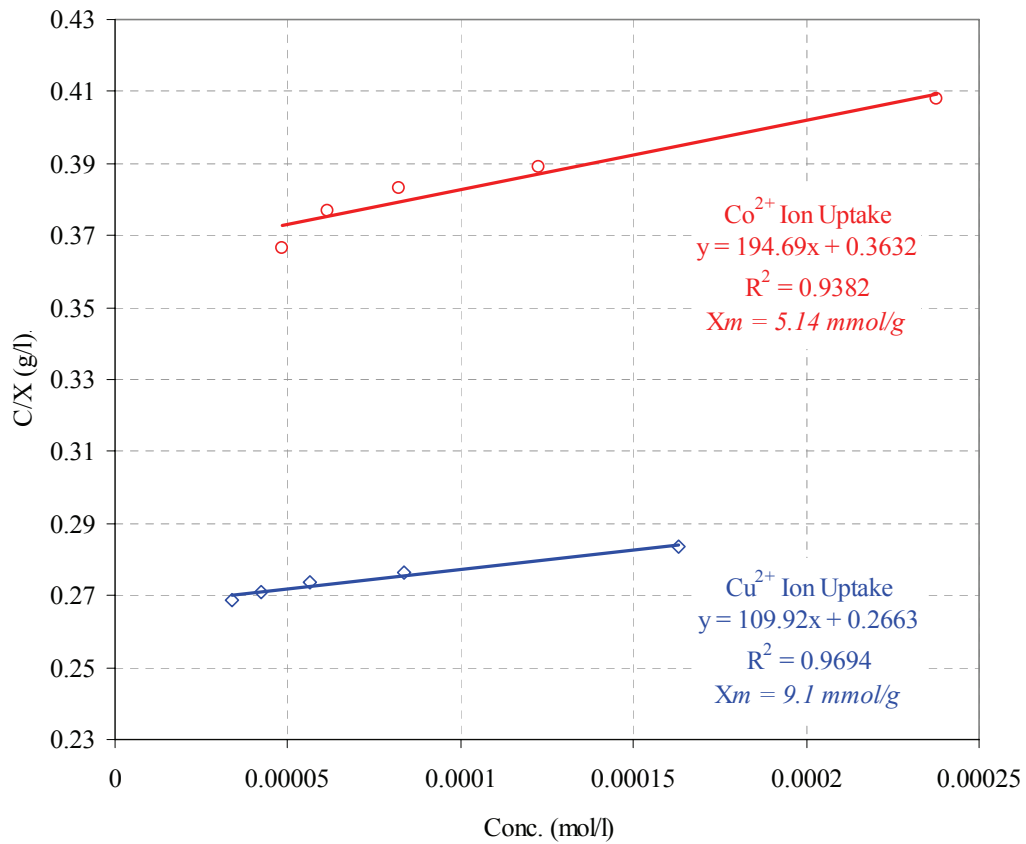
Figure 4.7. The Langmuir adsorption isotherms of Cu^{2+} and Co^{2+} ions adsorbed by OSU-6-W-TMSPEDA-2 adsorbent.

Since the average diamino-functional group content of the OSU-6-W-TMSPEDA-2 silica is 5.22 mmol/g, based on the above results, the uptake of Co^{2+} corresponds to the formation of a 1 Co^{2+}: 1 diamine complexes which indicate that each diamine group coordinates to one Co^{2+} ion. In the case of copper, the uptake of Cu^{2+} corresponds to the formation of 2 Cu^{2+}: 1 diamine group ratio. The latter indicates that each diamine-functional group coordinates to two Cu^{2+} ions, most likely a network of nitrogen-bridged metal complexes forms.

II. Radioactive Metal Ions Adsorption (UO_2^{2+} and Th^{4+})

The adsorption capacity of the modified mesoporous silica, OSU-6-W-TMSPEDA-2, toward radioactive metal ions was examined using five different amounts of adsorbent ranging from 25 to 125 mg and 100 ppm of UO_2^{2+} ions and Th^{4+} ions. The results are shown in Figures 4.8 and 4.9.

UO_2^{2+}
$y = 451.2x + 1.1619$
$R^2 = 0.9886$
$Xm = 2.22\ mmol/g$
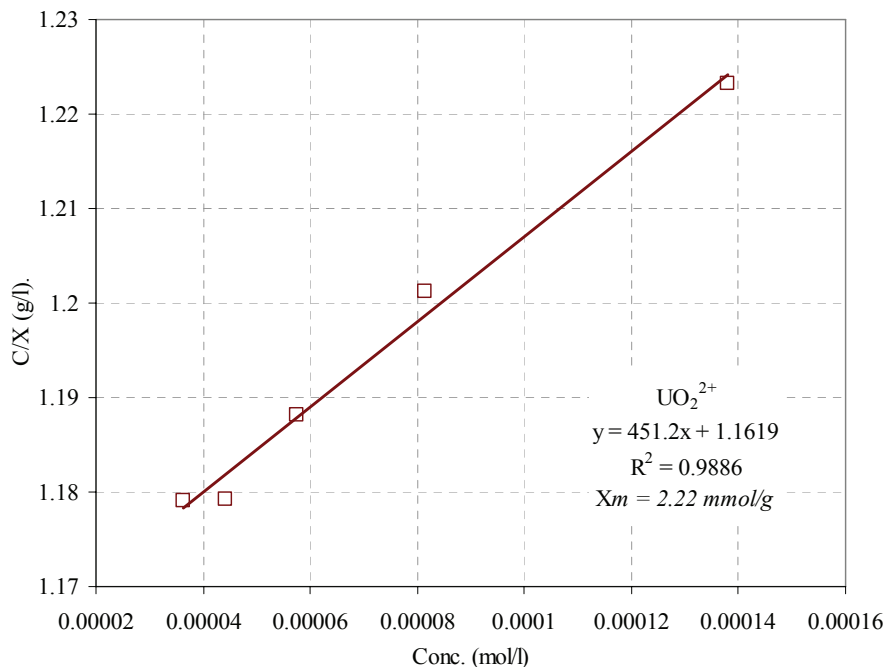
Figure 4.8. The Langmuir adsorption isotherm of UO_2^{2+} ions adsorbed by OSU-6-W-TMSPEDA-2 adsorbent
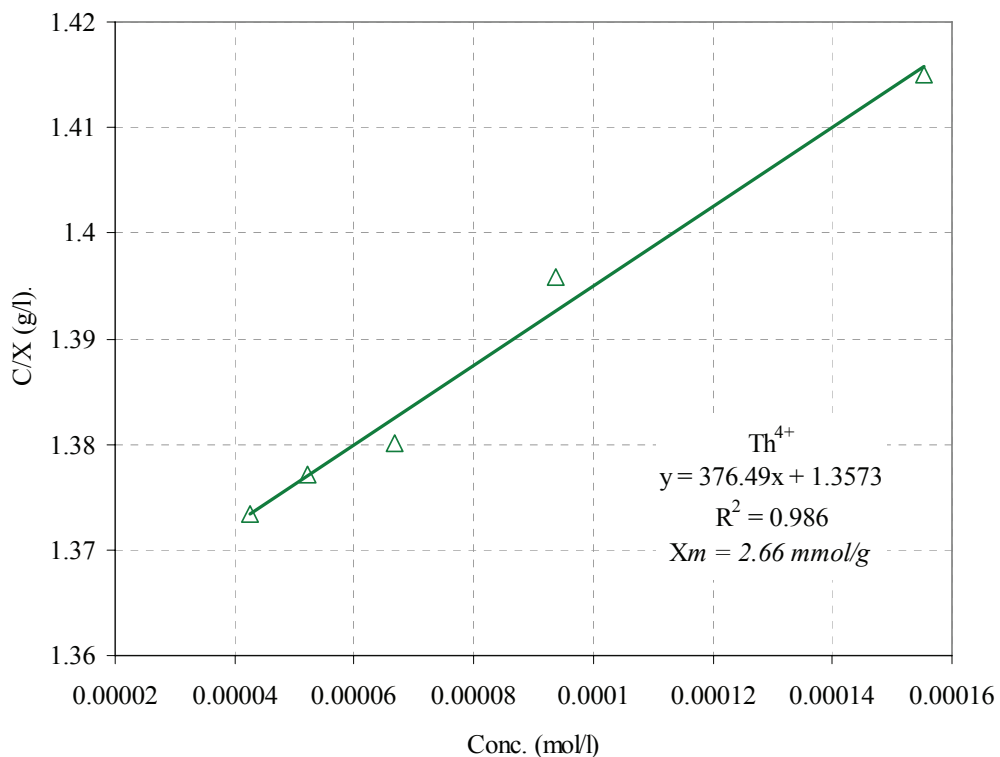
Figure 4.9. The Langmuir adsorption isotherm of Th4+ ions adsorbed by OSU-6-W-TMSPEDA-2 adsorbent

The uptake capacities calculated from the Langmuir adsorption isotherms were 2.22 mmol/g for UO_2^{2+} (527.5 mg/g) and 2.66 mmol/g for Th^{4+} (616.2 mg/g). This can be explained due to the formation of 1:2 complexes (metal to ethylenediamine ligand) at high concentrations of UO_2^{2+} and Th^{4+} ions.

III. Regeneration of the Absorbent

Treatment of the uranium-loaded material three times with stirred aqueous solution of 2.0 *M* HCl for 1 hour resulted in removal of the bound UO_2^{2+} from the structure, regenerating the adsorbent for further metal ion uptake. The regenerated

material, Figure 4.10, shows decrease in the uranium ion uptake capacity down to ~ 69% after the fourth regeneration.
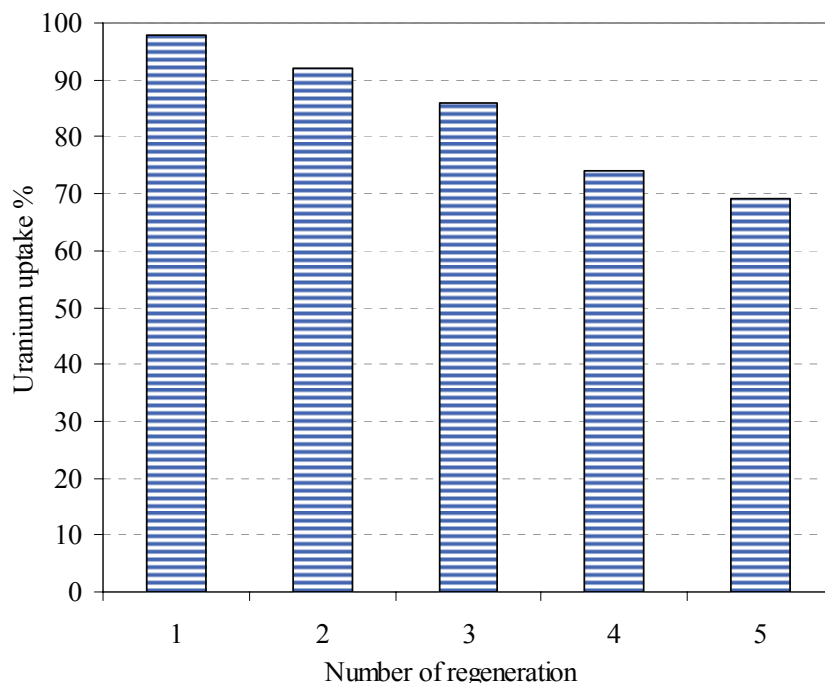
Figure 4.10. The regeneration experiments of UO_2^{2+} ions adsorbed by OSU-6-W-TMSPEDA-2 absorbent

The decreases may be due to loss of the immobilized groups with washing or a strong interaction of some UO_2^{2+} ions with the amine groups so that it can not be released with HCl washing. The latter, will lead to blocking of the available sites for chelating. Overall, this material shows excellent regeneration.

4.4. CONCLUSION

A novel approach to the preparation of functionalized ordered mesoporous materials for use in the selective adsorption of transition metal ions and radioactive materials is described. Both N_2 adsorption/desorption isotherms and XRD patterns of as-synthesized adsorbents showed that the ordered pore structure was retained during the

preparation steps and also showed that the functional group was immobilized mainly inside the mesopore channel. A remarkable degree of grafting has been achieved by the aid of an intermediate hydrolysis step.

Diamine-functionalized mesoporous adsorbent had a remarkable selectivity for transition metal ions (Co^{2+} and Cu^{2+}) and for radioactive material such as uranium (UO_2^{2+}) and thorium (Th^{4+}). The findings here show that the as-synthesized adsorbents prepared via a simple method without metal-imprinting had high adsorption capacities for Co^{2+}, Cu^{2+}, UO_2^{2+}, and Th^{4+} ions. In addition to being useful sorbates for metal ions, the new approach that was developed can also be applied to the preparation of transition metal catalysts.[36]

4.5. REFERENCES

1. Kim, J. S. A study on the heavy metal removal from aqueous solutions using chemically modified ceramic substrates. In: *Ph.D. Dissertation*, Seoul National University, Seoul **1999**, pp. 1–19.

2. Kim, J. S.; Yi, J.. Removal of copper ions from aqueous solutions using silica supports immobilized with 2-hydroxy-5-nonylacetophenoneoxime. *Separation Sci. Technol.* **1999,** *34*(15), 2957-2971.

3. J.S. Kim and J. Yi Selective removal of copper ions from aqueous solutions using modified silica beads impregnated with LIX 84. *J. Chem. Technol. Biotechnol.* **1999,** *74*(6), 544-550.

4. A.K. Sengupta, Y. Zhu and D. Hauze Metal(II) ion binding onto chelating exchangers with nitrogen donor atoms: Some new observations and related implications *Environ. Sci. Technol.* **1991,** *25*(3), 481-488.

5. J.S. Lee, N.V. Deorkar and L.L. Tavlarides Adsorption of copper cyanide on chemically active adsorbents. *Indus. Eng. Chem. Res.* **1998,** *37*(7), 2812-2820.

6. Khatib, I. S.; Parish, R. V.. *J. Organometallic Chem.* 369 (1989), p. 9.

7. J. Liu, X. Feng, G.E. Fryxell, L.-Q. Wang, A.Y. Kim and M. Gong Hybrid Mesoporous Materials with Functionalized Monolayers. *Adv. Mater.* **1998,** *10*(2), 161–165.

8. Feng, X.; Fryxell, G. E.; Wang, L.-Q.; Kim, A. Y.; Liu, J.; Kemner, K. M.. Functionalized Monolayers on Ordered Mesoporous Supports. *Science*, **1997,** *276*(5314), 923–926.

9. Mercier, L.; Pinnavaia, T. J.. A functionalized porous clay heterostructure for heavy metal ion (Hg^{2+}) trapping. *Micropor. Mesopor. Mater.* **1998**, 20(1-3), 101-106.

10. Brown, J.; Mercier, L.; Pinnavaia, T. J.. Selective adsorption of Hg^{2+} by thiol-functionalized nanoporous silica. *Chem. Commun.* **1999**, 5(1), 69-70.

11. Mercier, L.; Pinnavaia, T. J.. Heavy metal ion adsorbents formed by the grafting of a thiol functionality to mesoporous silica molecular sieves: Factors affecting Hg(II) uptake*Environ. Sci. Technol.* **1998**, 32(18), 2749-2754.

12. Mercier, L.; Pinnavaia, T. J.. Access in mesoporous materials: Advantages of a uniform pore structure in the design of a heavy metal ion adsorbent for environmental remediation. *Adv. Mater.* **1997**, 9(6), 500-503.

13. Fryxell, G. E.; Liu, J.; Hauser, T. A.; Nie, Z.; Ferris, K. F.; Mattigod, S.; Gong, M.; Hallen, R. T.. Design and Synthesis of Selective Mesoporous Anion Traps. *Chem. Mater.* **1999,** *11*(8), 2148-2154.

14. Brown, J.; Richer, R.; Mercier, L.. One-step synthesis of high capacity mesoporous Hg^{2+} adsorbents by non-ionic surfactant assembly. *Micropor. Mesopor. Mater.* **2000**, 37(1-2), 41-48.

15. Liu, A. M.; Hidajat, K.; Kawi, S.; Zhao, D. Y.. A new class of hybrid mesaporous materials with functionalized organic monolayers for selective adsorption of heavy metal ions. *Chem. Commun.* **2000**, 6(13), 1145-1146.

16. J.S. Beck, Method for synthesizing mesoporous crystalline material, US Patent 5,057,296 (1991).

17. Yanagisawa, T.; Shimizu, T.; Kuroda, K.; Kato, C.. The preparation of alkyltrimethylammonium-kanemite complexes and their conversion to microporous materials. *Bull. Chem. Soc. Jpn.* **1990,** *63*(4), 988-992.

18. Choudary, B. M.; Kantam, M. L.; Sreekanth, P.; Bandopadhyay, T.; Figueras, F.; Tuel, A.. Knoevenagel and Aldol Condensations Catalyzed by a New Diamino-functionalized Mesoporous Material. *J. Mol. Catal. A*, **1999,** *142*(3), 361-365.

19. Vrancken, K. C.; Possemiers, K.; Van Der Voort, P.; Vansant, E. F.. Surface modification of silica gels with aminoorganosilanes. *Coll. Surf., A: Physicochemical and Engineering Aspects* **1995,** *98*(3), 235-241.

20. Vrancken, K. C.; Van der Voort, P.; Gillis-D'Hamers, I.; Vansant, E. F.; Grobet, P.. Influence of Water in the Reaction of γ-Aminopropyltriethoxysilane with Silica Gel: a Fourier-transform Infrared and Cross-polarization Magic-angle-spinning Nuclear Magnetic Resonance Study. *J. Chem. Soc., Faraday Trans.* **1992,** *88*(21), 3197-3200.

21. R.M. Smith, *Gas and Liquid Chromatography in Analytical Chemistry*, J. Wiley, New York, 1988.

22. B. Porsch and J. Kratka, *J. Chromatogr.,* 543 (1991) 1.

23. T.J. Pinnavaia, J.G-S. Lee and M. Abedini, in D.E. Leyden and W.T. Collins (Eds.), Gordon and Breach Science Publ., New York, **1988,** p. 35.

24. Zhang, W. H.; Lu, X. B.; Xiu, J. H.; Hua, Z. L.; Zhang, L. X.; Robertson, M.; Shi, J. L.; Yan, D. S.; Holmes, J. D. Synthesis and Characterization of Bifunctionalized Ordered Mesoporous Materials. *Adv. Funct. Mater.* **2004,** *14*(6), 544-552.

25. Yoshitake, H.; Yokoi, T.; Tatsumi, T. Adsorption of Chromate and Arsenate by Amino-Functionalized MCM-41 and SBA-1. *Chem. Mater.* **2002,** *14* (11), 4603 - 4610.

26. Krasnoslobodtsev, Alexey V.; Smirnov, Sergei N.. Effect of Water on Silanization of Silica by Trimethoxysilanes. *Langmuir* **2002,** *18*(8), 3181-3184.

27. White, L. D.; Tripp, C. P. An Infrared Study of the Amine-Catalyzed Reaction of Methoxymethylsilanes with Silica. *J. Colloid Interface Sci.* **2000,** *227*(1), 237-243.

28. X. S. Zhao, G. Q. Lu, A. K. Whittaker, G. J. Millar, and H. Y. Zhu Comprehensive Study of Surface Chemistry of MCM-41 Using ^{29}Si CP/MAS NMR, FTIR, Pyridine-TPD, and TGA *J. Phys. Chem. B* **1997,** *101*(33), 6525-6531.

29. Jentys, A.; Pham, N. H.; Vinek, H. Nature of hydroxy groups in MCM-41. *J. Chem. Soc., Faraday Trans.* **1996,** *92*(17), 3287-3291.

30. Lee, B.; Kim, Y.; Lee, H.; Yi, J.. Synthesis of functionalized porous silicas via templating method as heavy metal ion adsorbents: the introduction of surface hydrophilicity onto the surface of adsorbents. *Micropor. Mesopor.* **2001,** *50*(1), 77-90.

31. Diaz, J. F.; Balkus, K. J., Jr. Synthesis and Characterization of Cobalt-Complex Functionalized MCM-41 *Chem. Mater.* **1997,** *9*(1), 61-67.

32. Park, D. H.; Park, S. S.; Choe, S. The formation of metal (M = Co(II), Ni(II), and Cu(II)) complexes by aminosilanes immobilized within mesoporous molecular sieves J. *Bull. Korean Chem. Soc.* **1999,** *20*(3), 291-296.

33. Sander, L. C.; Wise, S. A. Recent advances in bonded phases for liquid chromatography. *Crit. Rev. Anal. Chem.* **1987,** *18*(4), 299-415.

34. K.K. Unger, Packings and Stationary Phases in Chromatographic Techniques, Marcel Dekker, Moscow (1990).

35. Wouters, B. H.; Chen, T.; Dewilde, M.; Grobet, P. J.. Reactivity of the surface hydroxyl groups of MCM-41 towards silylation with trimethylchlorosilane. *Micropor. Mesopor. Mater.* **2001,** *44-45,* 453-457.

36. Cho, Y. S.; Park, J. C.; Lee, B.; Kim, Y.; Yi, J. Preparation of Nickel Catalyst Supported on SBA-15 Mesoporous Silica. *Catal. Lett.* **2002,** *81*(1-2), 89-96.

SYNTHESIS OF MESOPOROUS MATERIALS BEARING METHACRYLATE FUNCTIONAL GROUPS AND OTHER DERIVATIVES AND REMOVAL OF CONTAMINANTS

Abstract

Propylmethacrylate-functionalized mesoporous OSU-6-W materials were synthesized via post-synthesis grafting of 3-(trimethoxysilyl)propyl methacrylate (TMSPMA) onto OSU-6-W mesoporous silica. Two grafting procedures were used here based on the use of catalyst (triethylamine) and water for fast adsorption and hydrolysis of the methoxy groups. At the maximum level of silylation with TMSPMA, the solid state ^{29}Si CP/MAS NMR measurements of the two modified samples, OSU-6-W-TMSPMA-1 and OSU-6-W-TMSPMA-2, indicate that the Si atoms containing Si-C bonds are different in the two samples. These measurements also indicate that the surface coverage of propyl methacrylate anchored to silanol groups on the surface of OSU-6-W were not the same. Moreover, the results from the elemental analyses, UV-Vis and titration of the two modified samples show good agreement with that of the solid state ^{29}Si CP/MAS NMR. The propyl methacrylate-functionalized mesoporous material was subjected to a reaction with various active compounds (*e.g.,* lysine (2,6-diaminocaproic acid), β-alanine (3-aminopropionic acid), and glycine (aminoacetic acid)

in order to introduce new active groups into the modified sample.

These materials were characterized by Fourier transform infrared spectroscopy (FTIR), X-ray powder diffraction (XRD), scanning electron microscopy (SEM), ^{13}C and ^{29}Si solid state NMR spectroscopy, elemental analysis (EA), surface area analysis (BET), and UV-Vis spectroscopy.

The adsorption experiments of the radioactive ions, UO_2^{2+} and Th^{4+}, were conducted in order to investigate the capacity and selectivity of the synthesized modified samples.

5.1. INTRODUCTION

5.1.1. Contamination with Heavy Metal and Radioactive Materials

Heavy metals and radioactive materials are introduced into the environment through a number of industrial processes.[1] Depending on the chemical form and exposure level, these toxic materials can potentially be very harmful to humans and have a negative impact on the environment. Unlike organic pollutants, metal contamination is exacerbated by the fact that metals are nondegradable, thus recirculate and accumulate in the environment.[2,3] As a direct result of this, it is necessary to remediate heavily contaminated sites. This can only be accomplished by isolation and recovery of the contaminant since degradation is not an option. As a first attempt at remediation, bulk techniques, such as simple filtration or precipitation, are often utilized.[2,4] Although these techniques are useful in removing a significant fraction of the contaminant, they are unable to reduce the contaminant levels to meet environmental agency regulations for many of the more toxic metals. As a result, an ultimate step must be employed that is often in the form of a chemical extraction.

The ideal metal extraction and recovery technique must have selective binding toward metal of interest, thus allowing its separation from metals that are harmless or beneficial. Other wise, the latter ions could overcome the available binding sites and significantly reduce the efficiency or capacity of the extracting media. Also, strong binding is necessary for effective removal of contaminants and easy release of the metals is desirable for efficient concentration of the contaminant and reuse of the media. The extractant needs to be environmentally friendly to prevent further contamination when the media is ultimately discarded, and high stability to be reused with an extended lifetime, ensuring cost-effectiveness.[5]

5.1.2. Fabrication of the Mesoporous Silica Surface with a Propylmethacrylate Functional Group

The silylation reagents aminoorganosilanes discussed in chapter three, have the general formula $H_2N-R-Si-(OR')_3$. They differ from the general organosilanes by carrying an amino-functional group in the organic chain. This group is responsible for the high reactivity of the aminosilane molecules. The electron-rich nitrogen center of the amine group can enter into hydrogen bonding interactions with hydrogen donating groups, such as hydroxyl groups or other amines. Mixing of an aminosilane with silica gel results in fast adsorption, by hydrogen bonding of the amine to a surface hydroxyl group.[15] After adsorption, the amine group can catalyze the condensation of the silicon side of the molecule with a surface silanol. Thus siloxane bonds with the surface may be formed in the absence of water.[16,17] For other silanes (*e. g.,* 3-(trimethoxysilyl)propyl methacrylate) the siloxane bond formation requires an initial hydrolysis of the methoxy or ethoxy groups or the addition of an amine to the reaction mixture.[18]

Unfortunately, the addition of desirable functional groups to mesoporous silica is often impeded by the limited reactivity of silyl reagent (if available), a limited choice of organic silanes, and/or the often poor chemical stability of the surface grafted siloxane ligands. Functional groups introduced via silane grafting include alkylamines, epoxides, alkyl halides, and alkylthiols. In an effort to overcome the above limitations, subsequent reactions can be used to add the desired functional groups by reaction with previously grafted reactive groups.[19] In this investigation, the propyl methacrylate functional group served as an active site on the silica surface to bind other molecules. These molecules may impart new interaction capacities to the surface. Previously, propylmethacrylate-modified silica gel was used as a stationary phase in liquid and gas chromatography after a secondary modification treatment to place, for example, alcohol groups on the surface.[19]

To ensure the effectiveness of the hybrid materials in utilizing the intrinsic reactivity of the organofunctional groups, these moieties must keep their activity upon immobilization, they must be accessible to the external solution, and mass transfer to and from these active sites should be as fast as possible. As highlighted in recent investigations, this is especially important in heterogeneous catalysis for ensuring high efficiency and turnover,[12,25-30] as well as in removal of toxic substances to improve the performance of remediation processes and environmental containment technologies.[22,31-42] It is expected that the increase in the density of functional groups while retaining the open space would result in a higher activity. Therefore, high loading of functional groups in mesoporous silicas has received much attention.[43-46] Uniform surface modification

with functional groups is desired so that the coverage of functional groups on the surface may increase without adversely affecting the diffusion of molecules in the mesopore.[47-49]

5.1.3. Immobilization of Active Groups onto the Mesoporous Material Functionalized with Propylmethacrylate Groups

Currently, the most common chemical modes of metal removal include ion exchangers or removal by chelation with synthetic crown ethers or other macrocylic cage molecules.[50-54] The most significant drawback associated with typical ion exchangers is the lack of selectivity in metal binding and/or weak binding characteristics. While crown ethers are both selective and strong binders, due to polydentate chelation within a sized cavity, they often exhibit slow release kinetics.[50] This is a potential problem when metal recovery is required. In addition, many crown ethers are also very toxic, so using them may simply add to the problem of contamination. As a result of the inherent problems with most of the current metal remediation strategies, researchers are now turning toward natural systems. This study will focus on the potential utility of amino acids that have been immobilized on a substrate for general use in column applications.

A well-known class of metal binding proteins, the metallothioneins, is an example of such biomolecules that are characterized as having a high degree of metal binding specificity and have been isolated in a wide variety of organisms.[55-58] Their strong binding characteristics and selectivity seem to fit the criteria of the ideal metal chelator. Upon immobilization, these proteins seemed to lose the metal binding capabilities that they normally have within the cellular environment where they typically function in nature.[59] Examination of several metallothioneins showed that their sequences contained a significantly high percentage of cysteine residues and that sulfhydryl groups present on

these residues are primarily responsible for metal binding.[55,57] This suggests the possibility of using simpler amino acid chains (*e.g.,* poly-amino acids) as metal binding alternatives to natural peptides. Considering only the natural set of amino acids, one can readily recognize a variety of functionalities that could serve as coordination sites for metal chelation. Using amino acids, a wide variety of interesting chelators could be envisioned. More specifically, these chelators may exhibit the desired characteristics of specificity and have the added side benefit of being non-toxic when discarded.

5.2. AIM OF STUDY

This chapter reports the immobilization of a variety of amino acids on a methacrylate-functionalized mesoporous silica. The reaction of lysine (2,6-diaminocaproic acid), β-alanine (3-aminopropionic acid), and glycine (aminoacetic acid) to the alkene of the propylmethacrylate group via conjugate addition or the Michael addition.[60] *α,β*-unsaturated carbonyl compounds contain two electrophilic sites: the carbonyl carbon and the carbon atom that is *β* to it. Certain nucleophiles tend to react at the carbon-carbon double bond rather than at the carbonyl group. Such reactions proceed via enol intermediates and are described as conjugate addition, or 1,4-addition reactions.[60]

In addition to the synthesis and immobilization, these modified materials were tested as adsorbents for the separation and removal of harmful pollutants such as heavy metal and radioactive ions from water.

5.3. EXPERIMENTAL

5.3.1. Materials

The chemicals used are as follow: 3-(trimethoxysilyl)propyl methacrylate [$((CH_3O)_3Si(CH_2)_3OCO(CH_3)C=CH_2$ 98.0%, Aldrich], lysine, β-alanine, glycine, toluene 99.8% HPLC grade, ethyl alcohol, tetrahydrofuran (THF), triethylamine (TEA, 99%, Aldrich), bromine (Br_2), methylene chloride (CH_2Cl_2), 0.10 M KOH, and distilled water. The structures of some of these compounds are shown in Scheme 5.1.

3-(Trimethoxysilyl)propyl methacrylate
(TMSPMA)

Glycine

Lysine

β-Alanine
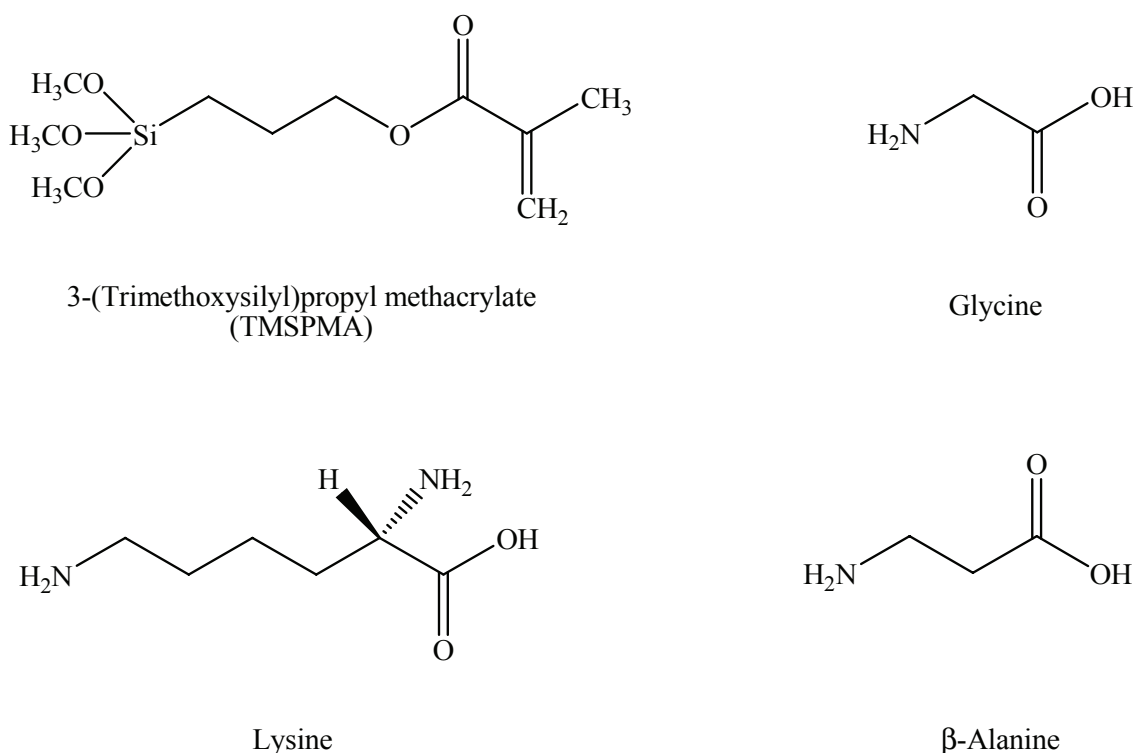
Scheme 5.1. The structures of some chemical used in this chapter.

5.3.2. Characterization

The modified mesoporous samples were characterized using a variety of techniques such as X-ray diffraction (XRD), surface area analysis (BET), elemental

analysis (EA), solid state ^{13}C and ^{29}Si NMR, and Fourier transform infrared (FT-IR) spectroscopies in order to confirm the attachment of the functional groups onto the surface and identify the texture properties. The full descriptions of all techniques were mentioned in both chapter two and three.

5.3.3. Preparation

5.3.3.1. Pretreatment of the Mesoporous OUS-6-W

The mesoporous silica material, OSU-6-W, was synthesized as discussed in chapter two of this thesis. It was activated by refluxing around 10.0 g of the mesoporous silica in 100 ml of dry toluene for 4 hours under dry atmosphere, followed by washing with dry toluene, and drying at 80 °C under vacuum. Next, 6.0 g (~ 100 mmol) of the dried material was mixed in 100 ml of dry toluene with twenty milliliters of triethylamine (TEA). The mixture was stirred for around one hour at room temperature and was then filtered off with a fine filter funnel and washed with dry toluene (3 X 50 ml). The activated material refered to as TEA-OSU-6-W.

5.3.3.2. Introduction of Propylmethacrylate Groups into the Mesoporous Surfaces

The propylmethacrylate group was attached to the mesoporous OSU-6-W material surfaces by means of the two post-synthesis grafting methods described in earlier chapters.

I. Grafting of the Mesoporous Silica with 3-(Trimethoxysilyl)propylmethacrylate in a One Step Reaction (OSU-6-W-TMSPMA-1)

OSU-6-W-TMSPMA-1 was prepared by refluxing 3.0 g (~ 50.0 mmol) of the activated mesoporous silica (TEA-OSU-6-W) with 50 mmol (~ 12.5 ml) of 3-

(trimethoxysilyl)propylmethacrylate (TMSPMA) in 100 ml of dry toluene in 250-ml

round-bottom flask under dry atmosphere (Scheme 5.2).

OSU-6-W   TMSPMA   OSU-6-W-TMSPMA
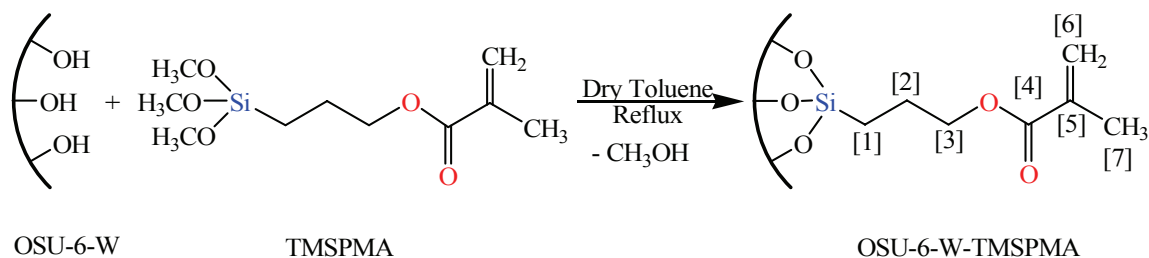
Scheme 5.2. The general chemical reaction of the functionalization process and carbon
atom position as described in the ^{13}C CP/MAS NMR.

After 48 hours, the mixture was cooled down to room temperature and the

resulting light brown solid was isolated by filtration. It was washed with 3 X 50 ml of

toluene and then methanol. The resulting white solid was then dried at 80 °C under

vacuum for 24 hours to yield 4.49 g of product.

The IR (cm^{-1}) (KBr) of the product contained absorptions at 3741(w), 3567(m),

3291(s, br), 2981(m, br), 2932(m), 2880(m), 2833(m), 1719(m, sh), 1634(m, sh),

1461(m, sh), 1346(w), 1315(w), 1211(s, br), 1083(s, br), 978(m, br), 804(m) 693(w),

574(w), and 467(s, sh). The solid-state ^{29}Si CPMAS NMR: δ (ppm) -48.0 (T^1), -56.8

(T^2), -91.6(Q^2), -102.5 (Q^3), and -109.8 (Q^4). Solid-state ^{13}C CPMAS NMR: δ (ppm) 8.9

(≡Si-*CH$_2$*-CH$_2$-)[1], 22.5 (≡Si-CH$_2$-*CH$_2$*-)[2], 66.7 (≡Si-CH$_2$-CH$_2$-*CH$_2$*-O-)[3], 168.3 (-

C(=O)-)[4], 137.3 (CH$_2$=*C*-)[5], 124.1 (*CH$_2$*=C-)[6], 18.2 (*CH$_3$*-C-)[7], and 30.3 (*CH$_3$*O-),

see Scheme 5. 2. Elemental analysis: C (19.14%) and N (0.18%).

II. Reaction of the Mesoporous Silica with 3-(Trimethoxysilyl)propylmethacrylate with the Mole Ratio of 1:1 in Three Modification Steps (OSU-6-W-TMSPMA-2)

Mesoporous silica grafted with propylmethacrylate groups was prepared as describe above. However, the product was then placed in a 125-ml Erlenmeyer flask then stirred with 50 ml of distilled water for five hours. The mixture was filtered off to recover the solid yield. The resulted product was dried at 80 $^{\circ}$C under vacuum for 24 hours then it went through another step in order to add more of the functional groups. In the last step, a 25 mmol of TMSPMA was refluxed with the result again in 100 ml of dry toluene under dry atmosphere. The resulting solid was filtered off, washed, and dried at 80 $^{\circ}$C under vacuum for 24 hours. The final product weight was 5.79 g.

IR (cm^{-1}) (KBr): 3420(s, br), 3309(s, br), 2934(s, sh), 2884(s, br), 1720(vs, sh), 1640(s, sh), 1459(m, sh), 1224(s, sh), 1081(s, sh), 965(w), 801(m, sh), 693(w), 574(w), and 464(s, sh). Solid-state ^{29}Si CPMAS NMR: δ (ppm) -56.7 (T^2), -65.5 (T^3), -101.9 (Q^3), and -109.7 (Q^4). Solid-state ^{13}C CPMAS NMR: δ (ppm) 9.0 (≡Si-CH$_2$-CH$_2$-)[1], 22.6 (≡Si-CH$_2$-CH$_2$-)[2], 66.8 (≡Si-CH$_2$-CH$_2$-CH$_2$-O-)[3], 169.6 (-C(=O)-)[4], 137.0 (CH$_2$=C-)[5], 125.8 (CH$_2$=C-)[6], 18.4 (CH$_3$-C-)[7], and 50.9 ppm (methanol solvent). Elemental analysis: C (24.59%) and N (0.24%).

5.3.3.3. Immobilization of Active Groups onto the Methacrylate-Functionalized Mesoporous Silica

A sample of 0.5 g of the modified mesoporous silica bearing propylmethacrylate functional groups, OSU-6-W-TMSPMA-2, was added to 50 ml of ethanol containing 5.0 ml of KOH (0.01 *M*) as a catalyst and 2.0 g of the amino acid in a 150 ml Erlenmeyer flask. The reaction mixture was stirred for 48 hours and the resulting solid was filtered

off, washed three times with 50 ml of THF, and dried under vacuum for 24 hours. The

general chemical reaction is illustrated in Scheme 5.3. The IR peaks in cm^{-1} (KBr) for

each immobilized group are listed in Table 5.1.

Table 5.1. The organic compound used and the FT-IR result of the final products.

Organic Compound	FT-IR (cm^{-1}) (KBr)
Lysine	3356, 3291, 2978, 2926, 2844, 1723, 1581, 1514, 1467, 1406, 1382, 1336
β-Alanine	3310, 2944, 2886, 1721, 1562, 1470, 1440, 1376, 1303
Glycine	3316, 2932, 2856, 1727, 1572, 1503, 1463, 1403, 1376, 1327
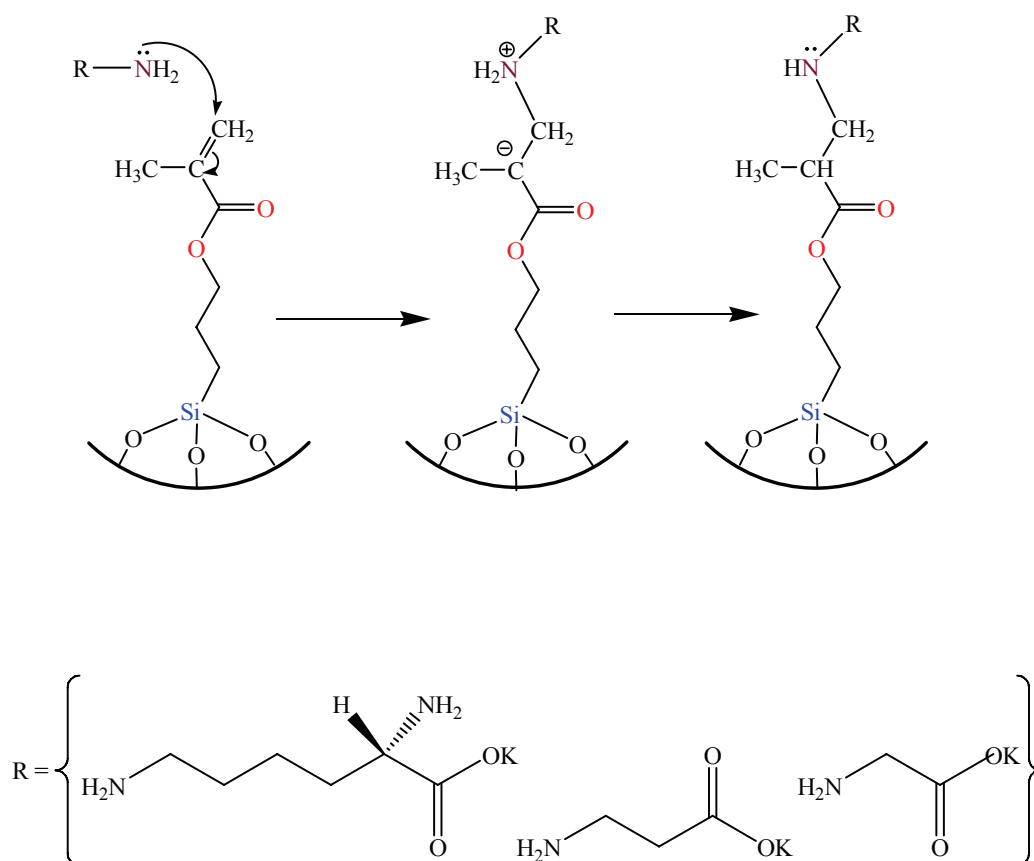
Scheme 5.3. The general chemical reaction of the functionalization process following Michael addition reaction.

5.3.4. Calculating the Total Surface Loading of the Ordered Mesoporous Silica with the Propylmethacrylate Functional Groups

The concentration of the functional groups was determined using several methods, that were discussed in the previous chapters.

I. Spectrophotometric Analysis Method

The amount of propylmethacrylate deposited on the surface was quantified using two variables. The surface loading (l) expresses the amount of deposited molecules in mmol/g. The number of molecules deposited per nm^2 is given by the surface coverage (C). Both values use the mass of the pure mesoporous silica before modification as a reference.[61]

I. A. Bromination Method

For the quantitative analysis of the propylmethacrylate in methylene chloride solution, a spectrophotometric analysis method was used. The determination of propylmethacrylate by means of a color reaction with bromine (Br_2), bromination reaction, Scheme 5.4, in an organic solvent such as methylene chloride is reported for the first time in this work. This reaction was left to for one week in order to ensure completion. In this method, an amount of 0.25 g of each modified sample was dissolved in 10 ml of 0.01 M of Br_2 in CH_2Cl_2. Immediately after the addition of Br_2, the solution was dark red. As time progressed, the color changed very slowly to orange, to yellow, and then to pale yellow.

OSU-6-W-TMSPMA   Brominated OSU-6-W-TMSPMA
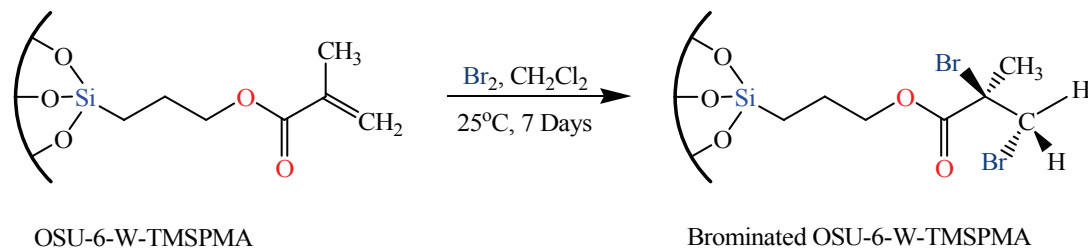
Scheme 5.4. Reaction of propylmethacrylate functional group with bromine.

The correlation between the standard solutions of bromide concentrations and the absorbance at $\lambda = 410$ nm was linear. The total deposited amount (l) was calculated by subtracting the residual amount of bromine in the solution after reaction from the initially added amount. The surface coverage (C) was calculated by dividing the loading (l) by the specific surface area (S_{BET}) of the sample. Multiplication by Avogadro's number (N_A = 6.022 X 10^{23} molecules/mole) yields units of molecules/nm^2:[61]

$$C = (l / S_{BET}) \cdot N_A$$

II. Elemental Analysis (Combustion Analysis)

Carbon analysis was carried out for both modified samples under study. The concentration of attached groups was determined as follows:[62,63]

$$C \text{ (groups/nm}^2) = 6 \times 10^5 \, P_C /[(1200 n_C - W P_C) S_{BET}]$$

where C is the concentration of attached groups, which contain carbon; P_C is the percentage of carbon in the sample, n_C is the number of carbon atoms in the attached group (counted as C_7), W is the formula mass of the modifier (counted as $C_7H_{11}O_5Si$), and S_{BET} is the initial specific surface area of the substrate (1283 m^2/g).

III. Solid State ^{29}Si CP/MAS NMR Spectrum

The solid state ^{29}Si CP/MAS NMR spectrum of the pristine OSU-6-W sample and the two modified samples OSU-6-W-TMSPMA-1 and OSU-6-W-TMSPMA-2 were used to evaluate the degree of silylation as described in chapter three.[64]

The difference in silanol concentration before and after silylation was approximately equal to the concentration of the functional groups.

5.3.5. Metal Ions Adsorption Study

The adsorption and separation experiments were conducted as follows; five different amounts (25-125 mg) of the functionalized mesoporous silica, OSU-6-W-TMSPMA-2-Glycine, was shaken for 4 hours with 10 ml of 100 ppm aqueous UO_2^{2+} in 20-ml glass vials. Measurement of the metal ion concentration was carried out by allowing the insoluble complex to settle, withdrawing a portion of the supernatant, and filtering using a 0.45µm membrane syringe. The metal ion uptake was calculated as mmol of M^{2+}/g of the grafted mesoporous silica. ICP spectroscopy was used to determine the concentration of uranium in the treated solutions.

5.4. RESULTS AND DISCUSSION

5.4.1. Mesoporous OSU-6-W Modified with Methacrylate Groups

OSU-6-W modified with propylmethacrylate functional group was prepared by post-synthesis method using 3-(trimethoxysilyl)propylmethacrylate (TMSPMA) and applying two different grafting procedures.

5.4.1.1. Identification of the Textural Properties (Physical Characterization)

I. X-ray Powder Diffraction (XRD)

The pristine ordered mesoporous material, OSU-6-W, and the functionalized samples with TMSPMA (OSU-6-W-TMSPMA-1 and OSU-6-W-TMSPMA-2) were characterized by XRD. The diffraction patterns are shown in Figure 5.1.
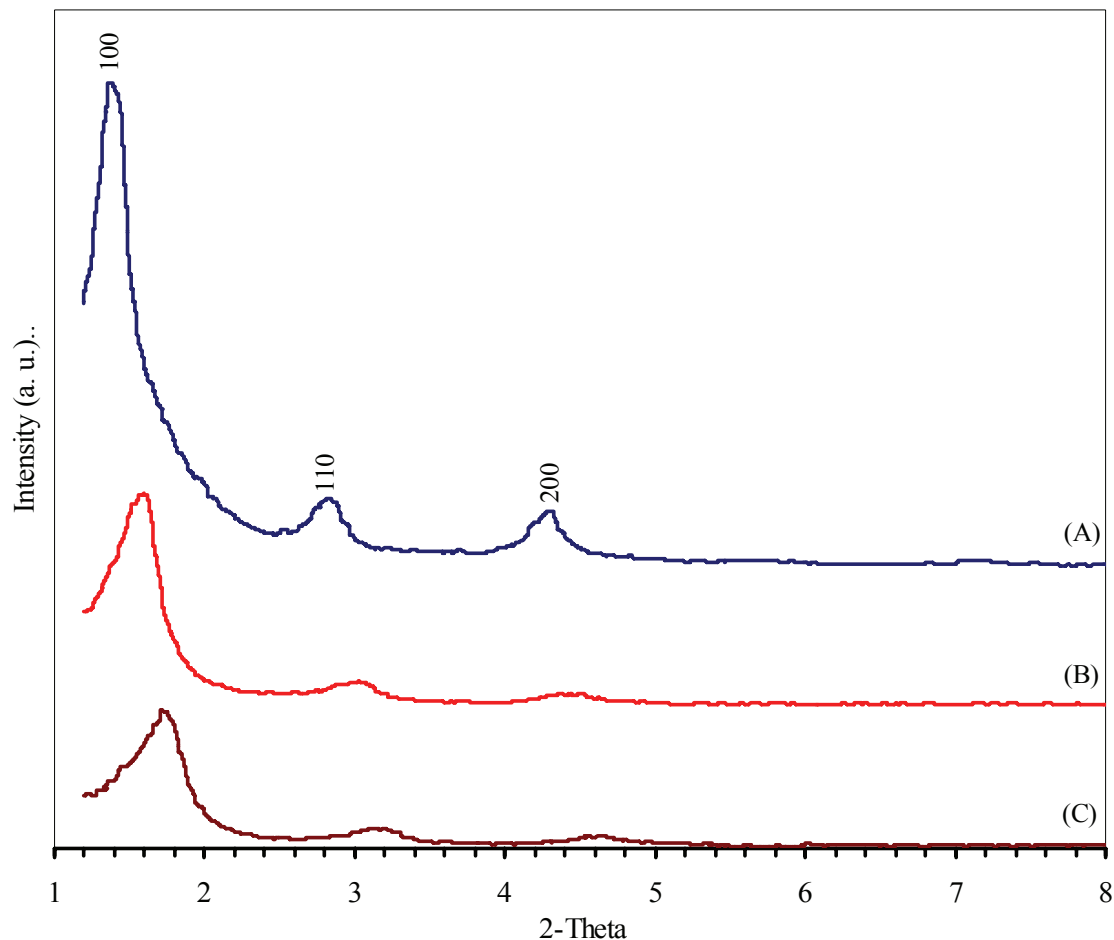
Figure 5.1. XRD patterns in the range of 1.0-10.0º of; (A) pristine ordered mesoporous material, OSU-6-W, (B) OSU-6-W-TMSPMA-1, and (C) OSU-6-W-TMSPMA-2. The spectra are shifted vertically for the sake of clarity.

The XRD patterns of the samples show strong (100) peaks and weaker (110) and (200) peaks. The (100) peak gradually shifts to higher angles with increasing amounts of the functional groups on the surface from OSU-6-W-TMSPMA-1 to OSU-6-W-TMSPMA-2, indicating an effective decrease of the pore diameter. According to the

average pore diameter of the material from the surface area measurements, this indicates an average thickening of the walls of about 25.8 Å in the case of OSU-6-W-TMSPMA-2, which statistically would correspond to an extra layer of Si-O-Si homogeneously spread on the original wall (20.9 Å). It also can be noticed that the d_{100} peak has become broader with higher loading of the functional groups, indicating a slight alteration of the ordering of the mesoporous structure.

II. Nitrogen Adsorption-Desorption Measurements

Figure 5.2 shows the nitrogen adsorption-desorption isotherms for the mesoporous silicas. The textural properties of the materials are summarized in Table 5.2.
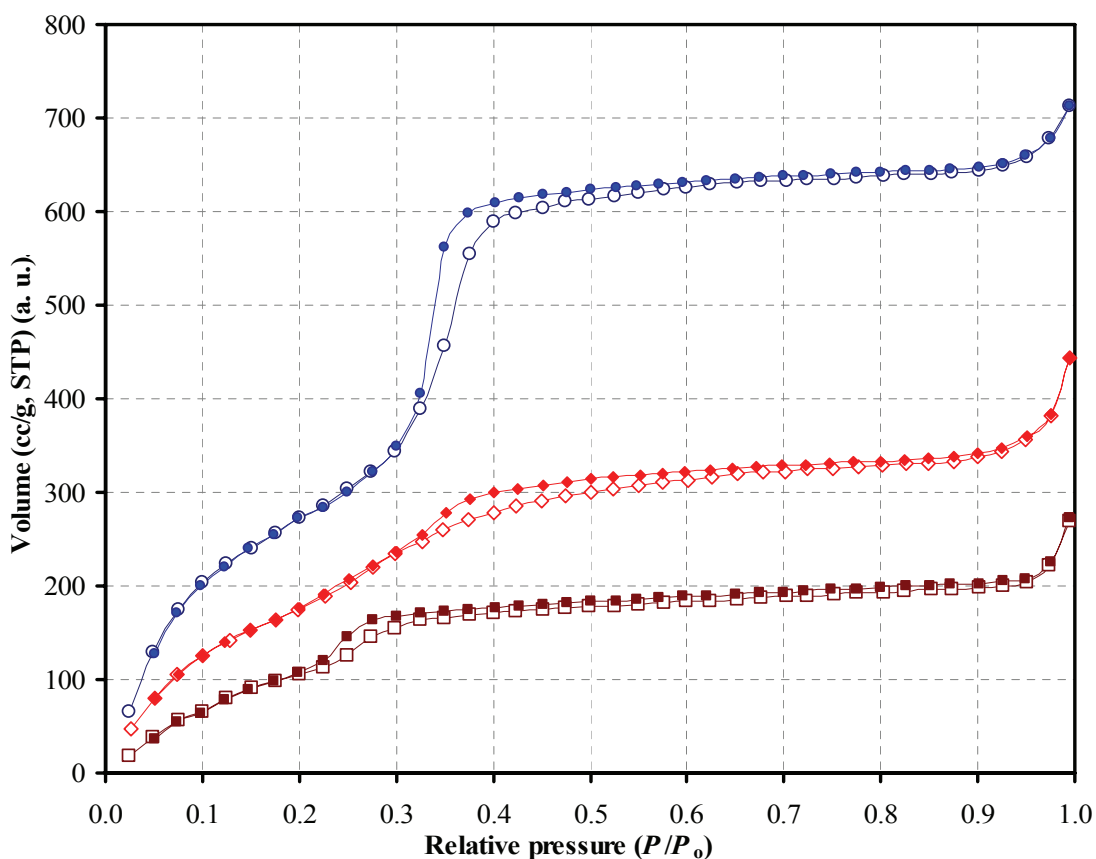
Figure 5.2. Nitrogen adsorption-desorption isotherms of (○) OSU-6-W, (◊) OSU-6-W-TMSPMA-1, and (□) OSU-6-W-TMSPMA-2. Open symbols: adsorption; closed symbols: desorption. The isotherm data are shifted vertically for the sake of clarity.

266

After reaction with the coupling agent, the surface area and pore volume of the mesoporous silicas was reduced from 1283 m^2/g to 956 m^2/g and 1.24 cm^3/g to 0.90 cm^3/g for OSU-6-W-TMSPMA-1 sample, and of 678 m^2/g and 0.61 cm^3/g for OSU-6-W-TMSPMA-2. The point at which the mesopores become fulled by nitrogen adsorption had shifted to lower relative pressures indicating a change in the pore diameter from 51.1 Å in the perant mesoporous silica to 41.2 Å for OSU-6-W-TMSPMA-1 and 34.1 Å for OSU-6-W-TMSPMA-2.

Figure 5.3 shows the pore size distribution of all three samples. It is clear that, the un-functionalized sample has the narrowest pore size distribution among the three samples. The modified samples OSU-6-W-TMSPMA-1 and OSU-6-W-TMSPMA-2 have a pore size distribution of 5.0±1.0 and 6.0±1.0 Å, respectively.
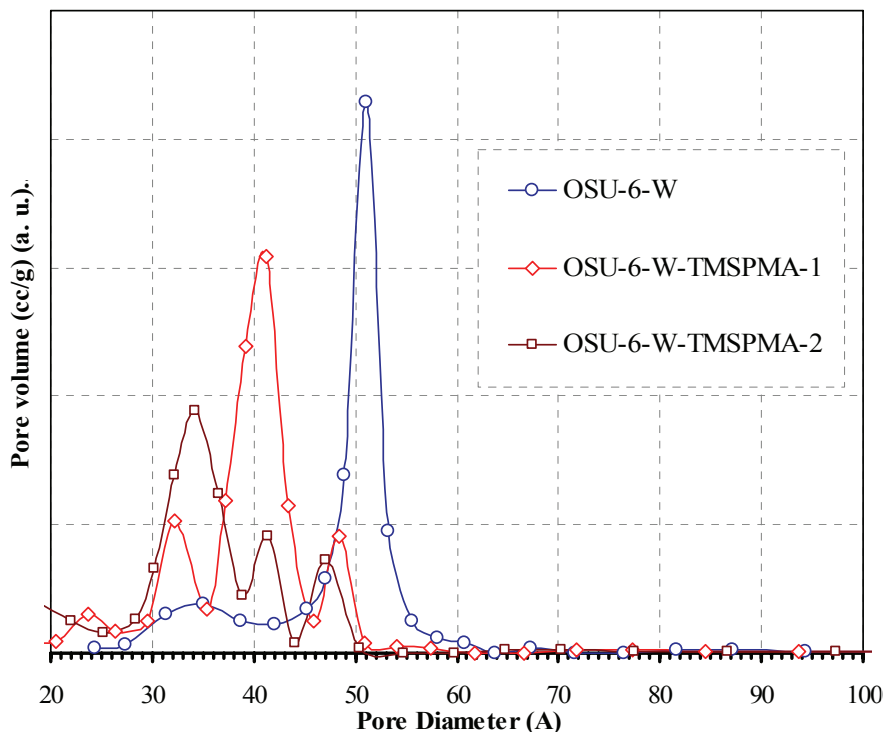
Figure 5.3. Pore size distribution of (○) OSU-6-W (max at 51.1 Å), (◊) OSU-6-W-TMSPMA-1 (max at 41.2 Å), and (□) OSU-6-W-TMSPMA-2 (max at 34.1 Å).

Table 5.2. Textural Properties Determined from Nitrogen Adsorption-desorption Experiments at 77 K and Powder XRD Measurements.

Sample	Specific surface area (m^2/g)	Total pore volume (cm^3/g)	Average pore size (Å)	d_{100} (Å)	Wall Thickness (Å)
OSU-6-W	1283	1.24	51.1	62.4	20.9
OSU-6-W-TMSPMA-1	956	0.90	41.2	56.1	23.6
OSU-6-W-TMSPMA-2	678	0.61	34.1	51.9	25.8

5.4.1.2. Identification of the Functional Groups (Chemical Characterization)

I. Solid State ^{29}Si CP/MAS NMR Spectroscopy

Figure 5.4 shows the ^{29}Si CP/MAS NMR spectra for the unmodified mesoporous silica, OSU-6-W, and the modified samples, OSU-6-W-TMSPMA-1, and OSU-6-W-TMSPMA-2.

The two functionalized samples, Figure 5.4 (B) and (C), show peaks with location at - 91.6, -102.5, -109.8 ppm, and -101.9, -109.7 ppm, corresponding to Q^2, Q^3, and Q^4 silicon environments for OSU-6-W-TMSPMA-1 and OSU-6-W-TMSPMA-2, respectively. These occur in similar locations to the corresponding three peaks of the starting material. In addition, the OSU-6-W-TMSPMA-1 spectrum contains an additional two peaks at -48.0, and -56.8 ppm corresponding to T^1, and T^2 silicon environments, while the OSU-6-W-TMSPMA-2 sample shows another two peaks at - 56.7 (T^2), and -65.5 (T^3). All peaks were identified by multipeak curve fitting.
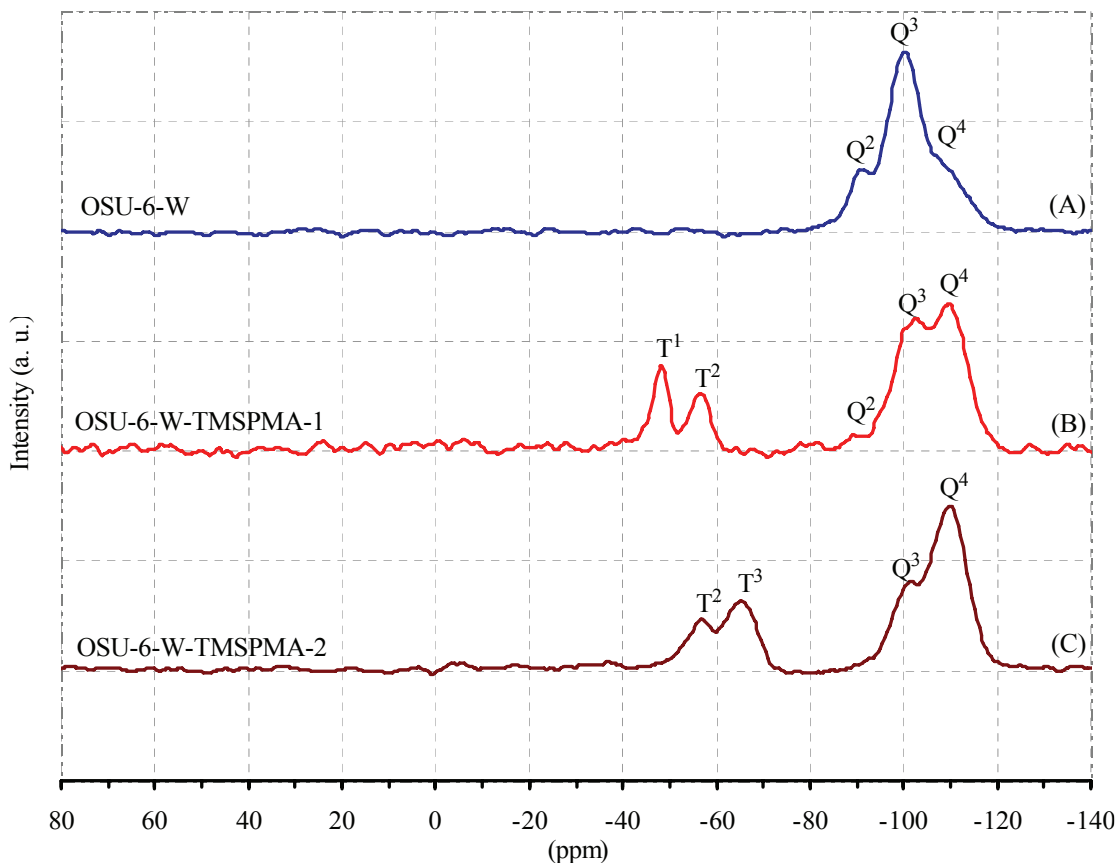
Figure 5.4. Solid state ^{29}Si CP/MAS NMR spectra of; (A) HCl-Ethanol washed mesoporous silica, OSU-6-W, (B) the modified OSU-6-W-TMSPMA-1, and (C) the modified OSU-6-W-TMSPMA-2.

The silylated samples with the propyl methacrylate functional groups, *i.e.,* OSU-6-W-TMSPMA-1 and OSU-6-W-TMSPMA-2, show changes in relative intensities of the Q^n resonances from those of OSU-6-W. In particular, the relative intensity for the Q^3 silicon resonance labeled at around -100 ppm undergoes a significant decrease as the number of functional groups increases while the Q^4 resonance increases in intensity. These changes are due to reaction of surface Si-OH groups with TMSPMA leading to the formation of more Si-O-Si bonds. The formation of a more uniform functionalized layer

in OSU-6-W-TMSPMA-2 as compared to OSU-6-W-TMSPMA-1 is reflected by an increases the peak intensity at around -65.5 ppm (T^3), a decrease in the peak at around -56.7 ppm (T^2), and disappearance of the peak at around -48 ppm (T^1).

The surface coverage of the functionalized monolayer of mesoporous OSU-6-W was greater in OSU-6-W-TMSPMA-2 sample than in OSU-6-W-TMSPMA-1 sample. This is basically due to the presence of the peak at T^3 in (C) which means more packing functional groups, also disappearance of the peak that arises from isolated SiO_3 groups. Solid state ^{29}Si NMR revealed a high degree of silane cross-linking and a surface population of 3.19 groups/nm^2, indicative of a good monolayer structure in the OSU-6-W-TMSPMA-2.

II. Solid State ^{13}C CP/MAS NMR Spectroscopy

The presence of covalently linked organic moieties bearing propylmethacrylate groups in the functionalized OSU-6-W mesoporous silicas was confirmed by ^{13}C CP/MAS solid-state NMR spectroscopy.[65,67] The spectra for propylmethacrylate-functionalized mesoporous materials, OSU-6-W-TMSPMA-1 and OSU-6-W-TMSPMA-2, showed resonances at δ (ppm) values of 8.9 ($\equiv$Si-CH_2-), 22.5 ($\equiv$Si-CH$_2$-CH_2-), 66.7 ($\equiv$Si-CH$_2$-CH$_2$-CH_2-O-), 168.3 (-C(=O)-), 137.3 (CH_2=C-), 124.1 (CH_2=C-), and 18.2 (CH_3-C-), and δ (ppm) of 9.0 ($\equiv$Si-CH_2-), 22.6 ($\equiv$Si-CH$_2$-CH_2-), 66.8 ($\equiv$Si-CH$_2$-CH$_2$-CH_2-O-), 169.6 (-C(=O)-), 137.0 (CH_2=C-), 125.8 (CH_2=C-), and 18.4 (CH_3-C-), respectively, Figure 5.5. Peaks corresponding to the organosiloxane moieties are relatively broad, indicating restricted mobility of the functional groups attached to the siloxane framework. The lower intensity of the peaks in OSU-6-W-TMSPMA-1 sample

compared to that in OSU-6-W-TMSPMA-2 indicate the low coverage, as can be seen in Figure 5.5.
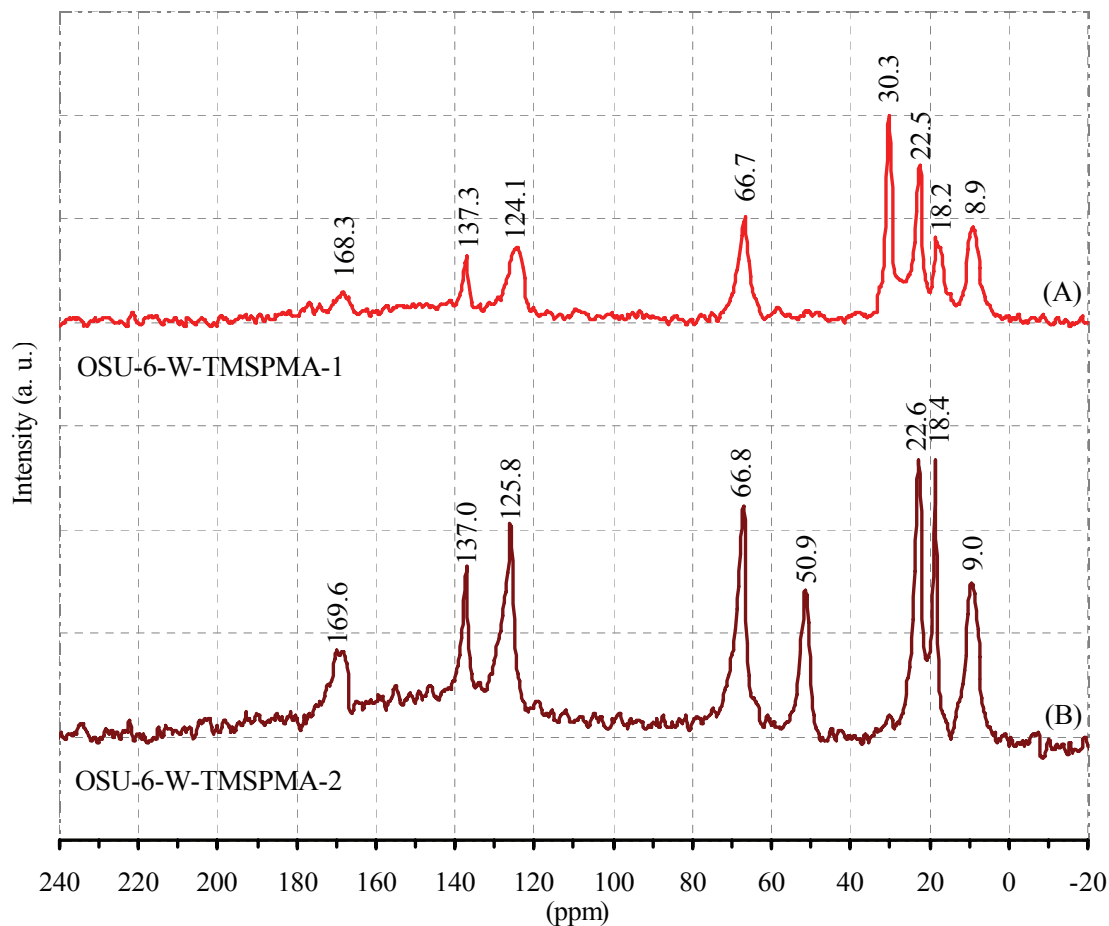
Figure 5.5. Solid state ^{13}C CP/MAS NMR spectra of the modified samples with propylmethacrylate functional groups, (A) OSU-6-W-TMSPMA-1, and (B) OSU-6-W-TMSPMA-2.

III. Fourier Transform Infrared Spectroscopy (FT-IR)

The vibrational spectra (Figure 5.6) confirmed the success of the grafting reactions. The observed spectra are very close to those reported, when propylmethacrylate was previously incorporated into similar materials.[65,67]
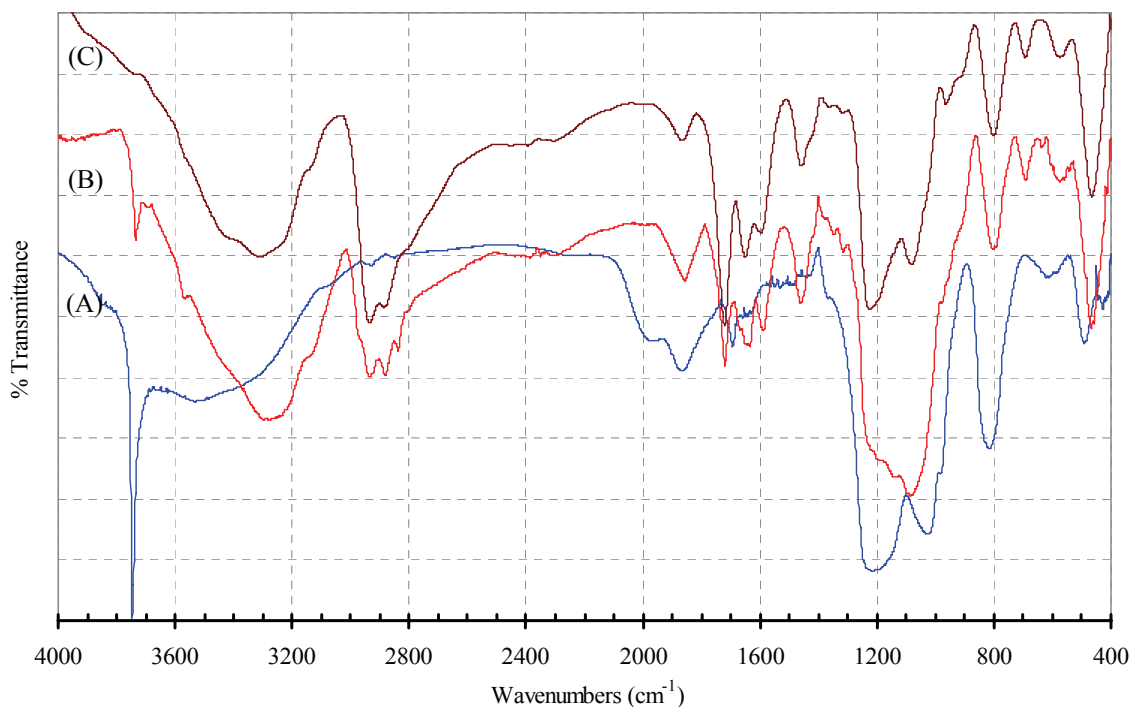
Figure 5.6. Infrared spectra of (curve A) OSU-6-W, (curve B) OSU-6-W-TMSPMA-1, and (curve C) OSU-6-W-TMSPMA-2.

The two modified silicas, OSU-6-W-TMSPMA-1 and OSU-6-W-TMSPMA-2 were characterized by infrared spectroscopy and compared to the corresponding unmodified solid materials, OSU-6-W. In such conditions all spectra showed a large band around 3000–3600 cm^{-1} most probably due to adsorbed water. The efficiency of the grafting process is demonstrated by a significant decrease in the silanol bands at around 3740 cm^{-1}, with an associated increase of new bands characteristics of the immobilized propylmethacrylate groups. These bands were attributed to both the symmetric and asymmetric stretching of active groups in OSU-6-W-TMSPMA-1; $v_{as}(CH_2) = 2944$ cm^{-1}, $v_s(CH_2) = 2891$ cm^{-1}, CH$_2$ scissor at 1454 cm^{-1}, $v_{as}(CH_3) = 2981$ cm^{-1}, $v_s(CH_3) = 2848$ cm^{-}1, CH$_3$ bending vibration at 1331 cm^{-1}, C=O stretching at 1719 cm^{-1}, and C=C vibration mode at 1634 cm^{-1}, in OSU-6-W-TMSPMA-2; $v_{as}(CH_2) = 2955$ cm^{-1}, $v_s(CH_2) =$

2892 cm^{-1}, CH$_2$ scissor at 1453 cm^{-1}, C=O stretching at 1720 cm^{-1}, and C=C vibration mode at 1640 cm^{-1}. When comparing the intensities of the IR peaks in the modified samples, we concluded that the second sample has a higher concentration of functional groups than the first modified sample which has been confirmed by the solid state ^{29}Si and ^{13}C NMR and elemental analysis. Silica fundamental bands were observed at ~ 1200 and ~ 1180 cm^{-1} (Si-O-Si stretch), ~ 800 cm^{-1} (Si-O-Si), and ~ 470 cm^{-1} (O-Si-O).[73,74] The presence of the CH$_3$ bending mode in the IR spectra of OSU-6-W-TMSPMA-1 suggests a small amount of remaining -OCH$_3$. 1347 and 1314 cm^{-1} were observed in the spectrum after grafting, which are attributed to CH$_3$ bending, and CH$_3$ bending vibrations, respectively.[75]

5.4.2. Characterization the Mesoporous Silicas Immobilized with Amino Acids

I. FT-IR Spectroscopy

The FT-IR spectra of all the amino acid containing samples confirm the success of the immobilization of the amino acid compound into the methacrylate-functionalized OSU-6-W material. In the FT-IR spectra of the immobilized lysine compound, the peak at 1723 confirms the presence of the C=O of the carboxylic acid. The peaks at 3356 and 3291 cm^{-1} correlate to the primary amine of the immobilized lysine. Other peaks at 1581 and 1467 cm^{-1} are related to the NH$_2$ bending vibration. The *β*-alanine immobilized ligand shows peaks at 3310, 1721, 1562, and 1470 cm-1 due to the secondary amine (N-H) vibration, C=O vibration and the NH bending vibration, respectively. The glycine immobilized ligand shows peaks at 3316, 1727, 1572, 1503, 1463 cm^{-1} that are associated with the secondary amine (N-H) vibration, C=O vibration and the NH bending vibration,

respectively. Moreover, in all immobilized samples the peak due to the C=C at 1640 disappears.[76]

II. Surface Area Analysis

The surface areas of all immobilized samples dropped significantly from 678 m^2/g to 244, 267, and 279 m^2/g for the immobilized lysine, β-alanine, and glycine, respectively. These results provide more evidence for the success of immobilization.

5.4.3. The Total Surface Loading of the Ordered Mesoporous Silica with the Propylmethacrylate Functional Groups

The concentration of the functional groups on the surface was determined. Table 5.3 shows the total coverage using three different determination methods. The results show high coverage when using a second grafting procedures with a hydrolysis step iintermediate. There are small differences in the results between all three methods that may be due to miscalculation in case of the spectrophotometric method, noise in case of the ^{29}Si NMR or impurities in case of elemental analysis. These results confirm the validation of the grafting procedure suggested here in this work to be good in increasing the total coverage.

Table 5.3. Total coverage from three different determination methods.

Sample	Surface Area (BET)	Spectrophotometric Analysis (SA) (mmol/g)	Elemental Analysis (EA)		^{29}Si NMR			Total Coverage (molecule/nm^2)		
			C %	N %	Q^2 (%)	Q^3 (%)	Q^4 (%)	SA	EA	NMR
OSU-6-W	1283	----	0.10	0.06	13.89	71.73	14.38	----	----	----
OSU-6-W-TMSPMA-1	956	3.68	19.14	0.18	3.73	44.55	51.72	2.32	1.98	1.71
OSU-6-W-TMSPMA-2	678	3.95	24.59	0.24	0.00	28.98	71.02	3.51	3.38	3.19

The OSU-6-W-TMSPMA-1 has an average coverage of 2.00 TMSPMA molecules per 100 Å^2, while the OSU-6-W-TMSPMA-2 sample has an average coverage of 3.36 TMSPMA molecules per 100 Å^2.

The slow reaction (seven days) compared to solution bromination of unsaturated organic compounds (hours) implies that the propylmethacrylate functional groups are mostly located on internal surfaces of the bulk sample, *i.e.,* within the mesopore channels.

5.4.4. Metal Ions Adsorption Study

I. Adsorption of Radioactive Metal Ions (UO_2^{2+})

The adsorption capacity of the modified mesoporous silicas, OSU-6-W-TMSPMA-2-Glycine, toward radioactive metal ions was examined using five different amounts of adsorbent (ranging from 25 to 125 mg) and a 100 ppm solution of the UO_2^{2+} ions at pH 5.5. The results are shown in Figure 5.7.
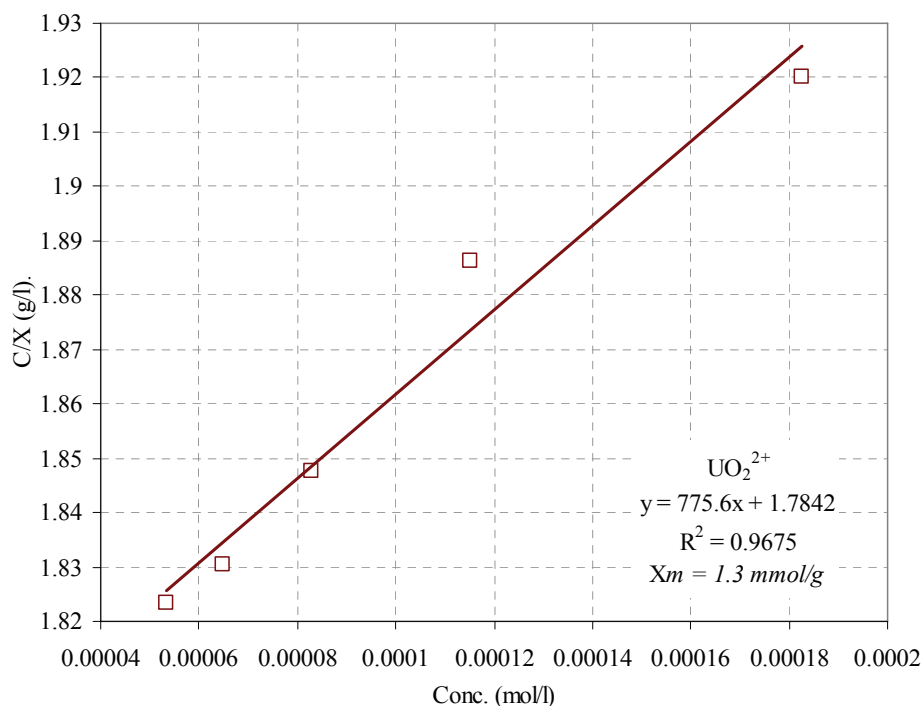
Figure 5.7. The Langmuir adsorption isotherm of UO_2^{2+} ions adsorbed by OSU-6-W-TMSPMA-2-Glycine absorbent

276

The maximum uptakes calculated from the Langmuir adsorption was 1.3 mmol UO_2^{2+}/g (or 307 mg/g) of the adsorbent. Assuming complet reaction of all methacrylate groups with glycine, the number of glycine groups is approxmatly 2.2 mmol/g. Thus, the results indicate the formation of approxmatly 3 UO_2^{2+} : 5 glycine complexes.

When comparing the uptake capacity of UO_2^{2+} by OSU-6-W-TMSPMA-2-glycine with that of OSU-6-W-TMSPEDA-2, the difference could be due to the high surface area of the latter and it may due to a low immobilization of the glycine groups. However, this result is outstanding and encouraging for more investigations in improvement of the immobilization process and the use of different active groups.

II. Regeneration of the Absorbent

Treatment of the uranium-loaded material by stiring three times with 2.0 M HCl for one hour resulted in the removal of the bound UO_2^{2+} from the structure and regeneration of the adsorbent for further metal ion uptake. The regenerated material, Figure 5.8, shows a decrease in the uranium ion uptake capacity down to ~ 55% after the fourth regeneration.

The decreases might be due to loss of the immobilized groups with washing or a strong interaction of the UO_2^{2+} ions with the carboxylic groups so that it is not released with HCl washing. The latter will lead to plugging of the available sites for chelating acids. Overall, this material shows relatively good regeneration.
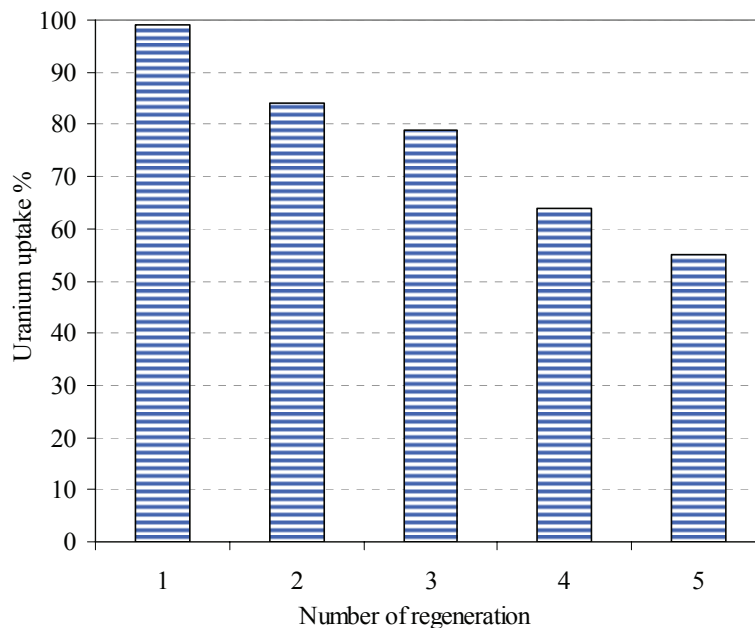
Figure 5.8. The regeneration experiments of UO_2^{2+} ions adsorbed by OSU-6-W-TMSPMA-2-Glycine adsorbent.

5.5. CONCLUSION

In this chapter, the synthesis and characterization of propylmethacrylate-functionalized mesoporous silica, OSU-6-W-TMSPMA-(1&2), prepared *via* post-synthesis grafting method using organoalkoxysilanes containing propylmethacrylate group was reported.

A significantly large coverage of functional groups (~ 3.36 group/nm^2) was realized. This high coverage can not be achieved without the aid of the amine catalyst and a two step silylation process with intermediate hydrolysis treatment.

In the first grafting procedure, the triethylamine along with the high hydroxyl (silanol) group concentration, high surface area, and large pore size worked very well in attaching a relatively high number of functional groups inside the pores and on the

surface. However, some of the silanol groups on the silica surface were still free and some of the methoxy groups from the attached groups were not hydrolyzed. Therefore, the use of a second silylation step was definitely required in order to increase the total coverage. Before this silylation step, a hydrolysis step with water is required in order to hydrolyze the methoxy groups left after the first silylation step. The hydrolysis step increases the amount of hydroxyl groups and facilitates the second condensation.

This investigation showed that immobilized amino acids are all capable of metal capacities in the range of mmole/g of adsorbant. In addition, metal selectivity and specificity could be achieved by altering the amino acid functionalities. There are still many directions that continuing research in this area could head, including the use of peptide libraries and more extensive metal-uptake studies.

5.6. REFRENCES

1. U. Forstner and G. T. W. Wittmann. *Metal Pollution in the Aquatic Environment*, Springer-Verlag, New York (1981).

2. M. P. Ireland. *Biological Monitoring of Heavy Metals*, Wiley, New York (1991).

3. J. P. Vernet. *Impact of Heavy Metals on the Environment*, Elsevier, New York (1992).

4. L. Friber, G. F. Nordberg, B. Vouk (Eds.). *Handbook on the Toxicology of Metals*, Elsevier, North-Holland, Biomedical Press, Amsterdam (1979).

5. Malachowski, L.; Stair, J. L.; Holcombe, J. A.. Immobilized peptides/amino acids on solid supports for metal remediation *Pure Appl. Chem.* 2004, 76(4), 777–787.

6. Vrancken, K. C.; Possemiers, K.; Van Der Voort, P.; Vansant, E. F. Surface modification of silica gels with aminoorganosilanes. *Colloids and Surfaces, A: Physicochemical and Engineering Aspects* **1995,** *98*(3), 235-241.

7. Vrancken, K. C.; Van der Voort, P.; Gillis-D'Hamers, I.; Vansant, E. F.; Grobet, P.. Influence of water in the reaction of γ-aminopropyltriethoxysilane with silica gel: a Fourier-transform infrared and cross-polarization magic-angle-spinning nuclear magnetic resonance study. *J. Chem. Soc., Faraday Trans.* **1992,** *88*(21), 3197-3200.

8. Kallury, K. M. R.; Macdonald, P. M.; Thompson, M.. Effect of Surface Water and Base Catalysis on the Silanization of Silica by (Aminopropyl)alkoxysilanes Studied by X-ray Photoelectron Spectroscopy and ^{13}C Cross-Polarization/Magic Angle Spinning Nuclear Magnetic Resonance. *Langmuir* **1994,** *10*(2), 492-499.

9. Blitz, J. P.; Murthy, R. S.; Leyden, D. E. Ammonia-catalyzed silylation reactions of Cab-O-Sil with methoxymethylsilanes. *J. Am. Chem. Soc.* **1987,** *109*(23), 7141-7145.

10. Ding, J.; Hudalla, C. J.; Cook, J. T.; Walsh, D. P.; Boissel, C. E.; Iraneta, P. C.; O'Gara, J. E. Synthesis and surface chemistry of spherical mesoporous organic-inorganic hybrid particles with an integrated alcohol functionality on the pore surface. *Chem. Mater.* **2004,** *16*(4), 670-681.

11. Brunel, D. Functionalized Micelle-templated Silicas (MTS) and their use as Catalysts for Fine Chemicals *Microporous Mesoporous Mater.* **1999,** *27*(2-3), 329-344.

12. Brunel, D.; Cauvel, A.; Fajula, F.; DiRenzo, F.. MCM-41 type silicas as supports for immobilized catalysts. *Stud. Surf. Sci. Catal.* **1995,** *97*, 173-180.

13. Corma, A.. From Microporous to Mesoporous Molecular Sieve Materials and Their Use in Catalysis. *Chem. Rev.* **1997,** *97*(6), 2373-2419.

14. Lim, M. H.; Stein, A.. Comparative Studies of Grafting and Direct Syntheses of Inorganic-Organic Hybrid Mesoporous Materials. *Chem. Mater.* **1999,** *11*(11), 3285-3295.

15. Price, P. M.; Clark, J. H.; Macquarrie, D. J.. Modified Silicas for Clean Technology. *Dalton* **2000,** *2,* 101-110.

16. Clark, J. H.; Macquarrie, D. J.; Wilson, K.. Functionalised Mesoporous Materials for Green Chemistry. *Stud. Surf. Sci. Catal.* **2000,** *129,* 251-264.

17. Cooper, C.; Burch, R. Mesoporous Materials for Water Treatment Processes *Water Res.* **1999,** *33*(18), 3689-3694.

18. Singh, R.; Khwaja, A. R.; Gupta, B.; Tandon, S. N.. Uptake and Extraction Chromatographic Separation of Mercury(II) by Triisobutylphosphine Sulfide (TIBPS) Sorbed on Silica Gel and Decontamination of Mercury Containing Effluent. *Talanta* **1999**, *48*(3), 527-535.

19. Kham, K.; Deratani, A.; Sebille, B. Kinetics of copper(II) ion fixation on modified silicas bearing some organic complexant functions *New J. Chem.* **1987**, *11*(10), 709-714.

20. Bresson, C.; Menu, M.-J.; Dartiguenave, M.; Dartiguenave, Y. Triethoxysilyl-substituted aminoethanethiol ligands for zinc and cadmium complexes and aminoethanethiol-modified silica gel. Evaluation of the corresponding supported molecular trap for metallic pollutant uptake (Cd^{2+}, Hg^{2+} and Pb^{2+}). *J. Environ. Monit.* **2000**, *2*(3), 240-247.

21. Dai, S.; Burleigh, M. C.; Shin, Y.; Morrow, C. C.; Barnes, C. E.; Xue, Z.. Imprint Coating: A Novel Synthesis of Selective Functionalized Ordered Mesoporous Sorbents *Angew. Chem., Int. Ed. Engl.* **1999**, *38*(9), 1235-1239.

22. Im, H.-J.; Yang, Y.; Allain, L.; Barnes, C.; Dai, S.; Xue, Z. Funtionalized Sol-Gels for Selective Copper(II) Separation *Environ. Sci. Technol.* **2000,** *34*(11), 2209-2214.

23. Dias Filho, N. L.. Adsorption of Copper(II) and Cobalt(II) Complexes on a Silica Gel Surface Chemically Modified with 3-Amino-1,2,4-triazole. *Colloids and Surfaces, A: Physicochemical and Engineering Aspects* **1998,** *144*(1-3), 219-227.

24. Mahmoud, M. E. Selective solid phase extraction of mercury(II) by silica gel-immobilized-dithiocarbamate derivatives *Anal. Chim. Acta* **1999**, *398*(2-3), 297-304.

25. Broudic, J.-C.; Conocar, O.; Moreau, J. J. E.; Meyer, D.; Wong Chi Man, M. New hybrid silica based materials for the solid–liquid extraction of actinides *J. Mater. Chem.* **1999**, *9*(10), 2283-2285.

26. Liu, A. M.; Hidajat, K.; Kawi, S.; Zhao, D. Y. A new class of hybrid mesoporous materials with functionalized organic monolayers for selective adsorption of heavy metal ions *Chem. Commun.* **2000**, 1145-1146.

27. Moller, K.; Bein, T. Inclusion Chemistry in Periodic Mesoporous Hosts. *Chem. Mater.* **1998**, *10*(10), 2950-2963.

28. Lim, M. H.; Blanford, C. F.; Stein, A. Synthesis of Ordered Microporous Silicates with Organosulfur Surface Groups and Their Applications as Solid Acid Catalysts *Chem. Mater.* **1998,** *10*(2), 467- 470.

29. Collinson, M. M. Analytical applications of organically modified silicates *Mikrochim. Acta* **1998**, *129*(3-4), 149-165.

30. Antochshuk, V.; Jaroniec, M.. 1-Allyl-3-propylthiourea Modified Mesoporous Silica for Mercury Removal *Chem. Commun.*, **2002,** *3,* 258–259.

31. Zemanian, T. S.; Fryxell, G. E.; Liu, J.; Mattigod, S.; Franz, J. A.; Nie, Z.. Deposition of Self-Assembled Monolayers in Mesoporous Silica from Supercritical Fluids. *Langmuir*, **2001,** *17*(26), 8172-8177.

32. Kruk, K.; Asefa, T.; Jaroniec, M.; Ozin, G. A.. Metamorphosis of Ordered Mesopores to Micropores: Periodic Silica with Unprecedented Loading of Pendant Reactive Organic Groups Transforms to Periodic Microporous Silica with Tailorable Pore Size. *J. Am. Chem. Soc.* **2002,** *124*(22), 6383-6392.

33. Mori, Y.; Pinnavaia, T. J.. Optimizing Organic Functionality in Mesostructured Silica: Direct Assembly of Mercaptopropyl Groups in Wormhole Framework Structures, *Chem. Mater.* **2001,** *13*(6), 2173-2178.

34. Díaz, J. F.; Balkus, K. J.; Bediouui, F.; Kurshev, V.; Kevan, L.. Synthesis and Characterization of Cobalt-Complex Functionalized MCM-41, *Chem. Mater.* **1997,** *9*(1), 61-67.

35. Fryxell, G. E.; Lin, Y.; Wu, H.; Kemner, K. M.. Environmental Applications of Self-Assembled Monolayers on Mesoporous Supports (SAMMS). *Stud. Surf. Sci. Catal.* **2002,** *141,* 583-590.

36. Bourlinos, A. B.; Karakostas, T.; Petridis, D.. "Side Chain" Modification of MCM-41 Silica through the Exchange of the Surfactant Template with Charged Functionalized Organosiloxanes: An Efficient Route to Valuable Reconstructed MCM-41 Derivatives, *J. Phys. Chem. B*, **2003,** *107*(4), 920-925.

37. Muñoz, A.; Rámila, A.; Pérez-Pariente, J.; Díaz, I.; Vallet-Regí, M.. MCM-41 Organic Modification as Drug Delivery Rate Regulator, *Chem. Mater.* **2003,** *15*(2), 500-503.

38. L. H. Chen and C. S. Chung. *Inorg. Chem.* **27**, 1880 (1988).

39. S. J. Franklin and K. N. Raymond. *Inorg. Chem.* **33**, 5794 (1994).

40. Z. Hou, C. J. Sunderland, T. Nishio, K. N. Raymond. *J. Am. Chem. Soc*. **118**, 5148 (1996).

41. Z. Hou, K. N. Raymond, B. O'Sullivan, T. W. Esker, T. Nishio. *Inorg. Chem.* **37**, 6630 (1998).

42. K. N. Raymond, T. M. Garrett, P. W. Miller. U.S. Patent No. 5049280 (Sept. 1991).

43. M. J. Stillman, C. F. Shaw, K. T. Suzuki (Eds.). *Metallothioneins, Synthesis, Structure and Properties of Metallothioneins, Phytochelatins and Metal-Thiolate Complexes*, VCH, New York (1992).

44. H. Sigel and A. Sigel. *Metal Ions in Biological Systems*, Marcel Dekker, New York (1989).

45. K. T. Suzuki, N. Imura, M. Kimura. *Metallothionein III: Biological Roles and Medical Implications*, Birkhauser Verlag, Boston (1993).

46. P. M. Harrison. *Metalloproteins*, Verlag Chemie, Weinheim (1985).

47. B. Anderson. *Evaluation of Immobilized Metallothionein for Trace Metal Separation and Preconcentration*, The University of Texas at Austin, Austin (1994).

48. Carey, F. A. *Organic Chemistry*, Fifth Edition, McGraw-Hill, 2003, p 777-790.

49. Vrancken, K. C.; Van Der Voort, P.; Possemiers, K.; Vansant, E. F. Surface and Structural Properties of Silica Gel in the Modification with γ-Aminopropyltriethoxysilane. *J. Colloid and Interface Sci.* **1995,** *174*(1), 86-91.

50. Sander, L. C.; Wise, S. A. Recent advances in bonded phases for liquid chromatography. *Crit. Rev. Anal. Chem.* **1987,** *18*(4), 299-415.

51. K.K. Unger, Packings and Stationary Phases in Chromatographic Techniques, Marcel Dekker, Moscow (1990).

52. Wouters, B. H.; Chen, T.; Dewilde, M.; Grobet, P. J.. Reactivity of the surface hydroxyl groups of MCM-41 towards silylation with trimethylchlorosilane. Micropor. Mesopor. Mater. 2001, 44-45, 453-457.

53. Nishiyama, N.; Horie, K.; Asakura, T.. Hydrolysis and condensation mechanisms of a silane coupling agent studied by carbon-13 and silicon-29 NMR. *J. Appl. Poly. Sci.* **1987,** *34*(4), 1619-1630.

54. Ding, J.; Hudalla, C. J.; Cook, J. T.; Walsh, D. P.; Boissel, C. E.; Iraneta, P. C.; O'Gara, J. E. Synthesis and surface chemistry of spherical mesoporous organic-inorganic hybrid particles with an integrated alcohol functionality on the pore surface. *Chem. Mater.* **2004,** *16*(4), 670-681.

55. Zhao, X. S.; G. Q. Lu, A. K. Whittaker, G. J. Millar, and H. Y. Zhu Comprehensive Study of Surface Chemistry of MCM-41 Using 29Si CP/MAS NMR, FTIR, Pyridine-TPD, and TGA J. Phys. Chem. B; 1997, *101*(33), 6525-6531.

56. Jentys, A.; Pham, N. H.; Vinek, H. Nature of hydroxy groups in MCM-41. *J. Chem. Soc., Faraday Trans.* 1996, 92(17), 3287-3291.

57. Yoshitake, H.; Yokoi, T.; Tatsumi, T. Adsorption of Chromate and Arsenate by Amino-Functionalized MCM-41 and SBA-1. *Chem. Mater.* **2002,** *14*(11), 4603-4610.

58. Socrates, G.. *Infrared Characteristic Group Frequencies: Tables and Charts,* second ed., Wiley, Chichester (1994).

CHAPTER
SIX

SYNTHESIS OF MESOPOROUS MATERIALS BEARING VINYL

FUNCTIONAL GROUPS AND CARBOXYL DERIVATIVE

6.1. INTRODUCTION

6.1.1. Fabrication of the Mesoporous Silica Surface with a Vinyl Functional Group

Various methods of functionalizing the surfaces of periodic mesoporous materials with organic groups have been investigated in recent years because surface modification permits tailoring of the surface properties for numerous potential applications including catalysis, ion exchange, encapsulation of transition-metal complexes or semiconductor clusters, chemical sensing, and nano-material fabrication.[1-7] As a support for organic functional groups, hexagonally ordered MCM-41[8,9] is particularly interesting due to its high surface area and uniform pore size distribution in the mesopore size range. Hybrid mesoporous sieves take advantage of the properties of the inorganic support, as well as of the organic surface groups. The polymeric silica framework of MCM-41 provides structural order, as well as thermal and mechanical stability, whereas organic species incorporated into the inorganic phases permit versatile control of interfacial and bulk materials characteristics, such as porosity, hydrophobicity, and optical, electrical, or magnetic properties.

Organic functionalization of the internal surface of a mesoporous silica host can be achieved either by covalently grafting various organic species onto the channel walls[4,9-13] or by incorporating functionalities directly during the preparation.[1-3,14-16] The first approach, a post-synthesis grafting process, has been widely employed to anchor specific organic groups onto surface silanols of diverse silica supports. Typically, organochlorosilanes or organoalkoxysilanes are used as precursors for the surface modification. In this method, the host materials should be dried carefully prior to adding precursors to avoid self-condensation of precursors in the presence of H_2O. Control over the concentration and distribution of organic moieties in MCM-41 by the post-synthesis grafting process is constrained by the number of surface silanol groups and by their accessibility. The grafting rates depend on the reactivity of precursors, diffusion limitations, and steric factors.

This chapter reports the structural, chemical, and physical properties of vinyl-modified OSU-6-W samples prepared by using the post-synthesis grafting process. The major features of this study are comparisons of products from two different synthetic methods with respect to efficiencies of the synthetic routes, precursor effects, vinyl group concentrations, the locations of vinyl groups in the mesoporous products, the hydrothermal stability of vinyl-functionalized samples, and qualitative observations of solvent absorption properties.

Unlike the case of amino silanes, the siloxane bond formation requires an initial hydrolysis of the methoxy or ethoxy groups or the addition of an amine to the reaction mixture.[17] Pure vinyl-modified silica gel has been used as a stationary phase in liquid and gas chromatography. The vinyl functional group serves as a reactive site on the silica

surface for biding of other molecules. That can, inturn, import new interaction capacities to the surface. All these applications explain the wide interest in the chemistry of vinyl-modified silica.

Functionalized mesoporous silica with a high density of vinyl groups and well-defined mesochannels that can enhance the accessibilities of molecules is required to achieve high production when applied as a catalyst and to reach high capacity and selectivity when applied as an adsorbent for harmful heavy metal cations, which cause environmental problems.

The syntheses of vinyl-functionalized mesoporous silicas prepared *via* direct co-condensation and post-synthesis grafting methods have been numerously demonstrated.[1,18] The unique feature in this investigation is the use of a thick-wall mesoporous material, OSU-6-W, with large pores and surface area, high silanol concentration, and superior thermal, hydrolytic and chemical stability than previously use MCM-41 materials for vinyl grafting.

6.1.2. Converting of Vinyl Groups on the OSU-6-W-VTMS to Carboxylic Groups

A large number of vinyl groups with high reactivity enables a variety of chemical modification by providing sites for immobilizing other ligands with high affinity for specific metal ions onto silica matrices by chemical modification. Such modification is expected to further improve the adsorption characteristics of the mesoporous materials.

Carboxylate groups have significant potential for the separation and removal of heavy and transition metal ions and radionuclides. To our knowledge no one has tried to convert vinyl groups directly attached to the silica surface to carboxyl groups. Sagiv *et al.,*[19] generated carboxylic acid groups from vinyl-terminated monolayers. Wasserman *et*

al.,[20] developed the oxidation procedure reported by Sagiv *et al.,*[19] in order to increase the performance and converting percentage. They converted 16-heptadecenyltrichlorosilane $(Cl_3Si(CH_2)_{15}CH=CH_2)$ attached to silicon-silicon dioxide (Si/SiO_2) substrates to a carboxylic acid by $KMnO_4$ and $NaIO_4$. As expected, the surface became more hydrophilic as vinyl groups were converted to carboxylic acid moieties.

In addition to the syntheses and characterizations of vinyl-functionalized mesoporous silica, OSU-6-W-VTMS-(1&2), we intend to convert the vinyl group to carboxylic groups in the vinyl-functionalized OSU-6-W materials. Moreover, other subjects such as bromination, kinetic, adsorption and group affinity to some solvents will be studied.

6.2. EXPERIMENTAL

6.2.1. Materials

Analytical grade chemicals from the following suppliers were used as purchased for all sample preparations: Vinyltrimethoxysilane $[((CH_3O)_3SiCH=CH_2)$ 98.0%, Aldrich], toluene 99.8% HPLC grade, ethyl alcohol, triethylamine (TEA, 99%, Aldrich), potassium permanganate $(KMnO_4)$, sodium metaperiodate $(NaIO_4)$, K_2CO_3, $NaHSO_3$, HCl (0.1 N), bromine (Br_2), dichloromethane (99.6%, Aldrich), and deionized water.

6.2.2. Instrumentation

The full descriptions of all techniques were mentioned in chapter two and three.

6.2.3. Preparation

6.2.3.1. Activation of the Mesoporous OSU-6-W

Activated OSU-6-W was prepared by the methods described in chapter three. After the activation step, the mesoporous silica underwent at treated to introduce an

amine compound onto the surface that would work as a catalyst. In this process, 6.0 g (~ 100 mmol) of the dried mesoporous material, OSU-6-W, was suspended in 100 ml of dry toluene. Twenty milliliters of triethylamine (TEA) was added to the suspension and the mixture was stirred for one hour at 25 $^\circ$C. The resulting mixture was filtered off using a fine filter funnel and washed with dry toluene (3 X 50 ml). This product will be refered to as TEA-OSU-6-W.

6.2.3.2. Grafting Vinyl Functional Groups into the Mesoporous Surfaces

The vinyl functional group was introduced and chemically attached to the mesoporous OSU-6-W material surfaces using the same two procedures described previously in chapter three and four for aminosilane reactions with the substitution of TEA-OSU-6-W for OSU-6-W.

I. Grafting of the Mesoporous Silica with Vinyltrimethoxysilane in a One Step Reaction (OSU-6-W-VTMS-1)

Mesoporous silica bearing vinyl functional groups was prepared using the same procedure as described for aminosilane in chapter three with substituting the activated mesoporous silica (TEA-OSU-6-W) for OSU-6-W and with 7.5 ml (~ 50 mmol) of vinyltrimethoxysilane (VTMS) for the aminosilane (Scheme 6.1). A white solid was isolated in a yield of 4.46 g. The IR peaks in cm^{-1} (KBr) are 3745(m), 3425(s, br), 3069(m), 2955(s, sh), 2852(s, sh), 1603(m, sh), 1463(vw), 1412(m, sh), 1250(s, br)(Si-C), 1084(s), 974(m), 808(m), 665(vw), 624(w), and 461(m). Solid-state ^{29}Si CP/MAS NMR resonances in δ (ppm) are -48.5 (T^1), -57.8 (T^2), -65.7 (T^3), -102.0 (Q^3), and 110.8 ppm (Q^4). Solid-state ^{13}C CP/MAS NMR resonances in δ (ppm) are 17.9, 60.9, 139.2

ppm (≡Si-*C*H=CH$_2$)[1], and 128.8 (≡Si-CH=*C*H$_2$)[2]. See Scheme 6.1. Elemental

analysis: C (9.37%) and N (0.09%).
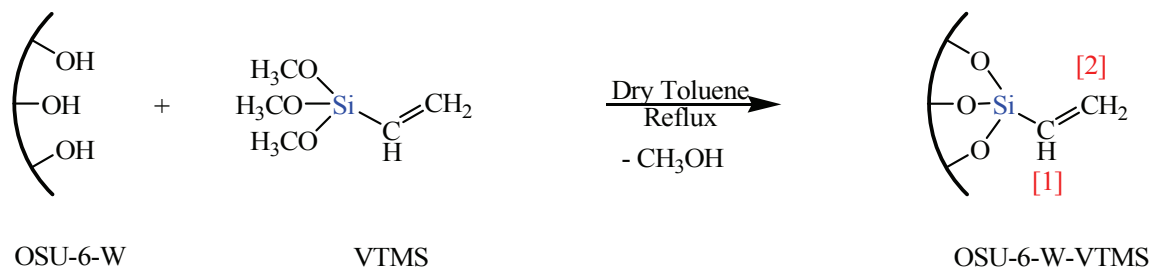
Scheme 6.1. Schematic illustration of the grafting reaction and the carbon atom position as described in the ^{13}C CP/MAS NMR

II. Grafting of the Mesoporous Silica Surface with Vinyltrimethoxysilane in Three Modification Reaction Steps (OSU-6-W-VTMS-2)

The mesoporous silica-supported vinyl groups was prepared following the same

procedure as described for the three step method in chapter three with the substitution of

the activated mesoporous silica (TEA-OSU-6-W) for OSU-6-W and 25 mmol (~ 3.7 ml)

of vinyltrimethoxysilane (VTMS) for the aminosilane. The final white solid was

obtained in a yield of 5.21 g. The IR peaks in cm^{-1} (KBr) are 3299(s, br), 3061(s, br),

2959(s, sh), 2856(s, sh), 1601(s, sh), 1458(m, sh), 1410(s, sh), 1276(s, br), 1171(s, br),

1087(s, br), 969(w), 812(m), 617(w), 594(m), and 474(m). Solid-state ^{29}Si CP/MAS

NMR: δ (ppm) -61.7 (T^2), -71.1 (T^3), -79.9, -102.5 (Q^3), and -109.8 (Q^4). Solid-state ^{13}C

CP/MAS NMR: δ (ppm) 50.2 (Methanol, solvent), 137.0 (≡Si-*C*H=CH$_2$)[1], and 130.0

(≡Si-CH=*C*H$_2$)[2]. See Scheme 6.1. Elemental analysis: C (12.40%) and N (0.10%).

6.2.3.3. Converting Vinyl Groups on the OSU-6-W-VTMS to Carboxylic Groups

The vinyl functional groups on the mesoporous OSU-6-W-VTMS-(1&2) were converted to the carboxylic acid groups following the procedure reported by Wasserman et al.[30] In this oxidation reaction, stock solutions of $KMnO_4$ (5 mM), $NaIO_4$ (195 mM), and K_2CO_3 (18 mM) in water were prepared. Immediately prior to the oxidation, 1.0 ml from each of these solutions was combined with 7.0 ml of distilled water to create the oxidizing solution ($KMnO_4$, 0.5 mM; $NaIO_4$, 19.5 mM; K_2CO_3, 1.8 mM). The vinyl-functionalized materials were placed in this solution for periods of 48 hours. The samples were removed from the oxidant and rinsed with 20 ml of each of $NaHSO_3$ (0.3 M), distilled water, 0.1 N HCl, distilled water, and ethanol. Then, the samples were dried under vacuum for 24 hours. Scheme 6.2 shows the oxidation reaction of the vinyl groups. The products were denoted as OSU-6-W-VTMS-1-Carboxyl and OSU-6-W-VTMS-2-Carboxyl and the IR in cm^{-1} (KBr) shows peaks in the region of 1720 cm^{-1}.

OSU-6-W-VTMS   OSU-6-W-Carboxyl
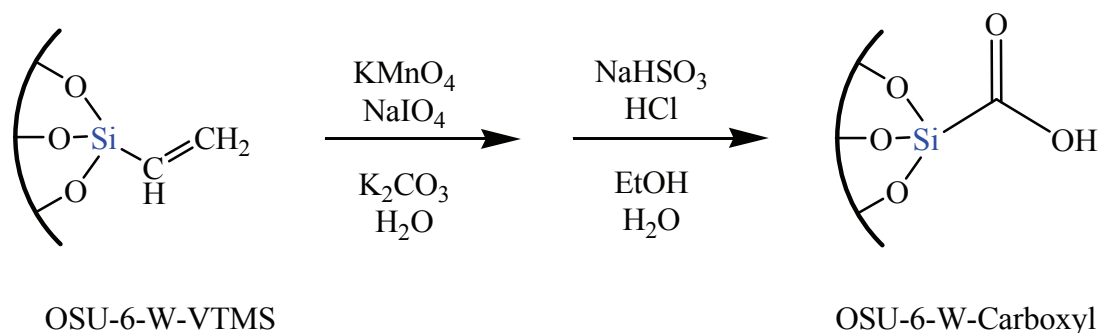
Scheme 6.2. Schematic illustration for the carboxyl converting reaction

6.2.4. Kinetic Study of the Bromination of Vinyl-Functionalized OSU-6-W Samples

The bromination reaction was monitored by UV-Vis spectroscopy, following the decay of the UV absorption of Br_2 at $\lambda_{max} = 410$ nm. An initial bromine stock solution was prepared by adding 0.5 ml of bromine to 100 ml of CH_2Cl_2. For each experiment, the concentration of the bromine stock solution was adjusted to give an initial UV absorbance value of approximately 1.0 at $\lambda = 410$ nm in a 1.0 cm quartz cuvette. Approximately 25 mg of vinyl-modified OSU-6-W was added to the cuvette and stirred. After given lengths of time, stirring was stopped, the cuvette was centrifuged for 3.0 minutes to separate all of the powder from the supernatant, and UV-Vis spectra of the supernatant bromine solution were obtained. A control experiment was carried out in a similar way using a sample of pure siliceous OSU-6-W.

6.2.5. Determination the Total Surface Loading of the Ordered Mesoporous Silica with the Vinyl Functional Groups

The amount of vinyl functional groups deposited on the surface was quantitatively determined using two variables. The surface loading (*l*) expresses the amount of deposited molecules in mmol/g. The number of molecules deposited per nm^2 is given by the surface coverage (*C*). Both values use the mass of the pure mesoporous silica before modification as a reference.[21] Different determination methods were used;

I. Spectrophotometric Analysis Method

The quantitative analysis of the concentration of vinyl groups was determined by means of a color reaction with bromine (Br_2) as shown in Scheme 6.3.
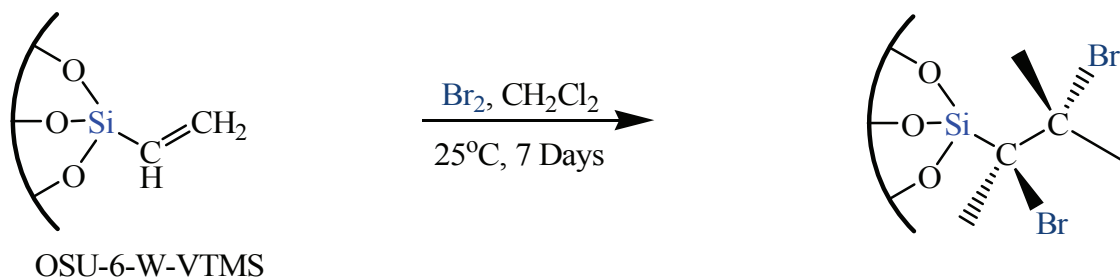
Scheme 6.3. Reaction of vinyl functional group with bromine.

In this method, an amount of 25 mg of each of the modified samples was dispersed in 10 ml of 0.03 M of Br_2 in CH_2Cl_2 in a 20-ml glass vial. An initial bromine stock solution was prepared by adding 1.0 ml of bromine to 100 ml of CH_2Cl_2. Immediately after the addition of Br_2, the solution was red. As time progressed, the color changed very slowly to orange, to yellow, and then to pale yellow. The mixtures were left under stirring for one week to ensure complete reaction. After that, the mixtures were centrifuged and the clear solution was transferred to a quartz cuvette, and the UV absorption was measured at the $\lambda_{max} = 410$ nm of the bromine solution to give the final concentration.

The correlation between the standard solutions of bromide concentrations and the absorbance at $\lambda = 410$ nm was linear. The total deposited amount (l) was calculated by subtracting the residual amount of bromine in the solution after reaction from the initially added amount. The coverage of the surface with vinyl groups (C) was calculated by dividing the loading (l) by the specific surface area (S_{BET}) of the sample. Multiplication by Avogadro's number ($N_A = 6.022 \times 10^{23}$ molecules/mole) gave units of molecules/nm^2:[21]

$$C = (l \, / \, S_{BET}) \cdot N_A$$

293

The spectrophotometric analysis method showed 5.47 mmol/g of the vinyl group for the OSU-6-W-VTMS-1 sample and 6.71 mmol/g of vinyl group for OSU-6-W-VTMS-2 sample.

II. Elemental Analysis (Combustion Analysis)

Carbon analysis was carried out for both modified samples. The concentration of attached groups was determined as follows:[22,23]

$$C \text{ (groups/nm}^2) = 6\text{x}10^5 \, P_C / [(1200n_C - WP_C)S_{BET}]$$

where C is the concentration of attached groups, which contain carbon; P_C is the percentage of carbon in the sample, n_C is the number of carbon atoms in the attached group (counted as C_2), W is the corrected formula mass of the modifier (counted as $C_2H_3O_3Si$), and S_{BET} is the specific surface area of the unbounded substrate (1283 m^2/g). The elemental analysis shows total carbon of 9.37% and 12.10% for OSU-6-W-VTMS-1 and OSU-6-W-VTMS-2, respectively. The results of the calculation of surface coverage are given in Table 6.4.

III. Solid State ^{29}Si CP/MAS NMR Spectrum

The solid state ^{29}Si CP/MAS NMR spectra of the vinyl modified silicas were analyzed as discussed in chapter three. Table 6.1 shows the solid state ^{29}Si CP/MAS NMR deconvolution results.

Table 6.1. Solid state ^{29}Si CP/MAS NMR deconvolution results

Sample	Q^4 (%)	Q^3 (%)	Q^2 (%)
OSU-6-W	14.38	71.73	13.89
OSU-6-W-VTMS-1	57.24	42.67	0.00
OSU-6-W-VTMS-2	85.86	14.14	0.00

6.3. RESULTS AND DISCUSSION

The ordered mesoporous silicas, OSU-6-W modified with a vinyl functional group were prepared by post-synthesis method from the reaction of OSU-6-W with vinyltrimethoxysilane (VTMS) using two different grafting procedures.

6.3.1. Identification the Textural Properties

I. X-ray Powder Diffraction

The X-ray powder diffraction (XRD) patterns of the organically functionalized samples are shown in Figure 6.1.
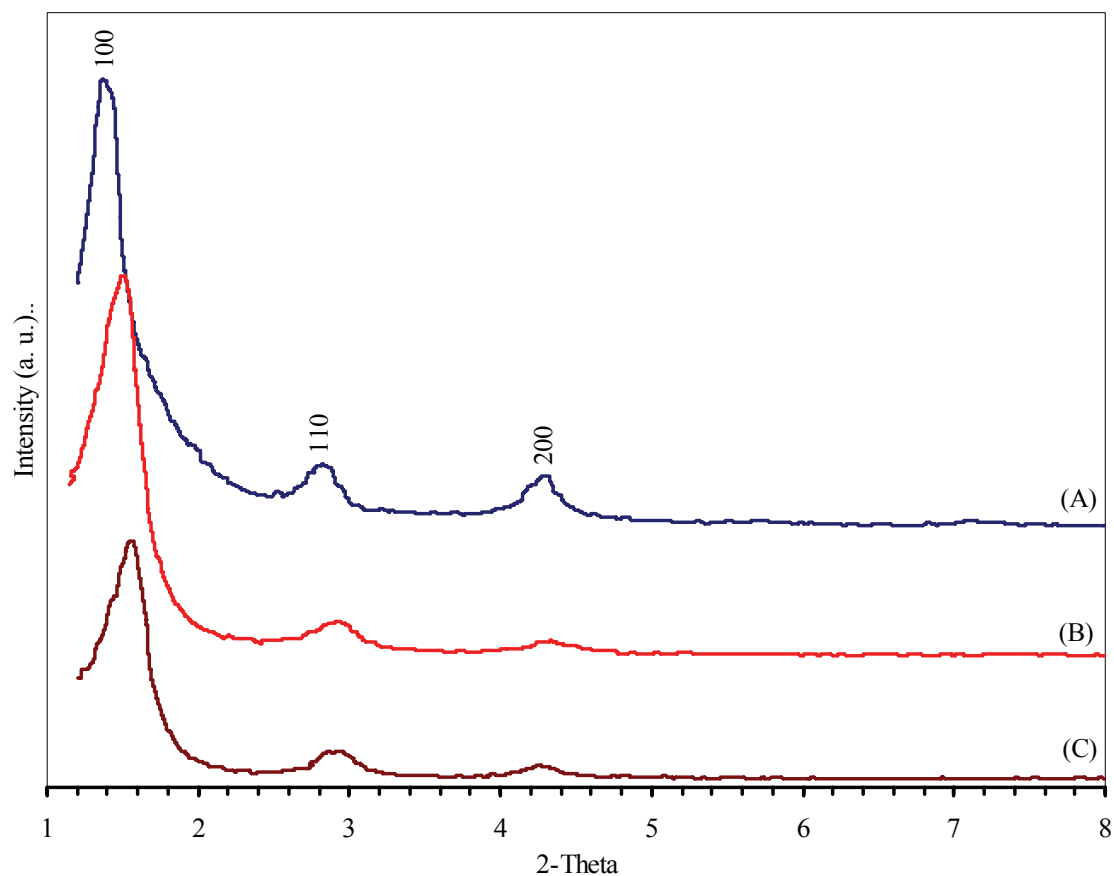
Figure 6.1. XRD patterns in the range of 1.0-10.0º of; (A) pristine ordered mesoporous material, OSU-6-W, (B) OSU-6-W-VTMS-1, and (C) OSU-6-W-VTMS-2. The spectra are shifted vertically for the sake of clarity.

After modification, and likely formation of a monolayer of silylation product on the surface walls, the overall order was only slightly reduced. It should be noted that the d_{100} spacing contracted very little during the modification processes (from 62.4 Å to 58.6 Å and to 56.3 Å for OSU-6-W-VTMS-1 and OSU-6-W-VTMS-2, respectively). The XRD patterns of the samples show strong (100) peaks and proportionally smaller (110) and (200) peak intensities, indicating that the modification process in the channels does not affect the framework integrity of the ordered siliceous OSU-6-W.

The average pore diameter of OSU-6-W-VTMS-2 from the surface area measurements, indicates an average thickening of the walls of about 25.5 Å this corresponds approximately to an extra one layer of Si-O-Si homogeneously spread on the original wall (20.9 Å). It also can be noticed that the d_{100} peak has become broader with the increase in the loading of the functional groups, indicating a slight alteration of the ordering of the mesoporous structure with more functional groups on the surface. Moreover, the relative intensities of higher angle peaks with respect to d_{100} decreased as the concentration of vinyl groups increased and decreased even further upon bromination. While the intensity reduction may be partially attributed to lower local order, such as variations in the wall thickness, it is mostly due to contrast matching between the amorphous silicate framework and the organic moieties that are located inside the channels of OSU-6-W.

Marler *et al.,*[24] observed that the XRD peak intensities of boron-containing MCM-41 (B-MCM-41) were related to the density of organic sorbates incorporated into the B-MCM-41. When organic sorbates having a higher density were loaded in B-MCM-

41, all XRD intensities systematically decreased due to the smaller difference of scattering contrast between the organic sorbates and the silicate walls of B-MCM-41.

The textural properties determined from Nitrogen adsorption-desorption experiments at 77 K and powder XRD measurements are shown in Table 6.2.

Table 6.2. Textural Properties Determined from Nitrogen Adsorption-desorption Experiments at 77 K and Powder XRD Measurements.

Sample	Specific surface area (m^2/g)	Total pore volume (cm^3/g)	Average pore size (Å)	d_{100} (Å)	Wall Thickness (Å)
OSU-6-W	1283	1.24	51.1	62.4	21.0
OSU-6-W-VTMS-1	1055	0.98	45.6	58.6	22.1
OSU-6-W-VTMS-2	873	0.79	40.7	57.3	25.5

II. Nitrogen Adsorption-Desorption Measurements

Nitrogen adsorption-desorption experiments, Figure 6.2, yielded Brunauer-Emmett-Teller (BET)[25,26] surface areas of 1055 and 873 m^2/g for the modified samples, OSU-6-W-VTMS-1 and OSU-6-W-VTMS-2, respectively, and total pore volumes of 0.98 and 0.79 cm^3/g, respectively.

After modification with the vinyl functional group, both the surface area and the total pore volume dropped significantly (BET surface area 1283 m^2/g; total pore volume 1.24 cm^3/g). The BET isotherm was similar to that of OSU-6-W. The reduction in total pore volume and shift in the pore size distribution peak from 51.1 to 45.6 and 40.7 Å imply a reduction in the free channel space as the vinyl groups were loaded. An opening

of *ca.* 40.7 Å is sufficiently large to allow all metal ions and most small organic

molecules to be incorporated into the functionalized OSU-6-W-VTMS-2.
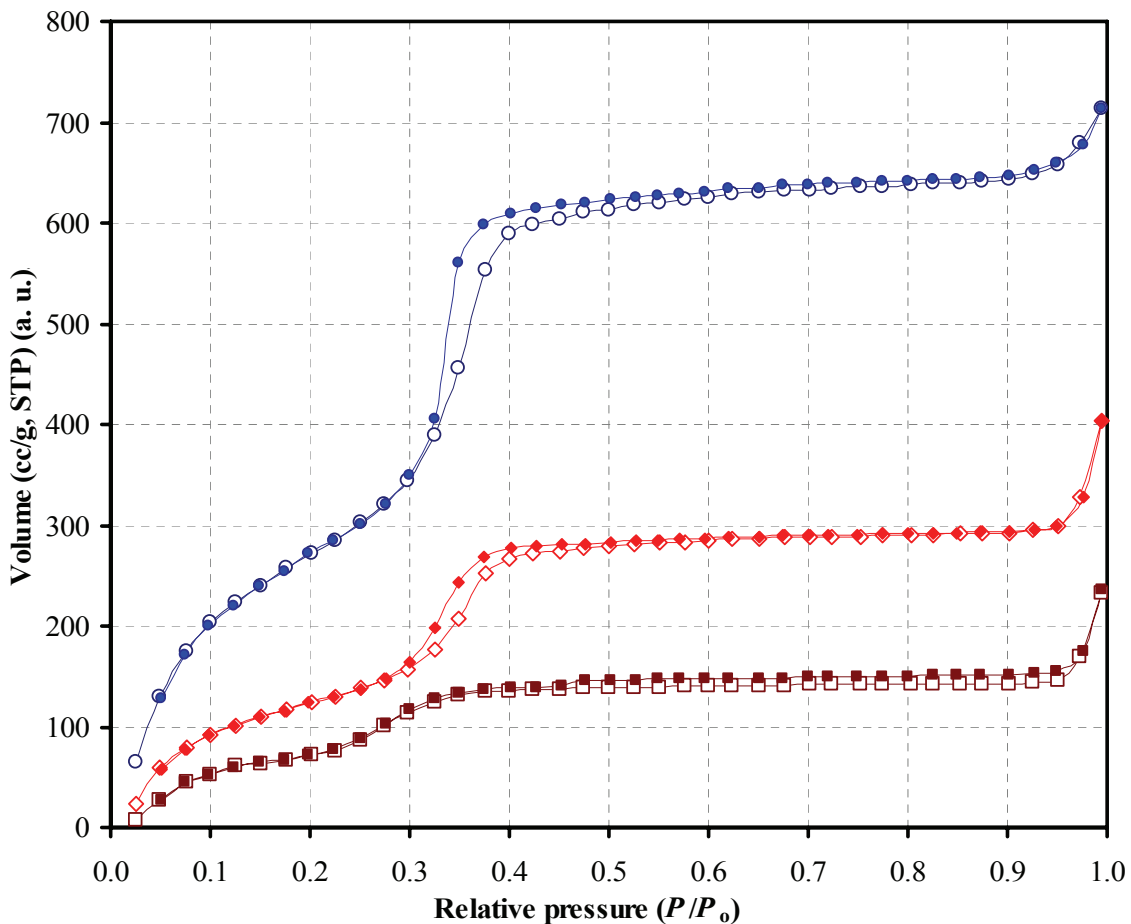
Figure 6.2. Nitrogen adsoption-desorption isotherms of (○) OSU-6-W, (◊) OSU-6-W-VTMS-1, and (□) OSU-6-W-VTMS-2. Open symbols: adsorption; closed symbols: desorption. The isotherm data are shifted vertically for the sake of clarity.

The vinyl-modified samples exhibited small hysteresis loops in the P/P_o region

between 0.3 and 0.45. While the hysteresis may be associated with capillary

condensation in ink-bottle pores, other effects such as network effects, the nature of the

framework, the adsorbate, and the temperature can influence the shape of the isotherm, so

that interpretation is difficult for this hybrid material.[27] It has been found that the relative

pressure (P/P_o) at which the adsorption reaches the last plateau shifts to the right for samples with larger pore diameter. This characteristic relative pressure (P/P_o) has been used to qualitatively compare the pore dimensions of different samples.[8,9,28] A higher value of the characteristic (P/P_o) indicates a larger pore size.[29] The mesoporosity of OSU-6-W sample consists of two parts: uniform framework-confined channels and non-uniform interparticle voids.[30]

From the pore size measurements, Figure 6.3, the pore size distributions of all samples were narrow, being less than 6.0 ± 1.0 Å wide.
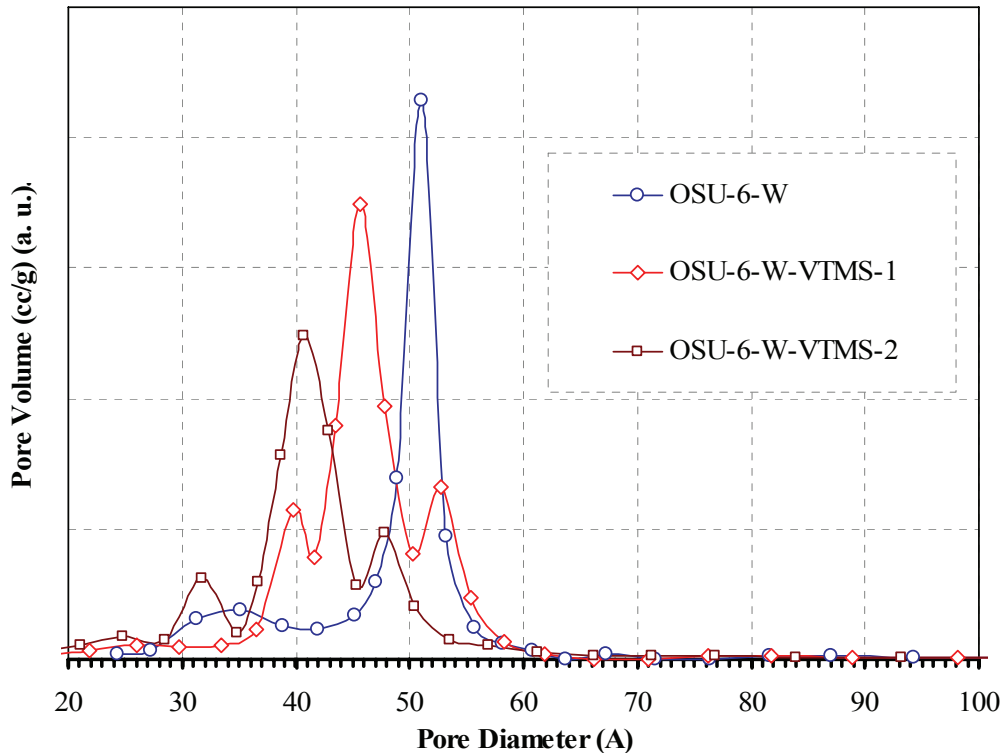
Figure 6.3. Pore size distribution of (○) OSU-6-W (max at 51.1 Å), (◊) OSU-6-W-VTMS-1 (max at 45.6 Å), and (□) OSU-6-W-VTMS-2 (max at 40.7 Å).

III. Thermogravimetric Analysis (TGA)

The thermal stability of the organic functional groups within the mesoporous materials (OSU-6-W-VTMS-1 and OSU-6-W-VTMS-2) was determined by thermogravimetric analysis (Figure 6.4). After initial loss of solvent, the removal of the vinyl groups started at 260-290 $^{\circ}$C and continued up to 400 and 450 $^{\circ}$C, respectively. An additional weight loss occurred at higher temperatures due to further condensation of the silicate walls, as observed in other mesoporous silicates.[31]
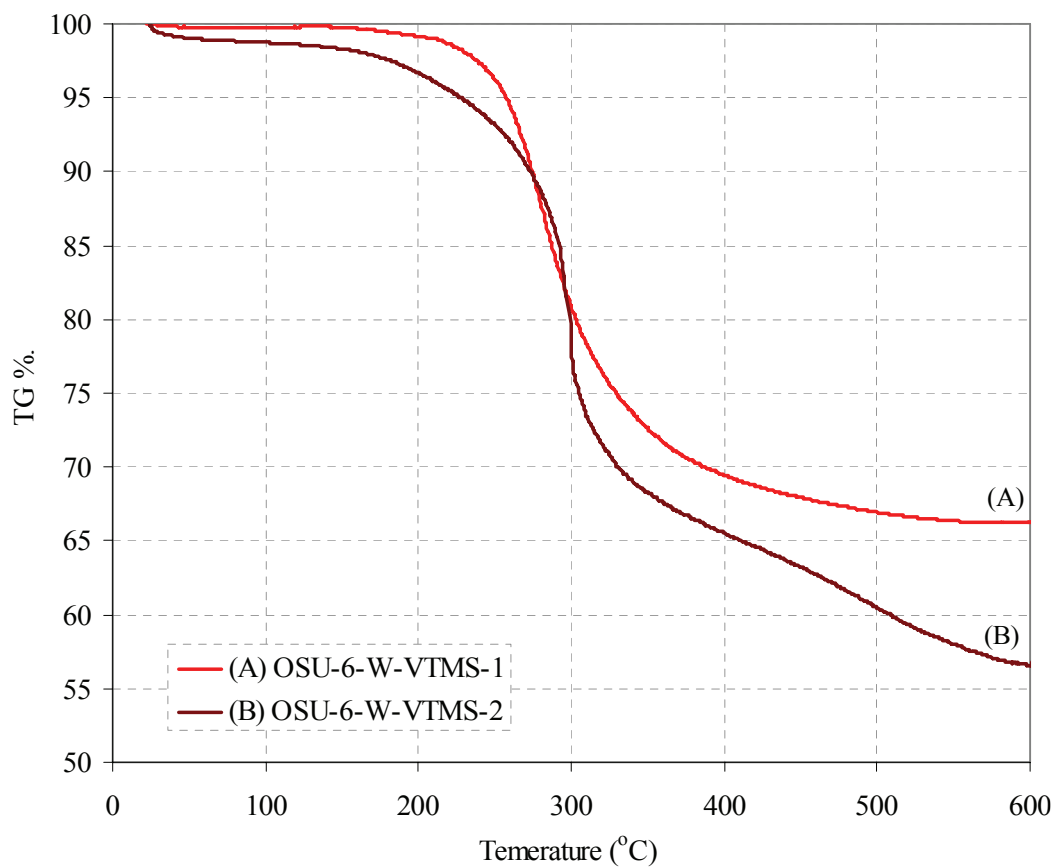
Figure 6.4. TGA curves of the modified samples, OSU-6-W-VTMS-1 and OSU-6-W-VTMS-2 (A and B, respectively).

6.3.2. Identification of the Vinyl Functional Groups

I. Solid State ^{29}Si CP/MAS NMR Spectroscopy

Figure 6.5 shows the solid state ^{29}Si CP/MAS NMR spectra for the unmodified mesoporous silica, OSU-6-W, and the two modified samples, (OSU-6-W-VTMS-1, and OSU-6-W-VTMS-2).
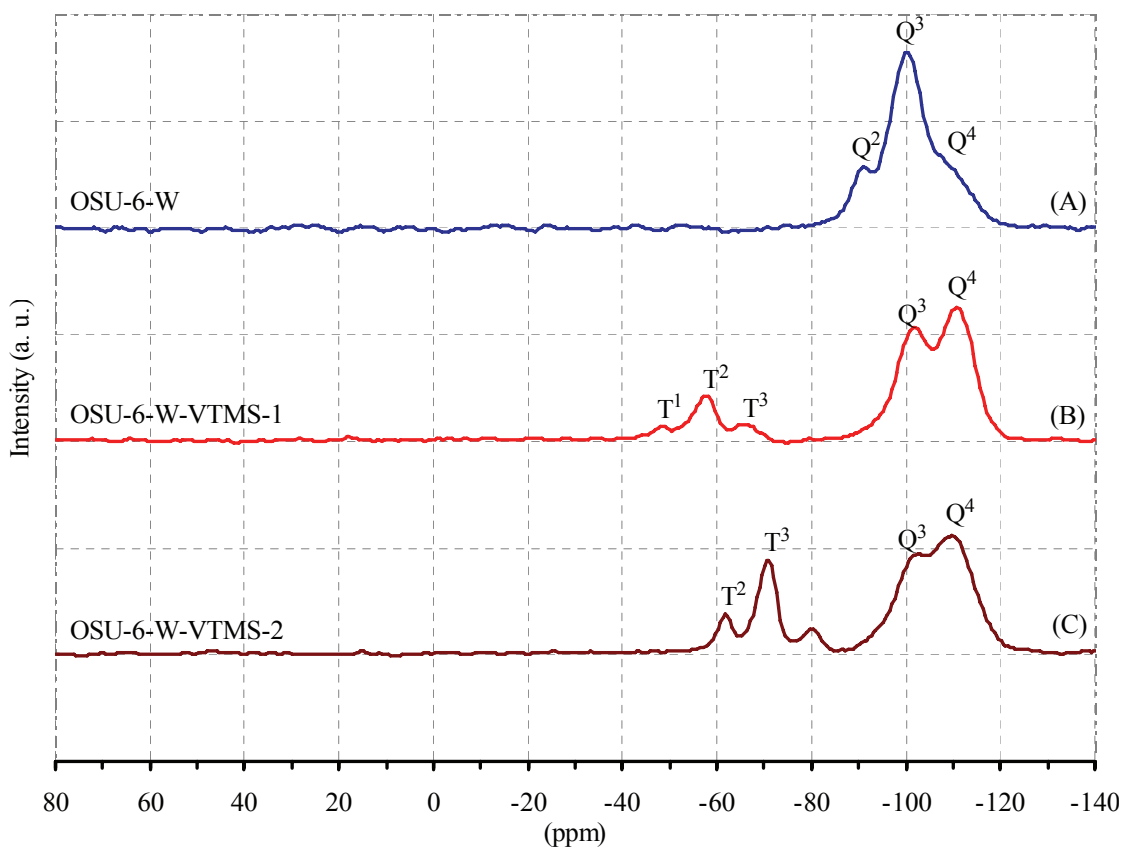
Figure 6.5. Solid state ^{29}Si CP/MAS NMR spectra of; (A) Un-modified mesoporous silica, OSU-6-W, (B) the modified OSU-6-W-VTMS-1, and (C) the modified OSU-6-W-VTMS-2.

As indicated in chapter two, OSU-6-W has three peaks in 29Si NMR spectrum. There is a low intensity peak at -91.2 ppm for the Q^2 silicons; a peak at -100.4 ppm

attributed to Q^3 silicons; and a resonance at -107.9 ppm attributed to Q^4 silicons, Figure

6.5. The two functionalized samples, Figure 6.5 (B and C), show similar peaks with

location at -102.0 and -110.8 ppm, and -102.5, -109.8 ppm, corresponding to Q^3, and Q^4

silicon environments for OSU-6-W-VTMS-1 and OSU-6-W-VTMS-2, respectively.

Derivtization of OSU-6-W led to the appearance of three new peaks at *ca.* -48.5, -57.8,

and -65.7 ppm corresponding to T^1, T^2, and T^3 silicon environment in case of the OSU-6-

W-VTMS-1, Figure 6.5(B). On the other hand, in the spectrum of OSU-6-W-VTMS-2,

Figure 6.5(C), there are only two resonances in the T^n silicon region. The resonance at

ca. -61.7 (T^2) ppm arises from terminal groups that are only bound to one neighboring

siloxane, and the resonance at *ca.* -71.1 (T^3) ppm arises from cross-linked groups that are

bound to two neighboring siloxanes. All peaks were identified by multipeak curve

fitting.

As expected, the grafting process resulted in a decrease in the intensity of the Q^3

resonance with an increase in the intensity of the Q^4 resonance of the mesoporous silica

framework. This difference in relative intensity is attributable to reactions of surface Si-

OH groups with VTMS molecules that lead to the formation of more Si-O-Si bonds. By

comparison between the two modified samples, the intensity of the peak at around -100

ppm decreases with the increase in the amount of functional groups on the surface. The

dominant peak on the OSU-6-W-VTMS-1 is attributed to the terminal groups (T^2) while

the dominant peak on the OSU-6-W-VTMS-2 is attributed to the cross-linked siloxane

group (T^3). The higher intensity of the peak at T^3 for OSU-6-W-VTMS-2 is indicative of

higher surface coverage as compared to OSU-6-W-VTMS-1. The increase in peak

intensity at around -71.1 ppm (T^3) compared with the peak at around -61.7 ppm (T^2) and

disappearance of the peak at around -48 ppm (T^1) demonstrates that the OSU-6-W-VTMS-2 has a surface that is mainly composed of cross-linked organosilyl groups. Solid state ^{29}Si NMR revealed a high degree of silane cross-linking and a surface population of 5.18 groups/nm^2, indicative of a good monolayer structure in the OSU-6-W-VTMS-2.

The integrated areas of these peaks are summarized in Table 6.3. The population of T^2 is larger than T^3 in OSU-6-W-VTMS-1, whereas T^3 is more abundant in OSU-6-W-VTMS-2. Also, the Q^3/Q^4 ratio in OSU-6-W-VTMS-1 is larger than OSU-6-W-VTMS-2. The differences in the ratios of T^2/T^3 and Q^3/Q^4 demonstrate that the population of silanol generated on the attached silane is larger in OSU-6-W-VTMS-2 than in OSU-6-W-VTMS-1.

Table 6.3. The integrated areas of the peaks from the solid state ^{29}Si CP/MAS NMR deconvolution results.

Sample	Q^3	Q^4	T^2	T^3	Q^3/Q^4	T^2/T^3
OSU-6-W-VTMS-1	42.76	57.24	69.38	18.48	0.75	3.75
OSU-6-W-VTMS-2	14.14	85.86	26.36	73.64	0.17	0.36

II. Solid State ^{13}C CP/MAS NMR Spectroscopy

The existence of covalently linked organic moieties bearing vinyl functional groups in the as-synthesized OSU-6-W mesoporous silicas was also confirmed by solid state ^{13}C CP/MAS NMR spectroscopy.[32] The solid state ^{13}C CP/MAS NMR spectrum, Figure 6.6, showed two resonances for the modified samples corresponding to vinyl carbons at 128.8 ($\equiv$Si-CH=CH$_2$) and 139.2 ppm ($\equiv$Si-CH=CH$_2$) and at 130.0 and 137.0

ppm for OSU-6-W-VTMS-1 and OSU-6-W-VTMS-2, respectively. These data

confirmed that vinyl groups were not damaged by either functionalization methods. The

intensities of the peaks related to the vinyl carbons are higher in OSU-6-W-VTMS-2 than

in OSU-6-W-VTMS-1 reflecting the higher total coverage. At higher population

densities, all of the carbon chains are near one another and have a more upright

orientation with respect to the silica surface. The molecules, therefore, have a higher

degree of ordering that narrows the line widths in the ^{13}C spectrum and allows better

resolution of the peaks.[12]
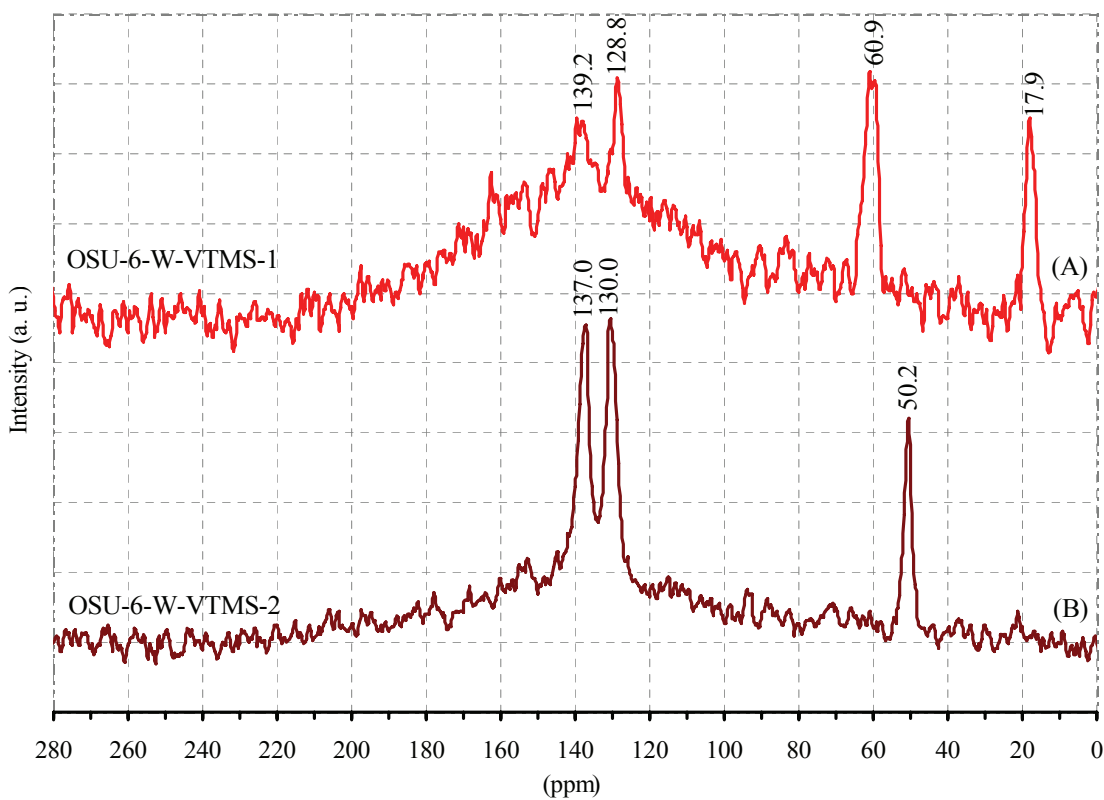
Figure 6.6. Solid state ^{13}C CP/MAS NMR spectra of the modified samples with vinyl
functional groups, (A) OSU-6-W-VTMS-1, and (B) OSU-6-W-VTMS-2

The resonances present at 17.9 and 60.9 ppm in the OSU-6-W-VTMS-1 sample are most likely due to the ethanol (solvent). The peak at 50.2 ppm in the OSU-6-W-VTMS-2 sample is probably due to methanol.

Peaks corresponding to the organosiloxane moieties are relatively broad, indicating restricted mobility of the functional groups attached to the siloxane framework.

III. Fourier Transform Infrared Spectroscopy (FT-IR)

The vibrational spectra, Figure 6.7, obtained from solid samples confirmed the success of the grafting reactions. The sequences of bands are very close to those observed, when vinyl functional groups were previously incorporated into similar materials.
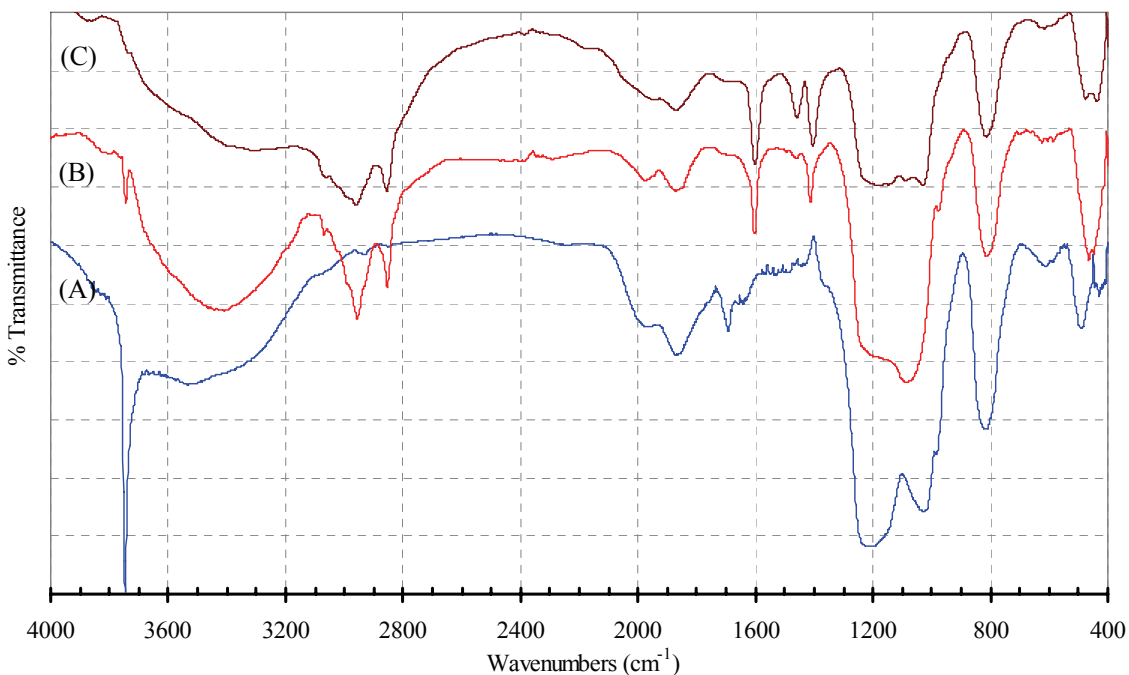
Figure 6.7. Infrared spectra of (curve A) OSU-6-W, (curve B) OSU-6-W-VTMS-1, and (curve C) OSU-6-W-VTMS-2.

The typical MCM-41 silica bands associated with the main inorganic backbone that have been discussed previously in chapter two are present. Additional bands are also observed in both spectra that confirmed the presence of organic pendant groups. The FT-IR absorption of the modified samples, OSU-6-W-VTMS-1 and OSU-6-W-VTMS-2, shows peaks at 1412 and 1410 cm^{-1} assigned to the =C-H bending mode of the vinyl group, and at 1603 and 1601 ppm assigned to C=C stretch. By increasing the deposited amount of VTMS on OSU-6-W using the second functionalization method in the synthesis of OSU-6-W-VTMS-2, an increase of the intensities of the peaks at 1410 (C-H), 1601 (C=C), and 1276 (Si-C) stretches was observed.

The efficiency of the grafting process is demonstrated by a significant decrease in the silanol bands at around 3740 cm^{-1}, that is associated with an increase of new bands characteristic of the immobilized vinyl functional groups.

6.3.3. Identification of Carboxylic Functional Groups in OSU-6-W-Carboxyl

The mesoporous material, OSU-6-W, functionalized with carboxylic acid directly attached to the surface was synthesized by oxidation of the vinyl groups of OSU-6-W-VTMS-(1&2). The new materials were characterized by the FT-IR spectroscopy. The FT-IR spectrum of the oxidized OSU-6-W-VTMS-1-Carboxyl and OSU-6-W-VTMS-2-Carboxyl, showed peaks that are specific for carboxylate groups located at 1721 and 1723 cm^{-1}, respectively. The disappearance of the peaks at 1603 and 1601 cm^{-1} due to C=C stretching confirms the successful conversion of the vinyl groups to carboxyl groups.

6.3.4. Kinetic Study of the Bromination of Vinyl-Functionalized OSU-6-W Samples

In the bromination study of OSU-6-W-VTMS-(1 and 2) in dichloromethane, a remarkably slow reaction rate was observed at room temperature such that complete

bromination required several days. The slow bromination was confirmed by FT-IR

spectra of both samples reacted with bromine for 1 and 4 days. After bromination, a

broad peak in the IR at 688 cm^{-1} confirmed the presence of C-Br bonds. Vibrations due

to vinyl carbon atoms were still present after a one day bromination but disappeared

completely after four days reaction, indicating that all vinyl groups were accessible to

bromine. This reaction was unusually slow compared to solution bromination of

unsaturated organic compounds even with bulky protecting groups.[33] However, the rate

was close to the rate of unhindered diffusion of Br_2 (kinetic diameter: 0.35 nm) through

2.2 nm diameter mesopore channels.[34]

   For qualitative measurements, the bromination reaction was monitored by UV-Vis

spectroscopy. In Figure 6.8, the intensity decreases of the bromine absorption at λ_{max} =

410 nm due to reaction with the two modified samples are comparable.
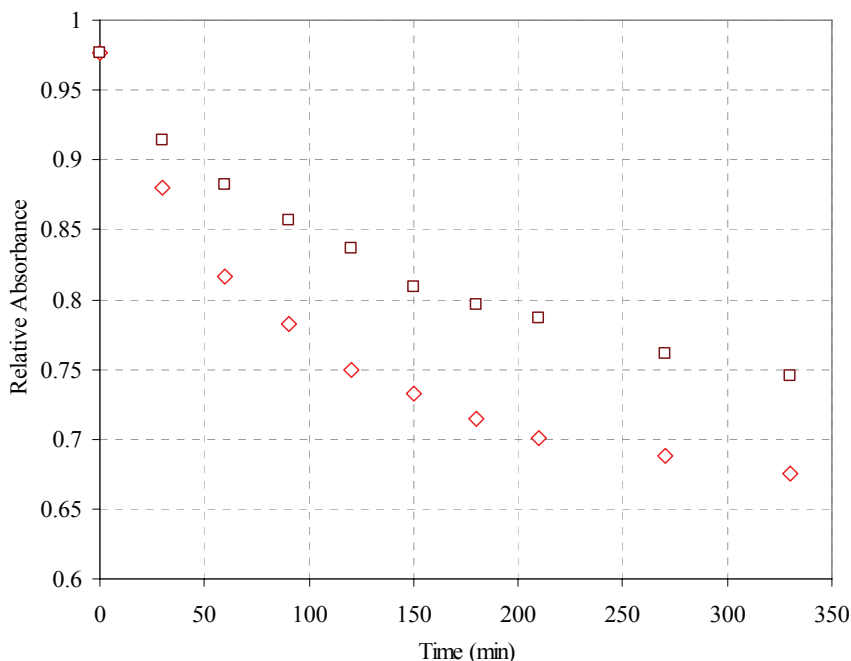
Figure 6.8. Plot of relative absorbance of Br_2/CH_2Cl_2 solutions (λ_{max} = 412 nm) vs. time
of stirring above vinyl-functionalized OSU-6-W samples: (◊) OSU-6-W-VTMS-1 and
(□) OSU-6-W-VTMS-2.
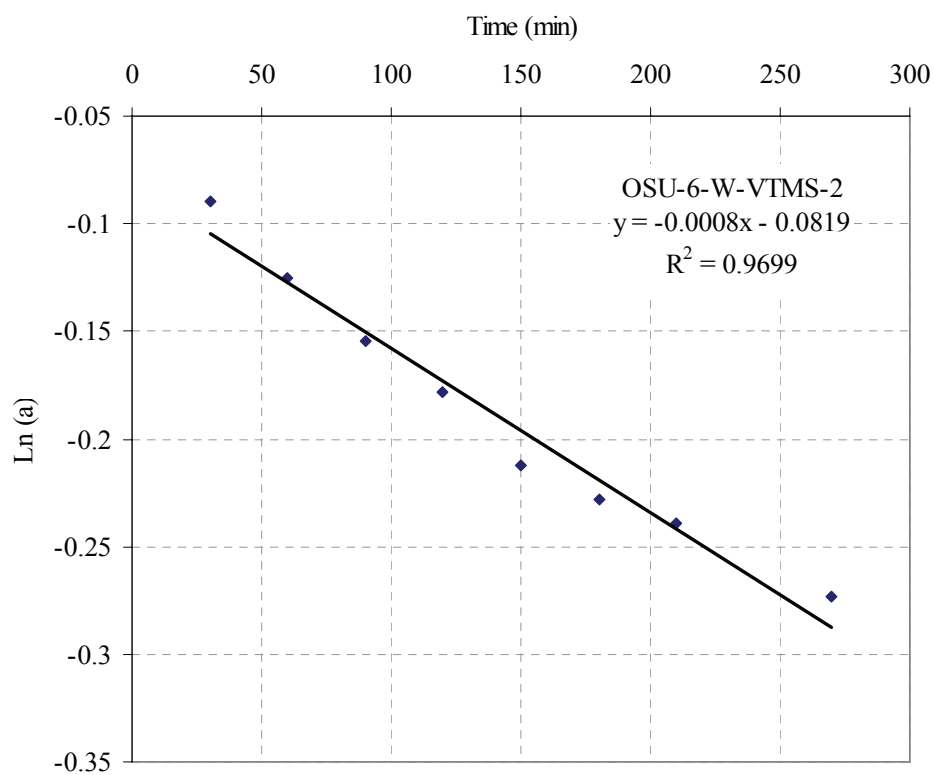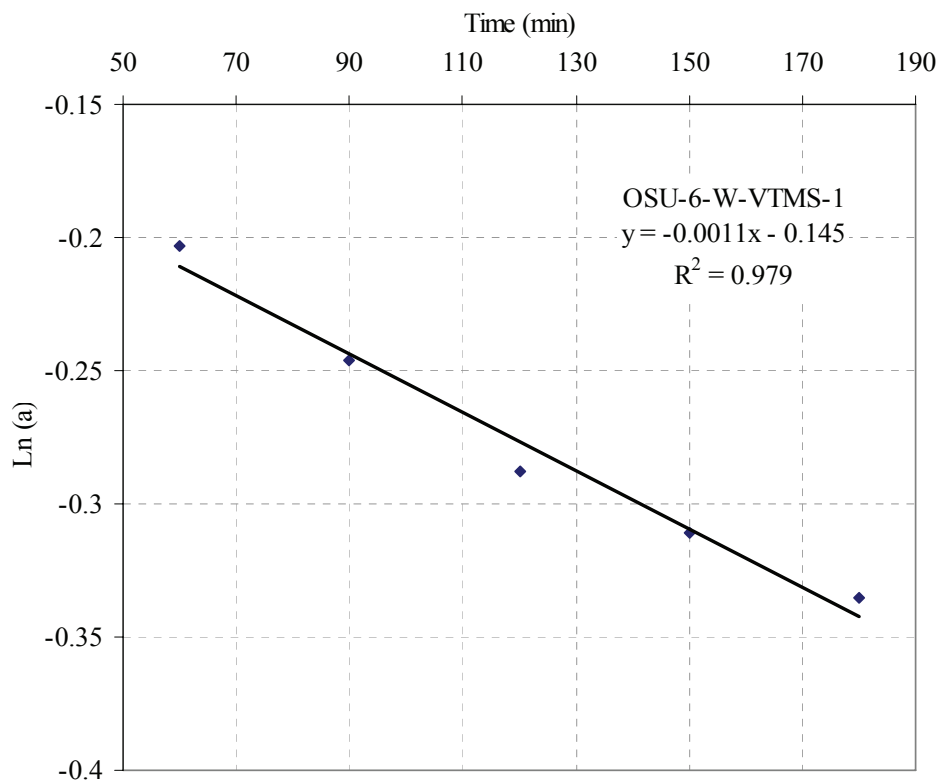
Figure 6.9. Plot of ln[Br$_2$] virsus time for OSU-6-W-VTMS-1 and OSU-6-W-VTMS-2.

The two samples, OSU-6-W-VTMS-1 and OSU-6-W-VTMS-2, had different

loadings of vinyl groups. The pore sizes calculated from the BJH method were 45.6 Å

for OSU-6-W-VTMS-1 and 40.7 Å for OSU-6-W-VTMS-2. The absorbance values of

both vinyl-modified samples dropped quickly during the first 30 minutes, suggesting that

reactions occurred on the external surfaces of those samples. As expected, the reaction

rate of the larger pore sample, OSU-6-W-VTMS-1, was faster than that of OSU-6-W-

VTMS-2. This pore size dependence of bromination provided evidence that limited

diffusion was one of the factors controlling the reaction rate.

On the basis of these observations, it is beleived that vinyl groups line the walls

throughout the channels, but groups on the external particle surface or near the channel

openings are brominated first. These can cause some hindrance for additional Br_2

molecules through steric effects, induced dipole interactions, and weak charge transfer

interactions. Solvent molecules present in the channels have also contributed to the

hindered diffusion of Br_2. The rate deceleration may therefore be attributed not only to a

decrease in the bromine concentration with time because this reaction is first order in Br_2

(Figure 6.9) but also to slower diffusion rates as the number of dibromoethyl sites

increases and the effective pore space decreases. The rate constants were 0.0011 and

0.0008 min-1 for OSU-6-W-VTMS-1 and OSU-6-W-VTMS-2, respectively.

6.3.5. Absorption of Nonpolar Solvents

Vinyl-modified OSU-6-W exhibited interesting sorption properties which were

investigated qualitatively at this point. Due to their hydrophobic surface and the small

particle size (a few micrometers), OSU-6-W-VTMS-(1&2) particles tended to float on

the surface of water. However, when OSU-6-W-VTMS-(1&2) were shaken with a

mixture of chloroform and water, the solids sank to the bottom of the flask as they absorbed the denser organic solvent. In mixtures of toluene and water (phase separated or as emulsions), toluene was absorbed by OSU-6-W-VTMS-(1&2), and the filled solids tended to form clusters. On the basis of their affinity for nonpolar solvents, OSU-6-W-VTMS-(1&2) and related materials may be useful for removing small amounts of organic fractions from water or for carrying out dry chemical reactions within the channels.

6.3.6. The Total Surface Loading of the Ordered Mesoporous Silica with the Vinyl Functional Groups

The amount of vinyl functional groups deposited on the surface was quantitatively determined using three different determination methods. Table 6.4 lists the results of the determination of the coverage of OSU-6-W with vinylsilyl groups.

The OSU-6-W-VTMS-1 sample has an average coverage of 3.04 VTMS molecule/100 $Å^2$, while the OSU-6-W-VTMS-2 sample has an average coverage of 4.91 VTMS molecule/100 $Å^2$.

Table 6.4. Total coverage from three different determination methods.

sample	Surface Area (BET)	Spectrophotometric Analysis (SA) (mmol/g)	Elemental Analysis (EA)		^{29}Si NMR			Total Coverage (molecule/nm^2)		
			C %	N %	Q^2 (%)	Q^3 (%)	Q^4 (%)	SA	EA	NMR
OSU-6-W	1283	----	0.10	0.06	13.89	71.73	14.38	----	----	----
OSU-6-W-VTMS-1	1055	5.47	9.37	0.09	0.00	42.67	57.24	3.12	3.06	2.95
OSU-6-W-VTMS-2	873	6.71	12.10	0.10	0.00	14.14	85.86	4.63	4.92	5.18

6.4. CONCLUSION

The grafting method applied in this research proved to be suitable for preparation of mesoporous silica with high loading with vinyl groups. Both modified samples, OSU-6-W-VTMS-1 and OSU-6-W-VTMS-2, have relatively well-ordered structures and high surface areas, on the basis of XRD and N_2 adsorption measurements. The average pore diameters lie in the range of mesoporous materials, thus permitting entry of large molecules or ions. The reactivity of the surface vinyl groups makes OSU-6-W-VTMS-(1&2) an ideal starting material for many other surface modifications.

The most critical differences between the two vinyl-grafted OSU-6-W samples appear to be the density of the functional groups and the mode of surface attachment of the majority of the vinyl groups.

For the first time, mesoporous materials with carboxylic groups directly attached to the surface have been synthesized. These materials will have huge impact on the adsorption and separation technology due to the high concentration of the carboxyl groups on the surface of high surface and robust materials.

6.5. REFERENCES

1. Lim, M. H.; Blanford, C. F.; Stein, A. Synthesis and Characterization of a Reactive Vinyl-Functionalized MCM-41: Probing the Internal Pore Structure by a Bromination Reaction. *J. Am. Chem. Soc.* **1997,** *119*, 4090-4091.

2. Lim, M. H.; Blanford, C. F.; Stein, A. Synthesis of Ordered Microporous Silicates with Organosulfur Surface Groups and Their Applications as Solid Acid Catalysts. *Chem. Mater.* **1998,** *10*, 467-470.

3. Burkett, S. L.; Sims, S. D.; Mann, S. Synthesis of hybrid inorganic-organic mesoporous silica by co-condensation of siloxane and organosiloxane precursors *Chem. Commun.* **1996,** 1367-1368.

4. Mercier, L.; Pinnavaia, T. J. Access in mesoporous materials. Advantages of a uniform pore structure in the design of a heavy metal ion adsorbent for environmental remediation. *Adv. Mater.* **1997,** *9*, 500-503.

5. Meziani, M. J.; Zajac, J.; Jones, D. J.; Roziere, J.; Partyka, S. Surface Characterization of Mesoporous Silicoaluminates of the MCM-41 Type: Evaluation of Polar Surface Sites Using Flow Calorimetry, Adsorption of a Cationic Surfactant as a Function of Pore Size and Aluminum Content. *Langmuir* **1997,** *13*, 5409-5417.

6. Diaz, J. F.; Balkus, K. J.; Bedioui, F.; Kurshev, V.; Kevan, L. Synthesis and Characterization of Cobalt-Complex Functionalized MCM-41 *Chem. Mater.* **1997,** *9*, 61-67.

7. Rao, S. Y. V.; De Vos, D. E.; Jacobs, P. A. 1,5,7-Triazabicyclo[4.4.0]dec-5-ene immobilized in MCM-41: a strongly basic porous catalyst. *Angew. Chem., Int. Ed. Engl.* **1997,** *36*, 2661-2663.

8. Kresge, C. T.; Leonowicz, M. E.; Roth, W. J.; Vartuli, J. C.; Beck, J. S. Ordered Mesoporous Molecular Sieves Synthesized by A Liquid-Crystal Template Mechanism. *Nature* **1992,** *359*(6397), 710-712.

9. Beck, J. S.; Vartuli, J. C.; Roth, W. J.; Leonowicz, M. E.; Kresge, C. T.; Schmitt, K. D.; Chu, C. T. W.; Olson, D. H.; Sheppard, E. W.; McCullen, S. B.; Higgins, J. B.; Schlenker, J. L. A new family of mesoporous molecular sieves prepared with liquid crystal templates. *J. Am. Chem. Soc.* **1992,** *114*(27), 10834-10843.

10. Sutra, P.; Brunel, D. Preparation of MCM-41 type silica-bound manganese(III) Schiff-base complexes *Chem. Commun.* **1996,** 2485-2486.

11. Moller, K.; Bein, T. Inclusion Chemistry in Periodic Mesoporous Hosts. *Chem. Mater.* **1998,** *10*, 2950-2963.

12. Feng, X.; Fryxell, G. E.; Wang, L.-Q.; Kim, A. Y.; Liu, J.; Kemner, K. M. Functionalized monolayers on ordered mesoporous supports. *Science* **1997,** *276*(5314), 923-926.

13. Shephard, D. S.; Zhou, W.; Maschmeyer, T.; Matters, J. M.; Roper, C. L.; Parsons, S.; Johnson, B. F. G.; Duer, M. J. Site-directed surface derivatization of MCM-41: use of high-resolution transmission electron microscopy and molecular recognition for determining the position of functionality within mesoporous materials. *Angew. Chem., Int. Ed.* **1998,** *37*(19), 2719-2723.

14. Moller, K.; Bein, T.; Fischer, R. X. Synthesis of Ordered Mesoporous Methacrylate Hybrid Systems: Hosts for Molecular Polymer Composites. *Chem. Mater.* **1999,** *11*, 665-673.

15. Fowler, C. E.; Burkett, S. L.; Mann, S. Synthesis and characterization of ordered organosilica-surfactant mesophases with functionalized MCM-41-type architecture *Chem. Commun.* **1997,** 1769-1770.

16. Babonneau, F.; Leite, L.; Fontlupt, S. Structural characterization of organically-modified porous silicates synthesized using CTA+ surfactant and acidic conditions *J. Mater. Chem.* **1999,** *9*, 175-178.

17. Blitz, J. P.; Murthy, R. S. Shreedhara; Leyden, D. E. Ammonia-catalyzed silylation reactions of Cab-O-Sil with methoxymethylsilanes. *J. Am. Chem. Soc.* **1987,** *109*(23), 7141-7145.

18. Lim, M. H.; Stein, A.. Comparative Studies of Grafting and Direct Syntheses of Inorganic-Organic Hybrid Mesoporous Materials. *Chem. Mater.* **1999,** *11*(11), 3285-3295.

19. Maoz, R.; Sagiv, J. Penetration-controlled reactions in organized monolayer assemblies. 1. Aqueous permanganate interaction with monolayer and multilayer films of long-chain surfactants. Langmuir 1987, 3(6), 1034-1044. Netzer, L.; Sagiv, J.. A new approach to construction of artificial monolayer assemblies. J. Am. Chem. Soc. 1983, 105(3), 674-676.

20. Wasserman, S. R.; Tao, Y. T.; Whitesides, G. M. Structure and reactivity of alkylsiloxane monolayers formed by reaction of alkyltrichlorosilanes on silicon substrates. *Langmuir* **1989,** *5*(4), 1074-1087.

21. Vrancken, K. C.; Van Der Voort, P.; Possemiers, K.; Vansant, E. F. Surface and Structural Properties of Silica Gel in the Modification with γ-Aminopropyltriethoxysilane. *J. Colloid and Interface Sci.* **1995,** *174*(1), 86-91.

22. Sander, L. C.; Wise, S. A. Recent advances in bonded phases for liquid chromatography. *Crit. Rev. Anal. Chem.* **1987,** *18*(4), 299-415.

23. Unger, K. K. Packings and Stationary Phases in Chromatographic Techniques, Marcel Dekker, Moscow (1990).

24. Marler, B.; Oberhagemann, U.; Vortmann, S.; Gies, H. Influence of the sorbate type on the XRD peak intensities of loaded MCM-41. *Microporous Mater.* **1996**, *6*, 375-383.

25. Barrett, E. P.; Joyner, L. G.; Halenda, P. P. The determination of pore volume and area distributions in porous substances. I. Computations from nitrogen isotherms. *J. Am. Chem. Soc.* **1951,** *73,* 373-380.

26. Horvath, G.; Kawazoe, K. Method for the calculation of effective pore size distribution in molecular sieve carbon *J. Chem. Eng. Jpn.* **1983**, *16*, 470-475.

27. Sing, K. S. W. Adsorption methods for the characterization of porous materials *Adv. Colloid Interface Sci.* **1998**, *77*, 3-11.

28. Zhao, X. S.; Lu, G. Q.; Millar, G. J. Advances in Mesoporous Molecular Sieve MCM-41. *Ind. Eng. Chem. Res.* **1996,** *35*(7), 2075-2090.

29. Zhu, H. Y.; Lu, G. Q.; Zhao, X. S. Thickness and Stability of Adsorbed Film in Cylindrical Mesopores. *J. Phys. Chem. B* **1998,** *102*(38), 7371-7376.

30. Tanev, P. T.; Pinnavaia, T. J.. Mesoporous Silica Molecular Sieves Prepared by Ionic and Neutral Surfactant Templating: A Comparison of Physical Properties. *Chem. Mater.* **1996,** *8*(8), 2068-2079.

31. Steel, A.; Carr, S. W.; Anderson, M. W.. ^{29}Si solid-state NMR study of mesoporous M41S materials. *Chem. Mater.* **1995,** *7*(10), 1829-1832.

32. Wang, L. Q.; Liu, J.; Exarhos, G. J.; Bunker, B. C.. Investigation of the Structure and Dynamics of Surfactant Molecules in Mesophase Silicates Using Solid-State ^{13}C NMR. *Langmuir* **1996,** *12*(11), 2663-2669.

33. Brown, R. S.; Slebocka-Tilk, H.; Bennet, A. J.; Bellucci, G.; Bianchini, R.; Ambrosetti, R.. Investigation of the early stages of electrophilic addition of bromine to olefins. Kinetic evidence for a reversibly formed bromonium ion in the reaction of bromine with tetraisobutylethylene *J. Am. Chem. Soc.* **1990**, *112*(17), 6310-6316.

34. Gupta, V.; Nivarthi, S. S.; McCormick, A. V.; Davis, H. T. Evidence for single file diffusion of ethane in the molecular sieve AlPO4-5. *Chem. Phys. Lett.* **1995**, *247*, 596-600.

PREPARATION OF MESOPOROUS MATERIALS BEARING GLYCIDOXYPROPYL FUNCTIONAL GROUPS AND IMMOBILIZATION OF ACTIVE GROUPS

Abstract

Hexagonal mesoporous silicas chemically modified with 3-Glycidoxypropyl moieties were synthesized through the post-synthesis of surfactant free mesoporous silica, OSU-6-W, with the silylating agent 3-Glycidoxypropyltrimethoxysilane (GPTMS). From this silylating agent the OSU-6-W-GPTMS-(1&2) inorganic-organic hybrids were synthesized. The solid state ^{29}Si NMR, titration method and elemental analysis of the two modified samples, OSU-6-W-GPTMS-1 and OSU-6-W-GPTMS-2, showed that the average number of pendant groups in these hybrids were around 2.17 and 3.49 group/nm^2 and from the surface area analysis these materials have pore diameters of 40.7 and 33.2 Å and surface areas of 966 and 720 m^2/g, respectively. Infrared spectroscopy, solid state nuclear magnetic resonance for ^{13}C and ^{29}Si nuclei and X-ray diffraction patterns are in agreement with the success of the proposed synthetic procedures, as confirmed for the formation of the mesoporous hybrids.

The functional group 3-Glycidoxypropyl has the epoxide ring opened by incorporating pyrazole (Py), 5-Aminotetrazole (ATZ), Adenine (Ad), and

ethylenediamine (Da) molecules under heterogeneous conditions, to yield a new functional groups anchored on the mesoporous surface. Based on elemental analysis for carbon and nitrogen a large degree of immobilization is observed, a drastic decrease in surface area of the original silica is observed for the immobilized surface. The heterogeneous route is an easier procedure to produce immobilization. All products were characterized through infrared spectroscopy, elemental analysis and surface area measurement.

The basic centers attached on pendant groups have the capacity to extract cations from aqueous solution, whose adsorption process is adjusted to the Langmuir model. Similar profile of adsorption was obtained on the isotherm with value 6.75 mmol g^{-1} in the maximum of the curve for copper.

7.1. INTRODUCTION

7.1.1. Grafting of the Functional Group

The covalent grafting of organic molecules with desired functions onto a variety of inorganic surfaces can be designed in order to embrace characteristics having significant practical advantages, such as improved structural and thermal stability, swelling behavior, accessibility to the reactive centers, and insolubility in organic and aqueous solvents.[1-3] The development of new inorganic-organic hybrids with the ability to synthesize porous solid structures on nanometer scale, resulting in mesoporous silicates, which available pendant groups are useful to coordinate metal ions. This behavior provides a special approach in the green chemistry field as catalysis and for removal of contaminants.[4-7] Among many inorganic materials able to bind covalently organic compounds, mesoporous silica material is highly explored not only due to its

high thermal and chemical stabilities, but also in considering its large surface area, and its associated properties.[1,6,7] Moreover, the success of such reactivity is due to the presence of high concentrations of silanol (Si-OH) groups on its surface, which enables the immobilization of a great number of organic molecules.[8] However, a series of mesoporous silicate structures can be available by exploring reaction conditions with appropriated structure directors.[9]

7.1.2. Immobilization of Organic Active Groups

Materials containing glycidyl functional groups have proven extremely popular for the attachment of various reactive groups and ligands due to the facile nucleophilic ring-opening reaction of the pendant epoxide functionality.[10-12] Amines react to yield materials with favorable ex-change kinetics for transition metal ions, due to the hydrophilic character of the resultant material, since the ring-opening reaction generates a hydroxyl group on the carbon atom β to the incoming amine.[13-16] This group makes this site rather hydrophilic, and is believed to make these materials particularly effective in applications involving the treatment of aqueous feed streams for metal-ion recovery. It is much less clear whether this hydroxy group is able to function as an additional binding site for chelation of metals.[17]

7.2. AIM OF STUDY

The purpose of this investigation was to develop a post-synthesis method to prepare mesoporous silica with grafted chelating agents for complexing metal ions. This post-synthesis method should increase the functional group coverage and maintain the pore size as large as possible. To realize these objectives, two synthetic procedures were developed using two different grafting methods. Moreover, the further modification of

the glycidoxypropyl functional groups with special active groups for specific application

such as adsorption of divalent transition metal from aqueous solution was targeted.

7.3. EXPERIMENTAL

7.3.1. Materials

All reagents and solvents were purchased from commercial sources and were used

as received unless otherwise mentioned. The chemical are 3-

glycidoxypropyltrimethoxysilane (GPTMS) [98.0% Aldrich], *N,N*-dimethylformamide

(DMF), 3-hydroxypropionitrile (3-HPN), pyrazole (Py), 5-aminotetrazole (ATZ), and

adenine (Ad), boron trifluoride diethyl etherate ($BF_3 \cdot OEt_2$), toluene (99.8% HPLC grade),

ethyl alcohol, dry methanol, triethylamine (TEA) [99% Aldrich], dichloromethane

(99.6% Aldrich), 96% sulfuric acid, thiourea, sodium carbonate (Na_2CO_3, 0.8 *M*), and

distilled deionized water. Molecular sieves (5A, beads, 4-8 mesh) were used to dry

solvents. The structures of some of these compounds are shown in Scheme 7.1.

3-Glycidoxypropyltrimethoxysilane (GPTMS)   Pyrazole

5-Aminotetrazole   Adenine
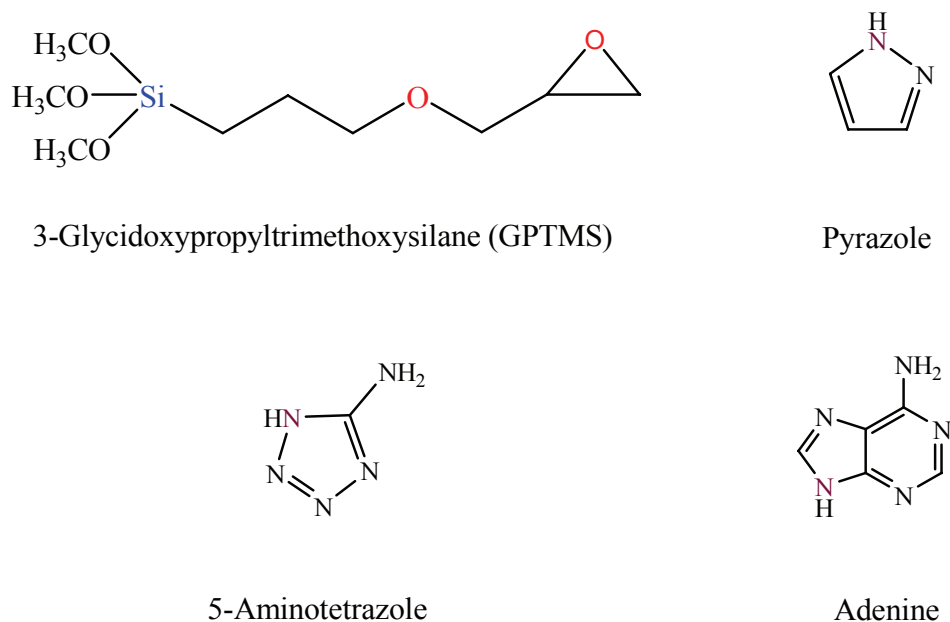
Scheme 7.1. The structures of some chemicals used in this work.

7.3.2. Characterization

The main products were characterized using several techniques including X-ray powder diffraction (XRD), N_2 adsorption-desorption analysis (BET), Solid-state ^{13}C and ^{29}Si MAS NMR spectroscopy, Diffuse reflectance infrared Fourier transform (DRIFT) spectroscopy, UV-Vis spectrometer, and Elemental analysis. The full details of sample preparation and instrument operation were mentioned previously in chapter two and three of this thesis.

7.3.3. Preparation

7.3.3.1. Activation of the Mesoporous OSU-6-W

OSU-6-W mesoporous silica material was synthesized as discussed in chapter two of this thesis. It was activated by refluxing with dry toluene and then reaction with triethylamine (TEA) as described in chapter five.

7.3.3.2. Surface Modification of Mesoporous Materials with Glycidoxypropyl Functional Groups

3-Glycidoxypropyl-functional group was chemically attached to the mesoporous OSU-6-W material surfaces by means of the post-synthesis grafting method. Two synthetic procedures were applied which are based on a combination of different synthetic methods used by previous researchers.

I. Grafted of the mesoporous silica with 3-Glycidoxypropyltrimethoxysilane (GPTMS) in a one step reaction (OSU-6-W-GPTMS-1)

Mesoporous silica-supported glycidoxypropyl groups was prepared by refluxing 3.0 g (~ 50 mmol) of the activated mesoporous silica (TEA-OSU-6-W) with 12.0 ml (~ 50 mmol) of 3-glycidoxypropyltrimethoxysilane (GPTMS) in 100 ml of dry toluene in a

250-ml round-bottom flask for 48 hours under dry atmosphere. An illustration of the

reaction is schematically represented in Scheme 7.2. The resulting solid mixture was

filtered off with a fine filter funnel, washed three times (3 X 50 ml) with toluene and then

ethanol, to rinse away any surplus GPTMS. The white solid was dried at 80 °C under

vacuum for 24 hours to yield 4.74 g. IR (cm^{-1}) (KBr): 3737(m), 3660(m, br), 3237(s, br),

2991(m), 2957(s, sh), 2893(m), 2853(m), 1630(m, sh), 1463(m, sh), 1372(w), 1266(s,

sh), 1224(s, br), 1148(s, br), 1061(s, br), 946(s), 808(s), 666(w), 574(w), and 490(w).

Solid-state ^{29}Si CP/MAS NMR resonances in δ (ppm) are -48.0 (T^1), -57.3 (T^2), -67.1

(T^3), -101.5 (Q^3), and -109.4 (Q^4). Solid-state ^{13}C CP/MAS NMR resonances in δ (ppm)

are 8.9 ($\equiv$Si-CH_2-CH_2-)[1], 21.7 ($\equiv$Si-CH_2-CH_2-)[2], 23.6 ($\equiv$Si-OCH_3), 72.1 ($\equiv$Si-CH_2-

CH_2-CH_2-O-)[3] and ($\equiv$Si-CH_2-CH_2-CH_2-O-CH_2)[4], 52.5 ppm ($\equiv$Si-$CH_2CH_2CH_2$-O-

$CH_2CH[O]CH_2$)[5], 42.0 ppm ($\equiv$Si-$CH_2CH_2CH_2$-O-$CH_2CH[O]CH_2$)[6], and 64.2 ppm,

see Scheme 7.2. Elemental analysis: C (17.36%) and N (0.08%).
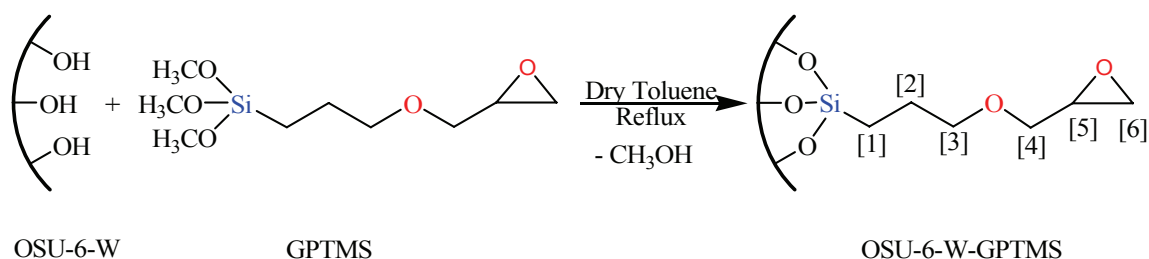
Scheme 7.2. The reaction scheme between GLYMO and silanol groups on the OSU-6-W
surface. The final product has numbers that illustrate carbon atoms positions as described
in the ^{13}C CP/MAS NMR.

II. Grafting of the Mesoporous Silica with 3-Glycidoxypropyltrimethoxysilane (GPTMS) in three Modification Reaction Steps (OSU-6-W-GPTMS-2)

A second glycidoxypropyl functionalized mesoporous silica was prepared using two silylation steps similar to that described above. In between the two silylation steps the material was stirred with 50 ml of distilled water for five hours, to hydrolysis the methoxy groups left from the fist step. The yield was dried at 80 °C under vacuum for 24 hours. The final yield was 5.98 g of white solid. IR (cm^{-1}) (KBr): 3628(m, br), 3376(m), 3295(m), 2923(s, sh), 2854(s, sh), 1456(m, sh), 1351(vw), 1249(s, sh), 1138(s, br), 1077(s, br), 969(m), 797(m, sh), 679(m), 575(m), and 499(m). Solid-state ^{29}Si CP/MAS NMR resonances in δ (ppm) are -57.2 (T^2), -65.0 (T^3), -100.4 (Q^3), and -108.7 (Q^4). Solid-state ^{13}C CP/MAS NMR resonances in δ (ppm) are 8.1 (≡Si-*C*H$_2$-CH$_2$-)[1], 22.1 (≡Si-CH$_2$-*C*H$_2$-)[2], 71.4 (≡Si-CH$_2$-CH$_2$-*C*H$_2$-O-)[3], 73.3 (≡Si-CH$_2$-CH$_2$-CH$_2$-O-*C*H$_2$)[4], 52.2 ppm (≡Si-CH$_2$CH$_2$CH$_2$-O-CH$_2$*C*H[O]CH$_2$)[5], 39.9 ppm (≡Si-CH$_2$CH$_2$CH$_2$-O-CH$_2$CH[O]*C*H$_2$)[6], and 56.6 ppm, see Scheme 7.2. Elemental analysis: C (22.24%) and N (0.11%).

7.3.3.3. Conversion of the Glycidyl Groups in the Modified OSU-6-W-GPTMS into A Thiirane Analogue

In a 250 ml Erlenmeyer flask, a 1.0 ml (20 mmol) solution of 96% sulfuric acid, H$_2$SO$_4$, in 100 ml of distilled water was stirred with 2.0 g of OSU-6-GPTMS-2 and 3.0 g (40 mmol) of thiourea at room temperature for 24 hours, Scheme 7.3 illustrates the chemical reaction. The solid product was filtered off and washed with distilled water (3 X 50 ml). It was then stirred gently in a solution of 0.8 *M* sodium carbonate, Na$_2$CO$_3$, (11.0 g, 100 mmol in 80 ml of distilled water) at room temperature for 24 hours. The

solid was collected again by filtration, washed with water (3 x 100 ml) and ethanol (50 ml) before drying initially at room temperature for 24 hours, and then at 70 °C under vacuum for 6 hours. The solid product was designated as OSU-6-W-Thiirane. The IR (cm^{-1}) (KBr): 1480, 1440, 1340, 1330, 910, 850, and 620 cm^{-1}.[17,18]
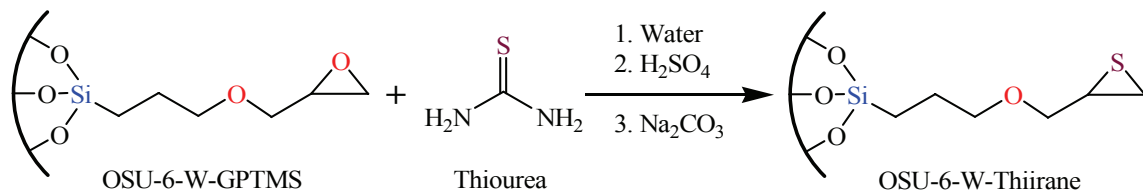
Scheme 7.3. Conversion of Epoxides Groups into Thiirane Analogue.

7.3.3.4. Modification of OSU-6-W-GPTMS-2 with 3-Hydroxypropionitrile (3-HPN)

Introduction of cyano function groups to the silica surface was prepared following the procedure by Allen *et al.,*[19] with minor changes. The preparation steps are as follows. A sample of 1.0 g of OSU-6-W-GPTMS-2 was added to 25 ml of *N,N*-dimethylformamide (DMF) in a 125-ml, Erlenmeyer flask and was stirred for one hour at room temperature. 0.5 g of 3-hydroxypropionitrile (3-HPN) and 0.2 g of boron trifluoride (BF$_3$) diethyl etherate were added to the mixture and stirring was continued for three hours at room temperature, Scheme 7.4. The reaction was stopped and the resulting solid was filtered off, washed three times with 25 ml of DMF, and dried under vacuum for 24 hours. The reaction yielded 1.13 g of the OSU-6-W-GPTMS-2-HPN product. IR (cm^{-1}) (KBr): 3556(m, sh), 3332(s, br), 2981(s), 2942(s), 2886(m), 2292(s), 1457, 1401, 1356, 1091, and 885.
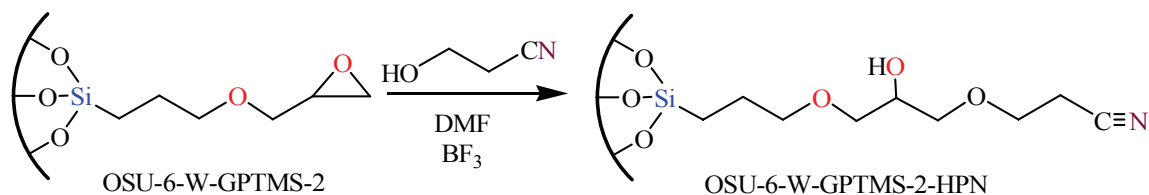
Scheme 7.4. Schematic illustration of the chemical reaction for the preparation of the OSU-6-W-GPTMS-2-HPN sample.

7.3.3.5. Modification of OSU-6-W-GPTMS-2 with Pyrazole (Py), 5-Aminotetrazole (ATZ), and Adenine (Ad)

Immobilization of the ligands pyrazole (Py), 5-aminotetrazole (ATZ), and adenine (Ad) took place in toluene and were performed using the same procedure reported by Moore *et al.,*[17,18] and yielded the chelating ion-exchange silicas OSU-6-W-GPTMS-2-Py, OSU-6-W-GPTMS-2-ATZ, and OSU-6-W-GPTMS-2-Ad, respectively, see Scheme 7.5.

The procedure used in attaching all the ligands is as follows; 1.0 g of OSU-6-W-GPTMS-2 was stirred with 5.0 g of the ligand in 100 ml of dry toluene in a 250-ml round-bottom flask at 100 ^{o}C for 24 hours. The modified solid was filtered off, washed with ethanol (3 x 50 ml) and water (3 x 50 ml), and then stirred with water (100 ml) at room temperature for 6 hours. The modified solids were collected and dried at room temperature for 24 hours and will be referred to as OSU-6-W-GPTMS-2-Py, OSU-6-W-GPTMS-2-ATZ, and OSU-6-W-GPTMS-2-Ad, respectively. IR spectrum (KBr, cm^{-1}) of OSU-6-W-GPTMS-2-Py: 1645, 1566, 1512 (C=C, C=N), 3517 (O-H), IR spectrum (KBr, cm^{-1}) of OSU-6-W-GPTMS-2-ATZ: 1632, 1579, 1501 (N-H, C=N), 3503 (O-H), and IR

spectrum (KBr, cm^{-1}) of OSU-6-W-GPTMS-2-Ad: 1625, 1558, 1514 (N-H, C=C, C=N), 3527 (O-H).
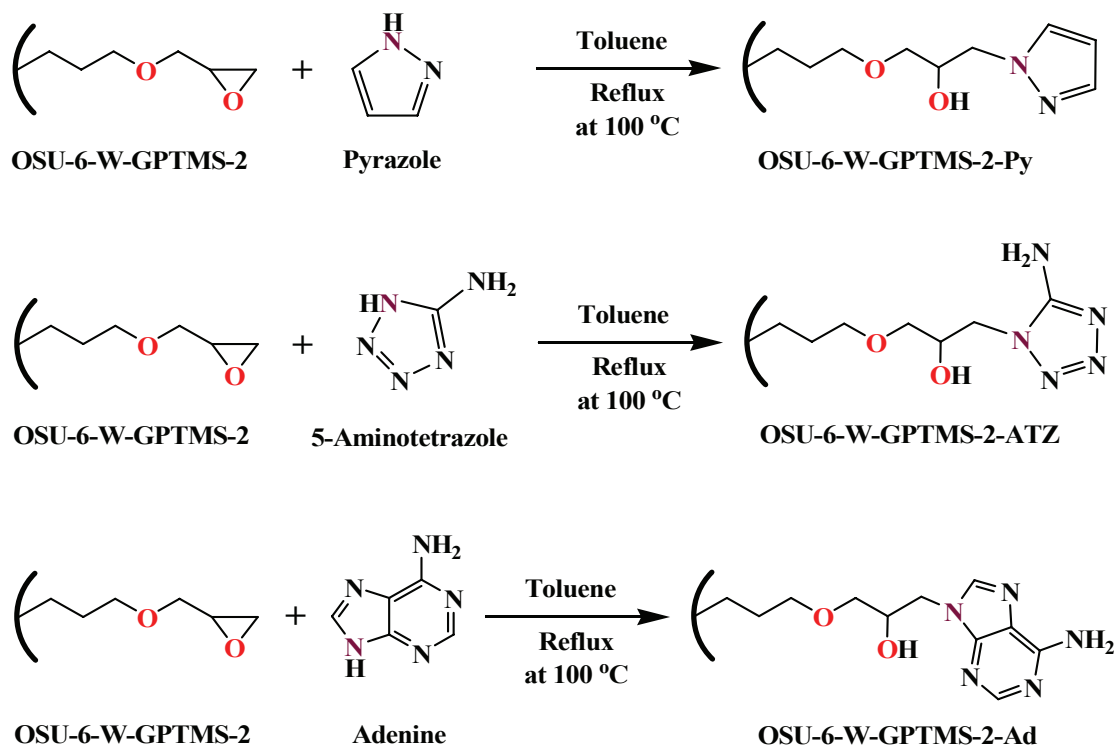
Scheme 7.5. Chemical reaction equations for the preparation of the modified samples.

7.3.3.6. Immobilization of Ethylenediamine (En)

The ethylenediamine molecule was incorporated onto the silica gel surface by a heterogeneous route.[20] This procedure consisted of suspending 0.5 g of OSU-6-W-GPTMS-2 in a solution of 1.5 ml (23.0 mmol) of the ethylenediamine and 50 ml of dry methanol. The mixture was refluxed under dry atmosphere for 48 hours. After words, the solid was filtered, washed with methanol and dried under vacuum for 24 hours, to

give the product named OSU-6-W-GPTMS-En. Scheme 7.6 illustrates the route employed in this preparation. The IR peaks in cm^{-1} (KBr): 3250, 1610, 1577, 1436 cm^{-1}.
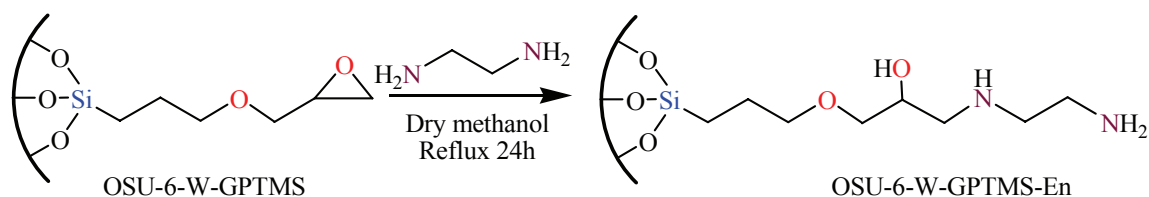
Scheme 7.6. Immobilization of the ethylenediamine on glycidoxy-functionalized mesoporous material.

7.3.4. Determination the Total Surface Loading of the Ordered Mesoporous Silica with the Glycidoxypropyl Functional Groups

I. Titration Method

There is a broad range of analytical techniques available for the quantitative determination of the glycidoxypropyl functional groups (oxirane functions).[21] In the case of surface-bonded groups, a decrease in reactivity had to be expected and, therefore, the most efficient procedure was selected after testing several possibilities found in the literature.[21,22]

I.1. Titration with Sodium Thiosulphate

This method was used only for epoxy-activated silicas. A 0.25 g amount of the modified samples were added to a saturated aqueous solution of sodium thiosulphate and stirred for 24 hours. The epoxide groups react as shown in Scheme 7.7.[23]

a)

Excess
Na$_2$S$_2$O$_3$
H$_2$O

OSU-6-W-GPTMS

OH

SSO$_3$Na

+

NaOH

b)

NaOH
+
phenolphthalein

0.01 M HCl

NaCl + H$_2$O

(Red)

(Colorless)
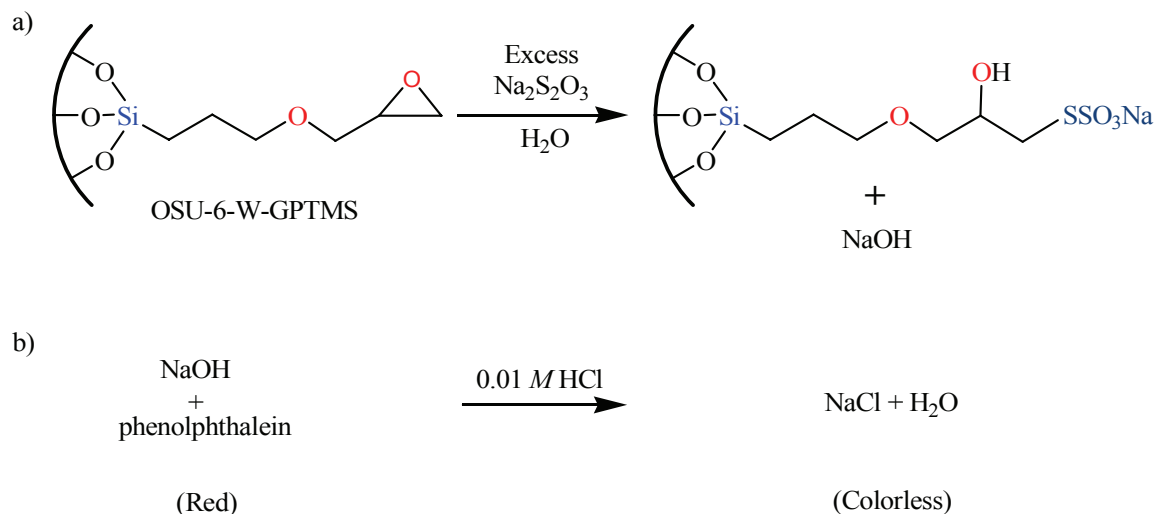
Scheme 7.7. Reaction of glycidoxypropyl functional group with sodium thiosulphate and production of sodium hydroxide (NaOH).

The resulting NaOH was titrated with 0.01 M HCl in the present of phenolphthalein indicator. The amount of HCl required for titration is equal to the amount of attached epoxides. The result showed good agreement with the results from other methods for determining the number of epoxides present.

In this method, the total amounts of hydrochloric acid used to reach the end point were 3.88 and 4.50 mmol/g for OSU-6-W-GPTMS-1 and OSU-6-W-GPTMS-2, respectively.

The surface coverage (C) was calculated by dividing the loading (l) by the specific surface area (S_{BET}) of the sample. Multiplication by Avogadro's number ($N_A = 6.022 \times 10^{23}$ molecules/mole) yielded units of molecules/nm^2:[24]

$$C = (l \,/\, S_{BET}) \cdot N_A$$

II. Elemental Analysis (Combustion Analysis) Method

Carbon analysis was carried out for both modified samples. The concentration of the attached groups was calculated as follows:[25,26]

$$C \text{ (groups/nm}^2) = 6 \times 10^5 \, P_C / [(1200 n_C - W P_C) S_{BET}]$$

where C is the concentration of attached groups, which contain carbon; P_C is the percentage of carbon in the sample, n_C is the number of carbon atoms in the attached group (counted as C_6), W is the corrected formula mass of the modifier (counted as $C_6H_{11}O_5Si$), and S_{BET} is the specific surface area of the unbonded substrate (1283 m^2/g). The total carbon concentrations are 17.36% and 22.24% for OSU-6-W-GPTMS-1 and OSU-6-W-GPTMS-2, respectively.

III. Solid state ^{29}Si CP/MAS NMR Spectrum

The solid state ^{29}Si NMR is used to determine the total coverage as described in chapter three. The relative peak areas of the ^{29}Si spectra required for this method are given in Table 7.1.

Table 7.1. Solid state ^{29}Si CP/MAS NMR deconvolution results

Sample	Q^4 (%)	Q^3 (%)	Q^2 (%)
OSU-6-W	14.38	71.73	13.89
OSU-6-W-GPTMS-1	50.68	49.32	0.00
OSU-6-W-GPTMS-2	69.23	30.77	0.00

7.3.5. Metal Uptake Experiments

The adsorption and separation experiments were conducted as follows; five different amounts in the range of 25-125 mg of the functionalized mesoporous silica, OSU-6-W-GPTMS-2, was shaken for 4 hours with 10 ml of a 100 ppm aqueous solution of Cu^{2+} in a 20-ml glass vial. Measurement of the metal ion concentration was carried out by allowing the insoluble complex to settle and filtering the supernatant with a 0.45μm membrane syringe filter. The metal ion uptake was calculated as mmol of M^{2+}/g of ligand. A linear range of the calibration curve was used in order to calculate the unknown concentration.

7.4. RESULTS AND DISCUSSION

GPTMS is exceptional among other silanes used to prepare bonded phases in the sense that the oxirane ring is highly reactive.[27] Functionalization with this reagent can be accompanied by formation of some by-products whose formation are highly pH and temperature dependent: All of the by-products may be expected to be less hydrophilic. For example, methanol formed by hydrolysis of GPTMS may participate in oxirane opening and form the corresponding glycol ethers that may further react with other oxirane rings leading to polymerization. Both bonded and unbonded GPTMS molecules may participate in these reactions. Initially, the starting silane is hydrolyzed to the trisilanol. Polymerization of these results in cyclic oligosiloxanes that could compete with the surface bonding reaction and these cyclic siloxane structures may be also became bonded to the silica surface.[28]

The complexity of the bonding reaction may be responsible for the differences in ionic and hydrophobic interactions among diol phases of a different origin.[29]

Hydrophobic interactions arise from hydrocarbon spacer groups with the number of hydroxy groups play a significant role in hydrophilicity.[30] Previously the functionalization reaction was studied in detail; bonded oxirane, vicinal diol, total hydroxy and CH contents were determined as a function of temperature, pH and time.[31] The aim was to find conditions giving the maximum surface coverage of oxirane groups on silica (epoxy activation).

The problems that lead to the unhydrolyzed and unreacted of the methoxy groups with surface hydroxyls may be due to the weak interaction of these groups with other silanes. These groups shield the surface hydroxyls to some extent from oncoming silanes as well. Therefore, the presence of an amine catalyst will facilitate the interaction and hydrolysis of the methoxy groups. Likewise, if water is present in the solution, hydrolysis of some methoxy groups will allow their polymerization in the solution or start vertical polymerization outward from the surface immobilized silanes. The new grafting procedure suggested here is basically concerned about hydrolysis of methoxy groups of only immobilized glycidoxypropyl functional groups after initial silanization and washing. The resulting hydroxyls resolve the two problems mentioned above as well as eliminate the unwanted vertical polymerization. Alternating silanization and washing in water enhances the maximum surface density of silanes by at least 30%.[32] Moreover, it appears that one treatment in water produces as large an effect as a few consecutive ones and the vertical polymerization, which could in theory start from unreacted methoxy groups after the second silanization, does not take place. Another problem is the steric hindrance of the incoming groups experianc from already bound groups that might

prevent them from reaching even higher surface concentration, *i.e.* surface coverage might not reflect the surface glycidoxypropyl concentration accurately.[33]

The ordered mesoporous silicas, OSU-6-W modified with glycidoxypropyl functional groups were prepared by post-synthesis method from the reaction of OSU-6-W with 3-glycidoxypropyltrimethoxysilane (GPTMS) using the two grafting procedures discussed in previous chapters.

7.4.1. Identification of Textural Properties

I. X-ray Powder Diffraction (XRD)

The pristine ordered mesoporous material, OSU-6-W, and the functionalized samples with GPTMS (OSU-6-W-GPTMS-1 and OSU-6-W-GPTMS-2) were characterized by the XRD. The X-ray diffraction patterns (XRD) in the range of 1.0-10.0º are shown in Figure 7.1. The XRD pattern of the unmodified OSU-6-W sample, as shown in figure 7.1 (A), shows three well-resolved diffraction peaks in the region of $2\theta = 1–5°$, which can be indexed to the (100), (110), and (200) diffractions, characteristic of the formation of well-arranged hexagonal mesostructure.[34] It can be noted that the (100) peak gradually shifts to higher angles with increasing of the functional groups on the surface from OSU-6-W-GPTMS-1 to OSU-6-W-GPTMS-2, indicating an effective decrease of OSU-6-W pore diameter. The pore size of OSU-6-W was narrowed from *ca.* 51.1 Å to *ca.* 40.7 Å in OSU-6-W-GPTMS-1 and to *ca.* 33.2 Å in OSU-6-W-GPTMS-2. The XRD patterns of the functionalized samples show less intense XRD peaks, suggesting that the modification process in the channels affects the framework integrity of the ordered mesoporous OSU-6-W. Nevertheless, the existence of characteristic diffraction peaks in both functionalized samples indicates the long-range order of

mesoporous hexagonal channels was still maintained after modification. Combination of

the XRD results with the average pore diameters from surface area measurements

demonstrates an average thickening of the walls of about 25.9 Å in the case of OSU-6-W-

GPTMS-2, which statistically would correspond to an extra one layer of Si-O-Si

homogeneously spread on the original wall (20.9 Å). It also can be noticed that the d_{100}

peak has become broader with the increase in the loading of the functional groups,

indicating a slight alteration of the ordering of the mesoporous structure as more

functional groups are added to the surface.
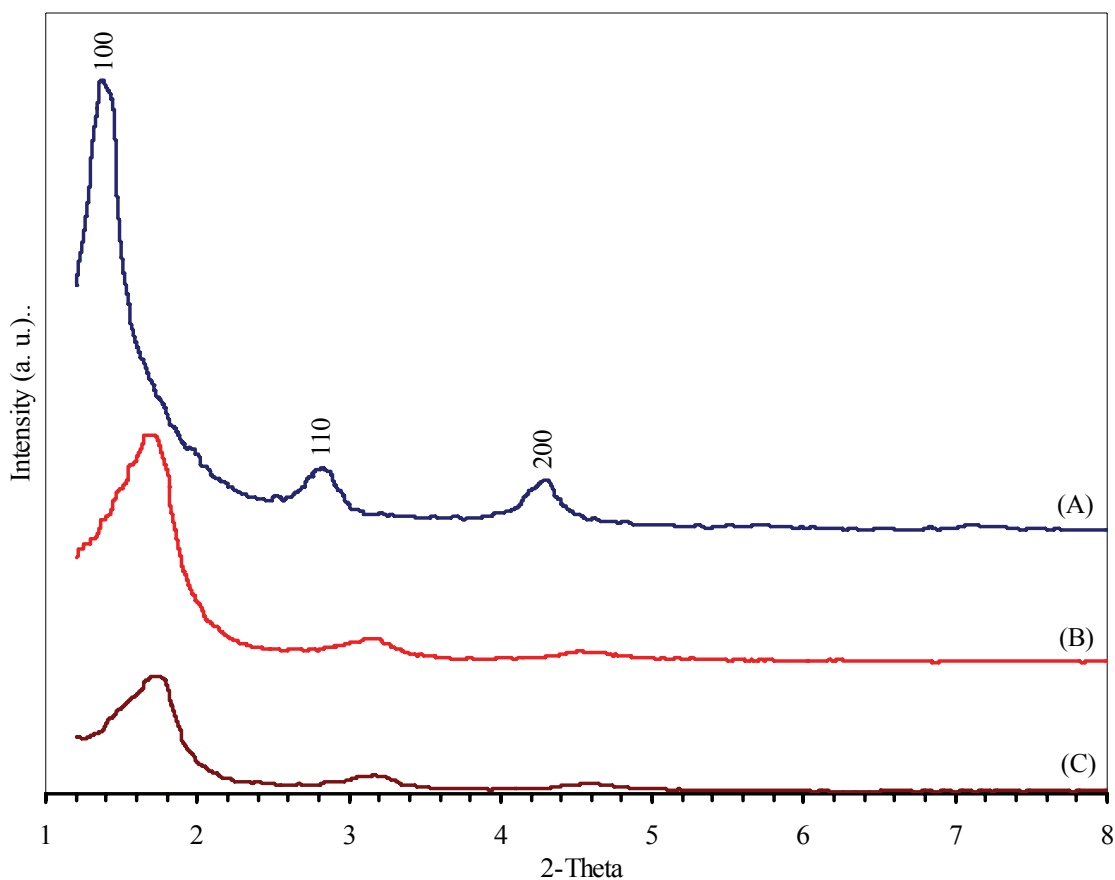
Figure 7.1. XRD patterns in the range of 1.0-10.0º of; (A) pristine ordered mesoporous
material, OSU-6-W, (B) OSU-6-W-GPTMS-1, and (C) OSU-6-W-GPTMS-2. The
spectra are shifted vertically for the sake of clarity.

II. Nitrogen Adsorption-Desorption Measurements

Figure 7.2 shows the nitrogen adsorption-desorption isotherms for the mesoporous silicas. The textural properties of the materials are summarized in Table 7.2. The curves are typical for mesoporous materials with hexagonal channel arrays.
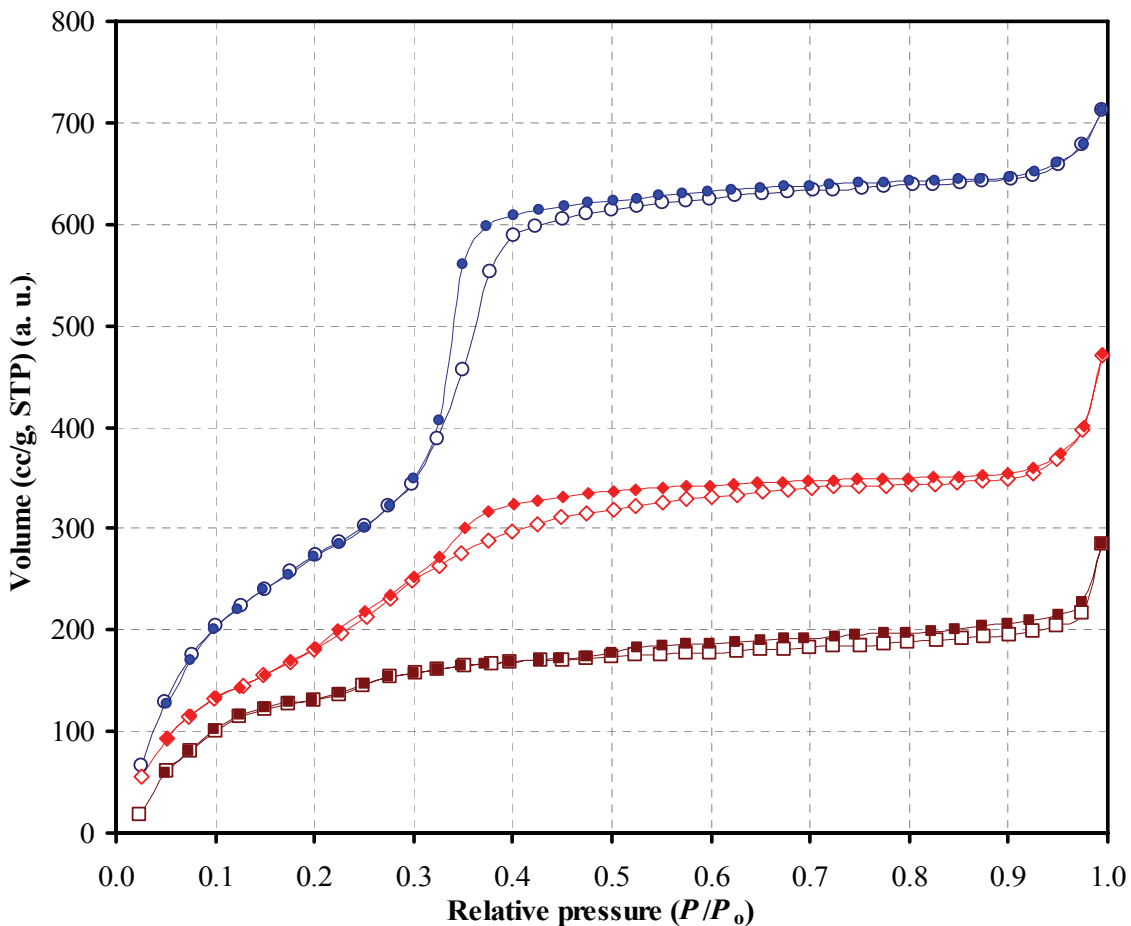
Figure 7. 2. Nitrogen adsorption-desorption isotherms of (○) OSU-6-W, (◊) OSU-6-W-GPTMS-1, and (□) OSU-6-W-GPTMS-2. Open symbols: adsorption; closed symbols: desorption. The isotherm data are shifted vertically for the sake of clarity.

After reaction with the coupling agent, the nitrogen adsorption-desorption experiments yielded a BET surface area of 966 m^2/g and a total pore volume of 0.92

cm^3/g for the OSU-6-W-GPTMS-1 sample, and a surface area of 720 m^2/g and a total

pore volume of 0.58 cm^3/g for the OSU-6-W-GPTMS-2 sample. The uptake

corresponding to the filling of the mesopores has shifted to lower relative pressures

indicating a reduction of the pore diameter (from 51.1 to 40.7 Å for OSU-6-W-GPTMS-1

and from 51.1 to 33.2 Å for OSU-6-W-GPTMS-2).

Table 7.2. Textural Properties Determined from Nitrogen Adsorption-desorption
Experiments at 77 K and Powder XRD Measurements.

Sample	Specific surface area (m^2/g)	Total pore volume (cm^3/g)	Average pore size (Å)	d_{100} (Å)	Wall Thickness (Å)
OSU-6-W	1283	1.24	51.1	62.4	21.0
OSU-6-W-GPTMS-1	966	0.92	40.7	54.6	22.4
OSU-6-W-GPTMS-2	720	0.58	33.2	51.2	25.9

Figure 7.3 presents the pore size distribution measurements of all three samples;

OSU-6-W, OSU-6-W-GPTMS-1, and OSU-6-W-GPTMS-2. It shows that for the un-

functionalized sample, OSU-6-W, the pore size distribution is a fairly narrow 3.5 Å wide.

After functionalization with the 3-glycidoxypropyltrimethoxysilane, the pore size

distributions of both functionalized samples were larger than the un-functionalized

sample. However, their pore size distributions consider to be narrow with about 7.0 Å

wide for both samples.
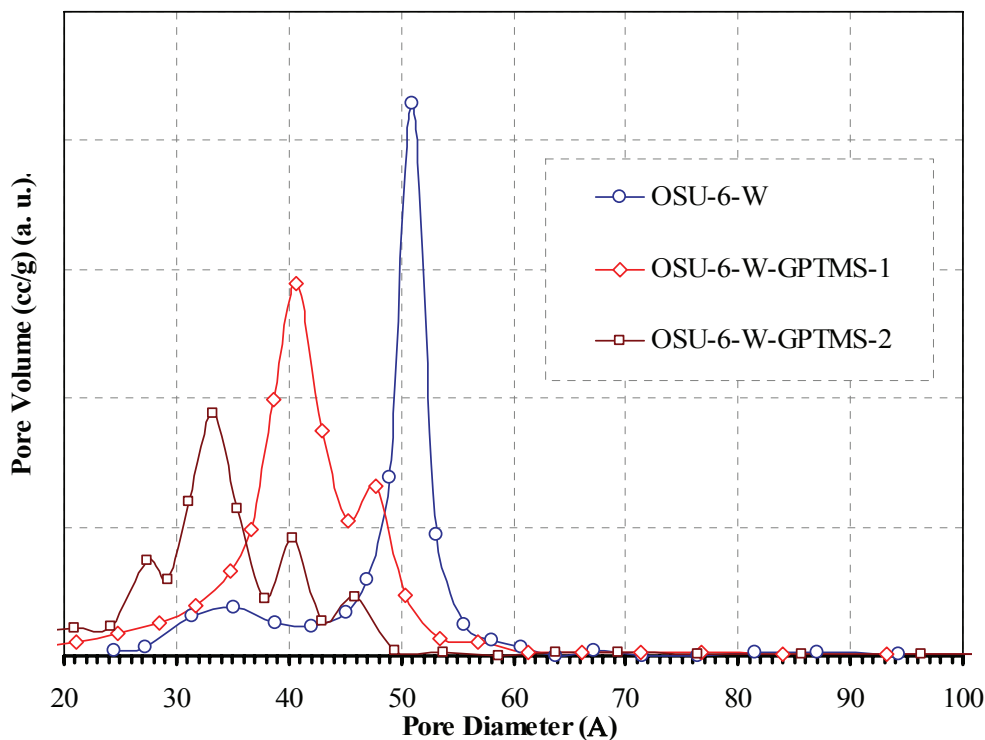
Figure 7. 3. The pore size distribution of (○) OSU-6-W (max at 51.1 Å), (◊) OSU-6-W-GPTMS-1 (max at 40.7 Å), and (□) OSU-6-W-GPTMS-2 (max at 33.2 Å)

7.4.2. Identification of the Functional Groups

I. Solid State ^{29}Si CP/MAS NMR Spectroscopy

Solid state ^{29}Si NMR measurements were performed in order to determine the surface structure of OSU-6-W after modification. Solid state ^{29}Si CP/MAS NMR peak assignments are described as previously reported by Glaser *et al.,*[35] for organically modified silicates. Figure 7.4 displays the solid state ^{29}Si CP/MAS NMR spectra of OSU-6-W without and with surface modification (OSU-6-W-GPTMS-1 and OSU-6-W-GPTMS-2), also with the chemical shift assignments for the observed resonances. The ^{29}Si CP/MAS NMR spectrum of OSU-6-W showed signals of Q^4 species (*Si*(OSi)$_4$) at *ca.*

-107.9 ppm, Q^3 species (Si(OSi)$_3$OH) at *ca.* -100.4 ppm, and shoulder Q^2 species

(Si(OSi)$_2$(OH)$_2$) at *ca.* -91.2 ppm.
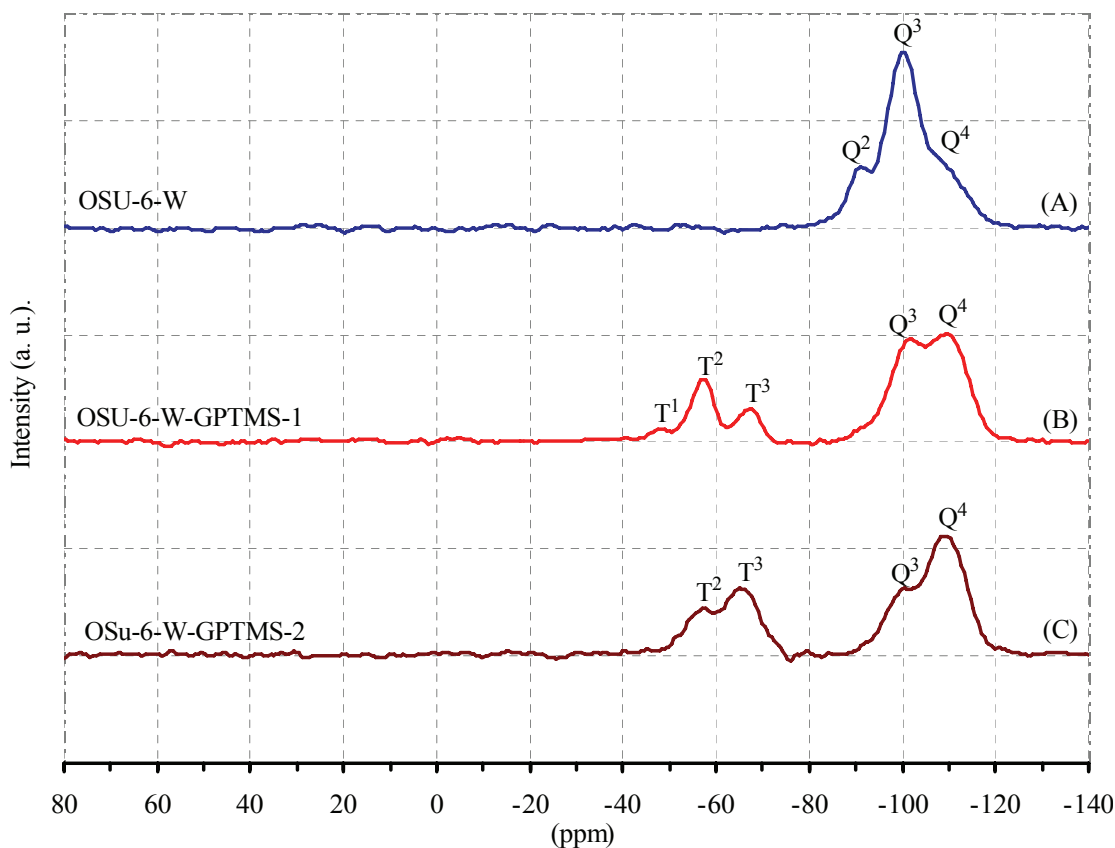
Figure 7.4. Solid state ^{29}Si CP/MAS NMR spectra of (A) Un-modified OSU-6-W, (B) OSU-6-W-GPTMS-1, and (C) OSU-6-W-GPTMS-2.

The ^{29}Si CP/MAS NMR spectrum of OSU-6-W-GPTMS-1 showed three signals

at -48.0(T^1), -57.3(T^2), and -67.1(T^3) ppm, while OSU-6-W-GPTMS-2 showed two

signals at -57.2 (T^2), -65.0 (T^3), corresponding to T^1 (RSi(OSi)(OH)$_2$), T^2 (RSi(OSi)$_2$OH),

and T^3 (RSi(OSi)$_3$) groups. R here represents the alkyl group belonging to GPTMS.

Besides those peaks, each modified sample also showed two peaks corresponding to Q^3

and Q^4 silicons. The OSU-6-W-GPTMS-1 modified sample shows relative intensity ratios for $T^1 : T^2 : T^3$ close to 1.0 : 9.6 : 5.1. However, the OSU-6-W-GPTMS-2 modified sample shows relative intensity ratio for $T^2:T^3$ close to 1.0:1.9. These NMR results reveal that the silanol groups on the OSU-6-W surfaces are highly accessible to the modification reagent, GPTMS.

II. Solid State ^{13}C CP/MAS NMR Spectroscopy

An important feature to enrich information about the attachment of the pendant groups in the inorganic structure of the hybrid is the ^{13}C NMR spectra in the solid state.[1,6,36] Solid state ^{13}C CP/MAS NMR peak assignments for glycidoxypropyl functional groups used in this study are based on those previously reported.[39]
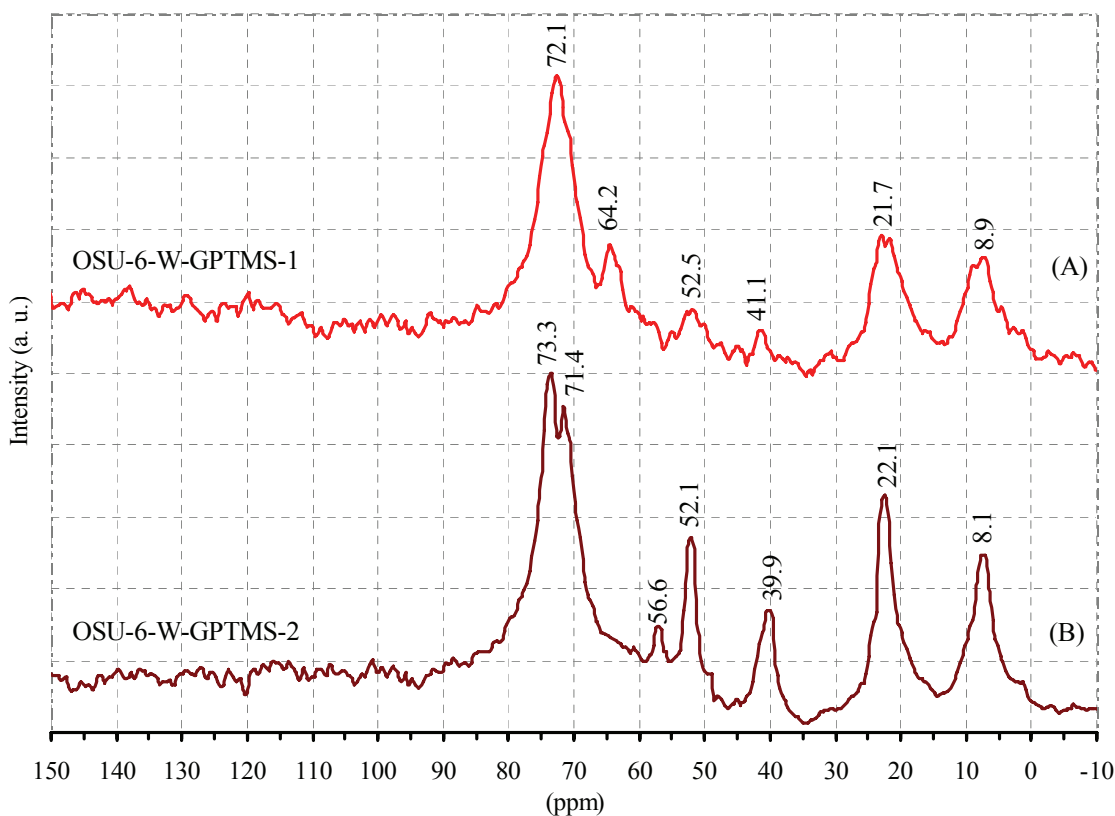
Figure 7.5. Solid state 13C CP/MAS NMR spectrum of (A) OSU-6-W-GPTMS-1, and (B) OSU-6-W-GPTMS-2.

Figure 7.5 shows the ^{13}C CP/MAS NMR spectrum of OSU-6-W-GPTMS-1 and OSU-6-W-GPTMS-2, together with the assignment of the main peaks. Two distinct peaks for the carbon atoms of the epoxy ring, of the glycidoxypropyl unit, were still observable at 42.0(C6) and 52.5(C5) ppm for OSU-6-W-GPTMS-1 sample and at 39.9(C6) and 52.2(C5) ppm for OSU-6-W-GPTMS-2 sample, indicating that most of the reactive epoxy rings were retained under the reaction conditions. Another remarkable feature was the appearance of the peak at 64.2 ppm and a broad shoulder at around 72.1 ppm, that can be assigned to either carbons of methylether and oligo- or poly(ethylene oxide) derivatives, respectively in case of OSU-6-W-GPTMS-1. These originate from the side reactions of the epoxy ring of GPTMS.[37] OSU-6-W-GPTMS-2 also displayed a peak at 56.6 ppm and one split peak at around 71.4 and 73.3 ppm, that can be assigned to either carbons of methylether and oligo- or poly(ethylene oxide) derivatives.[37]

III. Fourier Transform Infrared Spectroscopy (FT-IR)

Infrared spectroscopy was employed as an important tool to characterize the main products of such reactions.[38] The vibrational spectra obtained from solid samples confirmed the success of the grafting reactions, which sequence of bands are very close to those observed, when glycidoxypropyl functional groups was previously incorporated into a similar materials.

The infrared spectra, Figure 7.6, of OSU-6-W prior to and following grafting by 3-glycidoxypropyltrimethoxysilane (GPTMS) show several silanol bands at 3667, 3647, and 3436 cm^{-1} that are not well resolved in the spectrum of OSU-6-W and OSU-6-W-GPTMS-1 also have a sharp absorption is observed at 3746 cm^{-1} due to non-hydrogen bonded silanols.[39,40]
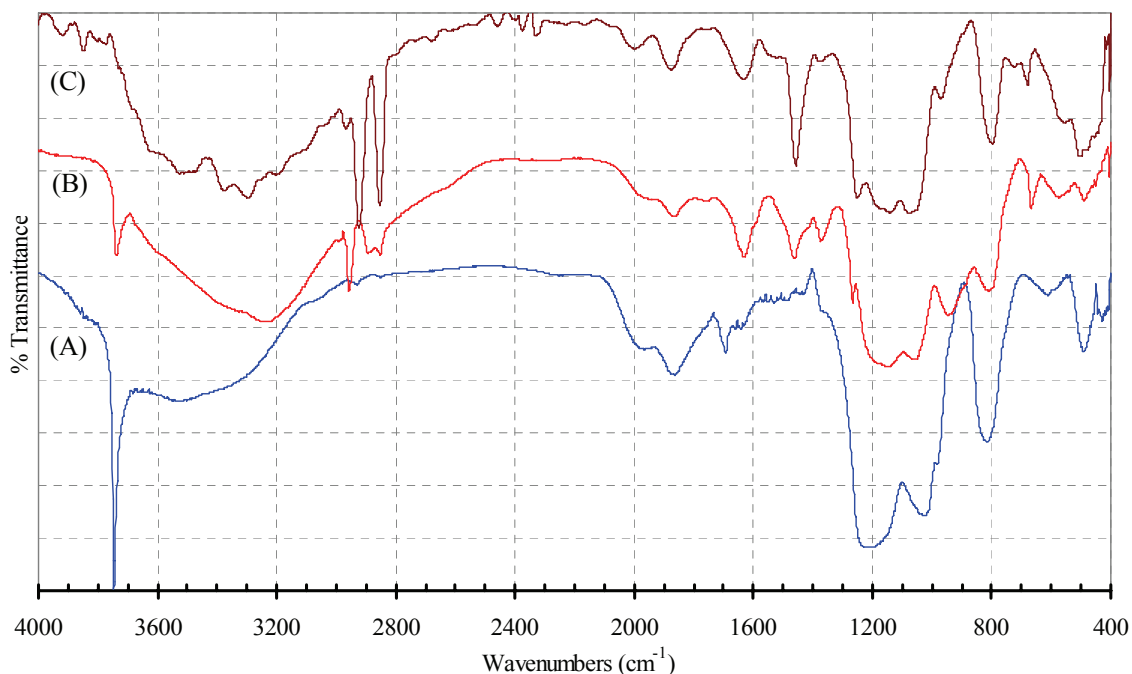
Figure 7.6. Infrared spectra of OSU-6-W (curve A), OSU-6-W-GPTMS-1 (curve B), and OSU-6-W-GPTMS-2 (curve C).

In the modified sample, OSU-6-W-GPTMS-1, bands at 3740, 2955, 2886, 1462, and 1375 cm^{-1} appear at the expense of the band at 3746 cm^{-1}. These bands are assigned to silanol (SiO-H) stretching, C-H asymmetric stretching $v_{as}(CH_2)$, C-H symmetric stretching $v_s(CH_2)$, CH$_2$ scissor, and CH$_3$ bending vibrations, respectively. The presence of the CH$_3$ bending mode suggests a small amount of remaining -OCH$_3$. Moreover, there are bands at 3053 and 2876 cm^{-1} due to the $v_{as}(CH_2)$ and $v_s(CH_2)$ vibration of the epoxy groups, respectively. The bands due to the $v_{as}(OC-H)$ and $v_s(OC-H)$ vibrations of the methoxy groups in GPTMS were at 2988 and 2855 cm^{-1}, respectively. The bands assignable to methoxy groups confirm that the OSU-6-W-GPTMS-1 has low coverage and give indication of the possibility of adding more functional groups onto the surface.

The FT-IR spectra of epoxides show characteristic bands at 1224 cm^{-1} (ring breathing), and 950-810 cm^{-1} (asymmetrical ring stretching).[41,42]

The OSU-6-W-GPTMS-2 modified sample has bands at 3628, 2946, 2880, and 1457 cm^{-1} who intensity increase at the expense of the band at 3746 cm^{-1} of OSU-6-W-GPTMS-1. These bands are assigned to silanol (SiO-H) stretching, C-H asymmetric stretching $v_{as}(CH_2)$, C-H symmetric stretching $v_s(CH_2)$, and CH_2 scissor, respectively. Moreover, there are bands at 3048 and 2871 cm^{-1} due to the $v_{as}(CH_2)$ and $v_s(CH_2)$ vibration of the epoxy groups, respectively. The bands due to $v_{as}(OC-H)$ and $v_s(OC-H)$ vibrations of methoxy groups in GPTMS were not observed. That means the OSU-6-W-GPTMS-2 has higher coverage and also gives an indication of formation of a highly ordered monolayer of the functional groups on the surface. The epoxides show characteristic bands at 1236 (ring breathing), 953 and 819 cm^{-1} (asymmetrical ring stretching).[41,42] The band positions are similar to those reported in the literature.[43] The bands in the two modified samples show shift to lower wavelength and increase in the intensities from the OSU-6-W-GPTMS-1 to OSU-6-W-GPTMS-2. These observations indicate high surface loading in the case of OSU-6-W-GPTMS-2 which has been confirmed by the solid state ^{29}Si and ^{13}C NMR and elemental analysis.

7.4.3. The Total Surface Loading of the Ordered Mesoporous Silica with the Glycidoxypropyl Functional Groups

The amount of glycidoxypropyl functional groups deposited on the surface was quantitatively determined using two variables. The surface loading (*l*) expresses the amount of deposited molecules in mmol/g. The number of molecules deposited per nm^2

is given by the surface coverage (C). Both values use the mass of the pure mesoporous silica before modification as a reference.

There is a broad range of analytical techniques available for the quantitative determination of the glycidoxypropyl functional groups (oxirane functions).[21] In the case of surface-bonded groups, a decrease in reactivity had to be expected and, therefore, the most efficient procedures were selected after testing several possibilities found in the literature.[21,22]

Table 7.3. Total coverage from three different determination methods.

Sample	Surface Area (BET)	Spectrophotometric Analysis (SA) (mmol/g)	Elemental Analysis (EA)		^{29}Si NMR			Total Coverage (molecule/nm^2)		
			C %	N %	Q^2 (%)	Q^3 (%)	Q^4 (%)	SA	EA	NMR
OSU-6-W	1283	----	0.10	0.06	13.89	71.73	14.38	----	----	----
OSU-6-W-GPTMS-1	966	3.88	17.36	0.08	0.00	49.32	50.68	2.42	2.09	1.99
OSU-6-W-GPTMS-2	720	4.50	22.24	0.11	0.00	30.77	69.23	3.76	3.53	3.17

Surface coverage was determined using the procedure described in previous chapters and the results are given in Table 7.3. All three methods show that OSU-6-W-GPTMS-1 modified sample has an average coverage of 2.2 GPTMS molecules/100 Å^2, while the OSU-6-W-GPTMS-2 sample has an average coverage of 3.5 GPTMS molecules/100 Å^2. Thus, a significantly large coverage of functional groups is obtained compare with the results in the literature (2.20 group/nm^2).[44] This difference probably arises from the difference in pore sizes, 51.1 Å vs 40.0 Å, respectively, the use of amine as catalyst, and the intermediate water treatment in the silylation process. The larger pores can avoid steric congestion of the silane molecules. The treatment with water induces full coverage with adsorbed water, that allows the formation of hydroxyl silanes and facilitates the assembly and aggregation of the incoming silyl groups on the surface. Thus, in the presence of water, the silane molecules are attached beyond the density of isolated silanols.

7.4.4. Conversion of the Glycidyl Groups in the Modified OSU-6-W-GPTMS-2 into a Thiirane Analogue

The availability of a sulfur analogue of a glycidyl functional material, *i.e.* a material with a pendant thiirane ring replacing the epoxide, would present enormous potential for the production of novel functional materials.[17,18,45] Ring-opening of the thiirane by a nucleophile containing hard donor atoms would be expected to generate the soft thiol donor at the β carbon atom. This interesting combination of hard and soft donor centres may give rise to interesting and unusual metal-ion chelation properties. A facile and efficient conversion of an epoxide into its thiirane analogue was employed that was previously developed by Moore *et al.*[17] In this investigation, the OSU-6-W-Thiirane was

prepared by converting the oxirane group in the OSU-6-W-GPTMS-2 material to the thiirane analogue, using thiourea in distilled water in the presence of dilute H_2SO_4 as a catalyst at room temperature. The direct conversion of epoxide into thiirane using thiourea is well documented for small molecules,[46] and a formal mechanism has been proposed (Scheme 7.8).
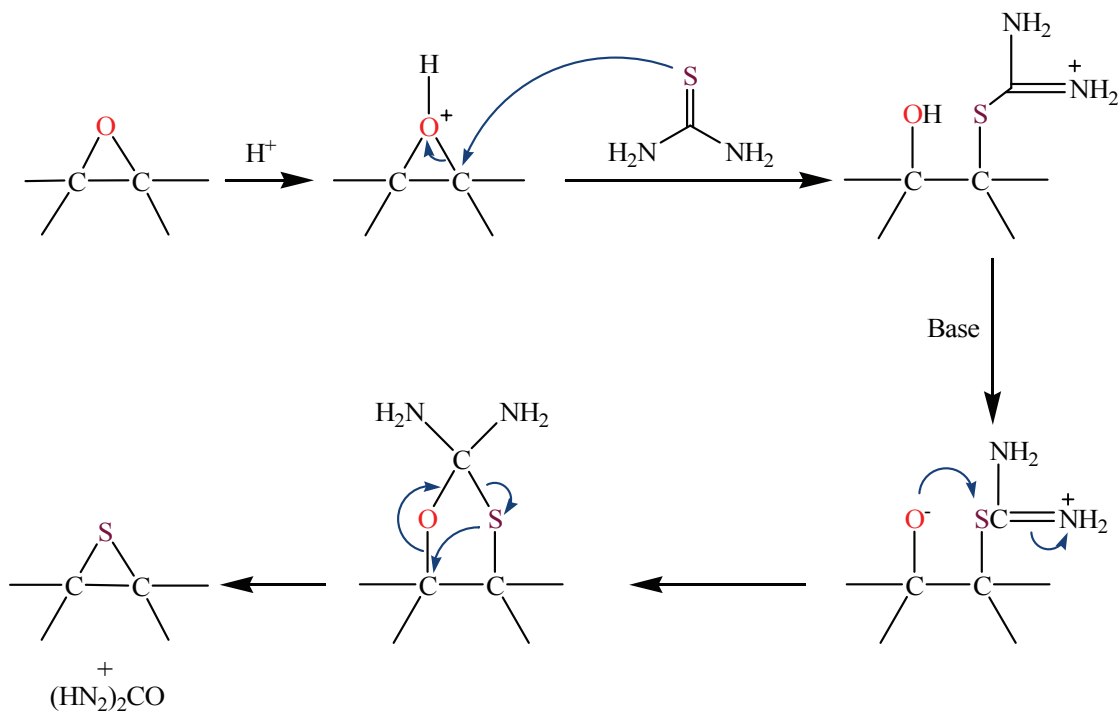
Scbeme 7.8. Mechanism of conversion of epoxide to thiirane groups using thiourea and H^+ catalyst.

The conversion reaction was not difficult to perform with the epoxide-containing OSU-6-W-GPTMS material. The data from FT-IR spectra show that this reaction yielded a relatively clean product. The peaks due to the epoxy functionality of OSU-6-W-GPTMS-2 were replaced by peaks at 622, 914, 1330, and 1440 cm^{-1} attributed to the

thiirane group. Thiourea was an efficient reagent and the results indicate that water was an appropriate solvent.

The FT-IR spectra of the two modified mesoporous silicas show difference between the oxirane and thiirane groups. The epoxy peaks and thiirane peaks, found in the spectra of OSU-6-W-GPTMS-2 and OSU-6-W-Thiirane respectively, at 810, 950 (epoxy ring vibration), 1340, 1480 (δ(CH) epoxy), 622, 914 (thiirane ring vibration), 1330 and 1440 cm^{-1} (δ(CH) thiirane).

7.4.5. Modification of OSU-6-W-GPTMS-2 with 3-Hydroxypropionitrile (3-HPN)

Introduction of cyano function groups onto the silica surface was preformed following the procedure by Allen *et al.,*[19] with minor changes. The resulting product was characterized using FT-IR spectroscopy and surface area measurement.

The FT-IR spectrum of pure 3-hydroxypropionitrile exhibited sharp IR bands at 3440, 2980, 2923, 2286(s), 1468, 1409, 1358, 1088, 874 cm^{-1}. Since the bands observed in the FT-IR spectra of the parent glycidoxypropyl-functionalized mesostructures (OSU-6-W-GPTMS-2) used for the immobilization reactions did not overlap with the characteristic bands of 3-hydroxypropionitrile, the presence or absence of bands in this region of the spectrum was used to determine whether successful inclusion of the nitrile into the mesostructures occurred. The process was indeed successful since the characteristic IR bands of these groups were observed in the resulting materials. Moreover, there was a noticeable decrease in the surface area (from 720 to 388 m^2/g) upon reaction with 3-hydroxypropionitrile. The pore size of the OSU-6-W-GPTMS-2 material is sufficiently large which in turn facilitate the incorporated of the 3-HPN

moieties inside the pores. The small and compact 3-HPN groups assist the immobilization inside the pore channels.

7.4.6. Modification of OSU-6-W-GPTMS-2 with Pyrazole (Py), 5-Aminotetrazole (ATZ), and Adenine (Ad)

Immobilization of the ligands pyrazole (Py), 5-aminotetrazole (ATZ), and adenine (Ad) took place in toluene and were performed using same procedure reported by Moore *et al.,*[17] yielding the chelating ion-exchange silicas OSU-6-W-GPTMS-2-Py, OSU-6-W-GPTMS-2-ATZ, and OSU-6-W-GPTMS-2-Ad, respectively, see Scheme 7.5.

Imidazole groups similar to the ligands used in this work have been bound to glycidyl methacrylate (GMA) resin before, but previous work involved a short spacer arm in the linkage.[13] Likewise pyrazole-containing ligands immobilized on a GMA resin have been reported,[15] but again this did not involve direct attachment of the simple azole unit. Moore *et al.,*[17] examined a number of solvents for the imidazole reaction with GMA resin and reported that, in the case of GMA the nonpolar aprotic solvent toluene proved to be optimum, with levels of bound imidazole up to 2.4 mmol/g being achieved.

The epoxy peaks found in the spectra of OSU-6-W-GPTMS-2 at 850, 910 (epoxy ring vibration), 1224, 1340, 1480 cm^{-1} (δ(CH) epoxy) disappear completely from the spectra of the modified OSU-6-W-GPTMS-2 after reaction with the various nuclephils. The appearance of peaks at around 3510-3525 cm^{-1} confirmed the generation of alcohol groups. Additional peaks due to heterocyclic aromatic ring vibrations were observed between 1500 and 1650 cm^{-1} (C=C, C=N) in the spectra of the modified oxirane mesoporous samples.[47]

The surface areas dropped from 720 m^2/g to 407, 369, and 384 m^2/g for the OSU-6-W-GPTMS-2-Py, OSU-6-W-GPTMS-2-ATZ, and OSU-6-W-GPTMS-2-Ad samples, respectively. It was thus concluded that the grafting methods was succeed in incorporating of pyrazole (Py), 5-aminotetrazole (ATZ), and adenine (Ad) moieties into the mesoporous structures.

7.4.7. Immobilization of Ethylenediamine (En)

The reaction between the epoxy moiety attached to the silylant agent GPTS, with a diamine molecule is based on a typical nucleophilic attack of the basic nitrogen atom on the strained acidic carbon atom of the ring[48], as represented in Scheme 7.9 when the 1,3-diaminoethane is involved. The non-bonded electron pair on the nitrogen of propane-1,3-diamine interacts initially with the acidic carbon atom of the epoxy ring (1); consequently the electrons of the bond between the carbon and oxygen of the epoxy ring are transferred to oxygen, opening the ring as represented in step (2). The excess of charge on the oxygen atom attracts the nearby hydrogen atom, once bonded to nitrogen, to form an oxygen-hydrogen bond (3), permitting electronic rearrangement (4) and producing the final, neutral product.
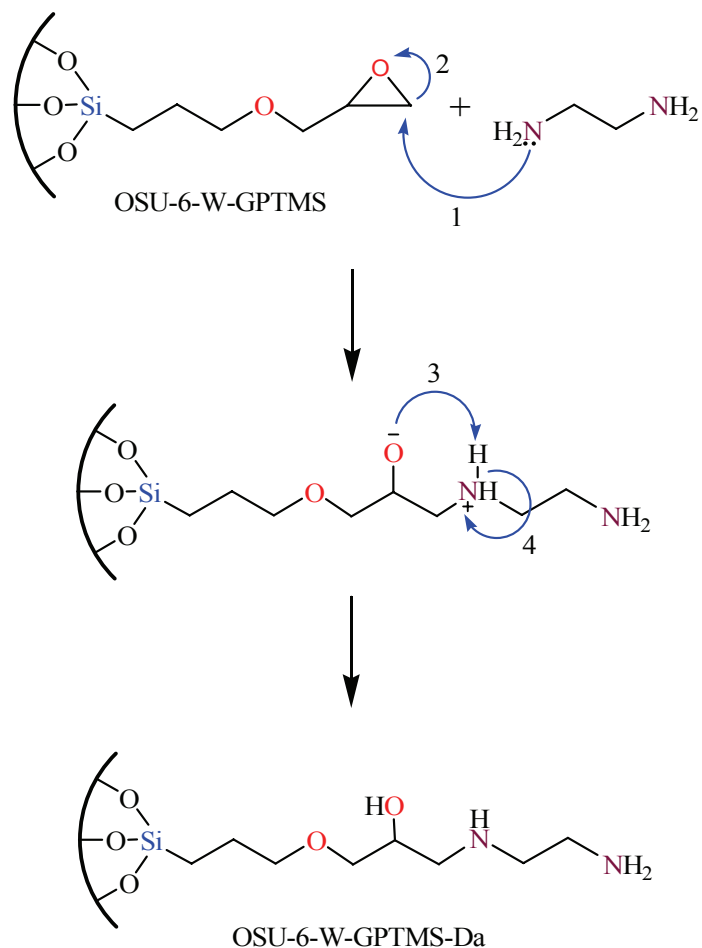
Scheme 7.9. Proposed mechanism of the reaction between the grafted epoxy moiety and propane-1,3-diamine.

An overview on the progress of the inorganic surface immobilization field is closely related to the advance of the synthetic chemistry involved. Relevant features associated with this subject are those that can cause expansion or insertion of the main organic chain precursor silylating agent, by exploring the presence of reactive centers on it. Glycidylpropyl functional group has available an epoxide group that can be opened. The three member cycle reacts with the nitrogen amine nucleophile centers of the

ethylenediamine molecule, as represented in the chemical reaction, Scheme 7.9, leading an increase in carbonic chain attached with additional two nitrogen basic centers.

Infrared spectroscopy was employed to characterize the reagents and the main product of the reaction of OSU-6-W-GPTMS-2 with ethylenediamine. The vibrational spectra obtained from the product confirmed the success of the insertion reaction, since bands that are very close to those observed, when propyl-1,3-diamine was previously incorporated into the same functional group were observed.[49] Clear evidence of the success of the reaction is given by the disappearance of the peak at 1249 cm^{-1} characteristic of the epoxy group. Another observation that supports the conclusion of a successful reaction is the appearance of a peak due to δNH_2 deformation at 1610 cm^{-1}. The presence of this band in this new synthesized silane spectrum established unequivocally the existence of an amine group in the framework of this compound.[49]

Some decrease in the surface area after functionalization is expected due to the presence of the immobilized groups, which can block the access of nitrogen molecules to the original structure of silica. However, in the present case, the drastic decrease from 720 to 343 m^2 g^{-1}, is related to both the number and also to the increased length of the pendant group attached to the inorganic backbone.

7.4.8. Metal Adsorption Study

I. Uptake Capacity

The uptake capacity of the modified OSU-6-W-GPTMS-2 silica was investigated using different amount of adsorbants interacting with 100 ppm solution of copper ions at pH 6.0. The results are shown in Figure 7.7. The maximum uptake, calculated from the Langmuir adsorption isotherms, was 6.75 mmol Cu^{2+}/g (or 438.5 mg/g). The glycidyl

concentration in the material is 3.09 mmol/g so the adsorption of copper is remarkably

high and can be explained due to the formation of 2.2:1 complex (metal to ligand).

The chart shows a plot of C/X (g/l) on the y-axis versus Conc. (mol/l) on the x-axis, with data points and a linear trend line. The following annotations appear:

$$y = 148.11x + 0.3943$$
$$R^2 = 0.9809$$
$$Xm = 6.75 \text{ mmol/g}$$
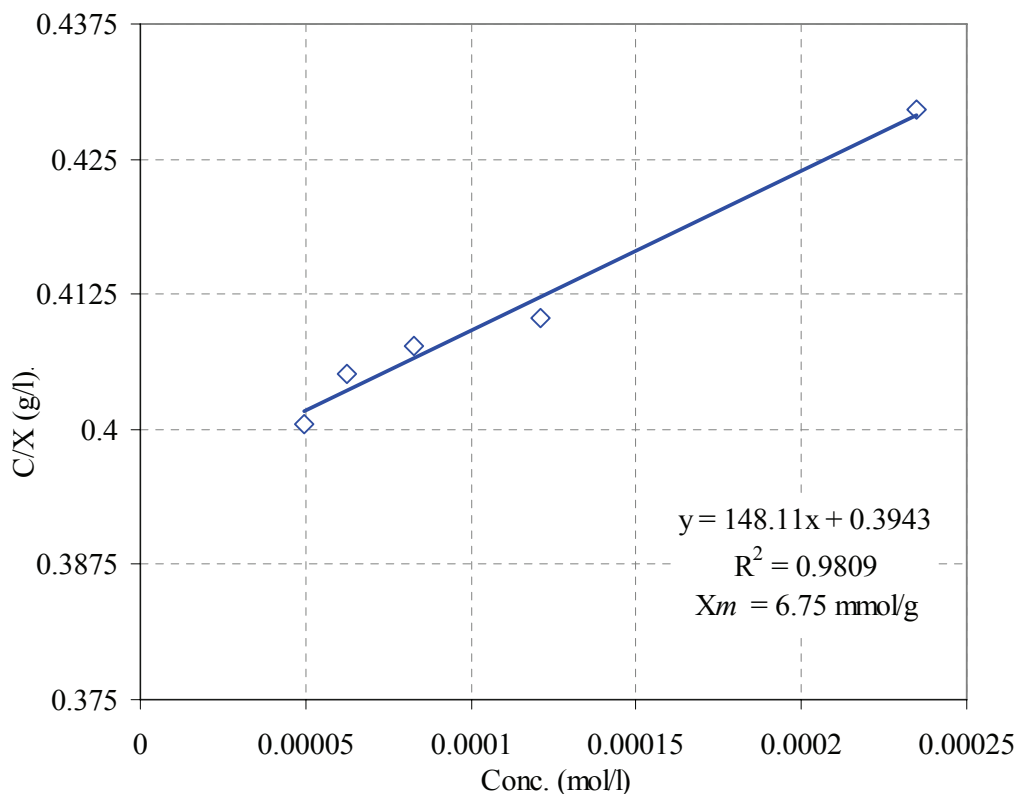
Figure 7.7. The Langmuir adsorption isotherms of Cu^{2+} ions adsorbed by OSU-6-W-
GPTMS-2 adsorbent.

II. Regeneration of the Absorbent

Treatment of the copper-loaded material with aqueous solution of 2.0 *M* HCl

three times each time stirring for around one hours resulted in the removal of the bound

Cu^{2+} from the structure, regenerating the adsorbent for further metal ion uptake. The

regenerated material, Figure 7.8, shows a decrease in the copper ion uptake capacity

down to ~ 76% after the third regeneration.
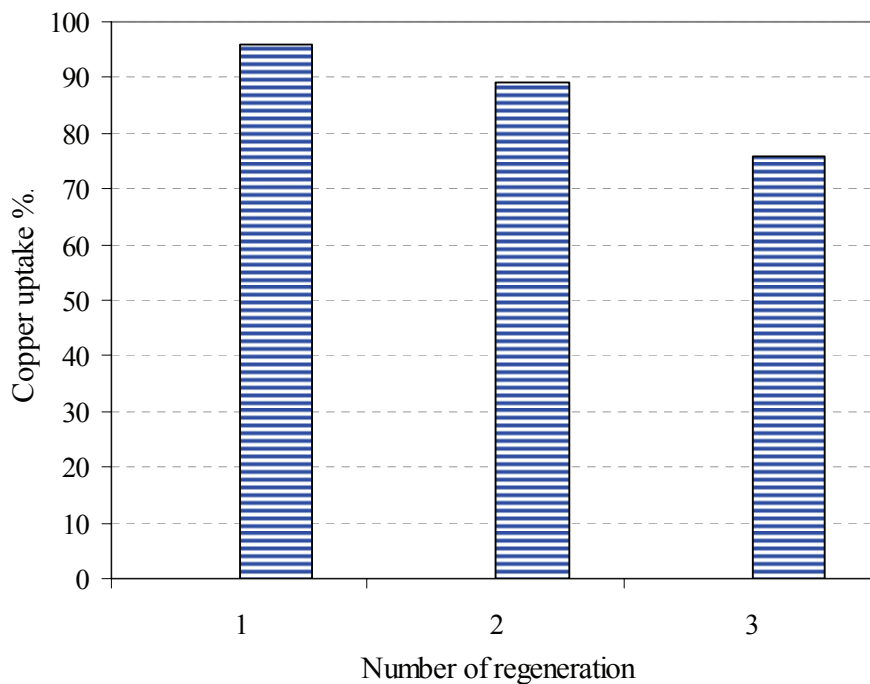
Figure 7.8. The regeneration experiments of Cu^{2+} ions adsorbed by OSU-6-W-GPTMS-2 absorbent

The decrease might be due to loss of the immobilized groups with washing or a strong interaction of the Cu^{2+} ions with the oxygen atoms that can not be released with HCl washing only. The later, will lead to blocking the available sites for chelating. Overall, this material shows excellent regeneration.

7.5. CONCLUSION

The 3-glycidoxypropylsilyl moiety was readily introduced onto the OSU-6-W mesoporous silica surfaces. Solid state ^{13}C and ^{29}Si NMR and infrared spectroscopy, X-ray powder diffraction, and surface area measurements confirmed the successful derivitization.

The hydrophilic GPTMS group on the surface of OSU-6-W plays an active role in the attachment of various reactive groups and ligands because of the facile nucleophilic

ring-opening reaction of the pendant epoxide functionality. The methods employed showed a significant incorporation of all active groups onto the mesoporous silica. This gave mesoporous silica hybrids with high surface areas and amounts of the active groups dispersed on the material.

The inorganic-organic hybrid, OSU-6-W-GPTMS-2 had a very high copper(II) ion adsorption. These characteristics in physical, chemical and structural properties and in adsorptive behavior indicate that further studies on the catalytic abilities of new solids should be undertaken.

7.6. REFERENCES

1. Jal, P. K.; Patel, S.; Mishra, B. K.. Chemical modification of silica surface by immobilization of functional groups for extractive concentration of metal ions. *Talanta* **2004,** *62*(5), 1005-1028.

2. Prado, A. G; Sales, L. A.; Carvalho, R. M.; Rubin, J. C.; Airoldi, C.. Immobilization of 5-amino-1,3,4-thiadiazole-thiol onto silica gel surface by heterogeneous and homogeneous routes. *J. Non-Cryst. Solids* **2004,** *33*(1), 61-67.

3. Van de Water, L. G. A.; Driessen, W. L.; Glenny, M. W.; Reedijk, J.; Schroder, M.. Selective and reversible extraction of heavy metal-ions by mixed-donor crown ether-modified oxirane and thiirane resins. *React. Funct. Polym.* **2002,** *51*(1), 33-47.

4. Macquarrie, D. Organically modified hexagonal mesoporous silicas . Clean synthesis of catalysts and the effect of high loading and non-catalytic second groups on catalytic activity of amine-derivatised materials. *Green Chem.* **1999,** *1*(4), 195-198.

5. Im, H. J.; Barnes, E.; Dai, S.; Xue, Z.. Functionalized sol–gels for mercury(II) separation: a comparison of mesoporous materials prepared with and without surfactant templates. *Micropor. Mesopor. Mater.* **2004,** *70*(1-3), 57-62.

6. Lin, Y.; Fiskum, S.; Yantase, W.; Wu, H.; Mattigod, S. W.; Vorpagel, E.; Fryxell, G. E.; Raymond, K. N.; Xu, J.. Incorporation of hydroxypyridinone ligands into self-assembled monolayers on mesoporous supports for selective actinide sequestration. *Environ. Sci. Technol.* **2005,** *39*(5), 1332-1337.

7. Fryxell, G. E.; Lin, Y.; Fiskum, S. K.; Birnbaum, J. C.; Wu, H.; Kemner, K.; Kelly, S.. Actinide sequestration using self-assembled monolayers on mesoporous supports. *Environ. Sci. Technol.* **2005,** *39*(5), 1324-1331.

8. Price, P. M.; Clark, J. H.; Macquarrie, D. J.. Modified silicas for clean technology. *J. Chem. Soc., Dalton Trans.* **2000,** *2,* 101-110.

9. Stein, A.; Melde, B.; Schroden, R.. Hybrid Inorganic-Organic Mesoporous Silicates-Nanoscopic Reactors Coming of Age. *Adv. Mater.* **2000,** *12*(19), 1403-1419.

10. Svec, F.. Reactive polymers. 56. Interaction of reactive sites of macroporous glycidyl methacrylate-ethylene dimethacrylate copolymers. *Angew. Makromol. Chem.* **1986,** *144,* 39-49.

11. Lindsay, D.; Sherrington, D.; Greig, J.; Hancock, R.. Novel chelating resins with remarkably high selectivities for copper(II) over zinc(II) ions. *J. Chem. Soc., Chem. Commun.* **1987,** *17,* 1270-1272.

12. Lindsay, D.; Sherrington, D. C.. Synthesis of chelating resins based on poly(styrene-co-divinylbenzene) and poly(glycidyl methacrylate-co-ethylene glycol dimethacrylate). *React. Polym., Ion Exchangers, Sorbents* **1985,** *3*(4), 327-339.

13. Verweij, P. D.; Driessen, W. L.; Reedijk, J.; Rowatt, B.; Sherrington, D. C. Selective and rapid uptake of copper(II) by a novel chelating resin containing imidazole groups. *React. Polym.* **1990,** *13*(1-2), 83-92.

14. Verweij, P. D.; Dugue, T.; Driessen, W. L.; Reedijk, J.; Rowatt, B.; Sherrington, D. C. Metal uptake by N,N'-bis(2-benzimidazolylmethyl)amine immobilized on poly(glycidyl methacrylate-co-ethylene glycol dimethacrylate). *React. Polym.* **1991,** *14*(3), 213-227.

15. Van Berkel, P. M.; Verweij, P. D.; Driessen, W. L.; Reedijk, J.; Sherrington, D. C. Metal uptake by didentate and tridentate pyrazole-containing ligands immobilized onto poly(glycidyl methacrylate-co-ethylene glycol dimethacrylate). *Eur. Poly. J.* **1992,** *28*(7), 747-754.

16. Verweij, P. D.; Van der Geest, J. S. N.; Driessen, W. L.; Reedijk, J.; Sherrington, D. C. Metal uptake by a novel benzimidazole ligand immobilized onto poly(glycidyl methacrylate-co-ethylene glycol dimethacrylate). *React. Poly.* **1992,** *18*(3), 191-201.

17. Moore, B. D.; Sherrington, D. C.; Zitsmanis, A.. Conversion of a glycidyl methacrylate resin into a thiirane analogue and subsequent immobilization of aliphatic amine and azole ligands. *J. Mater. Chem.* **1992,** *2*(12), 1231-1236.

18. Van Berkel, P. M.; Driessen, W. L.; Reedijk, J.; Sherrington, D. C.; Zitsmanis, A. Metal-ion binding affinity of azole-modified oxirane and thiirane resins. *React. Funct. Polym.* **1995,** *27*(1), 15-28.

19. Allen, D.; El Rassi, Z.. Capillary electrochromatography with monolithic silica columns III. Preparation of hydrophilic silica monoliths having surface-bound cyano groups: chromatographic characterization and application to the separation of carbohydrates, nucleosides, nucleic acid bases and other neutral polar species. *J. Chromatogr., A* **2004,** *1029*(1-2), 239-247.

20. Sales, J. A.; Prado, A. G.; Airoldi, C.. The incorporation of propane-1,3-diamine into silylant epoxide group through homogeneous and heterogeneous routes. *Polyhedron* **2002,** *21*(25-26), 2647-2651.

21. Cheronis, N. D.; Ma, T. S.. *Organic Functional Group Analysis by Micro and Semimicro Methods,* Wiley, New York, **1964.**

22. Engelhardt, H.; Mathes, D.. Chemically bonded stationary phases for aqueous high-performance exclusion chromatography. *J. Chromatogr.* **1977,** *142,* 311-320.

23. Oliver, R. W.; Editor. HPLC of Macromolecules: A Practical Approach. **1989,** pp. 2.

24. Vrancken, K. C.; Van Der Voort, P.; Possemiers, K.; Vansant, E. F. Surface and Structural Properties of Silica Gel in the Modification with γ-Aminopropyltriethoxysilane. *J. Colloid and Interface Sci.* **1995,** *174*(1), 86-91.

25. Sander, L. C.; Wise, S. A.. Recent advances in bonded phases for liquid chromatography. *Crit. Rev. Anal. Chem.* **1987,** *18*(4), 299-415.

26. Unger, K. K.. *Packings and Stationary Phases in Chromatographic Techniques,* Marcel Dekker, Moscow, **1990**.

27. Houben-Weil Methoden der Organischen Chemie, Band VI/la, Georg Thieme Stuttgart, **1979,** 357-382.

28. Plueddemann, E.. Silane Coupling Agents, 2nd Ed., Plenum Press, New York, **1991.**

29. Pfannkoch, E.; Lu, K.C.; Regnier, F.E.; Barth, H.G.. Characterization of some commercial high performance size-exclusion chromatography columns for water-soluble polymers. *J. Chromatogr. Sci.* **1980,** *18*(9), 430-441.

30. Roumeliotis, P.; Unger, K. K.. Assessment and optimization of system parameters in size exclusion separation of proteins on diol-modified silica columns. *J. Chromatogr.* **1981,** *218,* 535-546.

31. Bogart, G. R.; Leyden, D. E.; Wade, T. M.; Schafer, W.; Carr, P. W. Spectroscopic investigation of the hydrolysis of γ-glycidoxypropylsilane bound to silica surfaces. *J. Chromatogr.* **1989,** *483,* 209-219.

32. Krasnoslobodtsev, A. V.; Smirnov, S. N.. Effect of Water on Silanization of Silica by Trimethoxysilanes. *Langmuir* **2002,** *18*(8), 3181-3184.

33. Kao, Hsien-Ming; Tsai, Yi-Yuan; Chao, Shih-Wei. Functionalized mesoporous silica MCM-41 in poly(ethylene oxide)-based polymer electrolytes: NMR and conductivity studies. *Solid State Ionics* **2005,** *176*(13-14), 1261-1270.

34. Kresge, C. T.; Leonowicz, M. E.; Roth, W. J.; Vartuli, J. C.; Beck, J. S.. Ordered mesoporous molecular sieves synthesized by a liquid-crystal template mechanism. *Nature* **1992,** *359,* 710-712.

35. Glaser, R.H.; Wilkes, G.L.; Bronnimann,C. E.. Solid state silicon-29 NMR of TEOS-based multifunctional Sol-gel materials. *J. Non-Cryst. Solids* **1989,** *113,* 73-87.

36. Prado, A. G.; Airoldi, C.. Different neutral surfactant template extraction routes for synthetic hexagonal mesoporous silicas. *J. Mater. Chem.* **2002,** *12*(12), 3823-3826.

37. Templin, M.; Wiesner, U.; Spiess, H. W.. Multinuclear solid-state-NMR studies of hybrid organic-inorganic materials. *Adv. Mater.* **1997,** *9*(10), 814-817.

38. Socrates. G. *Infrared Characteristic Group Frequencies: Tables and Charts,* second ed., Wiley, Chichester **1994**.

39. Zhao, X. S.; Lu, G. Q.; Whittaker, A. K.; Millar, G. J.; Zhu, H. Y.. Comprehensive Study of Surface Chemistry of MCM-41 Using ^{29}Si CP/MAS NMR, FTIR, Pyridine-TPD, and TGA. *J. Phys. Chem. B*, **1997,** *101*(33), 6525-6531.

40. Jentys, A.; Pham, N. H.; Vinek, H. Nature of hydroxy groups in MCM-41. *J. Chem. Soc., Faraday Trans.* **1996,** *92*(17), 3287-3291.

41. Lwoswsi, W. *Comprehensive Heterocyclic Chemistr*y; Ed.; Pergamon Press: Oxford, U.K., 1984; Vol. 7, p 99.

42. Grasselli, J. G., Ritchey, W. M., Eds. *Atlas of Spectral Data and Physical Constants for Organic Compound*s, 2nd Ed., CRC Press Inc.: Cleveland, OH, **1975,** Vol. 1.

43. Piers, A. S.; Rochester, C. H. IR studies of adhesion promoters. Part 3. Adsorption and coupling of bifunctional silanes on silica at the solid/liquid interface. *J. Chem. Soc., Faraday Trans.* **1995,** *91*(8), 1253-1260.

44. Mingalyov, P. G.; Fadeev, A. Y. Activated silica supports for preparation of chromatographic sorbents. A comparative study of silicas containing attached epoxy, tosyloxy and halogen groups. *J. Chromatography, A* **1996,** *719*(2), 291-297.

45. Kalal, J.; Svec, F.; Marousek, V.. Reactions of epoxide groups of glycidyl methacrylate copolymers. *J. Polym. Sci., Polym. Symp.* **1974,** *47,* 155-166.

46. Reynolds, D. D.; Fields, D. L. *Heterocyclic Compounds with Three and Four-membered Rings Part 1 of The Chemistry of Heterocyclic Compounds,* ed. A. Weissberger, Wiley, New York, **1964,** p. 576.

47. (a) Otting, W.. Structure of the heterocyclic five-membered rings of pyrrole, imidazole, 1,3,4-triazole, and tetrazole. *Chem. Ber.* **1956,** *89,* 2887-2896. (b) Otting, W. Infrared spectra of reactive N-acyl compounds. *Chem. Ber.* **1956,** *89,* 1940-1945.

48. Solomons, T. W. G. *Fundamentals of Organic Chemistry,* 4th ed., Wiley, New York, **1994**.

49. Sales, J. A.; Airoldi, C.. Calorimetric investigation of metal ion adsorption on 3-glycidoxypropyltrimethylsiloxane + propane-1,3-diamine immobilized on silica gel. *Thermochim. Acta* **2005,** *427*(1-2), 77-83.

CHAPTER
EIGHT

FUNCTIONALIZED MESOPOROUS SURFACE WITH THIOL-FUNCTIONAL

GROUPS FOR HEAVY METAL RECOVERY

Abstract

Mesoporous materials have great potential for environmental and industrial processes, but many applications require the materials to exhibit specific surface chemistry and binding sites. Mesoporous silica materials with uniform channels containing functionalized organic monolayers have been synthesized by grafting a thiol functional group, (3-Mercaptopropyl)trimethoxysilane (MPTMS). A new approach to heavy metal ion adsorbents based on the covalent grafting of 3-mercaptopropylsilyl groups to the framework pore walls of mesoporous silica molecular sieves has been developed and investigated with regard to hydroxyl group densities, channel dimensions, morphologies, reaction conditions. Prior to thiol functionalization of the mesostructures by a grafting procedure, surfactant was removed from OSU-6 by solvent extraction. The grafting process was much more effective for the functionalization of OSU-6-W owing to a higher surface concentration of surface hydroxyl groups.

Results show that the ordered mesostructures of both functionalized samples, OSU-6-W-MPTMS-1 and OSU-6-W-MPTMS-2, were retained after modification and the thiol functional group was immobilized mainly inside the mesopore channel, as

evidenced by Brunauer-Emmett-Teller surface area, small-angle X-ray scattering, Fourier transform infrared, and elemental analyses. Solid-state nuclear magnetic resonance suggests that a cross-linked monolayer of mercaptopropylsilane was covalently bound to mesoporous silica and closely packed on the surface. The relative surface coverage of the monolayers can be systematically varied up to 95%. Consequently, the functionalized hybrid materials show exceptional selectivity and capacity for removing heavy metals from aqueous solution. Tailored hybrid materials have also shown potential to selectively bind transition metal ions. These materials are extremely efficient in removing mercury and other heavy metals from aqueous waste stream, with distribution coefficients up to 435,000. The Hg(II) adsorption capacities for OSU-6-W-MPTMS-2 were interpreted in terms of the size and accessibility of the framework pore structure.

The stabilities of these materials and the potential to regenerate and reuse them have also been demonstrated.

The surface modification scheme reported here enables rational design of the surface properties of tailored porous materials and may lead to the synthesis of more sophisticated functionalized composites for environmental and industrial applications. Rational design of the surface properties of mesoporous materials will lead to more sophisticated functional composites.

8.1. INTRODUCTION

8.1.1. Heavy Metal Ions Removing

Heavy metals, particularly mercury, are important environmental pollutants, that threater the health of human populations and natural ecosystems alike.[1] Removal of these species from the environment is thus a major focus of waste treatment and cleanup

efforts. An improvement in the removal of these contaminants from natural waters was definitely shown in recent years.[2] One of the major contributions is the development of new materials with the ability to remove wastes from water,[3] which is one of the principal goals of green chemistry.[4] Several adsorptive compounds are capable of capturing metal ions from aqueous solution, including activated charcoal,[5] zeolites,[6,7] and clays.[8,9] Among the inherent disadvantages of these materials are their wide distribution of pore size, heterogeneous pore structure, low selectivity for heavy metal ions, relatively low loading capacities, and somewhat small metal ion binding constants. In order to circumvent these limitations, some promising heavy metal sorbents have been prepared via the immobilization of ion-chelating agents on inorganic supports,[10,11] or via the coupling of chelating ligands (*e.g.,* thiol, or carboxyl functions) to support matrixes consisting of inorganic oxides (*e.g.,* silica, alumina, or clay)[12-20] or organic polymers (*e.g.,* polystyrene, cellulose, or poly(methyl methacrylate)).[21-26] Such functionalized materials have relatively high metal ion loading capacities and strong binding affinities for selected metal ions. This exceptional performance can be attributed to the presence of the surface-bound ligands, which can be specifically tuned to accommodate the selective adsorption of targeted metal ions. These functionalized oxides and polymers have been used in the preconcentration of metal ions for the analyzing of multicomponent solutions and for the removal of toxic species from wastewater streams, in particular, radionuclides.[20,26] Although superior in performance to conventional ion exchangers, functionalized matrixes remain relatively inefficient because only a fraction of the immobilized ligands are accessible for metal complexation.

8.1.2. Mesoporous Molecular Sieves Modification with Thiol-functional Groups

Inorganic–organic hybrids containing a variable number of simple or complex attached molecules bonded on inorganic surfaces are increasingly finding applications in several areas, mainly those related to sorbents for extraction or as supports for catalysts.[27,28] Among a large number of inorganic oxides, silica gel especially the recent discover mesoporous molecular sieves that has stimulated a new prospects for adsorbent and catalyst design.[29,30] They clearly accomplishes a significant role due to its ability to anchor organic chains designed to embrace desired functional groups.[31] This class of inorganic support supercedes organic polymers from the point of view of practicality with respect to structural stability, swelling behavior, thermal properties, high surface area and large and accessible pores, and aging, accessibility of reactive centers and insolubility in organic solvents. The new complexing agents bound to silica can be useful for a wide range of problems related to heterogeneous catalysis,[32] metal ion preconcentration,[33] ion-exchange,[34] pesticide preconcentration,[35] and stationary phases for chromatography,[36] and as well as in the use of these new materials to immobilize agrochemical compounds in order to anchor pesticides.[37]

For this purpose, the employment of silylating agents in many reactions is a commonly explored method to immobilize molecules. Such desired molecules covalently bonded on a surface can display chelating functional groups, which normally attain special properties.[31]

A logical strategy to increase the mercury adsorption capacity and to facilitate the adsorbent's regeneration is to increase the amount of the mercaptopropyl functional groups on the mesoporous surface and at the same time maintain the size of the pores as

large as possible in order to reduce or eliminate the mass transfer problem. These ligands, attached to a mesoporous silica support, should be stable under typical regeneration conditions, which will make them perfectly suitable for environmental applications due to the presence of a sulfur-containing functionality that exhibits high affinity toward mercury ions.

Recently, a direct derivatization of the porous silica surface with different organic molecules under various conditions has been reported.[38-40] Traditionally, the most common method used for surface derivatization of the crystalline silicon is the silanization reaction.[41]

Applications of mesoporous silicas as heavy metal ion adsorbents have also been studied recently.[42-50] Liu and Feng *et al.,*[42,43] reported on a heavy metal ion adsorbent (FMMS) based on the mercaptopropylsilyl functionalization of a calcined form of MCM-41. A high concentration of ligand was functionalized via the grafting process, which involved repeated surface hydrolysis and silylation cycles. The mercury loading of FMMS was high (2.5 mmol/g) (501 mg/g) in aqueous solutions. In this case, a surface hydrolysis step is necessary to generate surface hydroxyl groups, which are lost during the calcination. Mercier and Brown *et al.,*[44-47] used a neutral surfactant as a template to overcome this drawback. The neutral surfactant could be removed by solvent extraction. The amount of surface hydroxyl group loss by this procedure was much less than that by calcination or ion exchange. As a result, repeated hydrolysis and silylation reaction was not required for this procedure. The synthesized adsorbent (MP-HMS-C12) had a large pore size (2.7 nm), a high mercury loading capacity (1.5 mmol/g), and a high selectivity for mercury ions. Im *et al.,*[51] stated that the preparation of the ligand-coated mesoporous

powders usually involves at least two steps, and requires the use of surfactant templates followed by their extraction. Because of their sub-micron size, these powders are known to have faster adsorption kinetics than granules ones, where metal ions undergo longer internal diffusion to reach ligands.

In this chapter, the effectiveness of the silylation processes for the functionalization of mesoporous frameworks with mercaptopropyltrimethoxysilane, $(CH_3O)_3SiCH_2CH_2CH_2SH$, which has a strong binding affinity for mercury is reported. The Hg-binding properties of thiol-functionalized mesoporous molecular sieves with different pore dimensions and functional coverages were also explord. The efficiency toward Hg(II) binding is shown to depend critically on the pore size of the functionalized mesoporous molecular sieve. Also, OSU-6-W-MPTMS-2 is shown to be more densly functionalized with siloxane thiol groups compared to OSU-6-W-MPTMS-1, owing primarily to the higher surface density of functional groups. The results reported here should be useful in evaluating these materials for environmental cleanup and heavy metal ion recovery. Our attention was directed to the attachment of the mercaptopropyl functionality to the surface of ordered mesoporous silica, OSU-6-W.

8.1.3. Immobilization of Ethylchloroacetate Group

Insoluble porous materials bearing thiol-acetate ligands as chelating functional groups of the formula $\equiv Si\text{-}(CH_2)_3\text{-}SCH_2COOH$ have previously been prepared. The immobilized thiol-acetate ligand system was prepared by the reaction of the mesoporous silica immobilized thiol ligand (OSU-6-W-MPTMS-2) with ethylchloroacetate.[31] These ligand systems exhibit high potential for extraction and preconcentration of divalent metal ions such as Co^{2+}, Ni^{2+} and Cu^{2+}.[31]

8.2. EXPERIMENTAL

8.2.1. Chemicals

Analytical grade chemicals from the following suppliers were used as purchased

for all sample preparations: 3-mercaptopropyltrimethoxysilane [$((CH_3O)_3Si(CH_2)_3SH)$,

Gelest], ethylchloroacetate, toluene 99.8% HPLC grade, ethyl alcohol, triethylamine

(TEA, 99%, Aldrich), dichloromethane (99.6%, Aldrich), NaOH (0.025 M), HCl (2.0 M),

thiourea, and distilled deionized water.

8.2.2. Characterization

The main products were characterized using different techniques. The full details

of sample preparation and instrument operation were mentioned previously in chapter

two and three of this thesis.

8.2.3. Preparation

8.2.3.1. Activation of the Mesoporous OSU-6-W

The mesoporous silica, OSU-6-W, was synthesized as discussed in chapter two of

this thesis. The amine-activated mesoporous silica TEA-OSU-6-W was prepared as

described in chapter five.

8.2.3.2. Surface Modification of Mesoporous Materials with Mercaptopropyl

Functional Groups

Mercaptopropyl-functional group was chemically attached to the mesoporous

OSU-6-W material surfaces by means of the post-synthesis grafting method described in

previous chapters.

I. One-step Reaction of OSU-6-W with Mercaptopropyltrimethoxysilane (OSU-6-W-MPTMS-1)

3.0 g (~ 50 mmol) of the activated mesoporous silica (TEA-OSU-6-W) and 10 ml (~ 50 mmol) of mercaptopropyltrimethoxysilane (MPTMS) in 100 ml of dry toluene in a 250-ml round-bottom flask were refluxed for 48 hours under a dry atmosphere. An illustration of the reaction is schematically represented in Scheme 8.1. The resulting light gray solid was filtered off with a fine filter funnel, washed with toluene three times (3 X 50 ml), then ethanol, to rinse away any excess MPTMS. The solid then dried at 80 °C under vacuum for 24 hours to yield 4.76 g. IR peaks (cm^{-1}) (KBr): 3735(m, sh), 3510(m, br), 3281(m, br), 2927(m, sh), 2855(m, sh), 2558(m, sh), 1464(m, sh), 1373(m, sh), 1305(w), 1228(s, sh), 1143(s), 1066(s, sh), 967(m, sh), 801(s, sh), 694(m, sh), 582(m), and 461(m, sh). The solid-state ^{29}Si CP/MAS NMR resonances in δ (ppm) are -48.9 (T^1), -57.6 (T^2), -66.4 (T^3), -101.9 (Q^3), and -111.1 (Q^4). The solid-state ^{13}C CP/MAS NMR resonances in δ (ppm) are 11.8 (-CH$_2$-CH_2-Si≡)[1], 27.7 (-CH_2-CH$_2$-Si≡)[2] and (HS-CH_2-CH$_2$-CH$_2$-Si≡)[3], and 50.5 ppm (Methanol), see Scheme 8.1. Elemental analysis: C (10.64 wt %) and N (0.09 wt %).
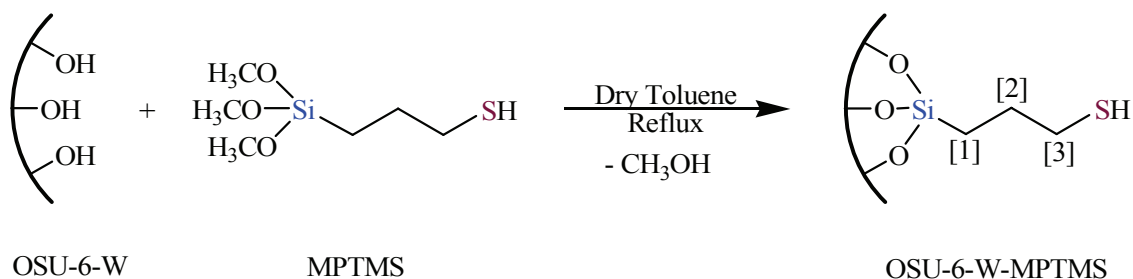
Scheme 8.1. An illustration of such grafting reaction. Carbon atoms are numbered to illustrate carbon atoms positions as described in the ^{13}C CP/MAS NMR.

II. Three-step Reaction of OSU-6-W with Mercaptopropyltrimethoxysilane (OSU-6-W-MPTMS-2)

Mesoporous silica-supported mercaptopropyl functional groups was prepared by refluxing 3.0 g (~ 50 mmol) of the activated mesoporous silica (TEA-OSU-6-W) with 5.0 ml (~ 25 mmol) of 3-Mercaptopropyltrimethoxysilane (MPTMS) in 100 ml of dry toluene in a 250-ml round-bottom flask for 48 hours under dry atmosphere. The resulting light gray solid was filtered off with a fine filter funnel, washed with toluene three times (3 X 50 ml) and then ethanol, to rinse away any surplus MPTMS. The resulting solid was then dried at 80 °C under vacuum for 24 hours. It was then placed in a 125-ml Erlenmeyer flask and stirred with 50 ml of distilled water for five hours. The mixture was filtered off to recover the solid which was then dried at 80 °C under vacuum for 24 hours. In the third step, a 5.0 ml (~ 25 mmol) of MPTMS was refluxed with the product from the previous step in 100 ml of dry toluene in a 250-ml round-bottom flask for 48 hrs under dry atmosphere. The resulting light gray solid was filtered off with a fine filter funnel, washed with toluene three times (3 X 50 ml) and then ethanol, to rinse away any excess MPTMS and dried at 80 °C under vacuum for 24 hours. The final product has a light gray color and weighed 5.81 g. The IR peaks (cm^{-1}) (KBr): 3641(m, br), 3296(s, br), 2920(s, sh), 2853(s, sh), 2561(m, sh), 1467(s, sh), 1373(w), 1305(m), 1237(s, sh), 1171(s, br), 1090(s, br), 954(m), 799(m, sh), 694(m, sh), 572(w), and 469(m). Solid-state ^{29}Si CP/MAS NMR resonances in δ (ppm) are -57.3 (T^2), -66.6 (T^3), -100.6 (Q^3), and -110.3 (Q^4). Solid-state ^{13}C CP/MAS NMR resonances in δ (ppm) are 12.3 (-CH_2-CH_2-Si≡)[1], 26.1 (HS-CH_2-CH_2-CH_2-Si≡)[3], and 29.4 (-CH_2-CH_2-Si≡)[2], see Scheme 8.1. Elemental analysis: C (14.61 wt %) and N (0.16 wt %).

8.2.3.3. Modification of OSU-6-W-MPTMS-2 with Acetic Acid

Insoluble porous materials immobilized ligand bearing thiol-acetate ligand as chelating functional groups of the formula $\equiv$Si-$(CH_2)_3$-SCH_2COOH were prepared as follows;[31] 1.0 g of OSU-6-W-MPTMS-2 was refluxed for 72 hours with an excess of ethylchloroacetate (10 ml) in a round bottom flask, in the presence of few drops of triethylamine. The solid product was filtered off, washed with successive 50 ml portions of 0.025 M NaOH, water, methanol and diethyl ether. The product was dried in vacuum for 24 hours. This product will be referred to as OSU-6-W-MPTMS-2-Acetate. Next, a 1.0 g of OSU-6-W-MPTMS-2-Acetate was refluxed with 50 ml of 2.0 M HCl for 10 hours in order to hydrolyze the ethoxy groups in the thiol-acetate ligands. The solid material was filtered, washed with successive portions, 50 ml, of 0.025 M NaOH, water, methanol and diethyl ether. The product was dried in vacuum for 24 hours and will be referred as OSU-6-W-MPTMS-2-Acac, Scheme 8.2.

OSU-6-W-MPTMS-2 + ClCH$_2$COOC$_2$H$_5$ $\xrightarrow[\text{Reflux} \\ \text{-HCl}]{(Et)_3N}$ OSU-6-W-MPTMS-2-Acetate

Ethylchloroacetate

OSU-6-W-MPTMS-2-Acetate $\xrightarrow[\text{Reflux}]{2.0\ M\ HCl}$ OSU-6-W-MPTMS-2-Acac
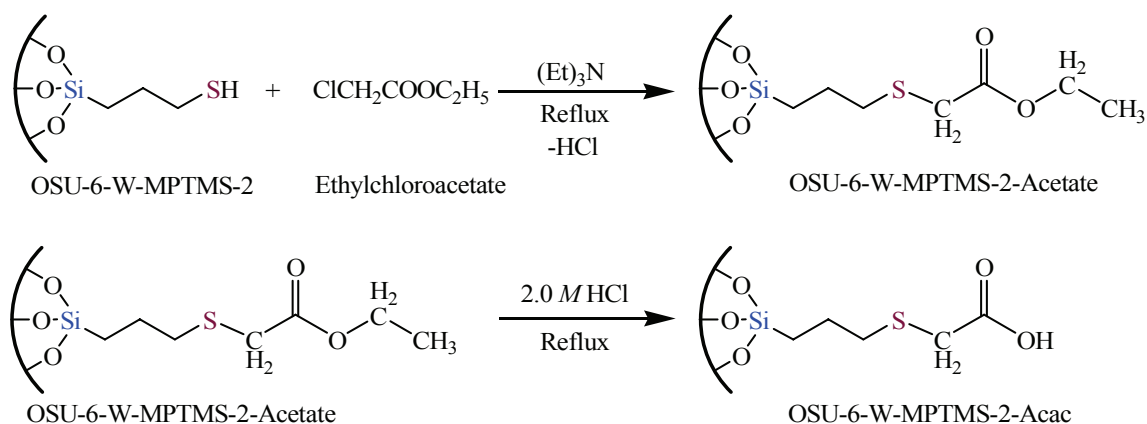
Scheme 8.2. Schematic diagram for the synthesis of adsorbents modified with acetic acid.

8.2.4. Application of the Synthesized Adsorbents

I. Heavy Metal Ions Adsorption

The adsorption process was conducted using batch experiments in water solution for the divalent cation (Hg^{2+}) at 25 °C. For the preparation of aqueous metal solutions, the metal nitrate salt was used (mercury(II) nitrate n-hydrate ($Hg(NO_3)_2 \cdot nH_2O$)). A buffer solution (pH 4) was prepared using potassium hydrogen phthalate and hydrochloric acid, and was used to prevent the precipitation of metal ion during the adsorption experiment. A series of samples of five different amounts of the thiol-functionalized mesoporous silicas (varying from 25 to 125 mg) were suspended in 10.0 ml of 100 ppm Hg^{2+} solutions in separate glass vial. The vials were then shaken on a mechanical laboratory shaker for 6 hour at room temperature. Afterwards a portion of the supernatant solution was removed for analysis. The metal ion uptake was calculated as mmol of Hg^{2+}/g ligand.

The same procedure was used to follow the effect of pH on cation adsorption, by using 10 ml of 100 ppm Hg^{2+} and 100 mg of OSU-6-W-MPTMS-2. In each case, the pH values were controlled with corresponding buffer solutions. For pH 1–3, Clark/Lubs buffers (HCl/KCl) were used, for pH 4 and 5, Na_3PO_4/H_3PO_4 buffers were used and for pH 6 and 7 $Na_3PO_4/NaOH$ buffers were used.[52]

The suspension was mechanically stirred for four hours in aqueous solution. The time required to reach equilibrium was first established through a series of experiments where the uptake of mercury by the functionalized material was monetored as a function of time. The samples were filtered and the residual metal concentration in the solutions was measured using an ICP spectrometer.[52]

II. Regeneration of the Adsorbents

The heavy metal ion absorbed on the surface of the adsorbent of the modified mesoporous silica with thiol-functionality was removed by placing and washing the adsorbents with acidified aqueous thiourea solution (2.0 M HCl) three times, each time stirring for around one hour. Subsequently the adsorbent was washed with distilled water, and finally it was dried in air before the second uptake-removal cycle.

8.3. RESULTS AND DISCUSSION

Heavy metal pollution, especially by mercury, is an important environmental concern due to the high toxicity of the metals. The harmful effects of mercury is manifested by hindered transport processes in living cells,[1] due to the high affinity of the element for sulfur-containing biological molecules. This high affinity can be exploited for removal of mercury ions from aqueous media by designing materials with sulfur-containing groups. Since the discovery of ordered silica-based materials with controllable mesoporous structure in early nineties,[29,53] there has been a great interest in their applications in environmental clean up. A special emphasis was given to the design and synthesis of nanostructured adsorbents with desirable surface properties and porous structures.[54,55] MCM-41 having high surface area and large and accessible pores,[29] is a good candidate for an insoluble matrix for the attachment of sulfur-containing groups, that possess the desired surface affinity toward mercury ions.[43,46,56]

Here, the preparation of mercaptopropyl-functionalized OSU-6-W and characterization of its structural and adsorption properties is reported. The experimental data demonstrate a high concentration of the functional group on the mesoporous surface and high affinity of this material toward mercury ions, that is reflected by a high

adsorption capacity approaching 3.26 mmol Hg^{2+} per gram of the adsorbent or *ca.* 0.7 g Hg^{2+}/g. The nitrogen adsorption study and a successful regeneration of the mercury-loaded mercaptopropyl-modified OSU-6-W demonstrate the accessibility of pores of this material to mercury ions. An efficient regeneration of this material was achieved with acidified aqueous thiourea solution. The regenerated material showed a significant mercury uptake (above 85% of the initial value).

Thiol functional groups were introduced to the pore surface of mesoporous silica as the terminal groups of organic monolayers. The hydrocarbon chains aggregated and formed close-packed arrays on the substrate. The siloxane groups then underwent hydrolysis and ultimately became covalently attached to the substrate and cross-linked to one another. The OSU-6-W modified with MPTMS material is a useful environmental remediation agent because it has a high affinity for binding mercury and other heavy metals.[43]

The pure mesoporous silica, OSU-6-W, and the two mesoporous silicas modified with 3-mercaptopropyltrimethoxysilane (MPTMS), OSU-6-W-MPTMS-1 and OSU-6-W-MPTMS-2, and OSU-6-W-MPTMS-2-Acac have been characterized using several techniques in order to confirm the attachment of the functional groups on the silica surface, to verify the structure, and determine the functional group concentration.

8.3.1. Identification the Textural Properties of the Thiol-modified Mesoporous Silica

I. X-ray Powder Diffraction (XRD)

Figure 8.1 compares the XRD patterns of the untreated mesoporous molecular sieves, OSU-6-W, and the two different modified samples with mercaptopropylsilyl, OSU-6-W-MPTMS-1 and OSU-6-W-MPTMS-2. The XRD pattern of OSU-6-W, which

contains a dominant d_{100} reflection and two reflections at higher diffraction angle, d_{110}

and d_{200}, is consistent with ordered hexagonal channel packing.[53]
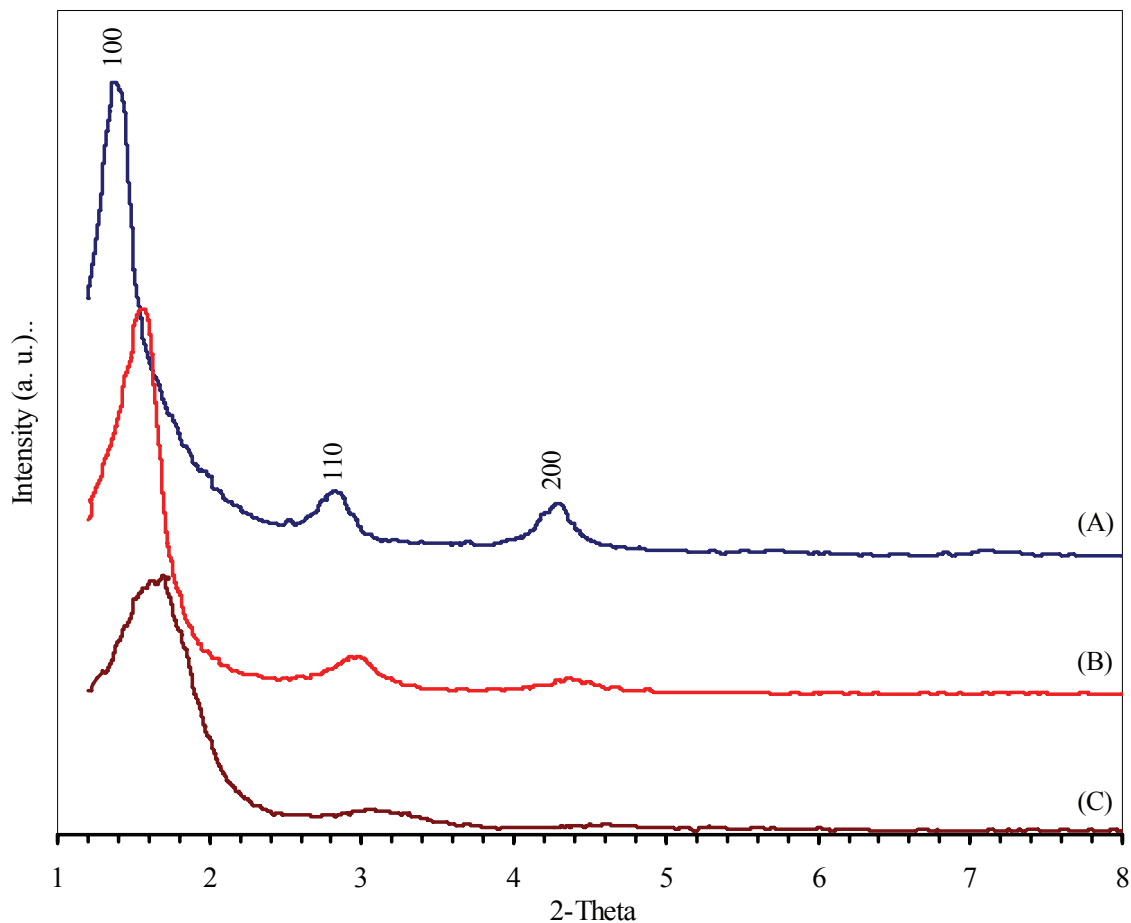
Figure 8.1. Powder X-ray diffraction patterns for OSU-6-W and their mercaptopropylsilyl-functionalized derivatives. (A) OSU-6-W, (B) OSU-6-W-MPTMS-1, and (C) OSU-6-W-MPTMS-2. The spectra are shifted vertically for the sake of clarity.

The XRD patterns of the modified samples show evidence for the conservation of

the structural order during the modification process steps. Each of the XRD patterns of

OSU-6-W-MPTMS-1 and OSU-6-W-MPTMS-2 showed three reflections. The X-ray

diffraction patterns of OSU-6-W-MPTMS-1 and OSU-6-W-MPTMS-2 show very intense

peaks (100) and two additional high-order peaks (110 and 200) with lower intensities. This result is characteristic of a hexagonal pore structure.

Organosilane grafting to the mesostructures causes a significant decrease in the XRD intensities. This is indicative of contrast matching between the silica framework and the grafted mercaptopropylsilyl groups. Contrast matching in OSU-6-W and related mesostructures has been observed previously upon filling the framework pores with organic guests.[57] The smaller contrast-matching effect in the case of OSU-6-W-MPTMS-1 probably results from the comparatively lower amount of mercaptopropylsilyl groups occupying the framework pore structure, whereas OSU-6-W-MPTMS-2 shows large contrast-matching which is most likely due to high loading of the functional groups on the surface.[46]

It should be noted that the decrease in the (100) peak intensity for OSU-6-W-MPTMS-1 and OSU-6-W-MPTMS-2 provides further evidence that grafting occurred mainly inside the mesopore channels because attachment of the organic functional groups onto the surface of the mesopore channels tends to reduce the scattering power (or scattering contrast) of the amorphous silicate wall.[46,57] These results indicate not only a significant degree of short-range ordering of the structure and well-formed hexagonal pore arrays of the samples but also the maintenance of the structural order of the synthesized adsorbents during functionalization. The cell parameters calculated from the d_{100} spacing value of OSU-6-W-MPTMS-1 was 57.3Å, whereas for OSU-6-W-MPTMS-2 it was 52.9 Å, and the wall thickness calculated from pore size measurement and XRD of OSU-6-W-MPTMS-1 was 23.8 Å whereas for OSU-6-W-MPTMS-2 it was 26.4 Å, see Table 8.1.

II. Nitrogen Adsorption-desorption Measurements

Nitrogen (N_2) adsorption/desorption isotherms for OSU-6-W-MPTMS-1 and OSU-6-W-MPTMS-2 showed irreversible type IV patterns with a H1 hysteresis loop between the adsorption and desorption branches as defined by IUPAC (Figure 8.2.). The physical properties of the unmodified OSU-6-W and the two modified samples, OSU-6-W-MPTMS-1 and OSU-6-W-MPTMS-2, such as surface area, pore size, pore volume, lattice spacing, and wall thickness, are listed in Table 8.1.

Table 8.1. Textural Properties Determined from Nitrogen Adsorption-desorption Experiments at 77 K and Powder XRD Measurements.

Sample	Specific surface area (m^2/g)	Total pore volume (cm^3/g)	Average pore size (Å)	d_{100} (Å)	Wall Thickness (Å)
OSU-6-W	1283	1.24	51.1	62.4	21.0
OSU-6-W-MPTMS-1	978	0.94	42.3	57.3	23.8
OSU-6-W-MPTMS-2	701	0.68	34.7	52.9	26.4

The calculated Brunauer-Emmett-Teller surface areas of OSU-6-W, OSU-6-W-MPTMS-1, and OSU-6-W-MPTMS-2 were 1283, 978, and 701 m^2/g, respectively. Thus the surface area decreased with an increase the extent of functional groups attached. The adsorption-desorption isotherms of OSU-6-W, OSU-6-W-MPTMS-1, and OSU-6-W-MPTMS-2 featured hysteresis loops with steep adsorption and desorption branches. The sharpness of the adsorption branches is indicative of a narrow mesopore size distribution. The position of the capillary condensation steps in the modified samples shifted to lower pressure values, suggesting a reduction in the mesopore size because the capillary

condensation pressure increases with the pore diameter. This was also confirmed by changes in the pore size calculated from the adsorption branch of the nitrogen adsorption/desorption isotherm using the Barrett-Joyner-Halenda formula.[58]
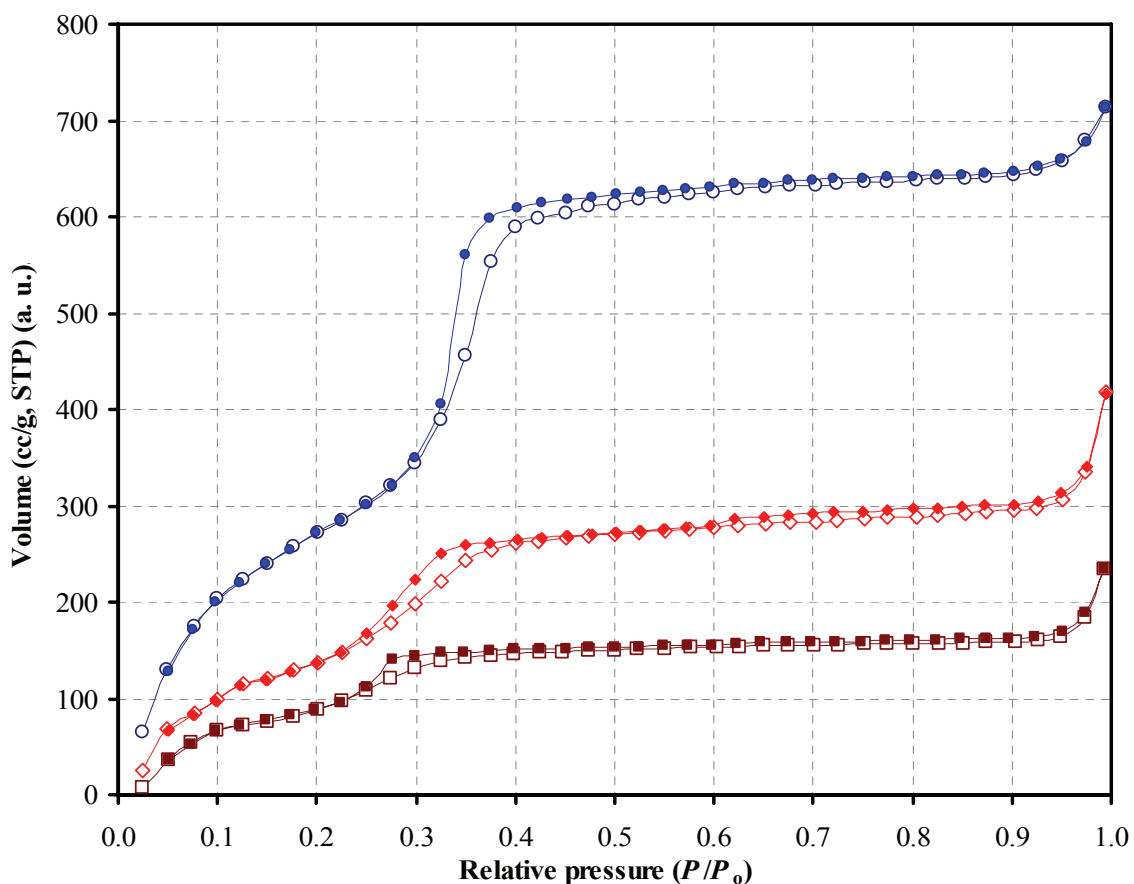
Figure 8.2. Nitrogen adsorption/desorption isotherms for (○) unmodified OSU-6-W and thiol-functionalized OSU-6-W ((◊) OSU-6-W-MPTMS-1 and (□) OSU-6-W-MPTMS-2). Open symbols: adsorption; closed symbols: desorption. The isotherm data are shifted vertically for the sake of clarity.

Upon grafting mercaptopropylsiloxane groups to the framework walls, a significant decrease in the surface area, pore volume, and pore diameter was observed for each sample as a result of the ligating thiol moieties present in the framework channels.

Nonetheless, significant surface areas and porosities were retained in all the mesostructures after mercaptopropylsilyl functionalization of the pore walls. The surface properties of the mercapto-functionalized adsorbents and their parent mesostructures are summarized in Table 8.1. The overall shape of the adsorption/desorption isotherms remained unchanged, and the pronounced steps of capillary condensation in primary mesopores were evident, indicating that the ordering of the OSU-6-W support was not affected by the modification.
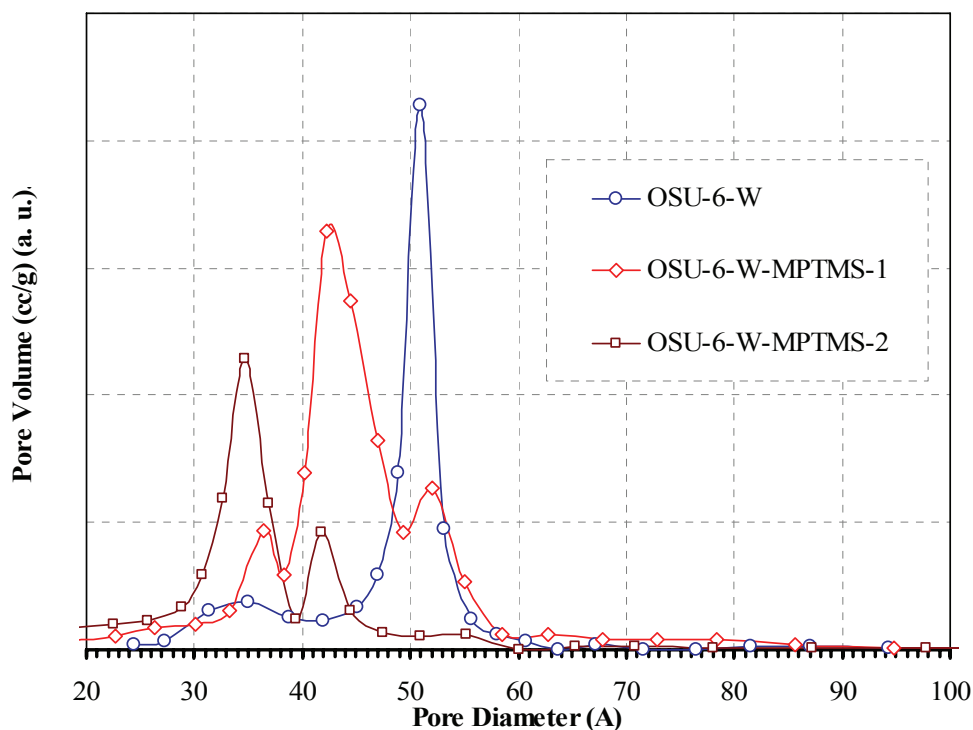
Figure 8.3. The pore size distribution of (○) OSU-6-W (max at 51.1 Å), (◊) OSU-6-W-MPTMS-1 (max at 42.3 Å), and (□) OSU-6-W-MPTMS-2 (max at 34.7 Å).

The adsorption isotherms were used for the calculations of the pore size distributions in OSU-6-W, OSU-6-W-MPTMS-1, and OSU-6-W-MPTMS-2.[59] The pore

size distributions (Figure 8.3) illustrate that all three silica gels are mesoporous materials with the maximum pore size distributions located at *ca.* 51 Å for OSU-6-W, 42.3 Å for OSU-6-W-MPTMS-1, and 34.7 Å for OSU-6-W-MPTMS-2, respectively. A broader maximum pore size distribution and a rather large width of half-height were observed for OSU-6-W-MPTMS-1 which has a lower loading of the functional group. Both mesoporous materials OSU-6-W and OSU-6-W-MPTMS-2, show relatively narrower maximum pore size distributions than OSU-6-W-MPTMS-1. Overall, all materials show narrow pore size distribution that are less than 7.0 Å.

8.3.2. Identification of the Thiol-functional Groups

I. Solid State ^{13}C CP/MAS NMR Spectroscopy

The structure of the functionalized monolayers and the chemical bonding can be studied by solid-state NMR experiments.[60] Single-pulse ^{13}C NMR spectra and peak assignments [Si-CH$_2$(1)-CH$_2$(2)-CH$_2$(3)-SH] for samples functionalized monolayers on mesoporous silicates, are shown in Figure 8.4. For OSU-6-W-MPTMS-1 (Figure 8.4(A)), the peak at 11.8 ppm was attributed to the methylene carbon group C1, directly bonded to the Si atom. The peak at 27.7 ppm was attributed to the other two methylene carbons (C2 and C3). For OSU-6-W-MPTMS-2 (Figure 8.4(B)), there are three peaks observed at 12.3, 26.1, and 29.4 ppm that are assigned to the methylene carbon (C1) directly bonded to the Si atom, to the middle methylene carbon (C2), and to the methylene carbon (C3) next to the -SH group, respectively, on the basis of the chemical shifts reported for CH$_3$(CH$_2$)$_7$SH.[60] The difference between Figure 8.4 (A) and Figure 8.4 (B) is attributable to a different molecular conformation for the organic monolayers at different coverages. At low surface coverage, the carbon chains can adopt a wide range of conformations;

therefore, the peaks for C2 and C3 cannot be distinguished because of conformational
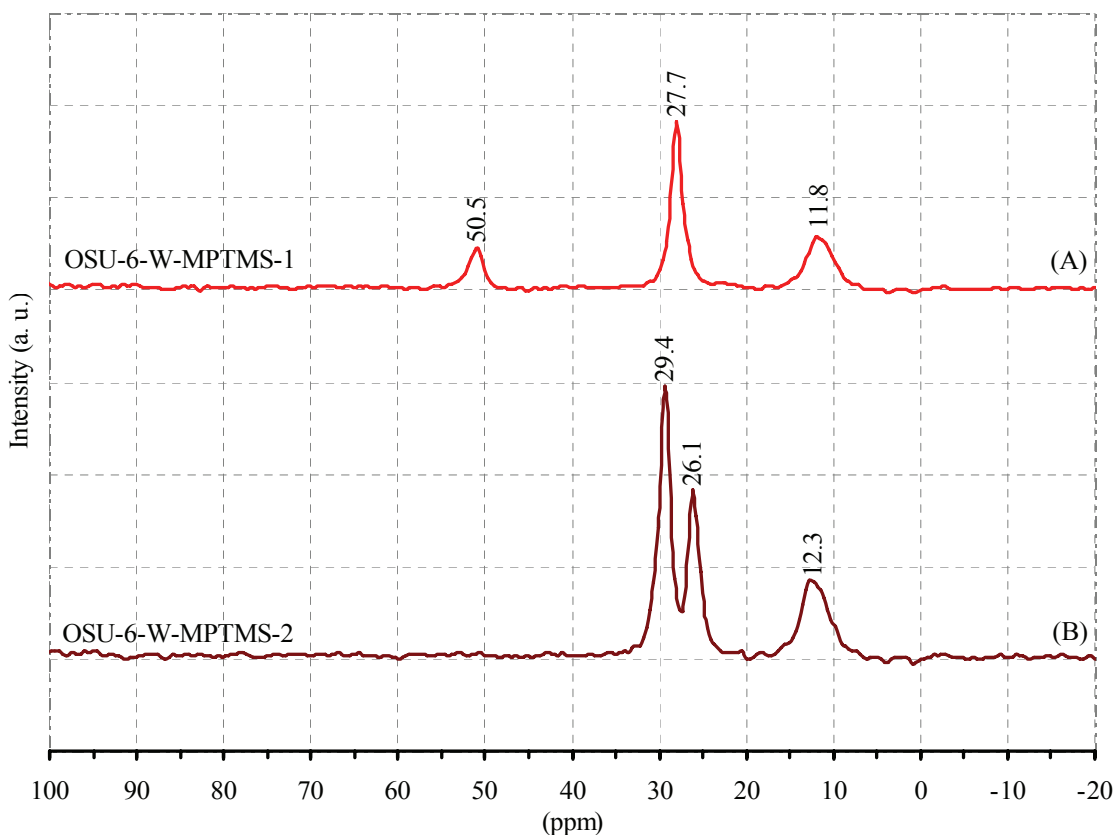
heterogeneity.

Figure 8.4. Solid state ^{13}C NMR spectra of organic monolayers on mesoporous silica, OSU-6-W, with the peak assignments. (A) OSU-6-W-MPTMS-1, C1 and C2 cannot be separated because of conformational heterogeneity. (B) OSU-6-W-MPTMS-2, C1 and C2 are clearly resolved, suggesting a more homogeneous environment.

At higher population densities, all of the carbon chains are near one another and

have a more upright orientation with respect to the silica surface, Scheme 8.2. The

molecules have a higher degree of ordering that narrows the line widths in the ^{13}C

spectrum and allows better resolution of the peaks for all three carbons. Moreover, the

existence of a ^{13}C CP/MAS NMR spectrum at 50.5 ppm in the OSU-6-W-MPTMS-1

could be from the presence of a small amount of methoxy groups (SiOCH$_3$) from the

functional group or may come from the methanol formed during the hydrolysis and condensation processes.

II. Solid State ^{29}Si CP/MAS NMR Spectroscopy

The close-packed conformation of the carbon chains is also evident in solid state ^{29}Si NMR results, Figure 8.5. Solid state ^{29}Si MAS NMR spectra of the unfunctionalized mesostructure (see Figure 8.5(A)) was obtained in order to estimate the Q^3 to Q^4 ratio and the fraction of framework silicon sites that have been silylated.
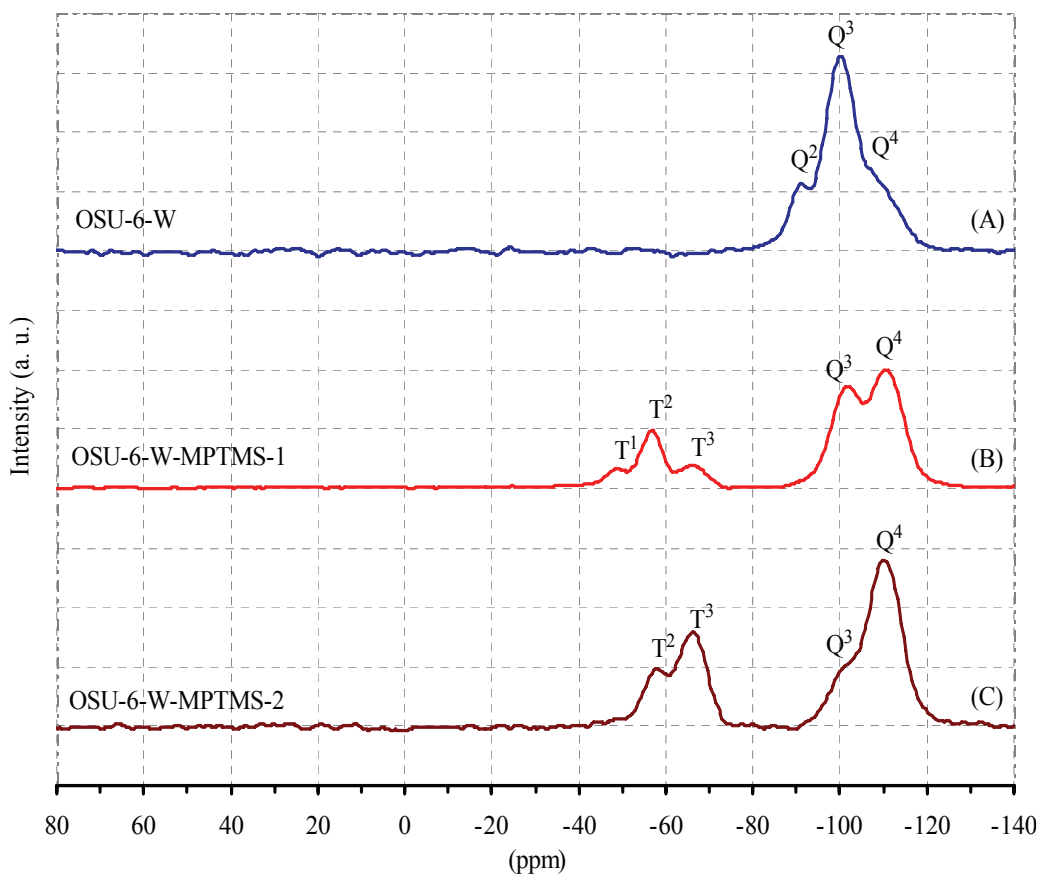
Figure 8.5. Solid state ^{29}Si NMR spectra of; (A) unmodified OSU-6-W and the two modified samples ((B) OSU-6-W-MPTMS-1 and (C) OSU-6-W-MPTMS-2).

Relative peak intensities in the solid state ^{29}Si cross-polarization magic angle spinning (CP/MAS) give indication of the surface loading and surface structure ordering.

In the unfunctionalized mesostructure, OSU-6-W, three signals were observed near -91.2, -100.4, and -107.9 ppm (Figure 8.5 (A)), corresponding to the Q^2 silanol sites $[(SiO)_2Si(OH)_2]$, Q^3 silanol sites $[(SiO)_3SiOH]$, and Q^4 framework silica sites $[(SiO)_4Si]$, respectively.[61] Grafting of the mercaptopropylsilyl moieties to these mesostructures causes the relative Q^3 and Q^4 signal intensities to decrease significantly. The large peaks at -101.9, -111.1 ppm, and at -100.6, -110.3 ppm for the modified samples, OSU-6-W-MPTMS-1 and OSU-6-W-MPTMS-2, respectively, are from the silica support. In Figure 8.5 (B), three additional peaks at -48.9 (T^1), -57.6 (T^2), and -66.4 (T^3) ppm are identified as corresponding to three different environments for the siloxane groups in the functionalized monolayers:[62] (i) isolated groups that are not bound to any neighboring siloxanes (T^1), (ii) terminal groups that are only bound to one neighboring siloxane (T^2), and (iii) cross-linked groups that are bound to two neighboring siloxanes (T^3). Among the three, the most dominant peak comes from the terminal group (T^2). In Figure 8.5 (C), the molecules are closer to one another, and the most predominant peak, at -66.6 ppm, corresponds to the cross-linked siloxane group; the isolated siloxane group is absent. The transition from disordered conformation at low surface coverage to close-packed conformation at high coverage is illustrated in Scheme 8.3.[43]

(A)

(B)
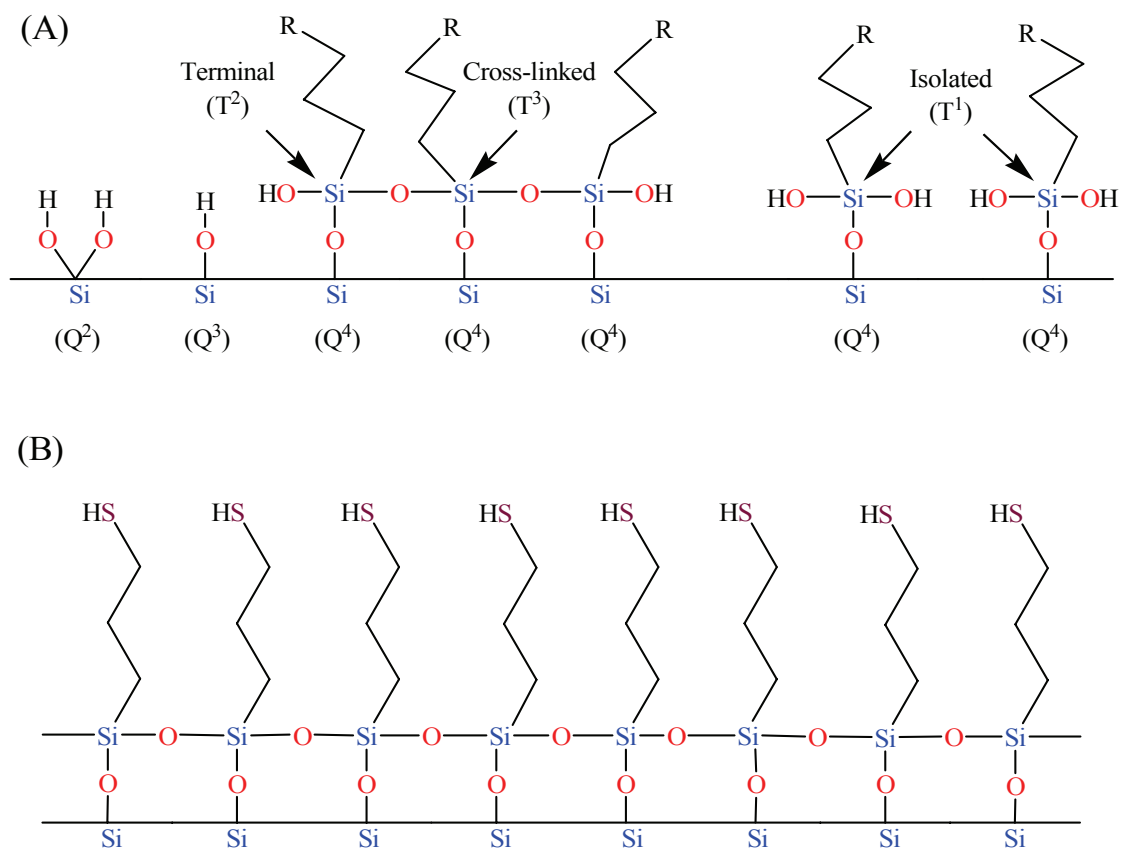
Scheme 8.3. Schematic conformations of functionalized monolayers on the surface under different conditions. (A) Disordered molecules at low surface coverage and (B) Close-packed at high surface coverage.

III. Fourier Transform Infrared Spectroscopy (FT-IR)

Figure 8.6 shows the FT-IR spectra of the untreated mesoporous silica and the two thiol-treated mesoporous samples, OSU-6-W-MPTMS-1 and OSU-6-W-MPTMS-2, in the low and high wavenumber ranges. Absorbance bands at 1100-1000 cm^{-1} and 800 cm^{-1} were observed for Si-O-Si and O-Si-O vibration modes of the silica lattice.[63-66] The shoulder at around 960-940 cm^{-1} has been reported to be associated with stretching mode of Si-OH.[63-66]
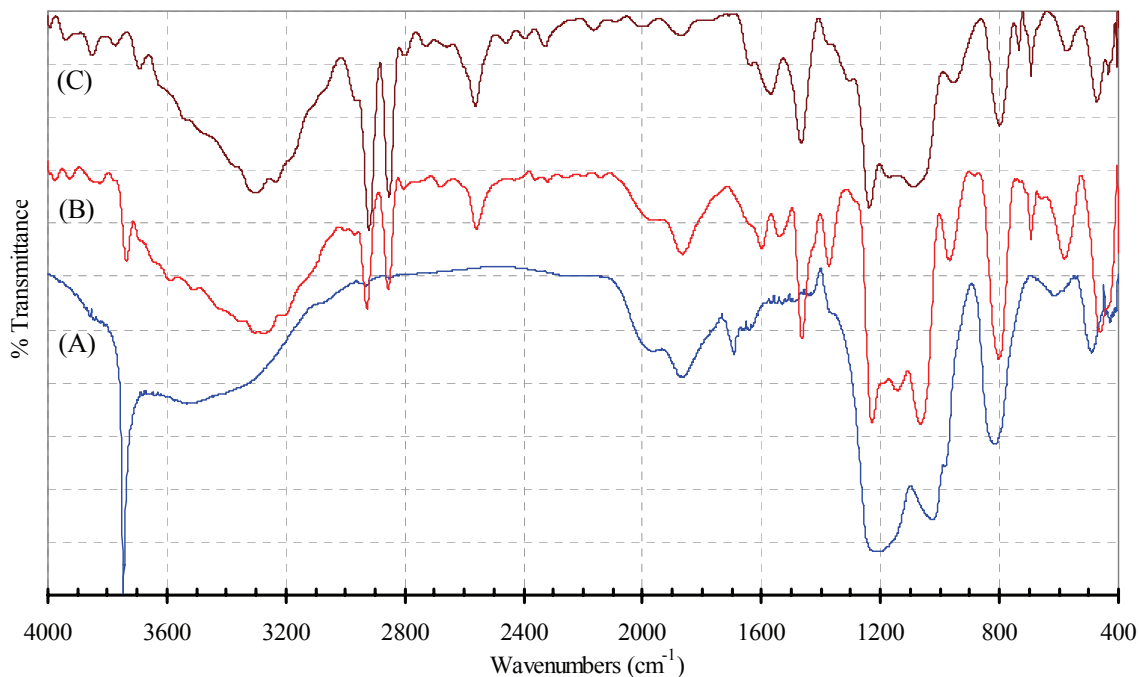
Figure 8.6. FT-IR spectra of; (A) the untreated mesoporous silica, OSU-6-W, (B) OSU-6-W-MPTMS-1, and (C) OSU-6-W-MPTMS-2.

The functional groups contained in the two samples were identified by FT-IR. The O-H bond stretching bands of the silanol groups of OSU-6-W were observed at 3200-3600 cm^{-1} and at 3746 cm^{-1}.[64] After immobilization of the thiol functionality, the intensity of the OH stretching band of silanol groups of OSU-6-W was decreased. After the thiol-attachment, FTIR spectra of OSU-6-W-MPTMS-1 shows two medium-intensity bands at 2561 cm^{-1} and 698 cm^{-1}, and two strong-intensity bands were observed at 2934 cm^{-1} and 2841 cm^{-1}. The former were attributed to thiol S-H stretch and C-S vibrations, respectively, and the letter bands were attributed to the C-H stretch of the methylenes of the alkyl chain.[67] The presence of a significant amount of mercaptopropylsilyl moieties in the modified OSU-6-W-MPTMS-2 sample was confirmed by the observation of

intense bands assigned to the C-H vibrations in the 2850-2930 cm^{-1} region and of stretching bands attributed to the S-H and C-S vibrations at 2558 and 699 cm^{-1}, respectively.[68] The FT-IR spectra indicate that an organic thiol monolayer was successfully immobilized inside the nanopores of the mesoporous silica.

On the basis of elemental analysis, the amounts of functional groups were calculated to be 2.50 and 4.92 groups/nm^2 for OSU-6-W-MPTMS-1 and OSU-6-W-MPTMS-2, respectively. The amount of grafted thiol functional groups was close to that of the other functional group containing nitrogen atoms. It has been reported that MPTMS [HSCH$_2$CH$_2$CH$_2$Si(OCH$_3$)$_3$], which has weaker basic catalytic properties than a nitrogen-based organosilanes (*i.e.,* amine, ethylenediamine, and diethylenetriamine) reacts via two-stage reactions.[69] These weakly basic characteristics of thiol functional groups were overcome by the use of an amine catalyst (triethylamine) which results in increase in the amount of grafted thiol functional groups. The relative surface coverage was estimated on the basis of the surface area of OSU-6-W and element analysis results after the thiol functional group was attached, and the full loading that could be achieved on the flat surface under the assumption of 5×10^{18} molecules/m^2 (5 molecule/nm^2) in a full surface coverage.[43] The fraction of surface coverage of OSU-6-W-MPTMS-1 and OSU-6-W-MPTMS-2 was about 50% and 98% of the full surface coverage, respectively. Spacing of each thiol functional group was about 2.0 nm.[70]

8.3.3. Identification of the Thiol-acetate Groups Immobilized into the Modified Mesoporous Silica

The thiol-acetate immobilized ligand system (OSU-6-W-MPTMS-2-Acac) was prepared by the reaction of mesoporous silica immobilized thiol ligand system (OSU-6-

W-MPTMS-2) with an excess of ethylchloroacetate in the presence of triethylamine to facilitate the removal of generated HCl, then the OSU-6-W-MPTMS-2-Acetate was hydrolyzed by an aqueous solution of 2.0 M HCl, Scheme 8.2.

I. Surface Area Analysis (BET)

The surface area of the mesoporous sample immobilized thiol-acetate group was less than that of the mesoporous OSU-6-W-MPTMS-2. The surface area dropped from 701 m^2/g to 473 m^2/g.

II. Fourier Transform Infrared Spectroscopy (FT-IR)

The FT-IR spectra for the OSU-6-W-MPTMS-2 and the OSU-6-W-MPTMS-2-Acac samples were obtained and compared to each other. Three characteristic regions at 3000-3500 cm^{-1}, 1500-1750 cm^{-1} and 900-1200 cm^{-1}, are identified corresponding to υ(OH), υ(C=O) and υ(SiO) vibrations.[63] These assignments were based on literature spectral data reported for similar systems.[71] The IR spectrum for the unhydrolyzed thiol-acetate ligand shows an absorbance band at 1721 cm^{-1} due to ester υ(C=O) stretching vibration. This band was not found in the IR spectrum of 3-mercaptopropylpolysiloxane. The IR spectrum for the hydrolyzed ligand system (OSU-6-W-MPTMS-2-Acac) shows two bands at 1724 cm^{-1} and 1640 cm^{-1} that are assigned to the asymmetric and symmetric stretching of the carboxylate.

III. Elemental Analysis (EA)

The total carbon contents (C%) of the new material after immobilizing the acetate group (OSU-6-W-MPTMS-2-Acac) is different from the thiol-functionalized sample (OSU-6-W-MPTMS-2). The total carbon content increased from 14.61% to 21.44%. This result indicates the attachment of the active groups on the thiol-functional groups.

8.3.4. Estimate the Total Surface Loading of the Mercaptopropyl Functional Groups on the Ordered Mesoporous Silica

The amount of mercaptopropyl deposited on the surface was quantified using two variables. The surface loading (l) expresses the amount of deposited molecules in mmol/g. The number of molecules deposited per nm^2 is given by the surface coverage (C). The surface coverage (C) was calculated by rationing the loading (l) to the specific surface area (S_{BET}) of the sample. Multiplication by Avogadro's number ($N_A = 6.022$ X 10^{23} molecules/mole) yields units of molecules/nm^2:[72]

$$C = (l \, / \, S_{BET}) \cdot N_A$$

Both values use the mass of the pure mesoporous silica before modification as a reference.

I. Elemental Analysis (Combustion Analysis)

The C and N analyses of the modified mesoporous materials were used to determine the quantity of mercaptopropylsilyl moieties grafted to the framework channels. The extremely low levels of nitrogen in the materials demonstrated the effectiveness of the ethanol extraction process in removing the amine surfactants from the OSU-6-W silicas. The SH group densities on the pore walls of the adsorbents (Table 8.2) were calculated on the basis of these loadings and the BET surface area of the unfunctionalized mesostructure.

Carbon analysis was carried out for all modified samples. The concentration of attached groups was determined as follows:[73,74]

$$C \, (groups/nm^2) = 6x10^5 \, P_C \, /[(1200n_C - WP_C)S_{BET}]$$

where C is the concentration of attached groups, which contain carbon; P_C is the

percentage of carbon in the sample, n_C is the number of carbon atoms in the attached

group (counted as C_3), W is the corrected formula mass of the modifier (counted as

$C_3H_7O_3SiS$), and S_{BET} is the specific surface area of the unbounded substrate (1283 m^2/g).

Table 8.2. Carbon and nitrogen elemental analysis, and concentration of mercaptopropyl functional groups

Sample	C %	N %	Surface Area (m^2/g)	MPTMS (group/nm^2)
OSU-6-W	0.10	0.06	1283	---
OSU-6-W-MPTMS-1	10.64	0.09	978	2.50
OSU-6-W-MPTMS-2	14.61	0.16	701	4.92

III. Solid State ^{29}Si CP/MAS NMR Spectrum

The relative ^{29}Si CP/MAS NMR peak areas, Table 8.3, were assigned and

determined as discussed in chapter three. The differences in the silanol concentration

before and after silylation were relatively equal to the concentration of the functional

groups.

Table 8.3. Solid state ^{29}Si CP/MAS NMR deconvolution results

Sample	Q^4 (%)	Q^3 (%)	Q^2 (%)	[SiOH] (mmol/g)	[SiOH] (molecule/nm^2)	[MPTMS] (group/nm^2)
OSU-6-W	14.38	71.73	13.89	14.43	6.77	---
OSU-6-W-MPTMS-1	55.57	44.43	0.00	6.94	4.27	2.49
OSU-6-W-MPTMS-2	82.99	17.01	0.00	2.76	2.08	4.69

A significantly larger coverage of functional groups (4.69 group/nm^2) has obtained compare to the results in the literature (3.80 group/nm^2).[43] This difference probably arises from the difference in the surface areas, 1283 vs. 900 m^2/g, respectively, the pretreatment of the mesoporous with amine and the intermediate water treatment in the silylation process. Also, the larger pore size can avoid a steric congestion of the silane molecules.

8.3.5. Application of the Adsorbents

8.3.5.1. Adsorption of Mercury Hg(II) Ions onto Thiol-grafted Mesostructures

In the present work, the Hg(II) adsorption study was carried out on thiol-grafted mesostructures for the purpose of illustrating the importance of pore size and functional group surface density on thiol group availability for Hg(II) binding. The studies by Mercier *et al.,*[47] and those of Feng *et al.,*[43] have shown that the heavy metal ion selectivity is not affected by the presence of the electrolytes normally associated with groundwater and waste streams. Also, no detectable amounts of Hg(II) was adsorbed by the unfunctionalized mesostructure.

I. Effect of pH

The effect of changing the solution pH on the uptake of mercury (Hg^{2+}) ion is shown in Figure 8.7. The results show an increase of metal ion uptake with increasing pH value that reaches a maximum at pH 7.5. Lower uptake occurs at lower pH values due to the protonation of the thiol moieties. The uptake study at high pH > 10 will lead to the dissolve of the mesoporous silica.[75-77]
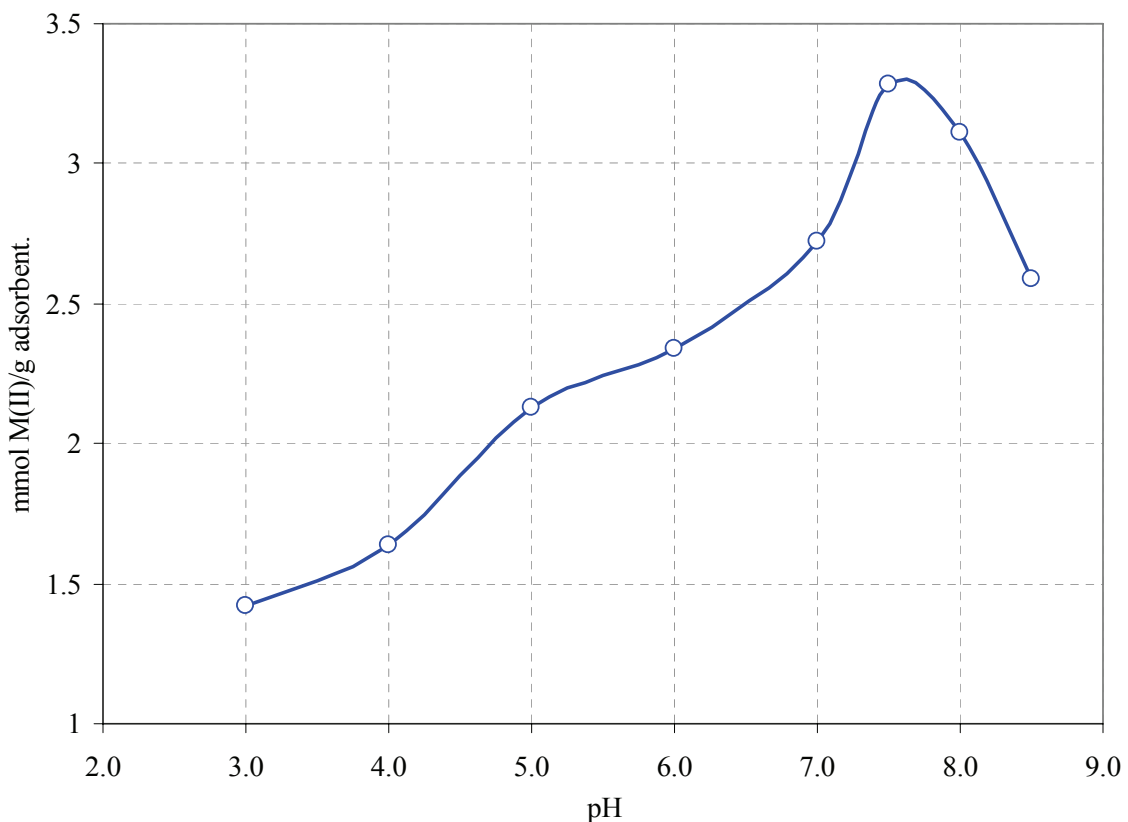
Figure 8.7. Mercury ion uptake versus pH using OSU-6-W-MPTMS-2

II. Effect of Exposure Time

The metal ion (Hg^{2+}) uptake rate as mmol M^{2+}/g ligand versus time (min), was determined by shaking the thiol-functional mesoporous materials (OSU-6-W-MPTMS-1 and OSU-6-W-MPTMS-2) in aqueous solution of the divalent metal ion at different time intervals. The result is given in Figure 8.8. It is shown that the metal ion uptake is increased as a function of exposure time in a nonlinear fashion. The increase of the metal ion uptake with time is attributed to diffusion factors. The adsorption of Hg^{2+} was found to be first order and rate constants were 0.0081 min^{-1} and 0.0059 min^{-1} for OSU-6-W-MPTMS-1 and OSU-6-W-MPTMS-2, respectively.
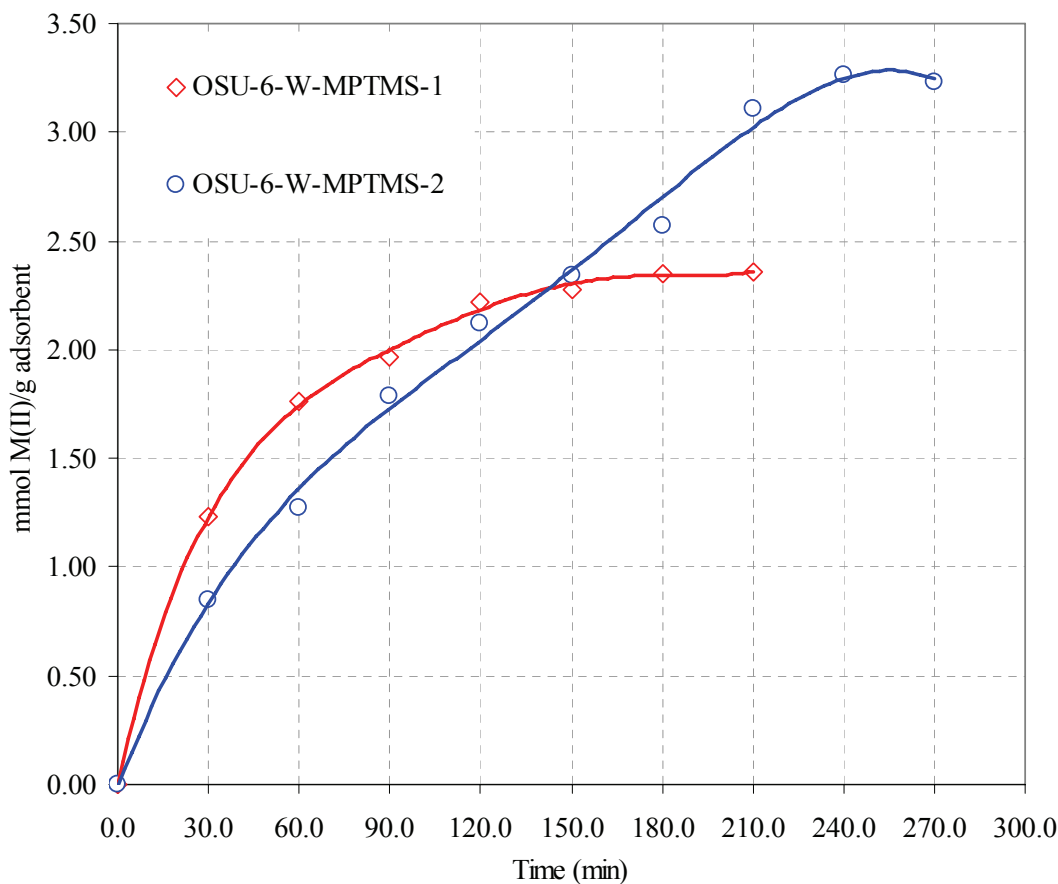
Figure 8.8. The uptake of Hg^{2+} ions by the mesoporous functionalized with thiol ligand system versus time at pH 7.5.

The uptake rate constant for Hg(II) by OSU-6-W-MPTMS-2 was smaller than that for OSU-6-W-MPTMS-1. This may be explained by the smaller pore size of the more highly functionalized material as compared to OSU-6-W-MPTMS-1. Nevertheless, overall the uptake rate is quite fast and can be attributed to the high surface area, the large pore size, and small particle size ($< 1.5\mu m$ from SEM).[78,79] Saturation by the mercury metal ion is found to occur after 3 and 4 hours for OSU-6-W-MPTMS-1 and OSU-6-W-MPTMS-2, respectively.

III. Mercury Ions Adsorption

The Hg^{2+} Langmuir adsorption isotherms of both adsorbents, Figures 8.9 and 8.10, exhibited typical Langmuir behavior. The maximum mercury ion adsorption capacities of these materials were 2.46 mmol/g (493.5 mg/g) and 3.32 mmol/g (665.9 mg/g) for OSU-6-W-MPTMS-1 and OSU-6-W-MPTMS-2, respectively, Table 8.4.
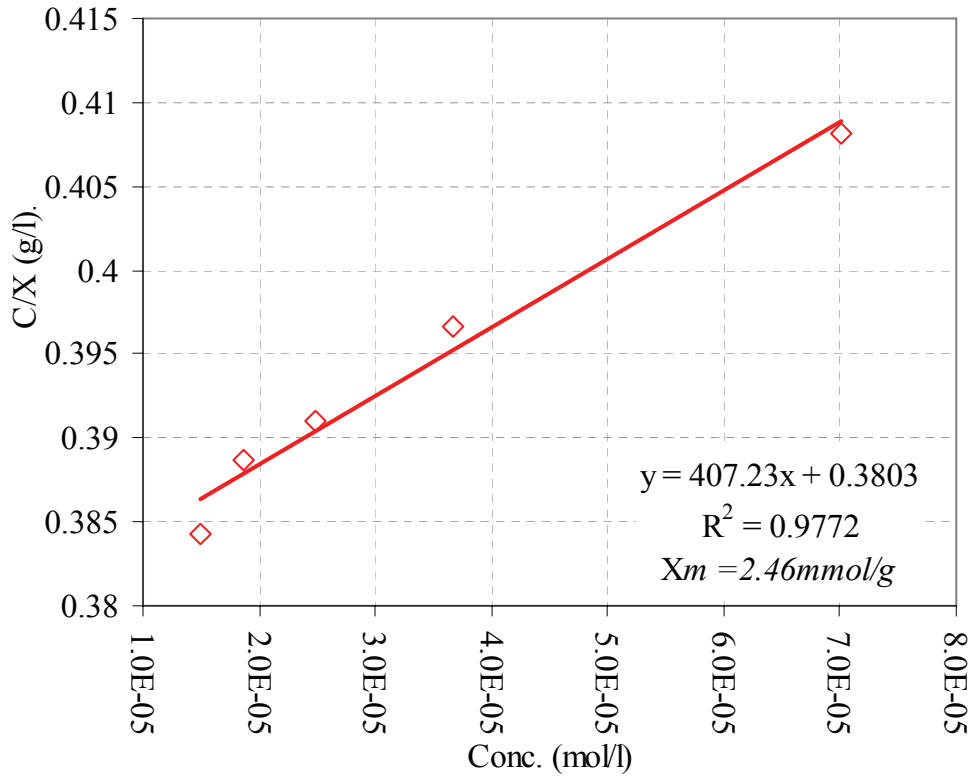
Figure 8.9. Hg^{2+} Langmuir adsorption isotherms for (◊) OSU-6-W-MPTMS-1.
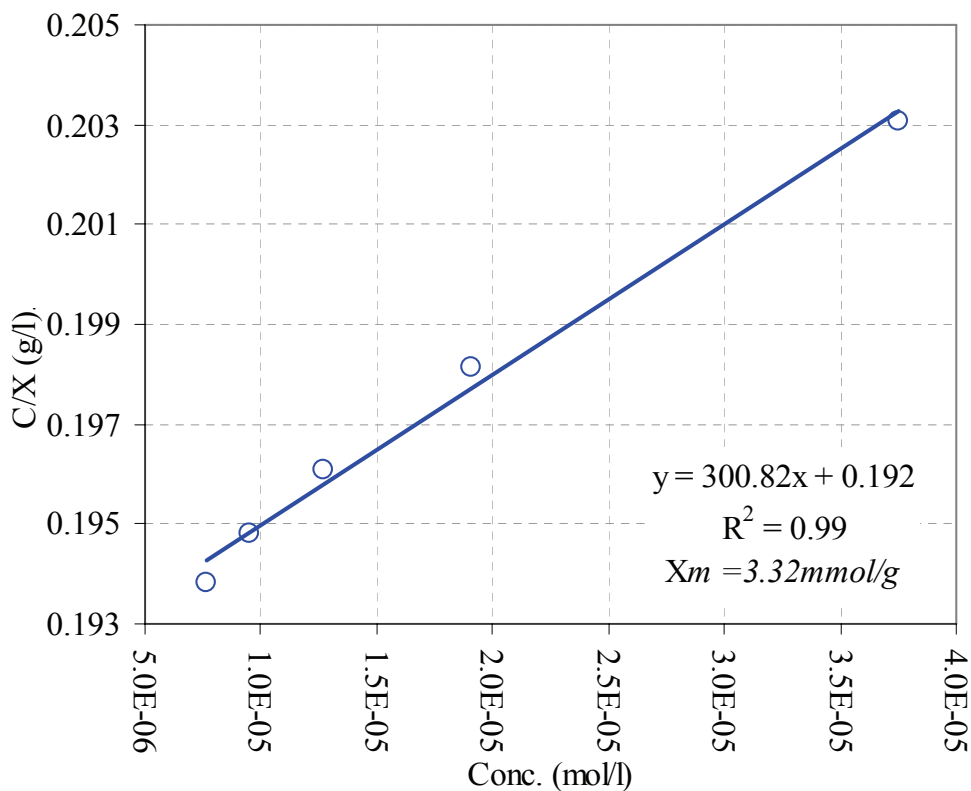
Figure 8.10. Hg^{2+} Langmuir adsorption isotherms for (○) OSU-6-W-MPTMS-2.

The number of thiol groups in each adsorbant are 2.95 and 4.05 mmol/g, respectively. Thus, about 82% of the available thiol groups are occupied by mercury ions (Table 8.4).[47]

The very high mercaptopropyl group content of OSU-6-W-MPTMS-2 resulted in an adsorption capacity that is markedly higher than that reported for MP-HMS (1.5 mmol/g, 300.9 mg/g)[46,47] and for FMMS (2.5 mmol/g, 501.5 mg/g),[43] therefore, the mesoporous OSU-6-W-MPTMS-2 has the highest capacity Hg^{2+} mesostructure-based adsorbent reported to date.

Table 8.4. Hg(II) Adsorption Data for Mercaptopropyl- Functionalized Mesoporous Molecular Sieves

Material	SH content (mmol/g)[a]	Hg(II) adsorbed (mmol/g)[b]	Hg/S molar ratio
OSU-6-W-MPTMS-1	2.95	2.46	0.83
OSU-6-W-MPTMS-2	4.05	3.32	0.82

[a] Millimoles of S per gram of Thiol-functionalized adsorbent from the titration method. [b] Millimoles of Hg adsorbed per gram of Thiol-functionalized adsorbent.

As seen from the results in Table 8.4, both thiol-functionalized samples, OSU-6-W-MPTMS-1 and OSU-6-W-MPTMS-2, allow Hg(II) ions to access all of the complexing thiol groups in the material (*i.e.,* Hg/S = 0.83 and 0.82, respectively). These derivatives retain large pore diameters (42.3 and 34.7Å) and significant pore volumes (0.94 and 0.68 cm^3/g), despite the high mercaptopropyl density (~ 2.95 and ~ 4.05 SH/nm^2, respectively) on the pore walls. These physical characteristics allow for the efficient binding of mercury to the mercaptopropyl groups grafted on the large, open and uniform pore channels of the adsorbent.

The mercaptopropylsilyl functionalized MCM-41 derivatives reported by Feng *et al.*,[43] are very effective heavy metal ion adsorbents, binding Hg(II) ions quantitatively to levels up to 501 mg/g. Their products, designated FMMS, have structural and reactivity features in common with our functionalized samples, such as the retention of framework mesoporosity and the ability to bind very high levels of Hg(II) ions to all of the thiol moieties present in the material, Table 8.5.

Table 8.5. Comparison between the physicochemical properties and mercury ion adsorption properties of reported thiol-functionalized mesostructures

Adsorbent	Synthesis Method	Pore diameter (Å)	Thiol content (mmol/g)	Hg^{2+} Adsorption capacity (mmol/g)	Hg/S molar ratio
FMMS[43]	Grafting	40.0	3.20	2.50	0.78
MP(2)-MSU-2[49]	One-step	28.0	2.30	2.30	1.00
MP-MCM-41[82]	One-step	14.0	4.70	2.10	0.45
MP-HMS-C12[47,46]	Grafting	27.0	1.50	1.50	1.00
MP-MSU-2[49]	One-step	42.0	0.90	0.90	1.00
MP-PCH[44]	Grafting	< 10.0	1.10	0.74	0.67
MP-MCM-41[46]	Grafting	20.0	0.57	0.59	1.00
MP-HMS-C8[46]	Grafting	15.0	0.90	0.55	0.61
OSU-6-W-MPTMS-1	Grafting	42.3	2.95	2.46	0.83
OSU-6-W-MPTMS-2	Grafting	34.7	4.05	3.32	0.82

The preparation of FMMS derivatives from calcined MCM-41, however, requires several rehydration and mercaptopropylsiloxane treatment steps to build up a mercaptopropyl monolayer on the framework walls. This multi-step process is necessary, in part, because the OH group population is substantially depleted by the surfactant calcination step. In contrast, the preparation of OSU-6-W-MPTMS-1 and OSU-6-W-MPTMS-2 are quite facile, involving only simple mercaptopropylsilyl grafting steps to afford the adsorbents. Moreover, the room-temperature synthesis used to prepare OSU-6 and the ability to recover the surfactant by ethanol extraction offer additional processing advantages.

Stein and coworkers[80] have recently reported the one-step synthesis of a very highly thiol-functionalized MCM-41-type framework, using an electrostatic surfactant

assembly strategy. The abundant thiol groups lining the inherently small diameters of such mesostructures, however, resulted in the constriction of their pore channels into the micropore size domain (1.4 nm diameter), thereby resulting in less-than-complete complexation with the material's thiol groups (Hg/S molar ratio = 0.45) (Table 8.5). On the other hand, the ambient temperature non-ionic surfactant assembly protocol presented in this work succeeded in producing a highly thiol-functionalized mesostructure (OSU-6-W-MPTMS-2) while maintaining pore channel mesoporosity. The greater pore diameter of OSU-6-W-MPTMS-2 affords complete access of mercury ions to its binding sites. As a result, the Hg^{2+} adsorption capacity of OSU-6-W-MPTMS-2 supercedes that of the other functionalized MCM-41 materials. Furthermore, the diffusion of the mercury ions into the OSU-6-W-MPTMS-2 pore channels is likely to be more favored owing to its significantly larger pore size.

Compared to mesostructured metal ion adsorbents, other solid-phase complexants exhibit substantially inferior metal-binding properties. When thiol groups are grafted into the interlamellar region of clay minerals, fewer than 10% of these sites are available for metal ion binding. The low utilization of the grafted ligand sites was attributed to the "stuffing" of the interlayer region of the clay, which precluded access of the target metal ions to most of the ligand sites.[19] Limited access was also observed for adsorbents prepared by the grafting of thiol moieties to the surface of porous silica gel. Although disordered (amorphous) silicas can exhibit surface areas and average pore diameters comparable to MCM-41, OSU-6-W, and HMS silicas, the broad pore size distributions and necking of the pores result in significant pore blockage functionalization.[47] The much higher metal ion loading levels observed for metal ion traps prepared from open-

framework mesoporous molecular sieve silicas can be attributed to their uniquely large and relatively uniform pore structures.

The results herein emphasize the advantages of molecular sieve silicas and the importance of the framework hydroxylation, nanoscale pore structure, and particle morphology in the design of efficient, high capacity heavy metal ion absorbents. When the channel pores are comparatively narrow (diameter < 20 Å) and abundant hydroxyl sites are present, the grafting of functional units is likely to result in highly congested environments within the pore networks, drastically reducing the surface areas, pore diameters, and pore volumes. As a consequence, the effective binding of adsorbate species to these functional sites may become significantly restricted. However, framework mesostructures that possess both large pore channel dimensions (diameters > 30 Å) and abundant surface hydroxyl groups are conducive to the formation of framework channels with both a large number of functional sites and the retention of appreciable open-framework characteristics (*i.e.,* high surface areas, pore diameters, and pore volumes). These latter features of mesoporous molecular sieve silicas, particularly as manifested in OSU-6-W material formed by neutral surfactant assembly, should favorably impact the field of absorbent technology and the ongoing efforts to design high-performance materials for environmental cleanup and heavy metal ion recovery.

IV. Adsorbent Regeneration

Treatment of the mercury-loaded material (OSU-6-W-MPTMS-2) with acidified aqueous thiourea solution (2.0 *M* HCl) three times each time stirring for around one hours resulted in the complete removal of the bound Hg^{2+} from the structure, regenerating the adsorbent for further metal ion uptake. The regenerated material show high mercury ion

uptake capacity of 2.87 mmol/g (~ 86.5%).   This result a lot much better than that reported for acid-regenerated FMMS [HCl (12.1 M)],[43] where the mercury ion uptake capacity of the acid-regenerated FMMS dropped dramatically to about 60% of its original adsorption capacity, which suggests that, the acid-leaching method with high concentration is at least partially destructive towards the mesostructures. These results suggest that, despite the effectiveness of the concentrated acid regeneration technique, acidified aqueous thiourea solution with moderate concentration of HCl should be used.

8.4. CONCLUSION

On the basis of the XRD patterns, N_2 adsorption isotherms, NMR and FTIR spectra, and elemental analyses presented above, we may conclude that the high surface area mesoporous silica with large pore size, pore volume, and narrow pore size distribution facilitate the incorporation of the mercapto-functional groups. However, the reaction conditions and the silanol group concentration play an important role in determine the amount of the functional groups. For instance, the use of an amine catalyst had shown to improve the coverage. Moreover, the use of water in an intermediate step, to hydrolyzed methoxy group left after first functionalization step, showed an improvement in the total surface coverage. The use of OSU-6-W silica prepared from C12 amine surfactants is a useful substrate for the design of functionalized mesoporous materials, because the neutral framework as assembled by the (S^oI^o) process optimizes the surface OH group density for reaction with siloxanes. This allows for the grafting of a large number of functional groups to the pore channel walls of the oxide, resulting in a highly functionalized pore wall surface.

This work has demonstrated a practical new synthesis strategy for the preparation of mesoporous adsorbant for mercury and other metal ion adsorbents. One material prepared by the new technique had a pore structure, composition and Hg loading capacity higher than that of FMMS (the highest capacity mesostructured mercury adsorbent previously reported).[43] For the first time, a combination of two synthesis procedures was used to yield a highly thiol-functionalized mesostructure which retained channels with mesopore-range dimensions (diameters > 20 Å). The synthesis method presented in this thesis may also prove to be more cost-effective than that used to prepare FMMS because it allows the recovery of the expensive assembly surfactant, requires fewer preparative steps and reagents, and is accomplished in a shorter time.

Functional groups (thiol groups in this case) were introduced to the pore surface of the mesoporous silica as the terminal groups of organic monolayers. The hydrocarbon chains aggregated and formed close-packed arrays on the substrate. The siloxane groups then underwent hydrolysis and ultimately became covalently attached to the substrate and cross-linked to one another. This material, OSU-6-W-MPTMS-(1&2), can efficiently remove mercury and other heavy metals (such as lead and silver) from contaminated aqueous solutions. The distribution coefficient, K_d, has been measured to be as high as 435,000. [K_d is defined as the amount of adsorbed metal (in micrograms) on 1.0 g of adsorbing material divided by the metal concentration (in micrograms per milliliter) remaining in the treated waste stream.]

Beyond their immediate applications in environmental cleanup, OSU-6-W-MPTMS-(1&2) provide unique opportunity to introduce molecular binding sites and to rationally design the surface properties (for example, wettability and charge density

distribution) of mesoporous materials. Specific groups in the functionalized monolayers can be used to attach new functional groups or to stimulate mineral deposition.[81,82]

The silanization reaction on the surface of freshly prepared mesoporous silica was achieved in an inert atmosphere in the presence of a trace of amine as catalyst. It also has been demonstrated that the amine provides the alkalinity for the hydrolysis of the $Si\text{-}H_x$ groups on the mesoporous silica surface, forming the intermediate $Si(OH)_x$ groups which subsequently undergo the silanization.[83]

8.5. REFERENCES

1. Manahan, S. E. *Environmental Chemistry*; 6th ed.; Lewis Publishers: Boca Raton, FL, 1994.
2. Thornton, J.. Implementing Green Chemistry. An Environmental Policy for Sustainability. *Pure Appl. Chem.* **2001,** *73*(8), 1231-1236.
3. Prado, A. G.; Arakaki, L. N.; Airoldi, C.. Adsorption and Separation of Cations on Chemically Modified Silica Gel Synthesized via the Sol-Gel Process. *J. Chem. Soc., Dalton Trans.* **2001,** *21,* 2206-2209.
4. Hjeresen, D. L.; Schutt, D. L.; Boese, J. M.. Green Chemistry and Education. *J. Chem. Edu.* **2000,** *77*(12), 1543-1544, 1547.
5. Faust, S. D.; Ali, O. M. *Chemistry of Water Treatment*; 2nd Ed. Chelsea, MI : Ann Arbor Press, 1998.
6. Huang, C. P.; Hao, O. J.. Removal of Some Heavy Metals by Mordenite. *Enviro. Tech. Lett.* **1989,** *10*(10), 863-874.
7. Zamzow, M. J.; Eichbaum, B. R.; Sandgren, K. R.; Shanks, D. E.. Removal of Heavy Metals and Other Cations from Wastewater Using Zeolites. *Sep. Sci. Technol.* **1990,** *25*(13-15), 1555-1569.
8. Sikalidis, C. A.; Alexiades, C.; Misaelides, P.. Adsorption of Uranium and Thorium from Aqueous Solutions by the Clay Minerals Montmorillonite and Vermiculite. *Toxicol. Enviro. Chem.* **1989,** *20-21,* 175-180.
9. Keizer, P.; Bruggenwert, M. G. M.. Adsorption of Heavy Metals by Clay-aluminum Hydroxide Complexes. *NATO ASI Ser. E* 1991, *190*, 177-203.
10. Kim, J. S.; Yi, J.. Removal of Copper Ions from Aqueous Solutions using Silica Supports Immobilized with 2-Hydroxy-5-nonylacetophenoneoxime. *Sep. Sci. Technol.* **1999,** *34*(15), 2957-2971.
11. Kim, J. S.; Yi, J.. Selective Removal of Copper Ions from Aqueous Solutions Using Modified Silica Beads Impregnated with LIX 84. *J. Chem. Technol. Biotechnol.* **1999,** *74*(6), 544-550.
12. Leyden, D. E.; Luttrell, G. H. Preconcentration of Trace Metals Using Chelating Groups Immobilized via Silylation. *Anal. Chem.* **1975,** *47*, 1612-1617.
13. Howard, A. G.; Volkan, M.; Ataman, D. Y.. Selective Preconcentration of Arsenite on Mercapto-modified Silica Gel. *Analyst* **1987,** *112*(2), 159-162.
14. Volkan, M.; Ataman, O. Y.; Howard, A. G.. Preconcentration of Some Trace Metals from Sea Water on a Mercapto-modified Silica Gel. *Analyst* **1987,** *112*(10), 1409-1412.
15. Andreotti, E. S.; Gushikem, Y.. Adsorption and Structure of Metal Ion Complexes with Piperazine Groups Grafted on Silica Gel Surface. *J. Colloid Interface Sci.* **1991,** *142*(1), 97-102.
16. Dias Filho, N. L.; Gushikem, Y.; Rodrigues, E.; Moreira, J. C.; Polito, W. L.. Structure of Copper Complexes Adsorbed on a Silica Gel Surface Chemically Modified with benzimidazole. *J. Chem. Soc., Dalton Trans.,* **1994,** *9,* 1493-1497.
17. Dias Filho, N. L.; Gushikem, Y.; Polito, W. L.. 2-Mercaptobenzothiazole Clay as Matrix for Sorption and Preconcentration of Some Heavy Metals from Aqueous Solution. *Analytica Chimica Acta* **1995,** *306*(1), 167-172.

18. Kudryavtsev, G. V.; Mil'chenko, D. V.; Yagov, V. V.; Lopatkin, A. A.. Ion Sorption on Modified Silica Surface. *J. Colloid Interface Sci.* **1990,** *140*(1), 114-122.
19. Mercier, L.; Detellier, C.. Preparation, Characterization, and Applications as Heavy Metals Sorbents of Covalently Grafted Thiol Functionalities on the Interlamellar Surface of Montmorillonite. *Environ. Sci. Technol.* **1995,** *29*(5), 1318-1323.
20. Izatt, R. M.; Bradshaw, J. S.; Bruening, R. L.. Accomplishment of Difficult Chemical Separations using Solid Phase Extraction. *Pure Appl. Chem.* **1996,** *68*(6), 1237-1241.
21. Phillips, R. J.; Fritz, J. S.. Chromatography of Metal Ions with Thioglycolate Chelating Resin. *Anal. Chem.* **1978,** *50*(11), 1504-1508.
22. Sugii, A.; Ogawa, N.; Hashizume, H.. Preparation and Properties of Macroreticular Resins Containing Thiazole and Thiazoline Groups. *Talanta* **1980,** *27*(8), 627-631.
23. Deratani, A.; Sebille, B.. Metal Ion Extraction with a Thiol Hydrophilic Resin. *Analytical Chem.* **1981,** *53*(12), 1742-1746.
24. Alexandratos, S. D.; Wilson, D. L.. Dual-mechanism Bifunctional Polymers: Polystyrene-based Ion-exchange/redox Resins. *Macromolecules* **1986,** *19*(2), 280-287.
25. Tzeng, D. L.; Shih, J. S.; Yeh, Y. C.. Adsorption of Heavy Metal Ions on Crown Ether Adsorbents. *Analyst* **1987,** *112*(10), 1413-1416.
26. Kantipuly, C.; Katragadda, S.; Chow, A.; Gesser, H. D.. Chelating Polymers and Related Supports for Separation and Preconcentration of Trace Metals. *Talanta* **1990,** *37*(5), 491-517.
27. Prado, A. G.; Airoldi, C.. Adsorption, Preconcentration and Separation of Cations on Silica Gel Chemically Modified with the Herbicide 2,4-Dichlorophenoxyacetic Acid. *Anal. Chim. Acta* **2001,** *432*(2), 201-211.
28. Clark, J. H.; Macquarrie, D. J.. Environmentally Friendly Catalytic Methods. *Chem. Soc. Rev.* **1996,** *25*(5), 303-310.
29. Beck, J. S.; Vartuli, J. C.; Roth, W. J.; Leonowicz, M. E.; Kresge, C. T.; Schmitt, K. D.; Chu, C. T. W.; Olson, D. H.; Sheppard, E. W.; et al. A New Family of Mesoporous Molecular Sieves Prepared with Liquid Crystal Templates. *J. Am. Chem. Soc.* **1992,** *114*(27), 10834-10843.
30. J.S. Beck, Method for Synthesizing Mesoporous Crystalline Material, US Patent 5,057,296 (1991).
31. El-Nahhal, I. M.; El-Shetary, B. A.; Salib, K. A. R.; El-Ashgar, N. M.; El-Hashash, A. M.. Uptake of Divalent Metal Ions (Cu^{2+}, Ni^{2+}, and Co^{2+}) by Polysiloxane Immobilized Triamine-thiol and Thiol-acetate Ligand System. *Analytical Letters* **2001,** *34*(12), 2189-2202.
32. Wilson, K.; Clark, J. H.. Solid Acids and Their use as Environmentally Friendly Catalysts in Organic Synthesis. *Pure Appl. Chem.* **2000,** *72*(7), 1313-1319.
33. Padilha, P. M.; De Melo Gomes, L. A.; Padilha, C. C. F.; Moreira, J. C.; Dias Filho, N. L.. *Anal. Lett.* **1999,** *32,* 1807.
34. Goswani, A.; Singh, A. K.. *Anal.Chim. Acta* **2002,** *454,* 229.
35. Prado, A. G.; Airoldi, C.. Adsorption and Preconcentration of 2,4-Dichlorophenoxyacetic Acid on a Chemically Modified Silica Gel Surface. *Fresenius J. Anal. Chem.* **2001,** *371*(7), 1028-1030.

36. Silva, C. R.; Jardim, I. C.; Airoldi, C.. Development of New Urea-functionalized Silica Stationary Phases Characterization and Chromatographic Performance. *J. Chromatogr. A* **2001,** *913*(1-2) 65-73.

37. Prado, A. G.; Airoldi, C.. A Toxicity Decrease on Soil Microbiota by Applying the Pesticide Picloram Anchored onto Silica Gel. *Green Chem.* **2002,** *4*(3), 288-291.

38. Buriak, J. M.. Organometallic Chemistry on Silicon Surfaces: Formation of Functional Monolayers Bound Through Si-C Bonds. *Chem. Commun* **1999,** *12,* 1051-1060.

39. Bateman, J. E.; Eagling, R. D.; Worrall, D. R.; Horrocks, B. R.; Houlton, A. Alkylation of Porous Silicon by Direct Reaction with Alkenes and Alkynes. *Angew. Chem., Int. Ed.* **1998,** *37*(19), 2683-2685.

40. Okubo, T.; Tsuchiya, H.; Sadakata, M.; Yasuda, T.; Tanaka, K. *Appl. Surf. Sci.* **2001,** *171*, 252.

41. Wang, J.; Zhu, T.; Song, J.; Liu, Z. F. *Thin Solid Films* **1998,** *327*, 591.

42. Liu, J.; Feng, X.; Fryxell, G. E.; Wang, L. Q.; Kim, A. Y.; Gong, M.. Hybrid Mesoporous Materials with Functionalized Monolayers. *Adv. Mater.* **1998,** *10*(2), 161-165.

43. Feng, X.; Fryxell, G. E.; Wang, L.-Q.; Kim, A. Y.; Liu, J.; Kemner, K. M.. Functionalized Monolayer on Ordered Mesoporous Supports. *Science* **1997,** *276*(5314), 923-926.

44. Mercier, L.; Pinnavaia, T. J.. A Functionalized Porous Clay Heterostructure for Heavy Metal Ion (Hg^{2+}) Trapping. *Micropor. Mesopor. Mater.* **1998,** *20*(1-3), 101-106.

45. Brown, J.; Mercier, L.; Pinnavaia, T. J.. Selective Adsorption of Hg^{2+} by Thiol-functionalized Nanoporous Silica. *Chem. Commun.***1999,** *5*(1), 69-70.

46. Mercier, L.; Pinnavaia, T. J.. Heavy Metal Ion Adsorbents Formed by the Grafting of a Thiol Functionality to Mesoporous Silica Molecular Sieves: Factors Affecting Hg(II) Uptake. *Environ. Sci. Technol.* **1998,** *32*(18), 2749-2754.

47. Mercier, L.; Pinnavaia, T. J.. Access in Mesoporous Materials: Advantages of a Uniform Pore Structure in the Design of a Heavy Metal Ion Adsorbent for Environmental Remediation. *Adv. Mater.* **1997,** *9*(6), 500-503.

48. Fryxell, G, E.; Liu, J.; Hauser, T. A.; Nie, Z.; Ferris, K. F.; Mattigod, S.; Gong, M .; Hallen, R. T.. Design and Synthesis of Selective Mesoporous Anion Traps. *Chem. Mater.* **1999,** *11*(8), 2148-2154.

49. Brown, J.; Richer, R.; Mercier, L.. One-step Synthesis of High Capacity Mesoporous Hg^{2+} Adsorbents by Non-ionic Surfactant Assembly. *Micropor. Mesopor. Mater.* **2000,** *37*(1-2), 41-48.

50. Liu, A. M.; Hidajat, K.; Kawi, S.; Zhao, D. Y.. A New Class of Hybrid Mesoporous Materials with Functionalized Organic Monolayers for Selective Adsorption of Heavy Metal Ions. *Chem. Commun.* **2000,** *13,* 1145-1146.

51. Im, H. -J.; Yang, Y. -H.; Allain, L. R.; Barnes, C. E.; Dai, S.; Xue, Z. -L.. Funtionalized Sol-Gels for Selective Copper(II) Separation. *Environ. Sci. Technol.* **2000**, *34*(11), 2209-2214.

52. Airoldi, C.; Santos, M. R. M. C.. Synthesis, Characterization, Chemisorption and Thermodynamic Data of Urea Immobilized on Silica. *J. Mater. Chem.* **1994,** *4,* 1479-1485.

53. Kresge, C. T.; Leonowicz, M. E.; Roth, W. J.; Vartuli, J. C.; Beck, J. S.. Ordered Mesoporous Molecular Sieves Synthesized by a Liquid-Crystal Template Mechanism. *Nature* **1992,** *359*, 710-712.

54. De Soler-Illia, G. J.; Sanchez, C.; Lebeau, B.; Patarin, J.. Chemical Strategies to Design Textured Materials: from Microporous and Mesoporous Oxides to Nanonetworks and Hierarchical Structures. *Chem. Rev.* **2002,** *102*(11), 4093-4138.

55. Anwander, R.. SOMC@PMS. Surface Organometallic Chemistry at Periodic Mesoporous Silica. *Chem. Mater.* **2001,** *13*(12), 4419-4438.

56. Nooney, R. I.; Kalyanaraman, M.; Kennedy, G.; Maginn, E. J. Heavy Metal Remediation using Functionalized Mesoporous Silicas with Controlled Macrostructure. *Langmuir* **2001,** *17*(2), 528-533.

57. Marler, B.; Oberhagemann, U.; Vortmann, S.; Gies, H. Influence of the Sorbate Type on the XRD Peak Intensities of Loaded MCM-41. *Micropor. Mater.* **1996,** *6*(5-6), 375-383.

58. Barrett, E. P.; Joyner, L. G.; Halenda, P. P.. The Determination of Pore Volume and Area Distribution in Porous Substances. I. Computations from Nitrogen Isotherms. *J. Am. Chem. Soc.* **1951,** *73*, 373-380.

59. Kruk, M.; Jaroniec, M.. Accurate Method for Calculating Mesopore Size Distributions from Argon Adsorption Data at 87 K Developed Using Model MCM-41 Materials. *Chem. Mater.* **2000,** *12*(1)*,* 222-230.

60. Badia, A.; Gao, W.; Singh, S.; Demers, L.; Cuccia, L.; Reven, L.. Structure and Chain Dynamics of Alkanethiol-Capped Gold Colloids. *Langmuir* **1996,** *12*(5), 1262-1269.

61. Cauvel, A.; Brunel, D.; DiRenzo, F.; Fajula, F.. Organic Lining of MCM-41-type Silicas *AIP Conf. Proc.* **1996,** *354*, 477-484.

62. Sindorf, D. W.; Maciel, G. E.. Solid-state NMR Studies of the Reactions of Silica Surfaces with Polyfunctional Chloromethylsilanes and Ethoxymethylsilanes. *J. Am. Chem. Soc.* 1983, 105, 3767-3776.

63. Socrates, G.. *Infrared Characteristic Group Frequencies: Tables and Charts,* second ed., Wiley, Chichester (1994).

64. Wood, D. L.; Rabinovich, E. M.. Study of Alkoxide Silica Gels by Infrared Spectroscopy. *Appl. Spectros.* **1989,** *43*(2), 263-267.

65. Almeida, R. M.; Guiton, T. A.; Pantano, C. G.. Characterization of Silica Gels by Infrared Reflection Spectroscopy. *J. Non-Cryst. Solids*, **1990,** *121*(1-3), 193-197.

66. Primeau, N.; Vautey, C.; Langlet, M. The Effect of Thermal Annealing on Aerosol-gel Deposited SiO_2 Films: a FTIR Deconvolution Study. *Thin Solid Films* **1997,** *310*(1,2), 47-56.

67. Silverstein, R. M.; Bassler, G. C.; Morrill, T. C. *Spectrometric Identification of Organic Compounds*, Wiley, New York, 5th edn., 1991.

68. Lagadic, I. L.; Mitchell, M. K.; Payne, B. D.. Highly Effective Adsorption of Heavy Metal Ions by a Thiol-Functionalized Magnesium Phyllosilicate Clay. *Environ. Sci. Technol.* **2001,** *35*(5), 984-990.

69. Husing, N.; Schubert, U.; Mezei, R.; Fratzl, P.; Riegel, B.; Kiefer, W.; Kohler, D.; Mader, W.. Formation and Structure of Gel Networks from $Si(OEt)_4/(MeO)_3Si(CH_2)_3NR'_2$ Mixtures ($NR'_2 = NH_2$ or $NHCH_2CH_2NH_2$). *Chem. Mater.* **1999,** *11*(2), 451-457.

70. Kang, T.; Park, Y.; Yi, J.. Highly Selective Adsorption of Pt^{2+} and Pd^{2+} Using Thiol-functionalized Mesoporous Silica. *Ind. Eng. Chem. Res.* **2004,** *43*(6), 1478-1484.

71. Zub, Y. L.; Parish, R. L.. Functionalized Polysiloxane Sorbents: Preparation, Structure, Properties and Use. *Studies in Surface Science and Catalysis* **1996,** *99*, 285-299.

72. Vrancken, K. C.; Van Der Voort, P.; Possemiers, K.; Vansant, E. F. Surface and Structural Properties of Silica Gel in the Modification with γ-Aminopropyltriethoxysilane. *J. Colloid and Interface Sci.* **1995,** *174*(1), 86-91.

73. Sander, L. C.; Wise, S. A. Recent Advances in Bonded Phases for Liquid Chromatography. *Crit. Rev. Anal. Chem.* **1987,** *18*(4), 299-415.

74. Unger, K. K.. Packings and Stationary Phases in Chromatographic Techniques, Marcel Dekker, Moscow (1990).

75. Khatib, I. S.; Parish, R. V.. Insoluble Ligands and Their Applications. I. A Comparison of Silica-immobilized Ligands and Functionalized Polysiloxanes. *J. Organomet. Chem.* **1989,** *369*(1), 9-16.

76. El-Nahhal, I. M.; Parish, R. V. Insoluble Ligands and their Applications. III. Polysiloxane Diaminoethane Derivatives. *J. Organomet. Chem.* **1993,** *452*(1-2), 19-22.

77. Parish, R. V.; Habibi, D.; Mohammadi, V.. Insoluble Ligands and their Applications. II. Polysiloxane-phosphine Ligands, their Complexes, and Hydrogenation Catalysts. *J. Organomet. Chem.* **1989,** *369*(1), 17-28.

78. Sayari, A. Catalysis by Crystalline Mesoporous Molecular Sieves. *Chem. Mater.* **1996,** *8*(8), 1840-1852.

79. Yang, R. T.; Pinnavaia, T. J.; Li, W.; Zhang, W.. Fe^{3+} Exchanged Mesoporous Al-HMS and Al-MCM-41 Molecular Sieves for Selective Catalytic Reduction of NO with NH_3. *J. Catal.* **1997,** *172*(2), 488-493.

80. Lim, M. H.; Blanford, C. F.; Stein, A.. Synthesis of Ordered Microporous Silicates with Organosulfur Surface Groups and Their Applications as Solid Acid Catalysts. *Chem. Mater.* **1998,** *10*(2), 467-470.

81. Bunker, B. C.; Rieke, P. C.; Tarasevich, B. J.; Campbell, A. A.; Fryxell, G. E.; Graff, G. L.; Song, L.; Liu, J.; Virden, J. W.; McVay, G. L.. Ceramic Thin-film Formation on Functionalized Interfaces Through Biomimetic Processing. Science 1994, 264(5155), 48-55.

82. Calvert, P.; Rieke, P.. Biomimetic Mineralization in and on Polymers. *Chem. Mater.* **1996,** *8,* 1715-1727.

83. Li, H. L.; Fu, A. P.; Xu, D. S.; Guo, G. L.; Gui, L. L.; Tang, Y. Q.. In Situ Silanization Reaction on the Surface of Freshly Prepared Porous Silicon. *Langmuir* **2002,** *18*(8), 3198-3202.

CHAPTER
NINE

PREPARATION OF MESOPOROUS MATERIALS BEARING BROMOPROPYL

FUNCTIONAL GROUPS AND AMINE DERIVATIVES FOR METAL

ADSORPTION

Abstract

Mesoporous silicas carrying di-, tri-, or penta-amine functional group of the

formula $(MeO)_3Si(CH_2)_3E$ [E = $NH(CH_2)_2NH_2$, $NH(CH_2)_2NH(CH_2)_2NH_2$,

$NH(CH_2)_2NH(CH_2)_2NH(CH_2)_2NH(CH_2)_2NH_2$] have been prepared by replacement of the

bromine in bromopropyl-functional group with ethylenediamine (EDA),

diethylenetriamine (DETA), or tetraethylenepentamine (TEPA), respectively.

The bromopropyl-functionalized mesoporous silica was prepared using two different

procedures that make use of the grafting technique of $(MeO)_3Si(CH_2)_3Br$ into the pores of

the mesoporous silica, OSU-6-W.

Batch tests were conducted to investigate the capabilities of the prepared

adsorbents to remove copper and other transition metal ions from aqueous solutions. The

mesoporous silicas with the di-, tri-, and pent-amine ligand systems exhibit high potential

for separation and preconcentration of divalent metal ions (Cu^{2+}, Zn^{2+}, and Cd^{2+}). The

tendency to chemisorb these divalent metal ions by these functionalized systems at the

optimum conditions was found in the order: $Cu^{2+} > Zn^{2+} > Cd^{2+}$. All the aminated

mesoporous silicas showed high resistance from leaching of ligand containing groups upon treatment with acidic solutions as noticed from the regeneration processes. A comparison of the different functionalized silica supports was performed with respect to copper adsorption capacity, copper adsorption rate, and nitrogen content. In addition, studies were carried out for the modified silica beads that showed highest copper ion removal capability among the three silica beads. From regeneration experiments it was found that copper ions which are adsorbed at the surface of the OSU-6-W-TCSPBr-2-EDA were recovered by washing with aqueous solution of 1.0 M HNO$_3$ and that the regenerated beads are reversible. The recovery ratios were between 80 and 90%. The results show that the OSU-6-W-TCSPBr-2-EDA prepared is feasible for the extraction of copper ions from aqueous solutions using a fixed-bed reactor.

9.1. INTRODUCTION

Mineral processing and metal finishing industries produce large amounts of waste effluents containing copper, nickel, cobalt, zinc, cadmium, and other harmful elements.[1] Metal ions are non-biodegradable in nature and, therefore, many metals attain toxicity at distinct levels.[2] Copper is both vital and toxic for many biological systems.[3] Therefore, increasing pressure from environmental authorities forces the establishment of discharge limits, which in turn, requires effective use of decontamination and purification methods. From the analytical point of view, it is known that solid phase extraction is an attractive technique based on the use of sorbent that chelates analytes.[4-7]

Promising sorbents can be prepared by anchoring chelating agents on mesoporous silica. In this chapter, immobilization of the bromopropyl functional groups and some derivatives is explored. The importance of such immobilization is related to the easy

addition of nucleophiles by attach at the terminal bromide active group.[8] The aim of the present investigation is to report the incorporation of di-, tri-, or pent-amine groups onto a previously modified silica gel surface and the ability of this new chelating moiety on this anchored surface for cation removal from water.

9.2. EXPERIMENTAL

9.2.1. Reagents and Materials

All chemical were purchased from commercial suppliers and used as received (unless otherwise mentioned) for all sample preparations. The chemicals are as follows. 3-bromopropyltrichlorosilane [$(Cl_3Si(CH_2)_3Br)$ 96.0%, Aldrich], anhydrous diethylamine, ethylenediamine, diethylenetriamine, tetraethylenepentamine, and glucose monohydrate were purchased from Aldrich and used as received. Toluene, 99.8% HPLC grade. Triethylamine [(TEA) 99%, Aldrich], acetone and diethyl ether were dried using anhydrous sodium sulfate for three days. Absolute ethanol and methanol, standard 0.1 M NaOH, standard 0.01 M HC1, methyl orange (0.1%) indicator, 2-propanol and pentane, and distilled deionized water were used as received. The structures of some of these compounds are shown in Scheme 9.1.

3-Bromopropyltrichlorosilane

Glucose monohydrate

Ethylenediamine

Diethylenetriamine

Tetraethylenepentamine
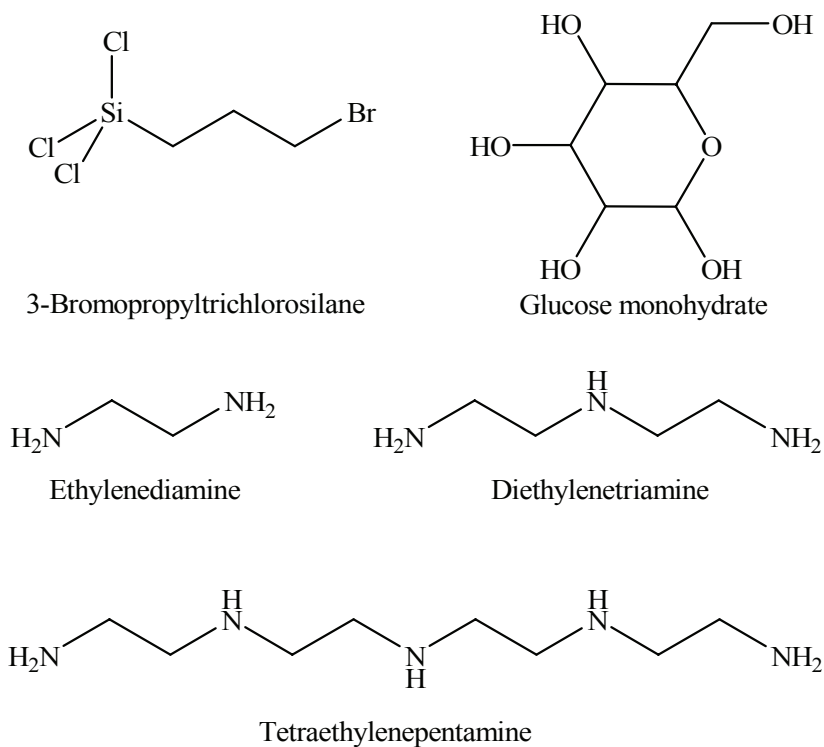
Scheme 9.1. The structures of some of the compounds used in this section

Solutions of divalent metals of the appropriate concentration were prepared by dissolving the metal(II) nitrates (analytical grade) in deionized water. Different pH ranges were prepared. Acetate solutions were prepared using hydrochloric acid/sodium acetate for pH 2-4, acetic acid/sodium acetate (buffer for pH 4-6), and acetic acid/NaOH for pH 6.5-8.0.[9-11]

9.2.2. Characterization

The synthesized products were characterized using several techniques including X-ray powder diffraction (XRD), surface area analysis (BET), solid state C-13 and Si-29

NMR spectroscopy, and Fourier transform infrared (FT-IR) spectroscopies. The full

descriptions are mentioned in chapter two and three of this thesis.

9.2.3. Preparation

**9.2.3.1. Surface Modification of Mesoporous Materials with Bromopropyl**

Functional Groups

Bromopropyl-functional group was chemically attached to the mesoporous OSU-

6-W material surfaces by means of the post-synthesis grafting method. The two synthetic

methodologies described in chapter five were used.

I. Reaction of the Mesoporous Silica with Bromopropyltrichlorosilane with the Mole

Ratio of 1:1 in One-step Reaction (OSU-6-W-TCSPBr-1)

50 mmol (~ 13.0 ml) of 3-bromopropyltrichlorosilane (TCSPBr) was dissolved in

10 ml of dry toluene, in a 50-ml round-bottom flask closed with rubber septa, under dry

atmosphere to prevent any hydrolysis prior to reaction with the mesoporous silica

surface. 3.0 g (~ 50.0 mmol) of the activated silica, TEA-OSU-6-W, was added to 50 ml

of dry toluene in a 125-ml round-bottom flask which was then closed with a rubber septa.

The solution of TCSPBr was added to the stirred mesoporous silica suspension dropwise

over 30 minutes using a syringe. The mixture was stirred gently for 48 hours at room

temperature to ensure complete reaction. The resulting solid was recovered by filtration

in a sintered funnel and washed with dry toluene (3 X 50 ml) to rinse away any surplus

TCSPBr. The resulting white solid, OSU-6-W-TCSPBr-1, was dried at 80 °C under

vacuum for 24 hours to give a yield of 4.97 g. IR (cm^{-1}) (KBr): 3734(m, sh), 3597(m,

br), 2923(m, sh), 2852(m, sh), 1436(m, sh), 1346(w), 1311(w), 1234(s), 1089(s, br),

978(m, br), 798(m, sh), 683(w), 574(w), and 450(m). Solid-state ^{29}Si CP/MAS NMR (δ,

ppm): -47.4 (T^1), -56.7 (T^2), -66.5 (T^3), -90.5 (Q^2), -101.4 (Q^3), and -108.2 (Q^4). Solid-state ^{13}C CP/MAS NMR (δ, ppm): 12.0($\equiv$Si-**C**H$_2$-)[1], 27.2($\equiv$Si-CH$_2$-CH$_2$-**C**H$_2$-Br)[3], and 34.5($\equiv$Si-CH$_2$-**C**H$_2$-)[2], Scheme 9.2. Elemental analysis yielded C (11.32 wt %) and N (0.09 wt %).
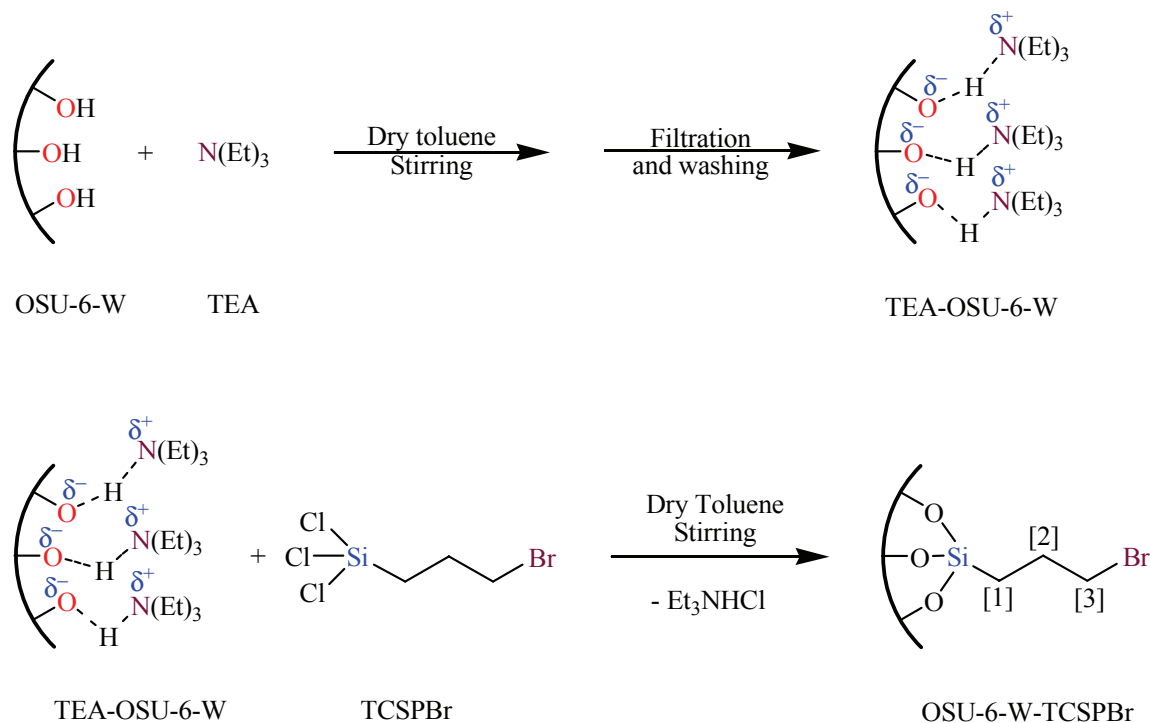
Scheme 9.2. Scheme to illustrate the chemical reaction involved and the number used in order to sign the carbon atom as described in the ^{13}C CP/MAS NMR.

II. Reaction of the Mesoporous Silica with Bromopropyltrichlorosilane with the Mole Ratio of 1:1 in Three Modification Steps (OSU-6-W-TCSPBr-2)

A multistep process was used to increase surface coverage with bromopropyl groups. The first step was the same as described above. In the second step the product

was placed in a 125-ml Erlenmeyer flask and stirred with 50 ml of distilled water for five hours. The mixture was filtered to recover the solid product which was then washed with dry toluene and dried at 80 ^{o}C under vacuum for 24 hours. In the third step, the reaction with 3-bromopropyltrichlorosilane (TCSPBr) was repeated. The final yield of white solid was 5.69 g. IR (cm^{-1}) (KBr): 3562(w, br), 3241(s, br), 2966(w), 2933(s, sh), 2892(w), 2856(s, sh), 1455(w), 1436(s, sh), 1350(w), 1303(m), 1245(s), 1097(s), 1045(m), 976(m), 804(m, sh), 692(m, sh), 614(w), 559(w), and 468(m). Solid-state ^{29}Si CP/MAS NMR δ (ppm) are -57.3 (T^{2}), -65.3 (T^{3}), -101.5 (Q^{3}), and -110.6 (Q^{4}). Solid-state ^{13}C CP/MAS NMR δ (ppm) are 12.0(≡Si-*C*H$_2$-)[1], 27.2(≡Si-CH$_2$-CH$_2$-*C*H$_2$-Br)[3], and 35.3(≡Si-CH$_2$-*C*H$_2$-)[2], Scheme 9.2. Elemental analysis yielded C (14.72 wt %) and N (0.16 wt %).

9.2.3.2. Preparation of the Immobilized Glucose Ligand System (OSU-6-W-TCSPBr-2-Glu)

Glucose-immobilized mesoporous silica was prepared according to a previously reported procedure.[12,13] The reaction involved addition of glucose monohydrate (2.0 g, 10.0 mmol) to a mixture of 0.5 g of the modified mesoporous OSU-6-W-TCSPBr-2 and 2.0 ml of triethylamine in 50 ml of dry toluene in a 125-ml round-bottom flask. The mixture was stirred and refluxed at ~ 100 ^{o}C for 24 hrs under dry atmosphere. The product was filtered and washed with 0.025 *M* NaOH, water, ethanol and diethyl ether, then dried under vacuum for 24 hrs. IR (cm^{-1}) (KBr): 3423, 1628. Elemental analysis: C (32.8 wt %) and N (0.09 wt %).

9.2.3.3. Preparation of OSU-6-W-TCSPBr-2 Immobilized Amine Ligand Systems

Preparation of mesoporous silica with immobilized amine functional groups was performed by utilizing nucleophilic displacements of the bromide by attach of the amine

group. The synthesis procedure is as follows; 1.0 g of mesoporous silica OSU-6-W-TCSPBr-2 was refluxed with an excess of 10 ml of target amine system (ethylenediamine, diethylenetriamine or tetraethylenepentamine) in 90 ml of dry toluene in a 250-ml round-bottom flask at 100 °C for 48 hours. The solid products were filtered, washed with successive portions of 50 ml of 0.025 M NaOH, water, methanol, and diethyl ether. The final products were dried in vacuum for 24 hours. The IR spectra (KBr, cm^{-1}) of all samples show peaks at around 1540-1640 cm^{-1} and no peaks were found due to the C-Br stretching vibration at around 660 cm^{-1}. Elemental analysis results are C% : 21.3, 29.67, 42.78 and N% : 19.74, 13.11, and 22.70, respectively.

9.2.3.4. Metal Uptake Experiments

The adsorption and separation experiments were conducted as follows; a 25 mg sample of the functionalized mesoporous silica-immobilized diamine ligand system, OSU-6-W-TCSPBr-2-Dien, was shaken for 4 hours with 10 ml of 100 ppm of aqueous solutions of the appropriate metal(II) ions (Cu^{2+}, Zn^{2+}, and Cd^{2+}), using 20-ml polyethylene bottles. Measurement of the metal ion concentration carried out by allowing the insoluble complex to settle down and filtering the supernatant using a 0.45μm membrane filter syringe. The metal ion uptake was calculated as mmol of M^{2+}/g ligand.

9.3. RESULTS AND DISCUSSION

9.3.1. Mesoporous Silica with Bromopropyl-Functional Groups

$RSi(OMe)_3$ and $RSiCl_3$ are usually used as silylating agents. The former has a low activity, leading to relatively low loading and a large number of residual silanol groups after silylation.[14,15] The residual silanol groups after silylation on the surface are

usually considered to lead to surface hydrophilicity[16] and may have a serious effect on

catalytic activity.[17,18] Therefore, they have to be end-capped with additional procedures.
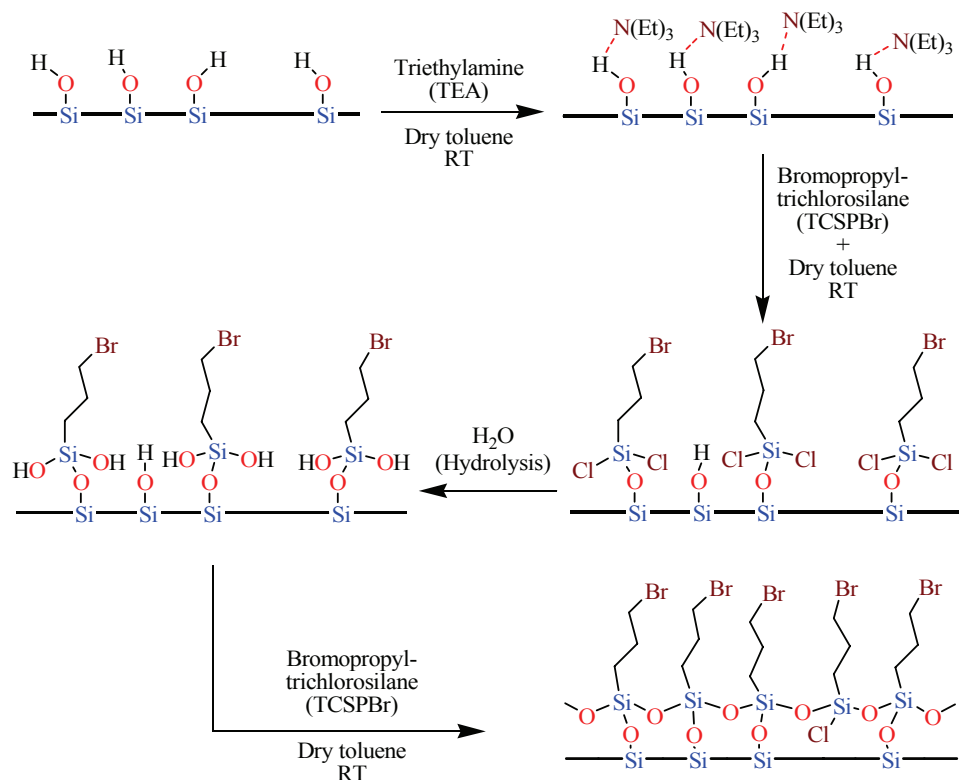
Scheme 9.3. Scheme of the proposed preparation reactions for the attachment of the coupling agent TCSPBr on the OSU-6-W surface

On the other hand, $RSiCl_3$ has high reactivity towards free silanol and hydrogen-

bonded silanol groups,[19] resulting in high loading and difficulty in controlling its

coverage to a homogeneous distribution. In addition, for preparation of organically

functionalized mesoporous materials, it is difficult to control the coverage of functional

groups in wide range regardless of post-synthesis or co-condensation method.[20]

3-Halogenpropyl-functionalized ordered mesoporous materials are a key

intermediate preferred by a lot of researchers for design and preparation of other

functionalized mesoporous materials, by nucleophilic displacement of the halogen atom.[21,22]

In the present work, because water can damage the walls of the silica structure, the nucleophilicity of the surface silanols was enhanced using triethylamine (TEA) without any trace of water. Thus, before grafting, the silica was heated at 100 °C for 2 hrs in order to remove the loosely bound water molecules. The grafting reaction of a coupling agent, γ-bromopropyltrichlorosilane (TCSPBr), to the surface silanols was enhanced by the pre-adsorption of triethylamine on the surface according to the mechanism first proposed by Blitz *et al.*,[23] and as shown by Tripp and Hair,[24] the possible interaction involved between the siliceous surface and the chlorosilanes at room temperature is hydrogen bonding, because covalent bonding ($Si_{surface}$-O-Si) would only occur above 300 °C.[25] However, they demonstrated that, by the use of triethylamine (TEA), covalent bonding can be made to occur at room temperature. After this first reaction was completed, the TEA-OSU-6-W mesoporous material was carefully washed to eliminate any TEA loosely bound to the silica surface.[26] A competition between the head trichlorosilyl and the tail bromoalkyl for the surface silanols is unlikely because the reactivity of chlorosilanes is known to be greater than that of bromoalkanes. Furthermore, a trichlorosilane was used rather than a monochlorosilane[27] to exclude any possible competition, even though; using a trichlorosilane, some lateral polymerization between silane molecules could not be excluded.[24] However, Azzopardi *et al.*,[28] reported that, under certain conditions, it is possible to react trichlorosilane with surface silanols without any significant polymerization. The FT-IR performed after the first step of the

synthesis showed that the reaction occurred on the trichlorosilyl side of the TCSPBr

molecules, as Br remains present in the solid.

In the second preparation method, a second modification step was performed after

treatment of the modified sample with water in order to hydrolyze the residual chloride

groups after the first modification step.[24]

9.3.1.1. Textural Properties of Functionalized Mesoporous Silicas (Physical

Characterization)

I. X-ray Powder Diffraction (XRD)

Low angle X-ray powder diffraction was performed and the results are shown in

Figure 9.1. The XRD of the pure mesoporous silica, OSU-6-W, as discussed previously

in chapter two, shows three diffraction peaks that can be indexed to a hexagonal

symmetry. As already well-described in the literature[29], this symmetry indicates the

ordering of cylindrical pores in a hexagonal array. The d_{100} value corresponds to the

distance between two successive walls (that is, one pore diameter plus a wall thickness).

After silanization, the two functionalized samples, OSU-6-W-TCSPBr-1 and

OSU-6-W-TCSPBr-2, have smaller d spacings than the starting materials. According to

the average pore diameters from the surface area analysis of both modified materials, this

indicates an average thickening of the walls to 22.9 and 26.8 Å, respectively, which

would correspond to addition of an extra layer of Si-O-Si homogeneously spread on the

original wall, in the case of OSU-6-W-TCSPBr-2. It can also be noted that the d_{100} peak

has become broader, indicating a slight alteration of the ordering of the mesoporous
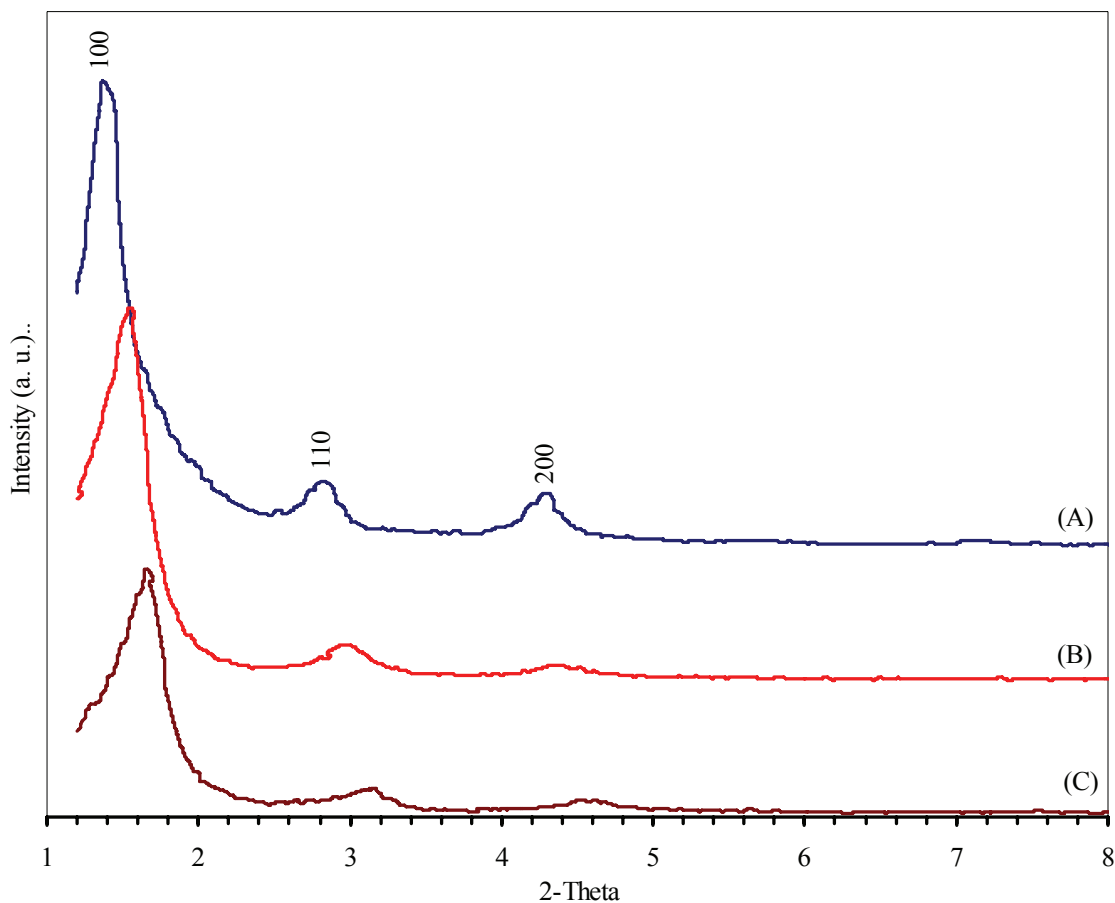
structure.

Figure 9.1. Powder X-ray diffraction patterns for OSU-6-W and their bromopropylsilyl-functionalized derivatives. (A) OSU-6-W, (B) OSU-6-W-TCSPBr-1, and (C) OSU-6-W-TCSPBr-2. The spectra are shifted vertically for the sake of clarity.

However, the decrease in diffraction intensities of 100, 110, and 200 reflections indicates that any structural order of the material did not extend over a long range, which is usually observed during modification of mesoporous materials.[30] It should be noted that there are no huge changes in the d_{100} before and after modification which can be used as an evidence of high chemical stability of both the parent mesoporous silica and the two modified samples.

II. Nitrogen Adsorption-Desorption Measurements

Figure 9.2 shows the nitrogen adsorption-desorption isotherms performed at 77 K

of the mesoporous silicas and the textural properties are summarized in Table 9.1.
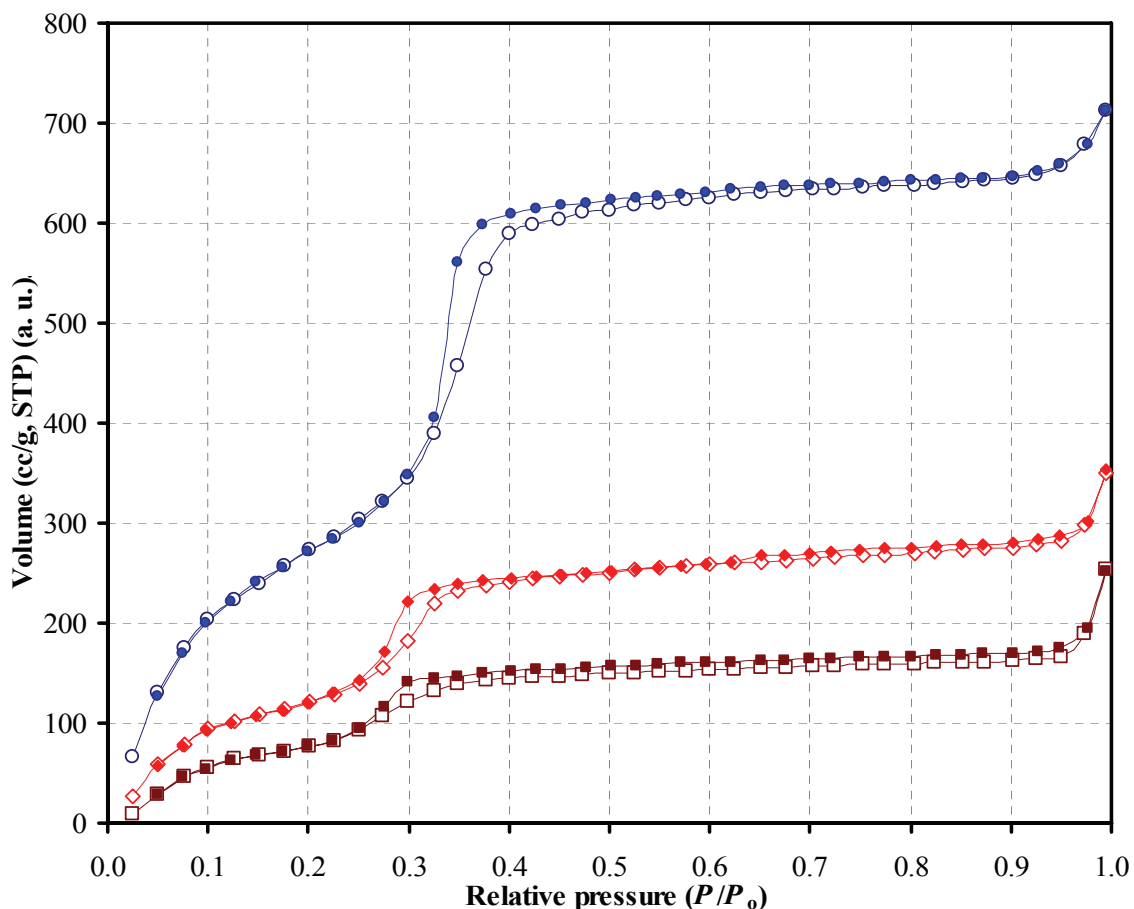
Figure 9.2. Nitrogen adsorption/desorption isotherms for (○) unmodified OSU-6-W and bromopropyl-functionalized OSU-6-W; (◊) OSU-6-W-TCSPBr-1 and (□) OSU-6-W-TCSPBr-2. Open symbols: adsorption; closed symbols: desorption. The isotherm data are shifted vertically for the sake of clarity.

After reaction with the coupling agent in both modified samples (OSU-6-W-

TCSPBr-1 and OSU-6-W-TCSPBr-2), the adsorption isotherm curves show that the total

adsorbed amount (taken at P/Po = 0.99) has diminished, as has the specific surface area, see Table 9.1. The uptake corresponding to the filling of the mesopores has shifted to lower relative pressures indicating a reduction of the pore diameter from 51.0 to 43.0 and 36.5 Å, respectively, Figure 9.3. The decrease of the mesoporous volumes of the materials after silanization is the direct consequence of the silanization process partially filling the pores.
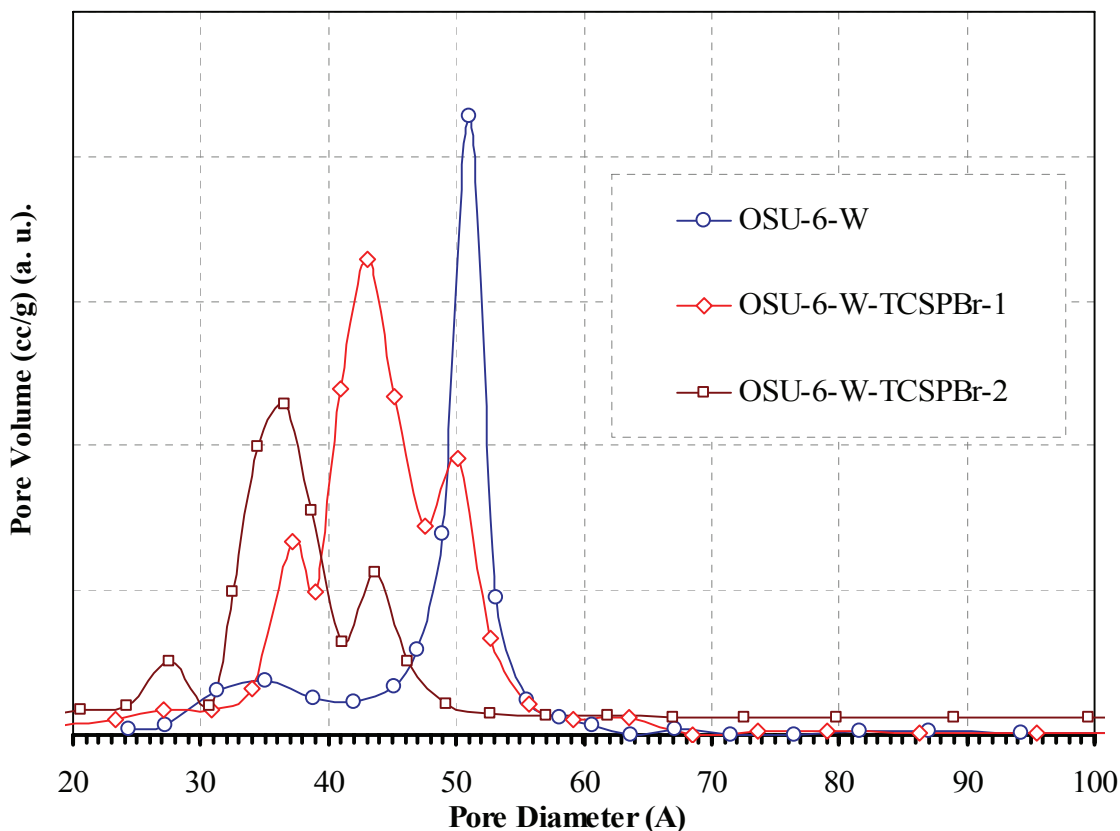

Figure 9.3. The pore size distribution of (○) OSU-6-W (max at 51.1 Å), (◊) OSU-6-W-TCSPBr-1 (max at 43.0 Å), and (□) OSU-6-W-TCSPBr-2 (max at 36.5 Å).

Table 9.1. Textural Properties Determined from Nitrogen Adsorption-desorption Experiments at 77 K and Powder XRD Measurements.

Sample	Specific surface area (m^2/g)	Total pore volume (cm^3/g)	Average pore size $(Å)$	d_{100} $(Å)$	Wall Thickness $(Å)$
OSU-6-W	1283	1.24	51.1	62.4	21.0
OSU-6-W-TCSPBr-1	1048	0.94	43.0	57.1	22.9
OSU-6-W-TCSPBr-2	719	0.76	36.5	54.8	26.8

9.3.1.2. Identification of the Bromopropyl-functional Groups in the Modified Mesoporous Silicas (Chemical characterization)

I. Solid State ^{29}Si CP/MAS NMR Spectroscopy

Solid state ^{29}Si CP/MAS NMR spectra of the bromopropyl-functionalized OSU-6-W samples along with un-functionalized OSU-6-W are shown in Figure 9.4. The peak around -110 ppm is assigned to the Q^4 atom $[(SiO)_4{}^*Si]$ of mesoporous silica. It is noted that there is a shoulder peak at -101.4 ppm in the solid state ^{29}Si CP/MAS NMR spectrum of OSU-6-W-TCSPBr-1, which is ascribed to the Q^3 environment $[(SiO)_3{}^*SiOH]$, while this peak was not observed in that of OSU-6-W-TCSPBr-2. This indicates that there were fewer silanol groups left in OSU-6-W-TCSPBr-2 and most of silanol groups were almost completely silylated. In addition, the ^{29}Si resonance peak observed around -65.3 ppm, which is ascribed to T^3 environment $[(SiO)_3{}^*SiR]$ has higher intensity than that in the OSU-6-W-TCSPBr-1 sample, indicating that the silyl groups in the OSU-6-W-TCSPBr-2 sample were present in higher concentration.
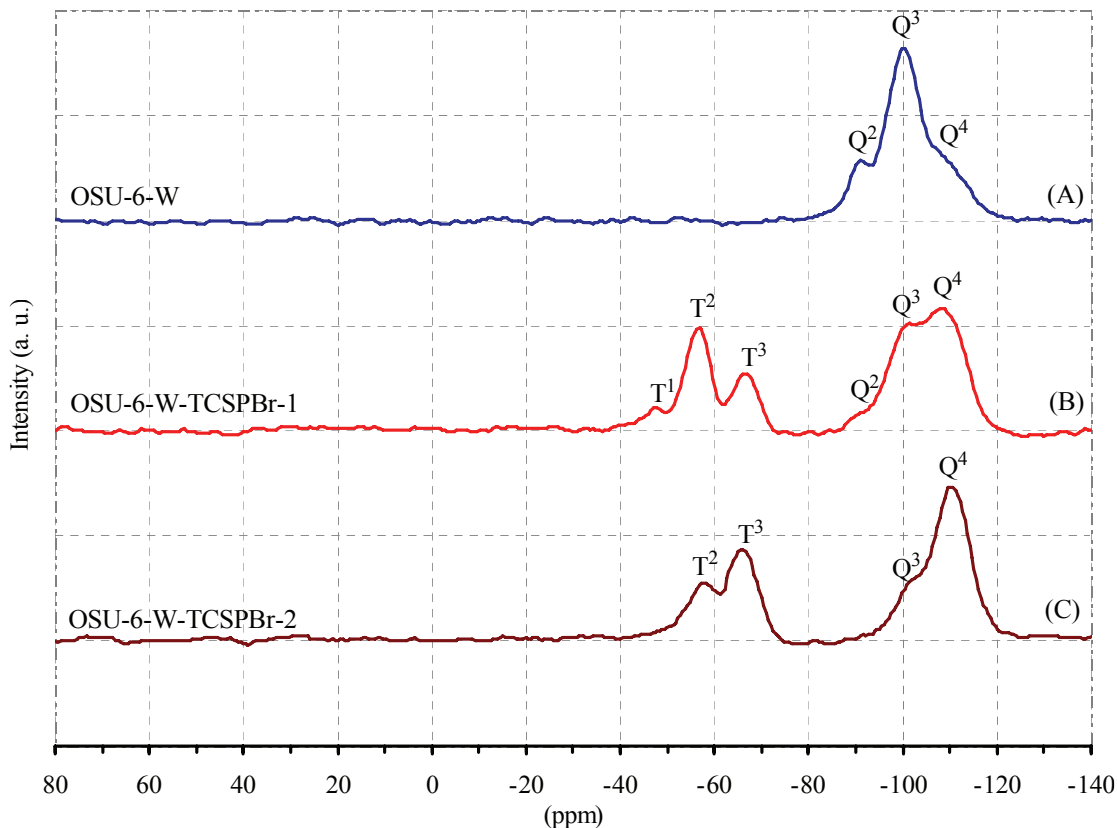
Figure 9.4. Solid state ^{29}Si NMR spectra of; (A) unmodified OSU-6-W, (B) modified OSU-6-W-TCSPBr-1, and (C) the modified OSU-6-W-TCSPBr-2.

II. Solid State ^{13}C CP/MAS NMR Spectroscopy

The presence of covalently linked organic moieties bearing bromopropylsilane chain groups in the as-synthesized OSU-6-W mesoporous silicas were also confirmed by ^{13}C CP/MAS solid-state NMR spectroscopy. ^{13}C CP/MAS NMR spectrum of OSU-6-W-TCSPBr is consistent with an anchorage of bromopropylsilane chains on the OSU-6-W surface.[14]
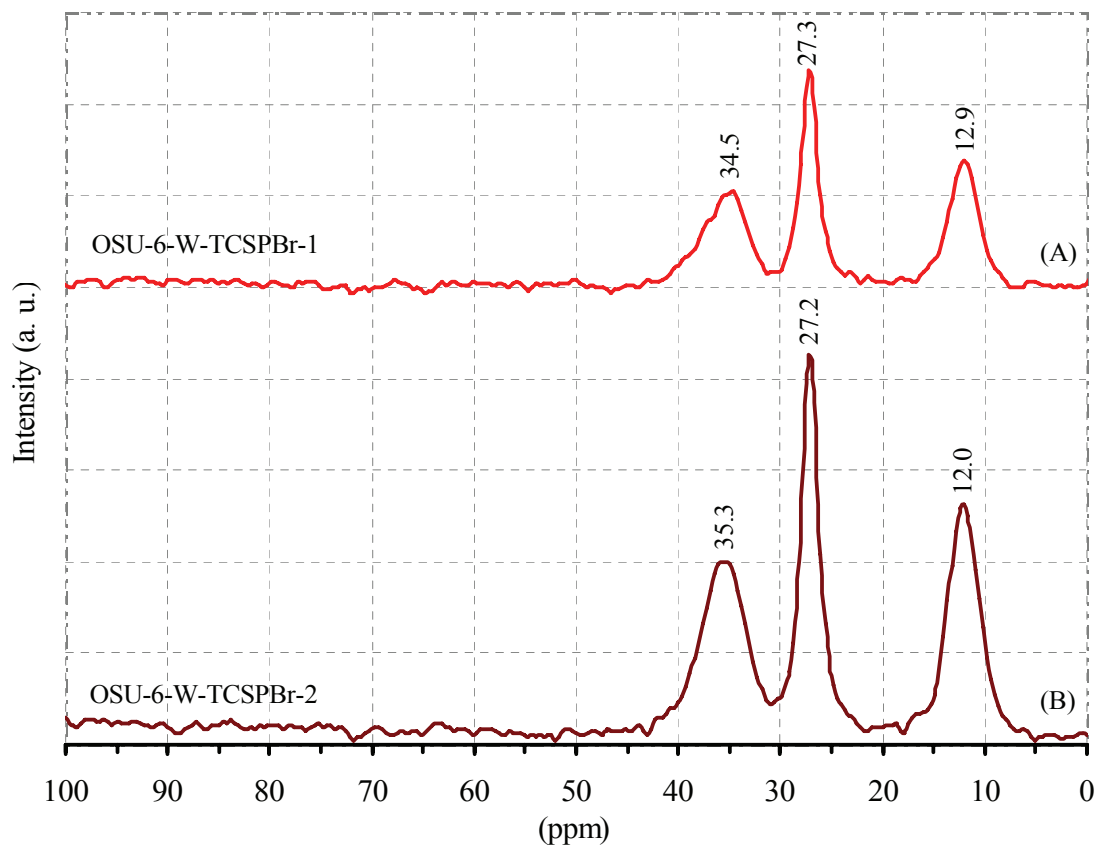
Figure 9.5. Solid state ^{13}C NMR spectra of organic monolayers on mesoporous silica, OSU-6-W, with the peak assignments. (A) OSU-6-W-TCSPBr-1, (B) OSU-6-W-TCSPBr-2.

Figure 9.5 shows resonances at δ (ppm) values of 12.0 ($\equiv$Si-CH$_2$-), 27.2 ($\equiv$Si-CH$_2$-CH$_2$-CH$_2$-Br), 34.5 ($\equiv$Si-CH$_2$-CH$_2$-) and δ (ppm) of 12.0 ($\equiv$Si-CH$_2$-), 27.2 ($\equiv$Si-CH$_2$-CH$_2$-CH$_2$-Br), 35.3 ($\equiv$Si-CH$_2$-CH$_2$-) corresponding to the functional groups in OSU-6-W-TCSPBr-1 and OSU-6-W-TCSPBr-2, respectively. Peaks corresponding to the organosiloxane moieties are relatively broad, indicating restricted mobility of the functional groups attached to the siloxane framework.

III. Fourier Transform Infrared Spectroscopy (FT-IR)

The vibrational spectra, Figure 9.6, obtained from solid samples confirmed the success of the grafting reactions, since the observed bands are very close to those reported, when bromopropyl groups were previously incorporated into similar materials.
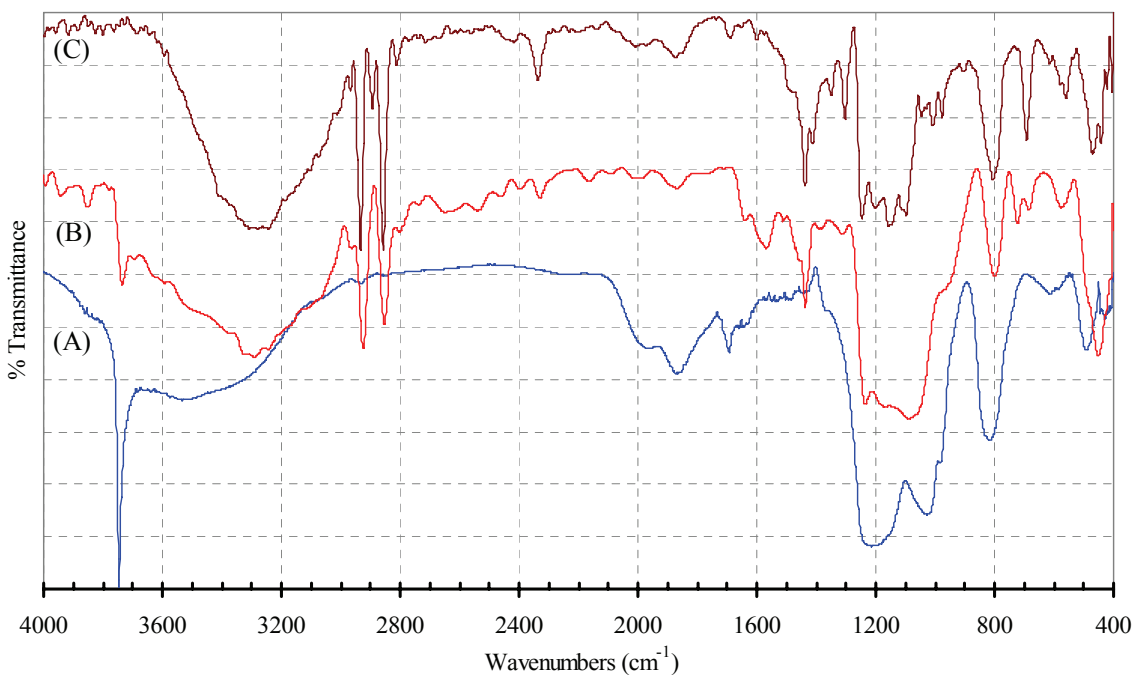
Figure 9.6. Infrared spectra of (curve A) OSU-6-W, (curve B) OSU-6-W-TCSPBr-1, and (curve C) OSU-6-W-TCSPBr-2.

All the spectra showed a large band around 3000-3600 cm^{-1} due to the present of small amount of silanol groups and most probably due to adsorbed water. The efficiency of the grafting process is demonstrated by a significant decrease in the silanol bands at around 3740 cm^{-1}, with an associated increase of new bands characteristics of the immobilized bromopropyl functional groups. These bands were attributed to both the symmetric and asymmetric stretching of active groups in OSU-6-W-TCSPBr-1; $v_{as}(CH_2)$

= 2934 cm^{-1}, v_s(CH$_2$) = 2889 cm^{-1}, CH$_2$ scissor at 1433 cm^{-1}, CH$_2$-Br stretching at 1233

and 1299 cm^{-1}, in OSU-6-W-TCSPBr-2; v_{as}(CH$_2$) = 2960 cm^{-1}, v_s(CH$_2$) = 2892 cm^{-1},

CH$_2$ scissor at 1455 cm^{-1}, and CH$_2$-Br stretching at 1238 and 1298 cm^{-1}.[31]

9.3.1.3. Calculate the Total Surface Loading of the Bromopropyl-Functional Groups on the Ordered Mesoporous Silicas

Determination the number of the functional group is one of the objects in order to evaluate the validation of the synthesis methods.

I. Titration Method

The amount of bromopropyl functional groups deposited on the surface was quantitatively determined using two variables. The surface loading (*l*) expresses the amount of deposited molecules in mmol/g. The number of molecules deposited per nm^2 is given by the surface coverage (*C*). Both values use the mass of the pure mesoporous silica before modification as a reference.[32]

There is a broad range of analytical techniques available for the quantitative analysis of the bromopropyl functional groups. In the case of surface-bonded groups, a decrease in reactivity had to be expected and, therefore, the most efficient procedures were selected after testing several possibilities found in the literature.

I.1. Titration with Diethylamine

The determination of the haloalkyl groups in inorganic compounds has generally involved reaction with excess anhydrous diethylamine. Since the reaction is slow, at least two days reaction time is generally allowed before titration.

The main criterion was the reproducibility of the end point determination as a function of the speed of the titration. Direct titration of tertiary amine groups of the

sample suspended in distilled water with standard (0.01 M) hydrochloric acid (HCl) in distilled water in the presence of methyl orange (0.1%) indicator was evaluated to be the best method.

A 0.25 g amount of each modified sample was added to 10 ml of anhydrous diethylamine and allowed to stand at room temperature for two days with stirring. The reaction between diethylamine and the bromoalkyl groups results in the formation of attached tertiary amines, Scheme 9.4.
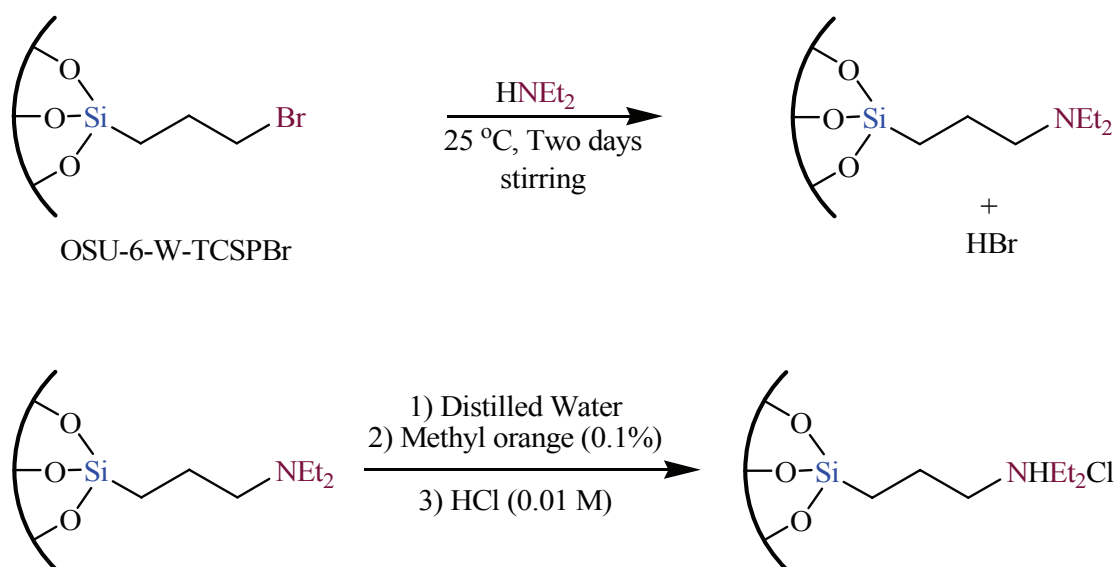
Scheme 9.4. Reaction of bromopropyl functional groups with secondary amine and titration reaction of tertiary amine with HCl.

The modified samples were extracted consecutively with distilled water, 2-propanol and pentane, and then dried at 50 °C for 2 hours.

421

A 0.25 g of each sample of diethylamine treated, OSU-6-W-TCSPBr-1 and OSU-6-W-TCSPBr-2, were separately suspended in 25 ml of distilled water. Three drops of methyl orange (0.1%) indicator were added to the mixture and titrate to a definite color change from orange to red color with standard $0.01M$ HCl was performed using a 50-ml burette. Very sharp visual end-points were generally obtained. The amount of attached amine (and therefore the amount of corresponding initial haloalkyl groups) is equal to the amount of HCl needed for titration. The result show relatively good agreement with other results from the other methods used for determination the number of functional groups.

In this method, the total deposited amount (l) was calculated from the amount of hydrochloric acid used to reach the end point. This value indicates the deposition in the surface of the mesoporous material. The surface coverage (C) was calculated by rationing the loading (l) to the specific surface area (S_{BET}) of the sample. Multiplication by the Avogadro's number ($N_A = 6.022 \times 10^{23}$ molecules/mole) yields units of molecules/nm^2:[32]

$$C = (l / S_{BET}) \cdot N_A$$

For the OSU-6-W-TCSPBr-1, an average coverage of 3.06 TCSPBr molecules/100 Å^2 was found, while the OSU-6-W-TCSPBr-2 sample had an average coverage of 5.22 TCSPBr molecules/100 Å^2.

II. Elemental Analysis (Combustion Analysis) Method

Carbon analysis of the mesoporous silica modified with bromopropyl functional groups was carried out for all types of sorbents studied. The concentration of attached groups was determined as follows:[33,34]

$$C \text{ (groups/nm}^2) = 6 \times 10^5 \, P_C / [(1200 n_C - W P_C) \, S_{\text{BET}}]$$

where C is the concentration of attached groups, which contain carbon; P_C is the percentage of carbon in the sample, n_C is the number of carbon atoms in the attached group (counted as C_3), W is the corrected formula mass of the modifier (counted as C_3H_6SiBr), and S_{BET} is the specific surface area of the unbonded substrate (1283 m^2/g), Table 9.2 shows the results.

Table 9.2. Carbon and nitrogen elemental analysis, and concentration of bromopropyl functional groups.

Sample	C %	N %	Surface Area (m^2/g)	TCSPBr (group/nm^2)
OSU-6-W	0.10	0.06	1283	---
OSU-6-W-TCSPBr-1	11.32	0.09	1048	2.78
OSU-6-W-TCSPBr-2	14.72	0.16	719	4.94

III. Solid state ^{29}Si CP/MAS NMR Spectrum

The Q^2, Q^3 and Q^4 of OSU-6-W are found at -91.2, -100.4, and -107.9 ppm respectively (Figure 9.4. (A)). The silicon atom of the silylating agent TCSPBr is seen at -47.4, -56.7, -66.5, -90.5, -101.4, -108.2 ppm and at -57.3, -65.3, -101.5, and -110.6 ppm for OSU-6-W-TCSPBr-1 and OSU-6-W-TCSPBr-2 functionalized samples, respectively (Figure 9.4.(B and C)). The relative peak areas from deconvolution of the spectra are given in Table 9.3.

Table 9.3. Solid state ^{29}Si CP/MAS NMR deconvolution results

Sample	Q^4 (%)	Q^3 (%)	Q^2 (%)	[SiOH] (mmol/g)	[SiOH] (molecule/nm^2)	[TCSPBr] (group/nm^2)
OSU-6-W	14.38	71.73	13.89	14.43	6.77	----
OSU-6-W-TCSPBr-1	52.83	47.17	0.00	7.34	4.22	2.55
OSU-6-W-TCSPBr-2	81.24	18.76	0.00	3.04	2.24	4.53

The difference in silanol concentration after silylation was equal to the concentration of the functional groups added. This indicates that each organosilyl group attaching to a single silanol site on the mesoporous silica.

The slight differences between all three determination methods (titration, elemental analysis, and solid state ^{29}Si NMR) could be due to one of the following reasons; In the case of titration method the end point could be missed and the solvent could be trapped inside the pores, whereas in the case of elemental analysis the presence of a trace amount of solvent could change the element percentage, while in the case of solid state ^{29}Si NMR the mistake could be from insufficient relation between pulses.

In this work a significantly large coverage of functional groups (~ 4.89 group/nm^2) have been obtained. This probably arises from the large pore size, 51.1 Å, the use of amine as catalyst, and the intermediate water treatment in the three-step silylation process.

9.3.2. Immobilized Glucose Ligand System OSU-6-W-TCSPBr-2-Glu

Glucose was chosen to modify the bromo-functionalized mesoporous system as it introduces multiple hydroxyl groups. In this study the immobilized glucose active group

was prepared and characterized using variety of physical techniques, including Fourier transform infrared (FT-IR) spectroscopy and elemental analysis.

As mentioned previously, this ligand was prepared by mixing glucose monohydrate with a mixture of the modified mesoporous OSU-6-W-TCSPBr-2 in dry toluene and triethylamine in a round-bottom flask and refluxing the mixture under dry atmosphere, Scheme 9.5.

OSU-6-W-TCSPBr-2   Glucose (Glu)   OSU-6-W-TCSPBr-2-Glu

R =
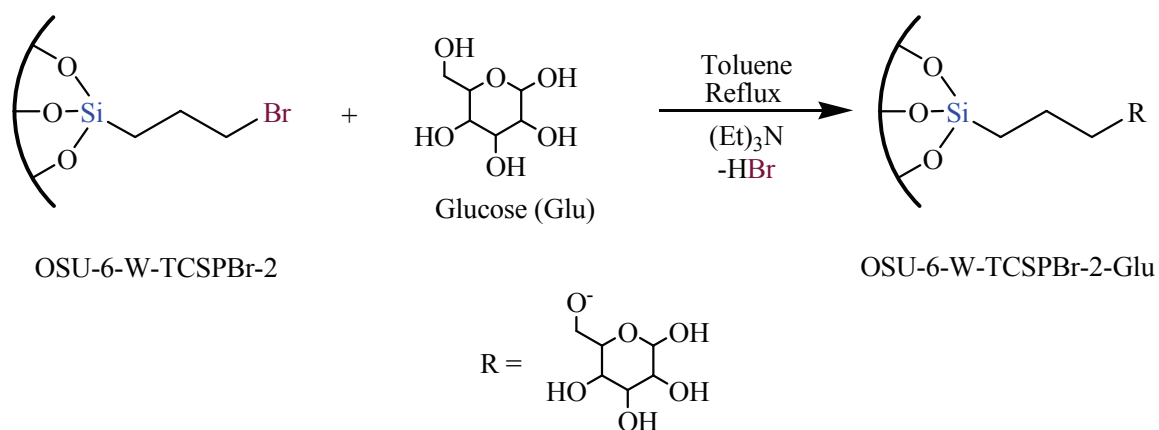
Scheme 9.5. Schematic diagram for the synthesis of adsorbent modified with glucose.

9.3.2.1. Identification of the Immobilized Glucose Ligand

I. Elemental Analysis

The carbon content is higher than that of the original material, OSU-6-W-TCSPBr-2. The total carbon content increased from 14.72% to 19.65%. This result gives indication of the incorporation of the active group into the functionalized mesoporous material.

II. FT-IR Spectroscopy

The FT-IR spectra of OSU-6-W-TCSPBr-2 and OSU-6-W-TCSPBr-2-Glu are show three characteristic absorption regions: 3500-3000 cm^{-1} due to ν(OH), 1743-1560 cm^{-1} due to δ(OH), and 1200-900 cm^{-1} due to ν(Si-O). The spectrum of OSU-6-W-TCSPBr-2-Glu also shows strong bands at 3423 cm^{-1} and 1628 cm^{-1} due to ν(OH) and δ(OH) vibrations, respectively. Moreover, the peak assigned for C-Br vibration at around 1290 cm^{-1} disappears. This confirms that the glucose functional group is chemically bonded to the surface.

III. Surface Area (BET)

The surface area of the mesoporous immobilized glucose ligand is much less than the of the bromo-functionalized mesoporous system. It dropped from 719 m^2/g to 334m^2/g.

9.3.3. OSU-6-W-TCSPBr-2 Immobilized with Di-, Tri-, and Pent-amine Functional Group[35]

These mesoporous inorganic-organic systems exhibit great potential in the extraction, recovery, and separation of metal ions from aqueous solution[9,10] and as supported ligands for catalysis.[11] Recently high resolution solid-state nuclear magnetic resonance (NMR) teqniques[36-38] and other chemical tools[16,39-42] have been used to examine their structural properties. Although the diamine ligand system is known for some time and its structure is now well established[36], there is a need for studying its metal binding chemistry in some detail. In this study, several factors were investigated to optimize its metal uptake capacities from aqueous solutions. These factors include

exposure time, pH, and competing ions. The chemical stability of the diamine ligand system was also investigated.

These amine immobilized mesoporous silicas were prepared by direct reaction of 3-bromopropyl-functionalized mesoporous silica with an excess of correspond amine ligand in the presence of N(Et)$_3$ (Scheme 9.6).[10] The triethylamine was used to combine with the generated HBr. The microanalytical data are given in Table 9.4.
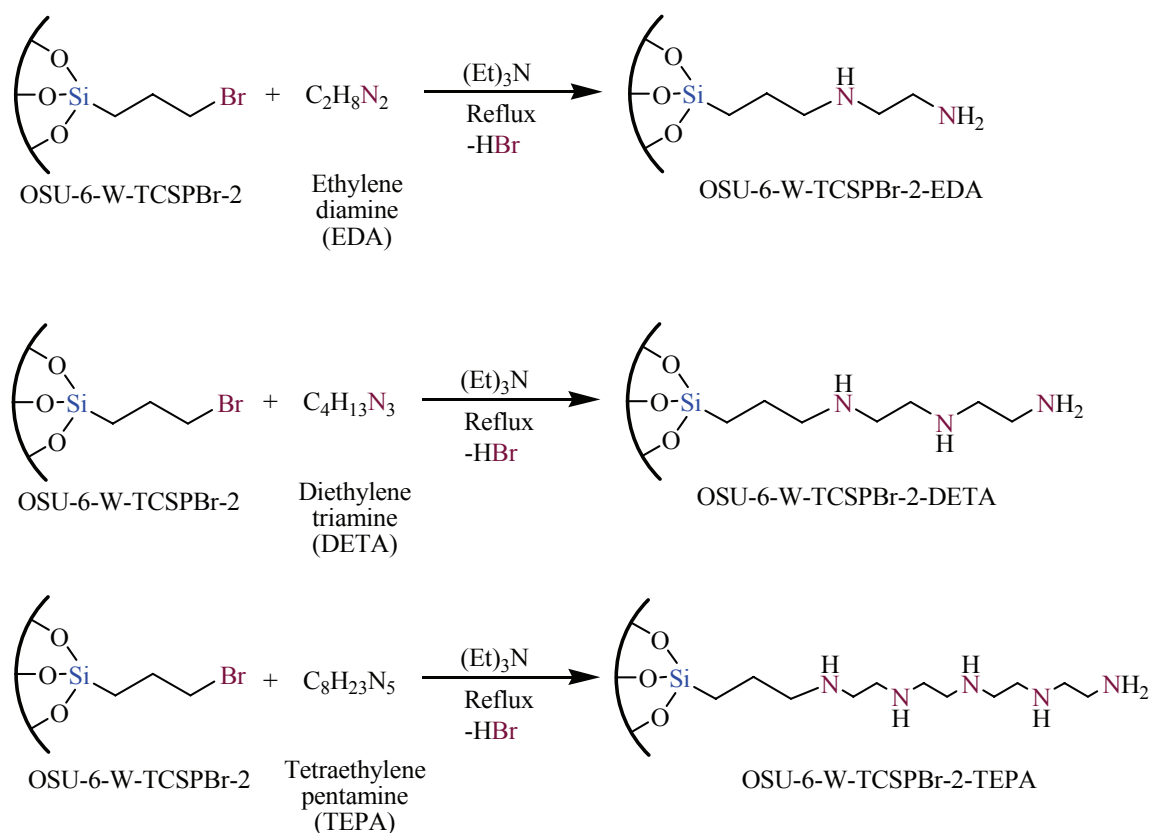
Scheme 9.6. Schematic diagram for the synthesis of adsorbents modified with EDA, DETA and TEPA.

9.3.3.1. Identification of the Immobilized Di-, Tri-, and Pent-amine Group

I. Elemental Analysis

Table 9.4 indicates that the reaction of di, tri, and pent-amine with bromofunctionalized mesoporous silica was complete and almost all bromine atoms were replaced by the amine functions. The lower percentages of C and N than the expected values may be due to the polyamine anchoring at more than one amine group.

Table 9.4. Elemental analysis data for OSU-6-W-TCSPBr-2 Immobilized Amine Ligand Systems

Immobilized Sample	C%	N%	C/N
OSU-6-W-TCSPBr-2-EDA	21.31	9.74	2.19
OSU-6-W-TCSPBr-2-DETA	29.67	13.11	2.26
OSU-6-W-TCSPBr-2-TEPA	42.78	22.70	1.88

II. FT-IR and ^{13}C Spectra

The FT-IR spectra for the immobilized diamine ligands were recorded at RT in the range 4000–400 cm^{-1}. There were four major regions of absorption at 3500–3000 cm^{-1}, 2980-2800 cm^{-1}, 1600–1500 cm^{-1}, and 1200–900 cm^{-1} due to ν(OH) stretching, δ(NH$_2$) deformations, and ν(Si-O) stretching vibrations.[43] The presence of peaks in the 1600-1500 cm^{-1} region confirm the attachment of the amine groups onto the functionalized OSU-6-W-TCSPBr-2.

III. Surface Area (BET)

The surface area of the three immobilized amine active groups, OSU-6-W-TCSPBr-2-EDA, OSU-6-W-TCSPBr-2-DETA, and OSU-6-W-TCSPBr-2-TEPA, are

409, 357, and 266 m^2/g, respectively. From the surface area measurements, it is clear that immobilization of amine groups inside the pores occured.

9.3.4. Metal Uptake Study

9.3.4.1. Effect of pH

The effect of changing the solution pH on the uptake of copper, zinc, and cadmium ions is shown in Figure 9.7. The results show an increase of metal ion uptake with increasing pH value reaching a maximum at pH 5.5 in case of copper, at pH 6.0 in the case of zinc, and at pH 7.0 in the case of cadmium.
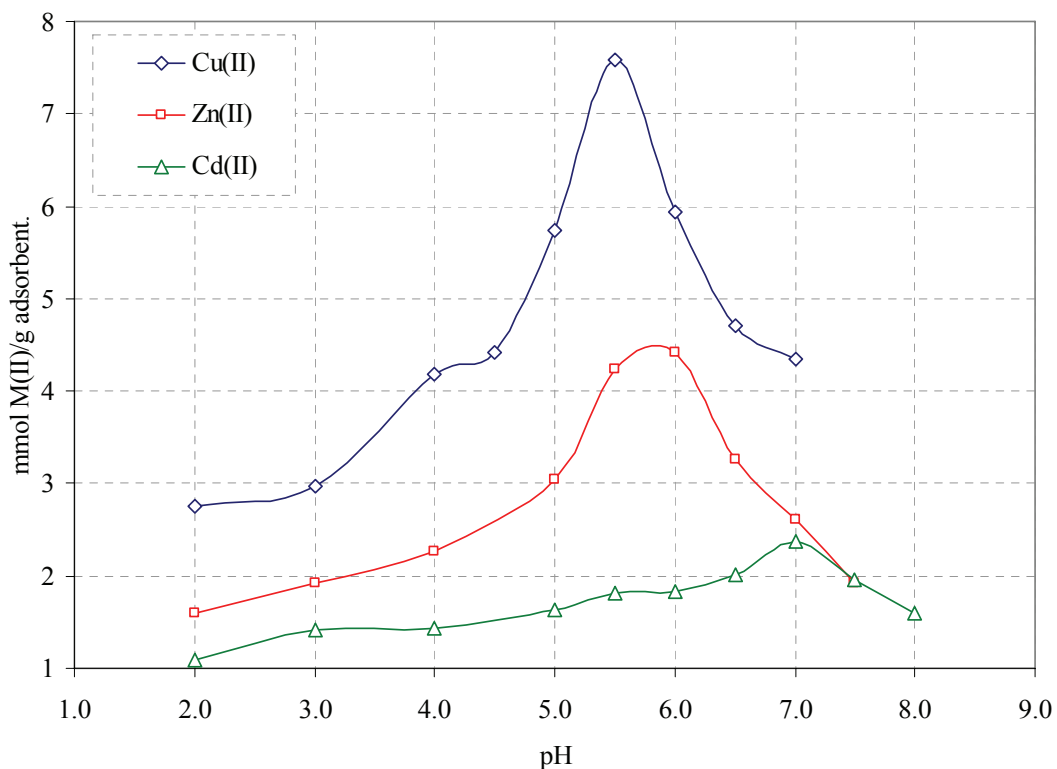

Figure 9.7. Metal uptake versus pH (pH 2–8, HCl/acetate solution, 4 hrs shaking time) using OSU-6-W-TCSPBr-2-EDA.

Lower uptake occurs at lower pH values due to the protonation of the amine moieties.[9-11,43,44] The uptake study at high pH > 10 will lead to the dissolving of the mesoporous silica.

9.3.4.2. Effect of Exposure Time

The metal ion (Cu^{2+}, Zn^{2+}, and Cd^{2+}) uptake rate as mmol M^{2+}/g ligand versus time (min), was determined by shaking the diamine ligand in aqueous solution of the divalent metal ion at different time intervals. The results are given in Figure 9.8.
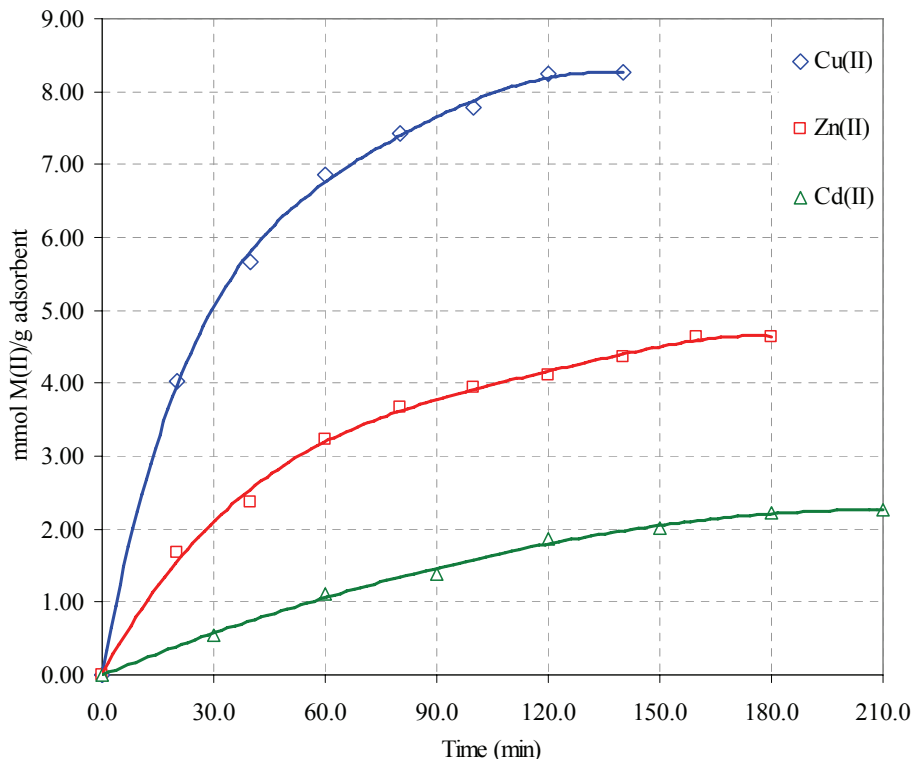

Figure 9.8. The uptake of Cu^{2+}, Zn^{2+}, and Cd^{2+} ions by the mesoporous immobilized diamine ligand system versus time.

It is shown that the metal ion uptake increased as a function of exposure time in a nonlinear fashion. This is consistent with the suggestions of El-Nahhal and coworkers.[36]

The rate of uptake of the different metal ions are faster than that reported by El-Nahhal *et al.*[36] This can be attributed to the high surface area and to the large pore size. Moreover, the adsorption rate is first order and the rate constant of the adsorption for the three metal ions, Cu^{2+}, Zn^{2+}, and Cd^{2+}, are 0.028, 0.019, and 0.014 min^{-1}, respectively.

9.3.4.3. Uptake Capacities

The uptake capacity of the modified mesoporous silicas immobilized di-, tri-, and pent-amine ligand systems was investigated using different amount of adsorbents and one constant concentration of copper, zinc, and cadmium ions (100 ppm) at pH 5.5, 6.0, and 7.0, respectively. The results are shown in Figure 9.9, 9.10, and 9.11. The maximum uptakes were calculated from the Langmuir adsorption isotherms and are listed in Table 9.5 and Table 9.6 lists the approximate formulas for the complexes formed.

Figure 9.9. The langmuir adsorption isotherms of Cu^{2+}, Zn^{2+}, and Cd^{2+} ions adsorbed by OSU-6-W-TCSPBr-2-EDA adsorbent.
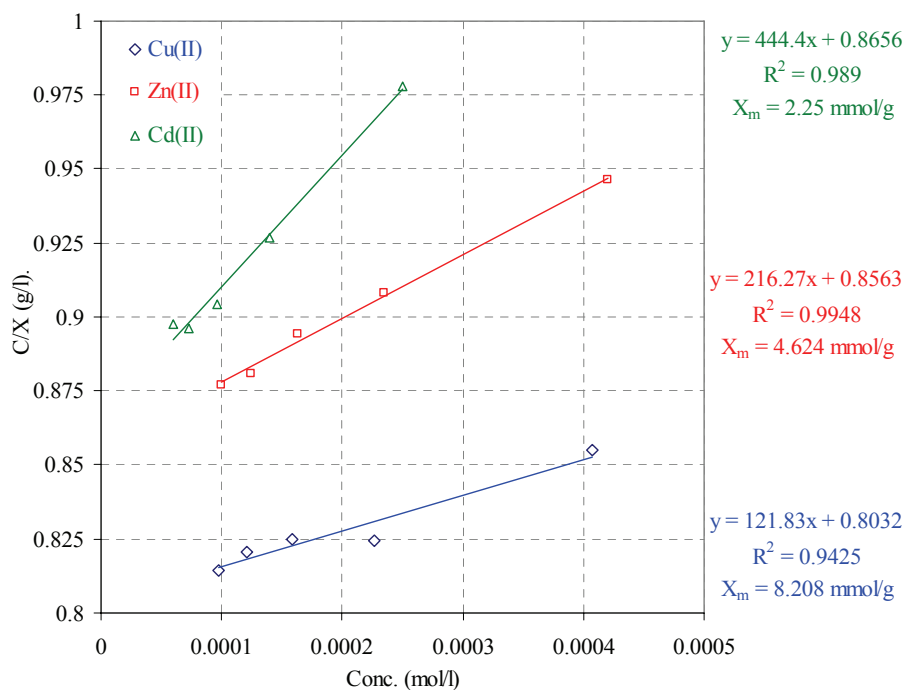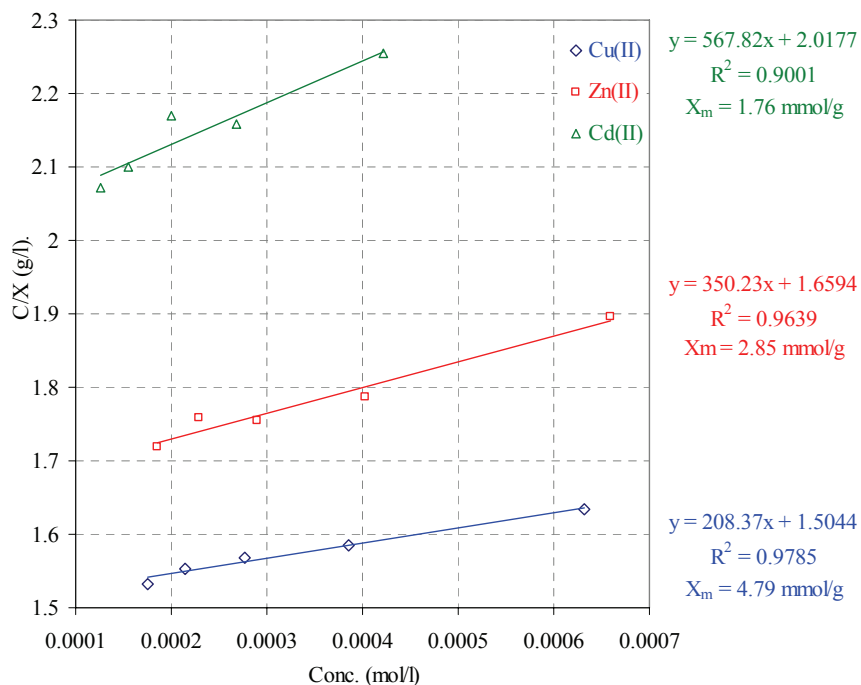
Figure 9.10. The langmuir adsorption isotherms of Cu^{2+}, Zn^{2+}, and Cd^{2+} ions adsorbed by OSU-6-W-TCSPBr-2-DETA adsorbent.
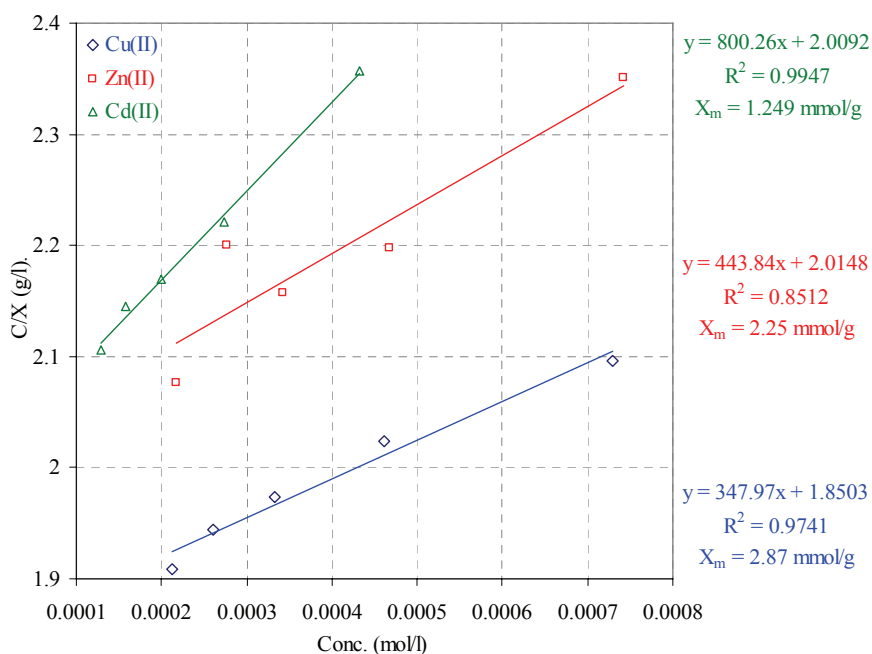

Figure 9.11. The langmuir adsorption isotherms of Cu^{2+}, Zn^{2+}, and Cd^{2+} ions adsorbed by OSU-6-W-TCSPBr-2-TEPA adsorbent.

Table 9.5. The uptake capacities from the Langmuir adsorption isotherms.

Adsorbent	Uptake capacity (mg/g)		
	Cu^{2+}	Zn^{2+}	Cd^{2+}
OSU-6-W-TCSPBr-2-EDA	522	302	253
OSU-6-W-TCSPBr-2-DETA	304	186	198
OSU-6-W-TCSPBr-2-TEPA	182	147	141

Table 9.6. The approximate formulas for the complexes formed.

Adsorbent	[group] mmol/g	Group : metal ion		
		Cu^{2+}	Zn^{2+}	Cd^{2+}
OSU-6-W-TCSPBr-2-EDA	3.38	(2:5)	(3:4)	(3:2)
OSU-6-W-TCSPBr-2-DETA	3.12	(2:3)	(1:1)	(2:1)
OSU-6-W-TCSPBr-2-TEPA	3.24	(1:1)	(3:2)	(2:1)

9.3.4.4. Effect of Competing Ions

The uptake of a mixture of copper, zinc, and cadmium (0.05 mmol each) by 150 mg of the mesoporous silica immobilized diamine ligand system was studied at three different pH values (5.5, 6.0, and 7.0). Maximum uptakes for copper, zinc, and cadmium ions were achieved at their optimum pH values (Table 9.6). For example, at pH 5.5, the uptake capacity is in the order: copper > zinc > cadmium, whereas at pH 6.0, the uptake is in the order of zinc > copper > cadmium and at pH 7.0 the order of uptake is zinc > cadmium > copper. Therefore the presence of competing ions does not affect considerably the maximum uptake that might be achieved at the optimum pH except for cadmium. Cadmium was affected significantly by the presence of the other competing

ions. This may be due to lower stability of the cadmium complexes compared to the

other metal ions.

Table 9.6. Metal Uptake (Per 150 mg Ligand) of Mesoporous-Immobilized Diamine for a Mixture of Metal Ions[a].

pH	Cu^{2+} (mmol)			Zn^{2+} (mmol)			Cd^{2+} (mmol)			Cu^{2+} + Zn^{2+} + Cd^{2+} (mmol)
	a	b	c	a	b	c	a	b	c	
5.5	0.050	0.044	47.31	0.042	0.032	34.41	0.024	0.017	18.28	0.093
6.0	0.046	0.036	36.00	0.050	0.039	39.00	0.037	0.025	25.00	0.100
7.0	0.033	0.023	26.44	0.039	0.035	40.23	0.049	0.029	33.33	0.087

[a] 0.05 mmol of each metal ion was used. a: The uptake of metal ion when exist alone; b: The uptake of metal ion from mixture of competing ions; c: Calculated percentage of each metal uptake based on the total amount of metal uptake

9.4. CONCLUSION

In conclusion, the synthesis of OSU-6-W-TCSPBr-1 and OSU-6-W-TCSPBr-2

provides a convenient method of tailoring the surface properties of mesoporous silicates

via organic functionalization and increase the surface coverage. The post-synthesis

grafting methods using this modification method applied here in this research work

proved to be suitable to overcome all problems mentioned previously such as low

loading. Both modified samples, OSU-6-W-TCSPBr-1 and OSU-6-W-TCSPBr-2, have

relatively well-ordered structures and high surface areas, on the basis of XRD, and N_2

adsorption measurements. The average pore diameters are in the range of mesoporous

materials, thus permitting size selectivity for large molecules. The reactivity of the

surface bromopropyl functional groups renders OSU-6-W-TCSPBr-2 an ideal starting

material for many other surface modifications, resulting in mesoscopic inorganic-organic hybrid materials with specific functional groups.

Mesoporous silicas carrying di-, tri-, or penta-amine functional group of the formula $(MeO)_3Si(CH_2)_3E$ [E = $NH(CH_2)_2NH_2$, $NH(CH_2)_2NH(CH_2)_2NH_2$, $NH(CH_2)_2NH(CH_2)_2NH(CH_2)_2NH(CH_2)_2NH_2$] have been successfully prepared by replacement of the bromine in bromopropylsiloxane (OSU-6-W-TCSPBr) with ethylenediamine (EDA), diethylenetriamine (DETA), or tetraethylenepentamine (TEPA), respectively. The mesoporous silicas with the di-, tri-, and pent-amine ligand systems exhibit high potential for separation and preconcentration of divalent metal ions (Cu^{2+}, Zn^{2+}, and Cd^{2+}). The tendency to chemisorb these divalent metal ions by these functionalized systems at the optimum conditions was found in the order: $Cu^{2+} > Zn^{2+} > Cd^{2+}$.

A comparison between the metal ion uptake using the modified samples prepared in this work and the modified samples used by Zaggout *et al.,*[35] group was performed. In general, our modified samples exhibit higher metal ion uptake than their samples. This is simply due to better diffusion of the metal ion which is a consequent of high surface area and large pore size, so the ligand groups become more accessible for the metal ions and therefore higher uptake was observed. Moreover, our sample has more functional groups on the surface than reported by Zaggout *et al.* Similar trends are reported for monoamine ligand systems.[43]

9.5. REFERENCES

1. Adjemian, A. In: *Hydrometallurgy' 94*, Chapman & Hall, Cambridge, UK **1994,** 3-11.
2. Sigel, H. Editor, *Metal ions in biological systems*, Dekker, New York **1988**, 24.
3. Scheinberg, I. H.; Morell, A. G.. Ceruloplasmin. *Inorg. Biochem.* **1973,** *1,* 306-319.
4. Dingman, J.; Siggia, Jr. S.; Barton, C.; Hiscock, K. B.. Concentration and separation of trace metal cations by complexation on polyamine-polyurea resins. *Anal. Chem.* **1972,** *44*(8), 1351-1357.
5. Moyers, E. M.; Fritz, J. B.. Preparation and Analytical Applications of A Propylenediaminetetraacetic Acid Resin. *Anal. Chem.* **1977,** *49*(3), 418-423.
6. Blount, C. W.; Leyden, D. E.; Thomas, T. L.; Guill, S. M.. Application of chelating ion exchange resins for trace element analysis of geological samples using X-ray fluorescence. *Anal. Chem.* **1973,** 45(7), 1045-1050.
7. Bohra, S.; Mathur, R.; Mathur, N. K.; Mathur, P. N.. Synthesis and application of guaran hydroxamic acid derivative. *J. Polym. Mater.* **1992,** *9,* 101-104.
8. Prado, A. G. S.; Airoldi, C.. Effect of the pesticide 2,4-D on microbial activity of the soil monitored by microcalorimetry. *Thermochim. Acta* **2000,** *349*(1-2), 17-22.
9. Khatib, I. S.; Parish, R. V.. Insoluble ligands and their applications. I. A comparison of silica-immobilized ligands and functionalized polysiloxanes. *J. Organomet. Chem.* **1989,** *369*(1), 9-16.
10. El-Nahhal, I. M.; Parish, R. V. Insoluble ligands and their applications. III. Polysiloxane diaminoethane derivatives. *J. Organomet. Chem.* **1993,** *452*(1-2), 19-22.
11. Parish, R. V.; Habibi, D.; Mohammadi, V.. Insoluble ligands and their applications. II. Polysiloxane-phosphine ligands, their complexes, and hydrogenation catalysts. J. Organomet. Chem. **1989,** *369*(1), 17-28.
12. Saadeh, S. M.; El-Ashgar, N.; El-Nahhal, I. M.; Chehimi, M.; Maquet, J.; Babonneau, F.. Synthesis, characterization and applications of polysiloxane networks with immobilized pyrogallol ligands. *Appl. Organometal. Chem.* **2005,** *19*(6), 759-767.
13. Harris, W. R.; Carrano, C. J.; Cooper, S. R.; Sofen, S. R.; Avdeef, A. E.; McArdle, J. V.; Raymond, K. N.. Coordination chemistry of microbial iron transport compounds. 19. Stability constants and electrochemical behavior of ferric enterobactin and model complexes. *J. Am. Chem. Soc.* **1979,** *101*(20), 6097-6104.
14. Cauvel, A.; Renard, G.; Brunel, D.. Monoglyceride Synthesis by Heterogeneous Catalysis Using MCM-41 Type Silicas Functionalized with Amino Groups. *J. Org. Chem.* **1997,** *62,* 749-751.
15. Sutra, P.; Fajula, F.; Brunel, D.; Lentz, P.; Daelen, G.; Nagy, J. B.. ^{29}Si and ^{13}C MAS-NMR characterization of surface modification of micelle-templated silicas during the grafting of organic moieties and end-capping. *Colloids Surf., A: Physicochemical and Engineering Aspects* **1999,** *158*(1-2), 21-27.
16. Caravajal, G. S.; Leyden, D. E.; Quinting, G. R.; Maciel, G. E.; Structural Characterization of (3-Aminopropyl)triethoxysilane-Modified Silicas by Silicon-29 and Carbon-13 Nuclear Magnetic Resonance. *Anal. Chem.* **1988**, *60*(17), 1776-1786.
17. Brunel, D.; Bellocq, N,; Sutra, P.; Cauvel, A.; Laspéras, M.; Renzo, F. D.; Galarneau, A.; Fajula, F.. Transition-metal ligands bound onto the micelle-templated silica surface. *Coord. Chem. Rev.* **1998,** *178-180,* 1085-1108.

18. Blanc, A. C.; Valle, S.; Renard, G.; Brunel, D.; Macquarrie, D. J.; Quinn, C. R.. The preparation and use of novel immobilized guanidine catalysts in base-catalyzed epoxidation and condensation reactions. *Green Chemistry* **2000,** *2*(6), 283-288.
19. Armistead, C. G.; Hockey, J. A.. Reactions of chloromethyl silanes with hydrated Aerosil silicas. *Trans. Faraday Soc.* **1967,** *63,* 2549-2556.
20. Park, M.; Komarneni, S.. Stepwise functionalization of mesoporous crystalline silica materials. *Micropor. Mesopor. Mater.* **1998,** *25*(1-3), 75-80.
21. Brunel, D.. Functionalized micelle-templated silicas (MTS) and their use as catalysts for fine chemicals. *Micropor. Mesopor. Mater.* **1999,** *27*(2-3), 329-344.
22. Song, C. E.; Lee, S. G.. Supported Chiral Catalysts on Inorganic Materials. *Chem. Rev.* **2002,** *102*(10), 3495-3524.
23. Blitz, J. P.; Murthy, R. S. S.; Leyden, D. E.. The Role of Amine Structure on Catalytic Activity for Silylation Reactions with Cab-O-Sil. *J. Colloid Interface Sci.* **1988,** *126*(2), 387-392.
24. (a) Tripp, C. P.; Hair, M. L.. Direct Observation of the Surface Bonds between Self-Assembled Monolayers of Octadecyltrichlorosilane and Silica Surfaces: A Low-Frequency IR Study at the Solid/Liquid Interface. *Langmuir* **1995,** *11*(4), 1215-1219. (b) Hair, M. L.; Tripp, C. P.. Alkylchlorosilane reactions at the silica surface. *Colloids and Surfaces, A: Physicochemical and Engineering Aspects* **1995,** *105*(1), 95-103. (c) Tripp, C. P.; Hair, M. L.. Reaction of Methylsilanols with Hydrated Silica Surfaces: The Hydrolysis of Trichloro-, Dichloro-, and Monochloromethylsilanes and the Effects of Curing. *Langmuir* 1995, 11(1), 149-155.
25. Tripp, C. P.; Hair, M. L.. Reaction of chloromethylsilanes with silica: a low-frequency infrared study. *Langmuir* **1991,** *7*(5), 923-927.
26. Pape, P. G.; Plueddemann, E. P.. Methods for improving the performance of silane coupling agents. *J. Adhes. Sci. Technol.* **1991,** *5*(10), 831-842.
27. Antochshuk, V.; Jaroniec, M. Simultaneous modification of mesopores and extraction of template molecules from MCM-41 with trialkylchlorosilanes. *Chem. Commun.* **1999,** *23,* 2373-2374.
28. Azzopardi, M. J.; Arribart, H.. In situ FTIR study of the formation of an organosilane layer at the silica/solution interface. *J. Adhes.* **1994,** *46*(1-4), 103-115.
29. Kresge, C. T.; Leonowicz, M. E.; Roth, W. J.; Vartuli, J. C.; Beck, J. S. Ordered Mesoporous Molecular Sieves Synthesized by a Liquid-Crystal Template Mechanism. *Nature* **1992,** *359*, 710-712.
30. Zheng, S.; Gao, L.; Guo, L.. Synthesis and characterization of copper(II)-phenanthroline complex grafted organic groups modified MCM-41. *Mater. Chem. Phys.* **2001,** *71*(2), 174-178.
31. Socrates, G.. *Infrared Characteristic Group Frequencies: Tables and Charts, second ed.*, Wiley, Chichester, **1994**.
32. Vrancken, K. C.; Van Der Voort, P.; Possemiers, K.; Vansant, E. F. Surface and Structural Properties of Silica Gel in the Modification with γ-Aminopropyltriethoxysilane. *J. Colloid and Interface Sci.* **1995,** *174*(1), 86-91.
33. Sander, L. C.; Wise, S. A.. Recent advances in bonded phases for liquid chromatography. *Crit. Rev. Anal. Chem.* **1987,** *18*(4), 299-415.
34. Unger, K. K.. Packings and Stationary Phases in Chromatographic Techniques, Marcel Dekker, Moscow (1990).

35. Zaggout, F. R.; El-Nahhal, I. M.; El-Ashgar, N. M.. Uptake of divalent metal ions (Cu^{2+}, Zn^{2+}, and Cd^{2+}) by polysiloxane immobilized diamine ligand system. *Analytical Letters* **2001,** *34*(2), 247-266.

36. Yang, J. J.; El-Nahhal, I. M.; Chuang, I.; Maciel, G. E.. Synthesis and solid-state NMR structural characterization of polysiloxane-immobilized amine ligands and their metal complexes. *J. Non-Cryst. Solids* **1997,** *209*(1,2), 19-39.

37. El-Nahhal, I. M.; Yang, J. J.; Chuang, I. S.; Maciel, G. E.. Synthesis and solid-state NMR structural characterization of polysiloxane-immobilized thiol and thiol-amine ligands. *J. Non-Cryst. Solids* **1996,** *208*(1-2)*,* 105-118.

38. Yang, J. J.; El-Nahhal, I. M.; Maciel, G. E.. Synthesis and solid-state NMR structural characterization of some functionalized polysiloxanes. *J. Non-Cryst. Solids* **1996,** *204*(2)*,* 105-117.

39. Chiang, C. H.; Ishida, H.; Koenig, J.. The Structure of γ-Aminopropyltriethoxysilane on glass surfaces. *J. Colloid Interface Sci.* **1980,** *74*(2), 396-404.

40. Ishida, H.; Chiang, C. H.; Koenig, J. L.. The structure of aminofunctional silane coupling agents. 1. γ-Aminopropyltriethoxysilane and its analogs. *Polymer* **1982,** *23*(2), 251-257.

41. Taylor, I.; Howard, A. G. Measurement of primary amine groups on surface-modified silica and their role in metal binding. *Anal. Chimica Acta* **1992,** *271*(1), 77-82.

42. El Nahhal, I. M.; Chehimi, M. M.; Cordier, C.; Dodin, G.. XPS, NMR and FTIR structural characterization of polysiloxane-immobilized amine ligand systems. *J. Non-Cryst. Solids* **2000,** *275*(1,2), 142-146.

43. El-Nahhal, I. M.; Zaggout, F. R.; El-Ashgar, N. M.. Uptake of divalent metal ions (Cu^{2+}, Zn^{2+} and Cd^{2+}) by polysiloxane immobilized monoamine ligand system. *Anal. Lett.* **2000,** *33*(10), 2031-2053.

44. Mahmoud, M. E.. Comparison of metal uptake properties of silica gel-bound ion exchangers and some amine derivatives. *Anal. Lett.* **1996,** *29*(10), 1791-1804.

VITA

Zeid Abdullah AL-Othman

Candidate for the Degree of

Doctor of Philosophy

Thesis: SYNTHESIS, MODIFICATION, AND APPLICATION OF MESOPOROUS
MATERIALS BASED ON MCM-41

Major Field: Chemistry

Biographical:

Personal Data: Born in Al Kharj, Kingdom of Saudi Arabia, on Jun 28, 1976.

The son of Abdullah Mohammad AL-Othman and Norah Zeid AL-Othman.

Education: Graduated from Al Delam High School, Al Delam, Kingdom of Saudi
Arabia in June, 1993; received Bachelor of Science degree with honor in
Chemistry from King Saud University (KSU), Riyadh, Kingdom of Saudi
Arabia in July, 1997;   Completed requirements for the Doctor of
Philosophy degree in Chemistry at Oklahoma State University, Stillwater,
Oklahoma, in December, 2006.

Experience: Employed by King Saud University, Riyadh, Kingdom of Saudi
Arabia as a teaching assistant from July 1997 to July 1998. Worked as a
graduate researcher in the department of chemistry, Oklahoma State
University, Stillwater, Oklahoma, USA, with scholarship from King Saud
University from January, 2000 to December, 2006.

Professional Membership: American Chemical Society (ACS), American
Association for the Advancement of Science (AAAS), Materials Research
Society (MRS), Saudi Chemical Society (SCS), American Ceramic
Society (ACerS), and Phi Lambda Upsilon (PLU, Honorary Chemical
Society).

Name: Zeid Abdullah AL-Othman   Date of Degree: December, 2006

Institution: Oklahoma State University   Location: Stillwater, Oklahoma

Advisor: Dr. Allen W. Apblett

Title of Study: **Synthesis, Modification, and Application of Mesoporous Materials Based on MCM-41**

Pages in Study: 438   Candidate for the Degree of Doctor of Philosophy

Major Field: Chemistry

Scope and Method of Study: The purpose of the investigation carried out in this research work was to synthesize mesoporous materials based on MCM-41 with high surface areas, large pore sizes, narrow pore size distributions, and high thermal, hydrothermal, and mechanical stabilities. This was completed by following the same procedures reported for the fabrication of the MCM-41 but with alterations in the surfactants and the additives used, and the reaction conditions employed such as the pH, the temperature, and aging time. Moreover, we aimed to modify these synthesized mesoporous materials with different functional groups of interest and evaluate their abilities in adsorption and separation of transition and heavy metal ions, and radioactive materials from aqueous medium. The functionalization of these mesoporous materials was done using different methods in order to maximize the number of groups on the surface and inside the pores. Different techniques such as infrared (IR), solid-state ^{29}Si and ^{13}C nuclear magnetic resonance (NMR), X-ray powder diffraction (XRD), thermal gravimetric analyses (TGA), and scanning and transmission electron microscopes (SEM and TEM) were used to confirm the production of the desired products. The surface area, pore size and pore size distribution were determined using the surface area analysis (BET) method. The surface properties (*e.g.,* number of groups on the surface) of these materials were determined by the adsorption of a proper probing molecule. The adsorption and separation abilities of these modified materials for the transition and heavy metal ions, and radioactive materials in aqueous solution were performed in the pH range from 2 to 8 at room temperature. The equilibrium concentration of the metal ions were determined using lead analysis test kit for the lead and using ultraviolet-visible (UV-Vis), inductive couple plasma (ICP), and atomic absorption spectroscopy (AAS) for the rest of materials.

Findings and Conclusions: The synthesized mesoporous materials possess high surface areas, large pore sizes, narrow pore size distributions, and high thermal, hydrothermal, and mechanical stabilities. The modified mesoporous materials were found to have high selectivity and capacity in the adsorption and separation of the transition and heavy metal ions in the aqueous solution. In addition, they showed great selectivity and capacity for the adsorption and separation of the radioactive materials in aqueous medium.

ADVISOR'S APPROVAL_____Dr. Allen Apblett_____